

AD-A247 666



①
DTIC
SELECTED
MAR 20 1992
S C D

NWC TP 6575

Parachute Recovery Systems Design Manual

by

Theo W. Knacke
Contractor
for the
Recovery Systems Division
Aerosystems Department

MARCH 1991

NAVAL WEAPONS CENTER
CHINA LAKE, CA 93555-6001



Approved for public release; distribution
is unlimited

U.S. Navy Edition

This manual may be distributed
only to U.S. Government personnel.

DEFENSE TECHNICAL INFORMATION CENTER

92 3 20 048



9207158

INITIAL DISTRIBUTION

- 9 Naval Air Systems Command
 - AIR-01 (1)
 - AIR-05 (1)
 - AIR-05TA (1)
 - AIR-42 (1)
 - AIR-42A (1)
 - AIR-421 (1)
 - AIR-5004 (2)
 - PMA-248 (1)
- 4 Chief of Naval Operations
 - OP-941J (1)
 - OP-944C (1)
 - OP-953F (1)
 - OP-983C (1)
- 3 Naval Sea Systems Command
 - PMS-422-2 (1)
 - Technical Library (2)
- 1 Naval Telecommunications Command (Code 124, C. Scallorn)
- 1 Space and Naval Warfare Systems Command (SPAWAR-310)
- 1 Commander in Chief, U. S. Pacific Fleet, Pearl Harbor (Code 325)
- 1 Commander, Third Fleet, San Francisco
- 1 Commander, Seventh Fleet, San Francisco
- 1 Cruise Missile Project (PDA-14)
- 4 Naval Warfare Assessment Center, Naval Weapons Station, Seal Beach, Corona
 - Code 821 (1)
 - Code 842 (1)
 - Code 8435 (1)
 - Code 8511 (1)
- 2 Naval Academy, Annapolis (Director of Research)
- 2 Naval Air Test Center, Patuxent River
 - TS-211, R. Olsen (1)
 - TS-222, S. Williams (1)
- 2 Naval Electronic Systems Security Engineering Center
 - Code 2102D, S. Kopyto (1)
 - Code 2201A, J. Care (1)
- 1 Naval Ship Weapon Systems Engineering Station, Port Hueneme (Code 4210)
- 1 Naval War College, Newport
- 1 Operational Test and Evaluation Force, Atlantic
- 8 Pacific Missile Test Center, Point Mugu
 - Code 0143 (1)
 - Code 1170 (1)
 - Code 3140 (1)
 - Code 3410 (1)
 - Code DP-1 (1)
 - Code DP-2 (1)
 - Code DP-3.2 (1)
 - Code DP-5 (1)
- 1 Headquarters, U. S. Army (DAMA-PPM-T, Block)
- 1 Army Ballistic Missile Defense Systems Command, Huntsville (BMDSC-RD, G. E. Wooden)
- 1 Army Communications Research and Development Command, Fort Monmouth (DRDCO-COM-RY-3, Coumeri)
- 2 Army Development and Readiness Command, Alexandria
 - DRCDE-RT, St. Jean (1)
 - DRCQA-S, Gonzales (1)

7 Air Force Wright Laboratories, Wright-Patterson Air Force Base
 WL/ENECA (4)
 WL/FIVR, B. Pinnell (2)
 WL/XOG, G. Loftin (1)
 1 Eastern Space and Missile Center, Patrick Air Force Base (ESMC/ROD, B. Loar)
 1 Rome Air Development Center, Hanscom Air Force Base (RADC/EEV, J. C. DiLeo)
 2 San Antonio Air Logistics Center, San Antonio (SA-ALC/MMILE, J. Foster)
 1 Western Space and Missile Center, Vandenberg Air Force Base (WSMC/RSDO, C. Brown)
 2 3246th Test Wing, Eglin Air Force Base
 TEERS, E. Poschell (1)
 TEIM, AMRAAM JTF (1)
 10 6510th Test Wing, Edwards Air Force Base (DOED, M. Wuest)
 1 6520th Test Group, Edwards Air Force Base (ENDD, J. Ramos)
 1 Defense Logistics Agency Headquarters, Alexandria (DLA-QP)

 3 Johnson Space Center (NASA), Houston, TX
 Code EG3, R. Meyerson (1)
 Code ET13, K. Hinson (1)
 Code SD4/K1, D. T. Flanagan (1)
 4 National Security Agency, Fort George G. Meade
 Code R-13, M. Bloom (1)
 Code S-13 (1)
 Code S-63, J. Stevenson (1)
 Code S-83, S. Tuss (1)
 1 Institut de Mechanique Des Fluides, Laboratoire Associe au C.N.R.S. (LA03)
 (P. M. Dutto)

ON CENTER DISTRIBUTION

1 Code 01
 1 Code 06
 1 Code 31
 1 Code 32
 4 Code 343 (3 plus Archives copy)
 2 Code 3463
 1 Code 38
 1 Code 61
 1 Code 62
 1 Code 623
 1 Code 64
 2 Code 641
 6 Code 6411
 1 Code 64113
 2 Code 6412
 6 Code 6414
 6 Code 6415, Kolb
 6 Code 642
 1 Code 643

Accession Per	
NTSC ORBRI <input checked="" type="checkbox"/>	
PTV TAB <input type="checkbox"/>	
Unnumbered <input type="checkbox"/>	
Justification	
By _____	
Distribution/ _____	
Availability Codes	
Dist	Avail and/or Special
A-1	

- 1 Army Electronics Research and Development Command, Adelphi (DRDEL-CT, Harden)
- 2 Army Materiel Command, Alexandria
 - AMCDE-F (1)
 - AMCICP-M (1)
- 1 Army Missile Command, Redstone Arsenal (DRCPM-PE-EA, Newton)
- 6 Army Test and Evaluation Command, Aberdeen Proving Ground
 - AMSTE-TE (4)
 - DRSTE-AD-I, Pancer (1)
 - DRSTE-LG-C, Frakes (1)
- 4 Army Training and Doctrine Command, Fort Monroe
 - ATDC-SL (2)
 - ATDC-T (1)
 - ATCD-TM-I, Branstetter (1)
- 4 Army Troop Support Command, St. Louis, MO (AMSTR-WD)
- 1 Aberdeen Proving Ground (STEAP-MT-G, Foote)
- 6 Army Airborne and Special Operations Test Board, Fort Bragg (ATCT-AB)
- 2 Army Combined Arms Combat Development Activity, Fort Leavenworth (ATZL-CAI-A)
- 1 Army Communications Security Logistics Activity, Fort Huachuca (SELCL-LM, Stewart)
- 8 Army Infantry Center and School, Fort Benning (ATSH-CD-MLS)
- 6 Army JFK Special Warfare Center, Fort Bragg (ATSU-CD-ML)
- 21 Army Natick Research, Development and Engineering Center, Natick, MA
 - STRNC-UAF, SMSgt. Hayes (1)
 - STRNC-UAP (20)
- 1 Army Operational Test and Evaluation Agency, Falls Church (CSTE-STS-1, Oldfield)
- 10 Army Quartermaster School, Fort Lee (ATSM-ABN)
- 1 Army Signals Warfare Laboratory, Vint Hill Farms Station, Warrenton (DELSW-SS, Paschal)
- 6 Army Yuma Proving Ground, Yuma, AZ (STEYP-MT-EP)
- 2 TEXCOM Airborne and Special Operations Test Board, Fort Bragg
 - ATCT-ABS, Capt. D. C. Bernard (1)
 - ACTC-ABT, Maj. J. Bryant (1)
- 1 Dugway Proving Ground (STEDP-PP, Peterson)
- 2 White Sands Missile Range
 - STEWS-ID-D
 - Bejarano (1)
 - P. D. Sharp (1)
- 1 Yuma Proving Ground (STEYP-MTS, Frnch)
- 6 1st SOCOM, Fort Bragg (AFVS-GCA)
- 6 XVIII Airborne Corps, Fort Bragg
 - AFZA-DPT-DI (4)
 - AFZA-GD-N (Natick LnO) (2)
- 3 Headquarters, U. S. Air Force
 - USAF/RDPT, Maj. T. Graham (1)
 - USAF/RDST, Maj. J. Galvez (1)
 - USAF/XOKCR, C. E. Edwards (1)
- 3 Air Force Systems Command, Andrews Air Force Base
 - AFSC/DCO, F. Bahrenburg (1)
 - AFSC/SDE, Capt. R. Smith (1)
 - AFSC/TB~~H~~, H. Elmore (1)
- 1 Air Force Systems Command, Space Division, Los Angeles (SD/DC, Maj. Murphy)
- 4 Air Force Acquisition Logistics Center, Pope Air Force Base (USAFAALCENT/TE)
- 2 Air Force Aeronautical Systems Division, Eglin Air Force Base (ASD/YBES, Capt. Rouse)
- 2 Air Force Armstrong Laboratories, Wright-Patterson Air Force Base (AL/CFA, S. Mehaffie)
- 3 Air Force Cryptologic Support Center, Kelly Air Force Base
 - AFCSC/EPED, Lt. Janisse (1)
 - AFCSC/EPPS, Lt. Evernham (1)
 - AFCSC/MMS, D. Hewitt (1)
- 1 Air Force Flight Test Center, Edwards Air Force Base (AFFTC/DXC, C. Heldreth)
- 1 Air Force Intelligence Agency, Bolling Air Force Base (AFIA/INTAW, Maj. R. Esaw)
- 2 Air Force Military Airlift Combat Operations Staff, Scott Air Force Base (MAC/XRT, C. Haines)
- 1 Air Force Munitions Systems Division, Eglin Air Force Base (MSD/DCO, J. Fagan)
- 4 Air Force Special Missions Operational Test and Evaluation Center, Hurlbert Field (SMOTEC/FW, SMSgt. Polek)

Parachute Recovery Systems

Design Manual

T.W. Knacke



Para Publishing, Santa Barbara, California

Parachute Recovery Systems Design Manual

by Theo W. Knacke

Published by



Para Publishing
Post Office Box 4232
Santa Barbara, CA 93140-4232, USA



Published by permission of the U.S. Navy (NWC TP 6575) at the Naval Weapons Center, China Lake, CA 93555-6001.

Right to publish granted to Para Publishing by the U.S. Navy. No part of this book may be reproduced or transmitted in any form or by any means, electronic or mechanical, including photocopying, recording or by any information storage or retrieval system without written permission from the author, except for the inclusion of brief quotations in a review.

Design copyright © 1992 by Para Publishing

First edition 1992

Library of Congress Cataloging-In-Publication Data

Knacke, T. W.

Parachute Recovery Systems Design Manual / by Theo W. Knacke. --

1st ed.

Includes bibliographical references and index.

1. Parachutes--Handbooks, Manuals, etc. I Title

ISBN 0-915516-85-3: \$49.95

TL752.K53 1992

629.134'386--dc20

91-43883

CIP

Printed in the United States of America

CONTENTS

Chapter 1 Introduction	1-1
Chapter 2 Parachute Recovery System Definitions and Description	2-1
2.1 Parachute Recovery System Definition	2-1
2.2 Parachute Recovery System Applications	2-3
2.3 Parachute Recovery System Boundaries	2-4
2.4 Parachute Recovery System Design Criteria	2-5
2.5 Reference Material	2-8
2.5.1 U.S. Air Force Reports	2-8
2.5.2 AIAA Papers	2-9
2.5.3 SAFE Symposia	2-9
2.5.4 University of Minnesota Extension Courses	2-10
2.5.5 Miscellaneous References	2-10
Chapter 3 Units of Measurement, Technical Tables, and Symbols	3-1
3.1 Units of Measurement	3-1
3.1.1 Basic Units	3-1
3.1.2 Derived Units	3-1
3.1.3 Engineering Units of Measurement	3-2
3.2 Conversion Tables	3-4
3.3 Technical Tables	3-4
3.3.1 Earth's Atmosphere	3-4
3.3.2 Dynamic Pressure	3-4
3.4 List of Symbols	3-16
3.5 Reference Material	3-20
Chapter 4 Aerodynamics as Related to Parachutes	4-1
4.1 Properties of the Atmosphere	4-1
4.1.1 Specific Weight of Air	4-1
4.1.2 Static Pressure	4-2
4.1.3 Temperature	4-2
4.1.4 Mass Density of Air	4-2
4.1.5 Gravity	4-2
4.1.6 Kinematic Viscosity	4-3
4.1.7 Reynolds Number	4-4
4.1.8 Mach Number	4-4
4.2 Continuity Law and Bernoulli Equation	4-5
4.2.1 Continuity Law	4-5
4.2.2 Bernoulli Equation	4-6
4.3 Newton's Three Laws of Motion	4-7
4.4 Forces Acting on a Body Moving Through Air	4-9
4.4.1 Symmetrical Body	4-9
4.4.2 Airflow Around an Asymmetrical Body (Airfoil)	4-10
4.5 Equilibrium of Forces in Steady Descent or Flight	4-14
4.5.1 Parachute in Steady Descent	4-14
4.5.2 Gliding Parachutes	4-17
4.5.3 Parasite Drag and Induced Drag	4-18
4.5.4 Aircraft in Horizontal Flight	4-20

4.6 Wind-Tunnel Testing of Parachutes	4-20
4.6.1 Blowers	4-21
4.6.2 Open-Throat, No-Return Wind Tunnels	4-21
4.6.3 Closed-Throat, Full-Return Wind Tunnel	4-22
4.6.4 General Comments for Wind-Tunnel Testing of Parachutes	4-22
4.7 Reference Material	4-23
Chapter 5 Parachute Characteristics and Performance	5-1
5.1 Parachute Decelerator Types	5-1
5.2 Parachute Drag and Wake Effects	5-14
5.2.1 Canopy Shape and Suspension Line Length Effects	5-16
5.2.2 Forebody Wake Effect	5-21
5.2.3 Measured Drag Coefficients of Various Types of Parachutes	5-24
5.2.4 Effect of Reynolds Number on Parachutes	5-29
5.3 Stability of Parachute Systems	5-30
5.3.1 General Definition	5-30
5.3.2 Parachute Stability	5-32
5.3.3 Stability of a Parachute Body System	5-36
5.4 Parachute Inflation Process	5-38
5.4.1 Opening Force Investigations	5-38
5.4.2 Parachute Canopy Inflation	5-41
5.4.3 Canopy Inflation Time	5-42
5.4.4 Parachute Drag-Area Increase During Canopy Filling Process	5-45
5.4.5 Effect of Canopy Loading, $W/(C_{DS})_p$, on Parachute Opening Forces	5-49
5.4.6 Methods for Calculating Parachute Opening Forces	5-53
5.4.7 Typical Parachute Opening-Force and Opening-Time Diagrams	5-62
5.5 Altitude and Canopy-Porosity Effects	5-67
5.5.1 Altitude Effects	5-67
5.5.2 Porosity Effects	5-71
5.6 Parachute Reefing	5-74
5.6.1 General Description and Application	5-74
5.6.2 Skirt Reefing	5-75
5.6.3 Skirt Reefing with Control Line	5-77
5.6.4 Vent Reefing	5-78
5.6.5 Slider Reefing	5-79
5.6.6 Continuous Disreefing	5-79
5.6.7 Drag-Area (Reefing) Ratio Versus Reefing-Line-Length Ratio	5-80
5.6.8 Forces in Reefing Lines	5-84
5.6.9 Fixed Pocketband Reefing	5-87
5.6.10 Reefing of Small-Diameter Parachutes	5-91
5.7 Canopy Shape and Canopy Pressure Distribution	5-91
5.7.1 Parachute Canopy Shape	5-91
5.7.2 Pressure Distribution in Parachute Canopies	5-93
5.8 Supersonic Inflatable Decelerators	5-97
5.8.1 Characteristics of Supersonic Flow	5-97
5.8.2 Supersonic Parachutes	5-98
5.8.3 Balloon-Type Inflatable Decelerators	5-106
5.8.4 Miscellaneous Decelerators	5-109
5.9 Maneuverable (Gliding) Parachutes	5-110
5.9.1 Parachute Types	5-110

5.9.2 Performance of Maneuverable Parachutes	5-116	
5.9.3 Opening Forces of Hi-Glide Parachutes	5-120	
5.10 Clustering of Parachutes	5-121	
5.10.1 General	5-121	
5.10.2 Loss of Drag in Cluster Applications	5-122	
5.10.3 Operational Cluster Experience	5-124	
5.11 Frequently Used Formulas in Parachute Design	5-128	
5.12 Reference Material	5-131	
 Chapter 6 Design of Parachute Assembly and Components		6-1
6.1 Parachute Deployment and Installation	6-1	
6.1.1 Parachute Deployment	6-1	
6.1.2 Uncontrolled Deployment	6-3	
6.1.3 Semicontrolled Deployment	6-3	
6.1.4 Static Line Deployment	6-4	
6.1.5 Controlled Deployment	6-5	
6.1.6 Canopy-First Deployment	6-6	
6.1.7 Drogue Gun Deployment	6-6	
6.1.8 Parachute Mortar Deployment	6-8	
6.1.9 Deployment by Rocket Extraction	6-10	
6.1.10 Cross-Wind Deployment	6-10	
6.1.11 Parachute Assembly Installation	6-11	
6.2 Parachute Design	6-13	
6.2.1 Parachute Assembly Configuration	6-13	
6.2.2 Parachute and Component Definition	6-14	
6.2.3 Design of Solid Material Parachutes	6-17	
6.2.4 Design of Slotted Parachutes	6-28	
6.3 Design of Parachute Assemblies and Components	6-38	
6.3.1 Parachute Clusters	6-38	
6.3.1.1 Cluster Configurations	6-38	
6.3.1.2 Effective Suspension-Line Riser Length	6-40	
6.3.1.3 Permanently Attached Pilot Chutes	6-40	
6.3.1.4 Canopy Ties	6-41	
6.3.1.5 Canopy Vent Size	6-41	
6.3.1.6 Cluster Parachute Deployment Bags	6-41	
6.3.1.7 Cluster Parachute Literature	6-41	
6.3.2 Pocket Bands	6-42	
6.3.3 Pilot Chutes	6-43	
6.3.4 Anti-Inversion Net	6-46	
6.3.5 Parachute Deployment Concepts	6-47	
6.3.5.1 Parachute Deployment Bags	6-48	
6.3.5.2 Banana-Peel Bag	6-50	
6.3.5.3 Deployment Sleeve	6-51	
6.3.5.4 Sacrifice Panel	6-52	
6.3.5.5 Skirt Hesitator and Quarter Deployment Bag	6-52	
6.3.5.6 General Comments on Deployment	6-54	
6.4 Parachute Stress Analysis	6-54	
6.4.1 Stress Analysis of Parachute Textile Components	6-54	
6.4.2 Load and Design Factors	6-55	

6.4.3	Preliminary Stress-Analysis Method for Solid-Material Canopies	6-58
6.4.4	Stressing of Horizontal Ribbons in Ribbon Parachutes	6-59
6.4.5	Stress Relief in the Canopy Crown Area	6-61
6.4.6	Dimensioning of Suspension Lines, Risers, and Canopy Vent and Skirt Tapes	6-61
6.5	Reefing System Design	6-61
6.5.1	General	6-61
6.5.2	Reefing System Installation	6-62
6.5.3	Reefing System Components	6-67
6.5.3.1	Reefing Rings	6-67
6.5.3.2	Reefing Line Cutters	6-69
6.5.4	Special Reefing Concepts	6-72
6.5.4.1	Continuous Disreefing	6-72
6.5.4.2	Fixed Reefing by Pocket Bands	6-73
6.5.4.3	Overinflation-Control Line (OC Line)	6-74
6.6	Designing and Fabricating in Textiles	6-74
6.6.1	Textile Materials	6-74
6.6.1.1	Natural Fibers	6-75
6.6.1.2	Man-Made Fibers	6-75
6.6.2	Spinning and Weaving of Textiles	6-78
6.6.2.1	Spinning	6-78
6.6.2.2	Fabric Weaving	6-80
6.6.3	Parachute Fabric Specifications	6-82
6.6.3.1	Parachute Cloth	6-82
6.6.3.2	Thread	6-83
6.6.3.3	Parachute Suspension Lines	6-83
6.6.3.4	Webbing and Tape	6-83
6.6.3.5	Related Specifications	6-84
6.6.4	Designing in Textiles	6-84
6.6.4.1	Measuring Textiles	6-84
6.6.4.2	Changes in Fabric Dimensions Caused by Sewing	6-85
6.6.4.3	Finished Versus Pattern Dimensions	6-85
6.6.4.4	Fullness	6-86
6.6.4.5	Tolerances	6-87
6.6.5	Designing in Kevlar	6-88
6.6.5.1	General Information	6-88
6.6.5.2	Kevlar Material	6-89
6.6.5.3	Kevlar Material Specifications	6-91
6.6.5.4	Design and Fabrication	6-92
6.7	Parachute Recovery System Weight and Volume	6-93
6.7.1	Importance of Minimum Weight and Volume	6-93
6.7.2	The Preliminary Design Method	6-94
6.7.3	The Drawing Method for Determination of Parachute Weight	6-98
6.7.4	The TWK Weight Determination Method	6-98
6.7.5	Pressure Packing of Parachute Assemblies	6-99
6.7.6	Investigation of Pressure Packing	6-101
6.8	Landing Impact Attenuation Systems	6-101
6.8.1	Landing Analysis	6-101
6.8.2	Relationship of Deceleration Stroke, Rate of Descent, and Allowable Impact Deceleration	6-103
6.8.3	Selection and Description of Impact Decelerators	6-105
6.8.3.1	General	6-105

6.8.3.2 Crushable Impact Attenuators	6-106
6.8.3.3 Air Bags	6-112
6.8.3.4 Retrorocket Landing Attenuation System	6-117
6.8.3.5 Skirt Jet Retrorocket System	6-120
6.8.3.6 Special Impact Attenuators	6-121
6.9 Reference Material	6-123
Chapter 7 Design of a Parachute Recovery and Landing System	7-1
7.1 Requirements	7-1
7.1.1 System Requirements	7-1
7.1.2 Requirements for Normal Operation	7-2
7.1.3 Requirements for Emergency Operation	7-2
7.1.4 Requirements Analysis	7-2
7.2 Landing Analysis and Impact-Attenuation System	7-3
7.2.1 Landing Analysis	7-3
7.2.2 Impact Attenuator System	7-4
7.3 Main Parachute System	7-6
7.3.1 Main Parachute System Requirements	7-6
7.3.2 Parachute Assembly Selection	7-6
7.3.3 Parachute Diameter	7-7
7.3.4 Parachute Deployment System	7-8
7.3.5 Extraction Parachute Assembly	7-10
7.3.6 Pilot Parachute Assembly	7-12
7.3.7 Main Parachute Forces	7-15
7.3.7.1 Requirements	7-15
7.3.7.2 Velocity-Altitude Profile	7-15
7.3.7.3 Force Calculation Methods	7-15
7.3.7.4 Reefed Opening Forces	7-16
7.3.7.5 Main Parachute Disreef Opening Forces	7-18
7.3.7.6 Comments on Calculated Opening Forces	7-21
7.3.7.7 Snatch Forces	7-23
7.3.8 Parachute Stress Analysis	7-24
7.3.8.1 Parachute Design Data	7-24
7.3.8.2 Parachute Forces	7-24
7.3.8.3 Main Parachute Safety and Design Factors	7-24
7.3.8.4 Suspension-Line Selection and Strength	7-25
7.3.8.5 Canopy Stress	7-26
7.3.8.6 Canopy Reinforcing Tapes	7-27
7.3.8.7 Design of Radials	7-28
7.3.8.8 Check for Proper Gore Fullness	7-29
7.3.9 Canopy Gore Shape	7-29
7.3.9.1 Vent Area	7-30
7.3.9.2 Vent Diameter	7-31
7.3.10 Pocket Bands	7-32
7.3.11 Parachute Reeling	7-33
7.3.11.1 Length of Parachute Reeling Line	7-33
7.3.11.2 Strength of the Reeling Line	7-34
7.4 High-Speed Drogue Chute Assembly	7-34
7.4.1 Requirements	7-34
7.4.2 Drogue Chute Selection	7-35
7.4.3 Required Drogue Chute Diameter	7-36
7.4.4 Computer Analysis of Drogue Chute Performance	7-38

7.4.5	Flight Emergency Recovery Conditions	7-38
7.4.6	Drogue Chute Opening Forces	7-39
7.4.6.1	Drogue Chute Reefed Opening Forces	7-39
7.4.6.2	Drogue Chute Disreef Opening Force	7-40
7.4.7	Drogue Chute Stress Analysis and Design	7-41
7.4.7.1	Drogue Chute Safety, Load, Loss, and Design Factors	7-41
7.4.7.2	Number of Gores and Suspension-Line Strength	7-41
7.4.7.3	Design of Radials, Vent and Skirt Tape, and Vent Lines	7-43
7.4.7.4	Drogue Chute Riser Design	7-44
7.4.8	Aerodynamic Design of Ribbon Parachute Canopies	7-44
7.4.8.1	Canopy Porosity	7-44
7.4.8.2	Vertical Ribbon Spacing	7-45
7.4.8.3	Drogue Chute Summary	7-47
7.4.9	Canopy Gore Design and Porosity Check	7-47
7.4.9.1	Canopy Gore Calculation	7-47
7.4.9.2	Preliminary Gore-Porosity Check	7-49
7.4.9.3	Recheck of Gore Dimensions with Vertical Ribbon Spacing, b, Equal to 1.1 Inches	7-50
7.4.9.4	Gore-Porosity Recheck	7-52
7.4.9.5	General Comments on Gore Design and Porosity Selection	7-54
7.4.9.6	Computer Programs for Determining Gore Design and Porosity Calculation	7-54
7.4.10	Ribbon Parachute Canopies with Continuous Horizontal Ribbons	7-54
7.4.11	Use of Kevlar Fabrics	7-55
Chapter 8	Parachute Recovery System Applications	8-1
8.1	Applications Analysis	8-1
8.2	Air and Space Vehicle Recovery	8-4
8.2.1	AQM-127A Supersonic Low-Altitude Target (SLAT)	8-4
8.2.2	CL 289 Reconnaissance Drone	8-5
8.2.3	Midair Retrieval of the USAF AGM-86B Air Launched Cruise Missile	8-8
8.2.4	Midair Retrieval System for the Navy AGM-109 Cruise Missile	8-10
8.2.5	Space Shuttle Solid Booster Rocket Parachute Recovery	8-12
8.3	Aircrew Emergency Escape Parachute Systems	8-13
8.3.1	Escape System Concepts	8-13
8.3.2	Military Personnel Emergency Parachute Types	8-15
8.3.3	Navy Aircrew Common Ejection Seat (NACES)	8-19
8.3.4	Aircrew Gliding Escape System (ACES)	8-21
8.3.5	Space Shuttle Crew Escape System	8-23
8.3.6	F-111 Crew Escape Module Parachute Recovery System	8-26
8.4	Airdrop of Cargo and Personnel	8-27
8.4.1	Scope of Airdrop Operations	8-27
8.4.2	Airdrop Aircraft and Procedures	8-28
8.4.3	Cargo Airdrop	8-31
8.4.4	Containers Used in Military Airdrop Operations	8-36
8.4.5	Airdrop Parachute Assemblies	8-36
8.4.6	Parachute Retrorocket Airdrop System	8-42
8.4.7	Cargo Point Delivery With Maneuverable Parachutes	8-43
8.4.8	Airdrop of Military Personnel	8-43
8.4.9	Multiple Personnel Drop	8-49
8.5	Aircraft In-Flight and Landing Deceleration by Parachute	8-49
8.5.1	General Application	8-49
8.5.2	Landing Deceleration Parachutes	8-49
8.5.2.1	Landing Roll Analysis	8-49
8.5.2.2	Landing Deceleration Parachute Design	8-51
8.5.2.3	Aircraft Installation	8-53

8.5.3	Landing Approach Parachutes	8-55
8.5.4	Aircraft Spin and Deep Stall Recovery Parachutes	8-55
8.5.4.1	Aircraft Spin Characteristics	8-55
8.5.4.2	Aircraft Deep Stall Characteristics	8-56
8.5.4.3	System Considerations	8-56
8.5.4.4	Aircraft Installation and Deployment	8-57
8.6	Ordnance Stabilization and Retardation by Inflatable Decelerators	8-60
8.6.1	Scope of Application	8-60
8.6.2	Stabilization and Retardation of Bombs, Mines, and Torpedoes	8-60
8.6.3	Bomb Retardation	8-62
8.6.4	Retardation of Aerial Mines	8-65
8.6.5	Stabilization and Retardation of Aerial Torpedoes	8-67
8.6.6	Retardation of Illuminating Flares	8-68
8.6.7	Sonar-Buoy Deceleration	8-69
8.6.8	Retardation of EC Jammers	8-70
8.6.9	Shell Recovery	8-71
8.6.10	Submunition Retardation by Parachute	8-71
8.6.11	Radar Reflecting Target Parachutes	8-73
8.7	Premeditated Parachute Jumping	8-74
8.7.1	Scope of Application	8-74
8.7.2	Military Test Jumpers	8-74
8.7.3	Paratroopers	8-77
8.7.4	Smoke Jumper Parachuting	8-78
8.7.5	Sport Parachuting	8-80
8.8	Reference Material	8-85

FIGURES

Chapter 2

2-1	System Integration and Components of a Parachute Recovery System	2-1
2-2	Schematic and Nomenclature of a Typical Ejection Seat Parachute Assembly	2-2
2-3	Parachute Applications	2-3
2-4	Parachute Performance Envelopes	2-4
2-5	Aerodynamic Decelerator Performance Range (1990)	2-5
2-6	Parachute Design Criteria	2-6

Chapter 3

3-1	Density Ratio, Temperature, and Speed of Sound Versus Altitude (Reference 3.4)	3-14
3-2	Dynamic Pressure Versus Altitude, Mach Number, and True Airspeed	3-15

Chapter 4

4-1	Typical Streamline	4-5
4-2	Pressure and Velocity Distribution in a Streamline Element	4-6
4-3	Rocket Principle	4-9
4-4	Stable Parachute in a Wind Tunnel	4-9
4-5	Airflow Around a Streamlined Body and an Open Hemisphere	4-10
4-6	Wind-Tunnel Forces Acting on an Airfoil	4-10
4-7	Aerodynamic Forces Acting on an Airfoil	4-12
4-8	Forces Acting on a Parachute	4-13
4-9	Coefficients C_D , C_T , and C_M Versus Angle of Attack, α , for a Stable and Unstable Parachute	4-13
4-10	Effect of Airflow Around a Cylinder and an Airfoil	4-15

4-11	Forces Acting on a Parachute in Steady Descent	4-16
4-12	Forces Acting on a Gliding Parachute	4-18
4-13	Forces and Moments Acting on an Aircraft in Steady Flight	4-20
4-14	Typical Air Blower	4-21
4-15	Open-Throat, No-Return Wind Tunnel	4-21
4-16	Closed-Throat, Full-Return Wind Tunnel	4-22
 Chapter 5		
5-1	Twenty-Eight-Foot-Diameter Circular, Flat Personnel Parachute	5-6
5-2	Two-Hundred-Foot-Diameter Circular, Flat Cargo Parachute	5-6
5-3	Army Paratrooper 35-Foot-Diameter Extended-Skirt Parachute	5-7
5-4	Twenty-Four-Foot-Diameter Hemispherical Parachute	5-7
5-5	Guide Surface Parachute	5-8
5-6	Seventy-Two-Foot-Diameter Annular Parachute With 24-Foot-Diameter Engagement Parachute in Midair Retrieval Configuration	5-8
5-7	Cross Parachute in Wind-Tunnel Test	5-9
5-8	Thirty-Two-Foot-Diameter Ribbon, Landing Deceleration Parachute	5-9
5-9	Ringslot Parachute	5-10
5-10	Sixty-Four-Foot-Diameter Mercury Ringsail Main Parachute	5-10
5-11	Rotofoil Parachute	5-11
5-12	Vortex Ring Parachute (Only Two of Four Adjacent Gores Are Shown)	5-12
5-13	Thirty-Five-Foot-Diameter T-10 (MC1-1B) Paratrooper Parachute, Modified With Slots and Control Lines for Glide and Controllability	5-12
5-14	Hi-Glide (Maneuverable) Parachutes	5-13
5-15	Ballute (Balloon-Type Decelerator)	5-14
5-16	Variation of Drag Coefficient With Cone Angle and Rate of Descent for Solid Fabric Parachutes	5-16
5-17	Variation of Drag Coefficient With Cone Angle and Rate of Descent for 28-Foot-Diameter Solid-Textile Parachutes	5-17
5-18	Drag Coefficient Versus Rate of Descent for Two Stable and Two Unstable Parachutes	5-18
5-19	Drag Coefficients, C_D , and C_D^* ; Canopy Area Ratio, S_p/S_c , and Diameter Ratio, D_p/D_c ; as a Function of Suspension-Line Ratio, L_e/D_c , for a One-Meter-Diameter Model Parachute	5-19
5-20	Variation of Drag Coefficient With Suspension-Line Ratio for Several Parachute Types	5-20
5-21	Parachute Drag Loss Caused by Forebody Wake	5-22
5-22	Drag Loss of the Apollo 16.5-Foot-Diameter, Ribbon Drogue Chute Caused by Different Forebodies	5-23
5-23	Determination of Effective Forebody Diameter	5-24
5-24	Drag Coefficient Versus Rate of Descent for Various Types of Solid Textile Parachutes	5-25
5-25	Drag Coefficient Versus Rate of Descent for Various Extended-Skirt Parachutes	5-26
5-26	Effect of Suspension-Line Ratio on an 1.8-Foot-Diameter Extended-Skirt Parachute	5-27
5-27	Drag Coefficient Versus Rate of Descent for Various Cross Parachutes	5-28
5-28	Drag Coefficient Versus Rate of Descent for Various Annular Parachutes	5-28
5-29	Effect of Reynolds Number on Drag Coefficient for a Sphere and Various Parachutes	5-30
5-30	Illustration of Static Stability	5-31
5-31	Graphical Illustration of Dynamic Stability	5-32
5-32	Relationship of Airflow and Stability for Various Parachutes	5-33

5-33	Moment Coefficients Versus Angle of Attack for Guide Surface; Ribbon, and Flat, Circular Parachutes, and for Porous and Nonporous Hemispheres	5-35
5-34	Various Configurations of Parachute Vehicle Attachments	5-37
5-35	Angle and Force Relationships for a Deceleration System Moving in Space	5-39
5-36	Parachute Canopy Inflation Process	5-41
5-37	Filling Distance of a Parachute Canopy	5-42
5-38	Typical Drag-Area-Versus-Time Increase for Various Parachute Types	5-45
5-39	Typical Drag-Area-Versus-Time Increase for Reefed Parachutes	5-46
5-40	Drag-Area Ratio Versus Dimensionless Filling Time	5-47
5-41	Drag-Area-Versus-Time Diagram for the Mercury Space Capsule	5-47
5-42	Drag-Area-Versus-Time Diagram for a Reefed 101-Foot-Diameter Triconical Parachute	5-48
5-43	Parachute Force Versus Time for a Wind-Tunnel Test (Infinite Mass Condition)	5-49
5-44	Force Versus Time for a Personnel Parachute Drop (Finite Mass Condition)	5-49
5-45	15.6-Foot-Diameter Ringslot B-47 Approach Parachute Opening Forces	5-51
5-46	Opening Process and Opening Force Versus Time for a Guide Surface Personnel Parachute Tested at the El Centro Whirl Tower at 250 Knots With a 200-Pound Torso Dummy	5-52
5-47	Rate of Descent Versus Canopy Loading and Parachute Applications	5-53
5-48	Opening-Force-Reduction Factor Versus Canopy Loading	5-55
5-49	Apollo Ribbon Drogue Chute Force Fluctuation Caused by Forebody Wake (Inflated Parachute Diameter, D_p , is 10.7 feet)	5-55
5-50	Opening-Force Factor Versus Mass Ratio	5-57
5-51	Opening-Force Reduction Factor, X_1 , Versus Ballistic Parameter, A	5-59
5-52	Drag-Area Profile for Parachute Inflation Sequence	5-61
5-53	Opening Forces of Various Personnel Parachutes	5-63
5-54	Snatch Force and Opening Force of the Air Force 28-Foot-Diameter Personnel Parachute, With and Without Quarter Deployment Bag	5-64
5-55	Opening Time Comparison of Three Configurations of the 28-Foot-Diameter Personnel Parachute: Standard, Standard With Pull-Down Vent Line, and Standard With Spreader Gun	6-65
5-56	Apollo Command Module, Block I, Reefed and Disreefed Opening Forces for a Single 88-Foot-Diameter Ringsail Parachute	5-65
5-57	Apollo Command Module Single Drogue Chute and Main Parachute Test Envelope	5-66
5-58	Nomenclature for Parachute Inflation Sequence	5-67
5-59	Opening Forces of Various Personnel Parachutes Tested at Altitudes from 7000 to 40,000 Feet at a Terminal Velocity of 102 KEAS	5-68
5-60	Parachute Opening Forces as a Function of Altitude for Various Types of Parachutes	5-69
5-61	15.6-Foot-Diameter Ringslot B-47 Approach Parachute Opening Forces as a Function of Altitude	5-70
5-62	Effect of Canopy Porosity on Drag Coefficient for Various Parachutes	5-72
5-63	Drag Coefficient and Oscillation as a Function of Total Porosity for 3.5-Foot-Diameter Flat and Conical Ribbon Parachutes as Measured in Wind Tunnel Tests	5-72
5-64	Opening-Force Coefficient as a Function of Total Porosity	5-73
5-65	Opening-Force Coefficient as a Function of Cloth Permeability for Cross Parachutes as Measured by the Naval Surface Warfare Center	5-74
5-66	Parachute Skirt Reeling	5-76
5-67	Parachute Skirt Reeling With Control Line	5-77

5-68	Parachute Vent Reefing	5-78
5-69	Total Parachute Force, Suspension-Line Force, and Vent-Line Force, as Functions of Vent-Line Retraction	5-78
5-70	Slider Reefing	5-79
5-71	Reefing Ratio Versus Reefing-Line Ratio for Various Parachutes	5-81
5-72	Reefing Ratio Versus Reefing-Line Ratio for Circular Flat, Conical, Triconical, and Extended-Skirt Parachutes	5-82
5-73	Reefing Ratio Versus Reefing-Line Ratio for 13.4-Foot-Diameter Conical Ribbon Parachute Tested in Aircraft Tow Test	5-83
5-74	Force Relationship in a Reefed Parachute	5-85
5-75	Reefed Canopy Profiles for Two Parachute Canopies of 0% and 20% Porosity	5-86
5-76	Ratio of Reefing-Line Force to Maximum Reefed Parachute Force Versus Reefing-Line Ratio	5-86
5-77	Definition of Inflated Canopy Dimensions	5-90
5-78	Canopy-Skirt Diameter as a Function of the Number of Gores for a Ribbon Parachute With $D_p = 0.67 D_0$	5-90
5-79	Canopy Cross Section of Two Ribbon Parachutes	5-92
5-80	Side Profiles of Ribbon Parachute Canopies With Porosities From 15 to 30%	5-93
5-81	Side Profiles of a Ribbon Parachute With Constant Canopy Porosity and Suspension-Line Ratios of 1.0, 1.5, and 2.0	5-93
5-82	Airflow and Pressure Distribution Around a Parachute Canopy	5-94
5-83	External Pressure Coefficient Versus Mach Number for a Ribbon-Type Metal Hemisphere	5-95
5-84	Inside, Outside, and Total Pressure Distribution Versus Mach Number for a Ribbon-Type Metal Hemisphere, Measured in Wind-Tunnel Tests	5-95
5-85	Pressure Distribution of a Ribbon Parachute at Various Times After Canopy Deployment	5-96
5-86	Supersonic Flow Around a Bullet-Type Body	5-97
5-87	Drag Coefficient, C_D , Versus Mach Number for an Ejectable Aircraft Nose Section	5-98
5-88	Supersonic Flow Field Around a Parachute Canopy	5-98
5-89	Supersonic Flow Around a Vehicle-Parachute System	5-99
5-90	Configurations of Three Supersonic Ribbon Parachutes	5-101
5-91	Drag Coefficient of Several Ribbon Parachutes as Function of Mach Number (1962 Data)	5-101
5-92	Demonstrated Mach Number/Altitude Range of Conical Ribbon Parachutes	5-102
5-93	Drag Coefficient Versus Mach Number for Conical Ribbon Parachutes	5-103
5-94	Demonstrated Altitude Versus Mach-Number Range of Hemisflo Ribbon Parachutes	5-104
5-95	Drag Coefficient Versus Mach Number for Hemisflo Ribbon Parachute	5-105
5-96	Drag Coefficient Versus Mach Number for Conical Ribbon and Hemisflo Parachutes (Recommended for Computerized Analysis of These Parachutes)	5-106
5-97	Ballute-Type Inflatable Decelerator	5-107
5-98	Drag Coefficient, C_D , Versus Mach Number for Goodyear Ballute	5-107
5-99	Force-Versus-Time Comparison Between a 5.5-Foot-Diameter Parasonic Parachute and a 3-Foot-Diameter Ballute Tested at Mach 2.6	5-108
5-100	Drag Coefficient, C_D , as Function of Mach Number for Various Aerodynamic Decelerators	5-109
5-101	Various Types of Decelerators	5-109
5-102	MC1-1B Parachute, the Maneuverable Version of the T-10 Paratrooper Parachute	5-111

5-103	The Pioneer Parachute Flying With a Gemini Spacecraft Model	5-113
5-104	Three Types of Advanced Maneuverable Parachutes	5-114
5-105	Forces Acting on a Ballistic and on a Maneuverable, Lifting Parachute	5-117
5-106	C_L/C_D Diagram and Glide Ratio L/D for Various Hi-Glide Parachutes and a Rigid Wing Parachute (Drag of Suspension Lines, Riser, and a Hypothetical Air Vehicle are Included)	5-118
5-107	Flight Performance of Maneuverable Parachute-Vehicle Systems	5-119
5-108	Increase in Vertical Velocity With Bank Angle	5-120
5-109	Typical Parachute Cluster Arrangement	5-123
5-110	Drag Loss in Parachute Clusters	5-124
5-111	Uniform Opening of a Cluster of Two 78-Foot-Diameter Extended-Skirt Parachutes	5-126
5-112	Y-Factor as Function of Drag Coefficient, C_D , and Velocity	5-130
Chapter 6		
6-1	Uncontrolled Deployment	6-3
6-2	Pilot Chute Deployment	6-4
6-3	Parachute Static-Line Deployment	6-5
6-4	Controlled Parachute Deployment Concept	6-6
6-5	Canopy-First Deployment Method Used on the Landing-Deceleration Parachute of the B-47 Bomber	6-7
6-6	Drogue Gun Deployment	6-7
6-7	Mortar Arrangement of the Apollo Command Module	6-8
6-8	Mortar Assembly of the Apollo Drogue Chutes	6-9
6-9	Two Typical Rocket-Extraction Methods	6-10
6-10	Cross-Wind Deployment Bag Ejection Methods	6-10
6-11	Typical Parachute Recovery System	6-14
6-12	Components of a Parachute	6-15
6-13	Typical Design of a Flat Circular Canopy	6-15
6-14	Gore Design of Bias and Block Construction	6-16
6-15	Circular Flat and Circular Conical Canopy Designs	6-18
6-16	Design of Extended-Skirt Parachutes	6-19
6-17	Typical Triconical Canopy Design Compared to Quarter-Spherical Shape	6-21
6-18	Typical Design of a Cross Parachute	6-22
6-19	Typical Design of Airfoil (Annular) Parachute	6-23
6-20	Ribbed Guide Surface Parachute Design	6-25
6-21	Ribless Guide Surface Parachute Design	6-26
6-22	Typical Gore Design of a Flat or Conical Ribbon Parachute	6-29
6-23	Recommended Total Canopy Porosity, λ_T , for Ribbon Parachutes as a Function of Parachute Diameter and Application (see Table 6-3 for Applications)	6-30
6-24	Change in Effective Porosity, λ_e , as a Function of Canopy Loading $W/(C_{DS})_p$ and Vertical Ribbon Spacing, a	6-32
6-25	Typical Design of a Hemisflo Parachute	6-34
6-26	Typical Design of Ringslot Parachute	6-35
6-27	Total Canopy Porosity, λ_T . Recommended for Ringslot Parachutes	6-36
6-28	Typical Design of Ringsail Parachute	6-37
6-29	Typical Parachute Cluster Arrangements	6-39
6-30	Pocket Band Design	6-42
6-31	MA-1 Pilot Chute in Vertical Wind-Tunnel Tests	6-44
6-32	Box-Type Pilot Chute	6-45
6-33	Canopy Gore With Anti-Inversion Net (Only One Gore Shown)	6-47

6-34	Typical Deployment-Bag Details	6-49
6-35	Typical Shear-Knife Design	6-50
6-36	Banana-Peel Bag Design	6-51
6-37	Typical Deployment Sleeve	6-51
6-38	Sacrifice-Panel Design	6-52
6-39	Skirt Hesitator	6-53
6-40	Deployment Bag Showing Suspension Lines in Stow Loops	6-53
6-41	Boundary Curves for Horizontal Ribbon Strength	6-60
6-42	Typical Skirt Reefing Installation	6-63
6-43	Reefing Cutter Installation	6-63
6-44	Three Methods of Reefing Cutter Installation	6-64
6-45	Cutter Installation for Two-Step Reefing	6-65
6-46	Standard Circular Reefing Rings	6-68
6-47	Dual Reefing Ring (Northrop Ventura Dwg. DR 8127)	6-68
6-48	Typical Commercially Available Reefing-Line Cutter	6-69
6-49	U.S. Army M21 Reefing Cutter	6-70
6-50	Sandia MC 3133 Reefing-Line-Cutter Installation	6-71
6-51	Diagram of Fixed Reefing by Pocket Bands	6-73
6-52	Tenacity in Grams Per Denier for Various Industrial Yarns	6-77
6-53	Loss of Tenacity in Nylon Caused by Exposure to Temperature	6-78
6-54	Melt-Spinning Process	6-79
6-55	Examples of Z Twists and S Twists in Filaments and Yarns	6-80
6-56	Typical Weave Patterns for Parachute Fabric	6-81
6-57	Changes in Fabric Length Caused by Sewing	6-85
6-58	Tolerances for Manufactured Textile Parts, Apollo Program	6-88
6-59	Tenacity of Four Kevlar Yarns as a Function of Yarn Twist	6-90
6-60	Loss in Strength of Six Different Kevlar Materials Caused by Weathering	6-91
6-61	Parachute Recovery System Weight as Percentage of Air Vehicle Weight	6-94
6-62	Weight of Final Descent Parachutes	6-95
6-63	Ribbon Parachute, Weight Versus Diameter and Horizontal Ribbon Strength	6-96
6-64	Weight of Ringsail Parachute as a Function of Parachute Diameter	6-97
6-65	Heavy Packing Presses Used for Packing the Apollo Main Parachutes	6-100
6-66	Apollo Main Parachute Pressure-Packed in its Storage Form	6-100
6-67	Pack Density as a Function of Pack Pressure and Packing Application Interval	6-101
6-68	Deceleration Stroke Versus Rate of Descent and Allowable Impact Deceleration	6-104
6-69	Ideal Energy Absorption Diagram	6-106
6-70	Typical Energy Absorption Diagram for Crushable Material	6-106
6-71	Typical Honeycomb Structure	6-107
6-72	AM551 Armored Reconnaissance Assault Vehicle Loaded on a Cargo Platform Using Paper Honeycomb as Impact Attenuator	6-107
6-73	Stress-Strain Diagram of Paper Honeycomb Pads	6-108
6-74	Paper Honeycomb Impact Attenuator	6-109
6-75	Effect of Density on Stress-Strain Curves for Polyurethane Foamed Plastic	6-110
6-76	Force-Stroke Efficiency of Various Crushable Materials	6-111
6-77	Energy Absorption Per Pound of Material Weight	6-112
6-78	Air Bag Pressure Versus Stroke Characteristics	6-113
6-79	Air Bag Configurations for Various Air Vehicles	6-114
6-80	USD-5 Air Bag Pressure Relief Valve With Blow-Out Diaphragm	6-116
6-81	Pressure Relief Valves for the CL-289 Air Bags Using Stretch Fabric Sleeves	6-116
6-82	Details of Rerocket Design and Installation	6-118

6-83	Weight Comparison of a Parachute-Air Bag and a Parachute-Retrorocket System for a 7800-Pound Crew Module	6-119
6-84	Design and Performance Details of the Skirt Jet Retrorocket System	6-120
6-85	Army CTU-2A High-Speed Aerial Delivery Container With Crushable Nose Cone and Impact Decelerating Force Versus Cone Deformation	6-121
6-86	Typical Nose Spike Impact Attenuator	6-121
Chapter 7		
7-1	Reconnaissance-Drone and Air Bag Configurations	7-5
7-2	Cluster of Two 72.7-Foot-Diameter Extended-Skirt Parachutes (Drawn to Scale)	7-9
7-3	Parachute Assembly Installation and Extraction Concept	7-10
7-4	Determination of Equivalent Forebody Diameter	7-11
7-5	Extraction Parachute Assembly	7-12
7-6	Pilot Chute Assembly	7-13
7-7	Main Parachute Assembly; Cluster of Two Parachutes	7-14
7-8	Velocity-Time Profile	7-15
7-9	Drag-Area-Versus-Time Profile for a Single Parachute and the Total Drone	7-21
7-10	Main Parachute Assembly	7-24
7-11	Vent-Tape Geometry	7-28
7-12	Bench Check on Gore Fullness	7-29
7-13	Gore Layout for Gore Dimensions	7-30
7-14	Vent Construction	7-31
7-15	Final Gore Dimensions	7-32
7-16	Pocket Band Arrangement	7-33
7-17	Drone Flight Envelope	7-35
7-18	Drogue Chute Arrangement	7-37
7-19	Venetian-Blind Effect of Horizontal Ribbon in a Ribbon Canopy	7-45
7-20	Canopy Gore Layout	7-46
7-21	Preliminary Gore Dimensions	7-49
7-22	Final Gore Dimensions	7-51
Chapter 8		
8-1	Slat Drone Parachute Recovery Sequence	8-5
8-2	Sequence of CL 289 Drone Recovery	8-6
8-3	Impact Attenuation Bag Configuration	8-7
8-4	Pressure Relief Valves for the CL-289 Airbags Using Stretch Fabric Sleeves	8-7
8-5	Midair Retrieval Parachute Assembly	8-8
8-6	Deployment Sequence of the MARS Parachute System	8-9
8-7	Parachute Deployment and Engagement Sequence	8-10
8-8	AGM-109 Tandem Parachute Assembly	8-11
8-9	Main Canopy Plan	8-12
8-10	Plan Form of the 6.2-Meter Aeroconical	8-20
8-11	Assembly Components of the 6.2-Meter Aeroconical	8-20
8-12	Opening Sequence of AGES Parachute Assembly	8-22
8-13	Side View of Escape Pole Deployed Through Side Hatch	8-24
8-14	Crew Bailout Mode – Crew Escape Pole	8-24
8-15	Navy Test Jumper Using Crew Escape Pole	8-26
8-16	Parachute Extraction System for Cargo Platforms	8-31
8-17	Standard Airdrop Method	8-32
8-18	The LAPES C-130 Platform Extraction System	8-34
8-19	High-Altitude Airdrop Resupply System (HAARS), First Stage Configuration	8-35

8-20	Parachute Extraction Force and Extraction Speed vs. Time for a 35-Foot Parachute Extracting a 50,000-Pound Load	8-42
8-21	T-10 Paratrooper Parachute	8-44
8-22	MC1-1B Maneuverable Paratrooper Parachute With Glide and Control Slots and Anti-Inversion Net	8-45
8-23	Aircraft Landing Roll as a Function of Parachute Diameter and Runway Conditions	8-50
8-24	B-52 With 44-Foot-Diameter Landing Deceleration Parachute	8-51
8-25	Typical Landing Deceleration Parachute Installation	8-51
8-26	Typical Spin/Stall Recovery Parachute Assembly and Deployment Concept	8-58
8-27	Deployment Sequence of the F-18 Spin-Recovery Parachute	8-59
8-28	Effect of Ratio Vehicle Weight, W, to Decelerator Drag Area ($C_D S$) on Down-Range Distance, Impact Angle, and Aircraft Separation Distance	8-61
8-29	Mark 83 Bomb With Ballute-Type Retarder	8-64
8-30	Typical Mine Cross Parachute Assembly in Flight	8-66
8-31	Torpedo With Ribbon Parachute Retarder in Flight	8-68
8-32	A Typical Sonar-Buoy-Parachute System in Stable Descent	8-70
8-33	Typical Configuration of an Extended Range Anti-Armor Mine	8-72
8-34	Radar Reflectivity of a 220-Degree Spherical Canopy, 36 Feet in Diameter Versus Aspect Angle	8-73
8-35	Parachutist Landing Parafoil With "Full Brakes"	8-77
8-36	Forest Service Smoke Jumper Ready to Jump	8-80

TABLES**Chapter 2**

2-1	Comparative Rating of Performance Characteristics for Various Parachute Recovery Systems Applications	2-7
-----	---	-----

Chapter 3

3-1	Conversion of English System to Metric System	3-5
3-2	Temperature Conversion Table	3-10
3-3	Properties of Earth's Atmosphere Versus Altitude	3-12

Chapter 5

5-1	Solid Textile Parachutes	5-3
5-2	Slotted Parachutes	5-4
5-3	Rotating Parachutes	5-4
5-4	Maneuverable (Gliding) Parachutes	5-5
5-5	Balloon-Type Decelerators	5-5
5-6	Canopy Fill Constant, n, for Various Parachute Types	5-44
5-7	Opening Forces and Canopy Loading of a 28-Foot-Diameter Parachute for Various Vehicle Applications	5-51
5-8	Canopy Loadings	5-71

Chapter 6

6-1	Determination of Gore Dimensions for Various Types of Parachutes	6-20
6-2	Roof Panel and Guide Surface Panel Pattern Dimensions	6-27
6-3	Recommended Porosity Range and Vertical Ribbon Spacing as a Function of Application and Velocity	6-31
6-4	Pocket Band Dimensions	6-43

6-5	Pilot and Main Parachute Drag-Area Ratios	6-45
6-6	Pilot Chute-Drag and Opening-Force Coefficients	6-46
6-7	Recommended Design Factors for Parachute Assemblies	6-56
6-8	Variation of Reefing Cutter Time as a Function of Temperature for a 10-Second Apollo Reefing Cutter	6-72
6-9	Dimensions for the Fixed Reefing of the 6.8-Foot-Diameter Conical Ribbon Parachute. (For nomenclature see Figures 6-51, 6-29, 6-30, and Section 3.4)	6-73
6-10	Characteristics of Various Materials	6-76
6-11	Allowable Impact Decelerations	6-104
6-12	Air Bag System Data Related to Figure 6-78	6-115
 Chapter 7		
7-1	Reefed Opening Force as a Function of Filling Time and Drag-Area Profile	7-18
7-2	Disreef Opening Force as a Function of Disreef Time and Drag-Area Profile	7-20
7-3	Comparison of Parachute Forces Calculated by the Three Methods	7-22
7-4	Determination of Design Factors for the Main Parachute Assembly	7-25
7-5	Suspension-Line Selection	7-25
7-6	Drogue Chute Candidates	7-36
7-7	Determination of Design Factors for the Drogue Chute	7-41
7-8	Effect of Number of Suspension Lines/Gores on Required Suspension-Line Strength, Gore Width, and Vent Diameter	7-42
7-9	Grid Porosity as Function of Horizontal Ribbon Distance, b	7-50
 Chapter 8		
8-1	Parachute Criteria	8-1
8-2	Drag Area/Weight Efficiency ($C_D S_p/W_p$) for Several Operational Parachutes	8-3
8-3	Navy Emergency Escape Parachute Information and Utilization	8-16
8-4	Air Force Personnel Emergency Parachutes, Man Mounted	8-18
8-5	Primary Aircraft Used in Military Airdrop Operations	8-29
8-6	Container Summary for Helicopter Airdrop	8-29
8-7	Airdrop Containers	8-36
8-8	Military Cargo Parachutes	8-38
8-9	Extraction Parachute Types	8-41
8-10	List of Military Premeditated Jump Parachutes	8-46
8-11	Basic T-10 Assembly Dimensions	8-47
8-12	Aircraft Deceleration Parachutes	8-52
8-13	Spin and Deep Stall Recovery Parachutes	8-57
8-14	Comparison of the 17-Foot-Diameter Nylon and the 24-Foot-Diameter Nylon/Kevlar Parachutes for the B-61 Nuclear Bomb	8-63
8-15	Military Maneuverable Parafoil Parachutes	8-76

About the Author



Theodor W. Knacke is the parachute engineer's engineer. He has spent a lifetime working in all phases of parachute research, development and application in both Germany and the United States. He is *the authority* on escape systems, landing deceleration canopies, aerial delivery clusters, personnel parachutes and spacecraft recovery systems.

Mr. Knacke has B.S. degrees in civil and aeronautical engineering and an M.S. degree in aeronautical engineering from the University of Stuttgart in 1939. After one year with Heinkel Aircraft, he joined the FIST Institute of the University of Stuttgart working primarily on the in-flight and landing deceleration of aircraft. This resulted in the creation of the ribbon canopy in 1938, of which he is a co-inventor.

After coming to the United States in 1946, Mr. Knacke served as a research engineer at the USAF Parachute Branch at Wright Field; from 1952 to 1957 as Technical Director of the USAF 6511th Test Group (Parachutes) at El Centro, California; from 1957-1961 as vice-president of engineering at Space Recovery Systems in El Segundo, California; and from 1962 through 1976 as Chief of the Technical Staff (Recovery Systems) at the Ventura Division of the Northrop Corporation in Newbury Park, California. His responsibilities during this time covered all areas of missile, drone, and spacecraft recovery, including the Mercury, Gemini and Apollo earth landing systems, ordinance retardation, aircraft escape and deceleration and related projects.

Since retiring from Northrop in 1977, Mr. Knacke has been a consulting engineer to the U.S. Army, Navy, Air Force and industry. He holds numerous patents, has published more than 30 papers and reports, and lectures extensively. He is known worldwide for his lectures sponsored by the American Institute of Aeronautics and Astronautics and hosted by the University of Minnesota.

Mr. Knacke was given the Achievement Award by the National Association for Remotely Piloted Vehicles in 1975. He is a Fellow of the AIAA and was awarded the AIAA Aerodynamic Decelerator and Balloon Technology Award in 1981.

The photographs on the cover of this manual were specially selected to represent some of the major projects of the author.

Naval Weapons Center

FOREWORD

This Parachute Recovery System Design Manual will provide parachute design engineers with up-to-date recovery system information and personnel entering the parachute design field with an all-inclusive training resource.

The manual was initiated by the Aerosystems Department of the Naval Weapons Center (NWC), China Lake, Calif. It is an extension of parachute recovery system engineering courses conducted by the author, Theo W. Knacke, at NWC; the Naval Surface Warfare Center, White Oaks, Silver Spring, Md.; and at extension courses conducted by the University of Minnesota, Minneapolis, Minn.

Don Goodrich and J. D. Johnson of the NWC Aerosystems Department served as project engineers.

The following organizations provided technical data and reviewed parts of the manual: The Aerosystems Department of NWC; The Army Natick Engineering, Development & Research Center at Natick, Mass.; The Air Force Crew Systems Division at Wright Patterson AFB, Ohio; and the Parachute Systems Division of the Sandia National Laboratories at Albuquerque, N. Mex. Personnel of Irvin Industries, Pioneer Parachute Co., and Paraflite, Inc., provided technical information.

Sandy Lane, Maggie Frazer, and Janice Kaspersen, of the NWC Technical Information Department, edited; and Susan Dunker, also of the Technical Information Department, provided graphic support for the manual.

This report has been reviewed for technical accuracy by the Recovery Systems Division, Aerosystems Department of NWC.

Approved by
M. K. BURFORD, Head
Aerosystems Department
31 December 1990

Under authority of
D. W. COOK
Capt., U.S. Navy
Commander

Released for publication by
W. B. PORTER
Technical Director

NWC Technical Publication 6575

Published by Technical Information Department
Collation Cover, 249 leaves
First printing 500 copies

Warning-Disclaimer

Whenever a person leaves the ground, he or she risks injury or even death. Whether to accept or reject this risk and its accompanying challenge must be a personal decision; one must weigh the risk and the reward. This book is designed to promote safety through education.

This is not a do-it-yourself text. The information contained here is intended as an introduction to parachute engineering and design and as a source of reference. It is not the only source of information.

This book is designed to provide accurate and authoritative information in regard to the subject matter covered. It is not the purpose of this manual to reprint all the information that is otherwise available, but to complement, amplify and supplement other courses and texts. For more information, see the many listed references.

The purpose of this manual is to educate and entertain. Every effort has been made to make this book as complete and as accurate as possible. However, there may be mistakes both typographical and in content. Therefore, this text should be used only as a general guide and not as the ultimate source of parachute information. Furthermore, this manual contains information only up to the printing date.

Para Publishing warrants this book to be free of defects in materials and workmanship. This warranty shall be in lieu of any other warranty, express or implied.

The author and Para Publishing shall have neither liability for, nor responsibility to, any person or entity with respect to any loss or damage caused or alleged to be caused directly or indirectly by the information contained in this book.

If you do not agree with the above, you may return this book to the publisher for a full refund.

CHAPTER I

INTRODUCTION

The purpose of this manual is to provide recovery system engineers in government and industry with tools to evaluate, analyze, select, and design parachute recovery systems. These systems range from simple, one-parachute assemblies to multiple-parachute systems, and may include equipment for impact attenuation, flotation, location, retrieval, and disposition. All system aspects are discussed, including the need for parachute recovery, the selection of the most suitable recovery system concept, concept analysis, parachute performance, force and stress analysis, material selection, parachute assembly and component design, and manufacturing.

Experienced recovery system engineers will find this publication useful as a technical reference book; recent college graduates will find it useful as a textbook for learning about parachutes and parachute recovery systems; and technicians with extensive practical experience will find it useful as an engineering textbook that includes a chapter on parachute-related aerodynamics. In this manual, emphasis is placed on aiding government employees in evaluating and supervising the design and application of parachute systems.

The parachute recovery system uses aerodynamic drag to decelerate people and equipment moving in air from a higher velocity to a lower velocity and to a safe landing. This lower velocity is known as rate of descent, landing velocity, or impact velocity, and is determined by the following requirements: (1) landing personnel uninjured and ready for action, (2) landing equipment and air vehicles undamaged and ready for use or refurbishment, and (3) impacting ordnance at a preselected angle and velocity.

The recovery cycle may include use of impact attenuation, flotation, and location equipment; retrieval by aircraft, boat, or ground vehicle; and delivery to an area for refurbishment and reuse.

Parachute recovery systems are required for emergency escape of personnel from aircraft, airdrops of troops and supplies, stabilization and retardation of ordnance, recovery of targets, sport parachuting, and similar applications. Optional uses include in-flight and landing deceleration of aircraft; recovery of missiles, spacecraft, and rockets; stabilization of falling bodies; and many others.

CHAPTER 2

PARACHUTE RECOVERY SYSTEM DEFINITIONS
AND DESCRIPTION

2.1 PARACHUTE RECOVERY SYSTEM DEFINITION

Defining the components and terminology of a parachute recovery system will help to avoid misunderstandings between Government agencies, prime contractors, and subcontractors.

Although a parachute recovery system is a subsystem or even a subsystem of a prime system, as shown in Figure 2-1, common usage refers to all parachute recovery subsystems and assemblies as systems. Figure 2-1 also shows the typical breakdown structure of a target drone recovery system containing—in addition to the parachute recovery system—sequencing, impact attenuation, flotation, location, retrieval, and docking equipment.

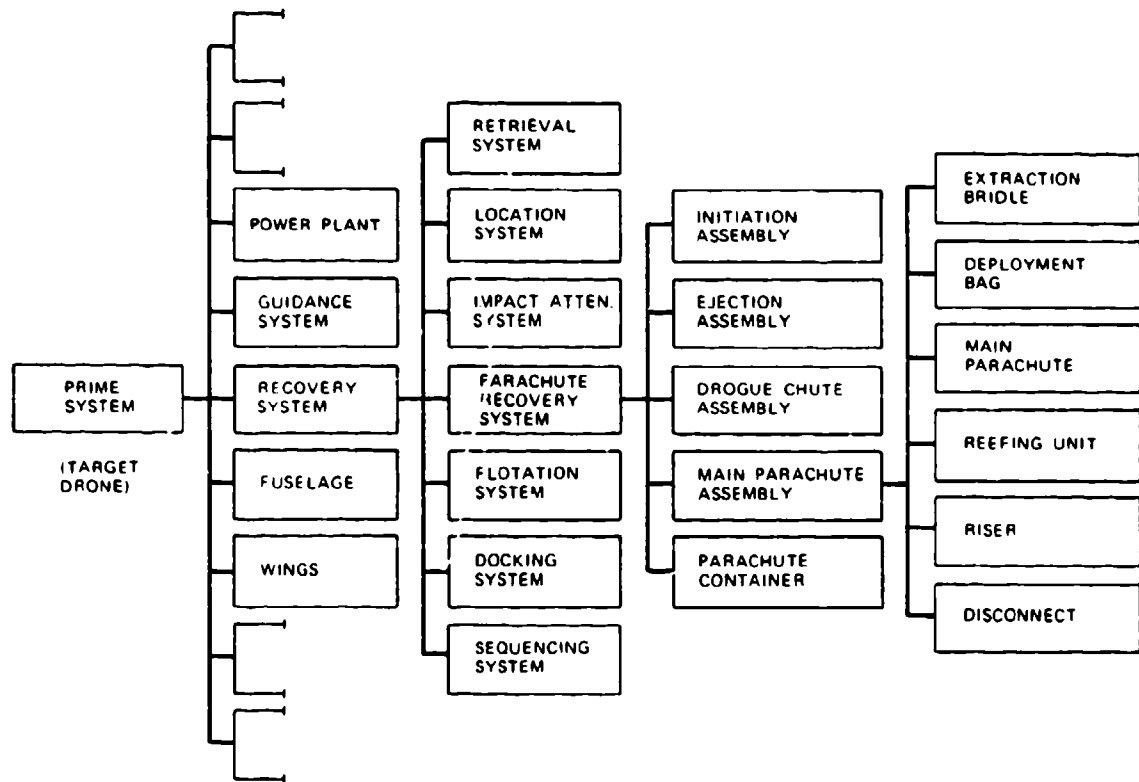


FIGURE 2-1. System Integration and Components of a Parachute Recovery System.

Many parachute recovery systems contain fewer components than are listed in Figure 2-1. For example, an aircraft landing deceleration parachute system consists of a compartment in the aircraft with door actuators and the parachute disconnect mechanism, and, separately within the compartment, a parachute assembly comprising an ejectable pilot chute, pilot-chute bridle, brake parachute, brake-parachute deployment bag, and riser with disconnect clevis.

Figure 2-2 is a schematic of a typical ejection seat parachute assembly with descriptive nomenclature. Many variations of the assembly are possible: independent main-parachute deployment, stabilized high-altitude descent on the drogue chute, seat stabilization by attitude sensors and reaction control system (RCS), velocity-altitude control of the parachute deployment sequence, and man-seat separation. The variations may result in more or fewer components and different component arrangements.

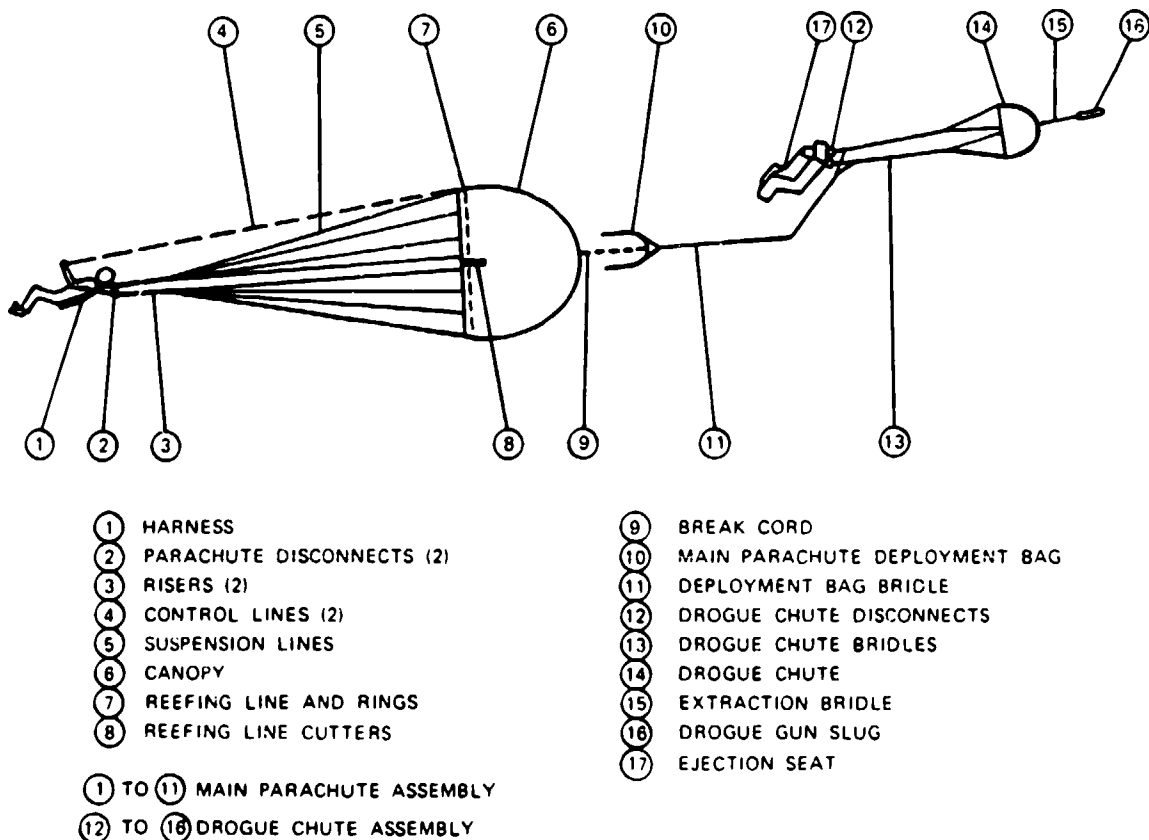


FIGURE 2-2. Schematic and Nomenclature of a Typical Ejection Seat Parachute Assembly.

2.2 PARACHUTE RECOVERY SYSTEM APPLICATIONS

The first recorded development and application of parachute-type devices involved the lowering of animals, and occasionally humans, during fairs and carnivals in 14th- and 15th-century Siam and China. Parachute development in Europe and the United States began in the 18th century for use in exhibits and shows. The first application of parachutes for saving the lives of aviators occurred during World War I. Since that time, parachutes have been used for the rescue of aviators; for premeditated jumps of military and civilian personnel; and by sport parachutists, smoke jumpers, and paramedic jumpers.

An airdrop of military personnel and equipment is the final phase of transport to a theater of operation. Personnel and equipment must land uninjured, undamaged, and ready for action or use.

Aircraft in-flight and landing deceleration involves termination of dangerous flight maneuvers, such as spin, deep stall, and high-speed flutter. In these cases, the parachute is disconnected after the aircraft reaches a controlled flight attitude. Many military and some civilian aircraft use parachutes as landing brakes to shorten the landing roll and save tires and brakes.

Many ordnance devices, such as bombs, mines, torpedoes, and submunitions, are parachute-retarded to let the aircraft escape the effective range of the weapon, to stabilize and retard the weapon before water entry, to obtain antiricochet impact angles, and to obtain a desired splinter-distribution pattern after impact.

Air vehicle recovery includes termination of flight, and recovery for reuse of targets, unmanned vehicle systems, booster rockets, and manned and unmanned spacecraft. Some of these are recovered by the Midair Retrieval System (MARS).

Parachutes are also used to decelerate high-speed land vehicles, rescue speedboat crews, and decelerate ships. Figure 2-3 lists today's primary parachute applications.

<u>PERSONNEL</u>	<u>AIRCRAFT VEHICLE RECOVERY</u>
1. PERSONNEL EMERGENCY	1. MISSILE/DRONE/LVS RECOVERY FOR REUSE, COMPONENT ANALYSIS, AND RANGE SAFETY
2. TRACTOR ROCKET ESCAPE SYSTEM	2. SOUNDING ROCKETS AND RE-ENTRY VEHICLES
3. CAPSULE AND EJECTION SEAT STABILIZATION AND DECELERATION	3. MANNED/UNMANNED SPACECRAFT
4. RESCUE MISSIONS	4. BOOSTER
5. SPORT PARACHUTING	
6. SMOKE JUMPERS	
<u>AIRDROP</u>	<u>ORDNANCE RETARDATION</u>
1. PARATROOPERS	1. BOMB/MINE/TORPEDO RETARDATION
2. ARMY COMBAT AND ENGINEERING EQUIPMENT	2. FLARES
3. AERIAL RESUPPLY	3. SUBMUNITION
4. SURVIVAL EQUIPMENT	4. SONAR BUOYS
<u>AIRCRAFT DECELERATION</u>	<u>SPECIAL</u>
1. APPROACH AND LANDING	1. AIR-TO-AIR RETRIEVAL
2. SPIN AND STALL RECOVERY	2. GROUND-TO-AIR RETRIEVAL
3. INFLIGHT DECELERATION	3. LAND/WATER SURFACE VEHICLE RETARDATION

FIGURE 2-3. Parachute Applications.

2.3 PARACHUTE RECOVERY SYSTEM BOUNDARIES

The application range of parachutes with regard to velocity and altitude was closely associated with the speed and altitude capability of aircraft until the 1950s. A research program conducted in the late 1940s and early 1950s established that parachutes could be used at supersonic speeds; parachutes developed specifically for supersonic application followed. Parachutes have been used successfully at speeds in excess of Mach 4.0, at altitudes up to the limits of the atmosphere, and at dynamic pressures to 15,000 psi. Parachutes have also been used to recover a rocket booster weighing 185,000 pounds. Figure 2-4 gives the required parachute performance envelopes for different applications.

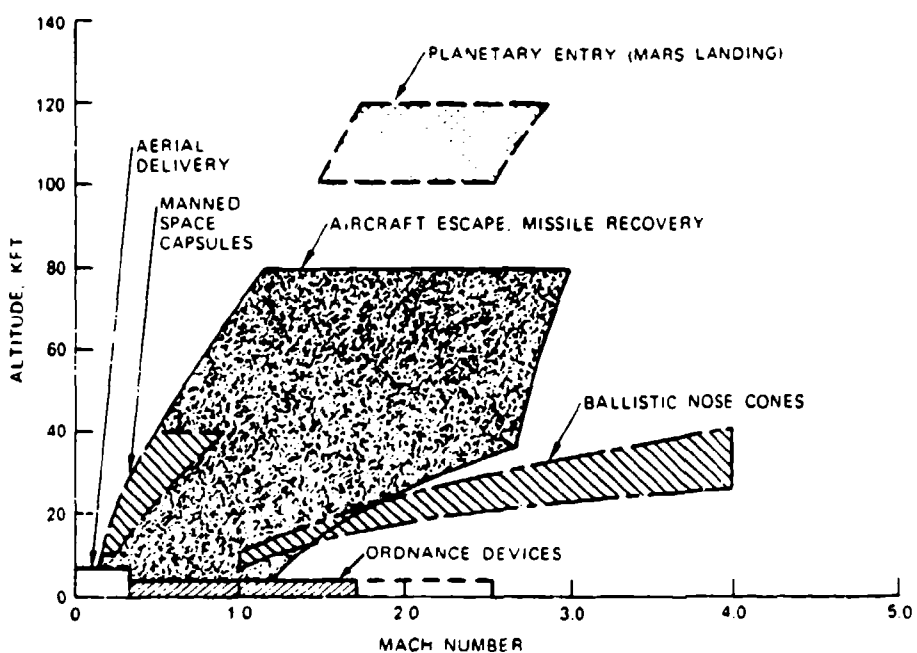


FIGURE 2-4. Parachute Performance Envelopes.

Figure 2-5 shows the approximate velocity and altitude boundaries of parachute systems that are presently in service or have been tested experimentally. Boundary limits are moved upward and outward as new materials are introduced that shift the aerodynamic heating limit to higher temperatures and make possible the recovery of heavier vehicles. Successful landings on Mars have been made, and vehicle landings by parachute on Venus and Jupiter are in preparation.

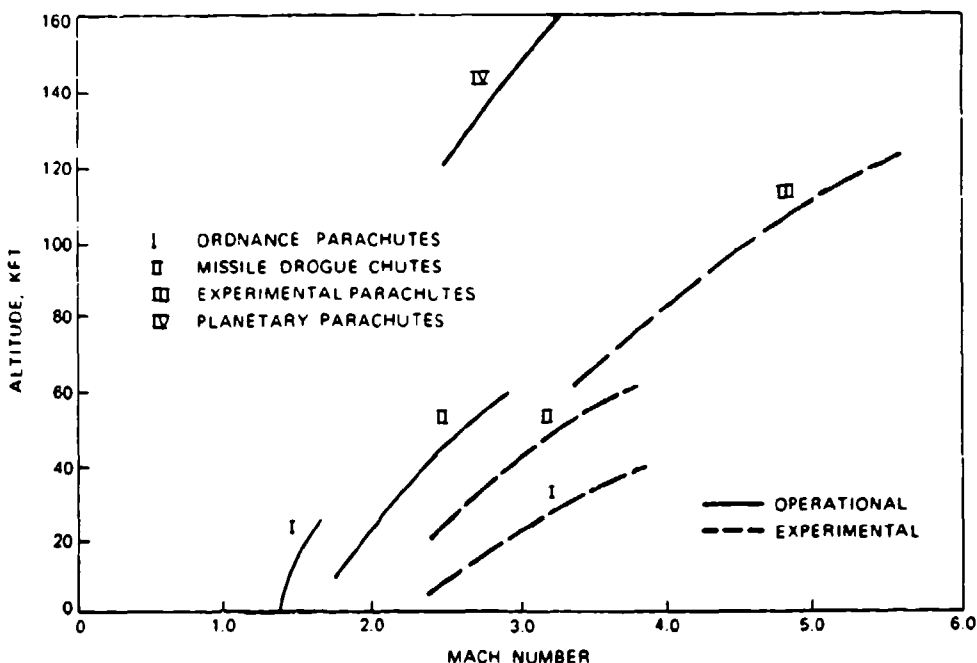


FIGURE 2-5. Aerodynamic Decelerator Performance Range (1990).

2.4 PARACHUTE RECOVERY SYSTEM DESIGN CRITERIA

Prerequisites for the design of a parachute recovery system are an understanding of the purpose of the system and its requirements, and a clear definition of the design criteria governing system and component selection. Figure 2-6 lists typical design criteria.

System reliability will always be of utmost importance. Parachute recovery systems have reached a high degree of reliability, as documented by the 31 consecutive, successful, manned spacecraft landings and the high reliability rate of paratrooper parachutes. In complex systems, it is mandatory to analyze and review all aspects and components of the total recovery system cycle. Failure to integrate the system totally can lead to the type of mishap experienced by Space Shuttle flight 7 in 1983, when a wrong sensor signal caused premature parachute disconnect, and the solid-fuel boosters were lost.

Weight and volume are important considerations. Parachute assemblies constitute approximately 5% of total vehicle weight for lightweight vehicles, and 3 to 4% for vehicles weighing several thousand pounds. A complete recovery system, including flotation, location, and retrieval assemblies, will weigh $10 \pm 2\%$ of the total vehicle weight. The 560-pound Apollo parachute assembly that was carried around the moon and back to Earth, where it was needed for landing, was a major expense in terms of weight, and much effort was dedicated to eliminating ounces to reduce overall spacecraft weight.

• RELIABILITY	• LOW ACQUISITION COST
• STABILITY	• LOW LIFE CYCLE COST
• HIGH DRAG	• WEIGHT EFFICIENCY $\frac{(C_D \cdot S)_o}{W_p}$
• LOW OPENING SHOCK	• VOLUME EFFICIENCY $\frac{(C_D \cdot S)_o}{V_p}$
• HIGH MACH CAPABILITY	• COST EFFICIENCY $\frac{(C_D \cdot S)_o}{\$}$
• LOW WEIGHT AND VOLUME	$(C_D \cdot S)_o$ PARACHUTE DRAG AREA - FT ²
• REPEATABILITY OF PERFORMANCE	W_p PARACHUTE WEIGHT - LB
• ENVIRONMENTAL ADAPTABILITY	V_p PARACHUTE VOLUME - FT ³
• GROWTH POTENTIAL	
• INDIFFERENCE TO DAMAGE	
• SIMPLICITY OF DESIGN AND MANUFACTURING	
• SIMPLICITY OF MAINTENANCE AND SERVICE	

FIGURE 2-6. Parachute Design Criteria.

For aerial targets, the recovery system is used only for recovery and retrieval in the last minutes of the mission. Each pound saved in the recovery system will either benefit the performance of the target or permit an increase in payload.

The selection of the parachute frequently begins with the stability requirement. Aircraft deceleration parachutes, first-stage drogue chutes, and most ordnance-retardation parachutes require a high level of stability—a requirement that automatically eliminates many high drag parachutes.

A final descent parachute, the high-weight item in any recovery system, is usually selected from high drag, solid textile parachutes that result in the smallest diameters and, consequently, the lowest weights and volumes. Limited parachute oscillation (0 to 10 degrees) of large final descent parachutes may be acceptable or may be eliminated by use of cluster parachutes.

A high drag coefficient is important in selecting the final descent parachutes. However, a better evaluation criterion is the weight-efficiency ratio, $(C_{DS})_o/W_p$, which shows how much parachute drag area, $(C_{DS})_o$, is produced per pound of parachute or parachute assembly weight, W_p . Where the cost of the parachute system may be higher than the cost of the payload (such as food or other low dollar-per-pound items), the deciding factor may be cost efficiency, $(C_{DS})_o/\$$.

Low opening shock is a valid selection criterion for unreefed parachutes, but loses its significance for large reefed parachutes where reefing controls the force-time history of the parachute opening process.

Growth potential is important in design. Most air vehicles that are recovered by parachute grow in weight during the development cycle because of design changes; changes in requirements; or, when in service, added payloads. An undamaged landing requires maintaining the rate of descent. This may mean increasing the size of the final descent parachute(s) with the concurrent increase in weight and volume of the parachute assembly. The parachute compartment size normally is fixed early in the design cycle of the vehicle and cannot be enlarged. The use of low-pressure packing at the start of the design for the parachute assembly allows storage of a larger parachute assembly later when higher-pressure packing can be incorporated. The use of high-pressure packing at the outset eliminates this possibility.

Repeatability of parachute performance is important for aircraft landing deceleration parachutes that are used 25 to 50 times. Repeatability is also a requirement for ordnance parachutes; parachutes manufactured to the same drawing must provide the same ballistic trajectory.

Table 2-1 is a guide for rating performance characteristics for different applications. Each application and each designer may use different rating values based on the special requirements of the particular application.

TABLE 2-1. Comparative Rating of Performance Characteristics
for Various Parachute Recovery Systems Applications.

Performance characteristics	Application					
	Spacecraft landing	Airborne troops	Aircraft escape	Aircraft landing deceleration	Ordnance	Aerial resupply
Reliability of operation	3	3	3	2	3	2
Repeatability of performance	2	2	2	3	3	1
Reuse	0	3	0	3	0	3
Low weight and volume	3	2	3	2	2	1
Stability	2	2	2	3	3	2
High drag	2	2	2	2	2	3
Low opening forces	1	3	2	3	2	3
Low maintenance/service	1	3	2	3	2	3
Cost	1	2	2	2	2	3

3 = high importance
2 = medium importance
1 = low importance
0 = not applicable

2.5 REFERENCE MATERIAL

The following reports and lecture and symposia papers and proceedings provide information on the analysis, design, testing, and use of parachute recovery systems.

Several parachute handbooks (References 2.1 through 2.4) have been published by the U.S. Air Force. Reference 2.1 covers developments after 1970, and References 2.2 through 2.4 cover the 1950 to 1970 developments.

The Aerodynamic Decelerator Systems Committee of the American Institute of Aeronautics and Astronautics (AIAA) conducts technical symposia. Papers presented at these symposia (References 2.5 through 2.15) are available as conference proceedings or as individual papers from AIAA headquarters in Washington, D.C.

Technical conferences of the Survival and Flight Equipment Organization (SAFE) are listed in Reference 2.16. These conferences cover the entire field of aircrew life-support equipment and aircrew escape.

The University of Minnesota conducts extension courses in aerodynamic decelerator systems technology. References 2.17 to 2.20 list the most recent lectures. Proceedings of these lectures are available from the Aerospace Department of the University of Minnesota in Minneapolis, Minn.

2.5.1 U.S. Air Force Reports

The following unclassified publications are recommended for individuals who want to obtain a general knowledge of parachutes and parachute recovery system application, performance, design, and components.

- 2.1 U.S. Air Force. *Recovery Systems Design Guide*, by H. W. Bixby, E. G. Ewing, and T. W. Knacke. USAF, December 1978. (USAF Report AFFDL-TR-78-151.) Available from the National Technical Information Service, Springfield, Va. 22161.
- 2.2 _____. *Performance of and Design Criteria for Deployable Aerodynamic Decelerators*. USAF, December 1963. (USAF Report ASD-TR-61-579.) Available from the Defense Technical Information Center, Cameron Station, Alexandria, Va. 22314.
- 2.3 _____. *USAF Parachute Handbook, Second Edition*. WADC Technical Report 55-265, ASTIA Document AD 118036, December 1956.
- 2.4 _____. *USAF Parachute Handbook*, ATI No. 35532, March 1951.

2.5.2 AIAA Papers

Proceedings and papers of AIAA conferences on aerodynamic decelerators and balloon technology are listed below.

- 2.5 Technical papers of the AIAA 10th Aerodynamic Decelerator Systems Technology Conference, Cocoa Beach, Florida, April 1989. Conference proceedings and individual papers are available from the American Institute of Aeronautics and Astronautics (AIAA), 370 L'Enfant Promenade, SW, Washington, DC 20024.
- 2.6 Various technical papers of the AIAA 9th Aerodynamic Decelerator and Balloon Technology Conference, Albuquerque, N. Mex., October 1986.
- 2.7 Proceedings of the 8th Conference, Hyannis, Mass., April 1984; available in report form from AIAA.
- 2.8 Papers of the 7th Conference, San Diego, Calif., October 1981; available as individual paper reprints from AIAA.
- 2.9 Papers of the 6th Conference, Houston, Tex., March 1979; available in report form from AIAA.
- 2.10 Papers of the 5th Conference, Albuquerque, N. Mex., October 1976; available as individual paper reprints from AIAA.
- 2.11 Papers of the 4th Conference, Palm Springs, Calif., May 1973; available as individual paper reprints from AIAA.
- 2.12 Papers of the 3rd Conference, Dayton, Ohio, September 1970; available as individual paper reprints from AIAA.
- 2.13 Papers of the 2nd Conference, El Centro, Calif., September 1968; available as USAF Report FTC-TR-69-11, Volumes I and II, from the Defense Technical Information Center, Cameron Station, Alexandria, Va. 22314.
- 2.14 Proceedings of the AIAA Aerodynamics Deceleration Systems Conference, Houston, Texas; September 1968, available in report form from AIAA.
- 2.15 Proceedings of the Symposium on Parachute Technology and Evaluation, El Centro, California, September 1964; available as USAF Report FTC-TR-64-12 from the Defense Technical Information Center, Cameron Station, Alexandria, Va. 22314

2.5.3 SAFE Symposia

- 2.16 Proceedings of the annual SAFE Symposia, covering all aspects of aircrew and cockpit bioengineering, aircrew escape, survival, and rescue. Yearly proceedings are available from the SAFE office, 15723 Van Owen St., Box 246, Van Nuys, Calif. 91406.

2.5.4 University of Minnesota Extension Courses

- 2.17 Lectures of the 1982 H. G. Heinrich Short Course on Parachute Systems Technology, University of Minnesota, Department of Aerospace Engineering, 110 Union St., S.E. Minneapolis, Minn. 55455.
- 2.18 Lectures of the 1985 H. G. Heinrich Short Course on Decelerator Systems Engineering, July 1985, University of Minnesota, Department of Aerospace Engineering, 110 Union St., S.E. Minneapolis, Minn. 55455.
- 2.19 Proceedings of the University of Minnesota/Carl Cranz Gesellschaft Course on Parachute Systems Technology, Fundamentals, Concepts, and Applications; Munich-Oberpfaffenhofen, June 1987. Available from the University of Minnesota, Department of Aerospace Engineering, 110 Union St., S.E. Minneapolis, Minn. 55455.
- 2.20 Lectures of the 1990 Short Course on Parachute Systems Engineering, May 1990, Boston, Massachusetts. Proceedings are available from the Department of Aerospace Engineering, University of Minnesota, Minneapolis, Minn. 55455.

2.5.5 Miscellaneous References

- 2.21 Proceedings of the 1986 and 1988 Parachute Manufacturing Seminars conducted by the Piedmont Community College, P. O. Box 1197, Roxboro, N.C. 27573.
- 2.22 D. Poynter, *The Parachute Manual*, published by Para-Publishing, P. O. Box 4232, Santa Barbara, Calif. 91340-4232.

CHAPTER 3

UNITS OF MEASUREMENT, TECHNICAL TABLES, AND SYMBOLS

Data presented in this chapter have been drawn from the *U.S. Standard Atmosphere, 1976*, the *Metric Design Guide*, the *Air Force Recovery Systems Design Guide* (Reference 2.1), Navy manuals, and other sources as referenced in section 3.5.

The symbols and abbreviations used in parachute recovery system design and analysis contained in section 3.4 agree with those listed in Navy manuals and the *Air Force Recovery Systems Design Guide*.

3.1 UNITS OF MEASUREMENT

3.1.1 Basic Units

Metric			English	
Quantity	Symbol	Name	Symbol	Name
Length	m	meter	ft	foot
Mass	kg	kilogram	lb	pound
Time	s	second	s	second
Temperature	K	Kelvin	R	Rankine
Electric current	A	ampere	A	ampere

3.1.2 Derived Units

Quantity	Symbol	Name	Dimension
Force	N	newton	$\text{kg}\cdot\text{m}/\text{s}^2$
Pressure	Pa	pascal	N/m^2
Work, energy	J	joule	$\text{N}\cdot\text{m}$
Rate of energy	W	watt	J/s

The metric units of measurement defined in sections 3.1.1 and 3.1.2 are used by physicists, but seldom by engineers who work with English units of measurement.

3.1.3 Engineering Units of Measurement

Length

One statute mile (mi) = 1760 yards (yd) = 5280 feet (ft)

One foot = 12 inches (in.)

One kilometer (km) = 1000 meters (m)

One meter = 100 centimeters (cm)

One centimeter = 10 millimeters (mm)

One millimeter = 10,000 microns

One meter = 10^3 millimeters = 10^7 microns = 10^{10} angstroms

Area

One square mile (mi^2) = 640 acres = 3,097,600 square yards (yd^2)

One square yard = 9 square feet (ft^2)

One square foot = 144 square inches (in^2)

One square kilometer (km^2) = 1,000,000 square meters (m^2)

One square meter = 10,000 square centimeters (cm^2)

One square centimeter = 100 square millimeters (mm^2)

Volume

One cubic yard (yd^3) = 27 cubic feet (ft^3)

One cubic foot = 7.48 gallons (gal) = 1728 cubic inches (in^3)

One cubic meter (m^3) = 1000 liters (L)

One liter = 1000 cubic centimeters (cm^3) = 1000 milliliters

One cubic centimeter = 1000 cubic millimeters (mm^3)

Weight

One English ton = 2000 pounds (lb)

One pound = 16 ounces (oz)

One ounce = 437.5 grains (gr)

One metric ton = 1000 kilograms (kg)

One kilogram = 1000 grams (g)

Force

One pound force = 4.44822 newtons (N)

One kilogram force = 9.80665 newtons

Pressure

One pound per square inch (psi) = 144 pounds per square foot (lb/ft²)

One atmosphere (atm) = 14.696 psi = 29.921 inches of mercury (in. Hg)

One kilogram per square centimeter (kg/cm²) = one technical atmosphere

One pascal (Pa) = one newton per square meter (N/m²)

Torr, millibar, and psi are used to define atmospheric pressure. See tables in section 3.2 for conversion between units.

Power

One horsepower (HP) = 0.7457 kilowatt (kW) = 550 foot-pounds per second (ft-lb/s)

One metric horsepower = 75 kg-m/s = 0.9863 English horsepower

Specific Weight

One pound per cubic inch (lb/in³) = 1728 pounds per cubic foot (lb/ft³)

One gram per cubic centimeter (g/cm³) = one kilogram per liter (kg/L) = one metric ton per cubic meter (ton/m³)

Density, Y, is expressed in lb/ft³

Specific weight, w, is expressed in g/cm³

Mass density, ρ, is expressed in slug/ft³ or kgs²/m⁴

Temperature

Absolute zero = zero degrees Kelvin (°K) = -273.16 degrees Celsius (°C); or -459.67 degrees Fahrenheit (°F) = zero degrees Rankine (°R)

Velocity

One knot = 1 nautical mile (nmi) per hour = 1852 meters per hour (m/h)

One mile per hour (mph) = 1.4667 feet per second (ft/s)

One kilometer per hour (km/h) = 0.27778 meter per second (m/s)

Acceleration

Acceleration is measured as velocity change per second (ft/s²)

Acceleration of gravity, g, (ft/s², m/s²) is the acceleration of any free-falling body toward the center of the Earth (see section 4.1.5).

3.2 CONVERSION TABLES

Conversion Table 3-1 is based on tables used in the aerospace industry and has been updated with information contained in References 3.1 to 3.4. Table 3-2 provides a convenient method to convert temperature data from Fahrenheit to Celsius, or vice versa.

3.3 TECHNICAL TABLES

3.3.1 Earth's Atmosphere

The Earth is surrounded by a blanket of gas pressing statically against its surface and making up its atmosphere. Atmospheric pressure, density, temperature, and the speed of sound vary with altitude.

Table 3-3 lists, versus altitude, the static pressure, p , in lb/ft^2 ; the mass density, ρ , in slugs/ft^3 ; the temperature, T , in $^{\circ}\text{F}$; and the speed of sound, C_s , in ft/s . These data are taken from the *U.S. Standard Atmosphere, 1976* (Reference 3.4). The altitude scale is represented by a vertical on the Earth's surface extending through the center of the Earth. The data in Table 3-3 are averages, varying with seasonal weather changes and the fact that the Earth is not a perfect sphere. The *U.S. Standard Atmosphere, 1976*, which contains a detailed discussion of these variations, includes data for higher altitudes.

Pressure and mass density decrease gradually with altitude. At an altitude of approximately 275,000 feet, continuum flow gradually changes to molecular flow, and, subsequently, to atomic flow. Sustained flight of aircraft with air-breathing engines ceases to be practical at altitudes approaching 100,000 feet because of the low density of the atmosphere.

The temperature gradually decreases with altitude to 37,000 feet, remains constant to 65,000 feet, and then increases again. A second temperature reversal occurs at approximately 160,000 feet (Reference 3.4). Figure 3-1 shows the altitude dependency of temperature and speed of sound. The close relationship between temperature and speed of sound is discussed in Chapter 4.

The value $1/\sqrt{\rho/\rho_0}$ permits the determination of rate of descent at any altitude. For example, a parachute with a sea-level rate of descent, v_{e_0} , of 20 ft/s has a rate of descent, v_e , at 40,000 feet of $20 \times 1/\sqrt{\rho/\rho_0} = 20 \times 2.0118 = 40.24 \text{ ft/s}$.

3.3.2 Dynamic Pressure

Chapter 4 contains an explanation of the importance of dynamic pressure, q , in all aerodynamic calculations. Figure 3-2 gives dynamic pressure in lb/ft^2 in relation to altitude, Mach number, and true airspeed. These graphic values should be used only for preliminary calculations. Final dynamic pressure values should be calculated using the method shown in Chapter 4.

TABLE 3-1. Conversion of English System to Metric System.

To convert from	To	Multiply by
atmosphere	pounds per square inch	14.69601
	kilograms per square centimeter	1.0332
	technical atmosphere	1.0332
	millimeters mercury	760
	inches mercury	29.9213
bar	newtons per square meter	101,325
	kilograms per square centimeter	1.0197
	inches of mercury	29.531
	pascal	10^5
British thermal units (Btu)	atmosphere	0.9869
	foot-pounds	777.98
centimeters	kilogram-calories	0.25198
	inches	0.39370
centimeters of mercury	feet	0.032808
	inches of water	5.35239
cubic centimeters	pounds per square inch	0.19337
	liters	0.001
cubic feet	cubic inches	0.06102
	cubic inches	1728
	cubic yards	9
	gallons	7.48052
	liters	28.31685
cubic feet per minute	cubic meters	0.02832
	cubic meters per minute	0.02832
cubic inches	cubic centimeters	16.38706
	liters	0.01639
	gallons	0.00433
cubic meters	cubic centimeters	10^6
	cubic feet	35.31445
	cubic yards	1.30794
	gallons	264.1776
cubic yards	cubic feet	27
	cubic meters	0.76456
degrees (arc)	radians	0.01745
dynes	grams (mass \times centimeters per second squared)	1

TABLE 3-1. (Contd.)

To convert from	To	Multiply by
fathoms	feet	6
	meters	1.82880
feet	inches	12
	yards	3
	centimeters	30.48
	meters	0.3048
feet per minute	miles per hour	0.01136
	kilometers per hour	0.01829
	meters per second	0.00580
	knots	0.00987
feet per second	miles per hour	0.68182
	kilometers per hour	1.09728
	meters per second	0.30480
	knots	0.59249
foot-pounds	kilogram-meters	0.13826
foot-pounds per second	horsepower	1/550 = 0.00182
gallons	cubic inches	231.04
	cubic feet	0.13368
	liters	3.78540
	imperial gallons	0.83268
grams	ounces	0.03528
	pounds	0.00221
	milligrams	1000
	kilograms	0.001
grams per cubic centimeter	kilograms per cubic meter	1000
	pounds per cubic foot	62.42833
horsepower	foot-pounds per second	550
	kilogram-meters per second	76.04039
	metric horsepower	1.01387
	kilowatts	0.7457
	British thermal units per second	0.7068
horsepower, metric	kilogram-meters per second	75
	horsepower, English	0.98632
	watts	735.499
inches	centimeters	2.54
inches of mercury	pounds per square inch	0.49116
	atmosphere	0.03342
	kilograms per square meter	0.03453

TABLE 3-1. (Contd.)

To convert from	To	Multiply by
inches of water	inches of mercury pounds per square inch	0.07349 0.03609
joules	newtons x meters watt-seconds foot-pounds	1 1 0.73756
kilograms	pounds grams	2.20462 1000
kilogram-meters	foot-pounds	7.23275
kilograms per cubic meter	pounds per cubic foot grams per cubic centimeter	0.06243 0.001
kilograms per square meter	pounds per square inch inches of mercury grams per square centimeter pounds per square foot	0.00142 0.002896 0.1 0.20477
kilometers	feet statute miles nautical miles	3280.839 0.62137 0.53996
kilometers per hour	feet per second miles per hour knots meters per second	0.91134 0.62137 0.53996 0.27778
knots	nautical miles per hour feet per second miles per hour kilometers per hour meters per second	1 1.68781 1.15078 1.852 0.51444
liters	cubic centimeters cubic inches cubic feet gallons	1000 61.02376 0.03532 0.26417
meters	inches feet yards	39.37008 3.28084 1.09361
meters per second	feet per second miles per hour kilometers per hour knots	3.28084 2.23693 3.6 1.94384

TABLE 3-1. (Contd.)

To convert from	To	Multiply by
microns	centimeters	0.0001
miles per hour	knots	0.86898
	feet per second	1.46667
	kilometers per hour	1.60934
	meters per second	0.44704
mils	inches	0.001
	millimeters	0.0254
nautical miles (U.K.)	feet	6080.20
nautical miles (USN, Intl)	meters	1852
	feet	6076.1155
	statute miles	1.15078
newtons	kilograms x meters per second squared	1
	pounds force	0.22481
	kilogram force	0.10197
ounces	pounds	16
	grams	28.3495
pascals	newtons per square meter	1
	pounds per square foot	0.02082
	kilograms per square meter	0.10197
pounds	kilograms	0.45359
pounds force	newtons	4.44822
pounds per cubic inch	pounds per cubic foot	1728
	grams per cubic centimeter	27.67974
pounds per square foot	inches of water	0.19242
	kilograms per square meter	4.88352
pounds per square inch	inches of water	27.7085
	atmosphere	0.06806
	kilograms per square meter	703.06687
quarts	gallons	4
	cubic inches	57.75
radians	degrees	57.29578
radians per second	degrees per second	57.29578
	revolutions per second	0.15916
slugs/ft ³	$\frac{\text{kg}}{\text{m}^3}$	52.554
square centimeters	square inches	0.155
square feet	square centimeters	929.0304

TABLE 3-1. (Contd.)

To convert from	To	Multiply by
square inches	square millimeters	645.16
square kilometers	square miles	0.38610
square meters	square yards	1.19599
square miles	square kilometers	2.58998
statute miles	feet	5.280
	nautical miles	0.86898
	kilometers	1.60934
tons, long	pounds	2240
	kilograms	1016.047
tons, short	pounds	2000
	kilograms	907.1847
tons, metric	kilograms	1000
	long tons	0.98421
	short tons	1.10231
torr	millimeters of mercury	1
watts	newtons × meters per second	1
yards	centimeters	91.44
	meters	0.9144

NWC TP 6575

TABLE 3-2 Temperature Conversion Table.

To convert from Fahrenheit to Celsius, go from center column to left column. To convert from Celsius to Fahrenheit, go from center column to right column. Conversion formulas:

$$C = \frac{5}{9}(F - 32); F = \frac{9}{5}C + 32$$

-100 to 25			26 to 61			62 to 97		
C.	F. C.	F.	C.	F. C.	F.	C.	F. C.	F.
-73	-100	-148	-3.3	26	78.8	16.6	62	143.6
-68	-90	-130	-2.8	27	80.6	17.1	63	145.4
-62	-80	-112	-2.2	28	82.4	17.7	64	147.2
-57	-70	-94	-1.6	29	84.2	18.2	65	149.0
-51	-60	-76	-1.1	30	86.0	18.8	66	150.8
-46	-50	-58	-0.6	31	87.8	19.3	67	152.6
-40	-40	-40	0.0	32	89.6	19.9	68	154.4
-34	-30	-22	0.5	33	91.4	20.4	69	156.2
-29	-20	-4	1.1	34	93.2	21.0	70	158.0
-23	-20	14	1.6	35	95.0	21.5	71	159.8
-17.7	0	32	2.2	36	96.8	22.2	72	161.6
-17.2	1	33.8	2.7	37	98.6	22.7	73	163.4
-16.6	2	35.6	3.3	38	100.4	23.3	74	165.2
-16.1	3	37.4	3.8	39	102.2	23.8	75	167.0
-15.5	4	39.2	4.4	40	104.0	24.4	76	168.8
-15.0	5	41.0	4.9	41	105.8	25.0	77	170.6
-14.4	6	42.8	5.5	42	107.6	25.5	78	172.4
-13.9	7	44.6	6.0	43	109.4	26.2	79	174.2
-13.3	8	46.4	6.6	44	111.2	26.8	80	176.0
-12.7	9	48.2	7.1	45	113.0	27.3	81	177.8
-12.2	10	50.0	7.7	46	114.8	27.7	82	179.6
-11.6	11	51.8	8.2	47	116.6	28.2	83	181.4
-11.1	12	53.6	8.8	48	118.4	28.8	84	183.2
-10.5	13	55.4	9.3	49	120.2	29.3	85	185.0
-10.0	14	57.2	9.9	50	122.0	29.9	86	186.8
-9.4	15	59.0	10.4	51	123.8	30.4	87	188.6
-8.8	16	61.8	11.1	52	125.6	31.0	88	190.4
-8.3	17	63.6	11.5	53	127.4	31.5	89	192.2
-7.7	18	65.4	12.1	54	129.2	32.1	90	194.0
-7.2	19	67.2	12.6	55	131.0	32.6	91	195.8
-6.6	20	68.0	13.2	56	132.8	33.3	92	197.6
-6.1	21	69.8	13.7	57	134.6	33.8	93	199.4
-5.5	22	71.6	14.3	58	136.4	34.4	94	201.2
-5.0	23	73.4	14.8	59	138.2	34.9	95	203.0
-4.4	24	75.2	15.6	60	140.0	35.5	96	204.8
-3.9	25	77.0	16.1	61	141.8	36.1	97	206.6

TABLE 3-2 (Contd.)

98 to 510			520 to 970			980 to 1000		
C.	F. C.	F.	C.	F. C.	F.	C.	F. C.	F.
36.6	98	208.4	271	520	968	526	980	1796
37.1	99	210.2	276	530	986	532	990	1814
37.7	100	212.0	282	540	1004	538	1000	1832
38	100	212	288	550	1022			
43	110	230	293	560	1040			
49	120	248	299	570	1058			
54	130	266	304	580	1076			
60	140	284	310	590	1094			
65	150	302	315	600	1112			
71	160	320	321	610	1130			
76	170	338	326	620	1148			
83	180	356	332	630	1166			
88	190	374	338	640	1184			
93	200	392	343	650	1202			
99	210	410	349	660	1220			
100	212	413	354	670	1238			
104	220	428	360	680	1256			
110	230	446	365	690	1274			
115	240	464	371	700	1292			
121	250	482	376	710	1310			
127	260	500	382	720	1328			
132	270	518	387	730	1346			
138	280	536	393	740	1364			
143	290	554	399	750	1382			
149	300	572	404	760	1400			
154	310	590	410	770	1418			
160	320	608	415	780	1436			
165	330	626	421	790	1454			
171	340	644	426	800	1472			
177	350	662	432	810	1490			
182	360	680	438	820	1508			
188	370	698	443	830	1526			
193	380	716	449	840	1544			
199	390	734	454	850	1562			
204	400	752	460	860	1580			
210	410	770	465	870	1598			
215	420	788	471	880	1616			
221	430	806	476	890	1634			
226	440	824	482	900	1652			
232	450	842	487	910	1670			
238	460	860	493	920	1688			
243	470	878	498	930	1706			
249	480	896	504	940	1724			
254	490	914	510	950	1742			
260	500	932	515	960	1760			
265	510	950	520	970	1778			

TABLE 3-3. Properties of Earth's Atmosphere Versus Altitude.

Altitude, Z (ft)	Pressure, P (lb/ft ²)	Mass density, ρ (slugs/ft ³)	$1/\sqrt{\rho/\rho_0}$	Temperature, T ('F)	Speed of sound, C_s (ft/s)
0	2116.22	.237689-2	1.0000	59.000	1116.45
1000	2040.86	.230812	1.0148	55.434	1112.6
2000	1967.69	.224088	1.0299	51.868	1108.75
3000	1896.67	.217516	1.0453	48.303	1104.88
4000	1827.75	.211093	1.0611	44.738	1100.99
5000	1760.87	.204817	1.0773	41.173	1097.10
6000	1696.00	.198685	1.0938	37.609	1093.19
7000	1633.08	.192695	1.1106	34.045	1089.26
8000	1572.07	.186845	1.1279	30.482	1085.32
9000	1512.93	.181133	1.1455	26.918	1081.37
10,000	1455.60	.175555-2	1.1636	23.355	1077.40
12,000	1346.24	.164796	1.2010	16.231	1069.43
14,000	1243.65	.154551	1.2401	9.107	1061.40
16,000	1147.50	.144802	1.2812	1.985	1053.30
18,000	1057.48	.135533	1.3243	-5.135	1045.15
20,000	9732.75-1	.126726-2	1.3695	-12.255	1036.93
22,000	8946.02	.118365	1.4171	-19.373	1028.65
24,000	8211.72	.110435	1.4671	-26.489	1020.30
26,000	7527.14	.102919	1.5197	-33.605	1011.89
28,000	6889.64	.958016	1.5751	-40.719	1003.40
30,000	6296.69-1	.890686	1.6336	-47.831	994.85
32,000	5745.85	.827050	1.6953	-54.942	986.22
34,000	5234.80	.766963	1.7604	-62.052	977.52
36,000	4761.28	.710284	1.8293	-69.160	968.75
38,000	4326.40	.646302	1.9177	-69.700	968.08
40,000	3931.29-1	.587278-3	2.0118	-69.700	968.08
42,000	3572.33	.533655	2.1105	-69.700	968.08
44,000	3246.20	.484936	2.2139	-69.700	968.08
46,000	2949.90	.440673	2.3224	-69.700	968.08
48,000	2680.70	.400458	2.4363	-69.700	968.08
50,000	2436.11-1	.363919-3	2.5556	-69.700	968.08
52,000	2213.67	.330721	2.6809	-69.700	968.08
54,000	2011.95	.300556	2.8121	-69.700	968.08
56,000	1828.47	.273148	2.9499	-69.700	968.08
58,000	1661.76	.248243	3.0943	-69.700	968.08

NWC TP 6575

TABLE 3-3. (Contd.)

Altitude, Z (ft)	Pressure, p (lb/ft ²)	Mass density, ρ (slug/ft ³)	$1/\sqrt{\rho/\rho_0}$	Temperature, T (°F)	Speed of sound, C_s (ft/s)
60,000	1510.28-1	.225614-3	3.2458	-69.700	968.08
62,000	1372.63	.205051	3.4046	-69.700	968.08
64,000	1247.55	.186365	3.5713	-69.700	968.08
66,000	1133.88	.169344	3.7464	-69.604	968.20
68,000	1030.76	.153513	3.9348	-68.514	969.55
70,000	9372.76-2	.139203-3	4.1322	-67.424	970.90
72,000	8938.59	.132571	4.3388	-66.334	972.24
74,000	8525.13	.126263	4.5550	-66.224	973.59
76,000	7058.82	.103970	4.7813	-64.155	974.93
78,000	6425.82	.943868-4	5.0183	-63.066	976.28
80,000	5851.20	.857110	5.2659	-61.977	977.62
82,000	5329.42	.778546	5.5255	-60.888	978.95
84,000	4855.49	.707382	5.7968	-59.799	980.29
86,000	4424.91	.642902	6.0805	-58.711	981.62
88,000	4033.60	.584461	6.3771	-57.623	982.95
90,000	3677.88-2	.531480-4	6.6876	-56.535	984.28
92,000	3354.42	.483433	7.0121	-55.447	985.61
94,000	3060.2	.439851	7.3513	-54.359	986.93
96,000	2792.56	.400305	7.7059	-53.272	988.26
98,000	2548.98	.364413-4	8.0762	-52.185	989.58
100,000	2327.25	.331829	8.4631	-51.098	990.90

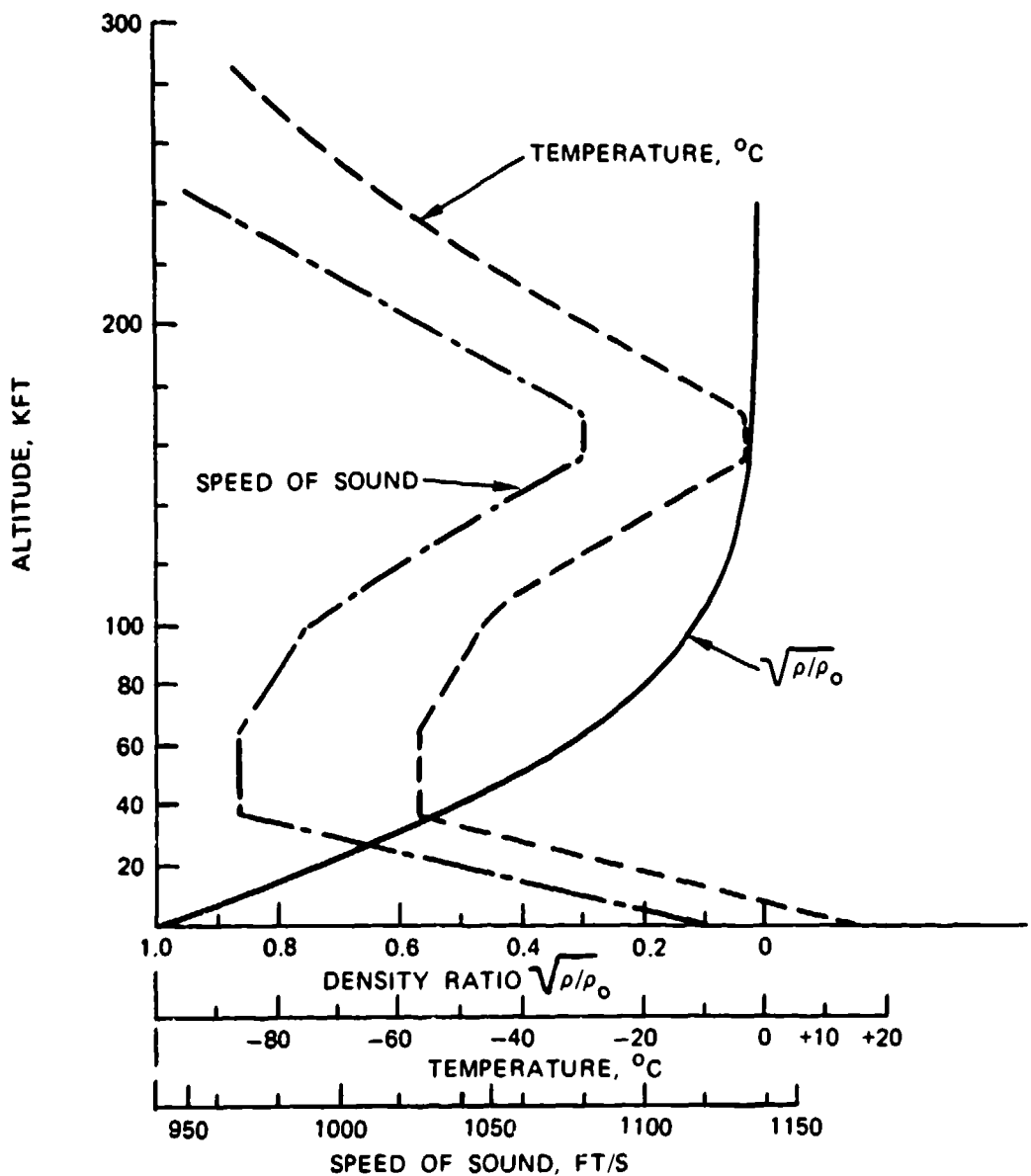


FIGURE 3-1. Density Ratio, Temperature, and Speed of Sound Versus Altitude (Reference 3.4).

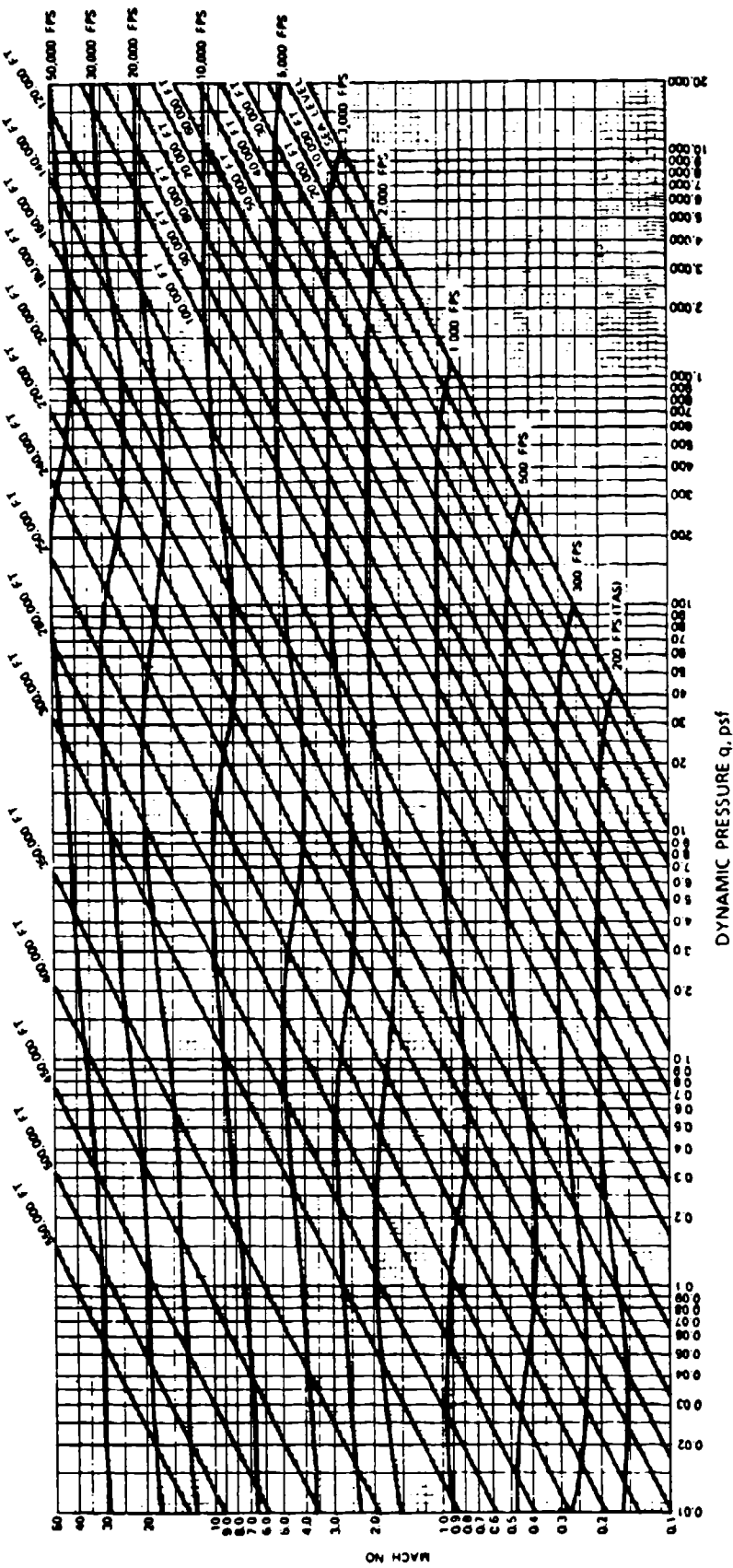


FIGURE 3-2. Dynamic Pressure Versus Altitude, Mach Number, and True Airspeed.

3.4 LIST OF SYMBOLS

A	Area
AR	Aspect ratio
a	Acceleration
b	Wingspan
C	Coefficient constant
C_A, C_R	Aerodynamic force coefficients
C_D	Drag coefficient
C_{Dc}	Drag coefficient of parachute cluster
C_{D_0}	Drag coefficient related to canopy surface area (S_0)
C_{D_p}	Drag coefficient related to inflated canopy area (S_p)
C_f	Coefficient of friction
C_L	Lift coefficient
C_m	Moment coefficient
C_N	Normal or side force coefficient
C_p	Pressure coefficient, specific heat
C_R	Resultant or radial force coefficient
C_x	Opening force coefficient (infinite mass)
c	Dimension of wing chord, factor to suspension line convergence
c_s	Velocity of sound
C_{DA}	Forebody drag area
$(C_{DS})_0$	Effective drag area of parachute related to canopy surface area (S_0)
$(C_{DS})_p$	Parachute drag area, general
$(C_{DS})_R$	Parachute drag area, reefed
D	Drag, diameter
D_B	Diameter of forebody
D_F	Design factor
D_o	Nominal diameter of parachute canopy = $(4S_0/\pi)^{1/2}$
D_p	Projected diameter of parachute = $(4S_p/\pi)^{1/2}$
D_R	Diameter of reefing-line circle
D_v	Diameter of canopy vent
E	Young's modulus of elasticity
E_K	Kinetic energy
e	Strength loss factor caused by abrasion, canopy gore width
e_s	Gore width at skirt of canopy
e_v	Gore width at vent of canopy

F	Force, structural load
F_c	Constant force, steady-state drag force
F_N	Normal force
F_o	Parachute opening force
F_x	Parachute maximum opening force
F_R	Reefed opening force
F_S	Parachute snatch force
F_{Ult}	Ultimate load
f	Unit stress, frequency, "a function of"
G	Load factor = a/g
g	Acceleration of gravity
g₀	Acceleration of gravity at sea level (MSL)
h	Height (general), height of canopy gore at any point
h_g	Height of canopy gore from vent to skirt
h_v	Height of vent
I	Impulse
i	Strength loss factor caused by vacuum
K	Constant (general)
K_f	Dimensionless filling time parameter
k	Strength loss factor caused by fatigue
L	Lift
L/D	Lift-to-drag ratio = glide ratio
L	Length (general)
L_e	Effective suspension-line length
L_R	Length of riser
L_r	Length of reefing line (installed length)
L_s	Length of suspension line
L_T	Distance between parachute canopy and forebody
M	Mach number, moment, system mass
M_s	Margin of safety
m	Mass
n	Canopy filling constant; strength loss factor caused by water absorption
N	Any number
N_G	Number of canopy gores
N_R	Number of risers
N_{SL}	Number of suspension lines
N_c	Number of parachutes in a cluster

p	Pressure, strength of material
Δp	Pressure differential
q	Dynamic pressure
R	Reliability factor
R_e	Reynolds number
R_m	Mass ratio
R_w	Weight ratio
r	Radius
S	Area (general)
S_F	Safety factor
S_f	Footprint area
S_g	Area of canopy gore
S_o	Surface area of parachute canopy including vent and slots
S_p	Projected frontal canopy area
S_r	Total open area of slotted canopy
s	Factor for asymmetrical canopy loading
s_d	Deceleration distance
s_f	Filling distance of parachute
T	Temperature, thrust
t	Time (general)
t_f	Parachute canopy filling time
u	Strength loss caused by seam connections
V	Volume
v	Velocity (general)
v_c	Equilibrium velocity, rate of descent
v_{c0}	Sea-level rate of descent
v_H	Horizontal velocity
v_V	Vertical velocity
v_s	Velocity at line stretch (canopy stretch)
v_T	Trajectory velocity
W	Weight (general)
W_p	Weight of parachute
W_{PA}	Weight of parachute assembly
W_R	Weight of parachute recovery system
w	Unit weight
x_1	Opening-force-reduction factor

Greek and Mathematical Symbols

α	Angle of attack as related to airflow
β	Angle of yaw, gore vertex angle
γ	Ratio of specific heat, flat canopy gore angle
Δ	Small increment of difference
δ	Angle between radials and suspension lines
ϵ	Relative elongation, drag area ratio $(C_{DS})_R/C_{DS}_0$ = reefing ratio
η	Efficiency
θ	Angle of flight path from horizontal
x	Spring constant
λ	Porosity or air permeability of parachute canopy
λ_g	Geometric canopy porosity
λ_m	Porosity of canopy material
λ_T	Total porosity of parachute canopy
μ	Viscosity, constructed angle between canopy radials and horizontal
ν	Kinematic viscosity
ξ_g	Ratio of gravitational acceleration (g/g_0)
ρ	Mass density of air
ρ_0	Mass density of air at sea level
Σ	Summation
σ	Air density ratio (ρ/ρ_0)
τ	Reefing-line ratio (D_R/D_0)
Φ	Angle between suspension lines and longitudinal axis (bank angle)
Φ_c	Angle between individual parachutes and cluster axis
\sim	Approximately
\approx	Approximately equal to
\equiv	Identical to

3.5 REFERENCE MATERIAL

- 3.1 *The International System of Units (SI)*, National Bureau of Standards Special Publication 330, issued December 1981, Superintendent of Documents, Government Printing Office, Washington D.C. 20404.
- 3.2 *Metric Practice Guide*, March 1970, ASTM Designation E-380-70, American Society for Testing and Materials, 1916 Race St., Philadelphia, Pa. 19103.
- 3.3 Lionel S. Marks, *Mechanical Engineers Handbook*, McGraw Hill Book Co.
- 3.4 *U.S. Standard Atmosphere*, 1976, published by National Oceanic and Atmospheric Administration, NASA, U.S. Air Force. Superintendent of Documents Stock No. 003-017-00323-0, Government Printing Office, Washington, D.C. 20402.

CHAPTER 4**AERODYNAMICS AS RELATED TO PARACHUTES****4.1 PROPERTIES OF THE ATMOSPHERE**

All forces acting on parachutes and all movements of parachutes are affected by the atmosphere, or air, surrounding the Earth. The air at the Earth's surface is approximately 78% nitrogen; 21% oxygen; and 1% a mixture of gases such as argon, neon, helium, water vapor, and carbon dioxide. This chemical composition remains relatively constant to an altitude of about 160,000 feet (50 kilometers). The following air qualities are of major significance in the dynamics of bodies moving in the atmosphere:

<u>Air quality</u>	<u>Symbol</u>	<u>Dimension</u>
Specific weight of air	w	lb/ft ³ , kg/m ³
Static pressure	p	atm, lb/ft ² , Pa, bar, torr
Temperature	T	°F, °C
Mass density	ρ	slugs/ft ³ , kg s ² /m ⁴
Gravity	g	ft/s ² , m/s ²
Speed of sound	C _s	ft/s, m/s

All of these qualities are altitude-dependent and may vary slightly on the Earth's surface with geographic latitude because of variations of the Earth's radius caused by the centrifugal forces of the rotation of the Earth. All standard data used herein refer to a latitude of 45 degrees. Sea level is defined as mean sea level (MSL). To compare performance data on an equal basis, the United States Bureau of Standards has defined standard day conditions as follows:

Temperature = 15 degrees Celcius (°C) or 59 degrees Fahrenheit (°F)
 Pressure = 760 millimeters (mm) of mercury (Hg) or 29.9213 inches (in.) Hg

4.1.1 Specific Weight of Air

For standard day conditions of 59°F temperature and a pressure of 29.9213 in. Hg, the specific weight of air, w, is 0.07648 lb/ft³ or 1.2250 kg/m³. The specific weight of air changes with pressure, temperature, and humidity. Further data can be found in References 3.4 and 4.1, and in technical handbooks.

4.1.2 Static Pressure

Static pressure depends on geographic latitude, weather conditions, and altitude. The static pressure at any altitude results from the weight of the air above that altitude. For MSL and standard day conditions, the pressure, p_0 , is 29.9213 in. Hg = 760 mm Hg = 1.0 atmosphere (atm). For conversion to Pascal, torr, or bar, see the conversion tables in section 3.2.

4.1.3 Temperature

Temperatures are defined in the English and metric systems in the so-called absolute and engineering scales. The absolute temperature minimum at 0 degrees pressure is $0^{\circ}\text{K} = -273.16^{\circ}\text{C}$, and $0^{\circ}\text{R} = -459.69^{\circ}\text{F}$. This is also written

$$\begin{aligned}\text{Degrees Kelvin} &= \text{degrees Celsius} + 273.16 \\ \text{Degrees Rankine} &= \text{degrees Fahrenheit} + 459.69\end{aligned}$$

The freezing point of water is 32°F or 0°C . The boiling point of water is 212°F or 100°C .

4.1.4 Mass Density of Air

Mass density defines the amount of mass contained in a unit volume of air. The mass density, ρ , of air is of special importance in aerodynamic calculations.

$$\rho = \frac{\text{specific weight of air, } w}{\text{acceleration of gravity, } g} = \frac{\text{lb}/\text{ft}^3}{\text{ft}/\text{s}^2} = \text{slug}/\text{ft}^3 = \frac{\text{kg s}^2}{\text{m}^4}$$

$$\text{slug} = \frac{\text{weight}}{\text{acceleration of gravity}} = \frac{\text{lb}}{\text{ft}/\text{s}^2}$$

Frequently the density ratio, σ , is used

$$\sigma = \frac{\text{ambient air density, } \rho}{\text{standard sea-level density, } \rho_0}$$

The factor $1/\sqrt{\rho/\rho_0}$ determines the increase in parachute rate of descent with altitude. The density at 40,000 feet is $\frac{1}{4}$ of the MSL density, and the density at 100,000 feet is $1/75$ of the MSL density. Therefore, the parachute rate of descent is about twice as high at 40,000 feet and about nine times as high at 100,000 feet. MSL density is 0.00237689 slugs/ ft^3 , or $0.1249 \text{ kg s}^2/\text{m}^4$.

4.1.5 Gravity

Any mass attracts another mass with a force called gravity. If the Earth were surrounded by a vacuum, a body suspended above the Earth and released would fall toward the center of

the Earth with increasing velocity caused by the acceleration of gravity, g . In reality, the falling body is decelerated by its air drag until the air drag, D , equals the weight of the body, W , and an equilibrium velocity is reached; for parachutes, this is called the steady-state rate of descent.

The acceleration of gravity, g , at sea level is

$$g = 32.174 \text{ ft/s}^2 \text{ or } 9.80665 \text{ m/s}^2.$$

The value $g = 9.80665 \text{ m/s}$ is standardized internationally but is accurate only for a latitude of 45 degrees.

With increasing altitude above the Earth's surface, the acceleration of gravity decreases in accordance with the equation

$$g = g_0 \left(\frac{r}{r + h} \right)^2$$

where

g = acceleration of gravity at any altitude, ft/s^2

g_0 = acceleration of gravity at sea level, ft/s^2

r = average Earth radius = $2.08556 \times 10^7 \text{ ft}$

h = altitude above sea level, ft

For other planets and heavenly bodies, the acceleration of gravity varies with the mass of the body. For example, the acceleration of gravity on Mars is about 1/3 of the acceleration of gravity on Earth. For more details on planets and heavenly bodies, see page XII of Reference 2.1.

4.1.6 Kinematic Viscosity

The coefficient of viscosity, μ , defines the shearing stresses in a gas or liquid and is sometimes called the resistance to continuous deformation. In aerodynamics, the coefficient of viscosity is combined with the mass density to form the kinematic viscosity, ν , where

$$\nu = \frac{\text{coefficient of viscosity, } \mu}{\text{mass density, } \rho} = 0.0001576 \text{ ft}^2/\text{s at sea level}$$

The kinematic viscosity, ν , is altitude dependent and is used to calculate the Reynolds number, Re .

4.1.7 Reynolds Number

The Reynolds number, Re , defines the relationship of mass forces to viscous friction forces in liquids and gases. It is calculated as

$$Re = \frac{v \cdot l}{\nu} = \frac{\text{velocity (ft/s)} \cdot \text{characteristic length (ft)}}{\text{kinematic viscosity (ft}^2/\text{s)}}$$

Reynolds number is an important criterion in subsonic, noncompressible flow, and allows comparison of model tests with full-scale flight tests. A Reynolds number effect on parachutes working in separated, turbulent flow has not yet been established, as shown in section 5.2. The following chart shows the Reynolds numbers for various air vehicles.

<u>Subject</u>	<u>Insect</u>	<u>Glider</u>	<u>DC-3</u>	<u>B-747</u>	<u>Drogue chute</u>	<u>Main parachute</u>	<u>WTT model</u>
Re	$6 \cdot 10^3$	$2.5 \cdot 10^6$	$24 \cdot 10^6$	$100 \cdot 10^6$	$50 \cdot 10^6$	$20 \cdot 10^6$	$2 \cdot 10^6$

4.1.8 Mach Number

Mach number is an important parameter of supersonic flight; it states how much faster than the speed of sound the air vehicle travels.

$$\text{Mach number, } M = \frac{\text{flight velocity, } v}{\text{speed of sound, } c_s}$$

The speed of sound is the velocity at which a pressure disturbance, such as the sound of the human voice, travels in any medium. The speed of sound varies considerably in different gases, liquids, and metals.

Speed of sound in air at MSL $c_s = 1116.46 \text{ ft/s} = 340.38 \text{ m/s}$

Speed of sound in water $c_s = 4749 \text{ ft/s} = 1461.21 \text{ m/s}$

Speed of sound in iron $c_s = 16,410 \text{ ft/s} = 5710.7 \text{ m/s}$

The speed of sound depends on temperature and the chemical composition of the medium. A widely used equation for speed of sound in air is

$$c_s = 41.4 \sqrt{\gamma \cdot T}$$

where

c_s = speed of sound in dry air, ft/s

γ = ratio of specific heat, equal to 1.4 for dry air, dimensionless

T = temperature in Fahrenheit absolute, equal to $459.67 + ^\circ\text{F}$

The speed of sound changes with altitude, as does temperature (see Figure 3-1). The drag of streamlined bodies such as missiles, airfoils, and airplanes increases considerably as their velocities approach Mach 1. Depending on the configuration of the body, supersonic compressibility effects may occur in the 0.75- to 0.85-Mach range, causing local supersonic flow, shock waves, flow separation, and concomitant increases in drag and changes in stability.

Parachutes that operate in separated flow over the entire velocity range do not show the typical drag increase when operating close to or beyond Mach 1. Supersonic parachute behavior is discussed in detail in section 5.8.

4.2 CONTINUITY LAW AND BERNOULLI EQUATION

4.2.1 Continuity Law

Air is thought to flow in layers called streamlines. Figure 4-1 shows streamlines as layers of air without air transfer between individual layers. The air is shown as being incompressible, a valid assumption for subsonic flow.



FIGURE 4-1. Typical Streamline.

If exchange of air does not occur across the streamline boundaries, the amount of air entering the streamline at point 1 must also exit at point 2, as shown in Figure 4-1. Because the cross section at point 2 is smaller than the cross section at point 1, the air must exit at a higher velocity. The following equation defines this condition:

$$v_1 \cdot S_1 \cdot \rho_1 = v_2 \cdot S_2 \cdot \rho_2$$

where

S = cross section of the streamline

v = velocity in the streamline

ρ = density of the air flowing in the streamline

This equation, which governs the flow in and around a body in gases and liquids, is important in aerodynamics and is called the Continuity Law. For incompressible subsonic flow, it can be simplified to

$$v_1 \cdot S_1 = v_2 \cdot S_2$$

Whenever the cross section narrows, the velocity increases; when the cross section widens, the velocity decreases.

4.2.2 Bernoulli Equation

Figure 4-2 illustrates a streamline with the cross section, S , the velocity, v , and the pressure, p . If the air is incompressible, the velocity downstream is $v + \Delta v$, and the pressure is $p + \Delta p$. If the air is inviscid, the inertia forces caused by the acceleration of air from v to $v + \Delta v$ must be balanced by differential pressure forces.

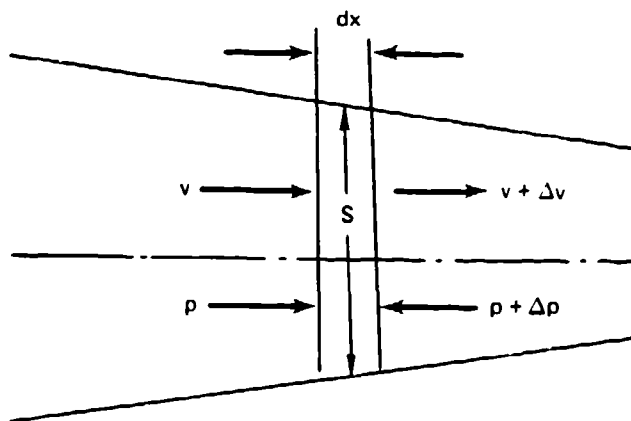


FIGURE 4-2. Pressure and Velocity Distribution in a Streamline Element.

The following equation can be written

$$p \cdot S - (p + \Delta p)S = m \cdot \frac{dv}{dt}$$

Simplified, the above equation yields

$$dp = -\rho v dv$$

and

$$p = -1/2 \rho v^2 + C$$

The above equation allows the following consideration: If p is pressure, then $1/2 \rho v^2$ and C must also be pressure. The equation $1/2 \rho v^2$ includes a velocity and is referred to as the dynamic pressure, or sometimes as velocity or impact pressure.

Pressure, p , is defined as static pressure; $1/2 \rho v^2$ as dynamic pressure; and the sum of both, C , as the total pressure or

$$p + 1/2 \rho v^2 = H$$

and

$$p_1 + 1/2 \rho v_1^2 = p_2 + 1/2 \rho v_2^2$$

where H is the total pressure of the system, lb/ft².

Dynamic pressure, q , is a frequently used quantity in aerodynamics:

$$q = 1/2 \rho v^2$$

where

q = dynamic pressure, lb/ft²

ρ = air density, slugs/ft³

v = velocity at a point of undisturbed flow, ft/s

The following formulas are used for calculating the sea-level dynamic pressure if the velocity is given in ft/s, knots, mph, or km/h, respectively:

$$q = \frac{v^2}{841.4} \text{ (ft/s)}, \quad q = \frac{v^2}{295} \text{ (knots)}, \quad q = \frac{v^2}{391.2} \text{ (mph)}, \quad q = \frac{v^2}{1013.1} \text{ (km/h)}$$

4.3 NEWTON'S THREE LAWS OF MOTION

Engineering mechanics are governed by the following three laws of Isaac Newton:

1. A body remains at rest or in an unaccelerated state of motion unless acted upon.
2. A force acting upon a body will produce an acceleration in the direction of the force.
3. An action in one direction will produce an equal reaction in the opposite direction.

The first law is self-explanatory. The second law may be expressed by the equation

$$F = m \cdot a$$

where

F = force in pounds acting on the mass, lb

m = mass of body that the force is acting upon, slugs

a = acceleration in ft/s^2 resulting from the force, F

The mass, m , of a body is obtained by

$$m = \frac{W}{g}$$

where

W = weight of the body, lb

g = acceleration of gravity, ft/s^2

The mass, therefore, has the dimension of

$$m = \frac{W}{g} = \frac{\text{lb}}{\text{ft/s}^2}$$

This unit of mass is the slug.

The equation of Newton's second law can now be written

$$F = \frac{W}{g} \cdot a, \text{ or } F = W \frac{a}{g}$$

The factor a/g is frequently called the load factor, G , and tells how much larger a force is than a force equivalent to the weight of the body. It is customary in parachute work to state that the maximum parachute force allowed is $G \cdot W$ or $(a/g) \cdot W$. It is appropriate to write

$$\text{Maximum allowable parachute force, } F = W \frac{a}{g}, \text{ or } F = W \cdot G$$

Figure 4-3 illustrates Newton's third law, explaining the principle of the rocket that can produce thrust in a perfect vacuum.

A mass, m , ejected from a rocket at the velocity, v , per unit time, t , will produce a force, F , which in turn will create a reaction force, R , of equal magnitude but acting in the opposite direction.

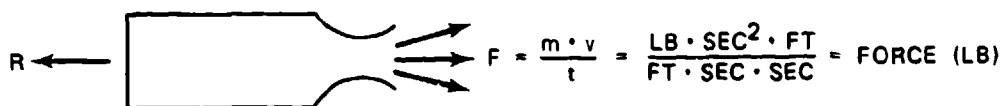


FIGURE 4-3. Rocket Principle.

4.4 FORCES ACTING ON A BODY MOVING THROUGH AIR

4.4.1 Symmetrical Body

A body moving through air experiences forces caused by air pressure acting on the body. The same forces exist if the body moves through air, such as a descending parachute, or if the body is fixed and the air moves against the body, such as a parachute or an airfoil in a wind tunnel (Figure 4-4).

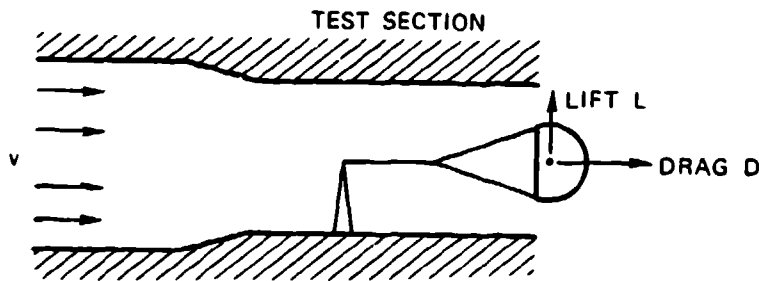


FIGURE 4-4. Stable Parachute in a Wind Tunnel.

A stable parachute in a wind tunnel experiences only the force called "drag" in the direction of the airflow. This drag force, D , is calculated to

$$D = q \cdot S \cdot C_D$$

where

D = drag, lb

q = dynamic pressure, lb/ft²

S = total surface area of the parachute canopy, ft²

C_D = coefficient of drag, dimensionless

The dynamic pressure, q , can be calculated from section 4.2.2. The surface area of the canopy, S , is selected as a reference area. The drag coefficient, C_D , is a form factor that indicates the drag characteristic of a specific shape. Most aerodynamic bodies are designed

for low drag or a low drag coefficient. Parachutes, generally, are designed for high drag; therefore, a high drag coefficient is desirable. This difference in drag is demonstrated by the two bodies shown in Figure 4-5.

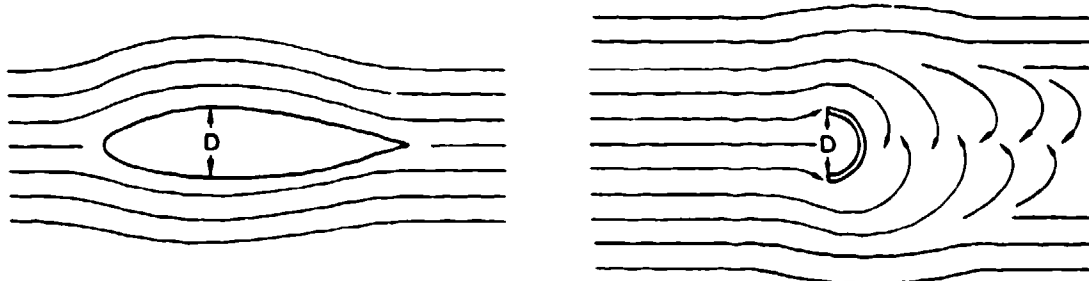


FIGURE 4-5. Airflow Around a Streamlined Body and an Open Hemisphere.

Both bodies have the same cross section perpendicular to the airflow. The cylindrical, streamlined body has a smooth airflow over its total body length, resulting in a drag coefficient, C_D , of 0.05 to 0.1, depending on slenderness ratio, surface roughness, and shape. The drag coefficient of all streamlined bodies is much affected by Reynolds number and Mach number. The open hemisphere, which is similar to a parachute canopy, has a drag coefficient, C_D , of 1.3 to 1.4 for the same body cross section. The difference in drag is explained by the smooth airflow around the streamlined body and a separated, turbulent flow around the open hemisphere. The drag of bodies with separated flow, like parachute canopies, is little affected by Reynolds number.

4.4.2 Airflow Around an Asymmetrical Body (Airfoil)

Figure 4-6 shows an airfoil fixed at an angle of attack, α , against the airflow in a wind tunnel. This airfoil creates a drag force, D , in the direction of the flow; a lift force, L , perpendicular to the direction of the flow; and a moment, M , around the attachment point of the airfoil. The sign convention of moments and forces shown are positive. Lift and drag can be combined for the resultant force, R .

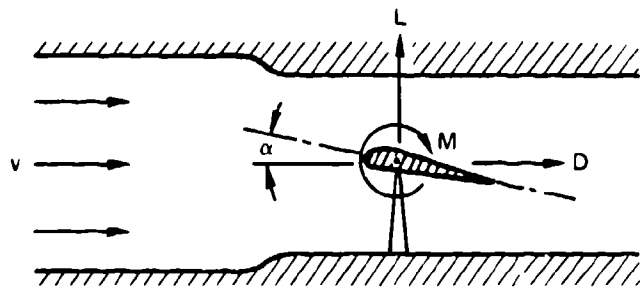


FIGURE 4-6. Wind-Tunnel Forces Acting on an Airfoil.

The lift, L, is calculated

$$L = q \cdot S \cdot C_L$$

where

L = measured lift, lb

q = dynamic pressure, lb/ft²

S = reference area, ft²

C_L = lift coefficient, dimensionless

The moment is

$$M = q \cdot S \cdot c_m \cdot c$$

where

M = moment, ft-lb

q = dynamic pressure, lb/ft²

S = reference area, ft²

c_m = moment coefficient, dimensionless

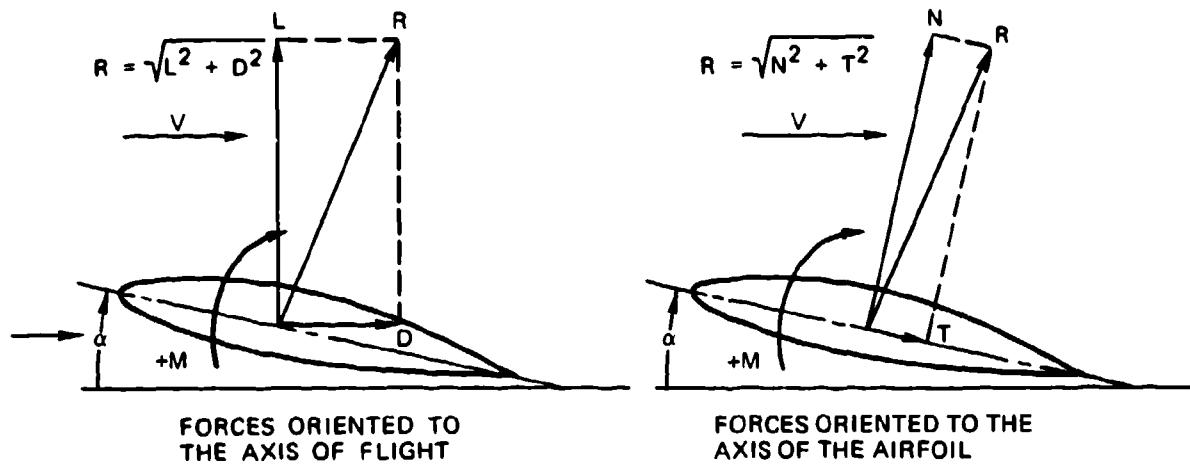
c = average chord width of the wing, ft

The reference area, S, is defined by agreement. For streamlined bodies, the maximum body cross section is used. Airfoils use the planform of the wing, and parachutes use the canopy surface area. The selection of the wing planform and the parachute surface area as references was made for practical reasons. The wing planform for a specific wing is fixed, whereas the cross section of the wing in the direction of the flow changes with the angle of attack. Similarly, the surface area of the parachute canopy is fixed; however, the frontal projected area of the inflated parachute canopy changes with airspeed, porosity, line length, and type of parachute.

Forces and moments acting on an airfoil or a parachute canopy may be presented in several ways. The two most frequently used methods, as shown in Figure 4-7, are with forces oriented to the axis of flight and with forces oriented to the axis of the airfoil.

The tangential force, T, and the normal force, N, are calculated

$$T = C_T \cdot S \cdot q$$



NOTES:

R = RESULTANT FORCE, LB	α = ANGLE OF ATTACK, DEG
L = LIFT, LB	N = NORMAL FORCE, LB
D = DRAG, LB	T = TANGENTIAL FORCE, LB
M = MOMENT, FT-LB	

FIGURE 4-7. Aerodynamic Forces Acting on an Airfoil.

and

$$N = C_N \cdot S \cdot q$$

where

C_T = tangential force coefficient, dimensionless

C_N = normal force coefficient, dimensionless

The resultant force, R, and the moment, M, in both presentations have the same direction and the same magnitude. The airflow fixed system is preferred for aerodynamic performance calculations, and the airfoil fixed system for wing stress calculations. The aerodynamic coefficients C_L , C_D , C_T , C_N , and C_m can easily be determined in wind-tunnel measurements.

Figure 4-8 shows the relationship of both force systems on a parachute. By definition, a negative moment is stabilizing, as illustrated in Figure 4-8. It is interesting to note that in Europe the stabilizing moment is defined as positive. Wind-tunnel installations frequently measure normal and tangential force instead of lift and drag. If α , T, and N are known, the drag, D, can be calculated

$$D = T \cos \alpha + N \cdot \sin \alpha$$

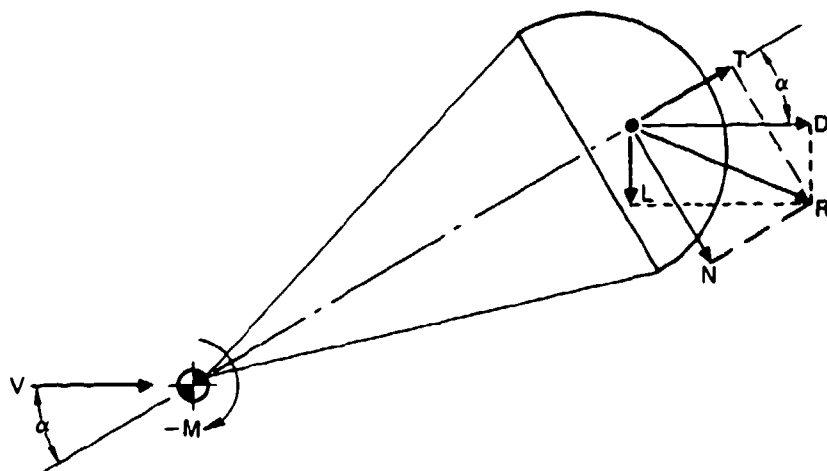
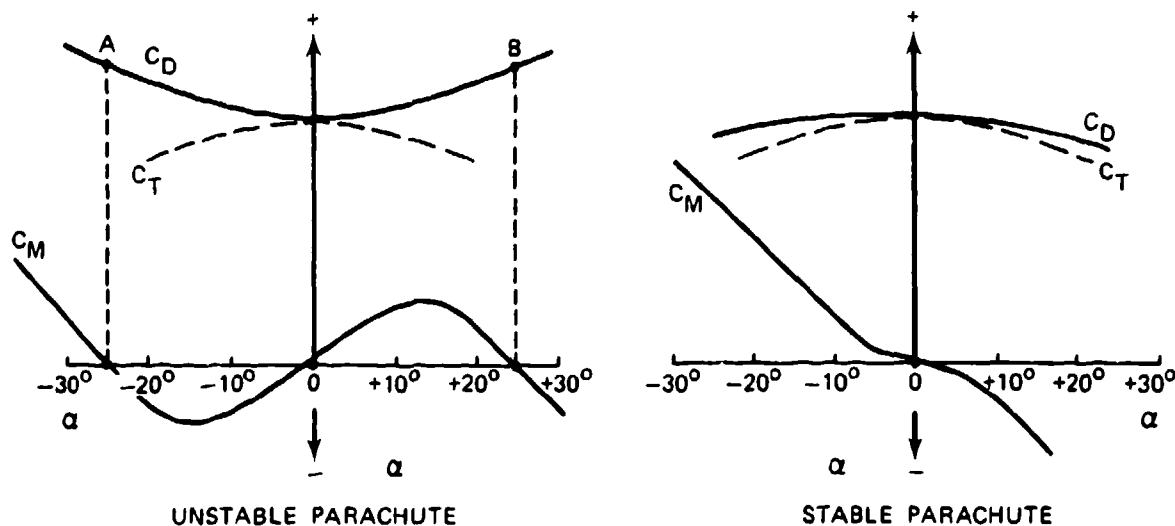


FIGURE 4-8. Forces Acting on a Parachute.

For a parachute with an angle of attack, α , equal to zero, the drag force and the tangential force are synonymous.

Figure 4-9 shows the coefficients C_D , C_T , and C_m versus angle of attack for stable and unstable parachutes.

The coefficient presentation shows two interesting facts. The slope of the moment coefficient curve, $dC_m/d\alpha$, for the unstable parachute is positive between -25 degrees and $+25$ degrees; this is, by definition, destabilizing. This parachute will oscillate approximately ± 25

FIGURE 4-9. Coefficients C_D , C_T , and C_m Versus Angle of Attack, α , for a Stable and Unstable Parachute.

degrees. The slope of the moment coefficient, $dC_m/d\alpha$, for the stable parachute is negative over the total angle of attack; this is, by definition, stabilizing. The steeper the negative $dC_m/d\alpha$ slope, the greater is the stabilizing tendency of the parachute, and the better is its damping capability against destabilizing forces such as sudden gusts of wind.

Figure 4-10, from Reference 4.1, demonstrates the effect of airflow around a cylinder and an airfoil. The circulation around a rotating cylinder creates lift caused by the increase in velocity on one side of the cylinder and a decrease on the opposite side. This is called the Magnus effect.

4.5 EQUILIBRIUM OF FORCES IN STEADY DESCENT OR FLIGHT

4.5.1 Parachute in Steady Descent

A stable parachute in unaccelerated descent has an equilibrium between the total drag of the parachute and the load, D_T , and the weight of the load and the parachute assembly, W_T (Figure 4-11). For steady descent

$$D_T = W_T \text{ or } D_p + D_L = W_p + W_L$$

where

D_T = total drag, lb

D_p = drag of parachute, lb

D_L = drag of load, lb

W_T = total weight, lb

W_p = weight of parachute, lb

W_L = weight of load, lb

In most cases, the drag of the load can be neglected in relation to the large drag of the parachute. With drag, $D = (C_D S)_p \cdot \rho/2 \cdot v^2$ and $D_T = W_T$, and solving for v , the important equation for rate of descent, v_e , is obtained.

Rate of descent,

$$v_e = \sqrt{\frac{2W}{S \cdot C_D \cdot \rho}}$$

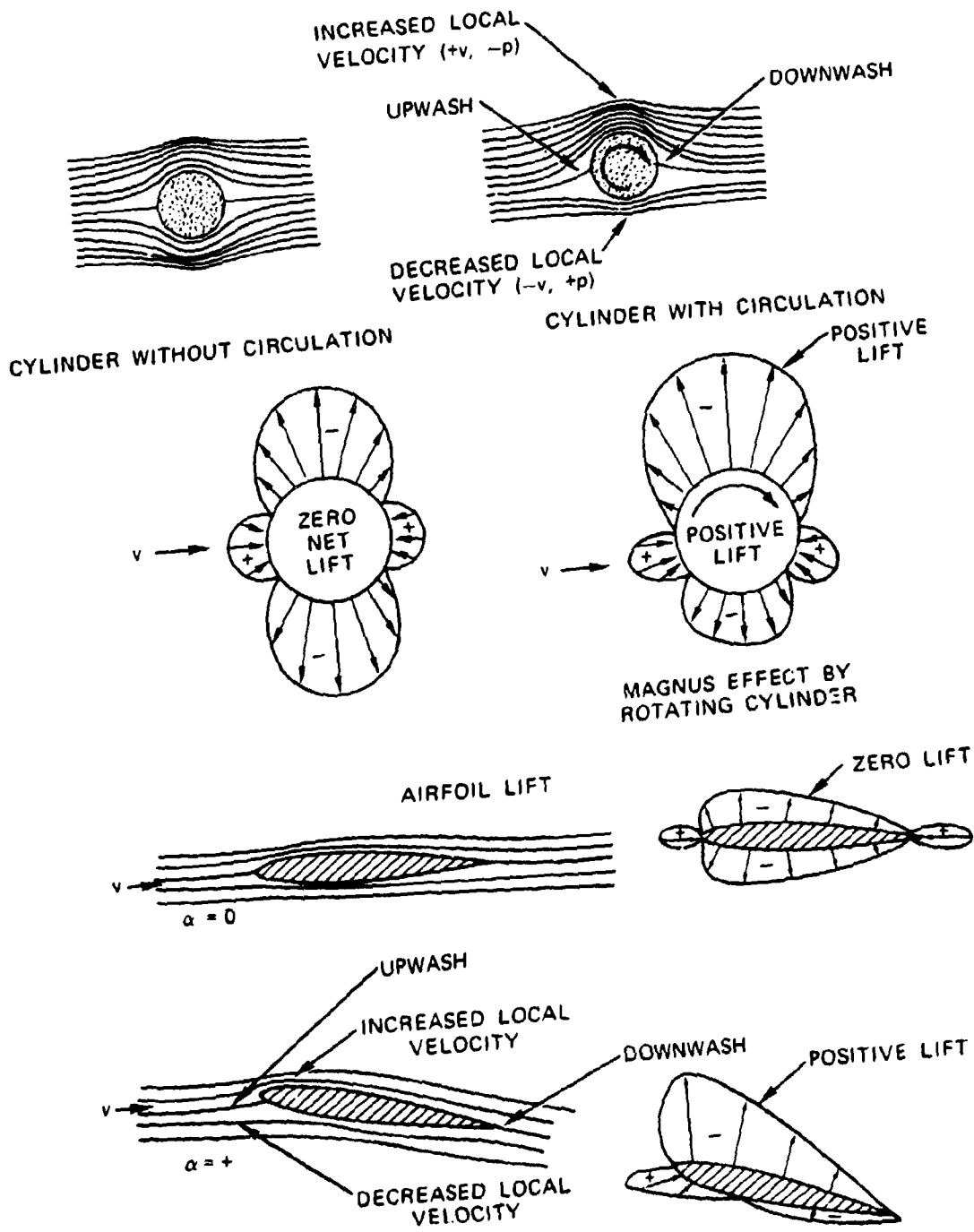


FIGURE 4-10. Effect of Airflow Around a Cylinder and an Airfoil.

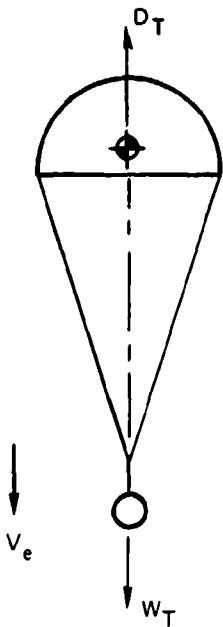


FIGURE 4-11. Forces Acting on a Parachute in Steady Descent.

or in parachute terminology for rate of descent at sea level

$$v_{e_0} = \sqrt{\frac{2W_T}{S_o \cdot C_{D_0} \cdot \rho_o}}$$

and rate of descent at any altitude

$$v_e = \sqrt{\frac{2W_T}{S_o \cdot C_{D_0} \cdot \rho_o}} \cdot \frac{1}{\sqrt{\rho/\rho_o}}$$

For $1/\sqrt{\rho/\rho_o}$, see column 4 in Table 3-3.

In the equation for rate of descent, v_e ,

W_T = weight of load and parachute assembly, lb

S_o = canopy surface area, ft²

C_{D_0} = parachute drag coefficient related to S_0

ρ = air density at a specific altitude in slugs/ft³, as shown in Table 3-3

During descent from altitude, the parachute system is constantly decelerated because of the increasing air density. This can be ignored for slowly descending main parachutes. However, for drogue chute systems that descend at 200 ft/s or faster, the constant deceleration may result in velocities 3 to 5% higher than the steady rate of descent.

4.5.2 Gliding Parachutes

Figure 4-12 shows the balance of forces on a gliding parachute. The total weight of the system, W_T , must be balanced by the resultant force, R . However, a lifting force is required for glide. To satisfy the force balance

$$R = W_T$$

$$R = \sqrt{L^2 + D^2}$$

$$R = C_R \cdot S \cdot \rho/2 \cdot v_T^2$$

$$C_R = \sqrt{C_L^2 + C_D^2}$$

Trajectory velocity, v_T , is calculated

$$v_T = \sqrt{\frac{2W}{S \cdot \rho} \cdot \frac{1}{\sqrt{C_L^2 + C_D^2}}}$$

or

$$v_T = \sqrt{\frac{2W}{S \cdot \rho} \cdot \frac{1}{C_R}}$$

Horizontal velocity is calculated

$$v_H = v_T \cdot \cos\phi, \text{ and vertical velocity, } v_V = v_T \cdot \sin\phi$$

The glide ratio is obtained from

$$\frac{L}{D} = \frac{v_H}{v_V} = \frac{C_L}{C_D}$$

Analysis of Figure 4-12 indicates that the larger the ratio of lift to drag, the better the glide ratio, L/D . A high resultant coefficient, C_R , results in a low glide or trajectory velocity, v_T , desirable for landing. A small C_R results in a high glide velocity, v_T , which is desirable for flying toward a target, compensating for head winds, or covering a distance quickly. Generally, gliding parachutes follow the same aerodynamic rules as low-aspect-ratio wings.

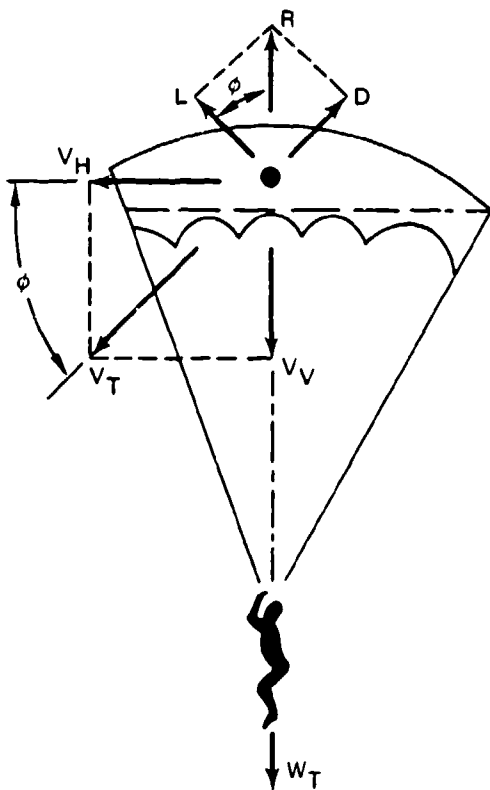


FIGURE 4-12. Forces Acting on a Gliding Parachute.

4.5.3 Parasite Drag and Induced Drag

The drag acting on a lift-producing air vehicle, such as a gliding parachute or an aircraft, has two primary components: the parasite drag, D_p , and the induced drag, D_i .

Parasite drag is produced by the form drag from individual components such as the suspension lines, canopy, and the jumper of a gliding parachute, and the fuselage, tail section, and control surfaces of an airplane. Large surfaces produce surface friction drag as part of the parasite drag.

Induced drag is caused by the lifting action of the parachute canopy or the aircraft wing. Section 4.7 includes books with detailed discussions of induced drag.

Total drag, D_T , can be defined as

$$D_T = D_p + D_i$$

or, in the coefficient form

$$C_{DT} = C_{Dp} + C_{Di}$$

The parasite drag, D_p , and the coefficient, C_{Dp} , can be determined in wind-tunnel tests or calculated as the sum of the individual component drags.

The induced drag coefficient, C_{Di} , of a gliding parachute canopy or a wing profile can be calculated

$$C_{Di} = \frac{C_L^2 \cdot S}{\pi \cdot b^2}$$

where

C_{Di} = coefficient of induced drag, dimensionless

C_L = lift coefficient, dimensionless

S = surface reference area, ft^2

π = 3.1415

b = span of the wing or parachute, ft

The expression b^2/S is defined as the aspect ratio of a wing or parachute with the notation $AR = b^2/S$. Therefore

$$C_{Di} = \frac{C_L^2}{\pi \cdot AR}$$

The equation for induced drag indicates that increasing the aspect ratio, AR , reduces the induced drag coefficient, C_{Di} , and therefore reduces the drag, D . This, in turn, increases the glide ratio, L/D . Increasing the glide ratio by increasing the aspect ratio is optimized on high-performance sailplanes with aspect ratios higher than 20. Increasing the glide ratio of gliding parachutes by increasing the aspect ratio has limitations, which are discussed in section 5.9.

4.5.4 Aircraft in Horizontal Flight

Figure 4-13 shows forces and moments on an aircraft in steady, horizontal flight. In steady, horizontal flight, an equilibrium exists between all forces and moments acting on the aircraft. Lift on the wing and tail, L_W and L_T , and the weight of the aircraft, W_A , balance in the vertical plane. Thrust, T , and drag, D , balance each other in the horizontal plane, and the positive or negative moment, M , is balanced by the positive or negative lift of the tail multiplied by the moment arm, L_T .

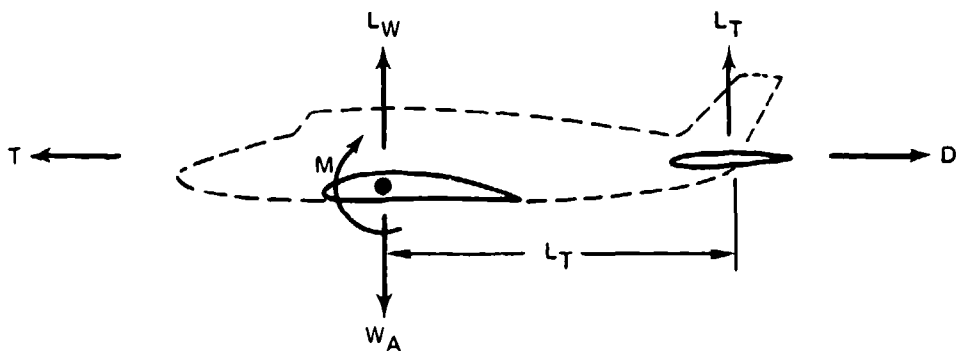


FIGURE 4-13. Forces and Moments Acting on an Aircraft in Steady Flight.

Any imbalance in these forces results in descent or climb in the vertical plane or faster or slower speed in the horizontal plane. A change in the lift of the elevator initiates climb or descent. Thrust, T , is the prime contributor for climb or descent and faster or slower speed. However, a balance of forces must always be maintained for horizontal flight or steady rate of climb or descent.

4.6 WIND-TUNNEL TESTING OF PARACHUTES

Wind tunnels are an effective tool for testing air vehicles and air-vehicle components and have been used successfully for testing parachutes and parachute systems. Experience has shown that certain rules apply for the wind-tunnel testing of parachutes. Small parachutes manufactured from textiles cannot be made sufficiently similar to large parachutes in geometric design and flexibility. Lightweight material, required to obtain design similarity, is difficult to manufacture or is unobtainable.

One cardinal rule has been established through many years of parachute wind-tunnel testing: A modification that changes the performance of a model parachute in wind-tunnel testing produces the same type and percentage of performance change in a large parachute. This rule is true for drag, stability, and opening-force characteristics.

4.6.1 Blowers

The simple air blower (Figure 4-14) is a proven tool for preliminary parachute testing of a chiefly qualitative nature. Unless special test conditions prevail, parachutes tested should be a minimum of 1.5 to 2 feet in diameter to obtain meaningful results.

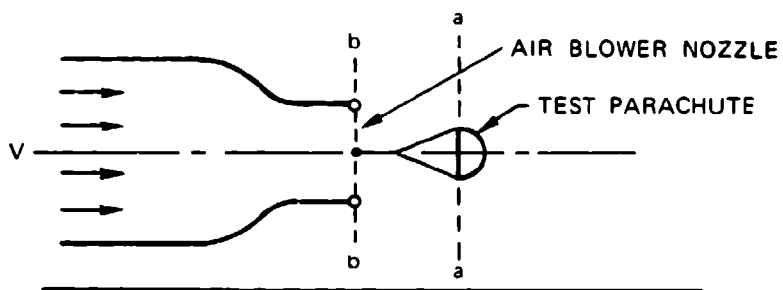


FIGURE 4-14. Typical Air Blower.

An air blower is a good preliminary test tool because it permits quick parachute-configuration changes and excellent visual observation.

4.6.2 Open-Throat, No-Return Wind Tunnels

The open-throat, no-return wind tunnel shown in Figure 4-15 permits exact measurements if parachutes of sufficient size are used. Parachutes 3 feet or more in diameter are well suited for obtaining good, quantitative test results.

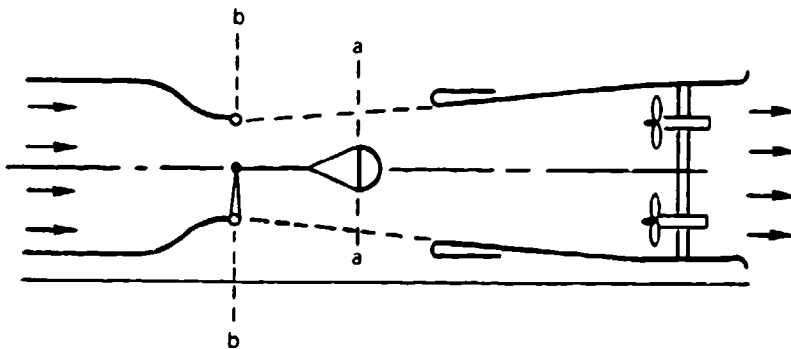


FIGURE 4-15. Open-Throat, No-Return Wind Tunnel.

In air blowers and open-throat wind tunnels, the velocity at the skirt of the parachute (Section a-a of Figures 4-14 and 4-15) is lower than the velocity at the nozzle exit of the wind tunnel (Section b-b of Figures 4-14 and 4-15). Care must be taken to measure the parachute test

velocity at Section a-a and not at Section b-b, the customary attachment point for airfoils and models.

Wind tunnels frequently cannot test at the descent velocity of most main parachutes of 20 to 30 feet per second. Obtaining proper test results at this low velocity is hampered by a poor velocity distribution in the wind-tunnel-test section, and by the weight of the test parachute. The latter has a tendency to pull the parachute downward, thereby providing a negative angle of attack. Testing unstable parachutes at higher velocities presents the problem that the drag coefficient, C_D , of unstable parachutes is velocity sensitive. The drag coefficient of unstable parachutes is described in section 5.2.

An open-throat wind tunnel permits quick changes in parachute configuration, such as changing the suspension and reefing line lengths. Large open-throat wind tunnels that are not sealed against outside elements suffer atmospheric problems such as fog formation in the test section.

4.6.3 Closed-Throat, Full-Return Wind Tunnel

Figure 4-16 is a drawing of a full-return, closed-throat wind tunnel. The full-return, closed-throat wind tunnel is generally considered best suited for obtaining good, qualitative, aerodynamic data, since it has a uniform velocity distribution in the test section. A disadvantage is the difficulty in gaining access to the test section for changing the parachute configuration.

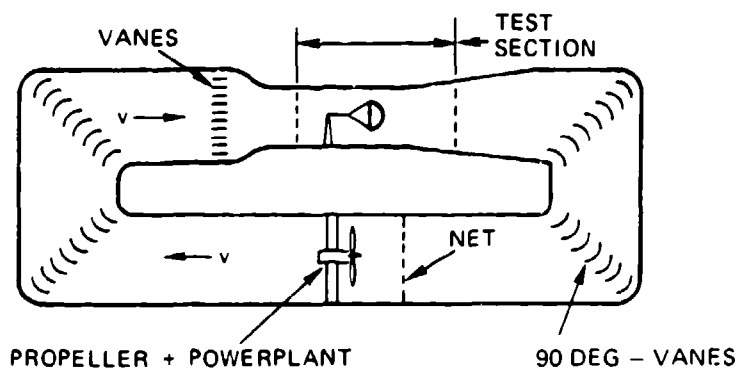


FIGURE 4-16. Closed-Throat, Full-Return Wind Tunnel.

4.6.4 General Comments for Wind-Tunnel Testing of Parachutes

1. Parachute models for wind-tunnel testing should be as large and as similar as possible in geometry and flexibility to full-scale parachutes. Parachutes of less than 1.5 feet in diameter

usually lack geometric similarity and material flexibility, which results in poor inflation characteristics and dissimilar inflated shapes.

2. The finished dimensions of model parachutes must be measured as accurately as possible to determine the nominal diameter, D_0 , and the surface area, S_0 . Model parachutes will shrink from 5 to 10% during manufacture because of sewing take-up, which results in a notable difference in the dimensions between the drawing and the completed parachute.

3. Wind-tunnel tests of parachutes are excellent for comparing different models and modifications; also, they are the most effective means for measuring coefficients of lift, drag, and normal and tangential forces, as well as for determining the load coefficient, C_x , for infinite load.

4. In wind-tunnel tests, velocity decay does not occur during parachute inflation and operation; this is defined as testing under "infinite mass condition." First-stage drogue chutes and parachutes with a canopy loading, $W/C_D S$, in excess of $100 \text{ lb}/\text{ft}^2$ approach this condition. Low-canopy-loading main parachutes with rates of descent of 20 to 30 ft/s have a large velocity decay during opening, which requires careful interpretation of the opening-force data obtained in wind-tunnel tests.

5. In the past, to avoid wind-tunnel blockage and questionable test data, the diameter of a test parachute could not exceed about 5 to 6% of the wind-tunnel test section area. Recent Sandia investigations of single and clustered ribbon parachutes with wind-tunnel blockage ratios of up to 30% have resulted in blockage correction methods that make it possible to test much larger parachutes (Reference 4.2).

4.7 REFERENCE MATERIAL

4.1 H. H. Hurt. *Aerodynamics for Naval Aviators*. Navy Manual NAVWEPS 00 80T 80, Chief of Naval Operations, Aviation Training Division.

4.2 J. M. Macha and R. J. Buffington. "Wall-Interference Corrections for Parachutes in a Closed Wind Tunnel." AIAA Paper, April 1989. (AIAA 89-0900-CP.)

For readers interested in a more detailed study of aerodynamics, the following books are recommended.

4.3 J. H. Dwindell. *Principle of Aerodynamics*. McGraw-Hill Book Co., New York, 1949.

4.4 J. Morane. *Introduction to Theoretical and Computational Aerodynamics*. John Wiley & Sons.

4.5 R.S. Shevell. *Fundamentals of Flight*. Prentice-Hall, 1983.

- 4.6 J. D. Anderson, Jr. *Introduction to Flight, Its Engineering and History*. McGraw-Hill Book Co., New York, 1978.
- 4.7 D. J. Cockrell. "The Aerodynamics of Parachutes." AGARDograph No. 6295, available from NASA Langley Research Center, M/S 180, Hampton, Va., 23665.

CHAPTER 5

PARACHUTE CHARACTERISTICS AND PERFORMANCE

Parachutes are the building blocks of any parachute recovery system. Their performance characteristics must be known and considered in selecting and designing a system. In the early 1920s, the circular, flat parachute manufactured from solid cloth was the primary parachute used for the rescue of aviators, for sport jumping, and for airdrop of light loads. In the 1930s, the military began using parachutes for the airdrop of troops and cargo and for the landing deceleration of aircraft. Beginning in the 1940s, parachutes were used for recovery of unmanned aircraft, missiles, ordnance devices, and, later, recovery of manned and unmanned spacecraft.

These new parachute applications resulted in, or were the result of, the development of numerous new types of parachutes. The new parachutes were superior to the circular, flat, solid textile parachutes in stability, opening forces, and drag. Some of the new types could be used for supersonic applications and others for descent in a gliding mode. However, the superior performance characteristics were not combined in one parachute. Prudent analysis, therefore, is a requisite for matching the appropriate parachute to the desired application.

5.1 PARACHUTE DECELERATOR TYPES

Common parachute types, varying in stability, drag, opening behavior, velocity capability, and other design and performance characteristics, are listed in Tables 5-1 through 5-5, which are updated from the tables in Reference 2.1. The performance data are to be used for preliminary considerations only. Detailed performance data are found in sections 5.2 through 5.10 and in the references (section 5.12). The following comments refer to the column headings in Tables 5-1 through 5-5.

Constructed Shape. The Plan and Profile columns define the constructed diameter and the cross section of the parachute canopy.

D_c , the constructed diameter of the canopy, can be obtained from the drawing of the specific parachute.

Nominal Diameter. D_o , the nominal diameter of the parachute, can be calculated from the total canopy surface area, S_o , including the area of the vent and all other openings:

$$D_o = \sqrt{4S_o/\pi} = 1.1284 \sqrt{S_o}$$

Inflated Shape. D_p , the projected diameter of the inflated parachute canopy, is best calculated from the projected or inflated canopy area, S_p , as measured in wind-tunnel tests. The projected diameter of a parachute varies with parachute type, canopy porosity, suspension-line length, velocity, and canopy design. A large projected diameter, D_p , will generally result in a large drag coefficient, C_{D_o} . The ratio of projected diameter to nominal diameter, D_p/D_o , is an indication of the drag effectiveness of the parachute design; the larger the projected diameter in relation to the nominal diameter, the larger the drag coefficient.

Drag Coefficient. C_{D_o} is the drag coefficient related to the total canopy surface area, S_o . The drag coefficient indicates how effectively a parachute canopy produces drag with a minimum of cloth area, thereby minimizing weight and volume.

Opening-Force Coefficient. C_x , the opening-force coefficient, indicates the difference between the instantaneous opening force and the steady drag force at constant speed. This condition, called the infinite mass case, is obtained in wind-tunnel tests and in parachute applications with high canopy loadings, $W/(C_d S)_p$, as exemplified by aircraft deceleration parachutes and first-stage drogue chutes.

Average Angle of Oscillation. The angle of oscillation is measured in wind-tunnel tests or during free-flight tests. Oscillation on most solid textile parachutes varies with size and descent velocity. Large parachutes oscillate less than small parachutes. Unstable parachutes tend to descend in an oscillating mode at rates of descent in excess of 25 ft/s, glide at descent rates below 15 ft/s, and mix glide and oscillation during medium rates of descent.

General Application. The general application column in Tables 5-1 through 5-5 indicates the primary use of the particular parachute type.

S_w in Table 5-4 is the wetted upper canopy surface area on gliding parachutes.

S_w/S_o in Table 5-4 is the ratio of the upper surface area to total cloth area, including all ribs and stabilizer panels.

Referenced reports for most of the listed parachutes will be found in subsequent sections of Chapter 5, but primarily in section 5.2, Parachute Drag and Wake Effects.

Figures 5-1 through 5-15 show some of the more common parachute-type decelerators listed in Tables 5-1 through 5-5.

TABLE 5-1. Solid Textile Pachutes.

TYPE	CONSTRUCTED SHAPE		INFLATED SHAPE $\frac{D_p}{D_o}$	DRAG COEF $C_D o$ RANGE	OPENING FORCE COEF C_X (INF MASS)	AVERAGE ANGLE OF OSCILLATION, DEGREES	GENERAL APPLICATION	
	PLAN	PROFILE						
FLAT CIRCULAR		— —	1.00	0.67 TO 0.70	0.75 TO 0.80	~1.7	±10 TO ±40	DESCENT, OBSOLETE
CONICAL			0.93 TO 0.95	0.70	0.75 TO 0.90	~1.8	±10 TO ±30	DESCENT, M < 0.5
BICONICAL			0.90 TO 0.95	0.70	0.75 TO 0.92	~1.8	±10 TO ±30	DESCENT, M < 0.5
TRICONICAL POLYCONICAL			0.90 TO 0.95	0.70	0.80 TO 0.96	~1.8	±10 TO ±20	DESCENT, M < 0.5
EXTENDED SKIRT 10% FLAT			0.86	0.66 TO 0.70	0.78 TO 0.87	~1.4	±10 TO ±15	DESCENT, M < 0.5
EXTENDED SKIRT 14.3% FULL			0.81 TO 0.85	0.66 TO 0.70	0.75 TO 0.90	~1.4	±10 TO ±15	DESCENT, M < 0.5
HEMISPERICAL			0.71	0.66	0.62 TO 0.77	~1.6	±10 TO ±15	DESCENT, M < 0.5, OBSOLETE
GUIDE SURFACE (RIBBED)			0.63	0.62	0.28 TO 0.42	~1.2	0 TO ±2	STABILIZATION, DROGUE, 0.1 < M < 1.5
GUIDE SURFACE (RIBLESS)			0.66	0.63	0.30 TO 0.34	~1.4	0 TO ±3	PILOT, DROGUE, 0.1 < M < 1.5
ANNULAR			1.04	0.94	0.85 TO 0.95	~1.4	< 6	DESCENT, M < 0.5
CROSS		— —	1.15 TO 1.19	0.65 TO 0.72	0.60 TO 0.85	1.1 TO 1.2	0 TO ±3	DESCENT, DECELERATION

NWC TP 6575

TABLE S-2. Slotted Parachutes.

TYPE	CONSTRUCTED SHAPE		INFLATED SHAPE $\frac{D_p}{D_o}$	DRAG COEF C_D RANGE	OPENING FORCE COEF C_X (INF MASS)	AVERAGE ANGLE OF OSCILLATION, DEGREES	GENERAL APPLICATION	
	PLAN	PROFILE						
FLAT (FIST) RIBBON		-----	1.00	0.67 TO 0.50	0.45 TO 0.50	-1.05	0 TO ±3	DROGUE, DESCENT, DECLERATION, OBSTACLES
CONICAL RIBBON		0.95 TO 0.97	0.70	0.50 TO 0.55	~1.05	0 TO ±3	DESCENT, DECCELERATION, $0.1 < M < 2.0$	
CONICAL RIBBON (VARIED POROSITY)		'	0.70	0.55 TO 0.60	1.05 TO 1.30	0 TO ±3	DROGUE, DESCENT, DECCELERATION, $0.1 < M < 2.0$	
RIBBON ¹ (HEMISFLD)		0.62	0.62	0.30 ¹ TO 0.46	1.00 TO 1.30	±2	SUPersonic, DROGUE, $1.0 < M < 3.0$	
RINGSLOT		1.00	0.67 TO 0.70	0.56 TO 0.65	~1.05	0 TO ±5	EXTRACTION, DECCELERATION, $0.1 < M < 0.9$	
RINGSAIL		0.84	0.69	0.75 TO 0.86	~1.10	±5 TO ±10	DESCENT, $M < 0.5$	
DISC - GAP - BAND		0.73	0.65	0.52 TO 0.58	-1.30	±10 TO ±15	DESCENT, $M < 0.5$	

¹FOR SUPERSONIC APPLICATION. SEE SECTION 5-8

TABLE S-3. Rotating Parachutes.

TYPE	CONSTRUCTED SHAPE		INFLATED SHAPE $\frac{D_i}{D_o}$	DRAG COEF C_D RANGE	OPENING FORCE COEF C_X (INF MASS)	AVERAGE ANGLE OF OSCILLATION, DEGREES	GENERAL APPLICATION	
	PLAN	PROFILE						
ROTAFOIL		—	1.0	~0.90	0.85 TO 0.99	1.05	0 TO ±2	DROGUE $D_o < 7$
VORTEX RING		— —	1.9	N/A	1.5 TO 1.8	1.1 TO 1.2	0 TO ±2	DESCENT SMALL D_o
SANDIA RFD		— —	1.0	~0.9	1.25	1.1	0 TO ±2	DROGUE

TABLE 5-4. Maneuverable (Gliding) Parachutes.

TYPE	CONSTRUCTED SHAPE PLAN	CONSTRUCTED SHAPE PROFILE	AREA RATIO $\frac{S_w}{S_n}$	AERODYNAMIC FORCE COEF C_R RANGE	GLIDE RATIO $(L/D)_{MAX}$	GENERAL APPLICATION
TOJO, TU SLOTS, ETC		— — —	1.0	0.85 TO 0.90	0.5 TO 0.7	DESCENT
LEMOIGNE (PARACOMMANDER)		— — —	1.0	0.90 TO 1.00	1.1	DESCENT
PARAWING (SINGLE KEEL)		— — —	1.0	0.90 TO 1.10	2.0 TO 2.5	DESCENT
PARAWING (TWIN KEEL)		— — —	1.0	1.00 TO 1.10	2.8 ^{1/2} TO 3.0	DESCENT
PARAFOIL		— — —	0.27	0.75 TO 0.85	2.8 ^{1/2} TO 3.5	DESCENT
SAILWING		— — —	0.80 TO 0.90	N A	2.8 ^{1/2} TO 3.5	DESCENT
VOLPLANE		— — —	0.60	N A	2.0 ^{1/2} TO 3.0	DESCENT

¹GLIDE RATIO IS AFFECTED BY ASPECT RATIO, AR, AND CANOPY LOADING, H/S.

Note: Maneuverable parachutes with a glide ratio L/D of 2.5 or better have been defined in the literature as "hi-glide parachutes." This includes the parawing, the parafoil, the sailwing, and the volplane.

TABLE 5-5. Balloon-Type Decelerators.

TYPE	CONSTRUCTED SHAPE PLAN	CONSTRUCTED SHAPE PROFILE	INFLATED SHAPE $\frac{D_p}{D_o}$	INFLATED SHAPE $\frac{D_p}{D_o}$	DRAG COEF C_D RANGE	OPENING FORCE COEF C_1 (INF. MASS.)	AVERAGE ANGLE OF OSCILLATION DEGREES	GENERAL APPLICATION
BALLUTE			0.51	0.51	0.51 ¹ TO 1.20	~1.05	-1	STABILIZATION, DROGUE, 0.8 - M - 4

¹FOR C_D VERSUS MACH NUMBER SEE SECTION 6.6.

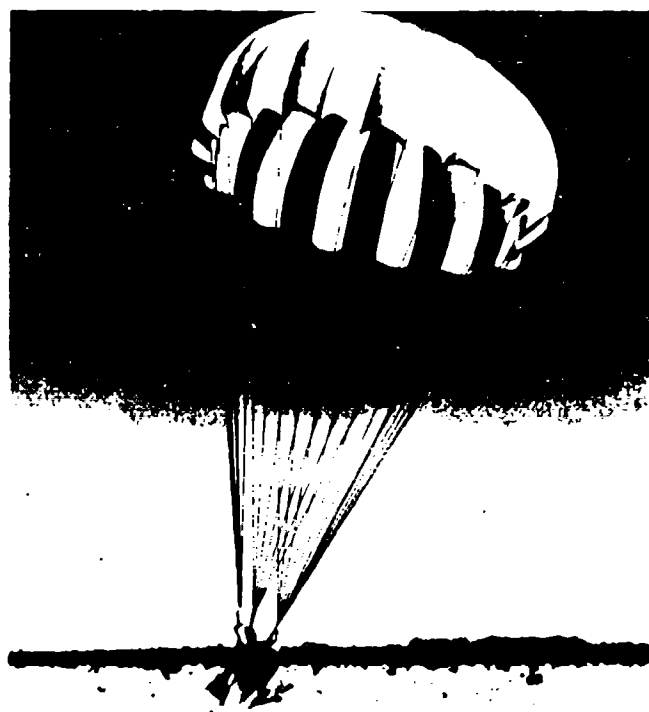


FIGURE 5-1. Twenty-Eight-Foot-Diameter Circular, Flat Personnel Parachute.

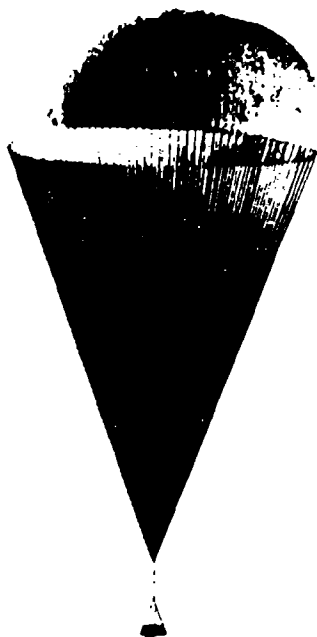


FIGURE 5-2. Two-Hundred-Foot-Diameter Circular, Flat Cargo Parachute.



FIGURE 5-3. Army Paratrooper 35-Foot-Diameter Extended-Skirt Parachute.

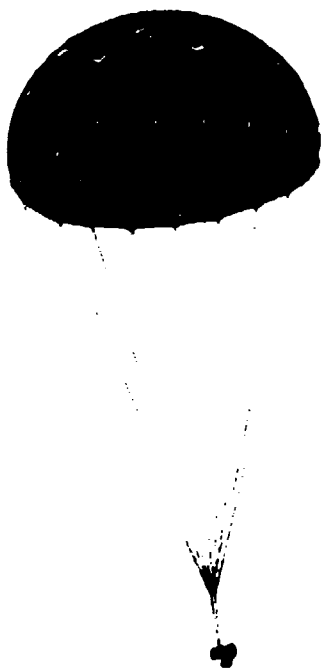


FIGURE 5-4. Twenty-Four-Foot-Diameter Hemispherical Parachute.



FIGURE 5-5. Guide Surface Parachute.

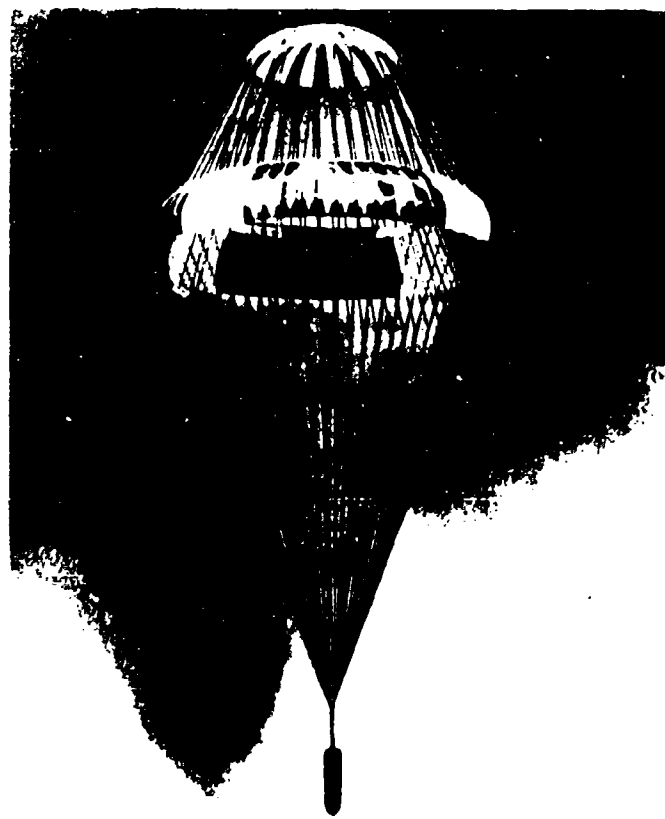


FIGURE 5-6. Seventy-Two-Foot-Diameter Annular
Parachute With 24-Foot Diameter Engagement
Parachute in Midair Retrieval Configuration



FIGURE 5-7. Cross Parachute in Wind-Tunnel Test.

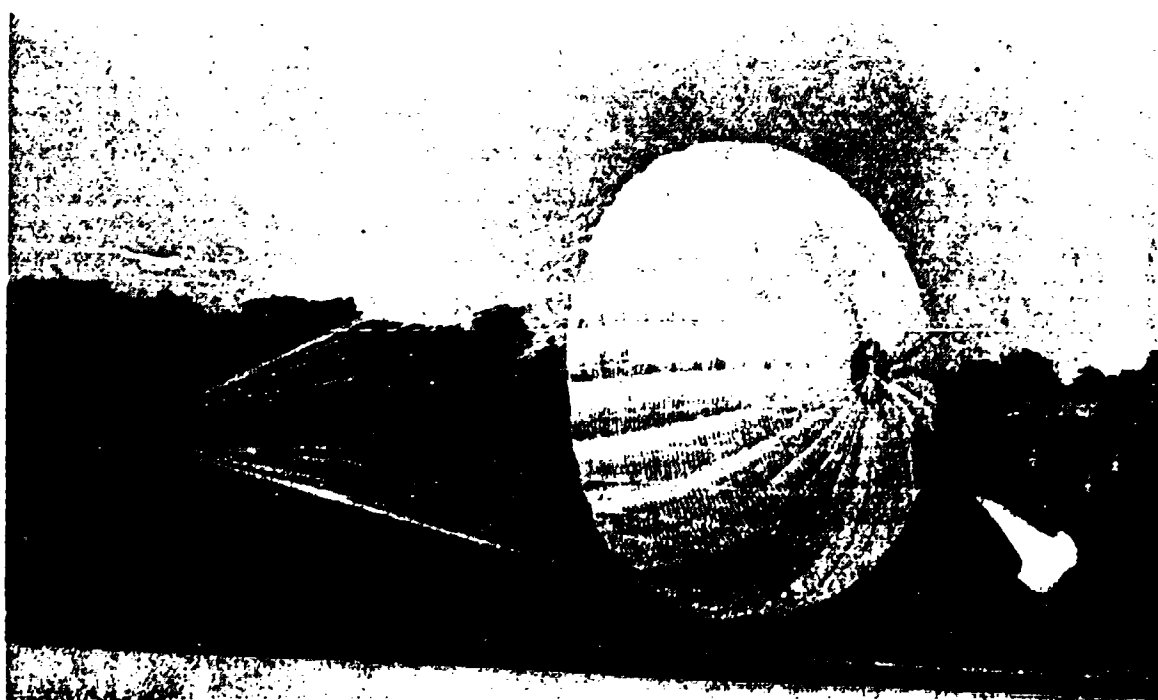


FIGURE 5-8. Thirty-Two-Foot-Diameter Ribbon, Landing Deceleration Parachute.

NWC TP 6525

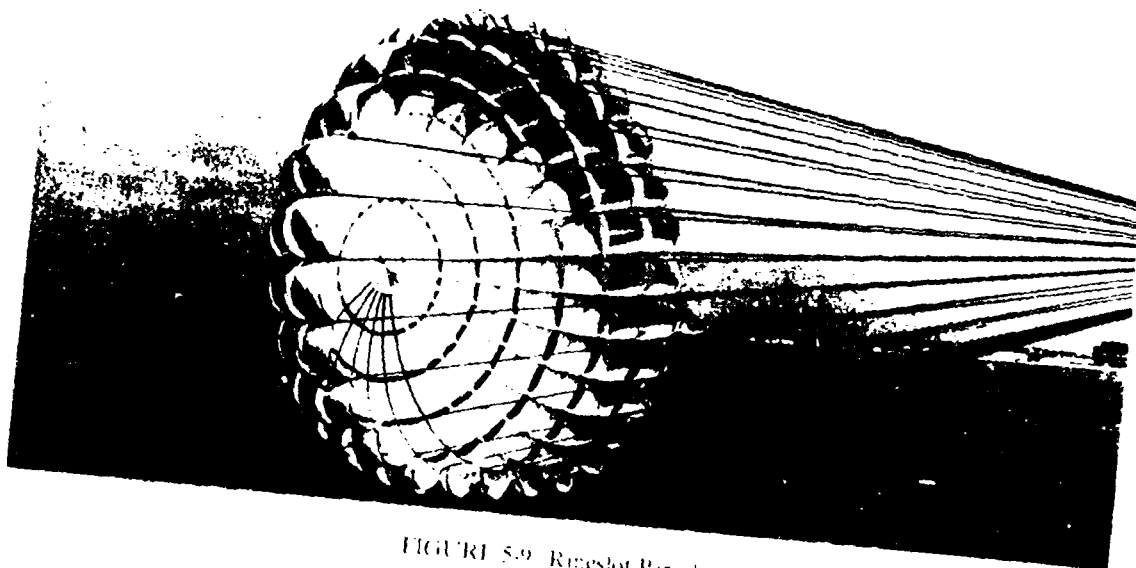


FIGURE 5-9. Ringslot Parachute

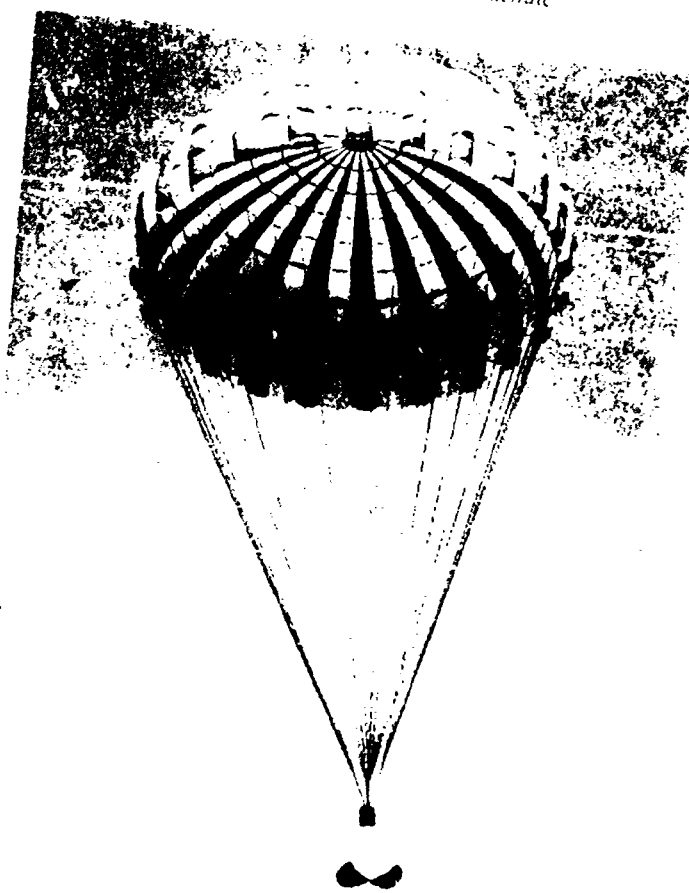


FIGURE 5-10. Six Foot Four Inch Diameter Mercury
Ringslot Main Parachute

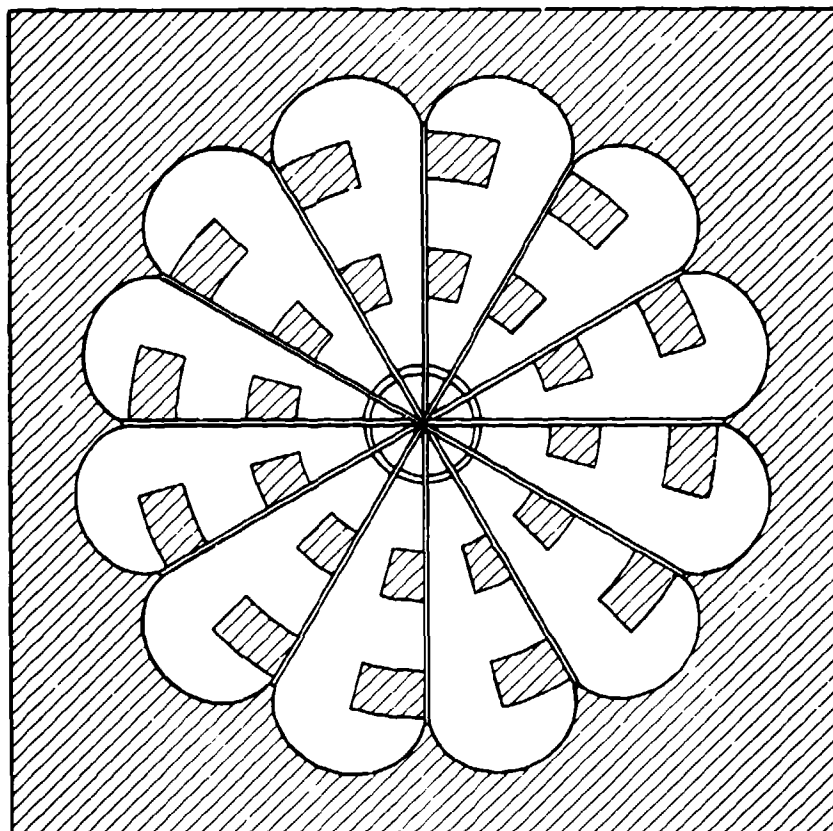


FIGURE 5-11. Rotofoil Parachute.

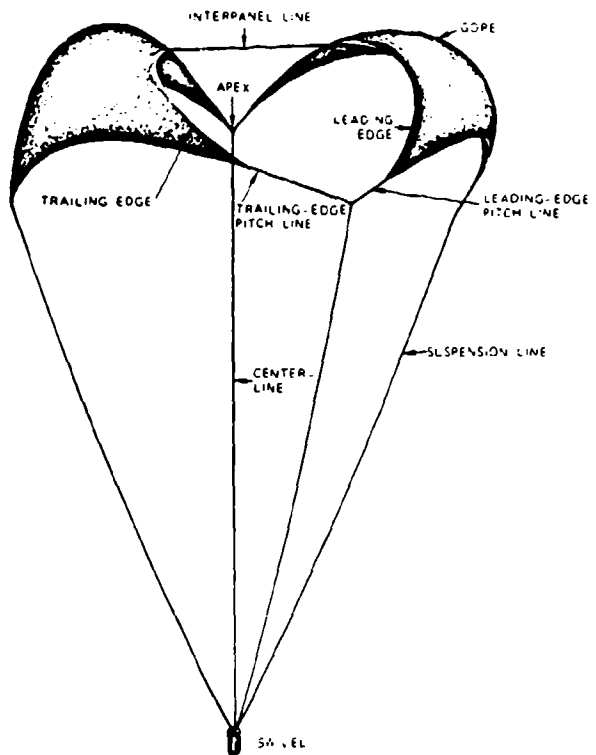


FIGURE 5-12. Vortex Ring Parachute (Only Two of Four Adjacent Gores Are Shown).

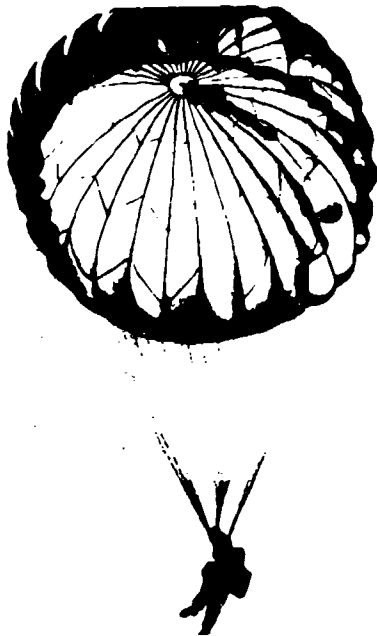


FIGURE 5-13. Thirty-Five-Foot-Diameter T-10 (MC1-1B) Paratrooper Parachute, Modified With Slots and Control Lines for Glide and Controllability.



(a) Parawing.



(b) Volplane.



(c) Parafoil.



(d) Sailwing.

FIGURE 5-14. Hi-Glide (Maneuverable) Parachutes.

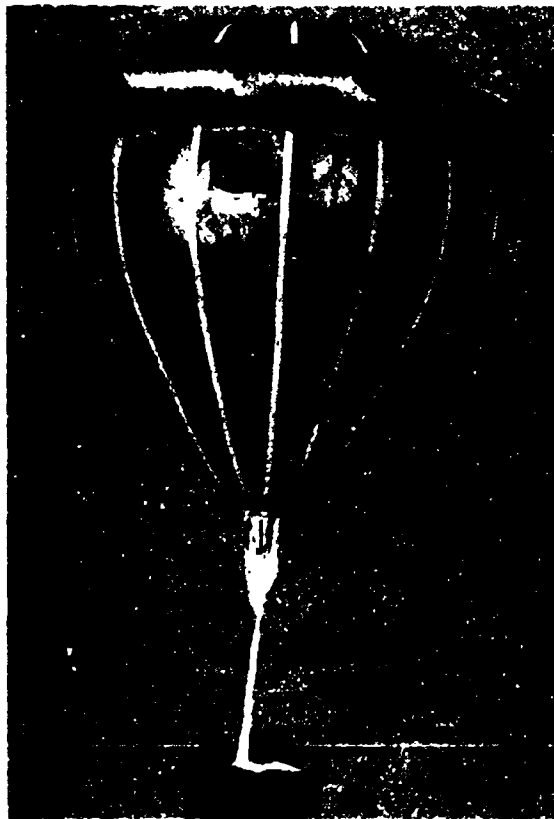


FIGURE 5-15. Ballute (Balloon-Type Decelerator).

5.2 PARACHUTE DRAG AND WAKE EFFECTS

Parachute drag is an important performance parameter, because it determines the rate of descent, generally a primary performance consideration in the design of a parachute system. To maintain a required constant rate of descent, the drag of the parachute must equal the weight of the total system, as discussed in Chapter 4. The parachute drag, D, is

$$D = C_{D_0} S_0 q, \text{ lb}$$

where

C_{D_0} is the parachute drag coefficient related to the canopy surface area, dimensionless

S_0 is the canopy surface area, including the vent area and all openings and slots in the canopy, ft^2

q is the dynamic pressure, equal to $1/2 \rho v^2$, lb/ft^2 .

For a given rate of descent, the dynamic pressure, q , is a fixed value. The product, $C_{D_0}S_o$, * is called the drag area of the parachute and is measured in square feet. A large drag coefficient, C_{D_0} , will result in a small canopy surface area, S_o , and a low parachute weight and volume. Because these characteristics are highly desirable for large-diameter, final descent parachutes, a large drag coefficient is frequently the deciding factor in the selection of a parachute. The following design features and parachute canopy characteristics are known to produce high drag coefficients:

1. Conical, multiconical, or quarter-spherical canopy shapes
2. Rectangular or triangular canopy shapes
3. Long suspension lines
4. Low canopy porosity
5. Annular canopy shapes
6. Rotating parachutes
7. Gliding parachutes

The drag coefficient, C_{D_0} , refers to the vertical component of the parachute velocity, as discussed in Chapter 4.

The glide velocity of a gliding parachute changes little with glide angle. However, the vertical component of the glide velocity (the rate of descent) decreases notably with an increasing glide ratio.

Rectangular and triangular parachutes up to personnel-parachute size have been used successfully at lower speeds. Deployment of large rectangular and triangular parachutes has caused problems. The noncircular canopy design makes it difficult to maintain tension on all canopy elements during deployment and inflation.

Long suspension lines increase the inflated diameter of the canopy and result in a larger drag coefficient, which, for a given rate of descent, produces a smaller diameter and a lighter parachute assembly.

Rotating parachutes have been used successfully with diameters up to 10 feet. Attempts to use larger rotating parachutes have resulted in poor deployment and canopy wrap-up before full inflation. Inaccuracies in the angle of pitch of individual gores cause variations in parachute rotation and drag coefficient.

Decreasing the porosity increases the drag coefficient but also produces a less stable parachute and a higher opening force.

Canopy profiles of quarter-spherical shapes and the similar triconical shapes have shown the highest drag coefficients for circular canopy designs.

* In this manual, $C_{D_0}S_o$, and $(C_D S)_o$, are interchangeable.

5.2.1 Canopy Shape and Suspension Line Length Effects

In 1949, the U.S. Air Force conducted model drop tests of 1600-square-inch parachutes under controlled conditions in the Lakehurst, New Jersey, airship hangar (Reference 5.1). These tests established several facts previously unknown or only suspected.

Solid textile parachutes of a round or cornered design and with a flat or shaped profile descended in a vertical line, but oscillated violently when dropped at rates of descent greater than 30 ft/s. The same parachutes, when dropped with a low weight, had a 10-ft/s rate of descent and descended in a stable, nonoscillating attitude, but glided at angles up to 45 degrees. In the 15- to 25-ft/s descent range, these parachutes combined oscillation with straight descent, or with glide but no oscillation. Gliding resulted in a low vertical velocity component and a high drag coefficient. Vertical descent with oscillation at the higher rates of descent resulted in lower vertical drag coefficients.

For the same surface areas, conical and quarter-spherical canopies had higher drag coefficients than circular flat canopies. Figure 5-16 shows that, at a rate of descent of 20 ft/s, a 30-degree conical parachute has a 9.5% higher drag coefficient than a flat, circular canopy, and

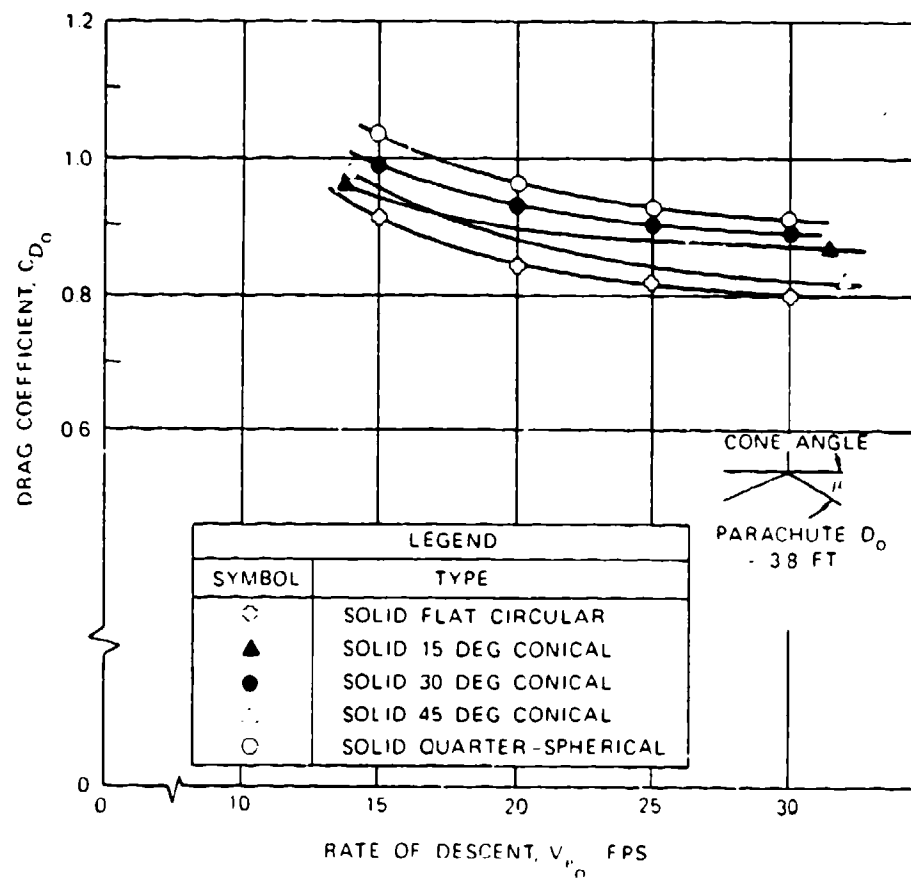


FIGURE 5-16. Variation of Drag Coefficient With Cone Angle and Rate of Descent for Solid Fabric Parachutes.

a quarter-spherical canopy has a 14.5% higher drag coefficient. These tests were the basis for the quarter-spherical profiles of the ringsail and the triconical parachute canopies.

The model test results were confirmed in full-scale drop tests conducted at El Centro, Calif., with modified 28-foot-diameter personnel parachutes. Successive gores were removed from a 28-foot-diameter, flat, circular canopy to convert it into a conical parachute of increasing cone angles. The vertical drag coefficient, C_{D_0} , increased with increasing cone angle and decreasing rates of descent. A cone angle of 25 to 30 degrees was the optimum angle, as shown in Figure 5-17 and Reference 5.2.

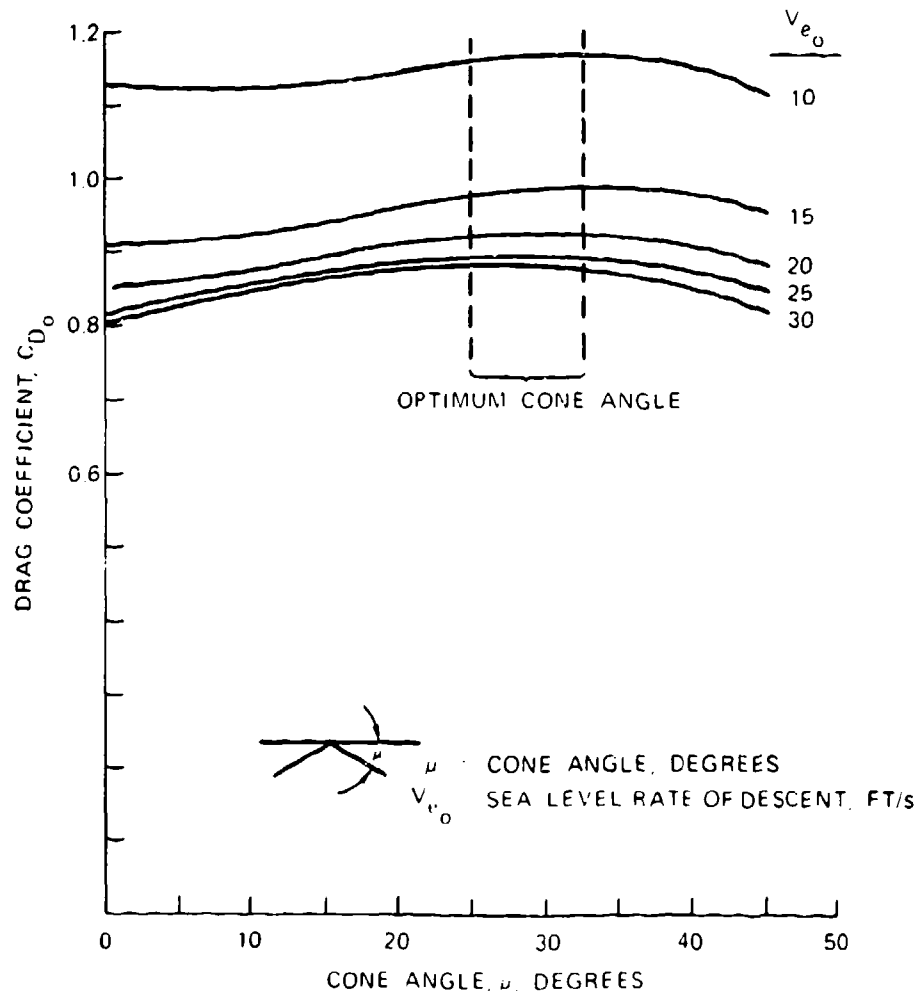


FIGURE 5-17. Variation of Drag Coefficient With Cone Angle and Rate of Descent for 28-Foot-Diameter Solid Textile Parachutes.

Data from Reference 5.1 (Figure 5-18) demonstrate the difference in drag coefficient, C_{D_0} , versus rate of descent for four parachute types. Two types are stable: a flat, circular, ribbon parachute and a guide surface parachute. Two types are unstable: a solid textile, circular, flat parachute and a solid textile, square, flat parachute. Figure 5-18 clearly shows the characteristic that unstable parachutes increase their drag coefficient with decreasing rates of descent because of the change in descent behavior from oscillation to glide.

An increase in drag coefficient for a specific parachute can be accomplished by increasing the length of the suspension lines (see Figure 5-19). The increase in suspension-line length causes the parachute to open wider with a larger inflated area, S_p , and inflated diameter,

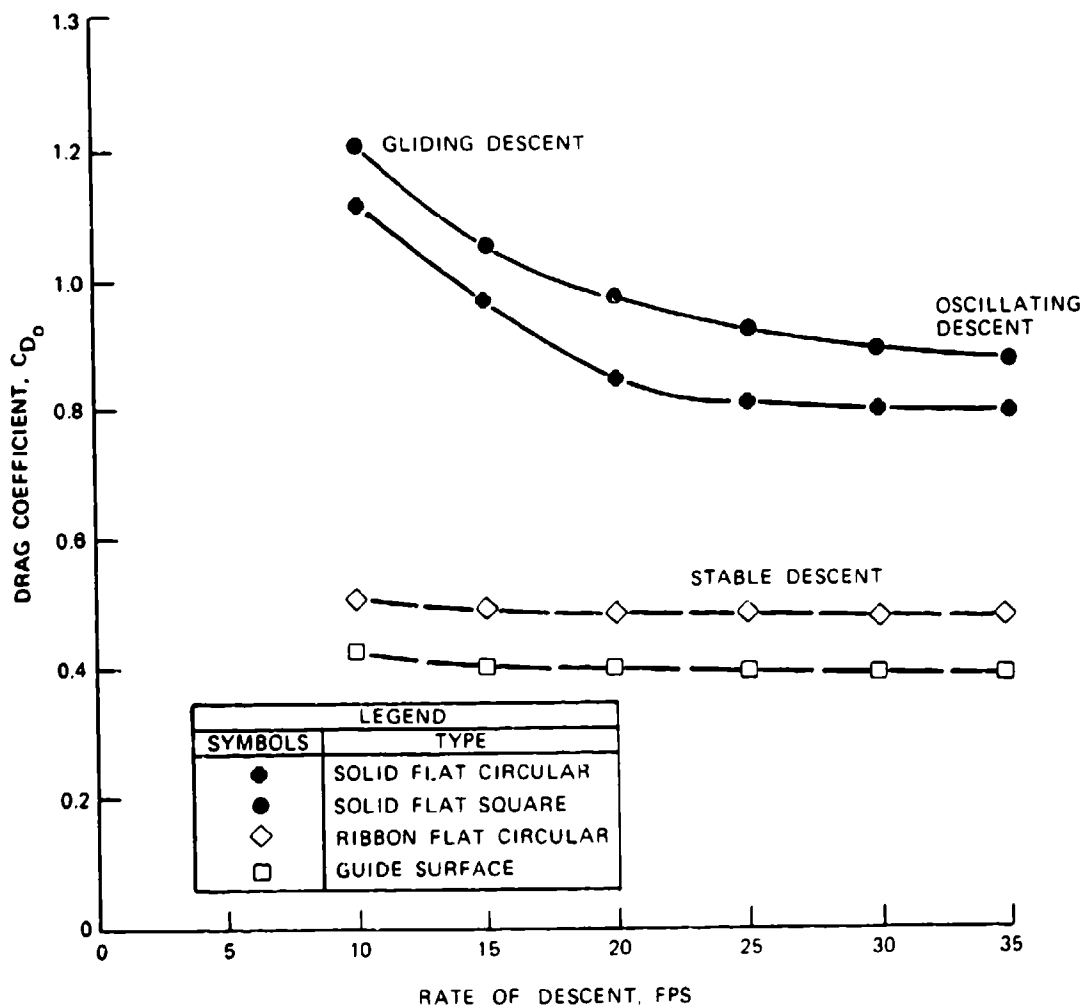


FIGURE 5-18. Drag Coefficient Versus Rate of Descent for Two Stable and Two Unstable Parachutes.

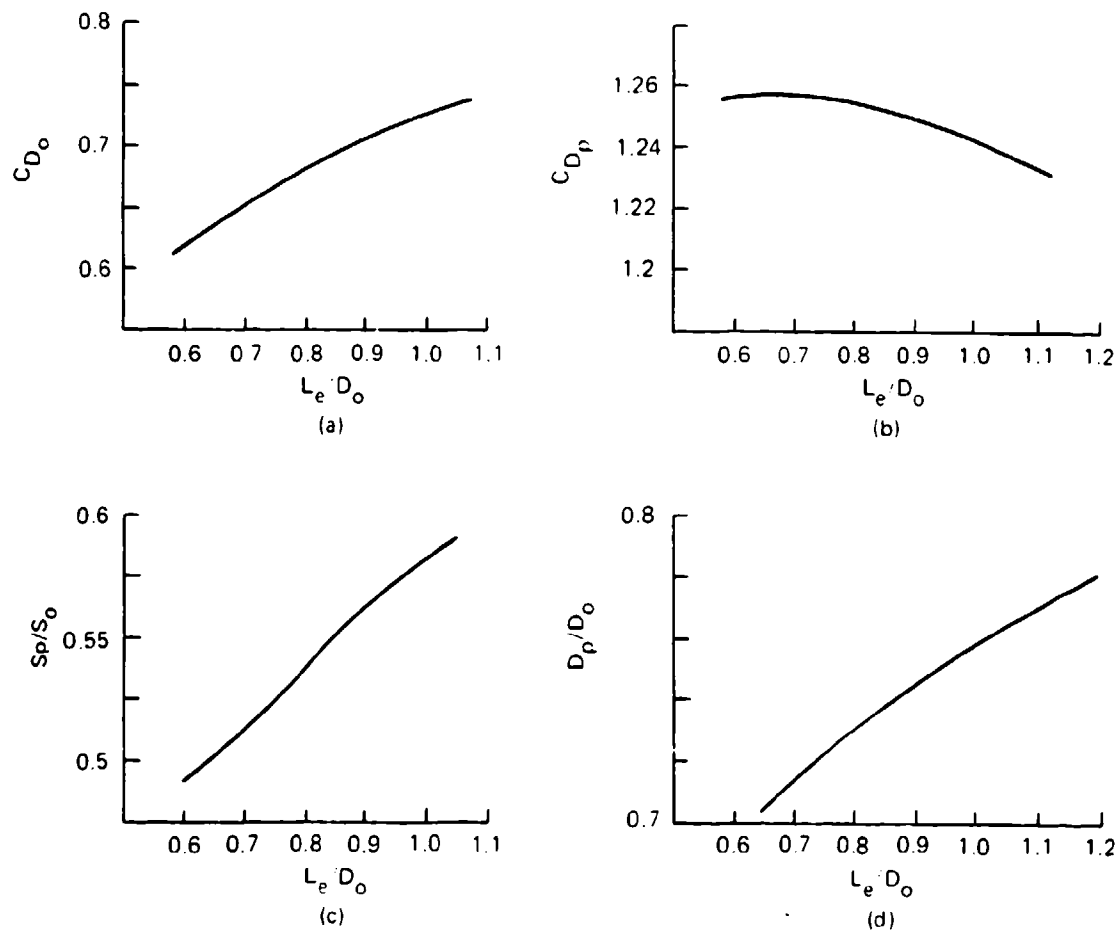


FIGURE 5-19. Drag Coefficients, C_{D_0} and C_{D_p} ; Canopy Area Ratio, S_p/S_0 ; and Diameter Ratio, D_p/D_0 ; as a Function of Suspension-Line Ratio, L_e/D_o , for a 1-Meter-Diameter Model Parachute.

D_p . The drag coefficient, C_{D_p} , related to the inflated (projected) area, S_p , decreases slightly with an increase in line length and a related increase in projected diameter (see Figure 5-19b). However, the drag coefficient clearly increases with an increase in suspension-line ratio, L_e/D_o (Figure 5-19a).

The slopes of the curves for area and projected diameter growth in Figure 5-19 indicate that using suspension-line ratios larger than 1.1 may have provided additional drag.

These data were obtained in model tests with 1-meter (3.3-foot)-diameter parachutes. Reference 5.3 provides background on the tests.

Figure 5-20 shows the possible increase in drag coefficient for line ratios, L_e/D_o , up to 2.0. Parachutes with no skirt restrictions, such as flat and conical circular parachutes, increase the drag coefficient up to line ratios of 2.0. Parachutes with skirt restrictions, such as extended skirts and hemispherical canopies, show little drag coefficient increase at line ratios above 1.1. The data in Figure 5-20, taken from United States, British, and German sources, show relatively good concordance.

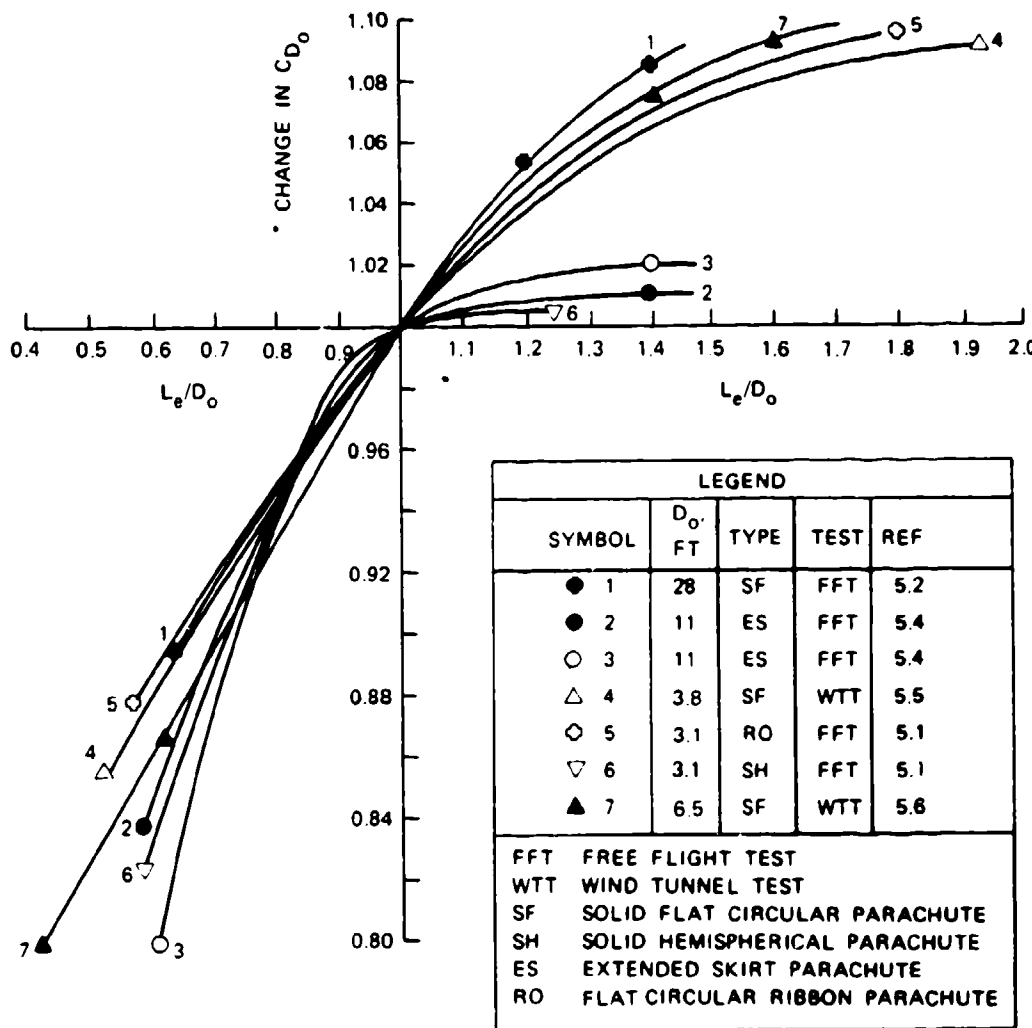


FIGURE 5-20. Variation of Drag Coefficient With Suspension-Line Ratio for Several Parachute Types.

Calculations indicate that line-length ratios above 1.5 may be detrimental because of the associated weight increase of the longer lines. Systems that employ parachutes in clusters or use first-stage drogue chutes require long risers. Parts of these risers may be replaced by longer suspension lines on the individual parachutes to increase parachute drag and decrease the required parachute diameter and parachute assembly weight.

5.2.2 Forebody Wake Effect

Parachutes are always used in connection with a forebody, such as a parachute jumper, an aircraft, a load platform, or an Apollo-type space capsule. Each forebody produces a wake that affects the parachute, depending on the relationship of the inflated parachute diameter, D_p , to forebody diameter, D_B , and the distance between the end of the forebody and the leading edge of the inflated parachute canopy. Figure 5-21 illustrates the drag loss. A cargo container descending on a 100-foot-diameter parachute produces little wake effect, because both the diameter ratio, D_p/D_B , and the distance between the container and the leading edge of the parachute, L_T , are large. The inflated diameter of the Apollo drogue chute was smaller than the diameter of the Apollo spacecraft. The distance between the leading edge of the parachute and the rear of the spacecraft was kept to a minimum to save weight. Many parachute jumpers have experienced the failure of a spring-loaded pilot chute that was ejected, but then collapsed and fell back on the jumper because of the blanketing or wake effect of the jumper's body.

Tests conducted in the NASA and Wright Field vertical wind tunnels determined that for vertical descending bodies, the parachute should be ejected to a distance equivalent to more than four times—and preferably six times—the forebody diameter, into good airflow behind the forebody. Applying the six-forebody-diameter rule has been successful on Apollo and other programs. Ejecting the parachute from a horizontal attitude or sideways out of the forebody wake can provide good inflation with shorter forebody-to-parachute canopy distances. However, successful inflation with shorter distances should be proven in tests of the most unfavorable—not the most favorable—deployment conditions.

Deploying a small parachute in the wake of a large forebody also causes considerable loss in parachute drag and may affect the stability of the parachute. Drag losses of up to 25% have been experienced in wind-tunnel and free-flight tests. Figure 5-21 presents parachute drag losses caused by forebody wake measured in wind-tunnel and free-flight tests. The two dotted lines (I in Figure 5-21) encompass parachute wake loss data measured in wind-tunnel tests by the University of Minnesota and the California Institute of Technology (Cal Tech) (References 5.7 through 5.9). Superimposed on this wind-tunnel data are free-flight test results obtained on the reefed 16.5-foot-diameter Apollo command module drogue chute tested behind three different forebodies. This drogue chute was tested behind (1) an 11.9-foot, boilerplate command module (CM) (II in Figure 5-21), (2) a 5.8-foot-diameter parachute test vehicle (PTV) (III), and (3) a 36-inch-diameter instrumented cylindrical test vehicle (ICTV) (IV)

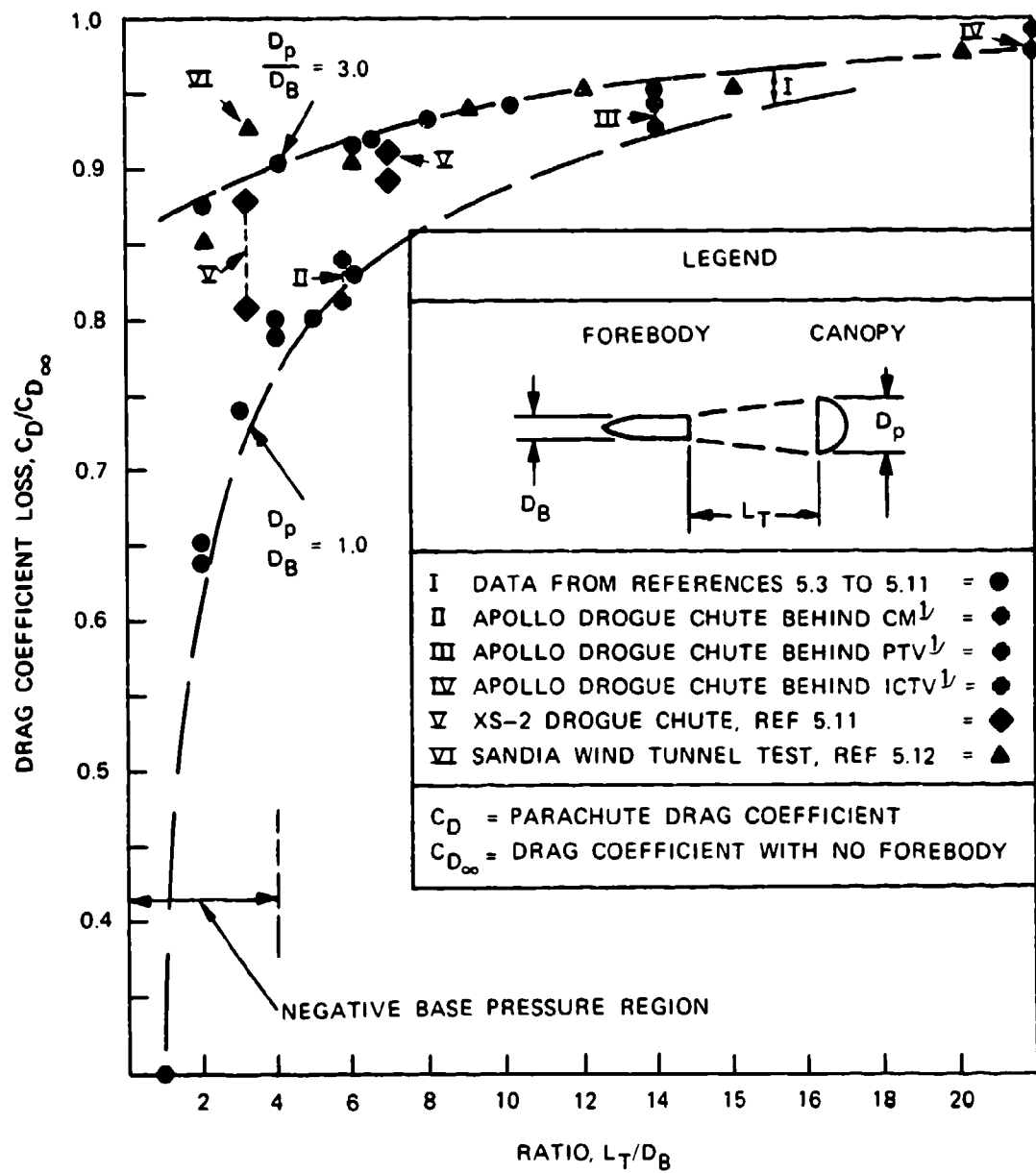


FIGURE 5-21. Parachute Drag Loss Caused by Forebody Wake.

(Reference 5.10). These measured Apollo parachute data agree well with data from the University of Minnesota and the Cal Tech wind-tunnel tests.

Parachute wake effect data measured in wind-tunnel tests behind a 3/8 scale model of the ejectable nose section of the XS-2 research aircraft (V) (Reference 5.11), and data measured on model parachutes by the Sandia National Laboratories (VI) (Reference 5.12), are included in Figure 5-21.

Figure 5-22 details the measured forebody wake effect on the 16.5-foot-diameter ribbon drogue chute of the Apollo Command Module shown in Figure 5-21.

Many forebodies, such as aircraft, have a noncylindrical cross section. Figure 5-23 demonstrates a method that has been used successfully to convert an odd-shaped cross section to a circular area. The area of the forebody, S_B , included in the inflated area of the parachute behind the forebody is converted into the area of an equivalent circle. The diameter of this circle, D_B , is then used as the reference forebody diameter.

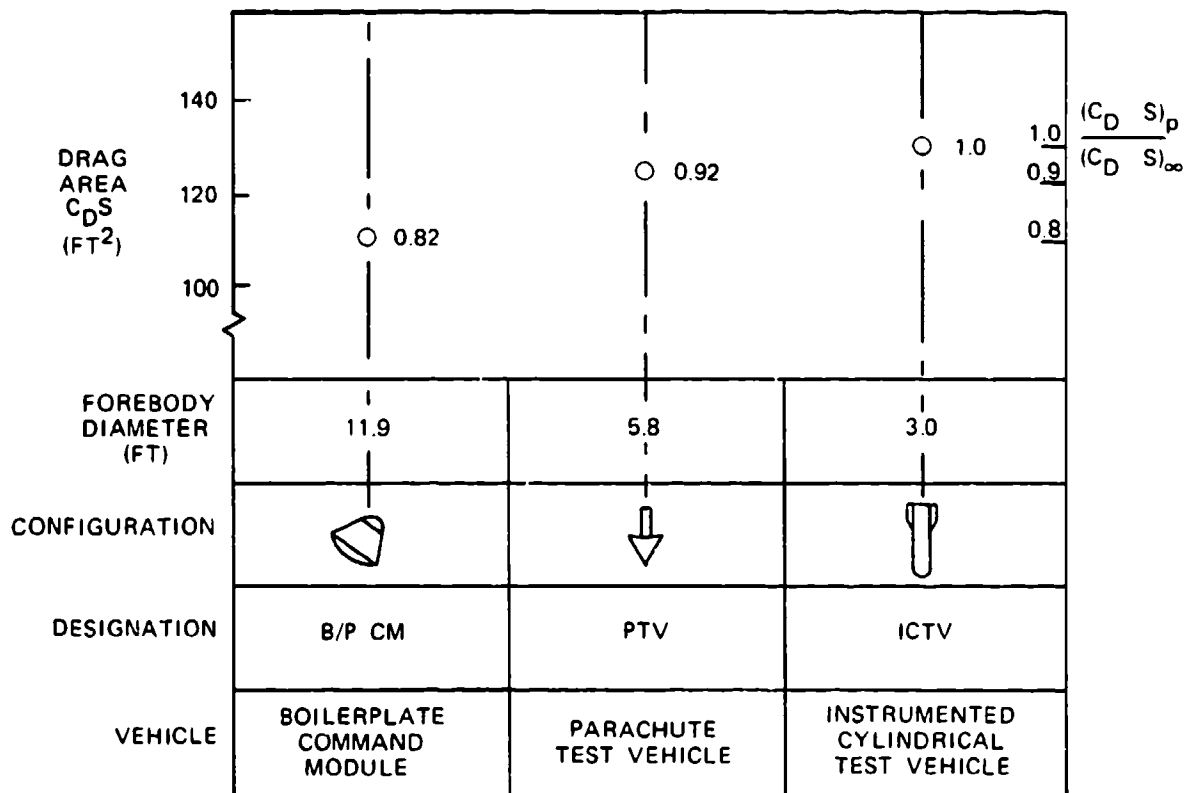
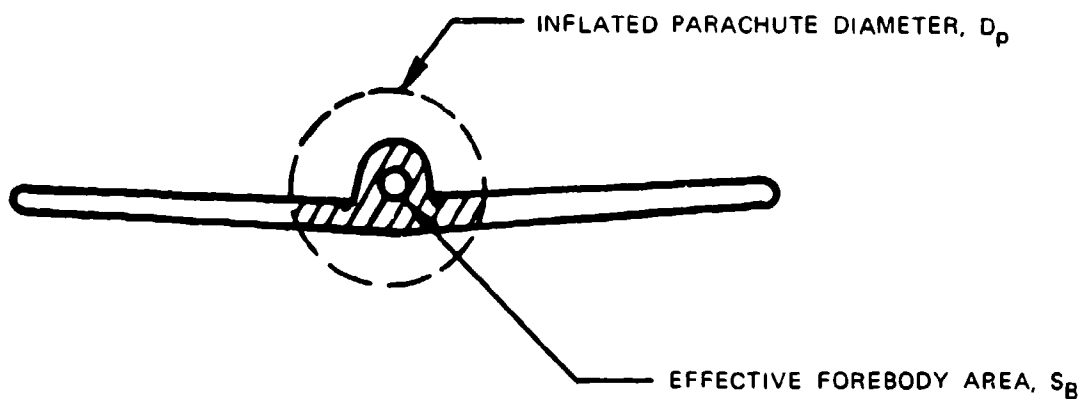


FIGURE 5-22. Drag Loss of the Apollo 16.5-Foot-Diameter, Ribbon Drogue Chute Caused by Different Forebodies.



$$\text{EFFECTIVE FOREBODY DIAMETER, } D_B = \sqrt{\frac{4 S_B}{\pi}}$$

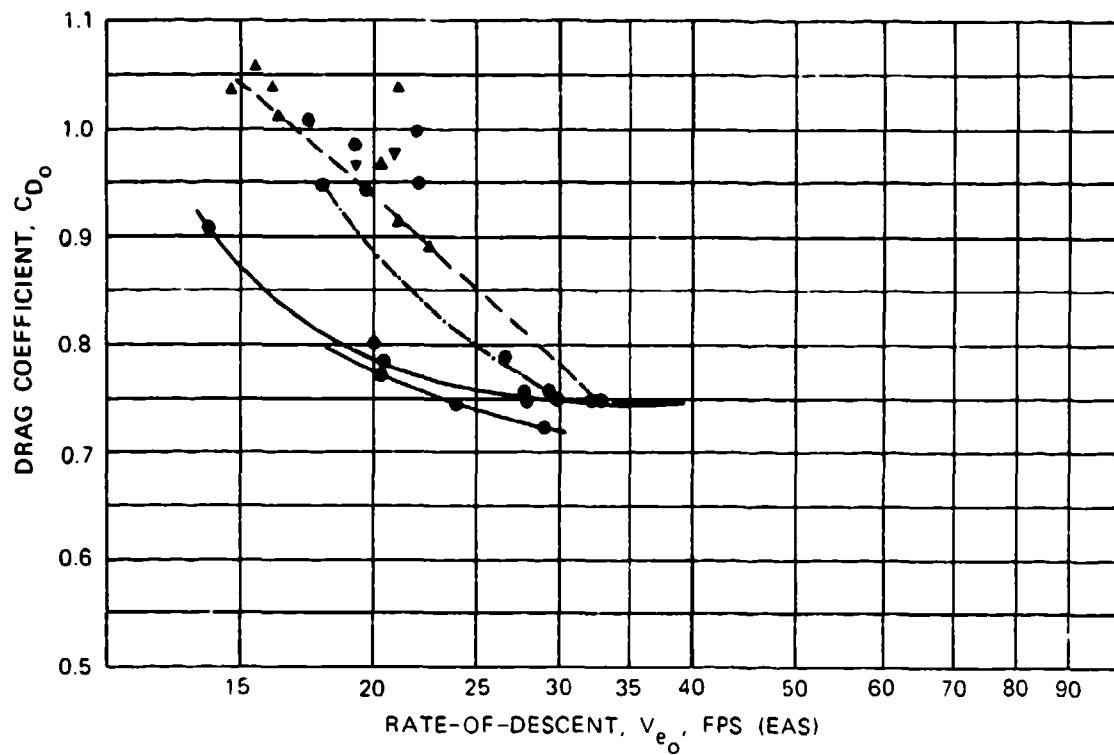
FIGURE 5-23. Determination of Effective Forebody Diameter.

5.2.3 Measured Drag Coefficients of Various Types of Parachutes

Drag coefficients are discussed in this section for solid flat, conical, triconical, extended-skirt, hemispherical, annular, and cross parachutes. These data were calculated from drop tests conducted over a period of time, primarily at the El Centro test facility. The main source for determining rates of descent were phototheodolite measurements, although some older tests used the 300-foot drop-line method. Most of the data were collected by the author; the summary data in Figure 5-24 were plotted by E. Ewing of Northrop-Ventura and presented in Figure 6-35 of Reference 2.1.

Figure 5-24 plots the measured drag coefficient data for solid, flat circular, circular conical, triconical, extended-skirt, ringsail, annular, and ringslot parachutes. The data confirm the previously stated fact that triconical, annular, and extended-skirt parachutes have the highest drag coefficients. The data also confirm that, similar to model parachutes (Figure 5-16), the drag coefficients of unstable, large parachutes decrease with increasing rates of descent.

References 5.13 through 5.20 refer to solid circular flat, circular conical, and triconical parachutes in general, and not to any specific parachute evaluated for the drag coefficient data in Figure 5-24.



PARACHUTE TYPE	D_o , FT	L_e / D_o
SOLID FLAT CIRCULAR	24-28	0.75-1.0
SOLID FLAT CIRCULAR	100	0.95-1.0
SOLID CONICAL CIRCULAR	95-100	0.95-1.0
▲ TRICONICAL	79.6-100	
— 14.3% EXTENDED SKIRT	60-67.3	0.92-1.0
" 10% EXTENDED SKIRT	56-67.2	1.0
— 10% EXTENDED SKIRT MC-1	35	0.85
" 10% EXTENDED SKIRT	34.5-38	0.87-0.94
—● RINGSAIL ($\lambda_T = 7-8\%$)	56.2-84.2	0.94-0.97
—● RINGSAIL ($\lambda_T = 7.2\%$)	88.1	1.4
● ANNULAR ($D_v / D_p = 0.63$)	42-64	1.25

FIGURE 5-24. Drag Coefficient Versus Rate of Descent for Various Types of Solid Textile Parachutes.

Extended-Skirt Parachutes. Figure 5-25 shows the drag coefficient versus rate of descent for various types of extended-skirt parachutes. These data are the result of numerous tests conducted with individual parachutes. The extended-skirt parachute was developed at Lakehurst, New Jersey, by the U.S. Navy in the late 1940s (Reference 5.21). In 1952, the U.S. Air Force used the extended-skirt design to develop the T-10 Troop Parachute (Reference 5.22). Extended-skirt parachutes designed for recovery of the Q-2 and the USD-5 drones achieved high drag coefficients combined with reasonably good stability of about 10 degrees of oscillation (References 5.23 and 5.24).

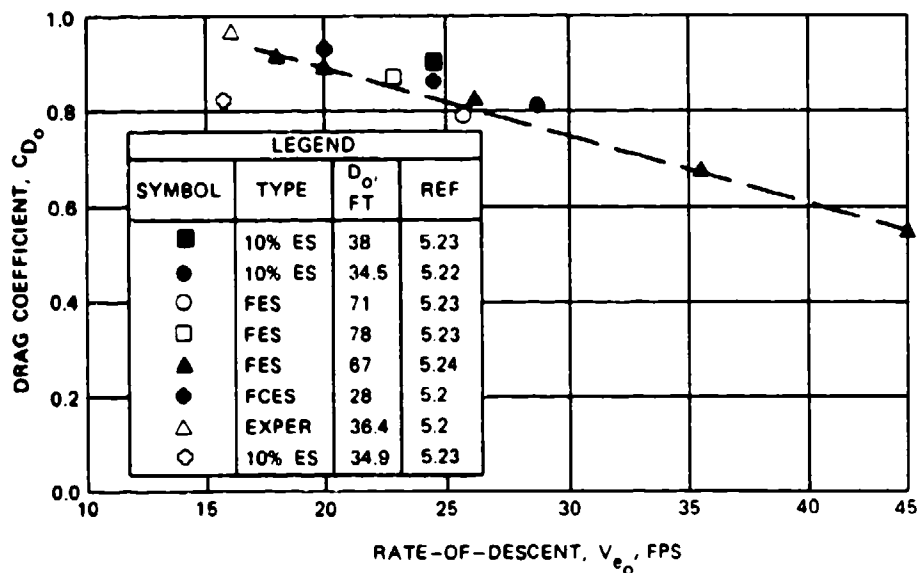


FIGURE 5-25. Drag Coefficient Versus Rate of Descent for Various Extended-Skirt Parachutes.

Combining the high drag effect of the triconical parachute with the good stability and low opening shock characteristics of the extended skirt design may produce a parachute combining the best features of both designs.

The sensitivity of extended-skirt parachutes to suspension-line length is shown in Figure 5-26. These tests were conducted with an 11.8-foot-diameter, 10% extended-skirt parachute in the Wright Field vertical wind tunnel. The data also demonstrate the effect of velocity on the drag coefficient.

Cross Parachute. In recent years, the cross parachute has been used for aircraft and ordnance deceleration as a low-cost replacement for the ringslot parachute. The cross parachute was first tested in 1947 by the Naval Ordnance Laboratory (Reference 5.25) and was reintroduced in 1962 as the French cross parachute (References 5.26 and 5.27). The Naval Surface Warfare Center (NSWC) at Silver Spring, Md., has conducted many aerodynamic and

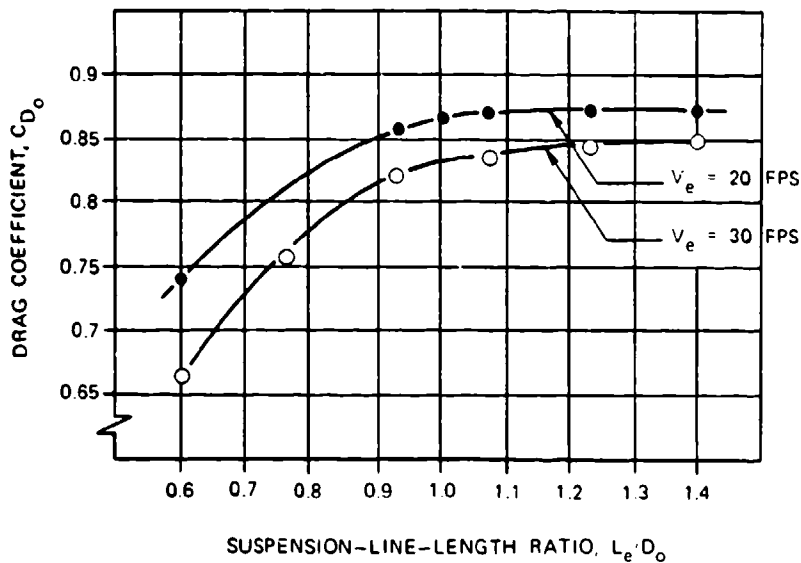


FIGURE 5-26. Effect of Suspension-Line Ratio on an 1.8-Foot-Diameter Extended-Skirt Parachute.

stress investigations on cross parachutes (References 5.28 to 5.32). NSWC is using the cross parachute for the stabilization and retardation of mines, see section 8.6.4. Reference 5.33 describes the use of a cross parachute as a final descent parachute. Figure 5-27 shows the cross parachute drag coefficient as a function of rate of descent evaluated from the NSWC programs. This stable parachute increases its drag coefficient with a decreasing rate of descent, a fact previously observed only on unstable parachutes. Drag and stability of the cross parachute depend on the arm's diameter-to-width ratio (W/L), on the number and length of suspension lines, and on cloth porosity. To conform to general use, the nominal diameter, D_o , is used in this manual instead of the arm length to define cross parachute diameter. Reports published primarily by the NSWC should be consulted before using this parachute. Wind-tunnel and water-tank tow tests on cross parachutes were conducted by the University of Leicester, England (Reference 5.34 and 5.35).

Annular Parachute. The annular parachute was developed in 1947 and named the airfoil parachute (Reference 5.36). Figure 5-28 shows its high drag coefficient. The parachutes with individual symbols in the figure are annular parachutes used in connection with a ringslot or ringsail engagement parachute for midair retrieval systems (References 5.37 and 5.38).

Ribbon Parachutes. Section 5.8 contains drag data on ribbon parachutes for the subsonic and supersonic range. Ribbon parachute performance depends to a large extent on selection of the right porosity. Design data, including the required porosity for a particular parachute size and application, are discussed in Chapter 6. References 5.39 through 5.47, published by various organizations, discuss performance, design details, and subsonic and supersonic applications of ribbon parachutes.

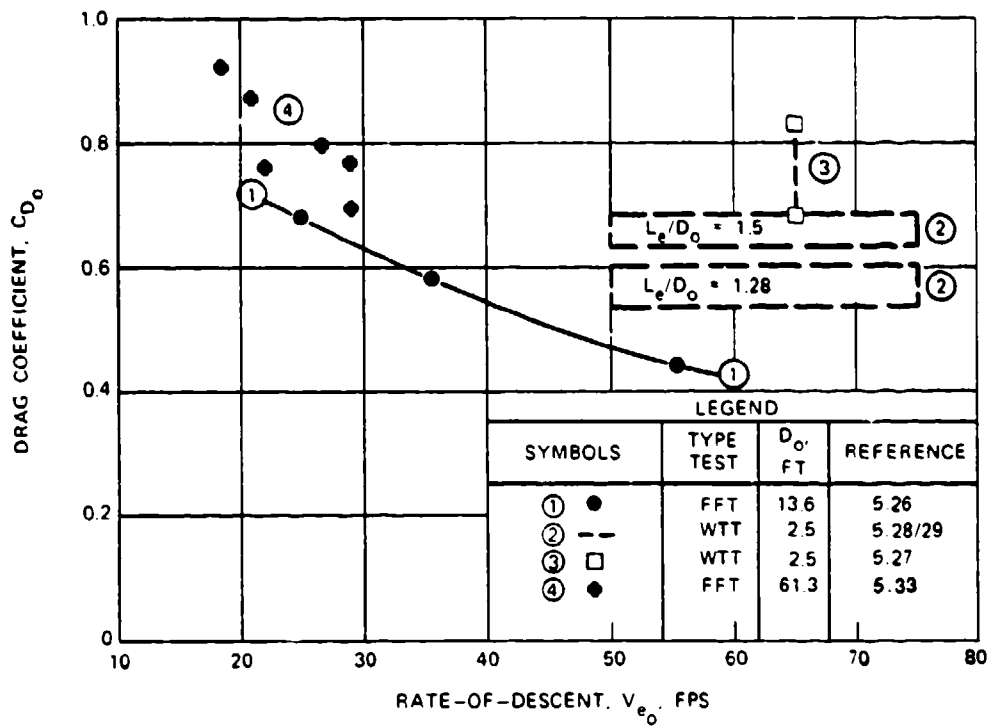


FIGURE 5-27. Drag Coefficient Versus Rate of Descent for Various Cross Parachutes.

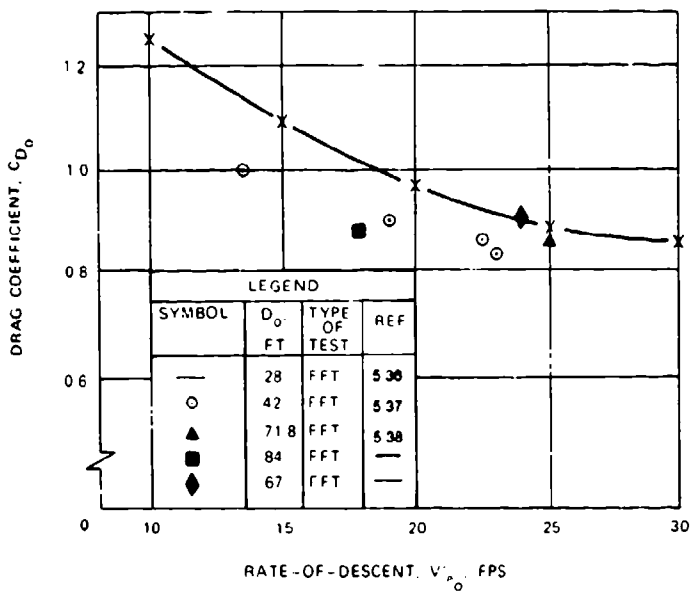


FIGURE 5-28. Drag Coefficient Versus Rate of Descent for Various Annular Parachutes.

The influence of Mach number on the drag of ribbon-type drogue chutes is discussed in section 5.8.

Ringslot Parachutes. References 5.48 and 5.49 give design details on ringslot parachutes. A drag coefficient, C_{D_0} , of 0.65 has been measured in free-fall tests. Selection of the proper total porosity, in accordance with Chapter 6, is important. Ringslot parachutes used as landing deceleration parachutes for aircraft experience a drag coefficient reduction from 0.65 to 0.60 because of the large wake behind the aircraft.

Ringsail Parachutes. Reference 5.50 is a summary report on ringsail performance, design, and application. These parachutes were used as the main descent parachutes for the Mercury, Gemini, and Apollo spacecraft and for the ejectable crew module of the F-111 aircraft.

Hemisflo Parachute. This supersonic ribbon parachute should be used at speeds of Mach 2 or higher. References 5.51 and 5.52 provide information on the development, design, and application of hemisflo parachutes.

Guide Surface Parachute. This parachute was developed as a high-stability, low drag parachute for the stabilization of bombs, mines, and torpedoes. It combines good stability with excellent damping characteristics. For details see References 5.53 and 5.54.

Disk-Gap-Band Parachute. Some information on this parachute, used successfully to land the Viking spacecraft on the planet Mars, is contained in References 5.55 and 5.56.

Rotating Parachutes. Several types of rotating parachutes have been used successfully. Angled vents in the parachute canopy rotate the parachute. Centrifugal forces acting on the canopy and suspension lines increase the projected diameter, resulting in a high drag coefficient. Attempts to use rotating parachutes with diameters greater than 10 feet have been unsuccessful because of deployment and canopy wrap-up problems. References 5.57 through 5.59 provide information on the three best known types of rotating parachutes.

Maneuverable (Gliding) Parachutes. Maneuverable gliding parachutes and their performance characteristics are discussed in section 5.9.

Balloon-Type Decelerators. These deceleration devices, including the Goodyear ballute, are discussed in section 5.8.

5.2.4 Effect of Reynolds Number on Parachutes

Chapter 4 states that parachutes, unlike airfoils, operate in turbulent flow because of the separation of the airflow at the leading edge of the parachute canopy. For this reason, the

Reynolds number does not appear to change the drag coefficient of parachutes. Measured data on parachute drag coefficient versus Reynolds number are compared in Figure 5-29 with the known Reynolds number effect on the drag coefficient of a sphere. These data are taken from Reference 2.1.

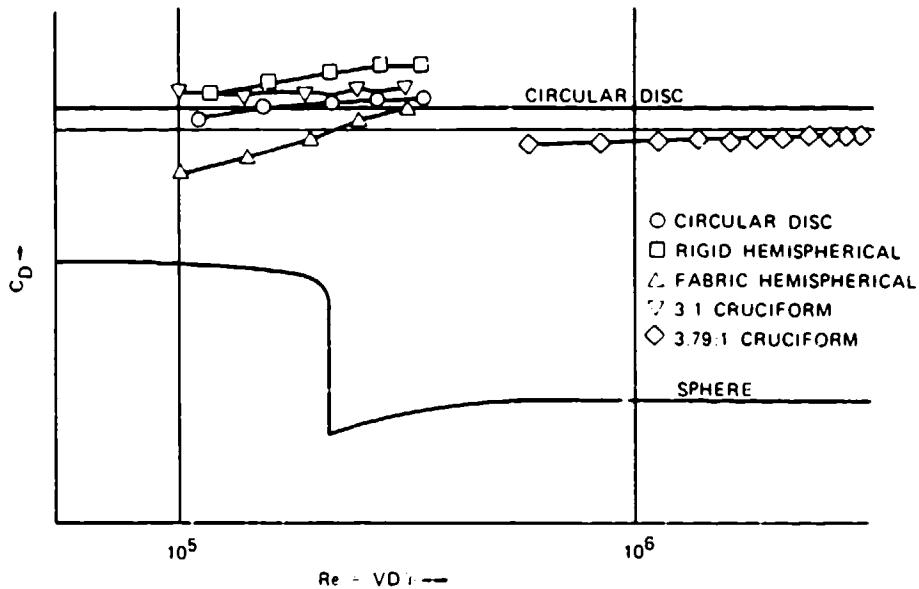


FIGURE 5-29. Effect of Reynolds Number on Drag Coefficient for a Sphere and Various Parachutes.

5.3 STABILITY OF PARACHUTE SYSTEMS

5.3.1 General Definition

Stability may be viewed as the tendency of a body to return to a position of balance or equilibrium after a displacement from that position. Controllability may be defined as the ease of causing that movement, or as the effectiveness of the mechanism used to cause the body to return to its original position. Various concepts of stability can be illustrated by simple examples. In Figure 5-30a, a ball is shown at rest in a concave depression. A displacement of the ball will result in gravity restoring it to its original position. This state is called "stable." If the ball is placed on a flat surface, a displacement of the ball from its position of rest will cause the ball to come to rest at a different location on the flat plate, with no tendency for the ball to return to its original position; this state is termed "neutrally stable" (Figure 5-30b). Figure 5-30c shows a ball placed in a state of equilibrium atop a larger spherical ball. Clearly, any displacement of the small ball on the large sphere causes the ball to continuously move away from its original position of stability. This condition is termed "unstable." In the three simple examples, we have considered the conditions connected with static stability.

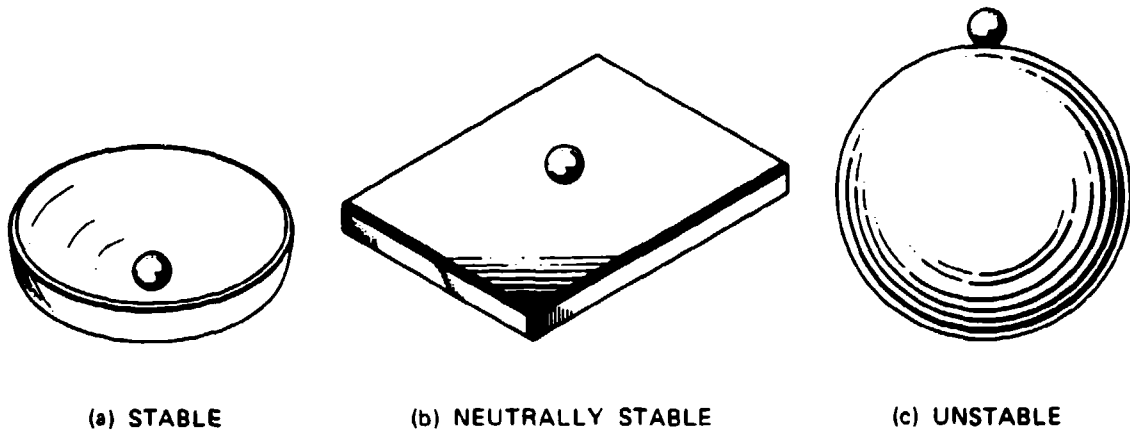


FIGURE 5-30. Illustration of Static Stability.

Dynamic stability refers to the continued motion of a moving body and may be illustrated by considering the ball on the concave surface in Figure 5-30a. The friction forces on the ball are always in a direction opposite to its motion. The friction forces, positive damping effect, together with the gravity component, make the ball tend to oscillate with a decreasing amplitude until it finally achieves the illustrated position of static stability. A ball in this dynamic environment is called "dynamically stable." If the aerodynamic forces of air resistance and the mechanical frictional forces could be reduced to zero—an impossible condition—there would be no damping force on the ball, and a small displacement of the force applied to the ball would cause an indefinite oscillation of constant amplitude. Such a condition is termed "neutrally dynamically stable." If friction force is overcome by some external force—for example, a propulsion force—the ball would oscillate with an increasing amplitude and would not return to its position of equilibrium; this condition is called "dynamically unstable."

These conditions of dynamic stability are graphically illustrated in Figure 5-31, which demonstrates the stability of three bodies. Body "a" is dynamically and statically unstable. Body "b" is statically stable but dynamically unstable, resulting in ever-increasing oscillations. Body "c" is dynamically and statically stable, resulting in oscillations damped with time.

The fact that a body is statically and dynamically stable is frequently not sufficient. For example, an automobile without shock absorbers is statically and dynamically stable in its spring motions, but may provide an uncomfortable ride because of insufficient damping of its body oscillations. Installation of shock absorbers increases positive damping and causes a rapid decrease of the body oscillations with time, thereby providing a comfortable ride.

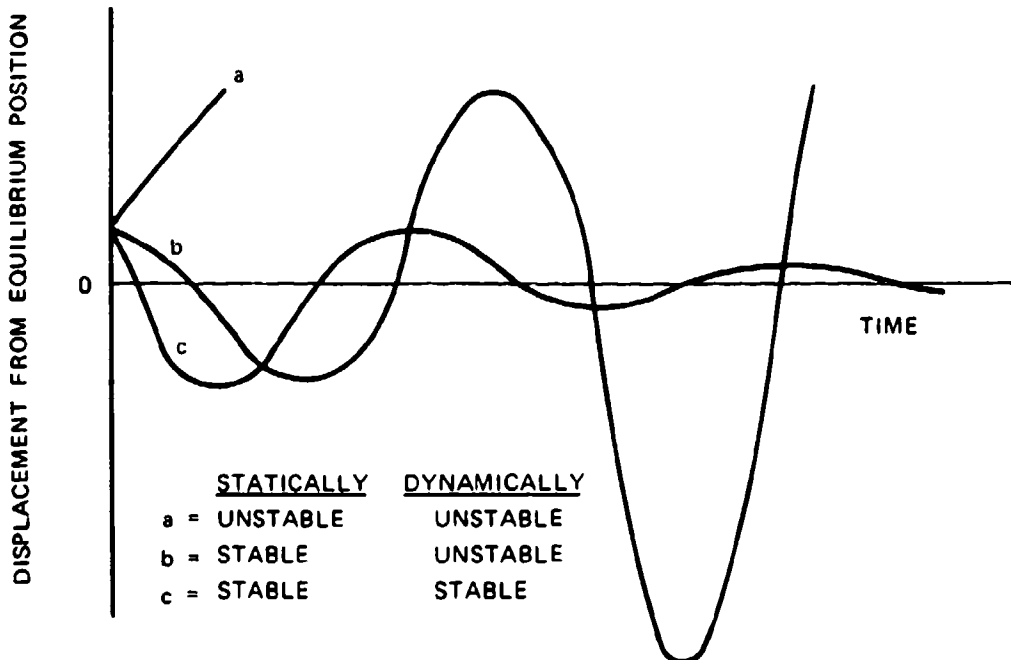


FIGURE 5-31. Graphical Illustration of Dynamic Stability.

A statically stable parachute may require excessive time to decrease its oscillation after an external disturbance, such as a wind gust, indicating that the parachute's damping characteristics are inadequate for stabilizing an unstable body.

In the case of an aircraft, good static and dynamic stabilities are desirable for large cargo-type aircraft, but this stability counteracts fast changes in attitude and position required for fighter aircraft, which are generally built with low or neutral static stability. In recent years, aircraft requiring a high degree of mobility have been designed with a slightly negative static stability, thus increasing mobility and decreasing the size and drag of the control surfaces.

5.3.2 Parachute Stability

Stability is defined as the tendency of a body to return to a position of equilibrium after displacement. Parachute engineers frequently use the term stability loosely. If two airdrop platforms descend, each on a 100-foot-diameter parachute, and one parachute oscillates ± 30 degrees and the other ± 5 degrees, observers frequently call the former parachute system unstable and the latter stable. In reality, both parachute systems are statically unstable in the oscillating mode but are sufficiently damped dynamically to stay within their ranges of oscillation without increasing the oscillation amplitude. It is more precise to define these parachutes as oscillating ± 30 degrees or ± 5 degrees; and, if possible, to state that

disturbances such as those caused by wind gusts are damped within a given number of full oscillations. The parachute oscillating ± 5 degrees most likely meets the requirements for airdrop; however, the same parachute is unsuitable for stabilizing airdropped bombs or torpedoes. For this application, a parachute with zero oscillation and good damping is required. As defined later in this section, a parachute meeting this requirement has a steep negative $dC_m/d\alpha$ over a wide range of angles of attack.

Why should one parachute have no oscillation and strong damping characteristics while another parachute oscillates violently? Figure 5-32 explains this difference by showing the airflow around several types of parachute canopies and rigid hemispheres. The airflow, made visible with smoke ejected from equally spaced nozzles in front of the parachute models, acts as streamlines, as explained in Chapter 4. Figure 5-32a shows the airflow around an imporous hemisphere. Airflow cannot get through the canopy but goes around and separates on the leading edge of the hemisphere in alternating vortexes, forming what is called the Karman

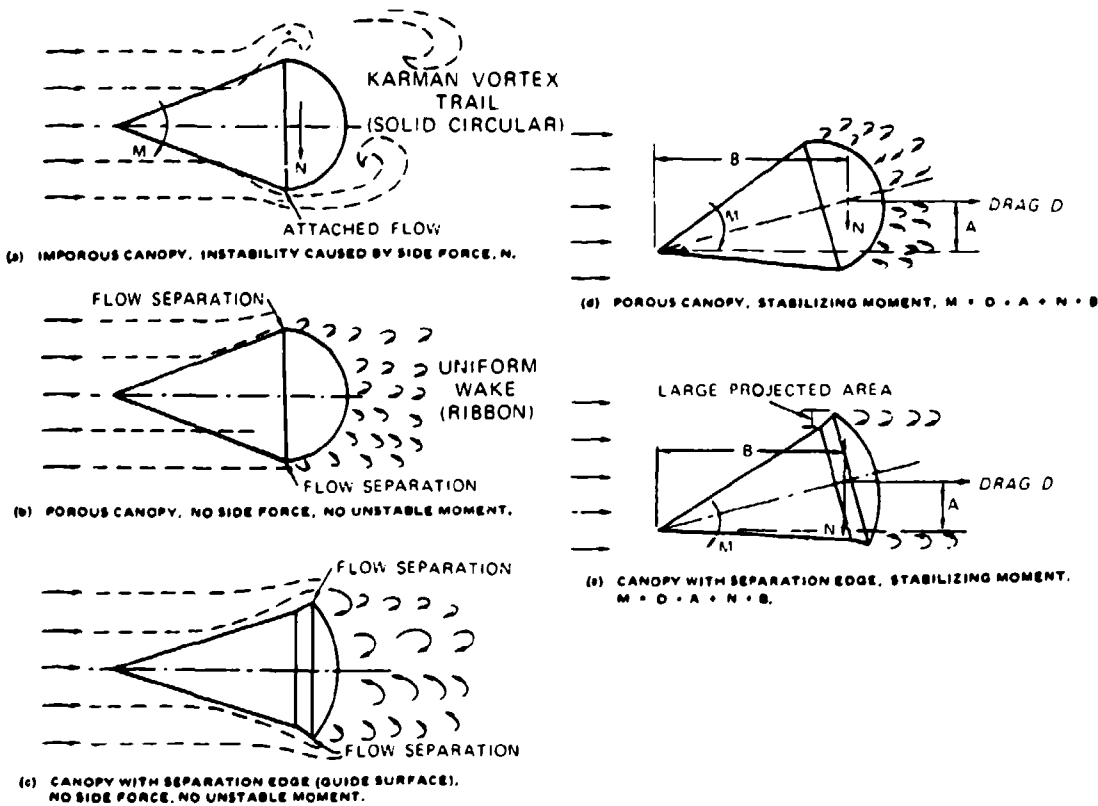


FIGURE 5-32. Relationship of Airflow and Stability for Various Parachutes.

Vortex Trail. The separation causes alternate pressure areas on opposite sides of the canopy, and these pressure areas produce the parachute's oscillations.

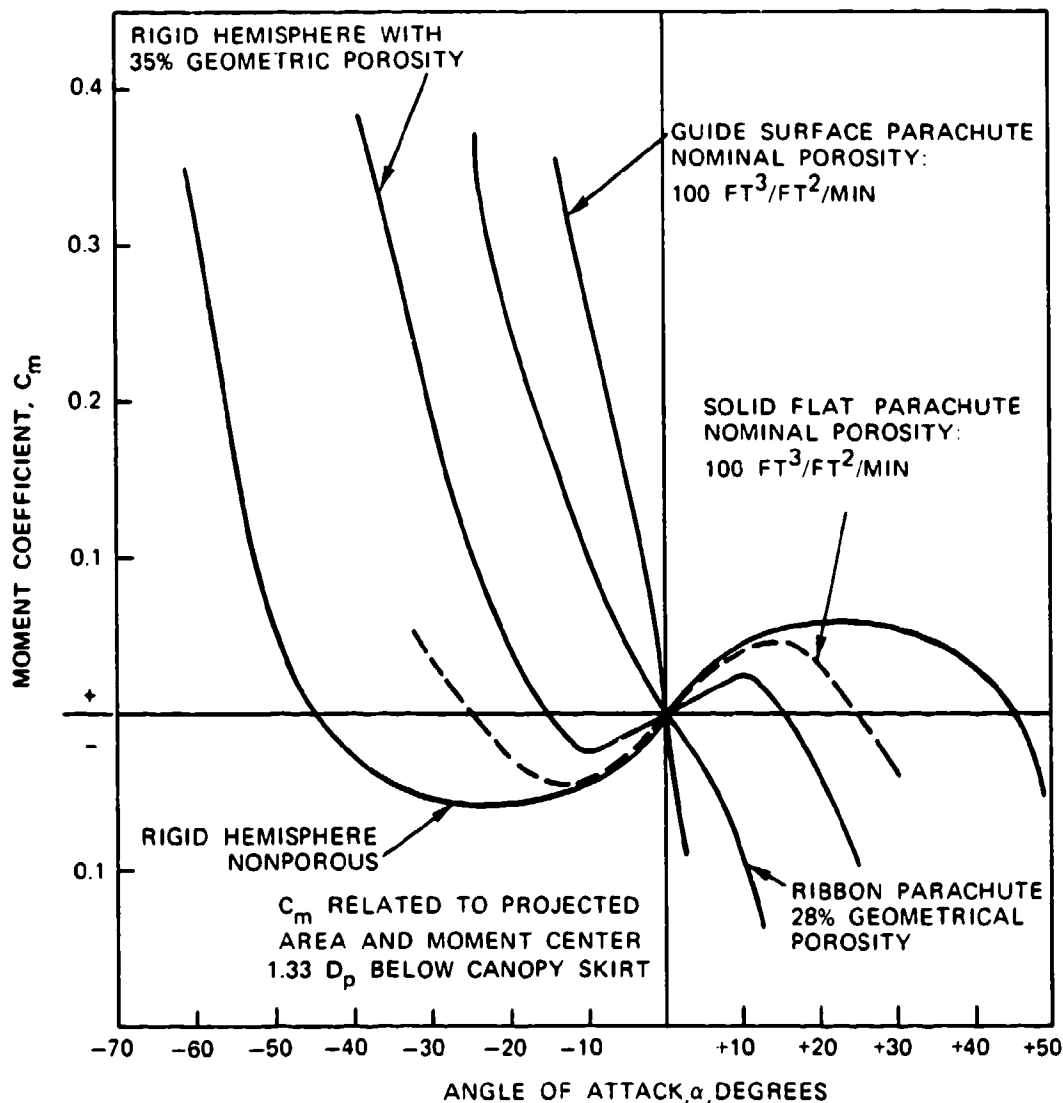
Figure 5-32b shows the effect of openings in the canopy. Part of the air flows through the canopy and forms a uniform wake consisting of small vortices. In addition, the airflow separates uniformly around the leading edge of the canopy, eliminating the destabilizing alternate flow separation of the Karman Vortex Trail. Uniform wake and airflow separation is the principle of the ribbon parachute and all slotted parachute canopies.

The guide surface parachute (Figure 5-32c) has a sharp separation edge around the skirt of the canopy, creating a strong, uniform airflow separation around the leading edge. In addition, the inverted leading edge (guide surface) creates a large, stabilizing normal force. Both the normal force, N, and the drag force, D, create a stabilizing moment if the parachute is displaced from its zero-angle-of-attack position (Figure 5-32e). The known main design features for creating stable parachutes are uniform airflow separation around the leading edge of the canopy, airflow through the canopy, and a large restoring moment such as that generated by a guide surface.

The static stability of various parachutes has been measured numerous times in wind-tunnel tests. Figure 5-33 plots the moment coefficient of several parachute types and of rigid hemispheres, as measured by the University of Minnesota (References 5.60 and 5.61). A negative $dC_m/d\alpha$ of the moment coefficient curve indicates that the parachute is stable and will return to its zero-angle-of-attack position after a disturbance. The solid, flat, circular canopy is a typically unstable parachute. It will oscillate between ± 25 degrees, but if deflected more than 25 degrees it will return to the 25-degree position. The ribbon and guide surface parachutes will return to their zero-angle-of-attack attitude if displaced, as indicated by the negative slope of the $dC_m/d\alpha$ curve going through the zero-angle-of-attack position for both parachute types.

The guide surface parachute has the steepest $dC_m/d\alpha$ and, therefore, the strongest stabilizing moment and best damping characteristics of all known parachutes.

Larger parachutes oscillate less than small parachutes. A 3-foot-diameter solid flat circular parachute manufactured from standard 1.1-oz/y² ripstop material, tested in a wind tunnel, will oscillate about ± 35 to 40 degrees. The standard 28-foot-diameter personnel parachute oscillates about ± 30 to 35 degrees. The 100-foot-diameter G-11 cargo parachute oscillates about 10 to 20 degrees. The 200-foot-diameter cargo parachute manufactured from 1.6-oz/y² material with about the same porosity as the other parachutes (described in Reference 5.14) oscillates less than 5 degrees. Ludtke discusses oscillation problems in Reference 5.62.



NOTE: IN THE U.S. A STABILIZING MOMENT IS DEFINED AS HAVING A NEGATIVE $dC_m/d\alpha$. IN EUROPE, A STABILIZING MOMENT IS DEFINED AS HAVING A POSITIVE $dC_m/d\alpha$.

FIGURE 5-33. Moment Coefficients Versus Angle of Attack for Guide Surface; Ribbon; and Flat, Circular Parachutes; and for Porous and Nonporous Hemispheres.

5.3.3 Stability of a Parachute Body System

Parachutes that are used with stable air vehicles must also be stable and not interfere with the inherent stability of the vehicle. Parachutes with good stability and high drag are used, such as the ribbon, ringslot, and cross parachutes. If a fast-falling, unstable body must be stabilized while maintaining a high rate of descent, a parachute with a strong negative $dC_m/d\alpha$, such as a guide surface parachute, may be preferable. For each parachute assembly, a compromise between required stability, weight, volume, and cost determines the final selection.

The following parachute application ranges have been established based on many years of practical experience.

Aircraft Landing Deceleration. Aircraft are inherently stable and do not require aircraft landing deceleration parachutes to contribute to their stability. Therefore, high drag stable parachutes that do not interfere with the aircraft controllability are used. Ribbon, ringslot, and cross parachutes are used primarily for aircraft landing deceleration.

Bomb Stabilization. During World War II, the Germans developed parachute-stabilized bombs that enabled them to shorten the length of the bomb and to store more bombs in existing aircraft bomb bays. These fast-falling bombs required a low drag, highly stable parachute with good damping capability to obtain the desired stability. The guide surface parachute was developed specifically for this application as a low drag, high-stability parachute (Reference 5.53). A single riser attachment did not provide a sufficiently stable parachute-bomb system, and a more rigid connection between the bomb and the parachute was required. Figure 5-34 contains two examples of rigid parachute-bomb connections: the multiple-point attachment on the circumference of the bomb and the geodetic attachment. The geodetic attachment is the best solution but is more complex.

Torpedo and Mine Stabilization. Mines and torpedoes that are airdropped from low altitudes are equipped with retardation parachutes to

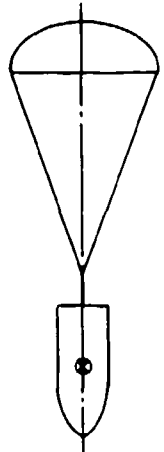
1. Decelerate the store to an acceptable water entry velocity, generally below 200 ft/s.
2. Obtain a water entry angle that avoids ricochet.
3. Avoid store oscillation and associated store damage at water impact.

Guide surface, ribbon, ringslot, and cross parachutes are being used successfully for this application.

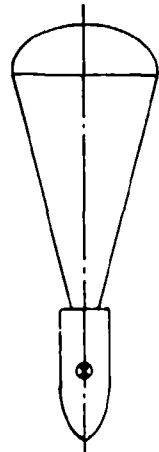
Bomb Retardation. Bombs dropped at high speeds from low-flying aircraft must be retarded to

1. Obtain a steep impact angle to avoid ricochet.
2. Permit the aircraft to escape the effective range of the exploding bomb.
3. Obtain a good fragmentation pattern associated with a steep impact angle.

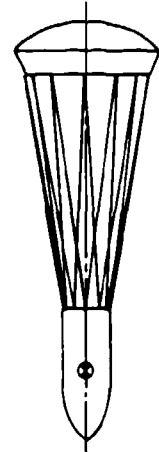
BOMBS



(a) SINGLE POINT

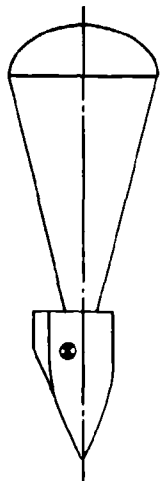


(b) MULTIPLE POINT

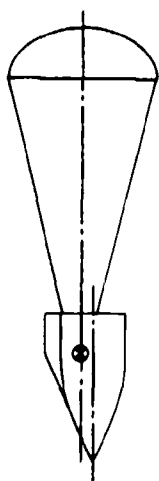


(c) GEODETIC

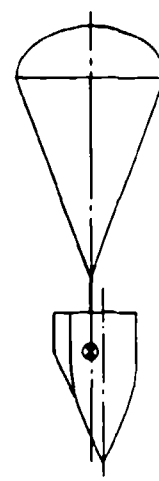
AIRCRAFT CREW MODULES



(d) CENTER LINE



(e) MULTIPLE POINT
CG ATTACHMENT



(f) SINGLE POINT
CG ATTACHMENT

FIGURE 5-34. Various Configurations of Parachute Vehicle Attachments.

Stable parachutes with good drag characteristics used for this one-time application include ribbon, ringslot, and cross parachutes as well as the inflatable ballute-type retarders.

Ejection Seat, Encapsulated Seat, and Crew-Module Stabilization and Retardation. All three aircraft escape systems need parachutes for stabilization and retardation. Stabilization is required in pitch, yaw, and roll; parachutes can provide stabilization in pitch and yaw, but are poor for roll control. For descent from a high altitude, a roll control of not more than 2 to 3 rpm is necessary for aviator comfort. This control can be obtained with a relatively large drogue chute with an equivalent sea-level rate of descent of 120 to 150 ft/s.

The aircraft crew-module stabilization in Figure 5-34 demonstrates the problem of stabilizing an asymmetrical body with the center of gravity (CG) off the center line of the vehicle. In the example shown, the drogue chute had to be attached offset to the nose section of the XS-2 research aircraft to ensure that the parachute force line would run through the CG of the crew module with the module hanging at a -2 degree zero lift attitude to eliminate destabilizing side forces (Reference 5.11).

The stability relationship of parachute and forebody is quite complex in systems where unstable forebodies must be stabilized by minimum size parachutes. Both the forebody and the parachute can oscillate in a 360-degree plane. The stability of such two-body, multi-degree-of-freedom systems has been investigated by several authors (References 5.63 through 5.67).

Neustadt showed that deploying a parachute opposite the oscillating motion of the forebody may increase the parachute force by as much as 20% (Reference 5.68).

5.4 PARACHUTE INFLATION PROCESS

5.4.1 Opening Force Investigations

Many attempts have been made to develop theoretical solutions to the parachute inflation process and obtain quantitative values for opening time and force. Investigations by Mueller, Scheubel, O'Hara, Rust, Heinrich, Wolf, and Purvis, defined in References 5.69 through 5.75, have increased the understanding of the parachute opening process, including the effect of apparent mass. However, no satisfactory practical solution for calculating filling time and parachute opening forces has evolved. The analytical solution of the opening process has been complicated in recent years by the development of means for controlling parachute inflation, such as reefing, sliders for steerable parachutes, pull-down vent lines, and related devices. While these methods provide control of parachute inflation, and thereby the opening forces, they also interfere with the parachute's natural inflation process. A good account of the present status of the parachute inflation theory was presented by D. Wolf in 1982 during the University of Minnesota Short Course on Parachute Systems Technology (Reference 2.17).

In 1942, Pflanz developed a numerical method for calculating parachute opening forces (References 5.76 and 5.77). He assumed that the drag area of the parachute or of any drag device increased from a low value to 100% in a given time and in a mathematically definable form, such as convex, concave, or linear. The parachute filling distance was assumed to be constant for a specific parachute. The Pflanz method includes altitude effects but does not include gravity effects or drag area overshoot after full opening.

Schuebel was the first to investigate the effect of the apparent mass on the parachute opening process. He defined apparent mass as both the air mass inside the inflating canopy and the air mass outside the canopy that is affected by the inflation process (Reference 5.70).

Modern, high-speed computers make it possible to calculate the time-dependent force-velocity-trajectory history of the parachute opening process for complex recovery systems. This calculation was first accomplished in 1960 by Space Recovery Systems, Inc. (Reference 5.23). The computer results agreed well with the forces measured in free-flight tests.

This force-velocity-trajectory approach was used in an extended form for predicting the parachute opening forces of the Gemini and Apollo drogue and main parachutes (References 5.78 and 5.79). McEwen gives an excellent review of previous efforts and recommends that inflation distance, not inflation time, be used as the reference for the inflation process.

For a parachute-vehicle system moving in space (Figure 5-35), the trajectory equations can be written in the form shown in the figure.

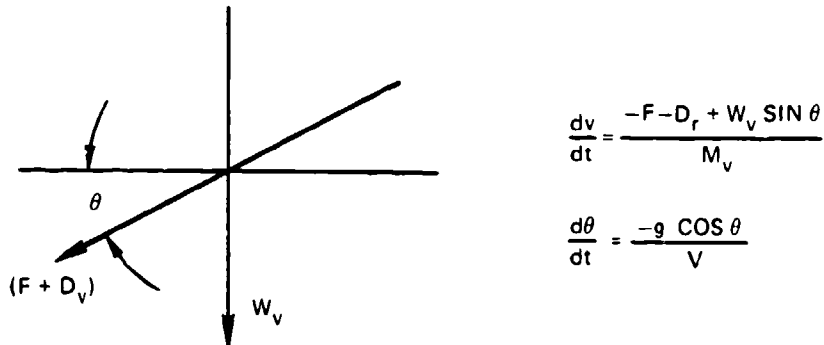


FIGURE 5-35. Angle and Force Relationships for a Deceleration System Moving in Space.

The parachute force, F, as a function of time is

$$F = (C_{DS})_p \rho / 2 v^2 + (m_a + m_v + m_p) \frac{dv}{dt} + v \frac{dm_a}{dt} + W_v \sin \theta$$

where

- F = parachute force acting parallel to the flight trajectory, lb
- D_v = drag of the vehicle (payload), lb
- W_v = weight of the vehicle or payload, lb
- θ = trajectory angle against the horizontal, degrees
- g = deceleration of gravity, ft/s²
- $(C_{DS})_p$ = parachute drag area, ft²
- ρ = density of air, slugs/ft³
- v = trajectory velocity, ft/s
- m_a = apparent mass (added mass), slugs
- m_p = mass of parachute, slugs
- m_v = mass of the vehicle or payload, slugs
- W_p = weight of the parachute, lb

The drag of the vehicle, D_v , depends on the drag area of the vehicle and on the instantaneous dynamic pressure, which changes during the opening process of the parachute.

The trajectory angle, θ , changes from the launch or deployment angle to vertical most rapidly during and after parachute inflation.

Changes in the value of the acceleration of gravity, g , do not affect the outcome at altitudes below 100,000 feet.

The parachute drag area, $(C_{DS})_p$, increases from close to zero at line stretch to 100% at full open canopy.

Density, ρ , changes with altitude; this change must be considered for longer trajectories. Both parachute and payload are assumed to have the same velocity and the same trajectory angle.

The apparent or added mass, m_a , is calculated by multiplying volume by density and by a form factor that depends on the particular parachute type. The apparent mass at an altitude of 40,000 feet is only one-quarter of the apparent mass at sea level, because apparent mass depends on density. Therefore, the apparent mass affects the magnitude of the parachute opening force at a given altitude.

In the parachute force equation, the vehicle weight is $W_v \cdot \sin \theta$. Using the sign convention of Figure 5-35, a parachute opening in a vertical attitude will have a force that is one unit weight higher than the force of a parachute opening in a horizontal attitude. This force difference must be considered in planning parachute test programs.

5.4.2 Parachute Canopy Inflation

Parachute inflation is defined as the time interval from the instant the canopy and lines are stretched to the point when the canopy is first fully inflated. Figure 5-36 shows the phases of canopy inflation. The canopy filling process begins when canopy and lines are stretched and when air begins entering the mouth of the canopy (a). After the initial mouth opening, a small ball of air rushes toward the crown of the canopy (b). As soon as this initial air mass reaches the vent (c), additional air starts to fill the canopy from the vent toward the skirt (d). The inflation process is governed by the shape, porosity, and size of the canopy and by air density and velocity at the start of inflation. Inflation is slow at first but increases rapidly as the mouth inlet of the canopy enlarges (e) and the canopy reaches its first full inflation (f). Most solid textile canopies overinflate and partially collapse because of the momentum of the surrounding air (g). Several factors contribute to an orderly, repeatable inflation process and to a low, uniform

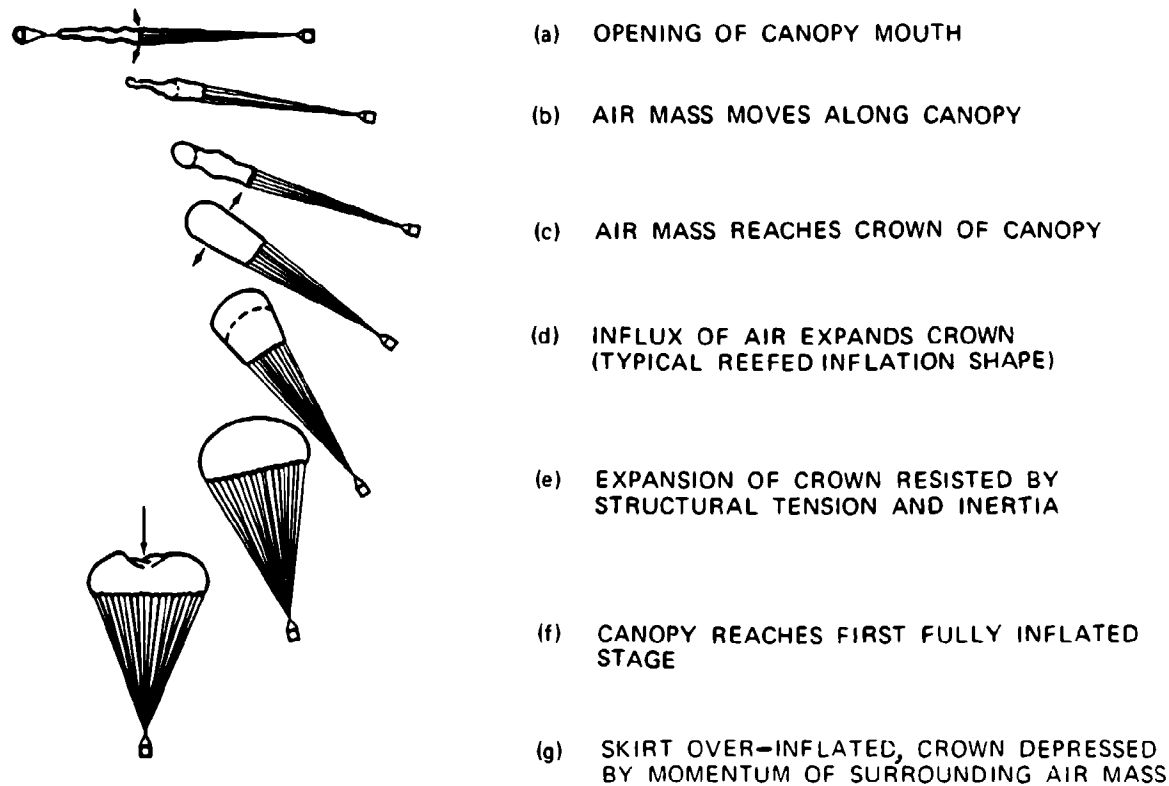


FIGURE 5-36. Parachute Canopy Inflation Process.

opening force. The amount of air moving toward the canopy vent at point (b) should be small to avoid a high-mass shock when the air bubble hits the vent of the parachute. The inflation of the canopy should occur axisymmetrically to avoid overstressing individual canopy parts. Overinflation of the canopy after the first initial opening should be limited to avoid delay in reaching a stable descent position.

Methods have been developed to control the inflation of the canopy; the most frequently used is canopy reefing. Reefing stops the inflation of the canopy at one or more steps between stages (c) and (f), thereby limiting the parachute opening force to a preselected level.

Reefing is also required for uniform inflation of parachutes in a cluster. Stopping the inflation of all cluster parachutes at a point close to stage (d) of Figure 5-36 allows all parachutes to obtain an initial uniform inflation—a prerequisite for a uniform final inflation—without running into a lead/lag chute situation with widely varying parachute forces. Other means for controlling the parachute opening include ballistic spreader guns, sliders for gliding parachutes, and pull-down vent lines.

5.4.3 Canopy Inflation Time

Knowledge of the canopy filling time, defined as the time from canopy (line) stretch to the first full open canopy position, is important. Mueller and Scheubel reasoned that, based on the continuity law, parachutes should open within a fixed distance, because a given conical column of air in front of the canopy is required to inflate the canopy (References 5.69 and 5.70). This fixed distance is defined as being proportional to a parachute dimension such as the nominal diameter, D_p . This assumption was reasonably confirmed in early drop tests with ribbon parachutes. French and Schilling, in papers published in 1968 and 1957, confirmed this assumption (References 5.80 and 5.81). Using the fixed-distance approach and the definitions in Figure 5-37, the filling distance for a specific parachute canopy can be defined as $s_f = n D_p = \text{constant}$.

With $s_f = n D_p$, the canopy filling time, t_f , can be defined as shown in Figure 5-37.

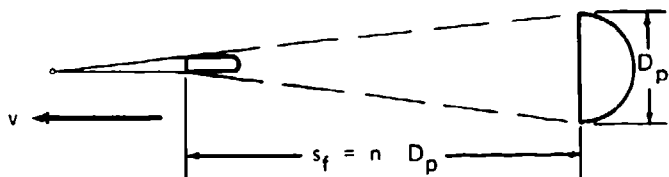


FIGURE 5-37. Filling Distance of a Parachute Canopy.

Because the parachute diameter, D_p , is variable, the fixed nominal diameter, D_o , is used to calculate canopy filling time

$$t_f = \frac{n D_o}{v}$$

where

D_o is the nominal parachute diameter, feet

v is the velocity at line stretch, ft/s

n is a constant, typical for each parachute type, indicating the filling distance as a multiple of D_o , dimensionless.

The constant, n , will be called "fill constant" in subsequent discussions. The basic filling-time equation, $t_f = n D_o/v$, has been extended by Knacke, Fredette, Ludtke, and others. The following formulations have provided good results.

Ribbon Parachute

$$t_f = \frac{n D_o}{\sqrt{0.9}}$$

where $n = 8$ (Knacke).

This equation gives accurate results with ribbon parachutes when the canopy porosities recommended in Chapter 6 are used. For small-diameter ribbon parachutes investigated in high-speed sled and rocket tests, Fredette found the following relationship:

$$t_f = \frac{0.65 \lambda_T D_o}{v}$$

where λ_T is the total canopy porosity expressed as a percent of the canopy surface area, S_o .

Solid Flat Circular Parachute

Wright Field investigations resulted in the following formulations:

$$t_f = \frac{n D_o}{\sqrt{0.85}}$$

where $n = 4.0$ for standard porosity canopies, and $n = 2.5$ for low porosity canopies.

Cross Parachute

An investigator at NSWC, Silver Spring, Md., recommends

$$t_f = \frac{(C_{DS})_p n}{v^{0.9}}$$

where $n = 8.7$. The author has evaluated parachute filling-time data from free-flight tests and found that a formulation for filling time, where the line-stretch velocity, v_s , is a linear function instead of an exponential function, gives satisfactory results in the medium-velocity range of about 150 to 500 ft/s. Table 5-6 lists the fill constant, n , in the equation $t_f = \frac{nD}{v}$ for a variety of parachutes.

TABLE 5-6. Canopy Fill Constant, n , for Various Parachute Types.

Parachute type	Canopy fill constant, n		
	Reefed opening	Disreef opening	Unreefed opening
Solid flat circular	ID*	ID	8
Extended-skin, 10%	16-18	4-5	10
Extended-skin, full	16-18	7	12
Cross	ID	ID	11.7
Ribbon	10	6	14
Ringslot	ID	ID	14
Ring sail	7-8	2	7
Ribless guide surface	4-6

* ID = Insufficient data available for meaningful evaluation.

Additional fill-factor data can be found in Table 6-1 of Reference 2.1.

The filling time of the various stages of reefed parachutes can be determined as follows:

$$t_{f1} = \frac{n D_o}{v_s} \left[\frac{(C_{DS})_R}{(C_{DS})_o} \right]^{1/2} \quad \text{and} \quad t_{f2} = \frac{n D_o}{v_r} \left[\frac{(C_{DS})_o - (C_{DS})_R}{(C_{DS})_o} \right]^{1/2}$$

where

t_{f_1} and t_{f_2} are the reefed and disreefed filling times,

v_s and v_f are the velocities at line stretch and at disreef, ft/s

$(C_dS)_R$ and $(C_dS)_o$ are the reefed- and full-open drag areas, ft².

Some solid textile, circular parachute types appear to have a critical opening velocity. At high velocities and high dynamic pressures, the canopy opens only partially. The drag of the partially opened parachute decelerates the parachute-vehicle system and the canopy opens fully. This type of opening can also occur on ribbon parachutes with porosities that are too high (Figure 6-23). Attempts to use this phenomenon for controlling the canopy inflation process, and thereby the parachute forces, have not been successful because of the variables involved and the difficulty of controlling the porosity of solid fabric canopies.

Some types of ribbon parachutes have been opened in the velocity range of up to Mach 4.0. Greene concludes that canopy filling time at supersonic speeds is constant, because the canopy operates behind a normal shock. Reference 5.82 presents test data that appear to confirm his investigations.

In a NASA test program to develop parachutes for planetary landing, ringsail, cross, and disk-gap-band parachutes were opened successfully at altitudes above 100,000 feet and at speeds exceeding Mach 3.0. Section 5.5 provides further details on high-altitude effects, and section 5.8 describes supersonic parachute applications.

5.4.4 Parachute Drag-Area Increase During Canopy Filling Process

The parachute drag area, $(C_dS)_p$, increases from 0 to 100% during canopy inflation. The drag-area-versus-time increase—linear, convex, concave, or random—is well known and has proven to be constant and repeatable for known parachute types (see Figure 5-38).

The drag-area-versus-time increase for reefed ribbon, ringsail, and extended-skirt parachutes is shown in Figure 5-39.

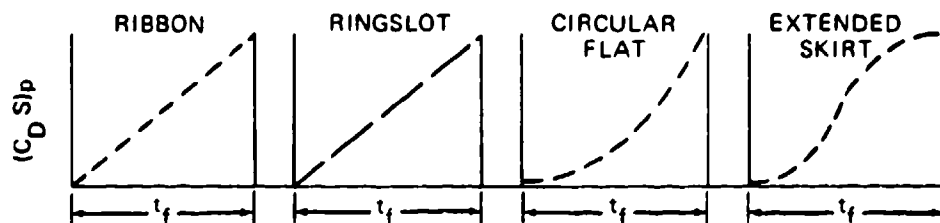


FIGURE 5-38. Typical Drag-Area-Versus-Time Increase for Various Parachute Types.

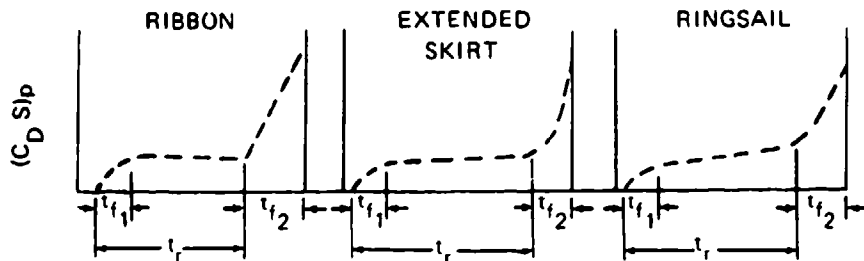


FIGURE 5-39. Typical Drag-Area-Versus-Time Increase for Reefed Parachutes.

The shape of the drag-area-versus-time curve may be somewhat drawn out or compressed by reefing, changes in porosity distribution in the canopy, wide slots, or other means; however, the basic configuration of the curve is maintained for a particular type of parachute.

Drag-area-versus-time curves are obtained from wind-tunnel or free-flight tests by dividing the measured instantaneous force by the instantaneous dynamic pressure. This, more precisely, should be called a dynamic drag area, because it includes characteristics that affect the opening process, such as apparent mass and altitude density.

The evaluated drag-area-versus-time increase for unreefed, solid flat circular, ringslot, and personnel guide chutes (Figure 5-40), is taken from Reference 5.83. The author has added the typical drag-area increase for ribbon and extended-skirt parachutes, determined from numerous tests. Ribbon and ringslot parachutes have a strictly linear drag-area-versus-time increase, and solid textile parachute types have a rather uniform, concave form of drag-area increase. Luttko found that this increase of solid textile parachutes could be expressed by

$$\frac{(CDS)_k}{(CDS)_o} = \left[\left(1 - \eta \right) \left(\frac{t}{t_f} \right)^3 + \eta \right]^2$$

where η is the ratio of the projected mouth area of the canopy at line stretch to the projected frontal area of the fully opened canopy.

Figure 5-41 plots drag-area increase for the 63-foot-diameter reefed ringsail main parachutes used with the Mercury space capsule. It shows a typical characteristic of ringsail parachutes—the increase in drag area during the reefed stage. The ringsail parachute inflates rapidly into an initial reefed stage and then grows slowly through inflation of additional rings. This characteristic is advantageous for single parachutes because it constitutes a form of continuous disreefing, a highly desirable feature.

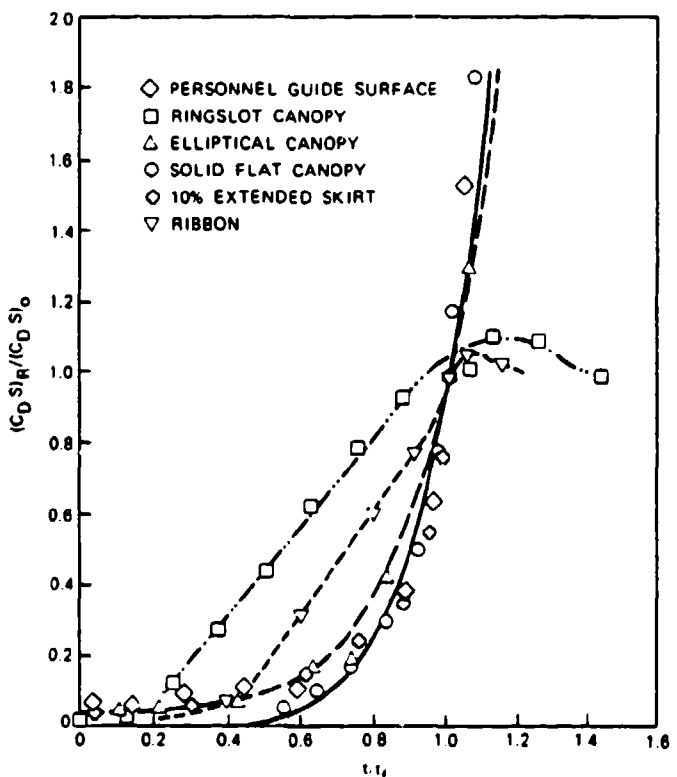


FIGURE 5-40. Drag-Area Ratio Versus Dimensionless Filling Time.

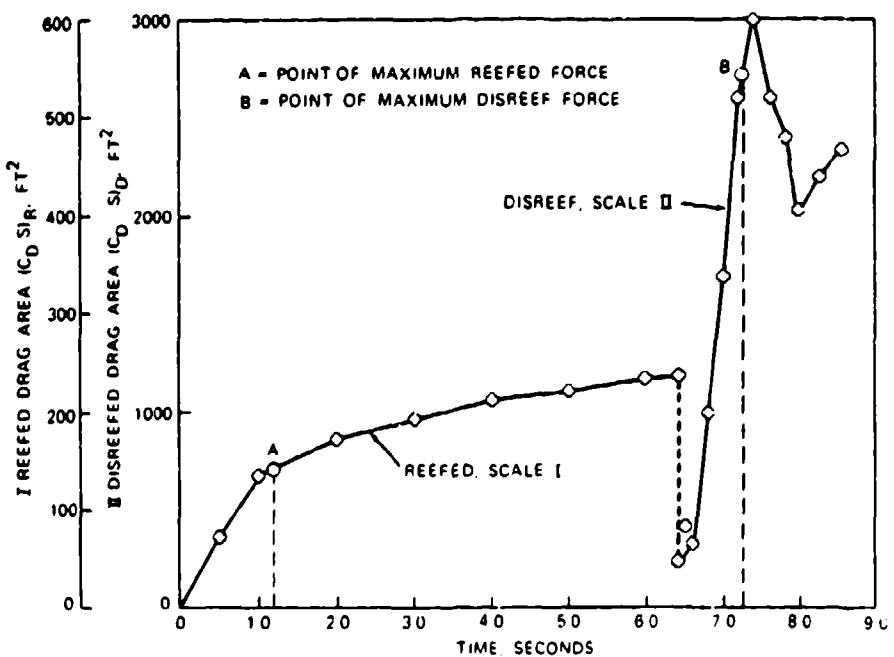


FIGURE 5-41. Drag-Area-Versus-Time Diagram for the Mercury 64-Foot Ringsail Parachute.

Figure 5-41 also demonstrates the extremely short disreefing time of 0.8 second. References 5.50 and 5.79 include figures that show the drag-area increase for a single 85-foot-diameter Apollo ringsail main parachute. The increase in drag area during the reefed stage proved detrimental for the cluster of the three Apollo main parachutes because it tended to support nonuniform inflation.

Reference 5.23 gives drag-area-versus-time data for reefed, extended-skirt parachutes. Several Sandia Reports (References 5.41 to 5.47) provide data on ribbon parachutes.

Drag-area-versus-time increase for a 101-foot-diameter, triconical parachute is shown in Figure 5-42. The drag area in the reefed stage remains constant, which is typical for all known types of parachutes except the ringsail. As shown in Figure 5-40, the disreef drag-area curve displays the same concave shape as other solid textile parachutes. The triconical parachute, in contrast to the ringsail parachute (Figure 5-41), has a long disreef time ($t_{f_2} = 7.5$ seconds), resulting in a relatively small canopy overshoot.

Data on drag-area-versus-time increase for the various parachute types are important for establishing the drag-area-versus-time diagrams required for the force-time-trajectory computer program described in this section and used in Chapter 7.

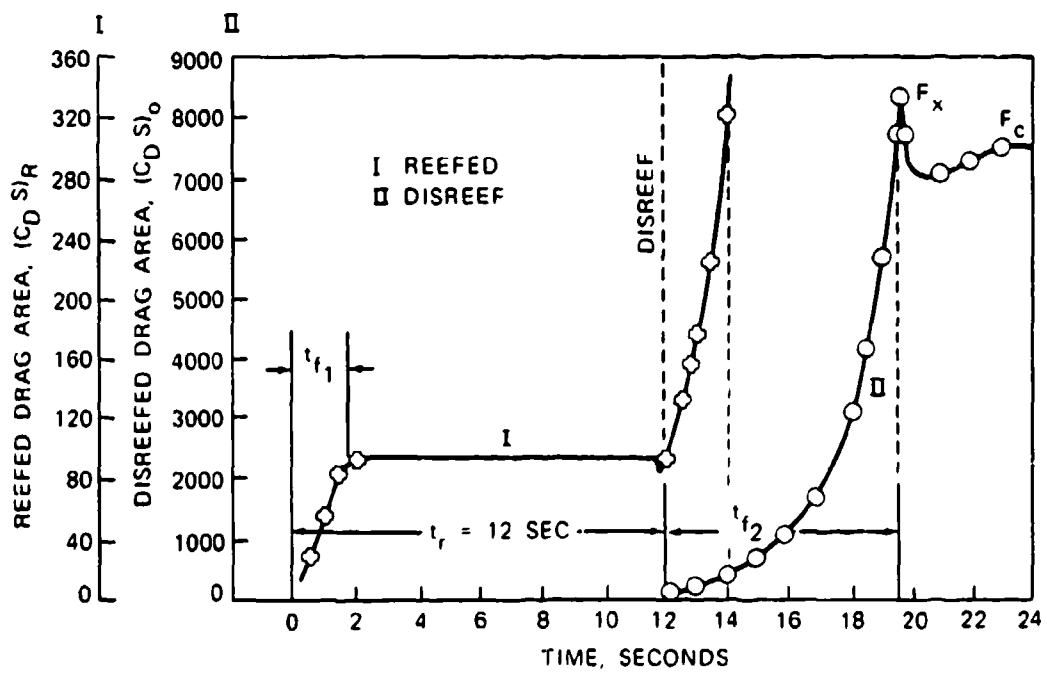


FIGURE 5-42. Drag-Area-Versus-Time Diagram for a Reefed 101-Foot-Diameter Triconical Parachute.

Recovery system engineers should evaluate and publish drag-area-versus-time diagrams to improve the database for computing the force-trajectory-time analysis of parachute recovery systems.

5.4.5 Effect of Canopy Loading, $W/(C_D S)_p$, on Parachute Opening Forces

Figure 5-43 is a force-time diagram of a parachute opening in a wind tunnel. This pattern is typical for parachutes without velocity decay during parachute inflation and is called the "infinite mass" condition, because the parachute acts as if it were attached to an infinite mass.

The same parachute dropped from an airplane and weighted for a 20 ft/s rate of descent will have the known force-time diagram of a personnel parachute (Figure 5-44).

The personnel parachute dropped from an airplane has a finite load and is referred to as being tested, or used, under a "finite mass" condition. The primary difference between infinite and finite mass conditions is that, under infinite mass conditions, the velocity does not decay during parachute opening; whereas, under finite mass conditions, the velocity during

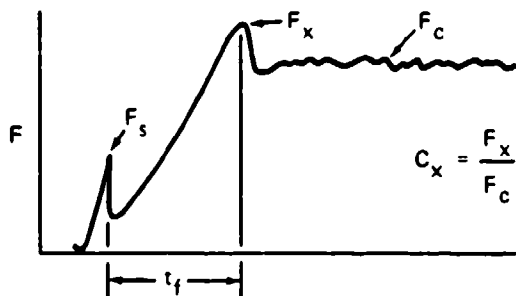


FIGURE 5-43. Parachute Force Versus Time for a Wind-Tunnel Test (Infinite Mass Condition).

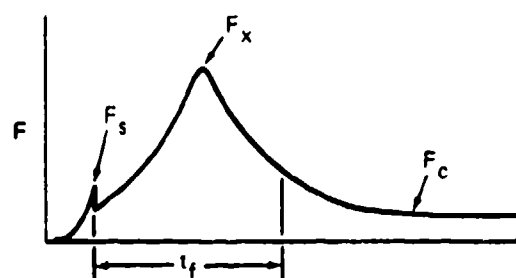


FIGURE 5-44. Force Versus Time for a Personnel Parachute Drop (Finite Mass Condition).

parachute opening decreases substantially. Infinite and finite mass conditions can also be defined as conditions of high and low canopy loading, $W/(C_{DS})_p$.

An additional typical difference between infinite and finite mass conditions is the location of the peak opening force, F_x . For a parachute opened under infinite mass conditions, or high canopy loading, peak opening force occurs at the first full canopy inflation. The peak opening force of a parachute opened at a finite mass condition will occur long before the parachute canopy is fully open.

The relationship of the peak opening force, F_x , to the steady-state drag force, F_c , in wind-tunnel tests is defined as

$$\text{Opening-force coefficient, } C_x = \frac{F_x}{F_c} \text{ (see Figure 5-43).}$$

C_x is a constant for a specific parachute type, as shown in Tables 5-1 through 5-5.

With the newly defined opening-force coefficient, C_x , the equation for the parachute force can be written

$$F_x = (C_{DS})_p q C_x X_1$$

where

$(C_{DS})_p$ = the drag area of the fully open parachute, ft^2

q = the dynamic pressure at line (canopy) stretch, lb/ft^2

C_x = the opening force coefficient at infinite mass, dimensionless

X_1 = opening-force-reduction factor, dimensionless.

The force-reduction factor, X_1 , is 1.0 for a parachute opened at the infinite mass condition; close to 1 for high canopy loading drogue chutes (close to the infinite mass condition); and as low as 0.02 for final descent parachutes with a low canopy loading (finite mass).

Table 5-7 shows the difference in opening forces and X_1 factor for a 28-foot-diameter parachute opened at 180 KEAS behind an aircraft as a landing deceleration parachute; behind an ordnance device such as a bomb, mine, or torpedo for retardation; and as personnel parachute for an aviator. The difference in the force reduction factor X_1 for the three applications is surprising. The primary reason for this effect is the difference in velocity decay during the parachute opening process.

Figure 5-45 shows the force-time record of a 15.6-foot-diameter ringslot parachute opened behind a B-47 bomber at a 30,000-foot altitude. This parachute, used as an approach brake for descent from high altitude, has a canopy loading close to infinite mass condition, resulting in an X_1 factor of 1.0.

TABLE 5-7. Opening Forces and Canopy Loading of a 28-Foot-Diameter Parachute for Various Vehicle Applications.

Application	Vehicle weight, lb	$(C_D S)_p, \text{ft}^2$	$W/(C_D S)_p, \text{lb}/\text{ft}^2$	C_x	F_x, lb	X_1	Mass condition
Aircraft	140,000	490	286	1.7	91,200	1.0	Infinite
Ordnance	2000	490	4.1	1.7	30,100	0.33	Intermediate
Personnel	250	490	0.51	1.7	2900	0.032	Finite

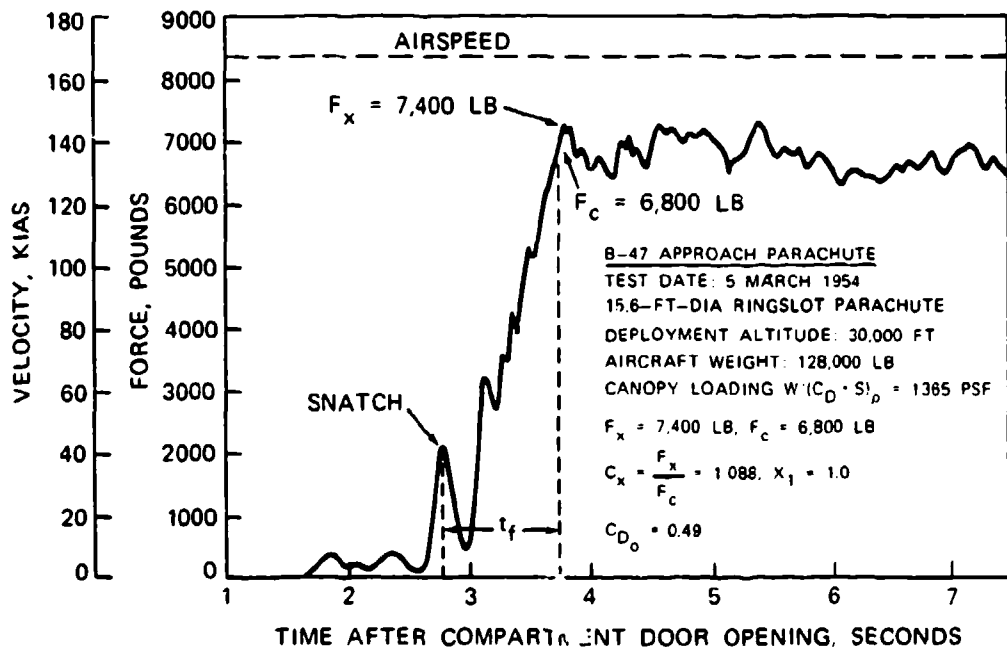


FIGURE 5-45. 15.6-Foot-Diameter Ringslot B-47 Approach Parachute Opening Forces.

The clean, aerodynamic configuration of the B-47 bomber produced a shallow approach angle, making a point landing difficult. A 15.6-foot-diameter ringslot parachute was used instead of wing brakes or spoilers to increase the drag on approach and thereby steepen the glide angle. At touchdown, a 32-foot-diameter ribbon parachute was deployed as a deceleration parachute side-by-side with the ringslot parachute. Deploying the parachutes at even skirt levels assured successful opening of the second parachute. Note that the aircraft velocity does not decay during parachute inflation.

Figure 5-46 shows the opening process and the opening force versus time for a 29-foot-diameter, guide surface personnel parachute tested at 250 knots at the El Centro, Calif., whirl tower. The difference in the force-versus-time diagram, with the ringslot

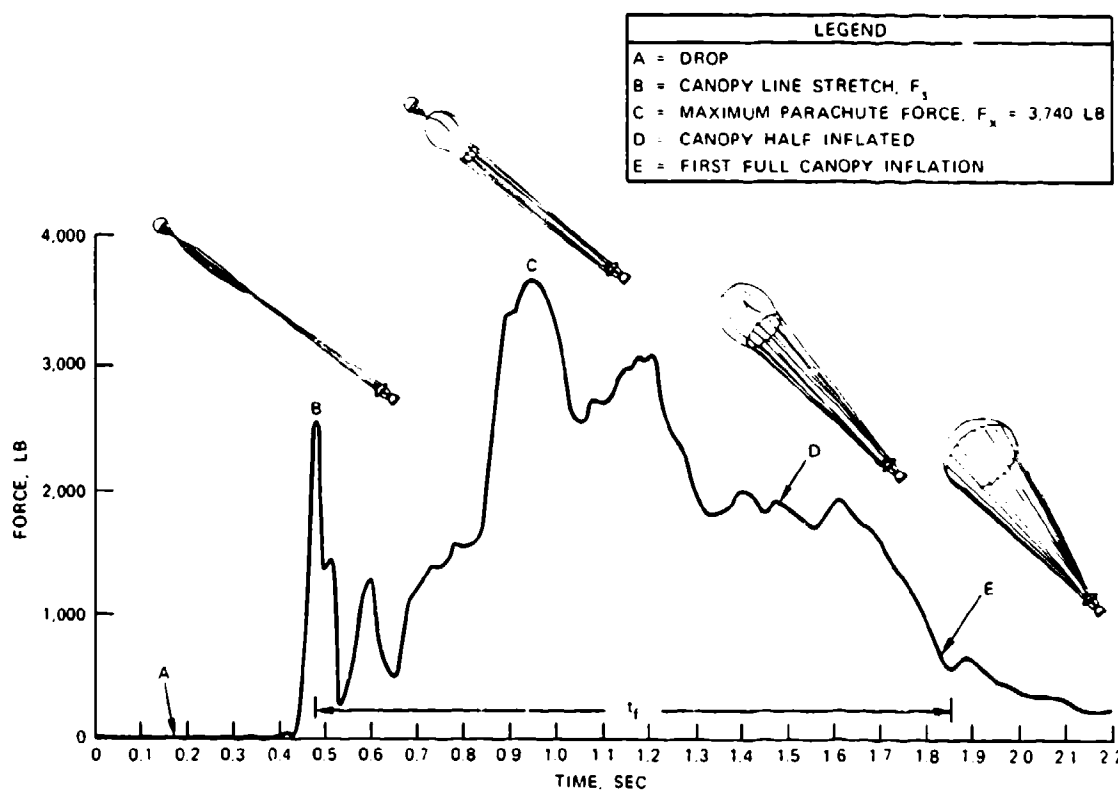


FIGURE 5-46. Opening Process and Opening Force Versus Time for a Guide Surface Personnel Parachute Tested at the El Centro Whirl Tower at 250 Knots With a 200-Pound Torso Dummy.

parachute opened behind the B-47 aircraft, is obvious. The maximum opening force, F_x , occurs when the parachute canopy has reached about one-third of its inflated diameter. The force at full open canopy has decreased to about 600 pounds, indicating that parachute velocity during opening has decreased almost to equilibrium velocity. The velocity decay during opening results in an opening-force-reduction factor, X_1 , of 0.0239.

Another important characteristic is the relative size of the snatch force. On high canopy loading parachutes, where the parachute mass is small compared to the mass of the vehicle to be decelerated, the snatch force is small if the deployment system is good, as described in Chapter 6. On low canopy loading parachutes, where the mass of the parachute can be 3 to 7% of the mass to be decelerated, the snatch force can reach or surpass the maximum opening force unless a proper deployment method is used.

All parachute applications fall into distinctive groups of canopy loading, $W/(C_{DS})_p$. Canopy loading is equivalent to dynamic pressure at equilibrium velocity and therefore relates to rate of descent. Figure 5-47 shows this relationship.

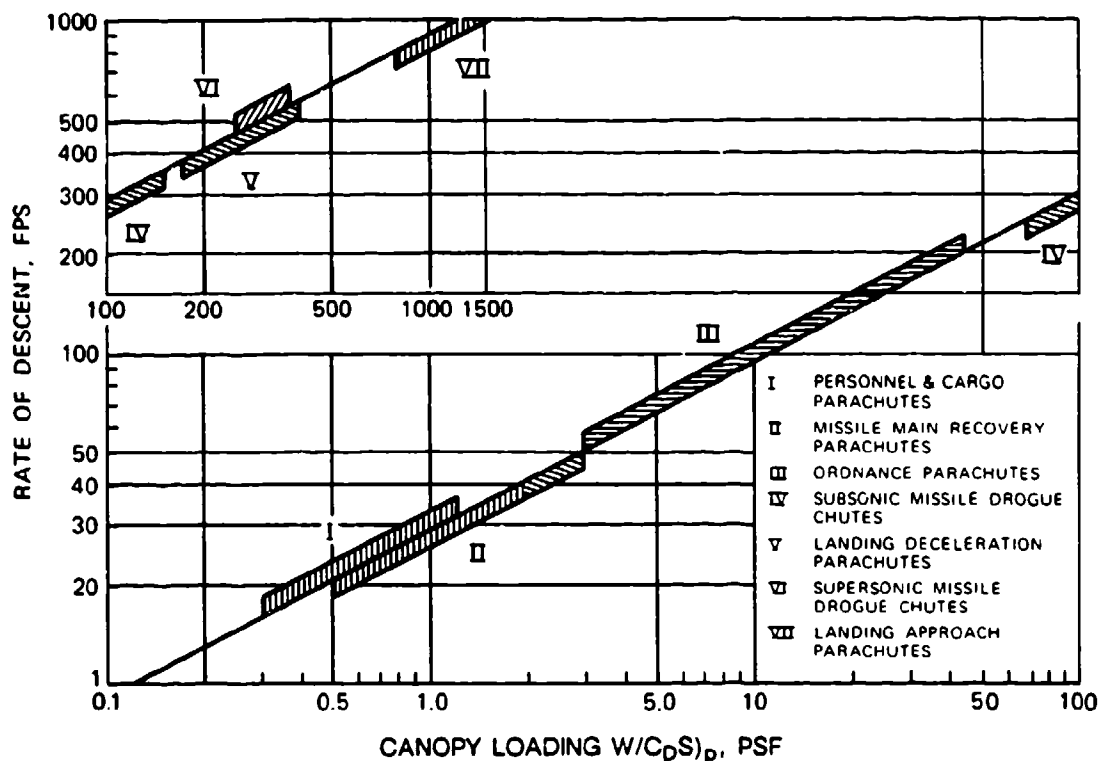


FIGURE 5-47. Rate of Descent Versus Canopy Loading and Parachute Applications.

The seven application groups in Figure 5-47 can be combined into three groups in relation to the force-reduction factor, X_1 . Groups I and II will have X_1 factors in the 0.02- to 0.25-range (personnel and cargo) parachutes. Group III (ordnance) parachutes have X_1 factors in the 0.3 to 0.7 range. These parachute groups operate at finite mass conditions. All parachutes in Groups IV to VII have X_1 factors close to or equal to 1.0 and operate at infinite mass conditions.

5.4.6 Methods for Calculating Parachute Opening Forces

Three methods for calculating parachute opening forces are discussed in this section. Method 1, the $W/(C_{DS})_p$ method, is fast but should be used for preliminary calculations only. Method 2, the Pflanz method, is mathematically exact and provides good results within certain application limits. Method 3, the previously mentioned computerized force-trajectory-time method, gives good results with no limitations. However, all three methods require knowledge of certain parachute and opening-process characteristics.

Method 1, $W/(C_{DS})_p$ Method. The equation for the parachute opening force, F_x , was defined in section 5.4.5 as

$$F_x = (C_{DS})_p q C_x X_1$$

where

$(C_{DS})_p$ = the drag area of the full open or reefed parachute, ft²

q = the dynamic pressure at line stretch or disreef, lb/ft²

C_x = the opening-force coefficient at infinite mass, dimensionless (Tables 5-1 through 5-5). Do not use C_x at low canopy loading

X_1 = the force-reduction factor (the unknown factor in this equation), dimensionless

For an unreefed parachute, the drag area, $(C_{DS})_p$, of the full open parachute is used. For a reefed parachute, a preliminary reefed drag area, $(C_{DS})_r$, can be calculated from the allowable maximum parachute force, F_x , and the dynamic pressure at line stretch:

$$(C_{DS})_R = \frac{F_x}{q C_x X_1}$$

For this preliminary calculation, an opening-force coefficient, C_x , of 1.0 should be used for the reefed parachute. The force-reduction factor, X_1 , can be estimated as 1.0 for reefed drogue chutes and 0.9 for reefed main parachutes.

For the actual force calculations for unreefed parachutes, the force coefficient in Tables 5-1 through 5-5 applies. Reefed parachutes have different opening-force coefficient factors for the reefed and disreefed stages. Figures 5-41 and 5-42 show the drag-area-versus-time diagrams for a reefed ringsail and a reefed triconical parachute. There is no drag overshoot for both parachutes when they open in the reefed stage. Therefore, the opening-force coefficient is 1.0. If evaluations from previous tests are not available, a C_x coefficient of 1.1 should be used. For the disreef stage, the force coefficient evaluated from test data should be used, if available; otherwise, Tables 5-1 through 5-5 will provide acceptable data.

For obtaining the opening-force reduction factor, X_1 , the canopy loading of the full open or the individual reefed stages is calculated and the appropriate X_1 factor as a function of canopy loading is found in Figure 5-48.

The amount of parachute force fluctuation in the wake of the forebody must be considered when calculating the opening force of a small drogue chute behind a large forebody. This fluctuation is illustrated in Figure 5-49, which shows the effect of the Apollo space capsule's wake on the opening force of the 16.5-foot-diameter ribbon drogue chute (Reference 5.10).

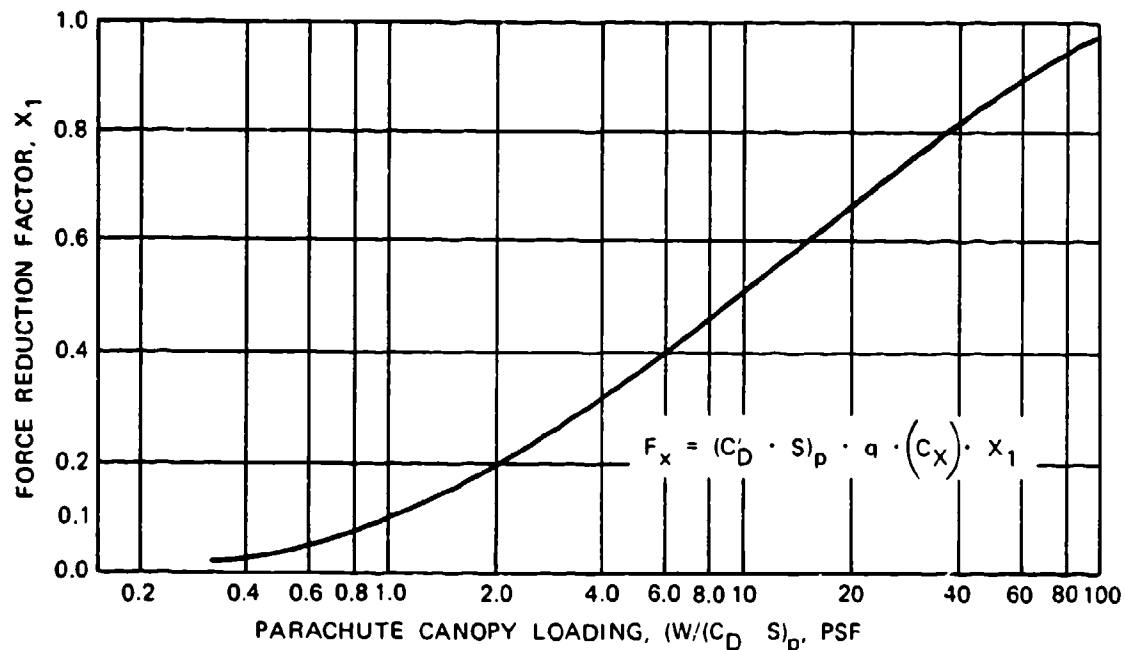
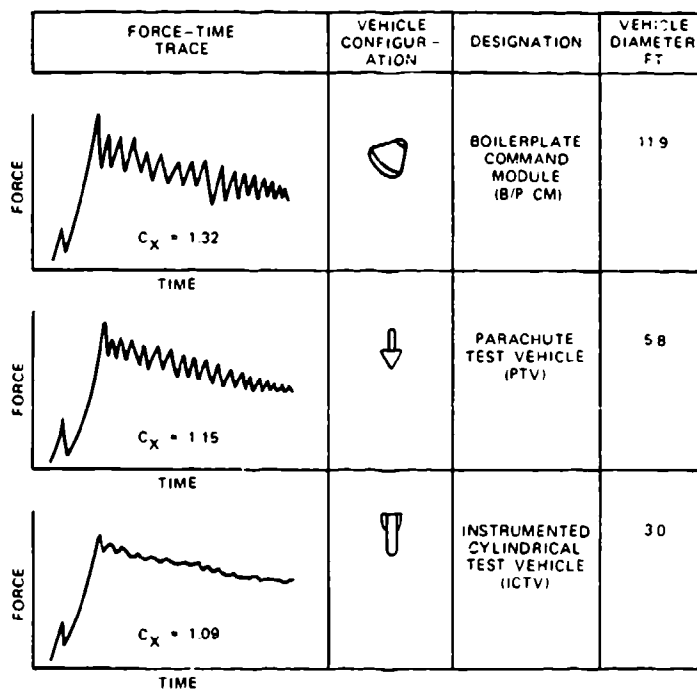


FIGURE 5-48. Opening-Force Reduction Factor Versus Canopy Loading.

FIGURE 5-49. Apollo Ribbon Drogue Chute Force Fluctuation Caused by Forebody Wake (Inflated Parachute Diameter, D_p , is 10.7 feet).

The increase in load fluctuation from the small ICTV to the large-diameter boilerplate command module (B/P CM) is apparent in the increase of the force coefficient, C_x , from 1.09 to 1.31. The force coefficient in Figure 5-49 is actually the product C_x times X_1 , called C_k . However, at the canopy loading of the drogue chute, X_1 will be close to 1.0, approaching the infinite mass condition.

The X_1 factor can be obtained from drop tests by calculating

$$X_1 = \frac{F_x}{(C_{DS})_p q}$$

and then plotting it versus $W/(C_{DS})_p$. The data in Figure 5-48 were obtained by this method. The X_1 factor in Figure 5-48 does not include the effect of altitude. Opening forces of high-canopy-loading parachutes change little with altitude. However, the effect of altitude on low-canopy-loading parachutes, such as personnel parachutes, is considerable. For low-canopy-loading parachutes, the X_1 factors should be used only for altitudes below 15,000 feet. Section 5.5 contains a discussion of the altitude effect on parachute forces.

Ewing evaluated and plotted the $C_k = C_x X_1$ factor from numerous tests of ringsail parachutes (Reference 5.50).

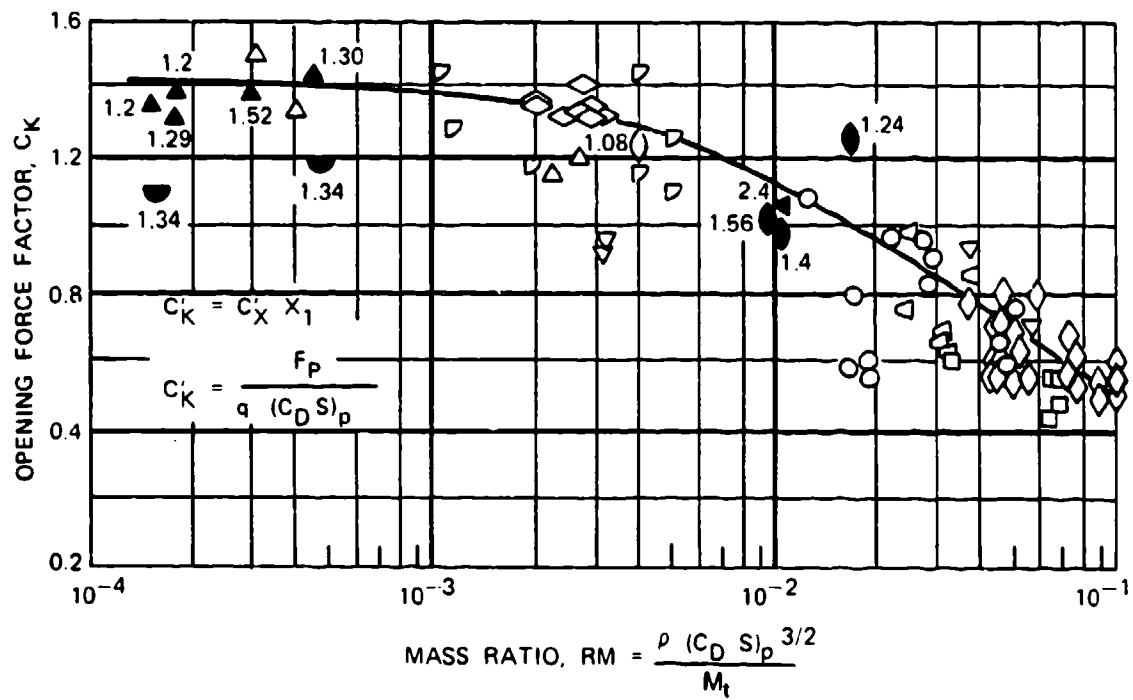
French recommends plotting a $C_k = C_x X_1$ factor versus a mass parameter in the form D_o^3/m , where D_o is the nominal diameter of the parachute and m is the mass of the vehicle and the parachute assembly (Reference 5.80).

Schilling recommends modifying this mass parameter to the form

$$R_m = \frac{\rho (C_{DS})_p^{3/2}}{m_t}$$

where m_t is the total mass of vehicle plus decelerator, ρ is the air density, and $(C_{DS})_p$ is the parachute drag area (Reference 5.81). The value $\rho \cdot (C_{DS})_p^{3/2}$ represents the volume of the air in and around the parachute canopy and has an obvious relationship to the apparent mass. The altitude effect is now included in plotting C_k factors versus this mass parameter, R_m . Figure 5-50, taken from a Northrop publication, shows C_k factors for reefed and unreefed ribbon and ringslot parachutes plotted versus the mass parameter. These data include supersonic deployment of ribbon parachutes.

Method 2, Pflanz Method. The Pflanz method was developed in Germany during World War II by E. Pflanz in cooperation with the author. It was based on the following concept. A body of known fixed weight and velocity is decelerated along a horizontal flight path by an aerodynamic drag device whose drag area increases from a small value to 100% in a known, mathematically definable form. This method is mathematically exact; however, no $(C_{DS})_p$ overshoot is included at the start of the reefed or disreefed inflation cycle. Details of this method may be found in References 5.76 and 5.77.



SYMBOL	PARACHUTE DATA				FOREBODY
	TYPE	D_0 , FT	REEFING RATIO	DEPLOY METHOD	
◊	APOLLO CONICAL RIBBON DROGUE	13.7	0.308	MORTAR	BUFF
◊	APOLLO CONICAL RIBBON DROGUE	16.5	0.428	MORTAR	BUFF
◊	ADDPEP HEMISFLO	16.0	0.22-0.41	CANISTER	STREAMLINED
◊	MERCURY CONICAL RIBBON	6.87	0.87	MORTAR	STREAMLINED
◊	SANDIA CONICAL RIBBON	20.0	0.186	DROGUE GUN	STREAMLINED
◊	COOK CONICAL RIBBON	84.4	0.20-0.30	PILOT CHUTE	STREAMLINED
◊	UAR RINGSAIL	20-30	0.16-0.31	PILOT CHUTE	STREAMLINED
◊	CENTURY RINGSAIL	128	0.125	PILOT CHUTE	STREAMLINED
◊	ASSET RINGSAIL	29.6	0.10-0.20	PILOT CHUTE	STREAMLINED
◊	APOLLO BLK II HEAVY RINGSAIL	83.5	0.08	FLOT CHUTE	STREAMLINED
◊	APOLLO BLK I AND II RINGSAIL	83.5	0.095	PILOT CHUTE	STREAMLINED

FILLED SYMBOLS INDICATE SUPERSONIC PARACHUTE DEPLOYMENT. NUMBERS ADJACENT TO DATUM POINTS IDENTIFY MACH NO. AT PARACHUTE LINE STRETCH

FIGURE 5-50. Opening-Force Factor Versus Mass Ratio.

A dimensionless ballistic parameter, A, is formed from known or calculated data

$$A = \frac{2W_t}{(C_{DS})_p \rho g v_1 t_f}$$

where

A = ballistic parameter, dimensionless

W_t = system weight, lb

(C_{DS})_p = parachute drag area, reefed or fully open, ft²

g = acceleration of gravity, ft/s²

v₁ = velocity at line stretch or start of disreef, ft/s

ρ = air density at altitude of parachute inflation, slugs/ft³

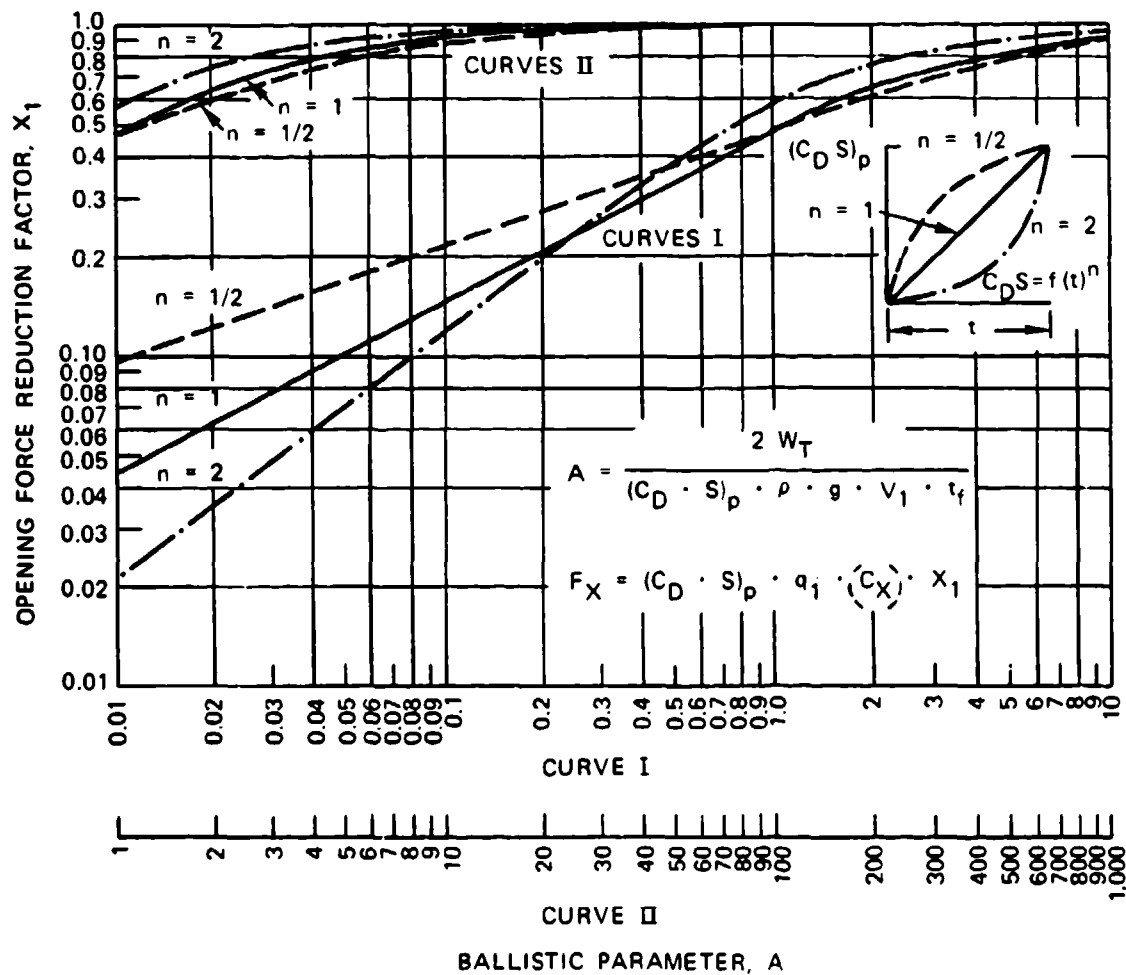
t_f = canopy inflation time

W_t, q, ρ are fixed values for each specific application, as is the drag area of the fully open parachute, (C_{DS})_p. A preliminary drag area of the reefed parachute, (C_{DS})_r, can be calculated as described in Method 1. The reefed filling time, t_{f1}, and the canopy disreefing time, t_{f2}, are calculated by the method given in section 5.4.3. After calculating the ballistic parameter, A, the force-reduction factor, X₁, is obtained from Figure 5-51. However, before determining X₁, the shape of the drag area increases versus time must be determined for the selected parachute. This drag-area-versus-time rise is denoted in Figure 5-51 by the letter n. The n = 1 curve is a straight line, typical for ribbon and ringslot parachutes. The concave curve, n = 2, is representative of solid cloth, flat circular, conical, extended-skirt, and triconical parachutes described in section 5.4.4. The convex form of (C_{DS})_p versus time occurs only in the reefed inflation of extended-skirt parachutes. Refer to the comments on the C_x factor of Method 1 for low-canopy-loading, unreefed parachutes.

The Pflanz report provides extensive information on forces, time of maximum force, and velocity decay versus time during the parachute inflation process for a variety of drag-area-versus-time increases other than those shown in Figure 5-51.

After the force factor, X₁, is determined from Figure 5-51, the opening force of the parachute is calculated as it was in Method 1

$$F_p = (C_{DS})_p q_1 (C_x) X_1, \text{ lb}$$

FIGURE 5-51. Opening-Force Reduction Factor, X_1 , Versus Ballistic Parameter, A .

where

$(C_D S)_p$ = the drag area of the fully open or reefed parachute

q_1 = the dynamic pressure at the start of inflation or at disreef

C_x = the opening-force coefficient for the reefed or unreefed parachute. To be used only for high canopy loading conditions

X_1 = the force-reduction factor determined from Figure 5-51

Frequently, a velocity decay occurs between vehicle launch and canopy (line) stretch, V_1 . This decay can be calculated for deceleration in a horizontal plane

$$V_1 = \frac{V_0}{1 + \left[\frac{(C_D S)_p \rho g t_f V_0}{2 W} \right]}$$

where

V_0 = velocity at the beginning of deceleration. All other notations are similar to those previously used

The second Pflanz report (Reference 5.77) expands on the first report by determining parachute forces and velocity versus time for straight-line trajectories of 30, 60, and 90 degrees.

Ludtke, in References 5.83 and 5.84, has somewhat generalized the Pflanz method and has included determination of parachute opening forces from deployment of any trajectory angle.

Method 3, Force-Trajectory-Time Method. The force-trajectory-time method is a computer approach to the parachute opening process. The recovery-system specification for an air vehicle, drone, missile, or aircrew escape system normally defines the starting and ending conditions of the recovery cycle, including weight of the vehicle, starting altitude, velocity, vehicle attitude; and for final recovery or landing, the specification defines the rate of descent at landing and the oscillation limitation. The maximum allowable parachute force is frequently expressed in g as a multiple of the vehicle weight. A typical requirement limits the parachute opening force to 3 to 5 g , necessitating a multiple-stage recovery system consisting of a reefed drogue chute and one or more reefed main parachutes.

These conditions require optimization of the total recovery cycle for minimum recovery time, altitude, and range within the allowable parachute force restraints. The computer, with its multiple-run capability that permits many variations in staging, timing, and altitude, is the ideal tool to accomplish this task.

A force-trajectory program best meets the above requirements for calculating the vehicle trajectory and deceleration as well as parachute forces as a function of time. The basic approach is somewhat similar to the Pflanz method. A drag-area-versus-time profile is formed for the total system vehicle plus decelerator. Multiple computer runs are made using the trajectory equations in section 5.4.1. The typical drag area for a main parachute-vehicle system is shown in Figure 5-52. This profile is used in Chapter 7 for dimensioning the main parachute assembly of a reconnaissance drone. Items that must be preselected are the drag area of the main descent parachute(s); the transfer velocity from the drogue chute to the main parachute(s); the filling times for the various parachute stages, reefed and disreefed; and a preliminary staging-timing sequence. The computer run will immediately determine whether the timing and staging are too short, too long, or correct for the force and altitude limitations.

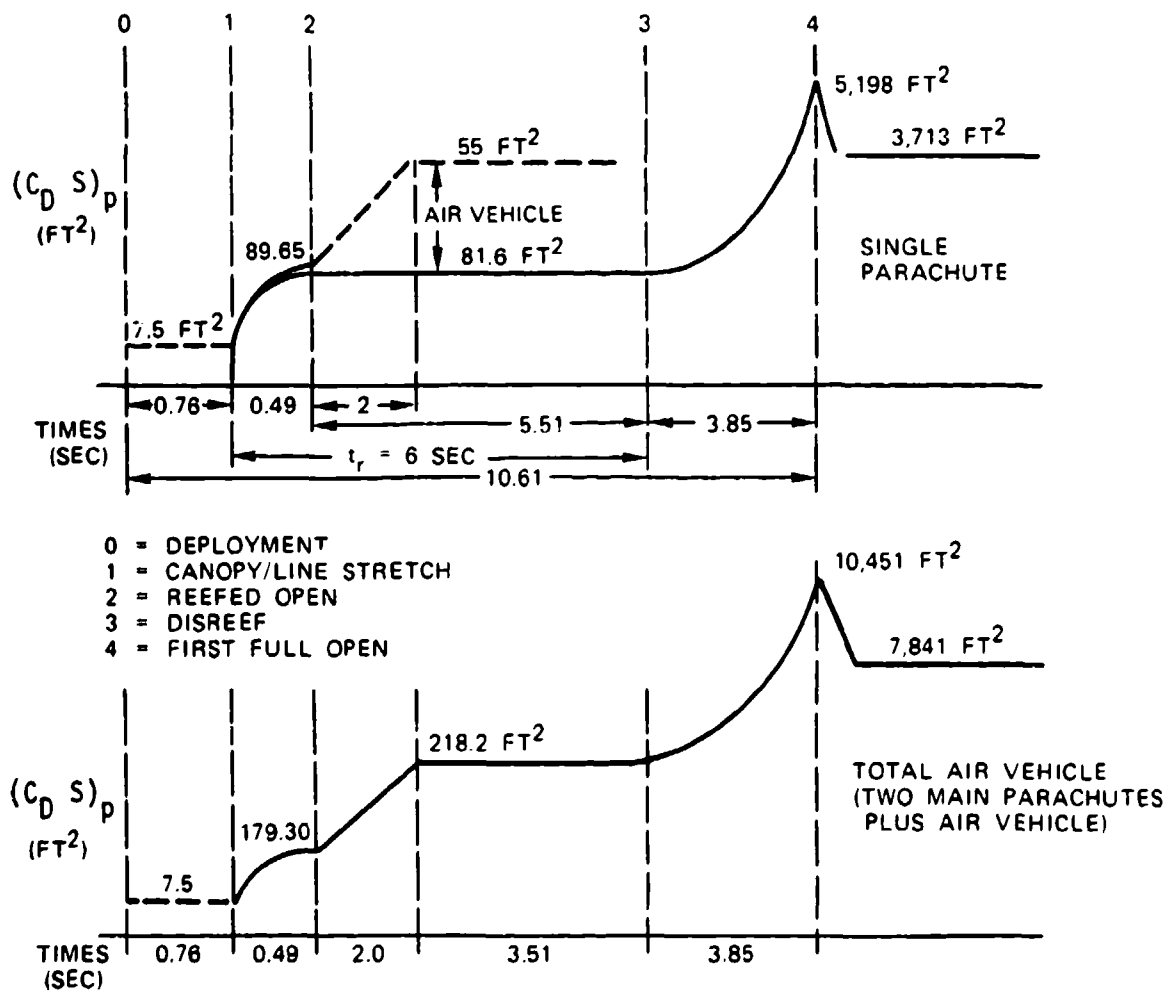


FIGURE 5-52. Drag-Area Profile for Parachute Inflation Sequence.

In addition to adjusting for force and altitude requirements, the computer program can easily investigate the effect of changing canopy fill time and slope of the drag-area-versus-time profile on parachute forces. If test data are available, the program can be fine-tuned to a high degree. It is even possible to include the snatch force in the form of a drag-area profile. A special computer program for calculating the deployment cycle and the snatch force is described in Reference 5.86. This program may be extended to include filling-time calculations by introducing the fill distance rather than the fill-time concept.

Figure 5-52 profiles the parachute drag-area-versus-time profile for a 4800-pound reconnaissance drone using a 7.2-foot-diameter conical ribbon drogue chute for high-speed deceleration, and two 72.8-foot-diameter conical, full-extended-skirt parachutes for final

recovery. The parachutes are used in conjunction with air bags for impact attenuation. The two main parachutes are deployed at altitudes up to 7000 feet in a vertical vehicle attitude after descending from higher altitude on the drogue chute. Maximum deployment velocity for the main parachute is 375 ft/s. This deployment condition assumes an emergency where recovery is initiated at high speed and high altitude. Normal recovery after mission completion will begin from a horizontal vehicle attitude at 2000 feet above ground and with a velocity below 375 ft/s, bypassing the drogue-chute-deceleration phase.

The upper part of Figure 5-52 shows the drag-area profile for a single main parachute. The drogue chute is disconnected at point zero, and main parachute deployment is initiated. During this time, the vehicle will accelerate while in a vertical attitude or decelerate while in a horizontal attitude. At point 1, canopy and suspension lines are stretched, inflation in the reefed stage begins, and the reefing cutters are initiated for a preselected reefing time. At point 2, the parachute is fully open in the reefed position; disreef begins at point 3. At this time, the pull of the main parachute, which is attached at the vehicle center of gravity with a V-riser for horizontal landing, may cause the vehicle, previously descending on the drogue chute in a vertical attitude, to change to a 90-degree attitude. A 90-degree attitude provides additional drag for deceleration of the vehicle, as indicated by the dotted line. The drag-area overshoot after full parachute inflation depends on the type of parachute used and its reefing conditions.

The lower drag-area curve in Figure 5-52 represents the total system: two main parachutes and the air vehicle. The individual parachute force is half the total calculated force if both parachutes open simultaneously and uniformly. Fast-opening parachutes often create a lead-lag chute condition. Reference 5.78 describes the calculation of opening forces for this condition.

5.4.7 Typical Parachute Opening-Force and Opening-Time Diagrams

Figure 5-53 compares opening forces versus velocity for the standard 28-foot-diameter personnel parachute; the aeroconical parachute used in the Martin-Baker Mark-10 ejection seat; the Irving-developed automatic inflation modulation (AIM) parachute; and the reefed, 28-foot-diameter personnel parachute used for the McDonnell-Douglas ACES II ejection seat.

Figure 5-54 documents the effect of a good deployment system, comparing snatch forces, F_s , and opening forces, F_x , for the standard 28-foot-diameter personnel parachute. Parachutes without quarter deployment bags (subscript 1) and with quarter deployment bags (subscript 2) are represented. The snatch force of the parachute without a deployment bag varies excessively and exceeds the opening forces. Use of the quarter deployment bag decreases the magnitude and the wide spread of the snatch force. The average opening force, F_x , is almost equal for both deployment systems (Reference 5.94).

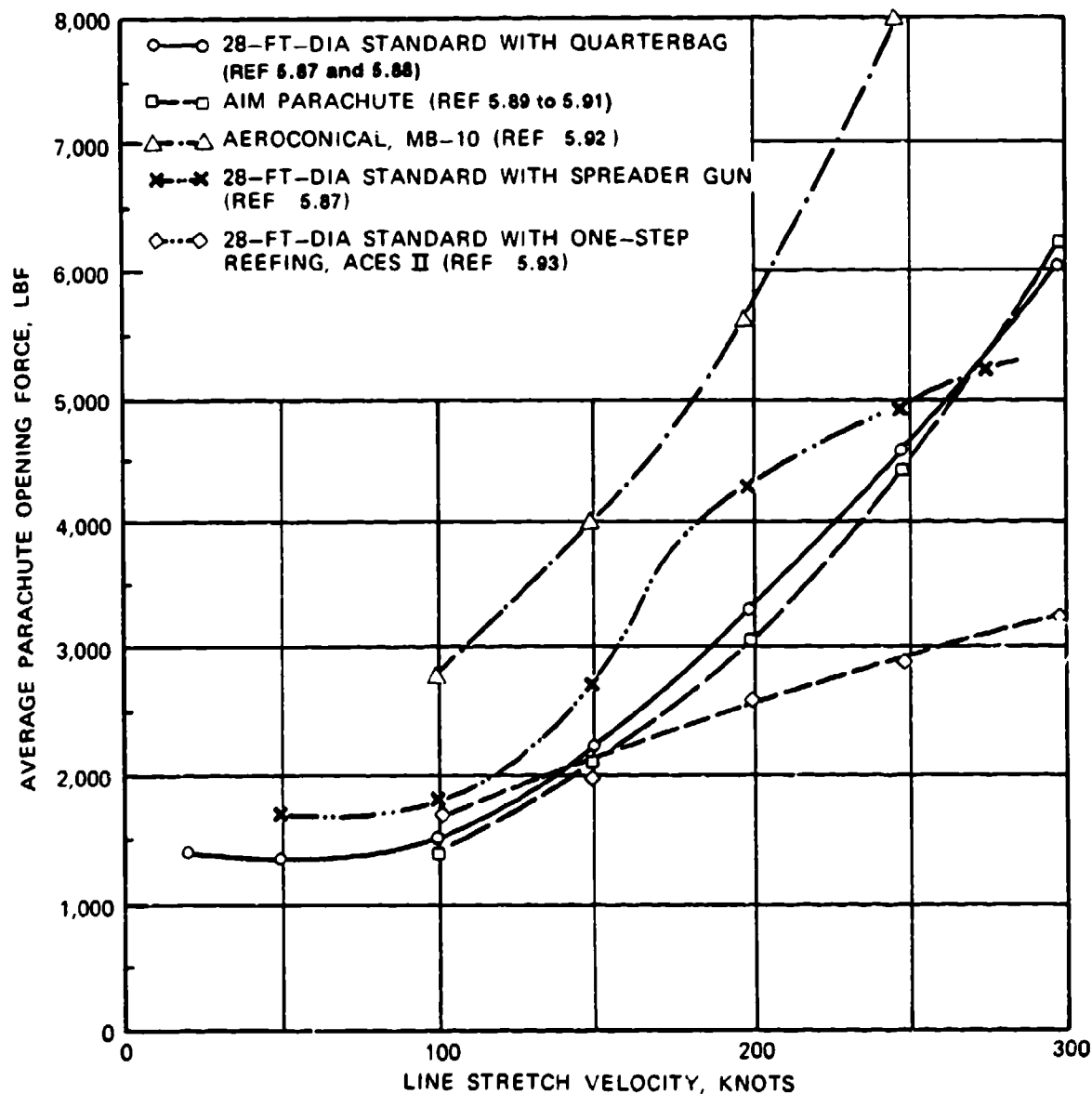


FIGURE 5-53. Opening Forces of Various Personnel Parachutes.

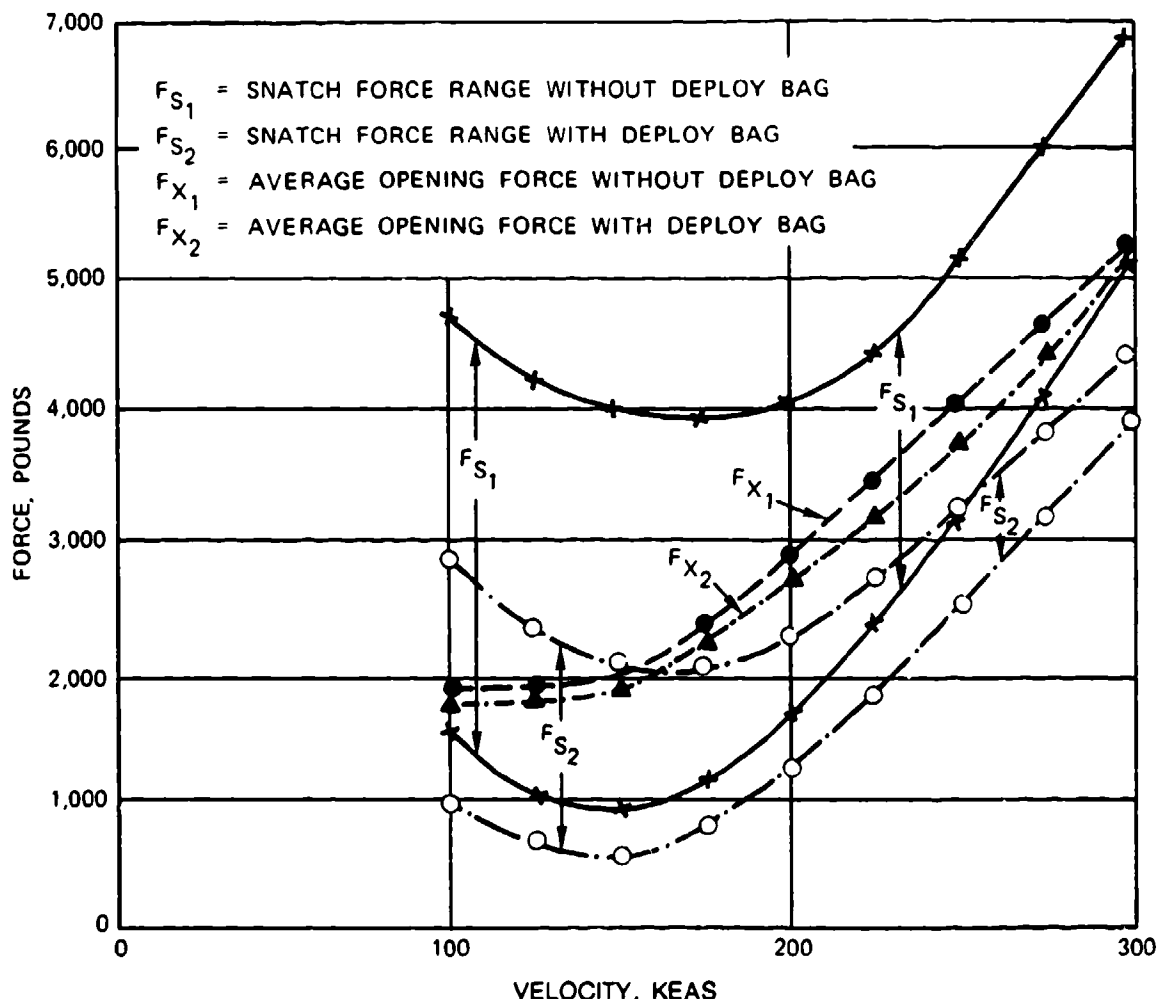


FIGURE 5-54. Snatch Force and Opening Force of the Air Force 28-Foot-Diameter Personnel Parachute, With and Without Quarter Deployment Bag.

Many methods have been investigated to decrease the parachute opening time, defined as the time from pack opening to first full open canopy. Figure 5-55 compares the opening time of the standard 28-foot-diameter personnel parachute with those of a 28-foot-diameter parachute equipped with pull-down vent lines (PDVL) and of a 28-foot-diameter personnel parachute equipped with a ballistic spreader gun (Reference 5.95). Both modified versions show shorter opening times in the 100- to 300-ft/s velocity range.

Changes that are advantageous in one area frequently result in deficiencies in another. In the case of the PDVL and the spreader gun, the changes result in higher snatch forces.

The force characteristics of reefed parachutes are shown in Figure 5-56, which plots the reefed and disreefed opening forces versus the opening velocity of a single, 88-foot-diameter

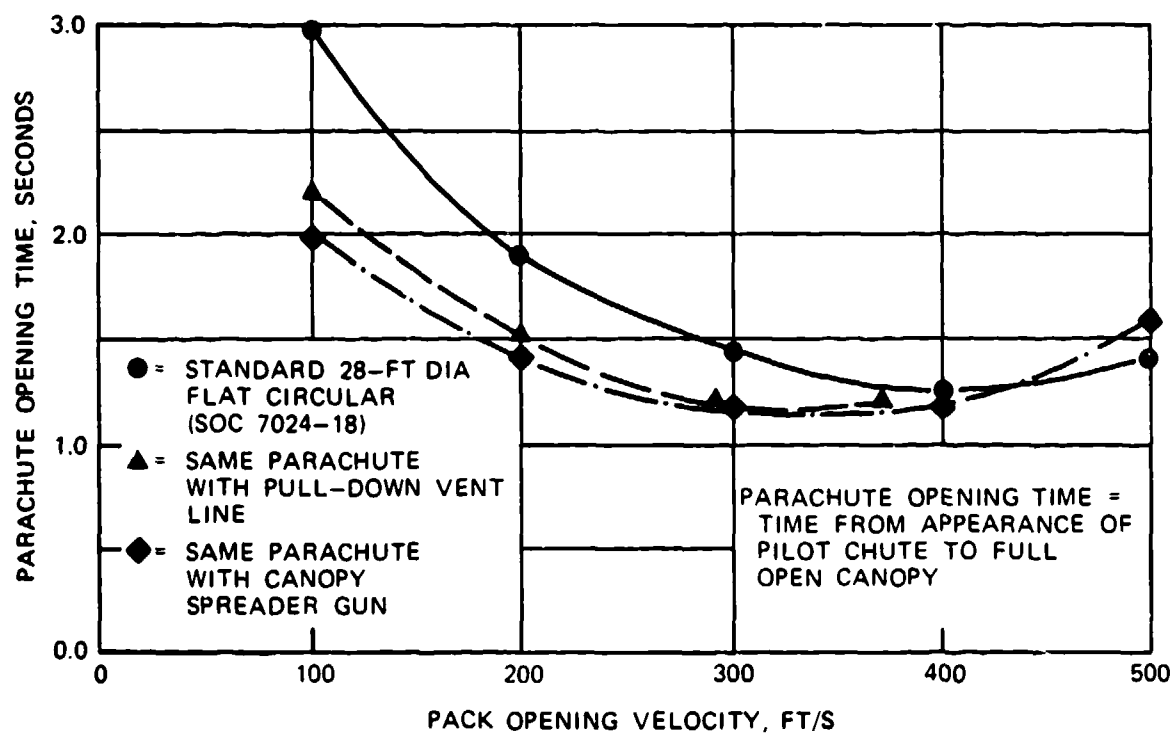


FIGURE 5-55. Opening Time Comparison of Three Configurations of the 28-Foot-Diameter Personnel Parachute: Standard, Standard With Pull-Down Vent Line, and Standard with Spreader Gun.

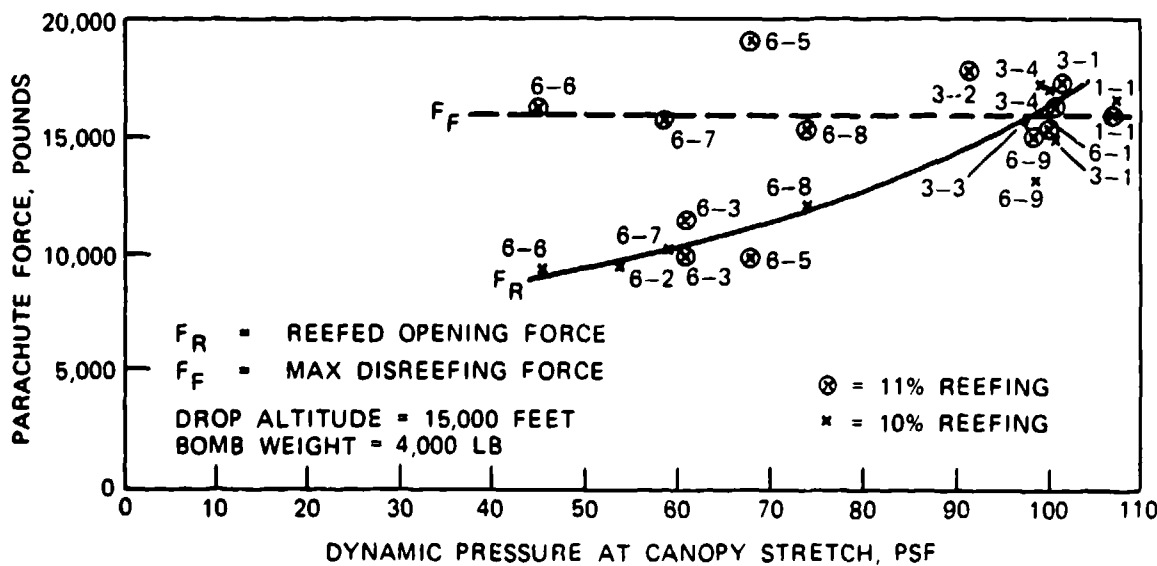


FIGURE 5-56. Apollo Command Module, Block I, Reefed and Disreefed Opening Forces for a Single 88-Foot-Diameter Ringsail Parachute.

Apollo Block I spacecraft main parachute. The reefed opening force, F_r , increases with velocity, whereas the disreefed force, F_f , remains constant, indicating that the reefing time is sufficiently long for the reefed parachute to reach its terminal velocity before disreef. Both force lines should meet at the point of maximum required velocity to give the best force and stress balance and, in return, the minimum-weight parachute assembly. The diagram illustrates another important point: if overload tests are required to demonstrate a margin of safety in the parachute design, only the reefed stage is overload-tested. Even in higher-velocity tests, the reefed parachute would probably reach its final velocity and the disreefed force would not increase.

This situation raises the question of how to conduct overload tests. The reefed parachute stage can be tested by increasing the test velocity to the desired level. The disreefed stage can be tested either by decreasing the reefing ratio of the reefed stage or by increasing the weight of the test vehicle. Both measures will increase velocity before disreef. For the Apollo program's extensive overload testing, the overweight method was selected because it did not change the end-item configuration of the parachute assembly. Three levels of testing were conducted on the Apollo parachute system. Level I used two drogue and three main parachutes to test the parachute forces expected at a normal landing after mission completion. Level II demonstrated the maximum design load occurring in a high-altitude abort case, with only one drogue and two main parachutes operating to a specification requirement. Level III demonstrated an overload capability of 1.35 against maximum design load. Figure 5-57 shows tests conducted on a single reefed drogue chute and a single main parachute reefed in two steps.

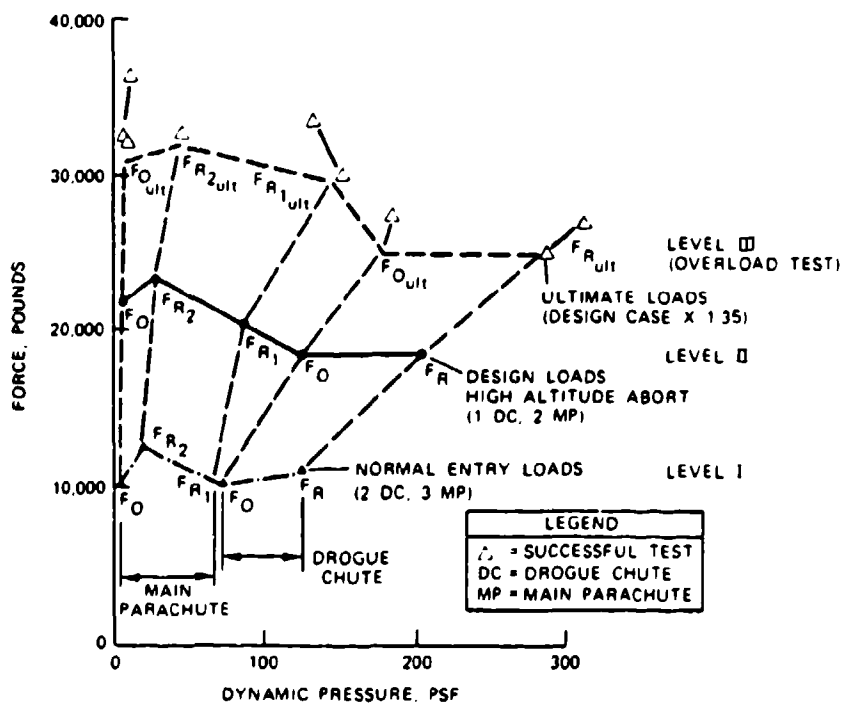


FIGURE 5-57. Apollo Command Module Single Drogue Chute and Main Parachute Test Envelope.

A recommended nomenclature for the parachute opening process is shown in Figure 5-58. Uniform definition of the various opening phases is important in verbal and written communication, especially in reports, so that the performances of different types of parachutes can be compared. Many reports fail to properly define filling time, deployment time, and other times essential for comparing opening characteristics.

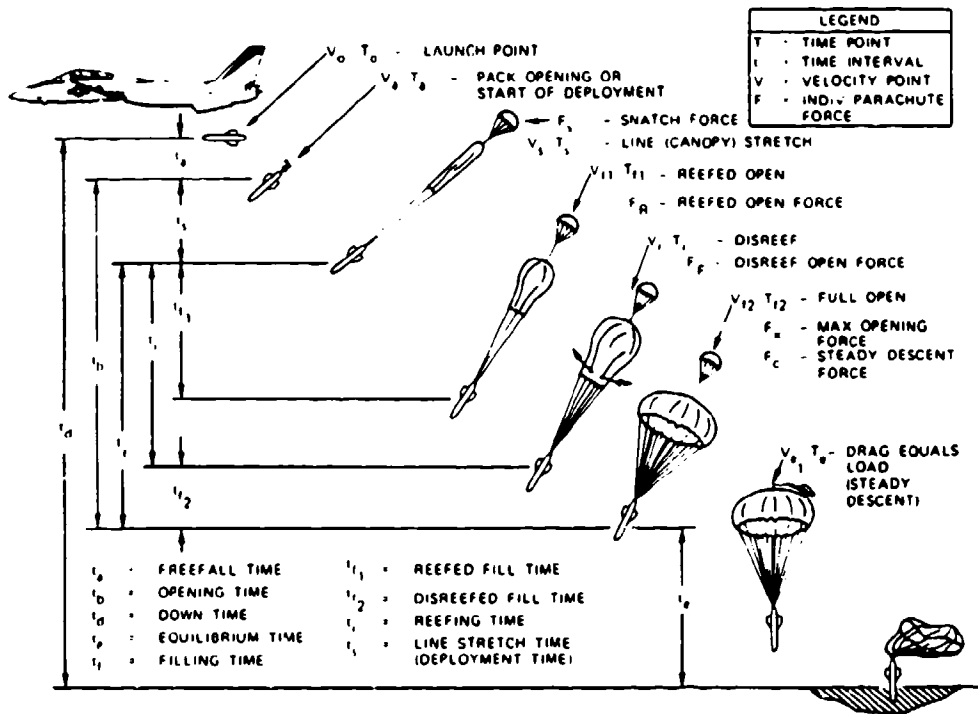


FIGURE 5-58. Nomenclature for Parachute Inflation Sequence.

5.5 ALTITUDE AND CANOPY-POROSITY EFFECTS

5.5.1 Altitude Effects

In 1944 the U.S. Army Air Corps conducted tests with five types of silk and nylon personnel parachutes dropped at indicated air speeds of 115 mph—the equilibrium velocity of a 200-pound torso dummy—and altitudes of 7000, 15,000, 26,000, and 40,000 feet. To the great surprise of the technical community, the parachute opening forces at 40,000 feet were about four times greater than the forces measured at 7000 feet, even though all parachutes were opened at the same dynamic pressure (indicated air speed). A second surprise was that nylon parachutes had considerably lower opening forces than the silk parachutes that were in extensive use at that time. Figure 5-59 shows the results of these tests (Reference 5.96).

The explanation for this force increase with altitude is that the true velocity is twice as high at 40,000 feet than at sea level for parachutes dropped at constant indicated air speed.

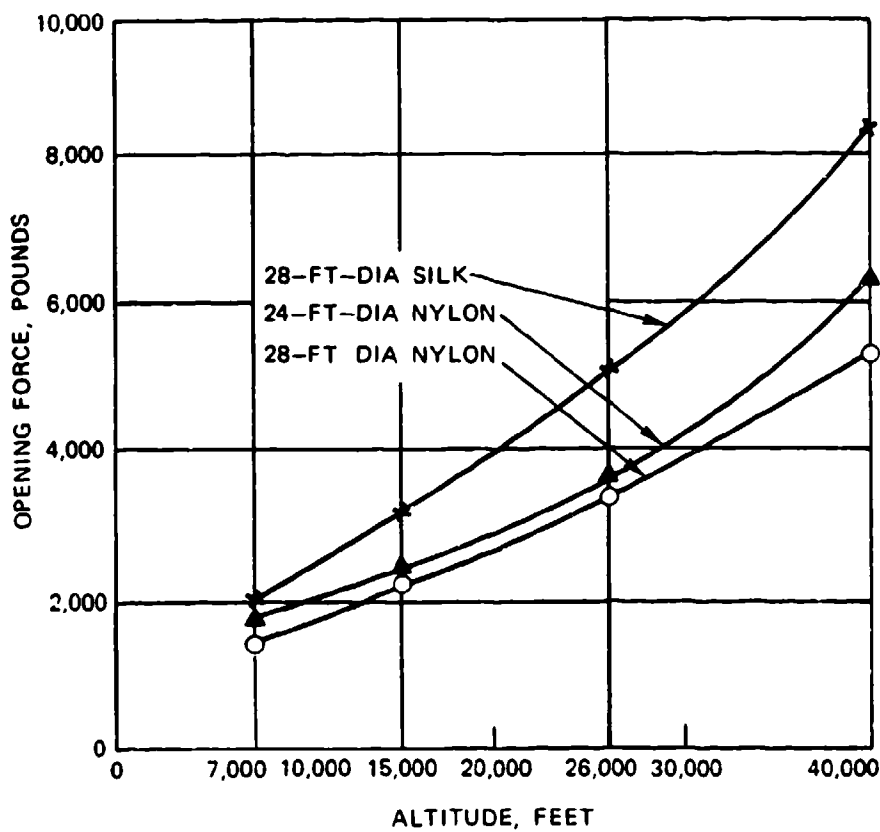


FIGURE 5-59. Opening Forces of Various Personnel Parachutes
Tested at Altitudes from 7000 to 40,000 Feet
at a Terminal Velocity of 102 KEAS.

Therefore, the kinetic energy to be absorbed during the inflation process is four times as high. In addition, the filling time of the canopy is only half as long at 40,000 feet as at sea level because of the 100-percent-higher true velocity. The higher forces on the parachutes manufactured from silk are explained by the higher elongation of nylon material. The higher forces on the 24-foot-diameter parachutes were caused by a slightly different design and the resultant shorter filling times.

In the 1950s the Air Force repeated these tests at altitudes up to 20,000 feet. Tests included the Navy 26-foot-diameter conical and the 35-foot-diameter T-10 extended-skirt parachutes used by paratroopers (Reference 5.97). In addition, high-altitude tests were performed on a reefed, 67-foot-diameter, extended-skirt parachute used as the main descent parachute for the Teledyne-Ryan Q-2 target drone (Reference 5.98). The test results are plotted in Figure 5-60. The opening forces of the four personnel parachutes increased with altitude as did the opening forces in the 1944 tests. The opening forces of the 35-foot-diameter T-10 extended-skirt parachute are considerably lower than the opening forces of the flat circular

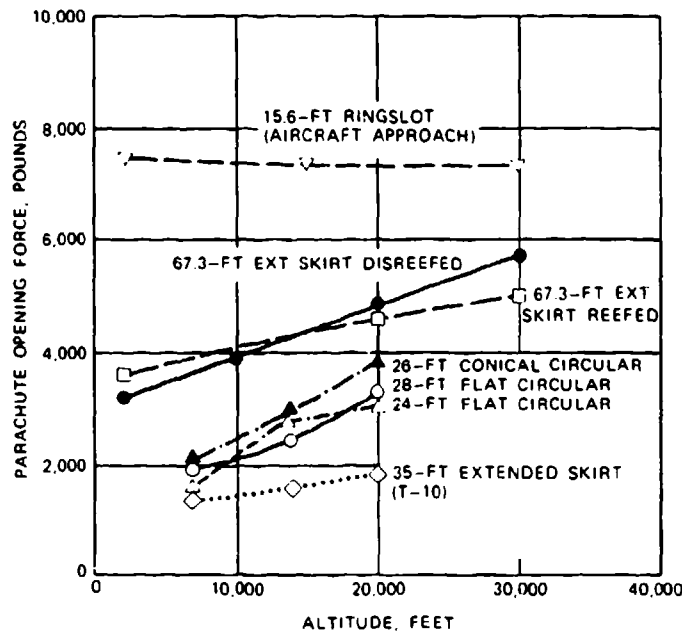


FIGURE 5-60. Parachute Opening Forces as a Function of Altitude for Various Types of Parachutes.

and conical parachutes. The tests with the reefed 67.3-foot-diameter extended-skirt parachute indicate that the reefed opening forces increase at a lesser rate with altitude than the disreefing forces because of the higher canopy loading of the reefed parachute (see section 5.4.5).

Parachute opening forces produced no force increase with altitude in tests conducted by the U.S. Air Force at Wright Field on the 15.6-foot-diameter ringslot parachute that was used as the approach brake for the B-47 bomber. Test results are shown in Figure 5-61 and plotted in the upper curve in Figure 5-60.

The primary difference in the force increase with altitude—a strong increase in the personnel parachutes, a medium increase in the reefed Q-2 drone parachute, and no increase in the B-47 approach parachute—is based on the canopy loading differences of the various parachutes. The high-canopy-loading B-47 parachute experiences no velocity decrease during parachute inflation at altitudes of either 2000 or 30,000 feet. The low canopy loading personnel parachutes experience a strong velocity decrease during opening at low altitude and a lesser velocity decrease during opening at altitude, resulting in a rapid force increase with altitude. The medium canopy loading, reefed Q-2 drone descent parachute has only a moderate force increase with altitude. The difference in opening force with altitude for parachutes with various canopy loadings is explained in Figure 5-51, where the force reduction factor, X_1 , is plotted as a function of the ballistic parameter, A . The ballistic parameter includes the density, ρ ; the true velocity at parachute line stretch, V_{O_i} ; and the canopy filling time, t_f . All three values

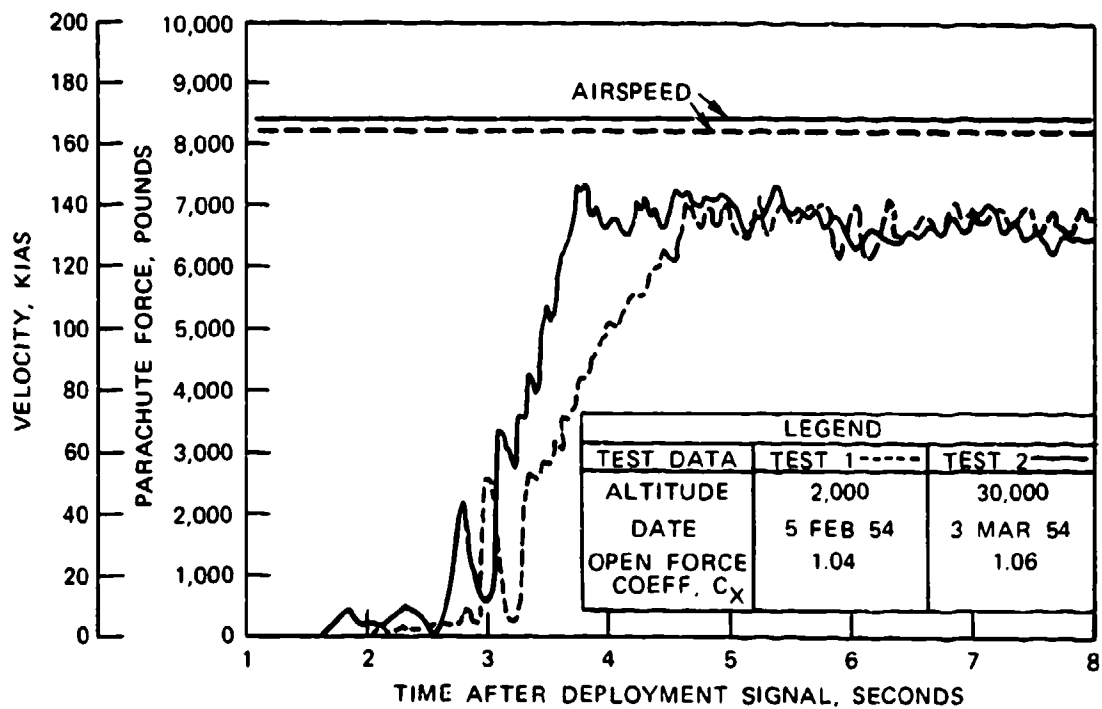


FIGURE 5-61. 15.6-Foot-Diameter Ringslot B-47 Approach Parachute Opening Forces as a Function of Altitude.

change with altitude. The low canopy loading personnel parachutes have ballistic parameter values in the 0.02 to 0.15 range, resulting in opening-force reduction factors approximately four to five times as high at 40,000 feet than at low altitude. The ballistic parameter value of the high canopy loading B-47 approach parachute is in the 200 to 1000 range, with little change in the resultant force reduction factor, X_1 . The reefed stage of the Q-2 main descent parachute has ballistic parameter value in the 3 to 10 range, producing only a small change in the force-reduction factor.

The canopy loading of the parachutes discussed in this analysis and plotted in Figures 5-60 and 5-61 are listed in Table 5-8.

References 5.99 and 5.100 discuss the general application of parachutes for high-altitude recovery and retardation, including the problem of aerodynamic heating and the effect of low canopy loading parachutes deployed after re-entry at high altitudes. In the late 1960s, NASA conducted an extensive program to develop a parachute system for landing the Viking spacecraft on Mars. This Planetary Parachute Entry Program (PPEP) included parachute tests at altitudes up to 139,000 feet and velocities in excess of Mach 3. The test results are summarized in Reference 5.101.

TABLE 5-8. Canopy Loadings.

Parachute application	Parachute type	Parachute diameter, ft	Parachute terminal velocity, ft/s	Canopy loading, $W/(C_0 S)_p$, lb/ft ²
Personnel	Flat circular	28.0	20	0.48
Personnel	Extended-skirt	35.0	18	0.38
Target drone recovery	Extended-skirt reefed	67.3	22	0.58
Target drone recovery	Extended-skirt reefed	6.0 (equivalent)	275	90.0
Aircraft approach	Ringslot	15.6	1007	1207.0

5.5.2 Porosity Effects

The porosity of parachute canopies influences parachute characteristics and parachute performance. For parachute canopies manufactured from solid fabric, the porosity is defined as the airflow through the canopy cloth in $\text{ft}^3/\text{ft}^2/\text{min}$, at a 1/2-inch water pressure. For slotted canopies such as ribbon, ringslot, and ringsail parachutes, porosity is defined in percent as the ratio of all open areas to the total canopy area. Most personnel parachutes and main descent parachutes for air vehicles, airdrop of equipment, and ordnance retardation use materials with porosities from 80 to 150 $\text{ft}^3/\text{ft}^2/\text{min}$. Gliding parachutes of the parawing, sailwing, and parafoil type use materials from 0 to 5 $\text{ft}^3/\text{ft}^2/\text{min}$, practically imporous. Slotted parachutes use geometric porosities in the 10 to 35% range.

Porosity affects parachute drag, stability, and opening forces. Parachute drag, opening forces, and oscillation decrease with increasing porosity. The decrease in oscillation and forces is a desirable characteristic but the decrease in drag is generally undesirable.

Figure 5-62, taken from Reference 2.1, plots the drag coefficients as a function of porosity for different parachute types. A cloth porosity of $27.4 \text{ ft}^3/\text{ft}^2/\text{min}$, at 1/2-inch water pressure is equivalent to 1% geometric porosity; this equivalency allows comparison of solid cloth parachutes and slotted parachutes. These data indicate a relationship among all parachutes. If the geometric porosity of a ribbon parachute is lowered to about 5%—the porosity of a flat circular, solid textile parachute—the ribbon parachute obtains the same drag coefficient, C_{D_0} , as the flat circular parachute; however, its stability decreases. This is demonstrated in Figure 5-63 by the drag coefficient increase and stability decrease of 3.5-foot-diameter flat and conical ribbon parachutes. The data were summarized from German and Wright Field

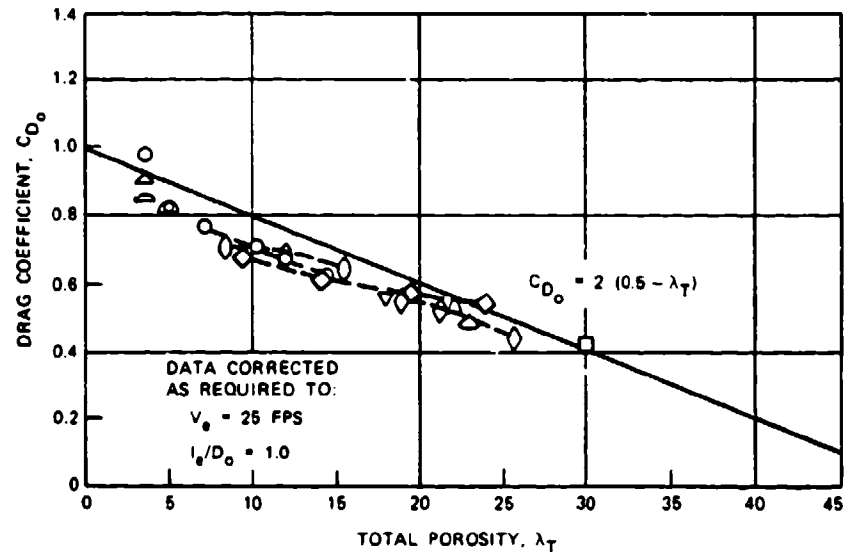


FIGURE 5-62. Effect of Canopy Porosity on Drag Coefficient for Various Parachutes.

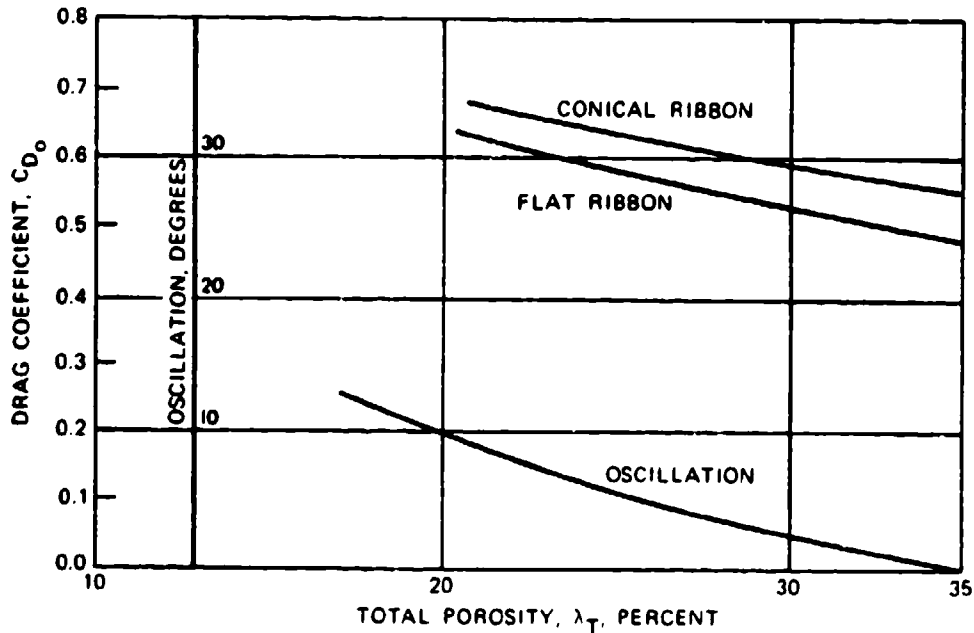


FIGURE 5-63. Drag Coefficient and Oscillation as a Function of Total Porosity for 3.5-Foot-Diameter Flat and Conical Ribbon Parachutes as Measured in Wind-Tunnel Tests.

wind-tunnel tests. A total porosity of 35% is required to obtain zero oscillation for a 3.5-foot-diameter ribbon parachute. Larger parachutes need a lower porosity to maintain proper inflation, zero oscillation, and the desired drag coefficient. The relationship of porosity versus diameter for maintaining proper performance for ribbon parachutes is discussed in Chapter 6.

The effect of porosity on the opening-force coefficient, C_x , is demonstrated in Figure 5-64. The data for the ribbon parachute were obtained by the Sandia National Laboratories in wind-tunnel tests (Reference 5.102). The author has supplemented the data range by plotting the opening-force coefficient value for circular solid textile parachutes and has extended the curve to include the range of parachutes manufactured from almost-zero-porosity material. This family of hi-glide parachutes includes the Rogallo parawing and the ram-air-inflated Jalbert parafoil. These parachutes have an opening-force coefficient of 2.5 to 2.8 (see section 5.9).

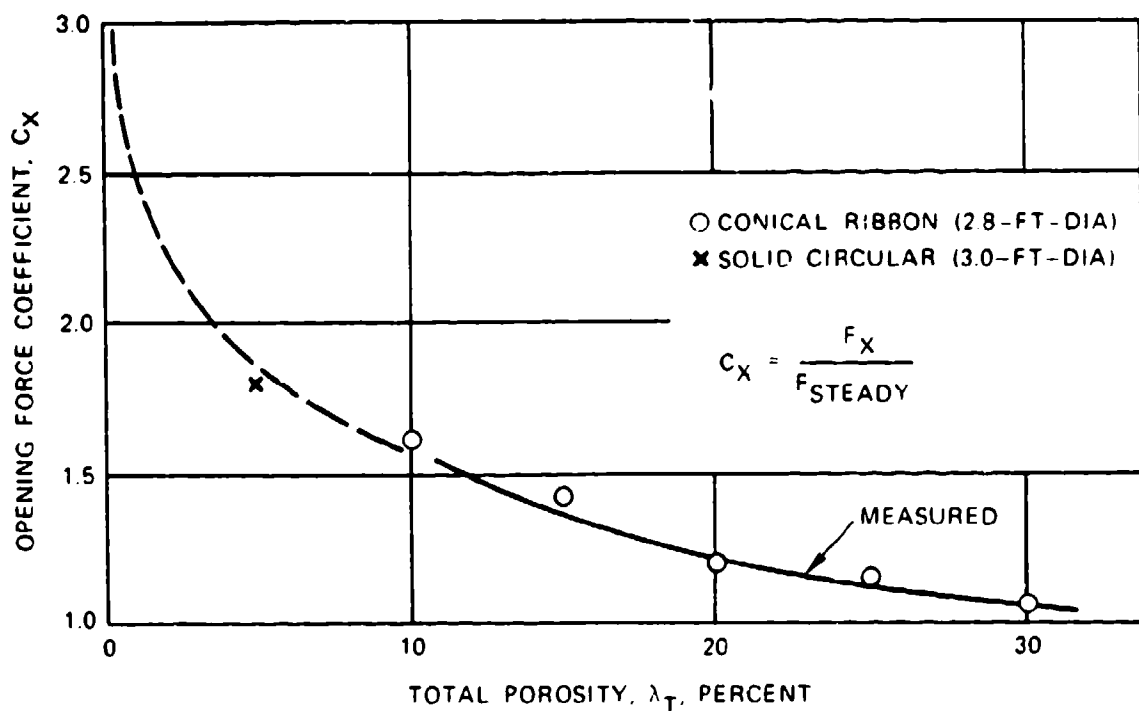


FIGURE 5-64. Opening-Force Coefficient as a Function of Total Porosity.

Figure 5-65 shows opening-force coefficient as a function of cloth permeability (porosity) for cross parachutes, as measured by the Naval Ordnance Laboratory (Reference 5.103). In the primary porosity range of 80 to 150 ft³/ft²/min, a force coefficient of 1.1 compares well with ribbon and ringslot parachutes which have a C_x of 1.05 to 1.1.

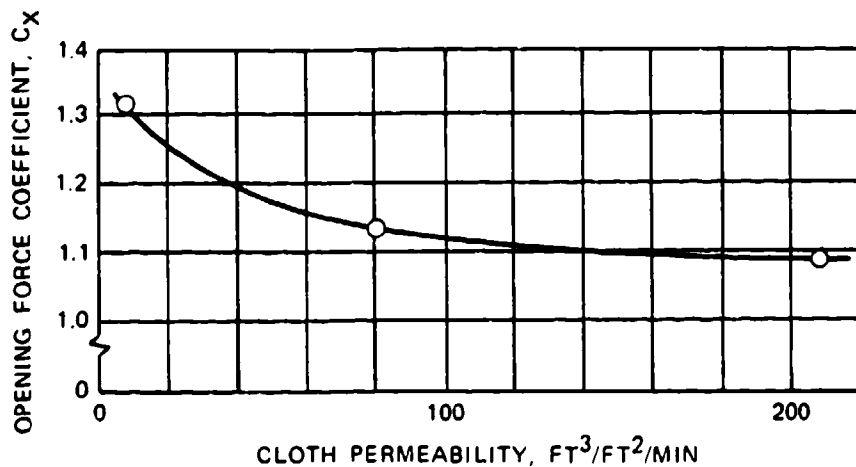


FIGURE 5-65. Opening-Force Coefficient as a Function of Cloth Permeability for Cross Parachutes as Measured by the Naval Surface Warfare Center.

5.6 PARACHUTE REEFING

5.6.1 General Description and Application

Parachute reefing permits the incremental opening of a parachute canopy, or restrains the parachute canopy from full inflation or overinflation. Reefing serves to

1. Limit the parachute opening forces to a predetermined value through successive steps of parachute opening, called reefing steps, at predetermined time intervals.
2. Obtain a temporarily high rate of descent. Reefing the parachute to a low drag area permits a more accurate drop from high altitude. Low-impact velocity is then obtained by disreefing the parachute shortly before ground impact.
3. Allow deployment of aircraft landing deceleration parachutes during approach for landing approach control. Disreefing the parachute at touchdown provides a powerful landing brake.
4. Increase parachute stability by a slight amount of fixed reefing.
5. Provide an overinflation control line (OC line) that lets the parachute open fully but prevents overinflation. The OC line decreases the parachute opening force by limiting the force overshoot at final parachute inflation.

Parachute reefing was developed in Germany during World War II, where many reefing methods were investigated. The parachute was restrained from opening fully by placing a line

around the canopy, the canopy skirt, and the suspension lines; by pulling down the vent of the parachute; and by releasing the parachute canopy only partially from the container or deployment bag. The skirt reefing method evolved as the most practical solution and is used in much the same form today (Reference 5.104).

Another investigation of various reefing methods was conducted in 1960 in Great Britain (Reference 5.105). Again, the skirt reefing method, called the rigging point reefing in Great Britain, proved to be the most practical system. Several attempts to develop other reefing methods were made. Two methods, vent reefing and slider reefing, have been used in some designs.

Reefing a parachute for use in a parachute recovery system starts with analytical determination of the various drag-area stages and the required timing steps. The analysis is best accomplished in computer runs. These computer runs determine the number of reefing stages; the timing of the stages; and the velocity, altitude, and trajectory increments based on maximum allowable parachute force, parachute force balance in the reefing stages, minimum recovery altitude, and other related requirements (Reference 5.106).

Four reefing methods are discussed in the following subsections.

5.6.2 Skirt Reefing

Skirt reefing, illustrated in Figure 5-66, is the most common reefing method.

Reefing rings are attached to the canopy skirt on the inside of the canopy at the connection point of each suspension line. The reefing line, a continuous line that restricts the opening of the canopy, is guided through the reefing rings and several reefing-line cutters. Each cutter contains a pyro-time train and a cutter knife and is initiated at canopy stretch by pull cords attached to the suspension lines or to the canopy. After a preselected time, the cutter fires and the knife severs the reefing line, allowing the parachute canopy to open fully or enter the next reefing stage.

The length of the reefing line is determined by the required reduction in parachute drag area, called reefing ratio. The required reefing ratio is obtained by proper selection of the reefing-line length. For design purposes, the reefing-line ratio is determined by relating the reefing-line length to the reefing-line length of a fully open parachute. In practice, the reefing-line ratio is defined as the ratio of the reefing-line circle diameter to the nominal diameter of the parachute. Section 5.6.7 gives, for various parachutes, the required reefing-line ratios as a function of the required drag area (reefing ratio). Section 6.5 contains details for proper dimensioning and installation of the reefing system.

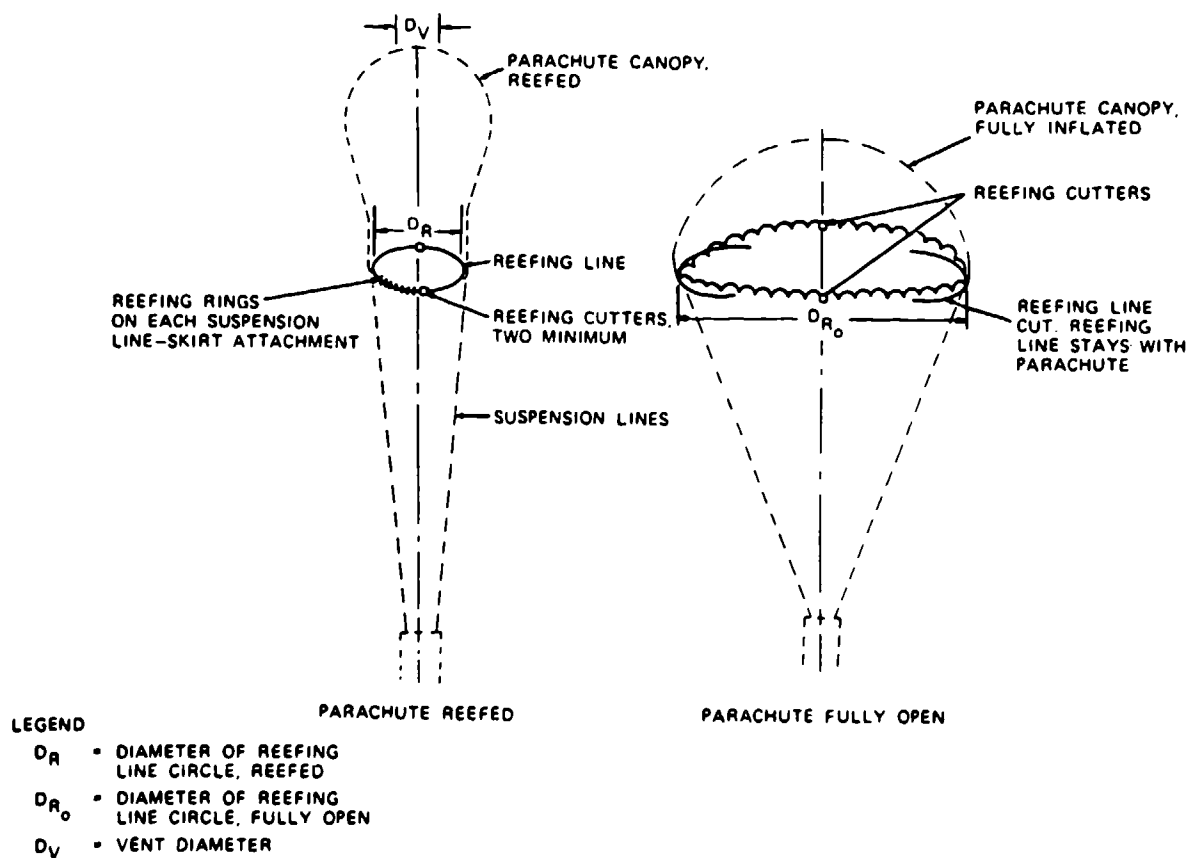


FIGURE S-66. Parachute Skirt Reefing.

When designing a skirt-reefing system, the designer must

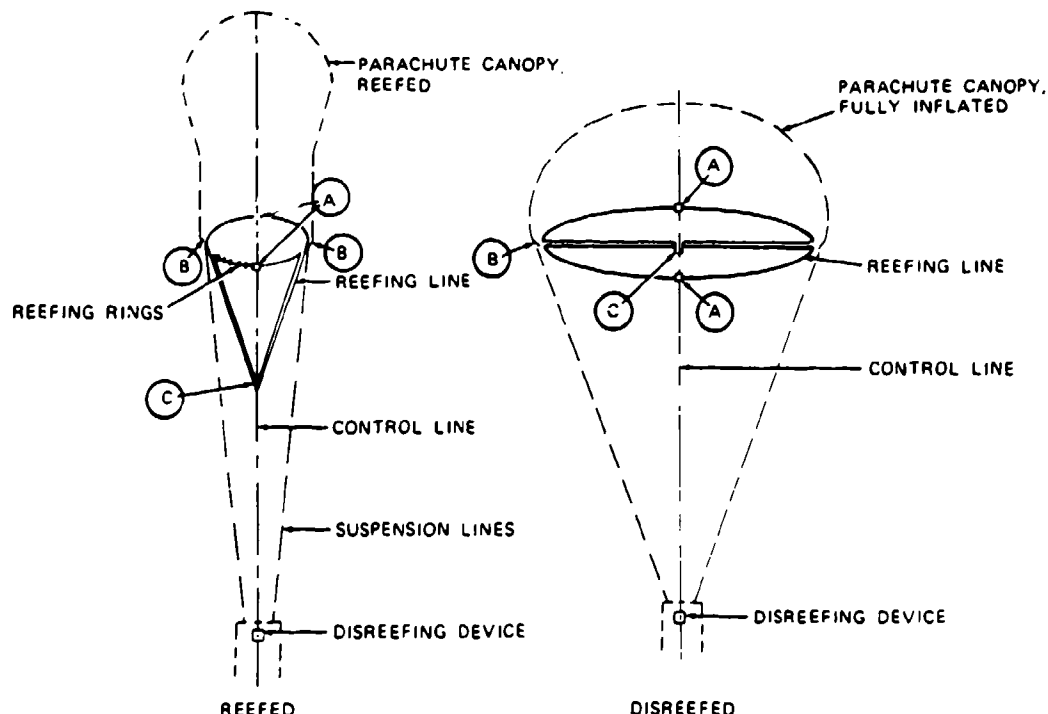
1. Define the length of the reefing line as the installed length.
2. Determine the forces in the reefing line and the resultant forces in the reefing system (see section 5.6.7).
3. Ensure that radial forces created by the forces in the reefing line are properly defined and that the reefing system does not overstress the parachute canopy.
4. Ensure that the vent diameter of the canopy, D_V , is smaller than the diameter of the reefing line circle, D_R (Figure 5-66). Reefing cutters with electronically controlled time delays have been developed by the Sandia National Laboratories. Actuating reefing cutters with RF signal from the command module was investigated by Northrop during the Apollo program. Both methods are discussed in section 6.5.

5.6.3 Skirt Reefing with Control Line

Skirt reefing with control line is illustrated in Figure 5-67. A two-section reefing line is attached to the canopy skirt at points A, guided around one-quarter of the skirt and out of the canopy at points B to a confluence point, C, returning the same way but around the adjacent quarter of the canopy. A second reefing line is run similarly around the second half of the canopy, and is connected with the first line at point C. The reefing system must allow full opening of the canopy. Pulling the control line toward the confluence point of the suspension lines reefs the canopy; paying out the control line disreefs it.

This method has been used for manually disreefing aircraft landing deceleration parachutes that were deployed reefed on landing approach and disreefed at touchdown.

This method was also investigated for continuous disreefing of parachutes. A disreefing device controlled the payout of the control line by using the force in one suspension line as a control sensor.



NOTE: A TWO-SECTION REEFING LINE IS ATTACHED TO THE CANOPY SKIRT AT POINTS (A), GUIDED AROUND ONE QUARTER OF THE SKIRT AND OUT OF THE CANOPY AT POINTS (B) TO A CONFLUENCE POINT, (C), RETURNING THE SAME WAY BUT AROUND THE ADJACENT QUARTER OF THE CANOPY (SEE 5.6.3).

FIGURE 5-67. Parachute Skirt Reefing With Control Line.

5.6.4 Vent Reefing

Vent reefing is illustrated in Figure 5-68. A line is attached to the center of the parachute vent. Pulling the vent line down toward the confluence point of the suspension line deforms the canopy. Pulling to about the level of the canopy skirt increases the inflated diameter and concurrently increases the drag coefficient, C_{D_0} , by about 30%. Continuing the downward pull decreases the canopy diameter and its drag area, creating a reefing condition. Extreme pull on the vent line may cause the suspension lines to wrap over the canopy. The increase in drag created by partial pull of the vent line is used in airfoil and annular parachutes for obtaining a high-drag canopy configuration. Vent reefing has been used for several special applications. Wind-tunnel and aircraft tow tests conducted with this configuration indicate a minimum useful reefing ratio of about 10% of the full-open drag area. Figure 5-69 shows total

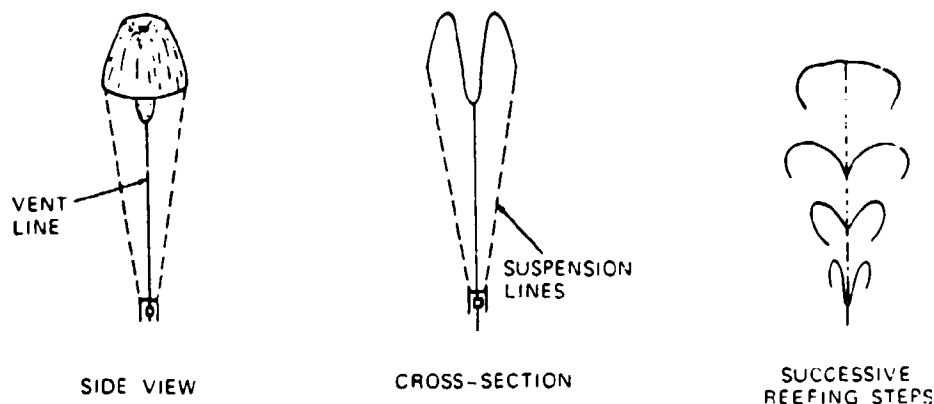


FIGURE 5-68. Parachute Vent Reefing.

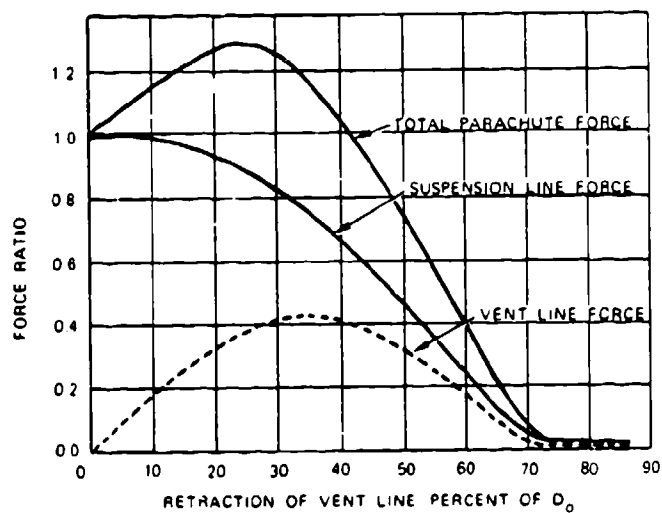


FIGURE 5-69. Total Parachute Force, Suspension-Line Force, and Vent-Line Force, as Functions of Vent-Line Retraction.

parachute, vent-line, and suspension-line forces of a vent-reefed parachute as a function of the vent-line retraction.

5.6.5 Slider Reefing

Slider reefing is shown in Figure 5-70. A slider, a square piece of cloth with grommets on each corner, is inserted in the center of the suspension lines. The suspension lines, bunched into four groups, pass through the grommets. During parachute packing, the slider is moved up to the parachute skirt. At initial deployment, the slider keeps the canopy closed and prevents a high snatch force. The spreading action of the inflating canopy forces the slider down the suspension lines, delaying and controlling canopy inflation. This method is used extensively on ram-air-inflated gliding parachutes used by sport parachutists.

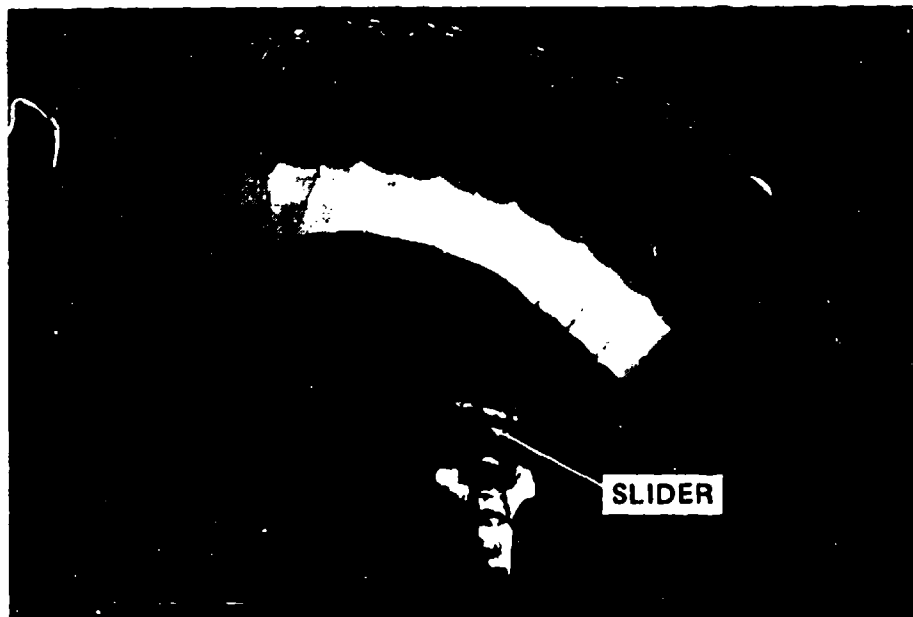


FIGURE 5-70. Slider Reefing.

A similar system, Schade ring reefing, was developed and used during World War II and retested in El Centro in 1953 (Reference 5.107).

5.6.6 Continuous Disreefing

Many attempts have been made to develop a reefing system where the opening of the parachute canopy is governed by a preselected force-time diagram. This approach has been called "continuous disreefing" in the literature. One of these investigations is described in Reference 5.108. However, none of these attempts has, so far, resulted in a practical solution.

5.6.7 Drag-Area (Reefing) Ratio Versus Reefing-Line-Length Ratio

Most reefing systems use an incremental opening of the parachute canopy to control the opening process. Knowledge of the required length of the reefing line is mandatory for designing the reefing system.

The drag-area decrease in relation to the decrease in the lengths of the reefing line has been determined in numerous wind-tunnel, aircraft tow, and freefall drop tests (Reference 5.109). Until 1960, the drag-area ratio was called the reefing ratio (Reference 5.104). When the parachute landing systems for the Mercury, Gemini, and Apollo spacecraft were designed, NASA called the reefing-line ratio the reefing ratio (References 2.1 and 5.79). This book, the *Parachute Recovery Systems Design Manual*, returns to the original definition, calling the drag-area ratio the reefing ratio. Figures 5-71 through 5-73 show the reefing ratio, ϵ (drag-area ratio), versus the reefing-line ratio, τ , for the most commonly used parachutes. These figures are taken from Reference 5.110, which contains a wealth of data on reefing-line versus reefing ratios for a variety of parachutes.

High canopy loading drogue and aircraft parachutes are generally reefed to about 30 to 60% of the full open drag area. Large main recovery parachutes, especially when two-stage reefing is required, must be reefed down to 2 to 5% of the full open drag area. This has been accomplished with circular solid textile and large ringsail parachutes.

In the early 1950s, the author conducted tests at El Centro with a standard 28-foot-diameter, flat circular parachute to determine the minimum obtainable drag area. A parachute without reefing, but with the suspension lines tied together at the skirt, had approximately 2% of the fully open drag area; the canopy descended vertically in a snake-like motion. A parachute with reefing rings and with the reefing line tied ring-to-ring had a 2.5% drag area, resulting in a canopy with a small-diameter, tube-type inflation but no bulbous crown. A 32-inch-long reefing line, giving a 10-inch-diameter reefing-line circle, produced a 4% drag area and a slightly bulbous crown. Small ribbon parachutes cannot be reefed below 4% of the fully open drag area, probably because of the rough surface of the ribbon canopy. Large parachutes can be reefed to lower values than small parachutes because of the relative size effect. Wind-tunnel models, smaller than about 3 feet nominal diameter, cannot be reefed much below 10% because of the relative stiffness of the model parachute. Tests for determining reefing characteristics, therefore, must be conducted on larger parachutes.

Skirt reefing has been used successfully on most circular parachute canopies, including disk-gap-band parachutes (Reference 5.111). Cross parachutes can be skirt reefed; however, inflation through the side pockets results in a bulbous crown and a minimum reefed drag area (reefing ratio) of about 10% of the fully open parachute (References 5.28 and 5.29). Guide surface parachutes are difficult to reef. Decreasing the skirt diameter with a reefing line flattens the canopy with little drag-area decrease followed by a sudden collapse of the canopy.

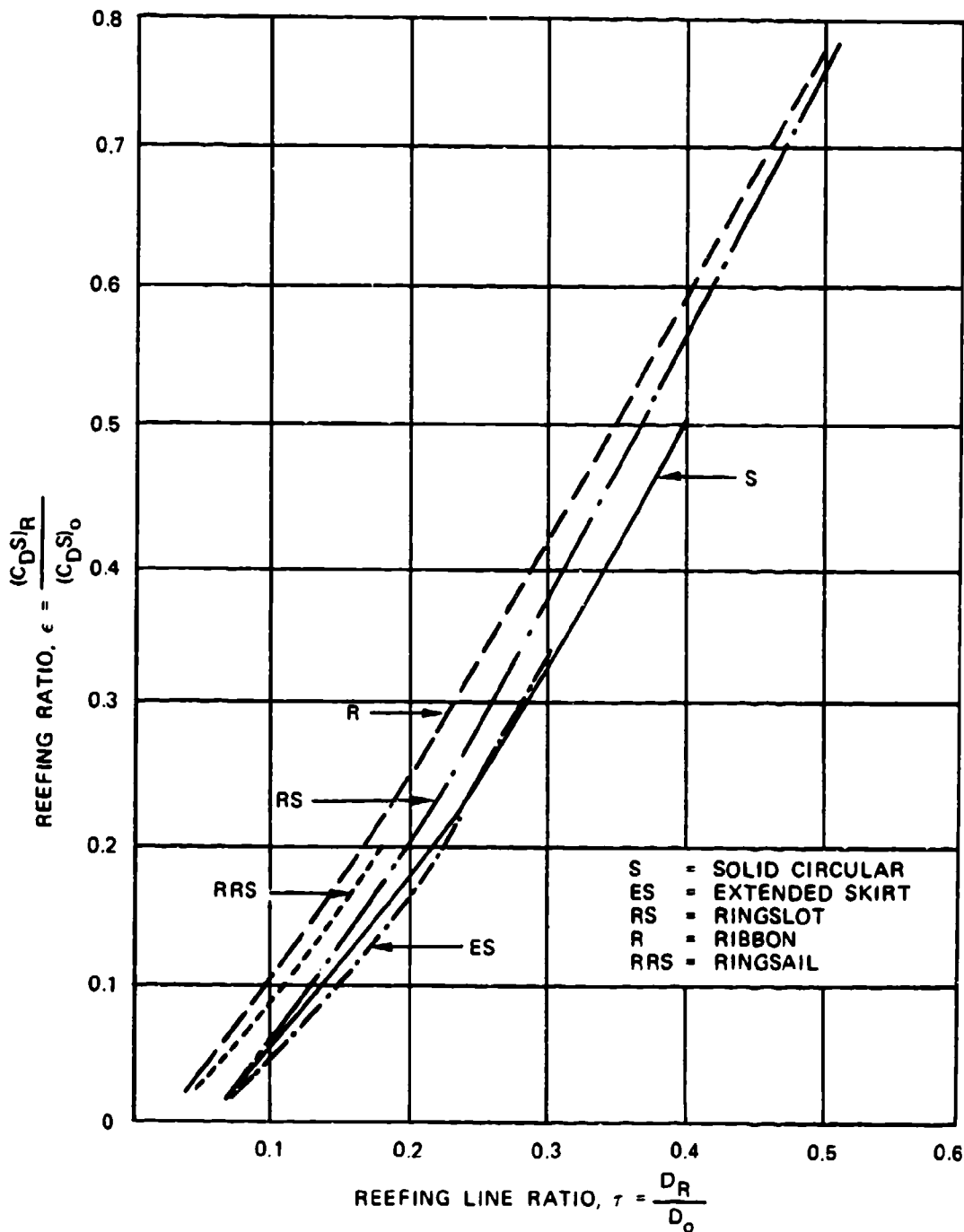


FIGURE 5-71. Reeling Ratio Versus Reeling-Line Ratio for Various Parachutes.

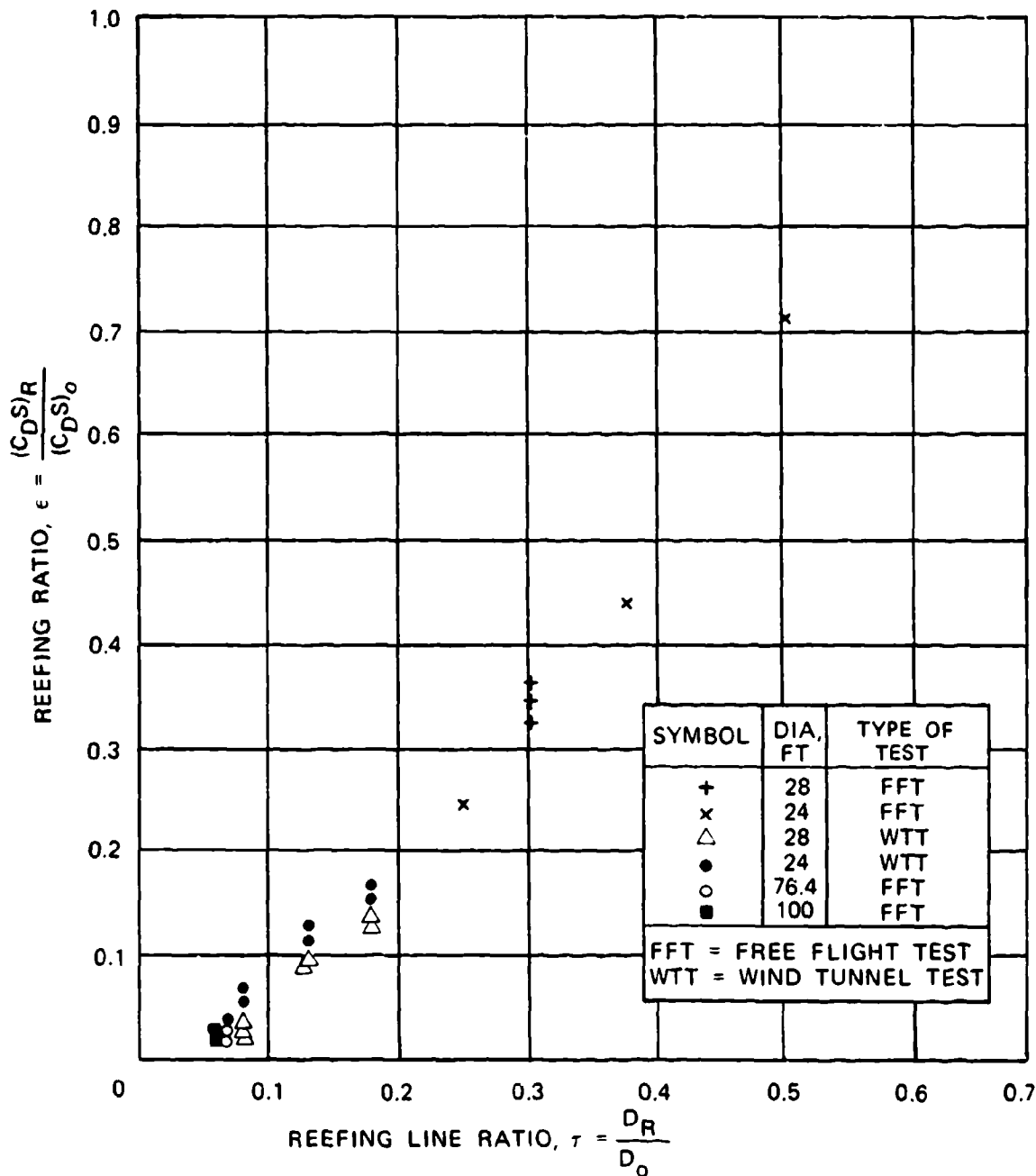


FIGURE 5-72. Reeling Ratio Versus Reeling-Line Ratio for Circular Flat, Conical, Triconical, and Extended-Skirt Parachutes.

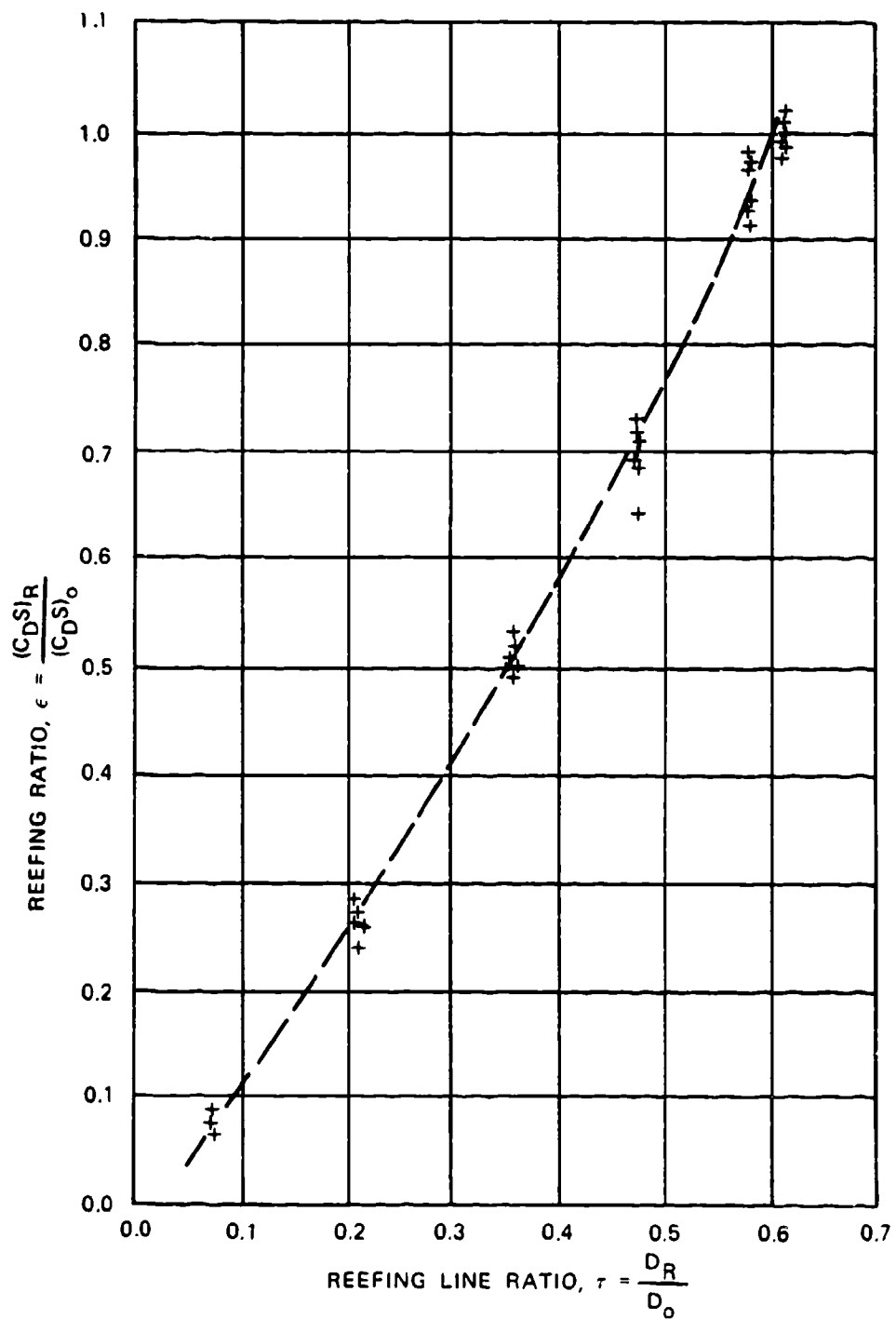


FIGURE 5-73. Reeling Ratio Versus Reeling-Line Ratio for 13.4-Foot-Diameter Conical Ribbon Parachute Tested in Aircraft Tow Test.

The required reefing-line length, L_R , for a specific reefed drag area, $(C_{DS})_R$, is determined as follows:

The required reefing ratio (drag-area ratio), ϵ , is obtained by dividing the reefed drag area by the drag area of the fully open parachute. Figures 5-71 through 5-73 show, for a given reefing ratio ϵ ,

$$\epsilon = \frac{(C_{DS})_R}{(C_{DS})_o} \text{ the required reefing-line ratio } \tau = \frac{D_R}{D_o}$$

where D_o is the known nominal diameter of the parachute and D_R is the diameter of the reefing-line circle. The length of the reefing line is now calculated to $L_R = D_o \pi \tau$, the installed length of the line. Additions must be made for the overlap, or Chinese finger splice, as explained in section 6.5.

5.6.8 Forces on Reefing Lines

The forces in the reefing line and its components must be known before the reefing system is designed. Force and trajectory calculations as a function of time determine the reefing stages and the parachute loads in the individual stages. It is practical to define the reefing-line force, F_{RL} , as a function of the known reefed parachute force, F_R , for the particular reefing stage.

Figure 5-74 shows that the force in the reefing line, F_{RL} , is related to the radial force, R , at the skirt of the parachute canopy. The radial force, in turn, depends on the parachute force, F_R , and the angle, δ , between the canopy radials and the suspension lines. The radial force and the force in the reefing line increase with an increase in the angle. A parachute with a bulbous inflation has a larger radial and reefing-line force, as does a parachute with longer suspension lines, because of the geometry of the system.

Figure 5-75, taken from Reference 5.112, shows the shape of a ribbon-parachute model during various stages of reefing as tested in a wind tunnel.

In a 1981 report, the author summarized all data available to that time on reefing-line forces (Reference 5.113). This report explains the difference between the reefing-line forces of a high-canopy-loading drogue-type parachute, where the maximum reefing-line force occurs at full reefed inflation, and a low-canopy-loading finz'-descent parachute. The maximum reefing-line force on the latter occurs before full reefed inflation because of the velocity decay during reefed opening (Figure 5-76). On unreefed, low-canopy-loading parachutes, the maximum force also occurs before full inflation. The high-canopy-loading parachute's

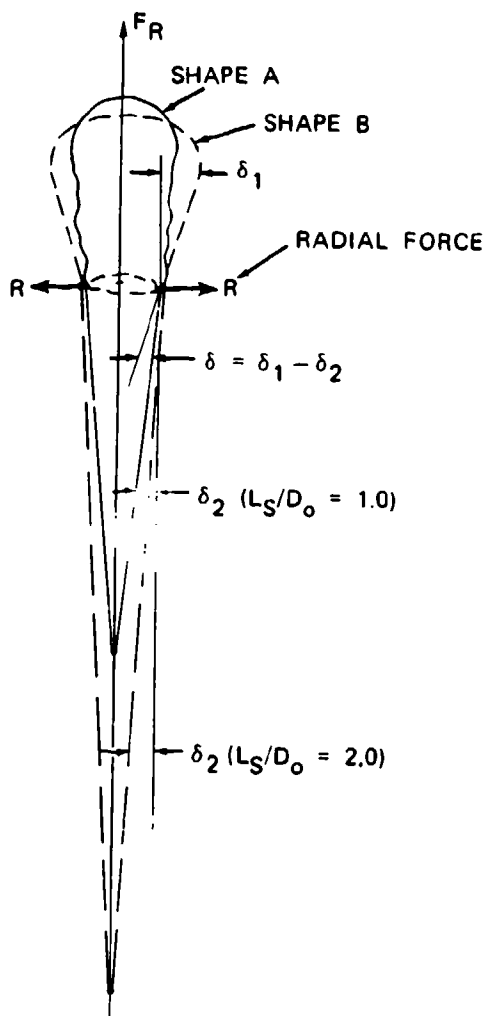
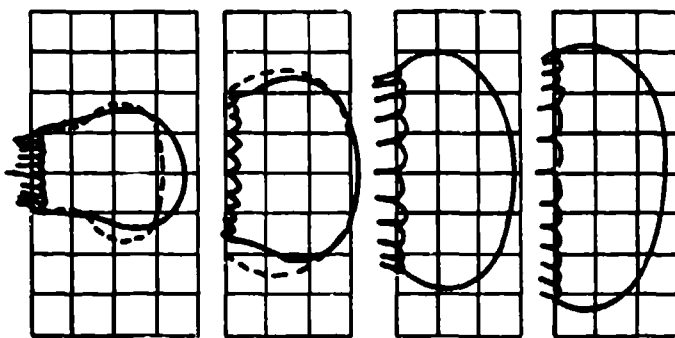


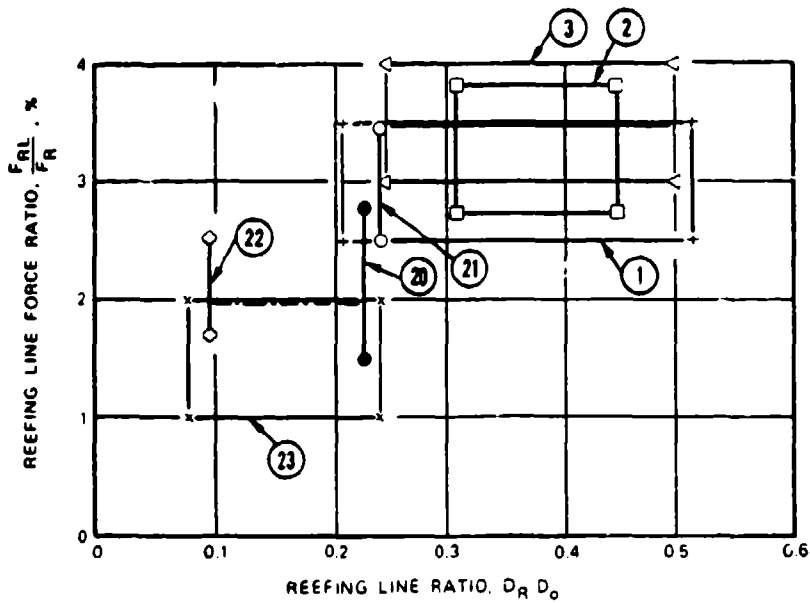
FIGURE 5-74. Force Relationship in
a Reefed Parachute.



LEGEND:

- POROSITY = 25 PERCENT
- - - POROSITY = 0 PERCENT

FIGURE 5-75. Reefed Canopy Profiles for Two Parachute Canopies of 0% and 20% Porosity.



LEGEND

$\frac{W}{C_D \cdot S}$	TYPE OF TEST	TEST ITEM ¹	D_o FT	$\lambda g.$ %	L_e/D_o	SYMBOL
HIGH	FFT	3	4-16	20-30	1.0	— △ —
HIGH	FFT	20	23	20-25	1.0	— ● —
HIGH	FFT	21	18.8	20-25	1.0	— ○ —
LOW	FFT	22	64	~8	1.0	— ◇ —
LOW	FFT	23	83.5	~9	1.41	— ✕ —
HIGH	A-LTT	1	10	~26	1.0	— + —
HIGH	WTT	2	3	34	1.0	— □ —

¹SEE REFERENCE 5.98.

FIGURE 5-76. Ratio of Reefing-Line Force to Maximum Reefed Parachute Force Versus Reefing-Line Ratio.

reefing-line forces are 3 to 4% of the reefed opening forces; whereas large-diameter, low-canopy-loading parachutes (Items 22 and 23 in Figure 5-76) have reefing-line forces of approximately 1 to 2.5% of the maximum reefed force. The item definition in Figure 5-76 is the same as in Table 1 of Reference 5.113. Recent reefing-line force measurements by the Sandia National Laboratories agree with the data plotted in Figure 5-76.

At Wright-Patterson Air Force Base, local accelerations on reefing cutters were measured in the 500- to 1000-g range at the time of line stretch. During the Apollo program, Northrop Corporation in California duplicated these measurements with similar results. These data must be considered in the design of the reefing-cutter installation.

The following recommendations are made regarding forces in reefing lines:

1. Use a reefing-line-to-maximum-reefed-parachute-force ratio of 0.03 to 0.04 for the design of a first-stage drogue chute in the medium-to-high subsonic range. Consider the effect of suspension-line ratios, L_e/D_0 , greater than 1.0; the effect of porosity; and the higher opening-shock factor, C_x , of transonic parachutes in the dimensioning of the reefing line.
2. Use a reefing-line-to-maximum-reefed-parachute-force ratio of 0.03 for ordnance retardation parachutes and parachutes with canopy loadings, $(W/C_D)_p$, in the 3- to 40-lb/ft² range.
3. Use a reefing-line-to-maximum-reefed-parachute-force ratio of 0.025 minimum for the design of large, final descent parachutes. This ratio should be increased for parachutes with unknown reefing characteristics, for small parachutes, and for parachutes with large reefing ratios.
4. A 2.5 safety factor is recommended for the design of all components of the reefing system.
5. Give special attention to ensure smooth reefing-cutter hole finishes, straight-through routing of reefing lines, proper reefing-ring attachment, and proper actuation of the reefing cutters.

5.6.9 Fixed Pocketband Reefing

Experience has shown that the required design porosity, λ_T , of slotted parachutes such as ribbon and ringslot is generally high enough to ensure positive inflation and good stability. However, under certain conditions, such as inflation in the wake of a large forebody, a higher porosity is necessary to ensure good stability. This porosity may be too high for proper inflation. The solution to this problem is fixed reefing.

Inflation is governed by the total canopy porosity, which ensures a positive pressure differential between the inside and outside of the canopy. The stability of the canopy is governed by the ratio of inflow into the canopy to outflow from the canopy. This ratio can be increased by reducing the canopy mouth area by a small amount of fixed reefing. This reefing does not change the canopy porosity and the positive pressure differential between the inside and outside of the canopy, but it increases the ratio of outflow to inflow into the canopy and improves the parachute stability. This method, which increases the effective porosity of the parachute, was used successfully on the supersonic drogue chute of the Mercury capsule. The 4-foot inflated diameter of the 6-foot-nominal-diameter drogue chute was smaller than the diameter of the Mercury capsule, which caused some instability and heavy canopy breathing. Using a 6.8-foot-diameter conical ribbon parachute reefed to the inflated diameter of a 6.0-foot-diameter parachute resulted in a stable parachute with reduced breathing. The effective porosity of the canopy, λ_{eff} , was increased by the ratio

$$\lambda_{\text{eff}} = \lambda_T \frac{S_2}{S_1}$$

where S_1 is the canopy area of the 6.0-foot-diameter parachute, and S_2 is the canopy area of the 6.8-foot-diameter parachute.

This ratio can be written in the form

$$\lambda_{\text{eff}} = \lambda_T \frac{D_o^2}{D_1^2}$$

where D_o is the nominal diameter of the unreefed parachute, and D_1 is the equivalent nominal diameter of the reefed parachute.

The required diameter for the unreefed parachute is calculated

$$D_o = D_1 \frac{\lambda_{\text{eff}}}{\lambda_T}$$

where

D_o = the nominal diameter of the parachute

D_1 = the nominal equivalent diameter of a parachute with the required drag area

λ_T = the porosity required to ensure proper inflation

λ_{eff} = the porosity required for good stability

In the case of the Mercury drogue chute, a 26% total porosity, λ_T , was selected for good inflation, resulting in an effective porosity

$$\lambda_{\text{eff}} = 26 \frac{6.8^2}{6.0^2} = 33.3\%$$

This type of fixed reefing is best achieved by pocketband reefing. Design details of the pocketband method are described in section 6.5.4.

Overinflation Control (OC) Line. The Apollo drogue chutes tested behind a small-diameter test vehicle were stable and exhibited no canopy breathing. However, the parachute exhibited heavy breathing in the wake of the large Apollo command module forebody (Figure 5-49). The breathing was considerably restrained by the installation of an OC line; the opening-force coefficient decreased from about 1.46 to 1.31 (Figure 5-49). This OC line is installed around the skirt of the parachute canopy in the same manner as a reefing line. The OC line permits full canopy inflation but not overinflation. To dimensionalize the OC line, the dimension of a fully inflated canopy must be analyzed (Figure 5-77). The skirt diameter, D_s , is slightly smaller than the projected or inflated canopy diameter, D_p . The projected diameter for a particular parachute type is independent of the number of canopy gores. The skirt diameter increases with the number of gores. The projected diameter varies with parachute type, canopy porosity, and suspension-line length. Average projected diameters for parachutes with normal porosity and line-length ratios of 1.0 are as follows:

$$D_p/D_o = 0.67 \text{ for ribbon parachutes}$$

$$D_p/D_o = 0.68 \text{ for flat, circular, fabric parachutes}$$

$$D_p/D_o = 0.70 \text{ for extended-skirt parachutes}$$

$$D_p/D_o = 0.72 \text{ for triconical parachutes}$$

Figure 5-78 shows the effect of the number of gores on the skirt diameter for a ribbon parachute with a projected diameter of 0.67 D_o . No equivalent data are available for other parachute types; it is therefore recommended that appropriate percentage values be used. OC-line installation is discussed further in section 6.5.4.

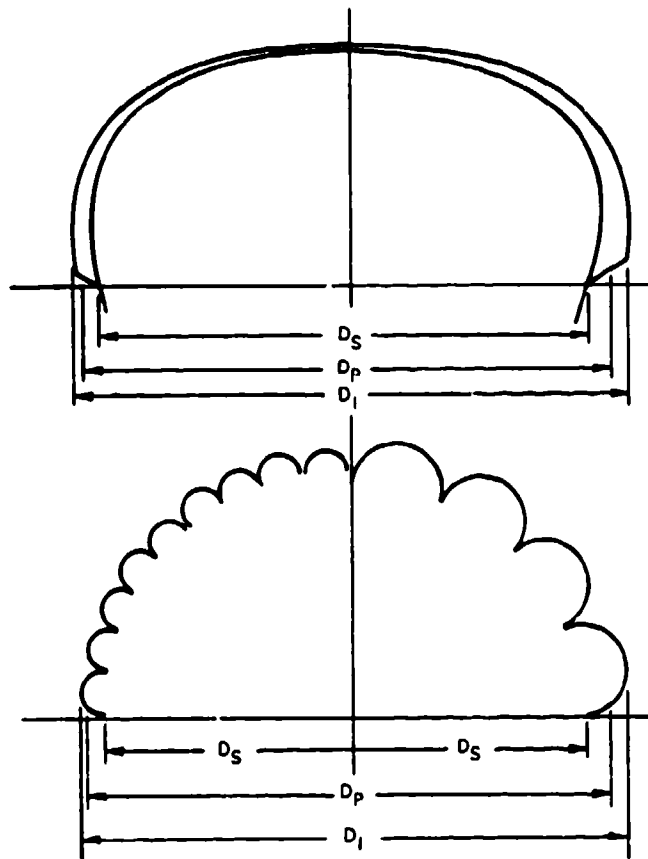
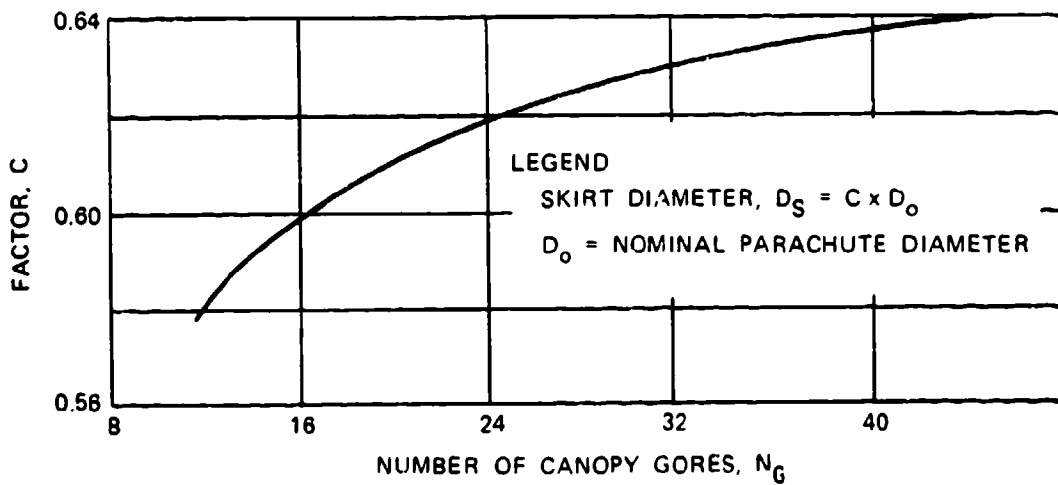


FIGURE 5-77. Definition of Inflated Canopy Dimensions.

FIGURE 5-78. Canopy-Skirt Diameter as a Function of the Number of Gores for a Ribbon Parachute With $D_p = 0.67 D_o$.

5.6.10 Reefing of Small-Diameter Parachutes

Small-diameter parachutes generally have few gores and a resultant low ratio of skirt diameter, D_s , to nominal diameter, D_o (Figure 5-77). The ratio of skirt diameter to nominal diameter versus number of gores for ribbon parachutes is shown in Figure 5-78 and defined as $C = D_s/D_o$. A similar relationship is valid for other types of parachutes. All data on reefing-ratio-versus-reefing-line-diameter ratios in Figures 5-71 through 5-73 are based on parachutes with 24 or more gores. For parachutes with fewer gores, these data result in reefing lines too long for the required drag area. The following approach is recommended for determining the reefing-line circle diameter, D_R , for parachutes with a small number of gores.

$$D_R = D_o \tau C$$

where

D_R = reefing-line circle diameter

D_o = nominal parachute diameter

τ = reefing-line-circle-diameter-to-reefing ratio, from Figures 5-71 through 5-73

$C = D_s/D_o$ ratio, from Figure 5-78, for parachutes with few gores

For parachutes with long reefing lines, the elongation caused by the force in the reefing line should be included in determining the required reefing-line length.

5.7 CANOPY SHAPE AND CANOPY PRESSURE DISTRIBUTION

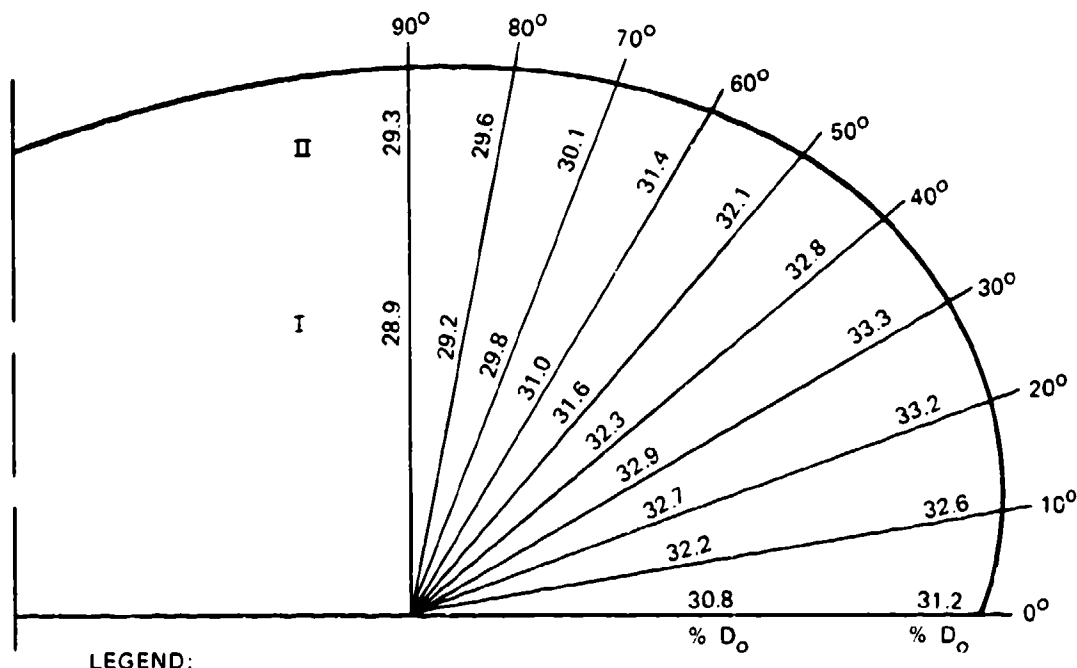
Knowledge of the parachute canopy shape and canopy pressure distribution are important for the design and stress analysis of parachutes, especially if the CANO or CALA computer programs are used for determining canopy stress. Both programs are discussed in section 6.4.

5.7.1 Parachute Canopy Shape

The inflated shape of a parachute canopy depends on the type and geometric design of the canopy (flat, conical, triconical, hemispherical, or other shaped-gore design), on the canopy porosity, and on the suspension-line length. Because the canopy shape depends on these factors, nonvariable, nominal parachute diameter, D_o , and the related surface area, S_o , are selected as references for such aerodynamic coefficients as C_{D_0} , C_L , C_m , and others.

Figure 5-79 shows the canopy cross sections along the radials for two ribbon parachutes with 9.9- and 9.6-foot diameters. These parachutes were tested in the Massie Memorial Wind Tunnel at Wright-Patterson Air Force Base, and in a large wind tunnel at Chalois Moudin, France. The shapes of the canopies are formed by the balance of internal pressure forces and the tension in the suspension lines. A higher internal pressure and longer suspension lines will result in larger inflated canopies.

The Sandia National Laboratories have measured the effect of canopy porosity and line length on canopy shape (Reference 5.114). These tests indicate that a decrease in canopy porosity and an increase in suspension-line length are the prime reasons for an increase in inflated canopy diameter and associated increase in drag coefficient. The increase in inflated canopy diameter with decreasing canopy porosity is shown in Figure 5-80, and the effect of suspension-line length in Figure 5-81. The increase in canopy diameter from a line-ratio increase of $L_e/D_o = 1.0$ to $L_e/D_o = 1.5$ is larger than the increase from a 1.5 to 2.0 ratio. This increase agrees with data plotted in Figure 5-20, where the increase in the drag coefficient is 7% for a line-ratio increase from 1.0 to 1.5 but only about 3% for a line-length increase from 1.5 to 2.0.

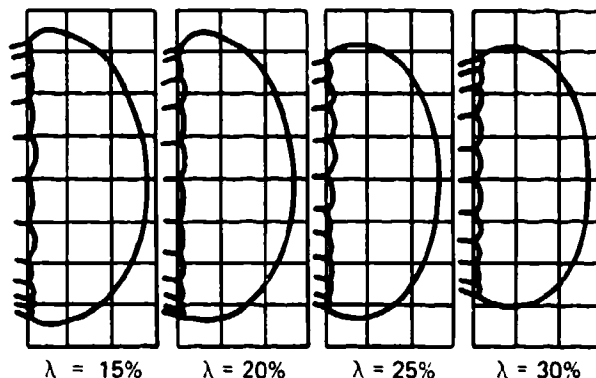


LEGEND:

I = 9.9-FT-DIAMETER FLAT RIBBON PARACHUTE, 20 GORES,
 $L_e/D_o = 1.0$

II = 9.6-FT-DIAMETER FLAT RIBBON PARACHUTE, 16 GORES,
 $L_e/D_o = 1.0$

FIGURE 5-79. Canopy Cross Section of Two Ribbon Parachutes.



NOTE: SUSPENSION-LINE RATIO, I_e/D_o , = 1.0

FIGURE 5-80. Side Profiles of Ribbon Parachute Canopies With Porosities From 15 to 30%.

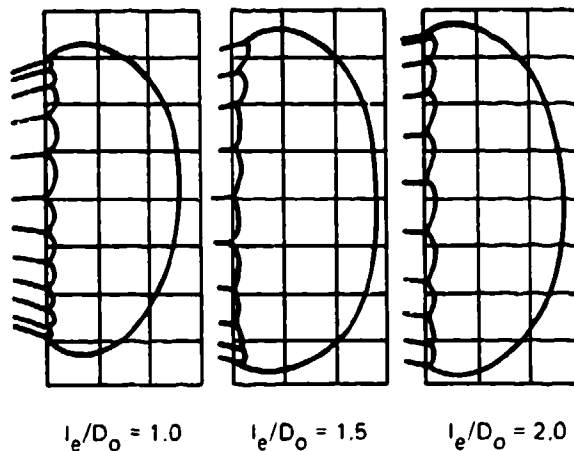


FIGURE 5-81. Side Profiles of a Ribbon Parachute With Constant Canopy Porosity and Suspension-Line Ratios of 1.0, 1.5, and 2.0.

5.7.2 Pressure Distribution in Parachute Canopies

Knowing the pressure distribution over the parachute canopy is important for analyzing the inflation characteristics of the canopy and for determining canopy stresses. Figure 4-10 shows the airflow and pressure distribution on several aerodynamic bodies. The general rule in aerodynamics is to prevent airflow separation and keep the airflow "attached" to the air vehicle to minimize air-vehicle drag. The opposite condition is desirable for parachutes in which uniform airflow separation around the leading edge of the canopy and uniform wake behind the canopy are required for obtaining high drag and good stability.

Figure 5-82 shows the airflow around a parachute canopy. The airflow in front of the canopy is decelerated to zero at the stagnation point, I. Behind the stagnation point, turbulent airflow occurs, resulting in a high static pressure inside the parachute canopy compared to the static pressure in the undisturbed flow of the free airstream around the canopy. The airflow around the edge of the canopy is accelerated by the compression of the streamlines, as described in Chapter 4, causing a negative pressure on the outside of the canopy. The positive inside pressure and the negative outside pressure form a strong outwardly directed pressure gradient that keeps the canopy inflated.

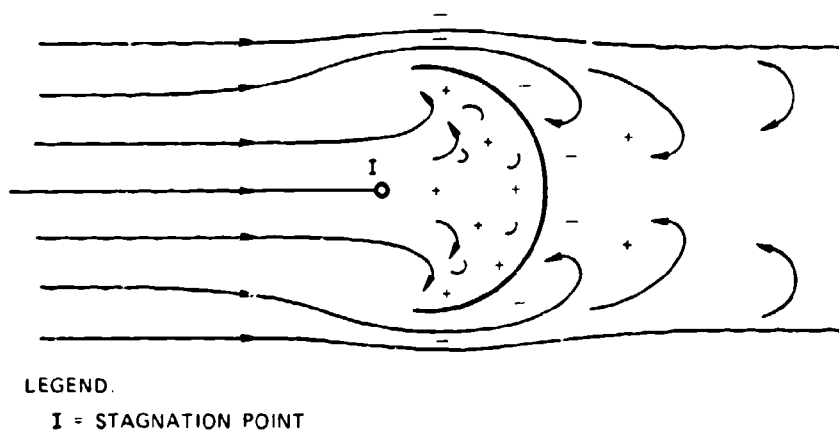


FIGURE 5-82. Airflow and Pressure Distribution Around a Parachute Canopy.

Bernoulli's Law states that $p + q = p_0$, where p is the static pressure, q the dynamic pressure, and p_0 the total pressure. From this equation we can derive the dimensionless pressure coefficient, c_p , with

$$c_p = \frac{p_0 - p}{q} \text{ or } C_p = \frac{\Delta p}{q}$$

Figure 5-83, from Reference 2.2, shows the external pressure coefficient, c_p , versus Mach number for a metal hemisphere with a geometric porosity of 20%, which simulates a ribbon-type parachute.

Figure 5-84, also from Reference 2.2, shows graphically the inside and the outside pressure coefficients versus Mach numbers, and shows numerically the total pressure differential coefficients for Mach 0.61 for a ribbon-type metal canopy. The strong pressure differential at the skirt of the canopy and the lower pressure differential at the vent are clearly indicated, as is the decrease in pressure gradient with a decrease in Mach number.

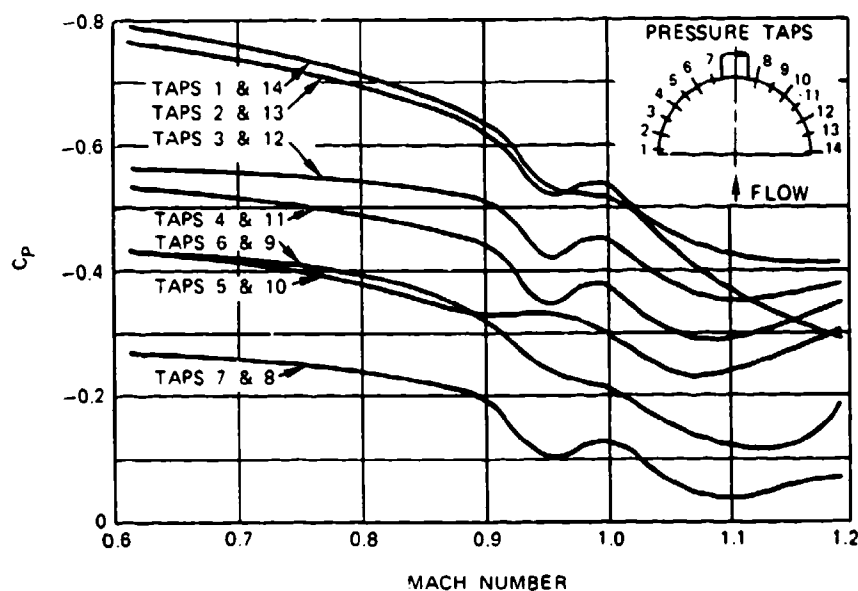


FIGURE 5-83. External Pressure Coefficient Versus Mach Number for a Ribbon-Type Metal Hemisphere.

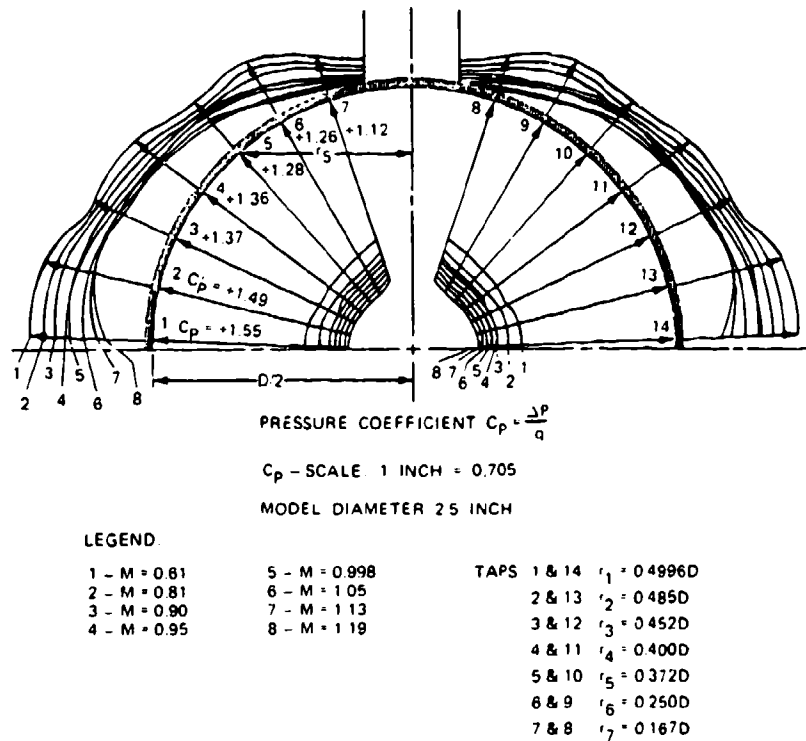


FIGURE 5-84. Inside, Outside, and Total Pressure Distribution Versus Mach Number for a Ribbon-Type Metal Hemisphere, Measured in Wind-Tunnel Tests.

Measuring pressure distribution in fully open flexible canopies and during inflation is quite difficult, especially for finite-mass conditions, which must be measured in free-flight tests. In the 1960s the University of Minnesota developed special pressure gages to be used with flexible textile parachutes. This work was continued and extended by the German Research Institute for Aeronautics and Astronautics (DVFLR) in Braunschweig, Germany, and by the Sandia National Laboratories. References 5.115 through 5.120 document these efforts. Figure 5-85 is from Reference 5.118, where Northrop, as a part of the Apollo program, replotted available pressure data for use in the development of the CANO program.

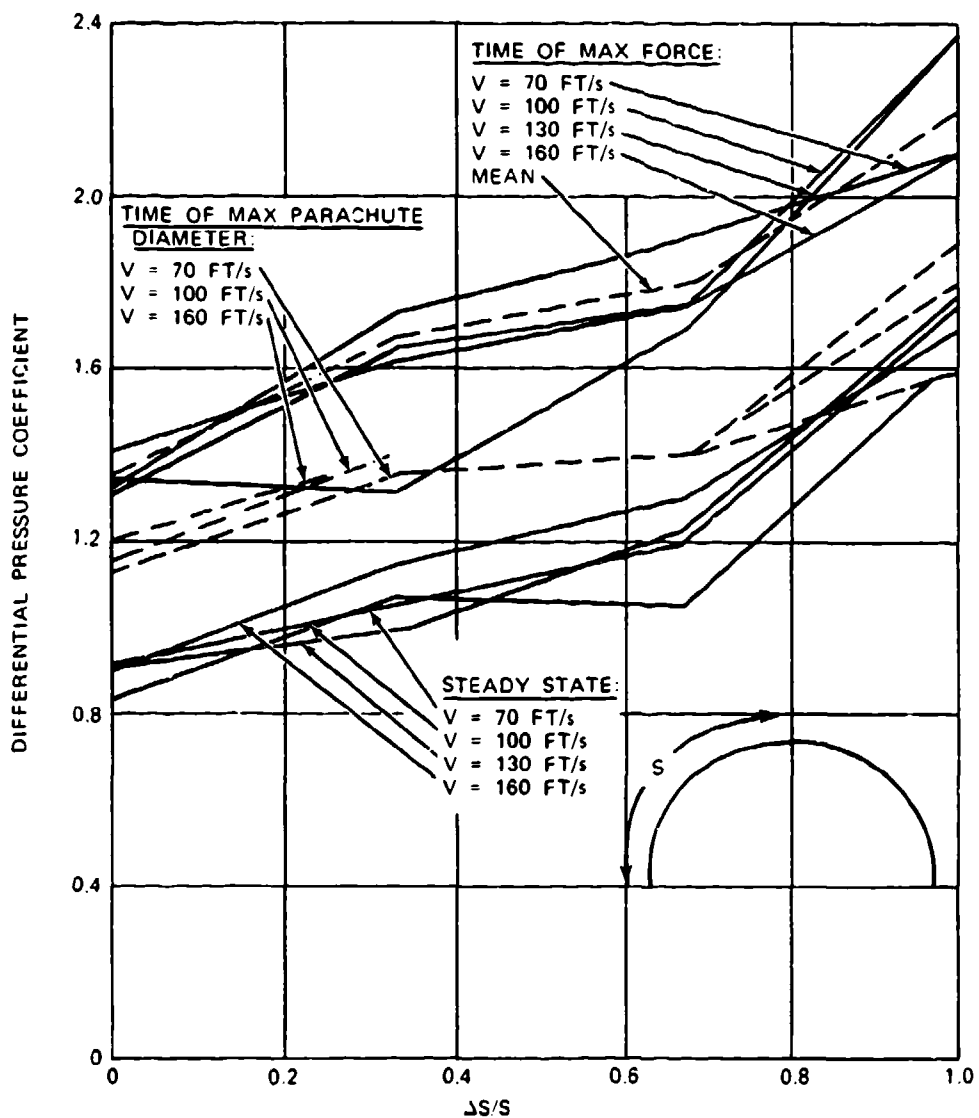


FIGURE 5-85. Pressure Distribution of a Ribbon Parachute at Various Times After Canopy Deployment.

5.8 SUPERSONIC INFLATABLE DECELERATORS

5.8.1 Characteristics of Supersonic Flow

Parachutes and balloon-type decelerators have been used successfully at speeds in excess of Mach 4, at altitudes up to the limit of the atmosphere, at dynamic pressures of 12,000 lb/ft², and on Earth as well as on other planets. Selecting the proper decelerator and analyzing its operational environment, supersonic inflation, aerodynamic heating, and flutter and stress problems are important because these decelerators are more complex than subsonic inflatable decelerators.

Section 4.1.8 defines supersonic speed by the associated Mach number, where Mach number is the ratio of the ambient velocity to the velocity of sound, c_s . The velocity of sound is 1116.46 ft/s at sea level and standard day condition. The air is considered incompressible by a body moving at a speed below Mach 1. When a body moving through air approaches the speed of sound, the air becomes compressible and starts to form compression waves in front of the body; this process is associated with local changes in velocity, pressure, and temperature. For detailed information on supersonic aerodynamics, see References 4.3 to 4.5 and the extensive literature.

Figure 5-86 shows the supersonic flow around a bullet moving at supersonic speed. A shock wave forms at the bow of the bullet, and expansion waves form at the protruding corners and the tail of the bullet. Reverse airflow and a long drawn-out, necked-in wake follow immediately behind the bullet. Most air vehicles flying at supersonic speeds are highly streamlined to minimize the drag increase that occurs when approaching Mach 1. Figure 5-87 shows this drag increase as a function of Mach number for an ejectable aircraft nose section. This drag increase is generally associated with a decrease in lift and stability.

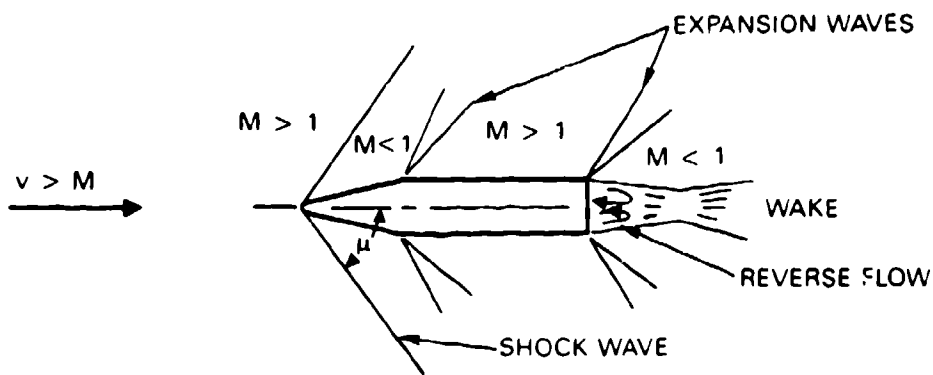


FIGURE 5-86. Supersonic Flow Around a Bullet-Type Body.

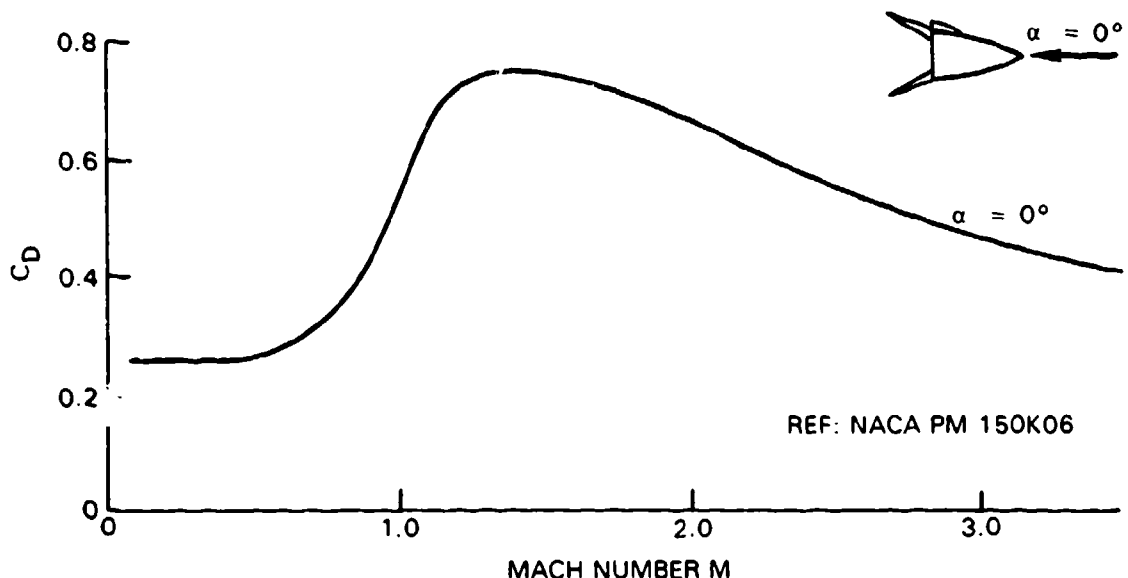


FIGURE 5-87. Drag Coefficient, C_D , Versus Mach Number for an Ejectable Aircraft Nose Section.

5.8.2 Supersonic Parachutes

The supersonic flow around a parachute canopy is distinctly different from the supersonic flow around a streamlined body, as shown in simplified form in Figure 5-88. A shock wave forms in front of the parachute canopy. As the supersonic velocity in front of the shock wave decreases to high subsonic velocity behind the shock wave, pressure, mass density, and temperature increase. Behind the canopy, a large wake forms with recirculation and negative pressure.

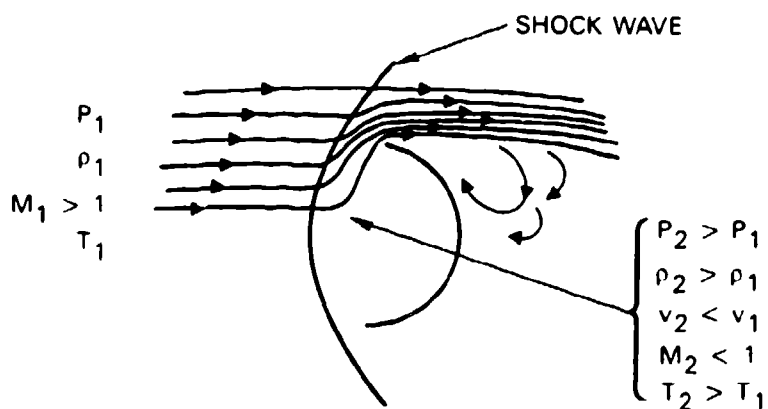


FIGURE 5-88. Supersonic Flow Field Around a Parachute Canopy.

A parachute canopy is never used by itself. In front of the canopy are suspension lines, a suspension line confluence point, and, generally, a riser and a forebody. Figure 5-89 shows the supersonic flow field around a streamlined forebody with an attached aerodynamic decelerator at a velocity of approximately Mach 3. The distance between the forebody and the leading edge of the parachute is equal to six times the maximum forebody diameter, and the suspension line length is equal to two times the nominal parachute diameter, D_0 .

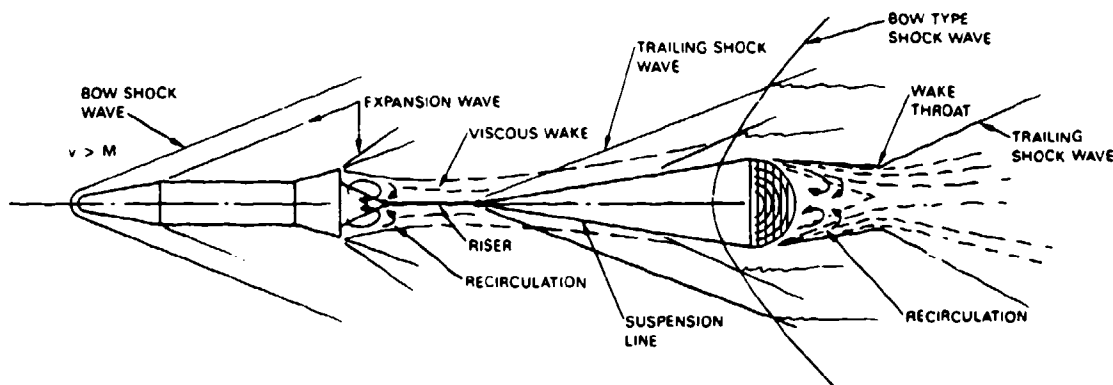


FIGURE 5-89. Supersonic Flow Around a Vehicle-Parachute System.

The flow field around the parachute canopy is seriously affected by the flow and the wake formed by the forebody, the riser, and the suspension lines. The relationship of forebody diameter to canopy diameter, the forebody shape, and the distance between forebody and leading edge of the parachute canopy cause considerable drag loss in the wake of the forebody.

In the early 1950s at Wright-Patterson Air Force Base, the Air Force started a research program to develop supersonic inflatable aerodynamic decelerators, including parachutes and, later, inflatable balloon-type devices. These investigations covered theoretical studies, wind-tunnel tests, sled tests, and free-flight tests that used rocket-boosted test vehicles.

Circular solid material types of parachutes were eliminated early in the program because of instability, canopy breathing, flutter, and stress problems. Flat ribbon parachutes in supersonic flow exhibited heavy breathing of the canopy leading edges, high-frequency flutter of canopy elements, and a tendency to close the mouth of the canopy at supersonic speeds.

Conical ribbon parachutes were suitable up to the Mach 2 to 2.5 range. Several new canopy designs were developed, including hemisflo ribbon, equiflo ribbon, and hyperflo parachutes. The hemisflo ribbon parachute proved to be the most practical design for velocities up to Mach 3.

In a follow-on program in the early 1960s, the Goodyear Aerospace Corporation developed the ballute (BALLoon-ParachUTE), an inflatable balloon-type decelerator discussed in detail in section 5.8.3.

At supersonic speeds, all parachutes exhibited canopy breathing, high-frequency ribbon flutter, and a progressive decrease in the canopy mouth area. The tested parachutes did not increase the drag coefficient while approaching Mach 1 but had a constant drag coefficient to about Mach 1.2 to 1.4. Thereafter, the drag coefficient decreased, because the gradual decrease in inflated parachute diameter acted as an automatic reefing system.

Parachute canopies of a spherical tension-s ^h shape, such as hemisflo and hyperflo designs, exhibited less breathing and flutter and a slower decrease in inflated diameter with increasing Mach number than did flat and conical parachutes.

Canopies with suspension lines twice as long as the nominal parachute diameter had higher drag and less tendency to gradual canopy closing.

A high canopy porosity is required to obtain sufficient airflow through the canopy to prevent canopy chocking. The three parachute types best suited for supersonic operations—the conical, hemisflo, and hyperflo ribbon parachutes— are shown in Figure 5-90.

Ribbed and ribless guide surface parachutes operated well at speeds up to Mach 1.4 but had high opening shocks and suffered structural damage caused by excessive flutter. Seam separation and material disintegration resulted.

Figure 5-91, taken from Reference 2.2, plots the drag coefficient, C_{D_0} , versus Mach number for four types of ribbon parachutes investigated in the Air Force program (References 5.121 to 5.124).

Since the Air Force research program, numerous supersonic wind-tunnel and free-flight tests have been conducted on parachutes. In wind-tunnel tests, canopy stress is very severe because of long exposure to high velocities. Heavy canopy breathing and high-speed flutter frequently result in material disintegration, seam separation, and canopy damage. In actual use, parachutes operate for only a short period of time in supersonic flow because of the normally high rate of deceleration typical of parachute systems. References 5.125 to 5.127 are three of the many reports available on the wind-tunnel and free-flight testing of parachutes deployed at supersonic velocities.

Low-altitude, high-dynamic-pressure application of nylon parachutes is limited to about Mach 2.2, because at higher speeds aerodynamic heating starts to melt the leading edge of the canopy and lightweight canopy parts, such as ribbons and tapes. Complete canopy destruction has been experienced on high canopy-loading ribbon parachutes deployed at Mach 3 at altitude and medium dynamic pressures.

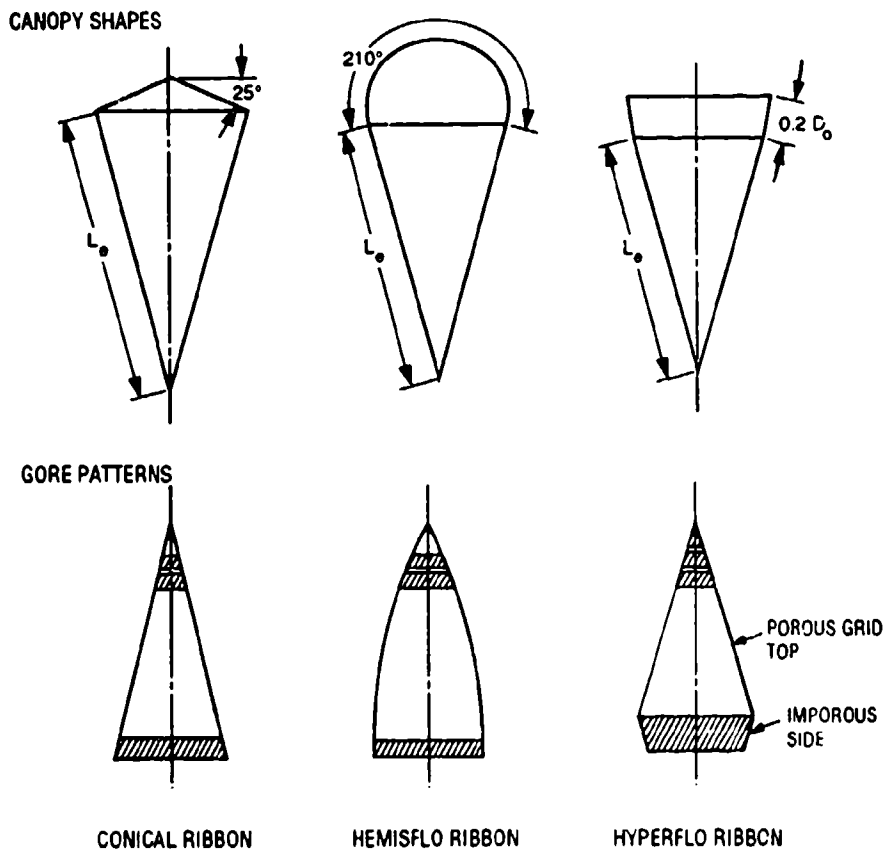


FIGURE 5-90. Configurations of Three Supersonic Ribbon Parachutes.

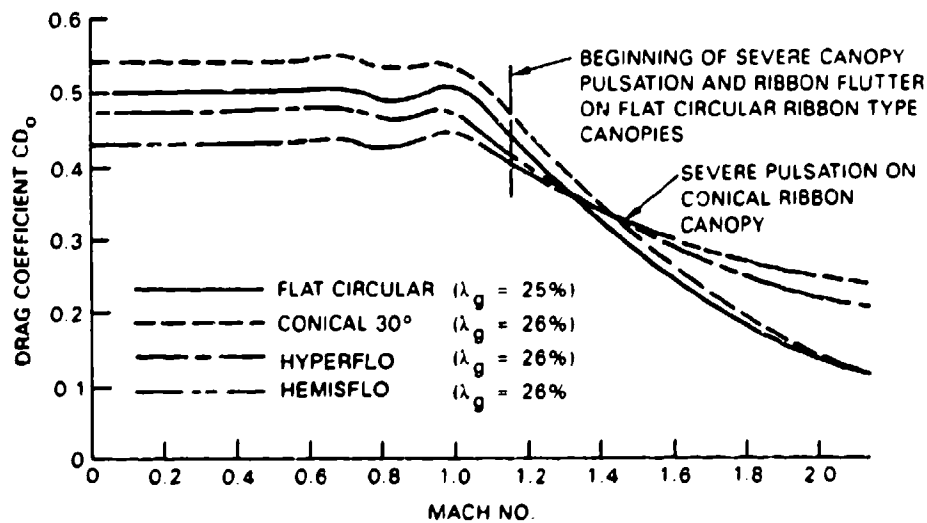


FIGURE 5-91. Drag Coefficient of Several Ribbon Parachutes as Function of Mach Number (1962 Data).

Slotted and solid material parachutes deployed at altitudes above 110,000 feet and at low dynamic pressures in NASA's PPEP program did not experience aerodynamic heating problems (Reference 5.101). References 5.128 and 5.129 discuss aerodynamic heating on parachutes and propose methods for calculating these transient temperatures. The forebody wake effect on supersonic decelerators is discussed in References 5.7 to 5.9, 5.130 and 5.131.

The Northrop Corporation summarized all available information on supersonic ribbon parachutes in the 1970s. The data in Figures 5-92 through 5-95 are from the Northrop report. References 5.132 through 5.134 confirm and supplement the Northrop data. The drag-area-versus-Mach-number graphs in Figure 5-96 have been successfully used in the computer analysis of time-velocity-force-position calculations of parachute recovery systems.

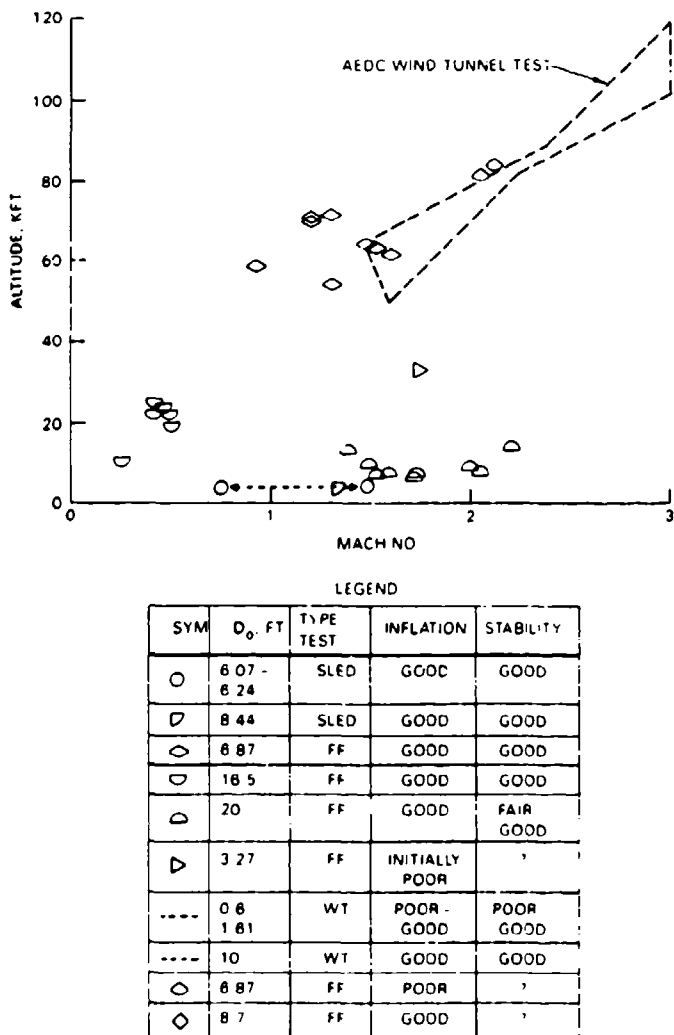
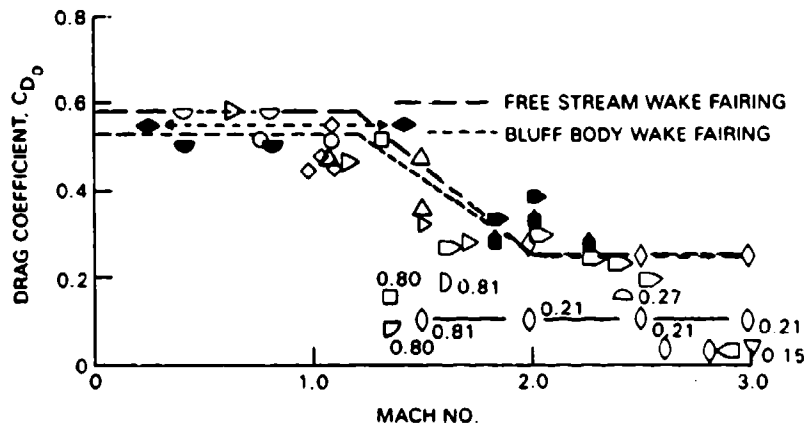


FIGURE 5-92. Demonstrated Mach Number/Altitude Range of Conical Ribbon Parachutes.



LEGEND

SYM	TYPE OF TEST	PARACHUTE PARAMETERS				
		D_o , FT	L_s/D_o	λ_o , %	μ , °	REEF RATIO
○	SLED	6.24	1.0	25.2	15	UNREEFED
□	SLED	6.24	1.0	25.8	20	UNREEFED
△	SLED	6.07	1.0	25.7	30	UNREEFED
◇	SLED	6.18	1.2	26.5	45	UNREEFED
◻	SLED	8.44	1.0	24	20	0.20
□	SLED	8.44	1.0	24	20	0.30
◇	WIND TUNNEL	1.0	2.34	28	?	UNREEFED
○	WIND TUNNEL	1.61	1.8	14	20	0.21
□	WIND TUNNEL	10	2.0	14	?	0.15
△	WIND TUNNEL	10	1.0	14	?	0.15
●	FREE FLIGHT* (MERCURY DROGUE)	6.87	0.88	27.2	30	FIXED REEFING
○	FREE FLIGHT (APOLLO DROGUE)	16.5	2.0	22.8	25	UNREEFED
□	FREE FLIGHT	20	1.3	28	20	0.27
○	FREE FLIGHT	23	1.0	24	30	31
□	WIND TUNNEL	0.6	?	20	?	UNREEFED
●	WIND TUNNEL	0.8	?	19	?	UNREEFED
△	FREE FLIGHT	3.27	1.0	20	30	UNREEFED

*PERMANENTLY REEFED TO 8.0 FT DIA

NOTES:

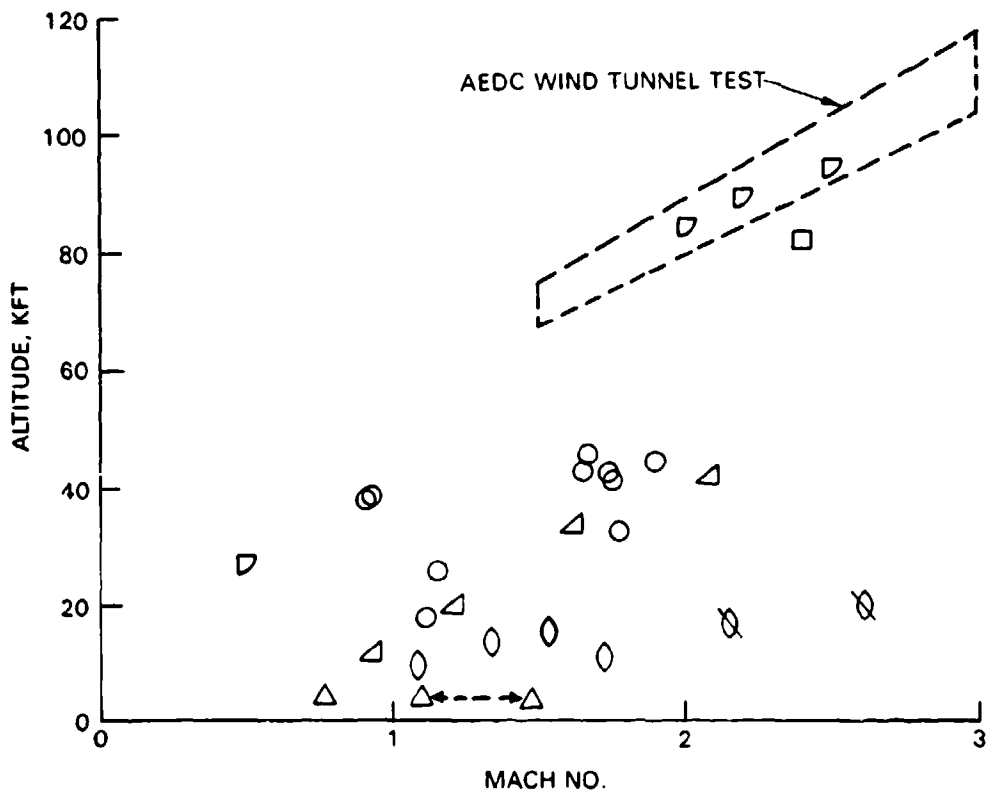
FILLED SYMBOLS REPRESENT C_D_0 VALUES MEASURED IN THE WAKE OF A BLUFF BODY

NUMBERS ADJACENT TO REEFED PARACHUTE DATA INDICATE REEFING RATIO

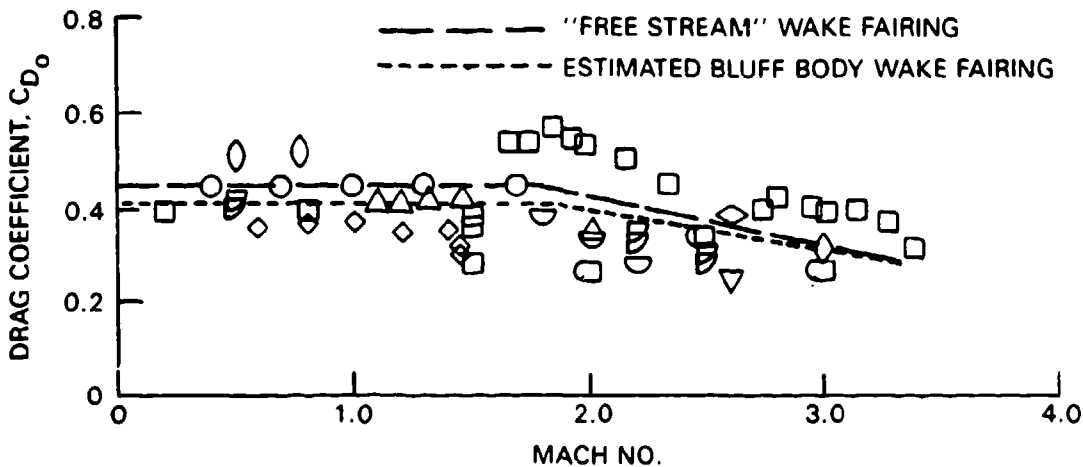
 μ = CANOPY CONE ANGLE

FIGURE 5-93. Drag Coefficient Versus Mach Number for Conical Ribbon Parachutes.

NWC TP 6575



FIGU. 14 Demonstrated Altitude Versus Mach-Number Range of Hemisflo Ribbon Parachutes.



NOTE: ALL DATA MEASURED IN THE WAKE OF
STREAMLINED BODIES

SYM	TYPE OF TEST	PARA PARAMETERS		
		D_0 , FT	L_s/D_0	λ_T , %
○	FREE FLIGHT	3.56	1.8	21
□	FREE FLIGHT	4.12	1.8	14.3
△	SLED	6.77	1.96	27.3
◊	WIND TUNNEL	1.15	1.8	21
▷	WIND TUNNEL	6.0	2.0	15&18
□	WIND TUNNEL	1.08	1.7	14
◊	WIND TUNNEL	6.0	2.0	8
○	SLED	6.24	1.96	25.4
□	WIND TUNNEL	1.07	2.0	28
▽	WIND TUNNEL	6.0	2.0	21
◊	WIND TUNNEL	6.0	2.0	10
□	WIND TUNNEL	5.5	2.0	18

FIGURE 5-95. Drag Coefficient Versus Mach Number for Hemisflo Ribbon Parachute.

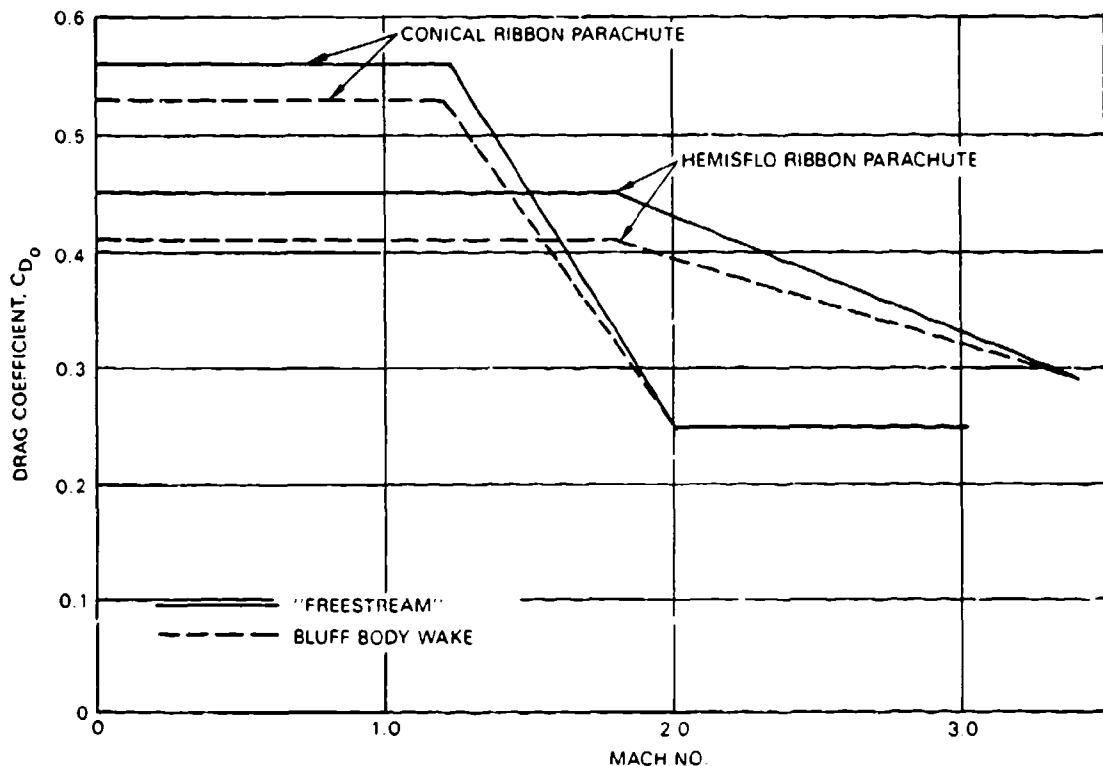


FIGURE 5-96. Drag Coefficient Versus Mach Number for Conical Ribbon and Hemisflo Parachutes (Recommended for Computerized Analysis of These Parachutes).

5.8.3 Balloon-Type Inflatable Decelerators

Several configurations of inflatable balloon-type decelerators have been investigated. So far only the ballute, developed by the Goodyear Aerospace Corporation under government contract (Reference 5.135), has been used operationally at subsonic and supersonic velocities. The configuration of the ballute, also called attached inflatable decelerator (AID), is illustrated in Figure 5-97. The balloon-shaped rear and center part is a tension shell; the conical forward part carries the loads to a junction point for connection with the forebody. A burble fence around the equator of the ballute creates a uniform flow separation, thereby eliminating destabilizing forces. The burble fence and the inverted conical front part together provide good stability. Air scoops in front of the burble fence ram-air inflate the ballute. Inflation with stored gas or gas generators has been investigated but was replaced with the simpler ram-air inflation method.

Figure 5-98 shows the ballute drag coefficient, C_{Dp} , as a function of a Mach number. The drag coefficient relates to the inflated area of the ballute, S_p , and not to the total surface area, S_o , as is customary on parachutes.

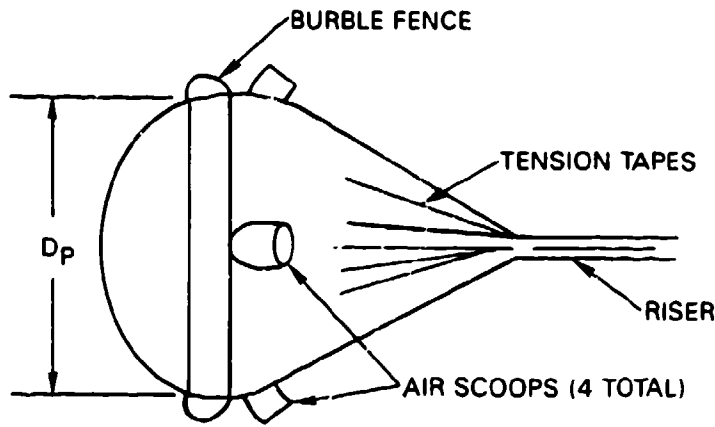
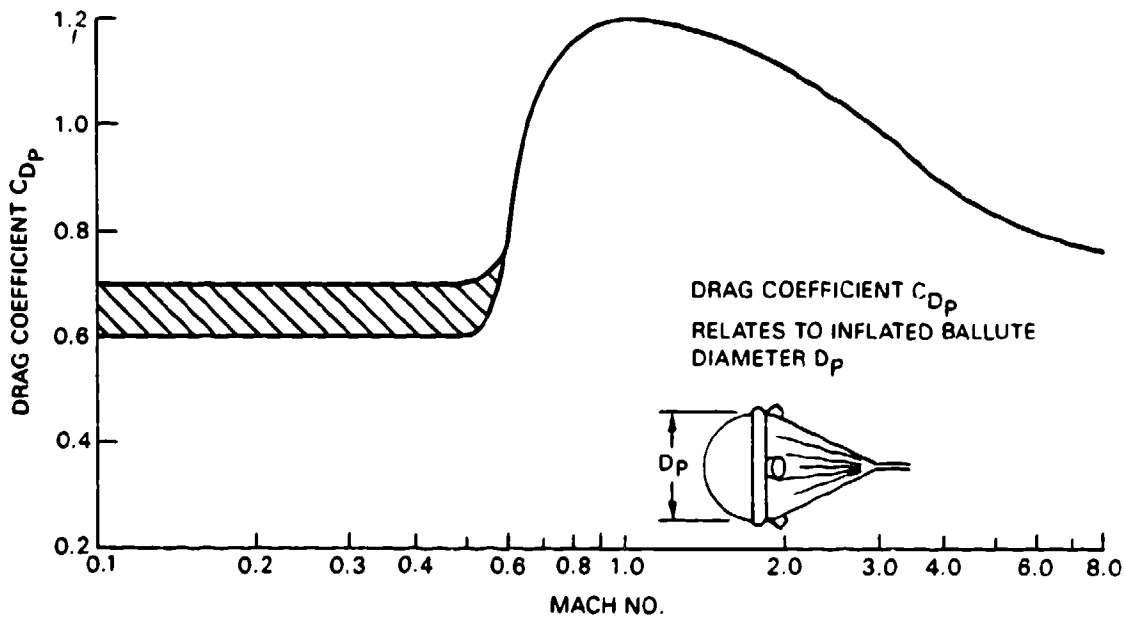


FIGURE 5-97. Ballute-Type Inflatable Decelerator.

FIGURE 5-98. Drag Coefficient, C_{D_0} , Versus Mach Number for Goodyear Ballute.

The inflation of the ballute is fast and uniform. Figure 5-99 compares force-time traces of a ballute and a parersonic parachute tested in the Tullahoma 16-foot supersonic wind tunnel at a constant velocity. The more uniform force, and the lower opening-force coefficient, C_x , of the ballute are shown. The parersonic parachute is related to the hemisflo parachute (Reference 5.136).

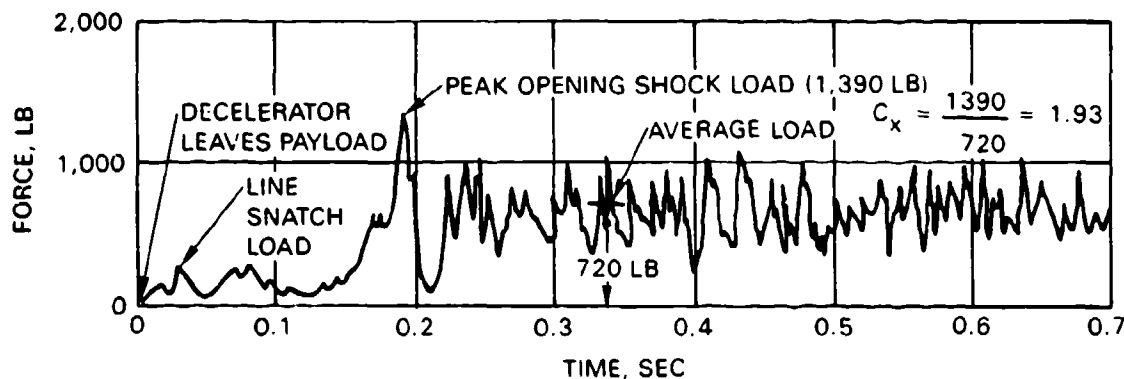
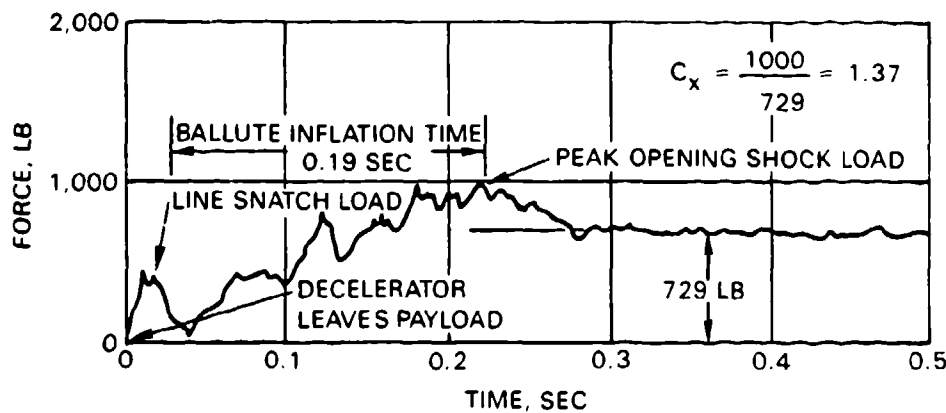
5.5 - FT D_0 PARASONIC PARACHUTE FORCE vs TIME AT MACH 2.6, $q = 220$ PSF.3 - FT DIAMETER BALLUTE, FORCE vs TIME AT MACH 2.6, $q = 220$ PSF.

FIGURE 5-99. Force-Versus-Time Comparison Between a 5.5-Foot-Diameter Parasonic Parachute and a 3-Foot-Diameter Ballute Tested at Mach 2.6.

Known applications of the ballute are the stabilization/retardation device for the Gemini spacecraft back-up ejection seat with an upper deployment limit of Mach 4 at 80,000 feet altitude, and the low-altitude retarder for the Mk 82 bomb.

Figure 5-100 compares the drag coefficient, C_{D_0} , of the conical ribbon, hemisilo ribbon, and guide surface parachutes with the ballute. The solid lines refer to the recommended application range, and the dotted lines indicate areas with limited data or areas where the decelerator should be used with caution. The drag coefficient of the ballute is referenced to the total surface area and not to the projected area as in Figure 5-98. References 5.137 to 5.139 are part of the literature available on ballute testing and application.

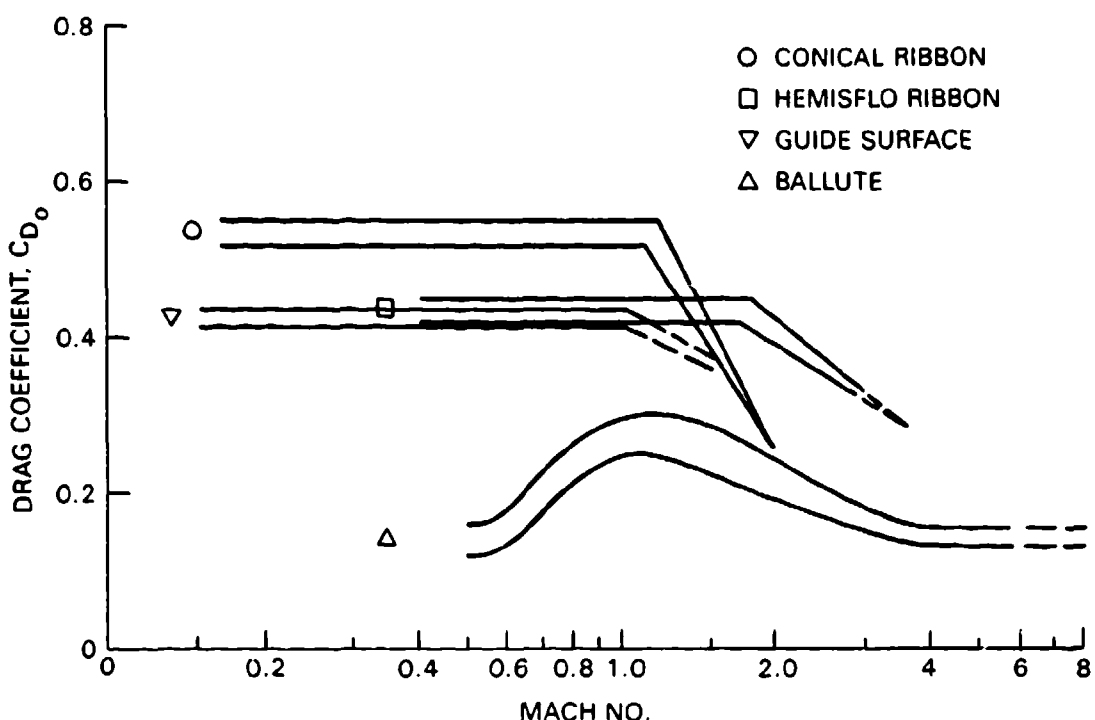


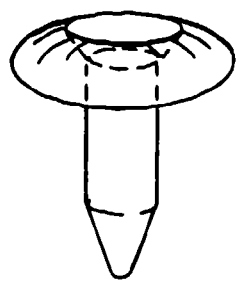
FIGURE 5-100. Drag Coefficient, CD_0 , as Function of Mach Number for Various Aerodynamic Decelerators.

5.8.4 Miscellaneous Decelerators

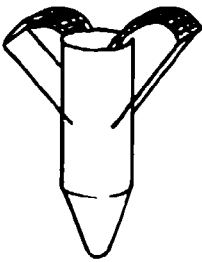
Various aerodynamic decelerators of rigid, semirigid, rotating, and inflatable design have been suggested or tested in the past. Figure 5-101 shows some of these decelerators, and Reference 5.140 compares some of the proposed supersonic decelerators.



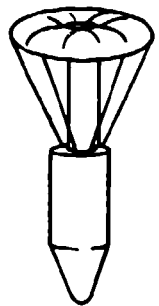
FIGURE 5-101. Various Types of Decelerators.



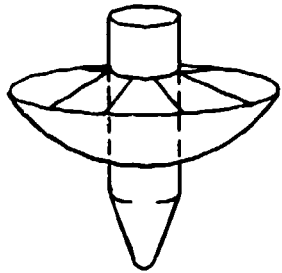
INFLATABLE DRAG RING



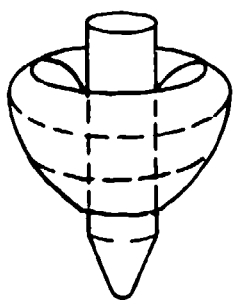
PARAFLAP



INFLATABLE PARASKIRT



AVCO DRAG BRAKE



INFLATABLE RING DECELERATOR

Figure 5-101. Various Types of Decelerators. (Contd.)

5.9 MANEUVERABLE (GLIDING) PARACHUTES

5.9.1 Parachute Types

Maneuverable parachutes in this manual refer to parachutes that can glide and turn and thereby provide the capability to fly toward a ground target or a selected landing area. Sport parachutists use these parachutes to perform aerial maneuvers.

The desire to make parachutes maneuverable is as old as the use of parachutes. The first recorded attempt is that of the Frenchman, Lateur, who was killed in 1856 while testing a maneuverable parachute of his own design. The American, DeGraff, suffered a similar fate in 1887.

In 1929, E. I. Hoffman, formerly Chief of the U.S. Army Parachute Test Group at McCook Field, Ohio, developed the Hoffman triangle parachute, the first practical

maneuverable parachute. It had a triangular canopy with two rounded corners and one cut-off corner, the latter forming an open scoop. Air exhausting horizontally from the scoop produced a thrust in one direction and a glide in the opposite direction. Pulling steering lines attached to both sides of the scoop deformed the canopy, causing air to be exhausted tangentially and the parachute to turn. The parachute's glide ratio was about 0.4 to 0.5 (Reference 5.141).

During World War II, the British developed the blank-gore parachute, a circular canopy with cloth removed from selected canopy gores to create thrust in one direction and glide in the opposite direction, as with the Hoffman triangle parachute. Turn control is again obtained by control lines and appropriate canopy deformation.

The best-known blank-gore-type parachute is the MC1-1B, a T-10 paratrooper parachute modified with double TU slots extending over 11 gores (see Figure 5-102). This parachute has a glide ratio L/D of 0.75 and a turn rate of 180 degrees in 5 seconds (Reference 5.142).

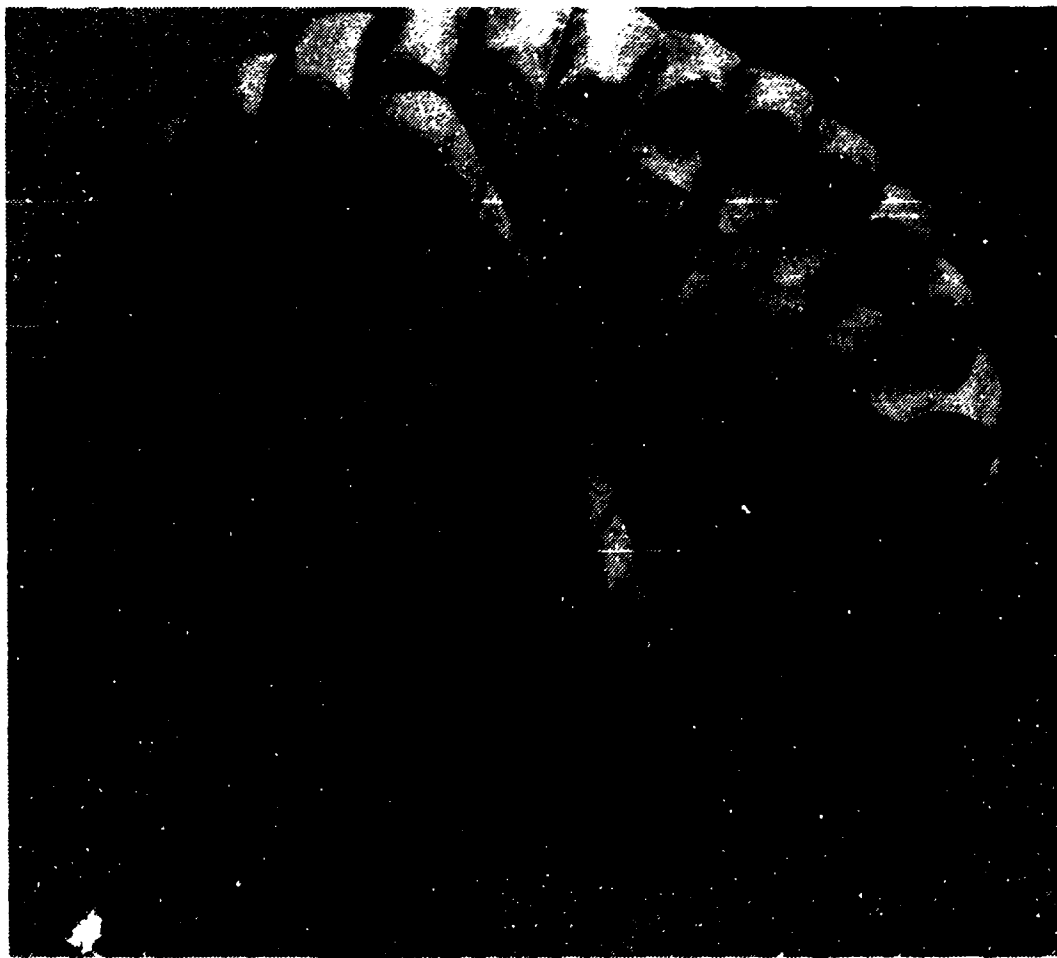


FIGURE 5-102. MC1-1B Parachute, the Maneuverable Version of the T-10 Paratrooper Parachute.

A notable increase in maneuvering performance was obtained by the French LeMoigne parachute, which combines multiple aerodynamically shaped canopy slots with stabilizer vanes and control lines. This parachute has obtained a glide ratio of 0.85 and a turn rate of better than 3 seconds for a 180-degree turn. The Pioneer Parachute Company improved the performance of the LeMoigne parachute in the paracommander (Figure 5-103), obtaining a glide ratio of 1.1 to 1.2, a high turn rate, and good landing control (References 5.143 and 5.144).

In 1972 the Naval Parachute Unit at El Centro, Calif., conducted extensive comparison tests with maneuverable personnel parachutes, including several types of blank-gore parachutes, the MC1-1B paratrooper parachute, and the paracommander. This program documented the high performance of the paracommander parachute (Reference 5.145).

The development of maneuverable personnel parachutes was greatly accelerated by the ever-increasing popularity of sport jumping and by the desire to land manned and unmanned spacecraft on land rather than in the ocean.

The following requirements were established for maneuverable sport-jumper and spacecraft parachutes:

Sport Parachuting

- 5.1. A glide ratio L/D of better than 1.5.
- 5.2. A turn rate of 3 seconds or less for a 180-degree turn.
- 5.3. A fast, uniform opening with opening forces limited to the equivalent of 10 g or less.

Spacecraft Landing

- 5.1. Capability to glide toward and land in a preselected landing area.
- 5.2. Capability to land in ground winds up to 30 knots.
- 5.3. Capability to avoid such ground obstacles as roads and high power lines.
- 5.4. Capability to limit parachute opening forces to 3 to 4 g and landing impact forces to 4 g.
- 5.5. Capability to land in all weather, day and night.

These requirements, especially those for spacecraft landing, led to the development of a number of high-performance maneuverable parachutes. These include the Rogallo wing (parawing) developed by NASA, the cloverleaf parachute developed by Northrop, the ram-air inflated parafoil developed by D. C. Jalbert, the volplane developed by Pioneer, and the Barish sailwing. Three of these parachutes are shown in Figure 5-104.

The cloverleaf parachute consists of a cluster of three parachutes combined into a single canopy, each with equal-length suspension lines. This arrangement of parachutes creates one

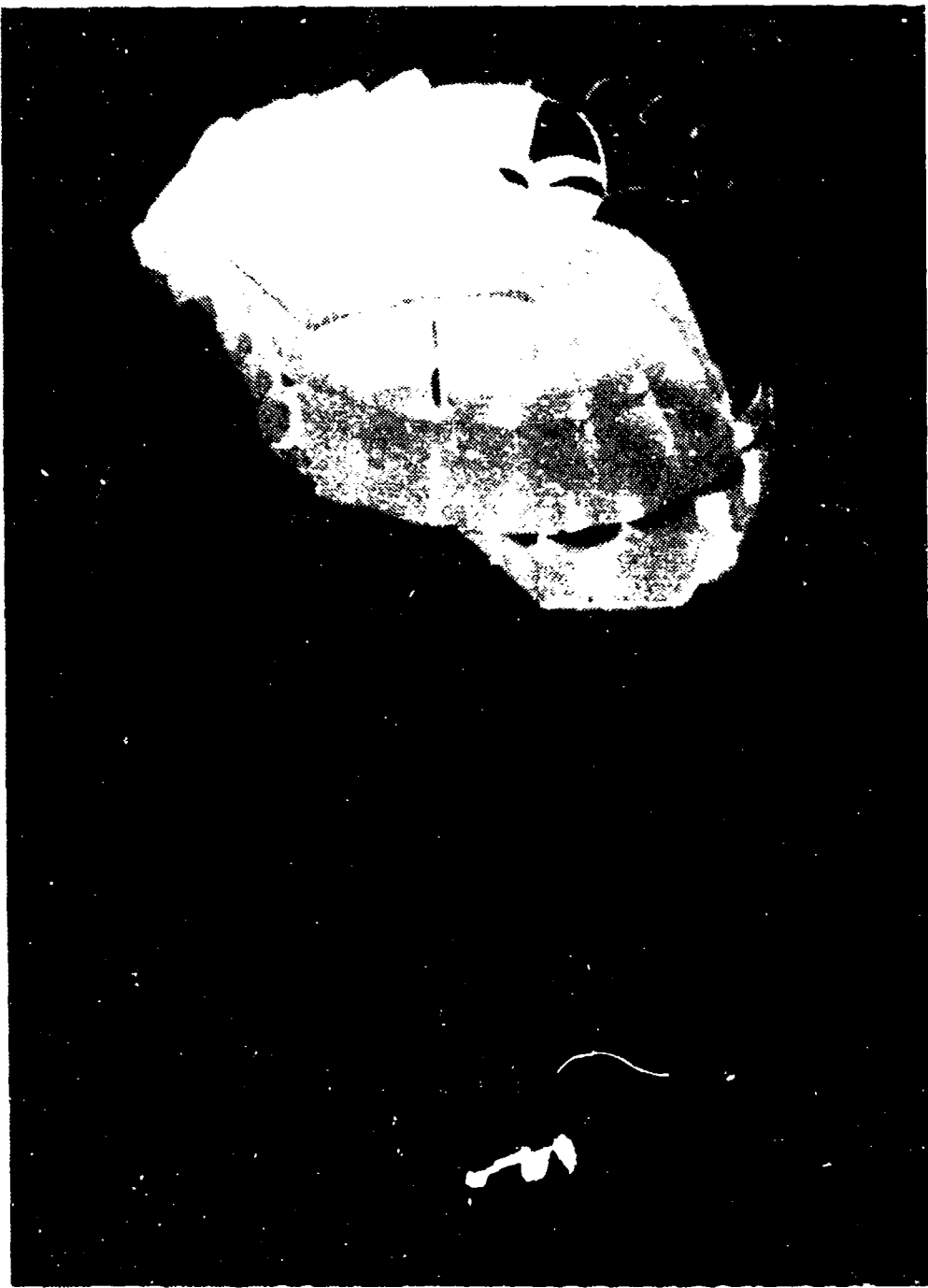


FIGURE 5.403 - The Pteranodon in flight Flying With a Gurney-Spivack Model

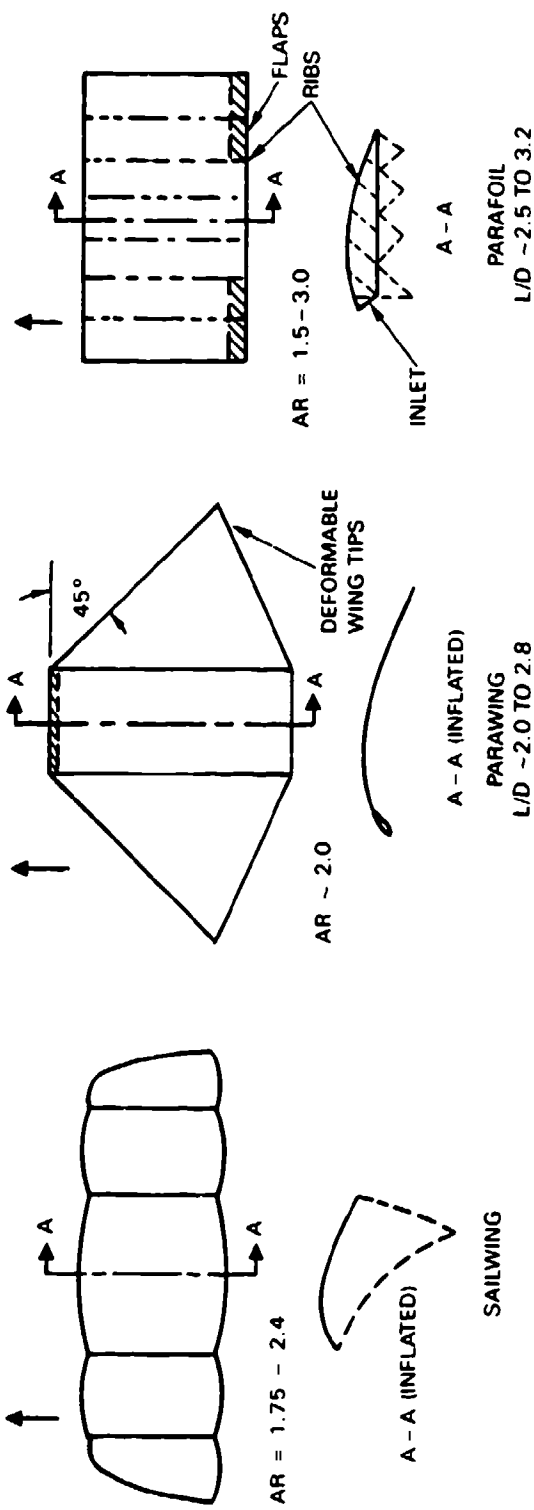


FIGURE S-104. Three Types of Advanced Maneuverable Parachutes.

parachute with an aspect ratio, AR, of about 2.0, reducing the induced drag and increasing the glide ratio. A rounded leading edge of the canopy is created by form ribs to avoid early flow separation and leading edge cave-in. Turn and landing control is obtained by alternate or simultaneous activation of two flaps on the trailing edges of the two rear canopy lobes. The canopy opens the same as a circular parachute. The use of imporous material results in a fast-opening parachute canopy and associated high opening forces. Northrop Corporation conducted an extensive development program on the cloverleaf parachute in the 1960s, starting with wind-tunnel model tests and ending with free-flight tests of a 56-foot-diameter parachute tested at 180 knots with a 3000-pound instrumented test vehicle. The cloverleaf parachute has a glide ratio up to 2.0 and good maneuver and landing capabilities. Opening forces can be limited to 4 g by use of multiple reefing, a somewhat complex method caused by the noncircular configuration of the canopy. References 5.146 and 5.147 give a detailed description of this development program.

The Rogallo wing or parawing is shown in Figure 5-104 in the twin-keel version. The canopy consists of two triangles in the single-keel version, and has a rectangular area between the two triangles in the twin-keel version. The twin-keel version can be equipped with rib-supported formed leading edges. Extensive development programs were conducted by industry, funded by NASA and the Air Force. Opening of the irregular-shaped canopy can be made uniform if controlled by multiple reefing. The single-keel version has a glide ratio L/D of 2.0 and the twin-keel version a glide ratio of 2.8. Deflection of the wing tips produces excellent maneuverability. The development programs included wind-tunnel model tests and flight tests of twin-keel parawings of up to 4000-square-foot wing area and 110-foot wing span tested with vehicles weighing up to 6000 pounds. A design drawback is the variation in suspension-line length around the canopy and the resulting uneven line loads. The high opening force of the nonporous material canopy requires three-step reefing to meet the load limitations for spacecraft applications when deployed at an altitude of 18,000 feet and a dynamic pressure of 90 lb/ft² (References 5.148 through 5.151).

The parafoil parachute, invented by D. Jalbert, consists of an all-flexible inflatable wing with an opening at the leading edge of the airfoil for ram-air inflation. For structural integrity and control of inflation, the wing is designed with individual cells (Figure 5-104). Suspension lines of equal length spanwise but various length cordwise give the wing an anhydral deflection, which provides stability and avoids end-cell collapse. Maneuverability is obtained by individual or simultaneous downward deflection of the outer trailing edges for turn or glide control (References 5.152 and 5.153). Opening forces are high because of the nonporous canopy material, similar to that of the parawing. (For a more detailed discussion of parawing and parafoil opening forces, see section 5.9.3). Sport parachutists use a suspension-line sliding keeper for opening-force control. Use of hi-glide parachutes for air vehicles and for aircraft escape requires multiple reefing. Lingard (References 5.154 and 5.155) provides a good

analysis of parafoil aerodynamics, design, and performance. References 5.156 through 5.161 describe individual development programs.

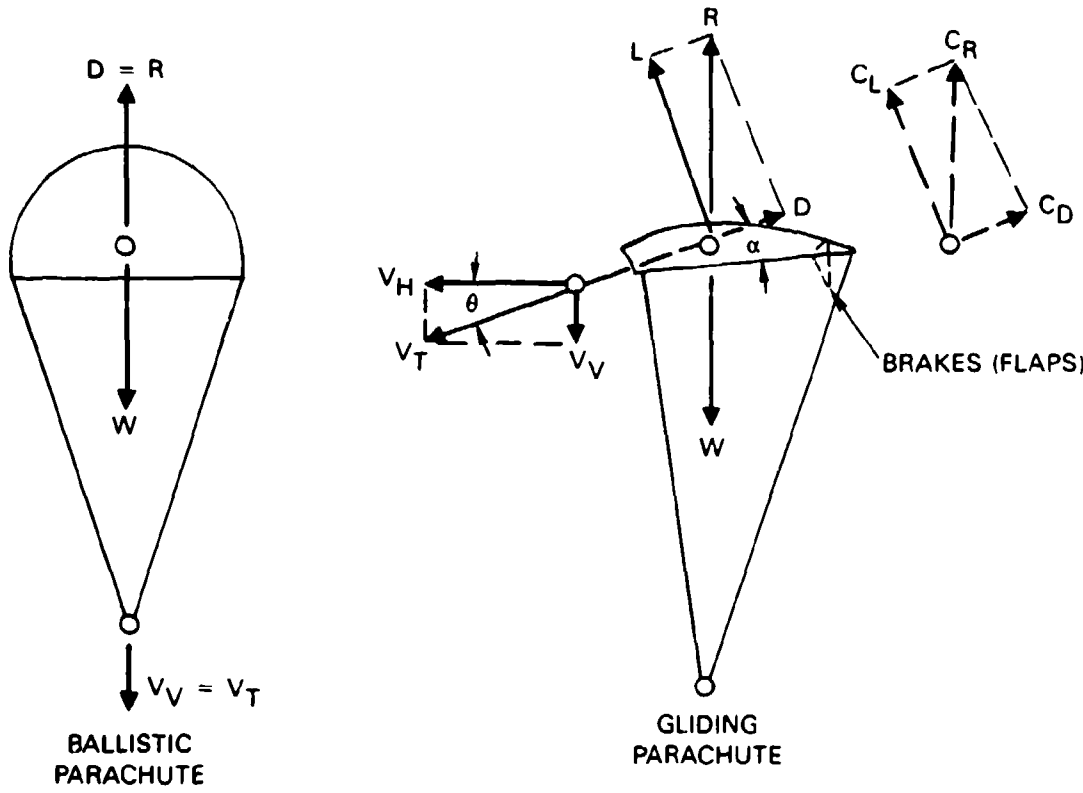
Two other hi-glide parachutes that have demonstrated high glide and maneuver performance are the Pioneer-developed volplane parachute and the Barish sailwing (Reference 5.162).

5.9.2 Performance of Maneuverable Parachutes

Lift and Drag. Lift and drag of hi-glide parachutes can be analyzed in the same way lift and drag of low-aspect-ratio aircraft wings are analyzed. Figure 5-105, taken from section 4.5, shows the balance of forces on a ballistic and on a gliding parachute. A ballistic parachute has only drag; lift is required to make a parachute glide. The higher the ratio of lift to drag, the better is the glide performance. Selection of an airfoil with a good glide ratio is important in designing the ram-air inflated wing. Another important airfoil characteristic is noncritical stall behavior. The parasite drag of suspension lines, risers, payload (jumper), and other nonlift-producing parts of the parachute system must be included in calculating the expected glide ratio.

An aircraft pilot controls the aircraft attitude and velocity by using the elevator and engine power. This control is not possible on gliding parachutes because of the lack of power and the long distance between the center of aerodynamic forces in the canopy and the center of gravity of the total system. The gliding parachute flies with a fixed angle, called the trim angle, between the wing and the vertical of the wing-payload system. This angle is generally the angle of optimum glide. Changing the angle of attack as it can be changed in airplanes requires changing the attitude and length of the suspension lines during flight, which is technically very difficult. Several hi-glide parachutes use flaps for lift and limited glide control. Sport parachutists use this method for landing in a controlled stall, a skillful but also critical maneuver.

Figure 5-106 shows the C_L/C_D diagram and the associated glide ratios for four vehicle-gliding parachute systems using a cloverleaf, a twin-keel parawing, a ram-air inflated parafoil, and a rigid wing with a NASA 4424 airfoil, each having an aspect ratio of 2.0. The rigid-wing vehicle reaches a glide ratio of 6.8, the optimum condition for an unpowered glide system. The parafoil parachute system obtains a glide ratio of 3.2, the parawing 2.9, and the cloverleaf 1.9. These performance data have been confirmed in free-flight tests. For rigid wings as well as gliding parachutes, two points in the C_L/C_D diagram are of special interest: the point of optimum glide and the point of maximum lift. Most hi-glide parachutes are trimmed for the point of optimum glide, as are most aircraft.



$$V_T = \sqrt{\frac{2W}{\rho S}} \quad C_R = \sqrt{C_L^2 + C_D^2}$$

GLIDE RATIO = L/D = C_L/C_D, V_H/V_V

HORIZONTAL VELOCITY V_H = V_T • COS θ

VERTICAL VELOCITY V_V = V_T • SIN θ

LEGEND

L, D, C_L, C_D SEE CHAPTER 4

R = RESULTANT FORCE

W = SYSTEM WEIGHT

V_T = TOTAL VELOCITY

V_V = VERTICAL VELOCITY

V_H = HORIZONTAL VELOCITY

FIGURE 5-105. Forces Acting on a Ballistic and on a Manueverable, Lifting Parachute.

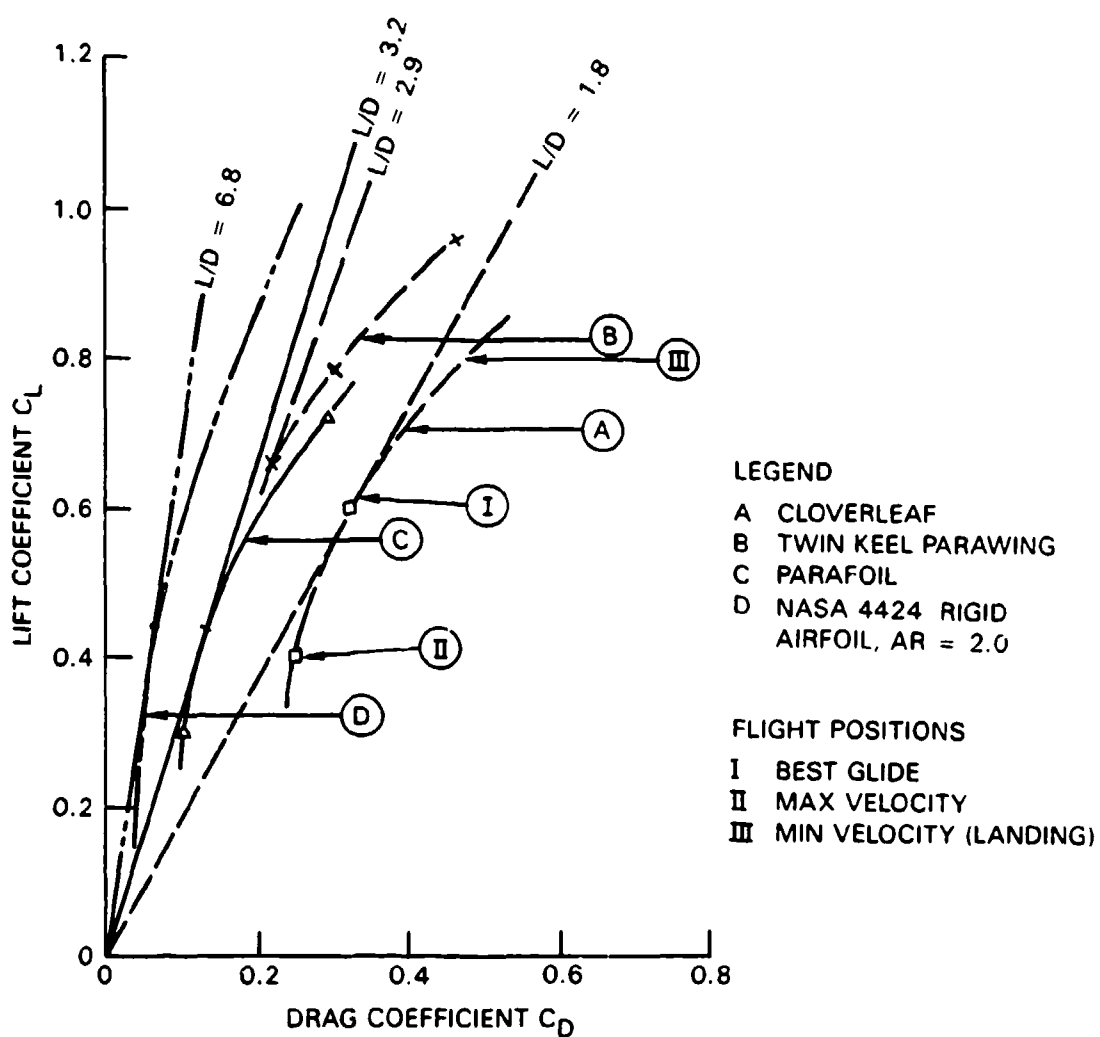


FIGURE 5-106. C_L/C_D Diagram and Glide Ratio L/D for Various Hi-Glide Parachutes and a Rigid Wing Parachute (Drag of Suspension Lines, Riser, and a Hypothetical Air Vehicle are Included).

Increasing the wing (parachute) aspect ratio reduces the induced drag and increases the glide ratio. But a more slender wing requires more and longer suspension lines, which increases the parasite drag. Slender wings are more difficult to deploy, more critical in stall, and less maneuverable. An aspect ratio of 3 appears to be an optimum for high-performance parafoil parachutes.

Vehicle Parachute System Performance. Figure 5-107 shows the glide performance of cloverleaf, parawing, and parafoil vehicle systems versus parachute wing loading, W/S , where W is the weight of the total system and S the area of the parachute. S is the surface area of the single-surface cloverleaf and parawing parachutes and the one-sided area of the parafoil. The diagram assumes that the parachute can be flown over most of the angle-of-attack range

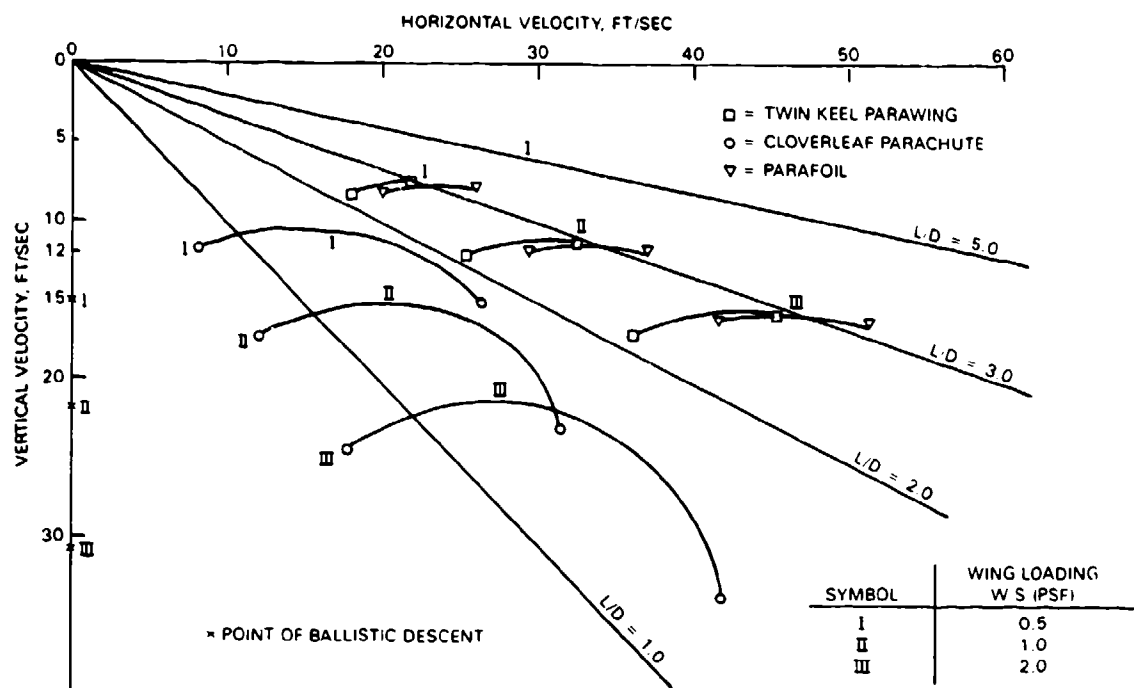


FIGURE S-107. Flight Performance of Maneuverable Parachute-Vehicle Systems.

investigated in wind-tunnel tests. In reality, as previously explained, gliding parachutes are designed for one trim angle, and angle-of-attack changes limited to those obtainable with flap deflection. This design provides a greater range on flap-equipped cloverleaf and parafoil parachutes than on parawings. The flight velocity changes with the square root of the wing loading. Any increase in wing loading slightly decreases the glide performance because of the proportionally larger increase in parasite drag. Spacecraft must be able to land in ground winds up to 30 knots; such a landing requires a high trajectory velocity and resultant high landing velocities.

D. B. Goodrich of the U.S. Army Natick Laboratories has investigated the dynamic flight and landing performance of hi-glide parachute vehicle systems (Reference 5.163).

Turn Control and Landing. All hi-glide parachutes use alternate deflection of the wing tips (parawing) or alternate deflection of the trailing edge flaps (cloverleaf and parafoil) for turn control. This decreases lift and increases drag on the inside wing, causing bank and turn of the wing and providing excellent turn control on all gliding parachutes. However, banking of the wing increases the vertical velocity by the cosine of the bank angle; for this reason, a landing should be made in horizontal attitude and not in a bank. The dependency between bank angle and increase in vertical velocity is shown in Figure 5-108.

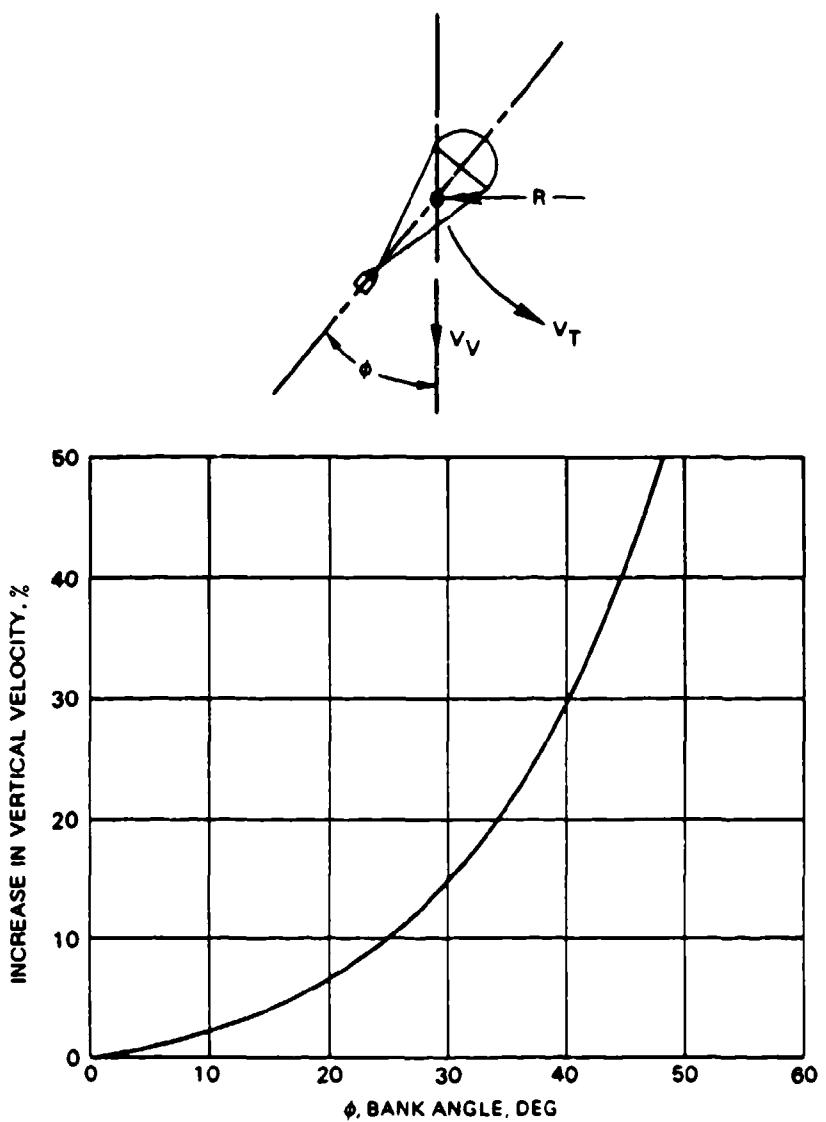


FIGURE 5-108. Increase in Vertical Velocity With Bank Angle.

5.9.3 Opening Forces of Hi-Glide Parachutes

All parachutes manufactured from low- or zero-porosity canopy material have higher opening forces than parachutes manufactured from standard material with porosities in the 100- to 150- $\text{ft}^3/\text{ft}^2/\text{min}$ range. Opening forces measured in free flight on large parawing parachutes were about 75% higher than those on equivalent area circular parachutes manufactured from standard material. These higher opening forces result in an opening-force coefficient, C_x , of 2.6 to 2.7 compared to a C_x coefficient of 1.8 for circular flat and 1.05 for

ribbon parachutes (see Figure 5-43). Force measurements conducted by the U.S. Navy on 350-ft² parafoil parachutes showed about 70 to 75% higher opening forces than those measured on the standard 28-foot-diameter personnel parachute (Reference 5.157). These data are very similar to those obtained on the parawing. Only limited data are available on filling-time and drag-area increase versus time; more information is required for accurate force calculations.

The sliding keeper, the reefing device used on most sport-jumper parafoil (square) parachutes, cannot be analyzed precisely because of variation in gliding friction, radial forces, and related factors.

A cursory analysis of available data on unreefed hi-glide parachutes suggests a filling-time constant, n, of 5 to 6 for the filling-time formulation $t_f = \frac{D_0 n}{V}$. Force calculations that used a filling-time constant of 5.5 and where the drag-area-versus-time curve has a convex shape (see Figure 5-40, section 5.4) gave opening forces in good agreement with those measured in the Navy program.

For velocities in excess of 150 knots, hi-glide parachutes require positive, time-controlled reefing such as the skirt-reefing method. Three reefing steps were required on the 4000-ft² parawing used for the recovery of a 6000-pound Apollo model with forces limited to 4 g. In the Aircraft Gliding Escape System (AGES) Program, the U.S. Navy needed two-step reefing to limit the opening forces to the equivalent of 15 g for bail-out at 300 knots and a 15,000-foot altitude (Reference 5.161).

5.10 CLUSTERING OF PARACHUTES

5.10.1 General

A parachute cluster consists of two or more parachutes used to stabilize, decelerate, or lower a payload or air vehicle. Large 100-foot-diameter G-11 parachutes have been used in clusters of 10 parachutes, and small parachutes have been used in clusters of up to 20 parachutes (Reference 5.164).

Parachute clusters have the following advantages:

1. Several small parachutes are easier to fabricate, store, maintain, rig, handle, and retrieve than a single large parachute.
2. Clustering permits use of the same type of parachute for a large range of weights. Typical is the 100-foot G-11 cargo parachute, which is used for a weight range from 3000 pounds to over 50,000 pounds.

3. A parachute cluster has less probability of a catastrophic system failure than a single large parachute, an important consideration in the recovery of manned and unmanned air and space vehicles.

4. A parachute cluster provides a stable descent system even when using individual, high-drag, unstable parachutes.

5. A parachute cluster has a shorter filling time than a single large parachute.

Parachute clusters can also have the following disadvantages:

1. It is impossible to obtain a perfectly synchronized opening of all parachutes in a cluster. Because unsynchronized opening causes a lead/lag parachute situation, with lead parachutes having shorter filling times and higher individual parachute loads, each parachute in the cluster must be designed to handle the maximum individual load. Therefore, the total strength of the parachutes in a cluster and their associated weight and volume are higher than the weight and volume of a single large parachute of equivalent drag area.

2. Parachute clusters experience a reduction in drag because of interference and systems geometry.

3. Parachute clusters in which individual parachutes have long reefing times (6 to 10 seconds) may experience variation in disreef times because of cutter-time inaccuracies.

4. Using fast-opening parachutes in a cluster promotes the lead/lag parachute inflation situation, resulting in canopy blanketing, delayed opening, and high forces on individual parachutes.

5.10.2 Loss of Drag in Cluster Applications

Figure 5-109 illustrates a typical parachute cluster and shows two different kinds of suspension-line/riser arrangements.

Wind-tunnel tests show that parachutes combined into clusters suffer a reduction in drag because of the geometry of the cluster system, which forces parachutes to fly at a large angle of attack. Reduction in drag probably also occurs because of mutual interference. Long suspension lines or a suspension-line-riser combination decreases the individual angle of attack and thereby increases the cluster drag. This is demonstrated in Figure 5-110, taken from Reference 2.1, which shows the reduction in drag measured in free-flight tests of large-diameter parachutes plotted as drag-coefficient ratio versus number of parachutes in the cluster. The Sandia National Laboratories performed extensive wind-tunnel tests on clusters of up to eight ribbon and solid flat circular 15-inch-diameter model parachutes (Reference 5.165). The ribbon parachute data are also plotted in Figure 5-110 and agree amazingly well with the data obtained in free-flight tests on large parachutes. The Sandia test data on solid flat circular models, although not plotted in Figure 5-110, are in agreement with the ribbon parachute data.

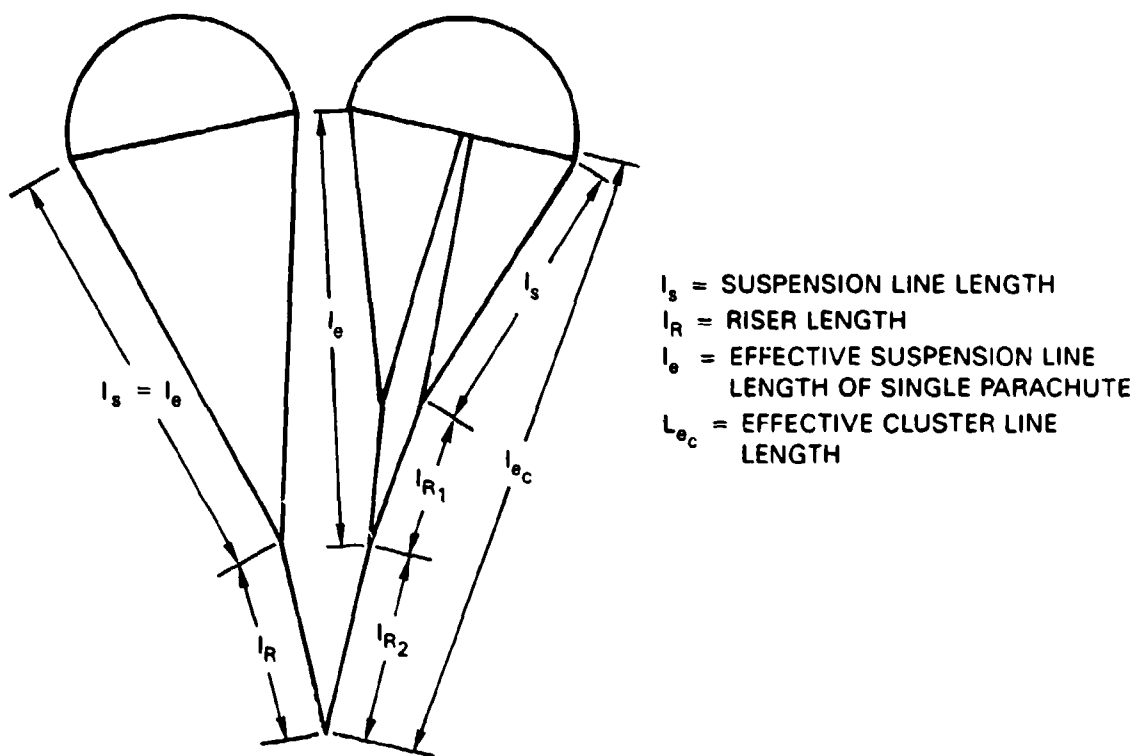


FIGURE 5-109. Typical Parachute Cluster Arrangement.

The lower group of large parachutes in Figure 5-110 consists of airdrop parachutes with short risers. The upper group, containing Apollo program parachutes, has an effective suspension-line/riser length, L_{e_c} , as recommended by Brown.

$$L_{e_c} = D_0 \sqrt{n_c}$$

where n_c is the number of parachutes in the cluster. Individual data measured on the Apollo parachute system were as follows:

Number of parachutes	1	2	3
L_{e_c}/D_0	1.41	1.54	1.54
$C_{D_{0c}}$	0.875	0.85	0.8
$C_{D_{0c}}/C_{D_0}$...	0.97	0.945

COMPOSITE DATA FROM DIFFERENT SOURCES

- 100 FT (D_o) G - 11 A ($l_o/D_o = 1.0$), REF. 2.2
- ◇ 100 FT (D_o) FLAT ($V_e < 25$ FTS), REF. 5.50
- ◊ 100 FT (D_o) FLAT ($V_e = 25 - 30$ FTS), REF. 5.50
- 88.1 FT (D_o) RINGSAIL ($l_o/D_o = 1.40$), REF. 5.50 *
- 85.6 FT (D_o) MODIF. RS ($l_o/D_o = 1.44$), REF. 5.50 *
- △ 128.9 FT (D_o) RINGSAIL ($l_o/D_o = 1.15$), REF. 5.50
- × 1.25 FT (D_o) RIBBON, NO RISER, REF. 5.165
- + 1.25 FT (D_o) RIBBON, LONG RISER, REF. 5.165 *

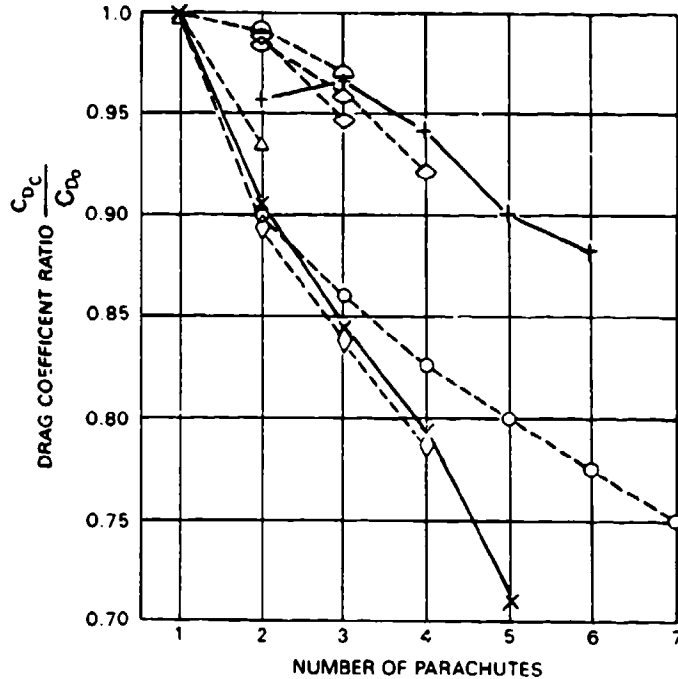


FIGURE 5-110. Drag Loss in Parachute Clusters.

5.10.3 Operational Cluster Experience

Proper operation of a parachute cluster depends on the configuration of the vehicle to be recovered, the prudent selection of the best suited type of parachute, the number of parachutes in the cluster, the diameter of the individual parachute, the selected cluster geometry, and the canopy loading (rate of descent) of the cluster assembly. Canopy loading, $W/(C_D S)_p$, has a distinct effect on uniform, simultaneous canopy inflation and related opening forces. The cluster of three unreefed 24-foot-diameter ringslot parachutes used for extracting airdrop platforms opens uniformly with only small differences in parachute opening forces (Reference 5.166). The cluster of three unreefed ribbon landing deceleration parachutes for the B-70 bomber inflated uniformly with uniform loads.

A cluster of three 24-foot-diameter parachutes manufactured from 0.25-oz/y² Mylar for a rate of descent of 5 ft/s would not operate properly. One or two parachutes inflated, but never all three. This difference in behavior is directly related to the canopy loading. The three platform extraction parachutes and the B-70 landing deceleration parachutes have a neglectable velocity drop during canopy inflation; therefore, sufficient dynamic pressure is available to inflate all three parachutes. When one of the three Mylar parachutes inflated ahead of the others, the velocity and dynamic pressure decreased so rapidly that the remaining pressure was insufficient to inflate the lag parachute(s).

Final-descent parachutes used for the airdrop of military equipment and the recovery of missiles and other air/space vehicles are generally in the 20- to 30-ft/s (0.4 to 1.0 lb/ft² canopy loading) range. This parachute group requires reefing of the parachute canopy to obtain reasonable, uniform canopy opening and uniform opening forces.

Early airdrop of military equipment using clusters of unreefed parachutes resulted in very irregular parachute operation. Parachutes opened sequentially, not uniformly, producing high opening loads, noninflation of lag parachutes, and destruction of the early inflating parachutes from overload. Reefing the individual parachutes in the cluster allowed all parachute canopies to obtain an initial reefed inflation followed by a reasonably uniform full inflation and inflation forces.

Reefing the individual parachutes made it possible to use parachute clusters for the recovery of equipment and manned and unmanned air and space vehicles (References 5.167 and 5.168).

The parachute cluster for the airdrop of military equipment uses a single or multiple parachute assembly for the extraction of the load platform. When the cluster is disconnected from the platform, the cluster lifts the main parachute bags off the platform and serves as pilot chute for the deployment of the main parachutes.

This deployment concept is not possible for the air vehicle shown in Figure 5-111. Extraction of the parachute bags from the vehicle compartment and parachute deployment by a single pilot chute would result in contact with the vertical stabilizer and would damage the parachute. In Figure 5-111, two pilot chutes were deployed by two drogue guns firing from the parachute compartment under 45 degrees upward, outward, and to the rear, providing for independent deployment of the two main parachute bags left and right of the vertical stabilizer (Reference 5.23).

The parachute cluster of the Earth landing system for the Apollo command module was designed so that no single component failure could cause a catastrophic system failure. This requirement ruled out all single-connection points and necessitated individual attachments and deployment of the two ribbon drogue chutes and the three ringsail main parachutes from

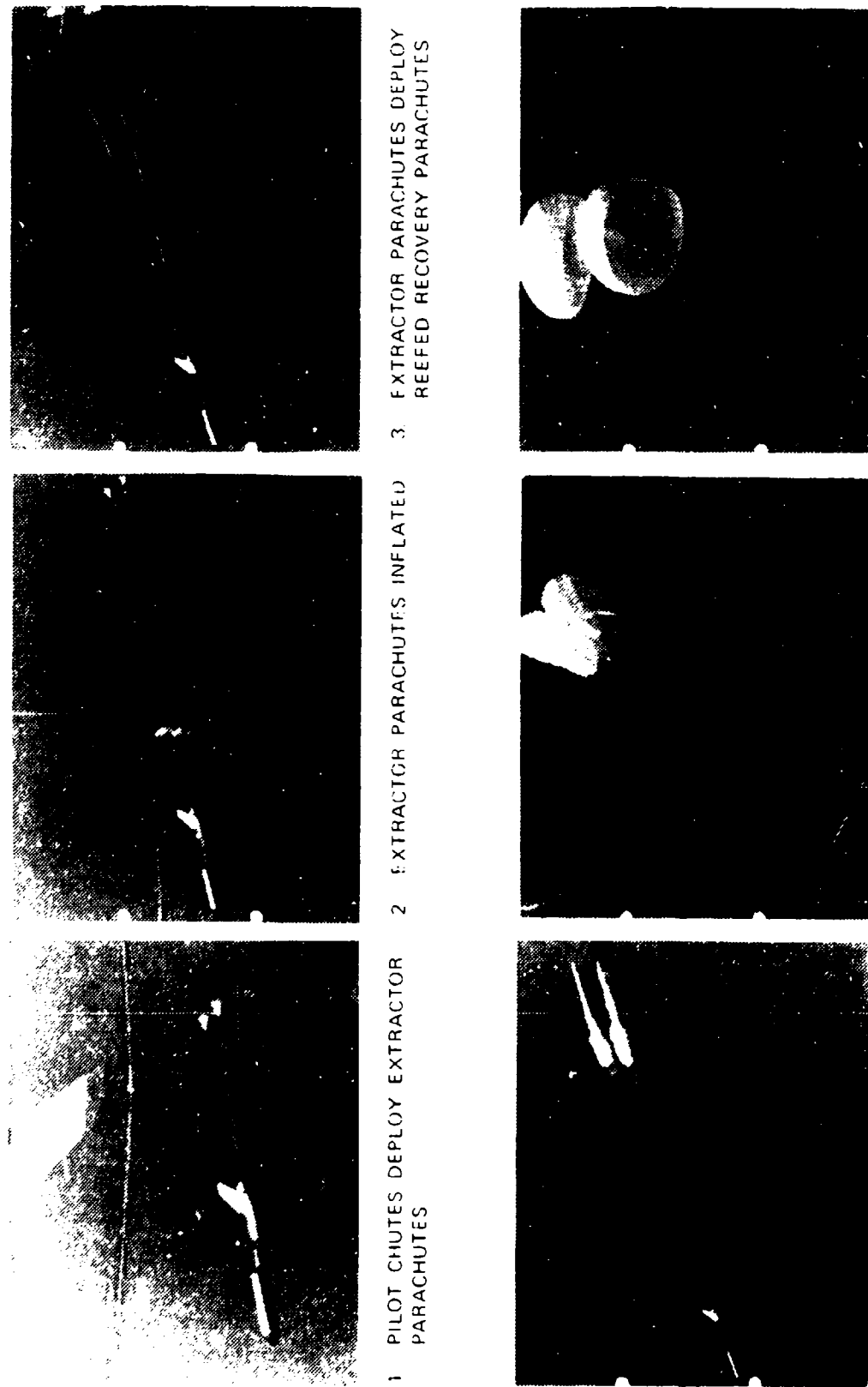


FIGURE 5-111. Uniform Opening of a Cluster of Two 78-Foot-Diameter Extended-Skirt Parachutes.

the unstable command module. This major analysis and design problem was made more difficult by the possibility of riser contact with the red hot heat shield.

Use of the ringsail parachute for the Apollo landing system presented another problem. Ringsail parachutes tend to grow in the reefed stage, crowding out the lag parachute or parachutes, causing a large force difference at disreef, and requiring all parachutes to be designed to accommodate the higher forces. Locating a wide slot at the first reefed inflation stage limited the growth of the reefed canopy stages and made inflation and forces more uniform. A force sharing of 40-40-20 was the best uniformity that could be obtained on the Apollo parachute cluster.

The cluster of three 70-foot-diameter ringsail parachutes for the crew module of the B-1 bomber used the independent parachute deployment concept of the Apollo system at the start of the program, but similar nonuniform inflation problems occurred. Two pilot chutes over a common junction point were permanently attached with long bridles to each main parachute assembly, notably improving the uniform inflation and load sharing of the three main parachutes (References 5.169 and 5.170). The single-failure-point aspect of the junction of the two pilot chutes was accepted, because parachute recovery of the crew module is already the backup and not the primary system.

Slow-opening extended-skirt parachutes have proven to be more uniform in cluster inflation (see Figure 5-111).

Limited experience indicates the fast-opening ringsail parachutes may be preferable for clusters using parachutes in the 120- to 138-foot-diameter range. Large parachutes manufactured from standard-porosity material open very slowly, resulting in false vents, canopy twisting, and other problems (References 5.14, 5.50, and 5.171).

Design, testing, operation, and problems with the cluster of three large ribbon parachutes for the water recovery of the solid-rocket boosters of the NASA space shuttle is discussed in considerable detail in papers presented at the 1979 AIAA conference on Aerodynamic Decelerator and Balloon Technology (see Reference 2.9).

As a rule, parachute clusters are stable assemblies even if the individual parachutes—such as circular flat, conical, or polyconical parachutes—are unstable. The moment coefficient graph (Figure 5-33) clearly shows that parachutes in a cluster operate at individual angles of attack where the destabilizing moment is close to zero. The dynamic stability of parachute cluster-vehicle systems is treated in References 5.172 and 5.173.

Detail design of parachute cluster assemblies is discussed in section 6.3.1. Additional cluster information is found in References 5.174 through 5.179.

5.11 FREQUENTLY USED FORMULAS IN PARACHUTE DESIGN

Dynamic Pressure

In equilibrium descent, parachutes descend at a constant dynamic pressure, q :

$$q = \frac{\rho v^2}{2} \text{ (lbs/ft}^2\text{)}$$

where

v = velocity in ft/s

ρ = mass density of air at ambient altitude in slugs/ft³

For velocity given in indicated air speed, dynamic pressure q can be calculated to

$$q = \frac{v^2}{x} \text{ (lbs/ft}^2\text{)}$$

where $x = \frac{v}{x}$

	knots	MPH	ft/s	km/h
x	295.9	391.2	841.4	1013.1

If the dynamic pressure is given, the equilibrium velocity, v , is

$$v = \sqrt{q x}$$

For true airspeed, the dynamic pressure is

$$q = \frac{v^2}{x} \sigma$$

where

$$\sigma = \frac{\rho}{\rho_0} \text{ (See Table 3-3)}$$

and the true airspeed is

$$v = \frac{\sqrt{q x}}{\sigma}$$

Parachute Rate of Descent and Diameter

$$v_e = \sqrt{\frac{2 W_T}{C_{D_0} S_0 \rho}}, \text{ ft/s}$$

where

W_T = weight of payload plus parachute assembly, lb

C_{D_0} = parachute drag coefficient related to s_0 , dimensionless

s_0 = canopy surface area = $\frac{\pi D_c^2}{4}$, ft²

v_e = equilibrium velocity (rate of descent), ft/s

ρ = mass density of air at desired altitude, slugs/ft³

For a given system weight, W_T ; a required rate of descent, V_e , at an altitude with the density, ρ , and using a parachute with a known drag coefficient, C_{D_0} , the required nominal parachute diameter is obtained by

$$D_0 = \sqrt{\frac{2.547 W_T}{C_{D_0} v_e^2 \rho}} \text{ ft}$$

The following simplified formulas can be used for determining parachute diameter and rate of descent at any altitude:

$$D_0 = \frac{\sqrt{W_T}}{v_{e0}} y \sqrt{\frac{\rho_0}{\rho}} \quad \text{and} \quad v_{e0} = \frac{\sqrt{W_T}}{D_0} y \sqrt{\frac{\rho_0}{\rho}}$$

The factor y as a function of parachute drag coefficient, C_{D_0} , is plotted in Figure 5-112, and the density ratio, σ , is plotted in Table 3-3.

For sea-level conditions

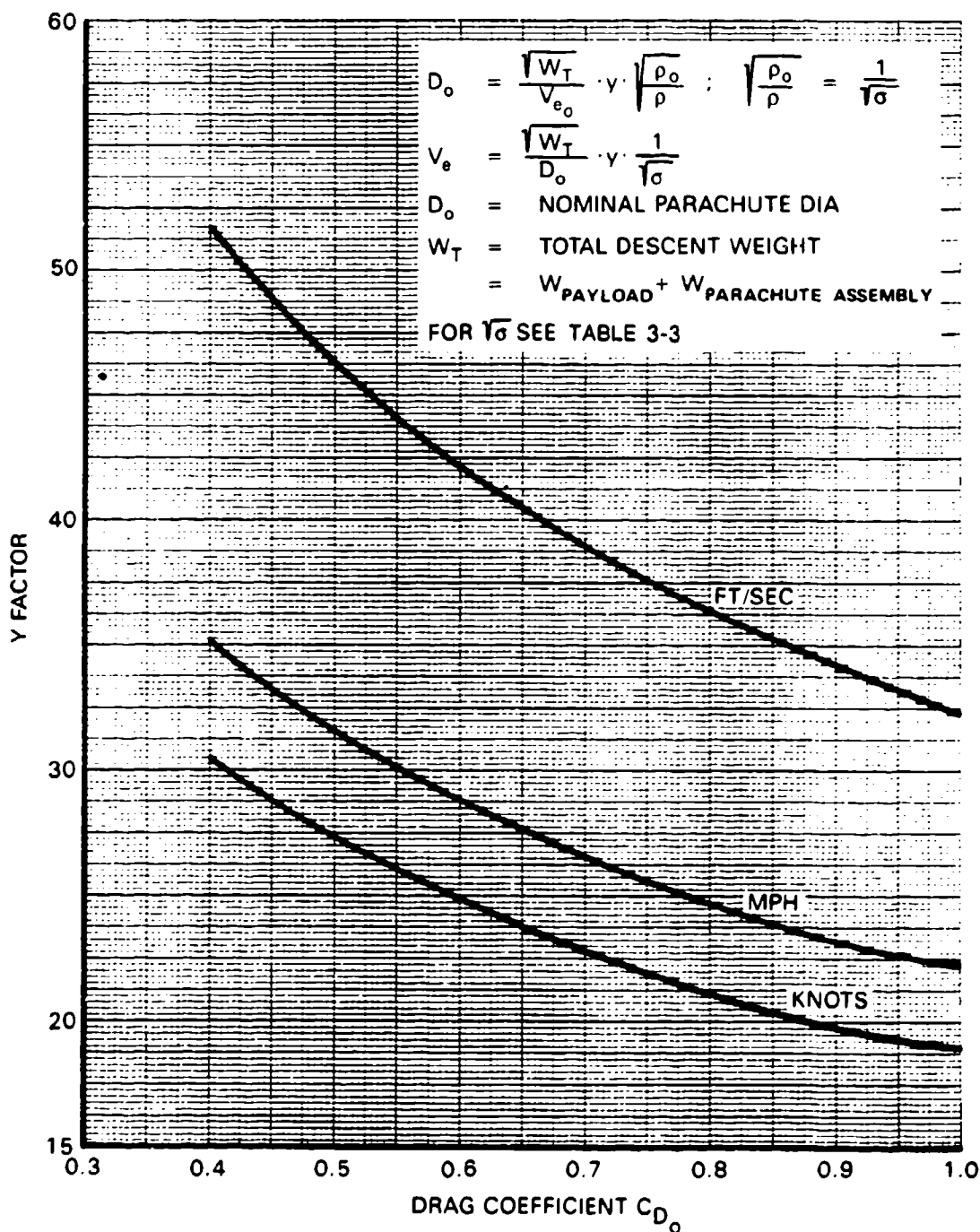
$$\sqrt{\frac{\rho_0}{\rho}} = 1.0$$

If V_{e0} is the sea-level rate of descent, then the rate of descent, V_e , at any altitude is

$$V_e = V_{e0} \frac{1}{\sqrt{\frac{\rho}{\rho_0}}} = V_{e0} \cdot \frac{1}{\sqrt{\sigma}}$$

To convert from rate of descent at altitude x_1 to rate of descent at altitude x_2 ,

$$V_{e_{x_2}} = V_{e_{x_1}} \sqrt{\frac{\sigma_{x_1}}{\sigma_{x_2}}}$$

FIGURE S-112. Y-Factor as Function of Drag Coefficient, C_{D_0} , and Velocity.

5.12 REFERENCE MATERIAL

- 5.1. U.S. Air Force. *Model Parachutes; Comparison Tests of Various Types*, by T. W. Knacke and A. M. Hegele. USAF, January 1949. (USAF Report MCREXE-672-12B.)
- 5.2. T. W. Knacke. Unpublished results of tests conducted by the U.S. Air Force 6511th Test Group (Parachutes), El Centro, Calif., 1953.
- 5.3. T. W. Knacke. Unpublished results of drop tests conducted with 1-meter D_0 model parachutes in a controlled environment, 1943.
- 5.4. U.S. Air Force. *Drop Tests of 16,000 In² Model Parachutes, Summary Report, Volume VII*, by J. F. Stimmier and R. J. Ross. USAF, April 1960. (USAF Report AF-TR-5867.)
- 5.5. ———. *CD Effects of Line Length and Number of Panels of a Flat, Circular Parachute*, by P. R. Doty. USAF. (USAF Report TSEAC14-672-3-3-4.)
- 5.6. Royal Aircraft Establishment. *The Effect of Various Factors on Parachute Characteristics*, by T. F. Johns and E. I. Auterson. RAE, Farnborough, England, January 1944. (R&M 2335.)
- 5.7. U.S. Air Force. *The Drag of Cones, Plates and Hemispheres in the Wake of a Forebody in Subsonic Flow*, by H. G. Heinrich and E. L. Haak. USAF, December 1961. (USAF Report ASD-TR-61-587.)
- 5.8. ———. *Drag Characteristics of Plates, Cones, Spheres and Hemispheres in the Wake of a Forebody in Transonic and Supersonic Flow*, by H. G. Heinrich and R. S. Hess. USAF, December 1964. (USAF Report RTD-TDR-63-4242.)
- 5.9. F. Dayman, Jr. and D. W. Kurtz. "Forebody Effects on Drogue Drag in Supersonic Flow." AIAA Paper, January 1968. (AIAA 68-8.)
- 5.10. T. W. Knacke. "The Apollo Parachute Landing System." Paper presented at the AIAA Aerodynamic Deceleration Systems Conference, El Centro, Calif., April 1968. (USAF Report FTC-TR-69-11.)
- 5.11. U.S. Air Force. *Wind Tunnel Tests for Defining the Parachute Retardation System for the Ejectable Nose Section of the XS-2 Research Aircraft*, by T. W. Knacke. USAF, June 1981. (USAF Report AFWAL-TM-81-130.)
- 5.12. C. W. Peterson and D. W. Johnson. "Reduction in Parachute Drag Due to Forebody Wake Effect." AIAA Paper. (AIAA 81-1939.)
- 5.13. U.S. Air Force. *Development Tests of a Low Altitude, High Speed Escape Parachute*, by I. Rosenberg. USAF. (USAF Report FTC-TN-58-11.)

- 5.14. U.S. Air Force. *200-Ft-Diameter Solid Flat Parachute, Engineering Tests*, by C. R. Graham. USAF, 6511th Parachute Development Test Group. February 1954. (USAF Technical Note FTL-54-1.)
- 5.15. National Parachute Test Range. *Results of Parachute Opening Force Test Program*, by J. W. Dahnke, J. F. Palmer, C. L. Ewing. N PTR. (Technical Report 2-76.)
- 5.16. U.S. Air Force. *G-11 A Parachute Ultimate Drop Test Conditions*, by C. R. Graham. USAF, September 1954. (USAF Report FTL-TN-54-23.)
- 5.17. ——. *High Altitude and Air Speed Tests of Standard Parachute Canopies*, by H. F. Freeman and I. Rosenberg. USAF, October 1958. (USAF Report AFFTC-TR-58-32.)
- 5.18. ——. *Performance Evaluation of Pioneer 23-Ft- D_0 Triconical Personnel Parachute*, by C. W. Fisher. USAF, July 1969. (USAF Report AFFTC-TR-69-28.)
- 5.19. Anonymous Pioneer Report. *Summary Report on the Pioneer 100-Ft- D_0 Triconical Parachute*. 1966. (Pioneer Report H-6014.)
- 5.20. W. Everett. "Development of an Improved Midair Retrieval Parachute System for Drone/RPV Aircraft." AIAA Paper. (AIAA 73-469.)
- 5.21. U.S. Naval Parachute Unit. *Test and Evaluation of a 26-Ft. Extended Skirt Personnel Parachute Canopy*, by H. R. Moy. USNPU, El Centro, Calif. (USNPU Technical Report 6-52.)
- 5.22. U.S. Air Force. *Test of Canopy, Extended Skirt Design (T-10)*, by H. R. Engel. USAF, May 1952. (USAF Report TN WCLE-52-16.)
- 5.23. ——. *Design Analysis of Final Recovery Parachutes for B-70 Encapsulated Seat and the USD-5 Drone*, by T. W. Knacke and L. L. Dimmick. USAF, April 1962. (USAF Report ASD-TDR-62-75.)
- 5.24. ——. *67.3-Ft. Nominal Diameter Fully Extended Skirt Parachute*, by K. W. Stevenson. USAF, April 1955. (USAF Report FTC-TN-55-9.)
- 5.25. Naval Ordnance Laboratory. *Model Parachute Wind Tunnel Tests of Several Different Types*, by G. L. Fogel. NOL, October 1954. (NOL TM 2872.)
- 5.26. U.S. Air Force. *Technical Evaluation of the French 'Cross' Parachute*, by C. E. Grinstoff. USAF, August 1963. (USAF Technical Memorandum ASTM-63-1.)
- 5.27. ——. *Drag and Stability of the Cross Type Parachute*, by R. J. Niccum and E. L. Haak. University of Minnesota. USAF, February 1965. (USAF Report AFFDL-TER-64-155.)

- 5.28. Naval Ordnance Laboratory. *Effect of Canopy Geometry on the Drag Coefficient of a Cross Parachute in the Fully Open and Reefed Condition for a W/L Ratio of 0.264*, by W. P. Ludtke. NOL, August 1971. (NOL TR 71-111.)
- 5.29. Naval Surface Warfare Center. *Effect of Canopy Geometry and Cloth Permeability on Drag Coefficient of a Cross Parachute in the Fully Open and Reefed Condition for a W/L Ratio of 0.3*, by W. P. Ludtke. NSWC, February 1982. (NSWC TR 81-441.)
- 5.30. Naval Ordnance Laboratory. *Effects of Canopy Geometry on the Infinite Mass Opening Shock of a Cross Parachute With a W/L Ratio of 0.264*, by W. P. Ludtke. NOL, July 1973. (NOL TR 73-157.)
- 5.31. ——. *Effects of Canopy Geometry on the Spinning Characteristics of a Cross Parachute with a W/L Ratio of 0.264*, by W. P. Ludtke. NOL, June 1972. (NOL TR 72-145.)
- 5.32. Naval Surface Warfare Center. *Wind Tunnel Measurements of the Variation of Suspension Line Forces in a Cross Parachute*, by W. P. Ludtke. NSWC, May 1990. (NSWC TR 89-306.)
- 5.33. U.S. Air Force. *Evaluation of the 73-Foot-Diameter Paraform Recovery Parachute System*, by R. S. Morrison. USAF, December 1979. (USAF Report AFFTC-TR-79-30.)
- 5.34. D. F. Jorgenson and D. J. Cockrell. "Aerodynamics and Performance of Cruciform Parachutes." AIAA Paper, October 1981. (AIAA 81-1919.)
- 5.35. C. Q. Shen and D. J. Cockrell. "Aerodynamic Characteristics of Flow Around Cross Parachutes in Steady Motion." AIAA Paper, October 1986. (AIAA 86-2458 CP.)
- 5.36. U.S. Air Force. *Parachute Airfoil Type, Design and Construction*, by W. C. Buhler. USAF, October 1947. (USAF Report TSEPE-672-19S.)
- 5.37. ——. *Feasibility Study of a Universal Aerial Recovery System, Volumes I and II*, by E. G. Ewing and J. Vickers. USAF, April 1966. (USAF Report SSD-TR-66-47.)
- 5.38. P. R. Delurgio, B. A. Engstrom, and W. C. Buhler. "The Mid-Air Retrieval System for the Air-Launched Cruise Missile." AIAA Paper, October 1981. (AIAA 81-1915.)
- 5.39. U.S. Air Force. *Design, Use and Construction of FIST Type Parachutes*, by T. W. Knacke. USAF, June 1948. (USAF Report MCREXE-672-19LL.)
- 5.40. ——. *Sample Calculation for a Deployable Aerodynamic Decelerator*, by R. J. Berndt and J. H. Dewesee. USAF. (USAF Report FDFR-TM-63-20.)
- 5.41. D. F. McVey, W. B. Pepper, and J. F. Reed. "A Parametric Wind Tunnel Study of Ribbon Parachutes." AIAA Paper, November 1975. (AIAA 75-1370.)

- 5.42. R. C. Maydew and D. W. Johnson. "Supersonic and Transonic Deployment of Ribbon Parachutes at Low Altitudes." *AIAA Journal of Aircraft*, Vol. 9, No. 7, July 1972.
- 5.43. Sandia National Laboratories. *Parachute Design and Performance for Supersonic Deployment and for the Recovery of Heavy Loads*, by W. B. Pepper. SNL, September 1969. (SNL Report SC-DC-69-1883.)
- 5.44. ——. *Design and Development of a Three-Stage Parachute System for Low Level Deployment at Mach 1.2*, by W. B. Pepper. SNL, May 1967. (SNL Report SC-DR-66-2707.)
- 5.45. ——. *Design and Development of a Heavy Duty 76-Ft Ribbon Parachute*, by I. T. Holt. SNL, September 1968. (SNL Report SC-R-68-1793.)
- 5.46. D. F. McVey and D. F. Wolf. "Analysis of Deployment and Inflation of Large Ribbon Parachutes." AIAA Paper, May 1973. (AIAA 73-451.)
- 5.47. D. W. Johnson and C. W. Peterson. "High-Speed, Low-Altitude Delivery Using a Single Large Ribbon Parachute." AIAA Paper, September 1984. (AIAA 84-0803.)
- 5.48. U.S. Naval Parachute Unit. *34-Foot Ringslot Parachute for Marine Resupply Container*, by W. C. Buhler. USNPU, El Centro, Calif, July 1954. (USNPU Technical Report 4-54.)
- 5.49. U.S. Air Force. *Performance Evaluation of a Cluster of Two 28-Foot D₀ Ringslot Extraction Parachutes Towed from a C-130 Aircraft*, by W. L. Brown and H. J. Hunter. USAF, September 1965. (USAF Report AFFTC-TR-65-25.)
- 5.50. ——. *Ringsail Parachute Design*, by E. G. Ewing. USAF, January 1972. (USAF Report AFFDL-54-72-3.)
- 5.51. ——. *Performance of Trailing Aerodynamic Decelerators at High Dynamic Pressure*, by B. A. Engstroem. USAF, January 1958. (USAF Report WADC-TR-58-284.)
- 5.52. ——. *Investigation of F-111 Crew Module Stabilization Parachute (Hemisflo) Model at Mach Numbers of 0.5, 2.0, and 2.5*, by L. L. Galagher. USAF, April 1960. (USAF Report AEDC-TR-65-83.)
- 5.53. ——. *Parachutes, Guide Surface (Ribbed Type)*, by H. G. Heinrich. USAF, February 1948. (USAF Report MCREXE-672-25F.)
- 5.54. Royal Aircraft Establishment. *The Design and Performance of the Ribless Guide Surface Parachute*, by G. G. Gale. RAE, Farnborough, England, November 1962. (Mech. Eng. Technical Note 362.)
- 5.55. H. N. Murrow and C. V. Eckstroem. "Description of a New Parachute for Use With Meteorological Rockets." Paper presented at the AIAA Sixth Conference on Applied Meteorology.

- 5.56. R. D. Moog and Assoc. "Qualification Flight Test of the Viking Decelerator System (DGB Parachute)." AIAA Paper, May 1973. (AIAA 73-457.)
- 5.57. Radioplane. *Aerodynamic Appraisal of the Rotafoil Parachute*, by A. Giffrin. Radioplane, March 1952. (Report 663.)
- 5.58. National Aeronautics and Space Administration. *Drag Characteristics of a Rotary Parachute (Vortex Ring) Tested in a Vertical Wind Tunnel*, by S. M. Burk, Jr. NASA, Langley 1962. (NASA Report D-1388.)
- 5.59. W. B. Pepper. "New High Performance Rotating Parachute." AIAA Paper, April 1984. (AIAA 84-0808.)
- 5.60. U.S. Air Force. *Some Research Efforts Related to Problems of Aerodynamic Retardation*, by H. G. Heinrich. USAF, November 1960. (USAF Report WADD-TN-60-276.)
- 5.61. ———. *Stability and Drag of Parachutes With Varying Effective Porosities*, by H. G. Heinrich and E. L. Haak. USAF. (USAF Report ADS-TDR-62-100.)
- 5.62. Naval Surface Weapons Center. *A View on the Cause of Parachute Instability*, by W. P. Lutke. NSWC, May 1983. (NSWC TR 83-28.)
- 5.63. Royal Aircraft Establishment. *Descent Characteristics of Parachutes*, by H. Henn. RAF translation of German Report ZWE/UM/6202, October 1944. RAE, Farnborough, England.
- 5.64. F. M. White and D. F. Wolf. "A Theory of Three-Dimensional Parachute Stability." AIAA *Journal of Aircraft*, Vol. 5, No. 1, January-February 1968.
- 5.65. D. F. Wolf. "The Dynamic Stability of a Nonrigid Parachute Payload System." AIAA *Journal of Aircraft*, Vol. 8, pp. 604-609, August 1971.
- 5.66. D. J. Cockrell, C. O. Shen, R. J. Harwood, and A. C. Baxter. "Aerodynamic Forces Acting on Parachutes in Unsteady Motion and the Consequential Dynamic Stability Characteristics." AIAA Paper, October 1986. (AIAA 86-2470 CP.)
- 5.67. K. F. Doherr and C. Saliaris. "On the Influence of Stochastic and Acceleration Dependent Aerodynamic Forces on the Dynamic Stability of Parachutes." AIAA Paper, October 1981. (AIAA 81-1941.)
- 5.68. M. Neustadt, et al. "A Parachute Recovery System Dynamic Analysis." *Journal of Spacecraft and Rockets*, Vol. 4, No. 3, March 1967.
- 5.69. National Advisory Committee for Aeronautics. *Parachutes for Aircraft*, by W. Mueller. NACA, October 1927. (NACA TM-450.)

- 5.70. F. N. Scheubel. "Notes on the Opening Shock of a Parachute." Progress Report IRE-65, April 1946, Foreign Exploitation Section, Intelligence (T-2).
- 5.71. F. O'Hara. "Notes on the Opening Behavior and the Opening Forces of Parachutes." *Royal Aeronautical Society Journal*, Vol. 53, November 1949. Pp. 1053-1062.
- 5.72. Northrop Corp. *Theoretical Investigation of the Parachute Inflation Process*, by L. W. Rust. Northrop Corp., Ventura Division, July 1965. (Report NVR-3887.)
- 5.73. U.S. Air Force. *Analysis of Parachute Opening Dynamics With Supporting Wind Tunnel Experiments*, by H. G. Heinrich and R. A. Norem. Proceedings of the 1969 Aerodynamic Deceleration Systems Conference. USAF. (USAF Report FTC-TR-69-11.)
- 5.74. D. F. Wolf. "A Simplified Dynamic Model of Parachute Inflation." AIAA Paper, October 1973. (AIAA 73-540.)
- 5.75. J. W. Purvis. "Theoretical Analysis of Parachute Inflation Including Fluid Kinetics." AIAA Paper, October 1981. (AIAA 81-1925.)
- 5.76. E. Pflanz. *Determination of the Decelerating Forces During the Opening of Cargo Parachutes*. ATI 26111, July 1942. USAF translation of German Report FGZ 231.
- 5.77. ———. *Retarding Forces During Unfolding of Cargo Parachutes*. ATI 20126, September 1943. USAF translation of German Report FGZ 331.
- 5.78. A. J. McEwen. "An Investigation of Parachute Opening Loads, and a New Engineering Method for Their Determination." AIAA Paper, September 1970. (AIAA 70-1168.)
- 5.79. Northrop Corp. *Investigation of Prediction Methods for the Loads and Stresses of Apollo Type Spacecraft Parachutes, Volume I*, by F. E. Mickey, A. J. McEwen, E. G. Ewing, E. C. Huyler, and B. Khajeb-Nouri. Northrop Corp., Ventura Division, June 1970. (Report NVR-6431.)
- 5.80. U.S. Air Force. *The Initial Phase of Parachute Inflation*, by K. E. French. Lockheed Aircraft Corp. Proceedings of the 1968 Aerodynamic Deceleration Systems Conference, El Centro, Calif. USAF, September 1968. (USAF Report FTC-69-11.)
- 5.81. Lockheed Aircraft Corp. *A Method for Determining Parachute Opening Shock Forces*, by D. L. Schilling. LAC, August 1957. (LAC Report 12543.)
- 5.82. G. C. Greene. "Opening Distance of a Parachute." *Journal of Spacecraft and Rockets*, Vol. 7, No. 1, January 1970.
- 5.83. Naval Surface Weapons Center. *Notes on a Generic Parachute Opening Force Analysis*, by W. P. Luttko. NSWC, March 1986. (NSWC TR 86-142.)

- 5.84. Naval Surface Weapons Center. *Notes on a Theoretical Parachute Opening Force Analysis Applied to a General Trajectory*, by W. P. Lutke. NSWC, May 1988. (NSWC TR 88-6.)
- 5.85. K. E. French. "Model Laws for Parachute Opening Shock." *AIAA Journal*, Vol. 2, No. 12, December 1964. Pp. 2226-2228.
- 5.86. J. W. Purvis. "Prediction of Parachute Line Sail During Lines-First Deployment." *Journal of Aircraft*, Vol. 20, November 1983. Pp. 940-945.
- 5.87. U.S. Air Force. *Performance of the BA-18, BA-18 With Spreading Gun and B-25 Parachute Assemblies*, by S. O. Hammond and R. D. Woolman. USAF, November 1976. (USAF Report AFFTC-TR-76-34.)
- 5.88. Naval Weapons Center. "Parachute Suitability Study for Navy Aircrew Common Escape System (NACES)." NWC, China Lake, Calif., July 1984. (Aerosystems Department Memorandum.)
- 5.89. D. B. Webb. "Development and Initial Test Results of a Parachute With Automatic Inflation Modulation (AIM)." AIAA Paper, March 1979. (AIAA 79-0467.)
- 5.90. U.S. Air Force. *Evaluation of Opening Characteristics, A.I.M. Parachute, Phase I and II and Addendum*, by T. J. Brosnahan. USAF, October 1981. (USAF Report AFFTC-TR-80-20.)
- 5.91. ———. *Evaluation of Opening Characteristics, Automatic Inflation Modulation Parachute, Phase III*, by T. J. Brosnahan. USAF, September 1982. (USAF Report AFFTC-TR-82-15.)
- 5.92. Naval Weapons Center. *GQ Aeroconical Personnel Maneuverable, Gliding Parachute Assembly, Type 1000*, by G. Menard. NWC, China Lake, Calif., December 1981. (NWC TP 6296.)
- 5.93. W. Chagaris. Data furnished by the Douglas Aircraft Co., Long Beach, Calif., on ACES II main parachute tests, basic and B-1 tests, February 1985.
- 5.94. U.S. Air Force. *28-Ft Standard Back Style Parachute Quarter Deployment Bag Comparison Test*, by Brooks. USAF, March 1952. (USAF Report AFFTC-TN-52-2.)
- 5.95. ———. *Performance Data for Four, Free-Type, Back-Style Automatic Personnel Parachute Assemblies*, by R. D. Woolman. USAF, January 1975. (USAF Report AFFTC-TR-74-35.)
- 5.96. U.S. Army Air Corps. *The Magnitude and Duration of Parachute Opening Shock at Various Altitudes and Air Speeds*, by G. A. Hallenbeck. USAAC, Engineering Division, July 1944. (Report ENG-49-696-66.)
- 5.97. U.S. Air Force. *High Altitude and High Airspeed Tests of Standard Parachute Canopies*, by H. F. Freeman and I. Rosenberg. USAF, October 1958. (USAF Report AFFTC-TR-58-32.)

- 5.98. U.S. Air Force. *67.3-Ft. D₀. Fully Extended Skirt Parachute, Drop Tests*, by K. W. Stevenson. USAF, April 1955. (USAF Report AFFTC-TN-55-9.)
- 5.99. T. W. Knacke. "High Altitude Parachute Recovery." Paper presented at the 1952 Symposium on Physics and Medicine of the Upper Atmosphere. Reprinted as "Physics and Medicine of the Upper Atmosphere." Univ. of N. Mex. Press, 1952.
- 5.100. Royal Aircraft Establishment. *The Use of Parachutes at High Speeds and High Altitude*, by M. H. L. Waters and A. C. Browning. RAE, Farnborough, England, August 1961. (Mech. Eng. Technical Note 340.)
- 5.101. U.S. Air Force. *Summary of Experimental Results Obtained From the NASA Planetary Entry Parachute Program*, by H. N. Murrow and J. C. McFall, Jr., NASA, Langley. Paper presented at the 1968 Aerodynamic Deceleration Systems Conference, El Centro, Calif. USAF, September 1968. (USAF Report FTC-69-11.)
- 5.102. W. B. Pepper and J. F. Reed. "Parachute Study of Pressure Distribution in Wind Tunnel Testing," *Journal of Aircraft*, Vol. 10, No. 11. Pp. 895 to 900, November 1976.
- 5.103. Naval Ordnance Laboratory. *Effects of Canopy Geometry on the Infinite Mass Opening Shock of a Cross Parachute With a W/L Ratio of 0.264*, by W. P. Luttko. NOL, July 1973. (NOL TR 73-157.)
- 5.104. U.S. Air Force. *Reefing Methods, Parachutes*, by T. W. Knacke. USAF, October 1947. (USAF Report TSEPE-672-25D.)
- 5.105. Royal Aircraft Establishment. *Some Wind Tunnel Experiments on the Reefing of Parachutes*, by M. H. L. Waters and D. B. Cobb. RAE, Farnborough, England, November 1963. (Mech. Eng. Technical Note 329.)
- 5.106. M. W. Higgins. "Recovery System Preliminary Design. A Simplified Approach to Determining Drogue Chute Staging, Timing, and Altitude Requirements." AIAA Paper, March 1979. (AIAA 79-0446.)
- 5.107. U.S. Air Force. *Controlled Opening Parachute (Schade)*, by D. Gold. U.S. Air Force 6511th Test Group (Parachutes), El Centro, Calif., 1956. (USAF Report TN-56-1.)
- 5.108. ——. *The University of Kentucky Continuous Disreefing Device*, by J. F. Lafferty and K. O. Lange. USAF, May 1959. (USAF Report WADC TN 58-177.)
- 5.109. ——. *Determination of the Aerodynamic Drag and Static Stability of Reefed Parachute Canopies*, by A. P. Riffle. USAF, January 1965. (USAF Report AFFDL-TR-64-164.)
- 5.110. ——. *Reefing of Parachutes-Drag Area Ratios Versus Reefing Line Ratios*, by T. W. Knacke. USAF, July 1976. (USAF Report ASD-TR-76-2.)

- 5.111. P. J. Bobbitt, R. J. Mayhue, G. L. Faurote, and L. L. Galigher. "Supersonic and Subsonic Wind Tunnel Tests on Reefed and Unreefed Disk-Gap-Band Parachutes." AIAA Paper, September 1970. (AIAA 70-1172.)
- 5.112. D. F. Wolf and R. H. Croll. "Wind Tunnel Measurements of Dynamic Reefing Line Tension in Ribbon Parachutes." AIAA Paper, March 1979. (AIAA 79-465.)
- 5.113. U.S. Air Force. *Reefing of Parachutes-Forces in Reefing Line*, by T. W. Knacke. USAF, October 1981. (USAF Report ASD-TR-81-5029.)
- 5.114. W. M. Pepper and J. F. Reed. "Parametric Study of Parachute Pressure Distribution by Wind Tunnel Testing." AIAA Paper. (AIAA 75-1366.)
- 5.115. U.S. Air Force. *Pressure Distribution During Parachute Inflation Phase I, Infinite Mass Opening Case*, by H. D. Melzig and P. K. Schmidt. USAF, March 1966. (USAF Report AFFDL-TR-66-110.)
- 5.116. ———. *Pressure Distribution During Parachute Opening*, by H. D. Melzig and C. Salaris. USAF, February 1969. (USAF Report AFFDL-TR-68-135.)
- 5.117. Sandia National Laboratories. *Pressure and Profile Data of 20° Conical Ribbon Parachutes*, Volumes I and II, by H. G. Heinrich. SNL, May 1977. (SNL Report 77-7005.)
- 5.118. Northrop Corp. *Investigation of Prediction Methods for the Loads and Stresses of Apollo Type Spacecraft Parachutes, Volume II Stresses*, by W. M. Mullins, D. T. Reynolds, K. G. Lindh, and M. R. Bottorf. Northrop Corp., Ventura Division, June 1970. (NVR-6432.)
- 5.119. J. F. Henfling and J. W. Purvis. "Pressure Distribution on Parachute Ribbon Shapes." AIAA Paper, September 1984. (AIAA 84-0815.)
- 5.120. K. K. Muramoto and W. L. Garrard. "Method for Calculating the Pressure Field About a Ribbon Parachute Canopy in Steady Descent." AIAA Paper, September 1984. (AIAA 84-0794.)
- 5.121. U.S. Air Force. *Recovery Systems for Missiles and Target Aircraft*, by J. R. Downing, J. H. McClow, R. O. Fredette, and H. V. Hawkins. Part I, II, and III. USAF, March 1954 to December 1958. (USAF Report TR-58-53.)
- 5.122. ———. *Study of Parachute Performance and Design Parameters for High Dynamic Pressure Operation*, by P. F. Pederson. USAF, May 1964. (USAF Report FDL-TDR-64-66.)
- 5.123. ———. *Study and Exploratory Freeflight Investigations of Deployable Aerodynamic Decelerators Operating at High Altitudes and High Mach Numbers*, by W. E. Nikel and W. M. Gran. USAF, July 1964. (USAF Report FDL-TDR-64-35.)

- 5.124. U.S. Air Force. *Supersonic Parachute Research*, by R. Berndt. USAF, July 1966. (USAF Report ASD-TR-66-236.)
- 5.125. Arnold Engineering Development Center. *Performance of Flexible Aerodynamic Decelerators at Mach Numbers From 1.5 to 6*, by J. S. Deitering. AEDC, July 1963. (Report AEDC-TDR-63-119.)
- 5.126. ——. *Aerodynamic Performance of Various Hyperflo and Hemisflo Parachutes at Mach Numbers From 1.8 to 3*, by D. E. Beichenau. AEDC, March 1965. (Report AEDC-TR-65-57.)
- 5.127. ——. *Wind Tunnel Investigations of Flexible Aerodynamic Decelerator Characteristics at Mach Numbers From 1.5 to 6*, by J. S. Deitering. AEDC, June 1965. (Report AEDC-TR-65-110.)
- 5.128. U.S. Air Force. *Transient Temperatures of Parachutes During Descent*, by E. Eckert, et al. USAF, August 1957. (USAF Report WADC-TN 57-320.)
- 5.129. ——. *Instantaneous Local Temperatures of Aerodynamic Decelerators; Part I, Methods of Prediction*, by G. Engholm, et al. USAF, September 1960. (USAF Report WADC-TR-60-670.)
- 5.130. R. M. Nerem and D. W. Henke. "Theoretical and Experimental Studies of Supersonic Turbulent Wakes and Parachute Performance." AIAA Paper, September 1968. (AIAA 68-947.)
- 5.131. R. M. Nerem and T. W. Brunner. "Initial Results on the Theoretical Prediction of Drag for a Trailing Decelerator at Supersonic Speeds." AIAA Paper, September 1970. (AIAA 70-1177.)
- 5.132. C. W. Peterson, D. E. Waye, L. R. Rollstein, and I. T. Holt. "Design and Performance of a Parachute for Supersonic and Subsonic Recovery of an 800-lb Payload." AIAA Paper, October 1986. (AIAA 86-2435-CP.)
- 5.133. X. Lin. "The Gun-Launched Tests for Supersonic Parachutes." AIAA Paper, October 1986. (AIAA 86-2474-CP.)
- 5.134. W. B. Pepper, R. J. Buffington, and C. W. Peterson. "Exploratory Testing of Supersonic Ribbon Parachutes in the NASA 9-Ft by 7-Ft Wind Tunnel." AIAA Paper, October 1986. (AIAA 86-2446.)
- 5.135. U.S. Air Force. *Investigation for Determining the Feasibility of Using Inflatable Balloon Type Drag Devices for Recovery Applications in the Transonic, Supersonic and Hypersonic Flight Regime; Part II, Mach 4 to 10 Feasibility Investigation*, by the Goodyear Corp. USAF, December 1962. (USAF Report ASD-TDR-62-702.)

- 5.136. W. R. Pinnell and F. Blotacher. "Correlation of Analytical and Empirical Techniques for Designing Supersonic and Hypersonic Decelerators." Proceedings of the 1966 AIAA Conference, Houston, Tex., September 1966.
- 5.137. A. C. Aebisher and E. S. Sutters. "Development Status of Ballute System for Stabilization and Retardation of Aircraft Stores." AIAA Paper, September 1970. (AIAA 70-1200.)
- 5.138. M. M. Mikulas and H. L. Bohan. "Summary of the Development Status of Attached Inflatable Decelerators." Proceedings of the 1968 Aerodynamic Deceleration Systems Conference, El Centro, Calif., September 1968.
- 5.139. H. L. Bohan and R. Miserentino. "Attached Inflatable Decelerator Performance Evaluation and Application Study." AIAA Paper, September 1970. (AIAA 70-1163.)
- 5.140. T. T. Blanco, et al. "Recovery of High Performance Reentry Vehicles." Proceedings of the 1966 AIAA Conference, Houston, Tex., September 1966.
- 5.141. Naval Weapons Center. *A Look at the Hoffman Triangle Parachute—The First Successful Gliding Parachute*, by D. Gold. NWC, China Lake, Calif., 1982. (Aerosystems Department publication.)
- 5.142. Naval Aerospace Recovery Facility. *Performance Evaluation, 35-Foot Diameter Extended Skirt Personnel Parachute Canopy Assembly With 'TU' Orifice*, by G. L. Menard. NARC, El Centro, Calif., April 1967. (NARC Report 8-66, AD815808L.)
- 5.143. W. J. Everett. "The Design and Development of the Parasail Parachute." Paper presented at the University of Minnesota Course on Aerodynamic Deceleration, July 1965.
- 5.144. E. D. Vickers. "Aerodynamics of the Parasail (Paracommander)." Paper presented at the University of Minnesota Course on Aerodynamic Deceleration, July 1965.
- 5.145. Naval Aerospace Recovery Facility. *Performance Investigation of Various Configurations of Personnel Maneuverable Parachute Canopy Assemblies*, by G. L. Menard. NARC, El Centro, Calif., February 1971. (NARC Report 5-71.)
- 5.146. U.S. Air Force. *Investigation of Various Textile Parachutes and Control Systems to Achieve Steerability, Parts I to III*, by E. M. Linhart, V. F. Riley, and C. R. Graham, Northrop Corp. USAF, January 1964. (USAF Report FDL-TDR-64-81.)
- 5.147. Northrop Corp. *Development of a Large Controllable Parachute, 56-Ft Diameter Cloverleaf*, by E. M. Linhart and C. R. Graham. Northrop Corp., Ventura Division, March 1967. (Northrop Report NVR-5064.)
- 5.148. F. Rogallo. "Flexible Wings." *AIAA Astronautics and Aeronautics*, August 1968.

- 5.149. U.S. Air Force. *Status of Research on Parawing Lifting Decelerators*, by W. C. Sleeman and T. G. Gainer, NASA, Langley. Proceedings of the 1968 Aerodynamic Deceleration Systems Conference, El Centro, Calif., September 1968. (USAF Report FTC-TR-69-11.)
- 5.150. J. H. Moeller and E. M. Linhart. "Parawing Technology for Spacecraft Land Landing, a Progress Report." AIAA Paper, September 1970. (AIAA 71-1187.)
- 5.151. National Aeronautics and Space Administration. *Free-Flight Investigation of Large All-Flexible Parawings and Performance Comparison with Small Parawings*, by J. H. Moeller. NASA. March 1970. (NASA CR 66918.)
- 5.152. C. D. Jalbert. "Multi-Cell Wing Type Aerial Device." U.S. Patent No. 3,285,546 granted 15 November 1966.
- 5.153. U.S. Air Force. *A Review of Parafoil Programs*, by J. D. Nicolaides, R. J. Speelman, and G. L. Menard. Proceedings of the 1968 Aerodynamic Deceleration Systems Conference, El Centro, Calif., September 1968. (USAF Report FTC-TR-69-11.)
- 5.154. Royal Aircraft Establishment. *The Performance and Design of Ram-Air Gliding Parachutes*, by J. S. Lingard. RAE, Farnborough, England, August 1981. (Technical Report 81103.)
- 5.155. J. S. Lingard. "The Aerodynamics of Gliding Parachutes." AIAA Paper, October 1986. (AIAA 86-2427.)
- 5.156. National Aeronautics and Space Administration. *Wind Tunnel Investigation of Ram-Air Inflated All-Flexible Wings of Aspect Ratios 1.0 to 3.0*, by G. W. Ware. NASA, 1969. (NASA Report TM SX-4187.)
- 5.157. Naval Aerospace Recovery Facility. *Performance Evaluation Tests, Parafoil Maneuverable Personnel Parachute Assembly, Final Report*, by G. L. Menard. NARC, El Centro, Calif., September 1969. (NARC Report 2-69.)
- 5.158. U. S. Air Force. *Parafoil Steerable Parachute, Exploratory Development for Air Drop System Application*, by R. J. Speelman, C. A. Babish, and R. J. Berndt. USAF. (USAF Report AFFDL-TR-71-37.)
- 5.159. Naval Weapons Center. *Basic Performance, Design, and Construction of Ram-Air Inflated Gliding Parachute Wings*, by M. C. Butler. NWC, China Lake, Calif. (NWC TM 5739.)
- 5.160. R. J. Speelman, C. Bradshaw, J. Sobczak, and G. L. Menard. "Hi-Glide Personnel Canopies: Effort Toward Identification of Requirements." AIAA Paper. (AIAA 70-1194.)
- 5.161. Naval Weapons Center. *In-Flight Ejection Seat Test Using the Aircrew Gliding Escape System (AGES) Parachute*, by M. C. Butler, Jr. NWC, China Lake, Calif., September 1986. (NWC TP 6741.)

- 5.162. National Aeronautics and Space Administration. *Wind Tunnel Investigation of the Static Aerodynamic Characteristics of a Multilobe Gliding Parachute (Sailwing)*, by G. W. Ware and C. E. Libbey. NASA. (NASA Technical Note TND-4672.)
- 5.163. D. B. Goodrich. "Theoretical Study of the Longitudinal Stability of High-Performance Gliding Airdrop Systems." AIAA Paper. (AIAA 75-1394.)
- 5.164. W. D. Brown. *Parachutes*. Pub. by Sir Isaac Pitman & Sons, LTD, London, July 1948.
- 5.165. B. K. Baca. "An Experimental Study of the Performance of Clustered Parachutes in a Low Speed Wind Tunnel." AIAA Paper, April 1984. (AIAA 84-0822.)
- 5.166. U.S. Air Force. *Extraction Parachute Clustering Techniques*, by C. W. Marshall. USAF, October 1958. (USAF Report FTC-TN-58-18.)
- 5.167. ———. *G-12B 64-Ft Cargo Parachute Cluster Tests*, by C. W. Marshall. USAF, March 1958. (USAF Report FTC-LR-58-102.)
- 5.168. ———. *G-11, A Parachute Retardation System*, by I. Svoboda. USAF, February 1961. (USAF Report FTC-TN-61-102.)
- 5.169. W. C. Buhler. "Development of a High Performance Ringsail Parachute Cluster." AIAA Paper, May 1973. (AIAA 73-468.)
- 5.170. Pioneer Parachute Co. *B-1 Crew Module, Parachute Recovery System Qualification Tests*, by W. C. Buhler. BBC, April 1974. (Document 1155.)
- 5.171. E. D. Vickery and M. Eldredge. "Development of a System of Six Clustered 137-Ft Diameter Parachutes to Recover 60,000 Pounds." AIAA Paper, October 1986. (AIAA 86-2445-CP.)
- 5.172. D. F. Wolf and H. R. Spahr. "A Parachute Cluster Dynamic Analysis." AIAA Paper, November 1975. (AIAA 75-1398.)
- 5.173. U.S. Air Force. *Drag and Dynamics of Single and Clustered Parachutes in Freestream and With Wake and Ground Effects*, by H. G. Heinrich and R. A. Norem. USAF, November 1966. (USAF Report AFFDL-TR-66-104.)
- 5.174. H. G. Heinrich and J. C. Schmitt. "Measurement of Aerodynamic Coefficients of Twin Parachute Clusters." AIAA Paper, March 1979. (AIAA 79-0461.)
- 5.175. J. W. Stone. "The Performance of Large Cluster Parachutes." Paper presented at the University of Minnesota Course on Aerodynamic Deceleration, July 1965.

- 5.176. U.S. Air Force. *Wind Tunnel Study of Parachute Clustering*, by J. F. Braun. USAF, April 1963. (USAF Report ASD-TRD-63-159.)
- 5.177. J. H. Moeller. "A Method of Load Prediction for Parachutes in Clusters," *Journal of Aircraft*, Vol. 4, No. 4, July-August 1967. Pp. 339-342.
- 5.178. U.S. Air Force. *Investigation of the Flow Field During the Inflation of Clustered Parachutes*, by R. J. Niccum and N. D. Kovacevic. USAF, November 1966. (USAF Report AFFDL-TR-66-106.)
- 5.179. D. J. Kolega, W. D. Woodis, and J. D. Reuter. "Vent Modification of Large Ribbon Parachutes to Enhance Cluster Performance." AIAA Paper, October 1986. (AIAA 86-2433.)

CHAPTER 6

DESIGN OF PARACHUTE ASSEMBLY AND COMPONENTS

The prime contractor, generally in cooperation with a Government agency, defines the load, personnel, ordnance, and air or space vehicle that must be recovered. The prime contractor specifies the vehicle weight and configuration, the recovery velocity and altitude envelope, the landing conditions, and the environment in which the recovery system must operate.

The recovery system contractor, usually a subcontractor, develops and tests the parachute system and, if required, the impact-attenuation system. The components of this task may range from a single parachute assembly for parachutists to a multiple parachute assembly for the recovery of a space vehicle.

The systems analyst, the systems engineer, and the aerodynamicist then define the required recovery system that may include a drogue chute and main parachute assembly, an impact-attenuation system, and other components. They define the type and number of parachutes required, and the necessary reefing stages. They also define the installation, deployment, and recovery signal method. These tasks should all be done in close cooperation with the prime contractor. The design engineer then converts the calculated data into reliable, workable hardware that will meet the recovery specification.

The parachute design engineer must learn to design in textiles, the primary material of parachute assemblies. Textile fabrics are subject to the same laws of stress and strain as metals or composites. However, many differences exist in the nonlinear elastic characteristics of natural and man-made fibers that are woven and braided into cloth, tapes, and suspension lines and are then connected by sewing to form parachute assemblies.

6.1 PARACHUTE DEPLOYMENT AND INSTALLATION

6.1.1 Parachute Deployment

Parachute deployment denotes the sequence of events that begins with the opening of a parachute compartment or parachute pack attached to the body to be recovered. Deployment

continues with extraction of the parachute until the canopy and suspension lines are stretched behind the body and the parachute canopy is ready to start the inflation process. This deployment is associated with a mass shock (snatch force) created by the acceleration of the mass of the parachute to the velocity of the body to be recovered. The task of a good deployment system is to limit the mass shock to an acceptable level. Shock limitation is accomplished by controlling the parachute deployment process and providing means for progressive incremental acceleration of all parts of the parachute to the velocity of the forebody. A high snatch force is usually the result of a poor deployment system. The need for a controlled progressive parachute deployment increases with parachute size and deployment velocity, and with the number of parachutes in the assembly. An uncontrolled high acceleration of the canopy skirt may also cause reefing cutters to rip away from their anchor points and damage the reefing installation.

A good parachute deployment system provides the following benefits:

1. Minimizes the parachute snatch force by controlling incrementally the deployment of the parachute, and by keeping the parachute canopy closed until line stretch occurs. Acceleration of the air mass in a partially inflated canopy before line stretch is a main contributing factor to high snatch loads.
2. Keeps tension on all parts of the deploying parachute. Tension prevents fluttering of the canopy. Fluttering causes entanglement, canopy damage, line-overs, and canopy inversions.
3. Minimizes opening time and opening-force scatter caused by irregularities and delayed action during parachute deployment and inflation.
4. Supports uniform deployment and subsequent inflation of parachute clusters. This is of utmost importance in clusters to avoid wide discrepancies in forces and opening times of the various parachutes. Design approaches for preventing these problems are discussed in section 6.3.1.

Means for obtaining a good, controlled parachute deployment include a positive method for parachute extraction by a mechanically or pyro-ejected pilot or drogue chute. Aerodynamically deployed spring-loaded pilot chutes, used successfully for personnel parachutes, are generally not satisfactory for deployment of large final descent parachutes for air vehicles and ordnance devices.

Parachute and riser should be stored in a textile envelope for protection during deployment and to ensure a controlled deployment that keeps tension on all parts of the parachute and riser. The textile envelope, called the deployment bag, should have separate compartments for the canopy, suspension lines and, if required, for the riser. These components should be secured in their individual compartments in sequential steps (folds) in

stow loops or retention ties. The pull of a pilot or drogue chute first extracts the main parachute from the parachute compartment and then from the deployment bag in a controlled incremental sequence, thereby maintaining order and tension on all parts of the deploying parachute assembly.

Questionable deployment methods should be avoided or thoroughly tested. Bench deployment tests are an essential part of the design-and-development cycle. During the bench test, the engineer should try to make the deployment system malfunction. If the system does malfunction in bench tests, the same malfunction will certainly occur some time when the parachute is being used; the malfunctioning part should be redesigned.

6.1.2 Uncontrolled Deployment

In an uncontrolled deployment, the parachute is released or ejected into the airstream without a pilot chute, drogue chute, or deployment bag (Figure 6-1). Uncontrolled deployment may be acceptable for small parachutes less than 5 feet in diameter, but is unacceptable for larger parachutes because it results in high snatch forces and partial canopy inflation before line stretch. If tension on the canopy and lines is not controlled, line-overs, inversions, entanglement between parts of the parachute, and associated parachute damage can occur.

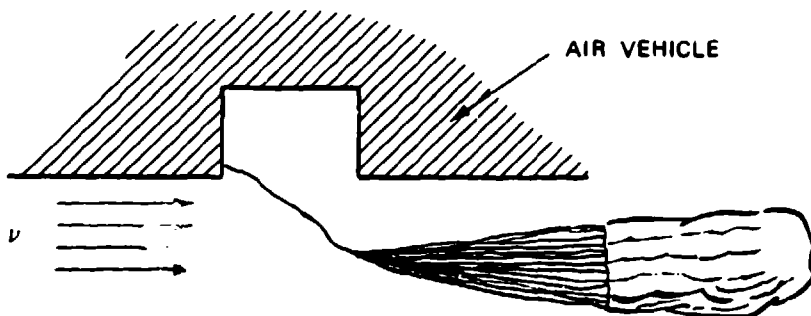


FIGURE 6-1. Uncontrolled Deployment.

6.1.3 Semicontrolled Deployment

Semicontrolled deployment uses a pilot chute for extracting the main parachute (Figure 6-2).

The semicontrolled concept has worked with medium-sized parachutes deployed at low velocities. If deployment occurs over a large velocity range, the pilot chute may be powerful enough at high speeds to cause high snatch loads, and not powerful enough at low speeds to avoid sail formation. Partial canopy inflation before canopy stretch may still occur with this deployment. Use of a deployment bag is a better solution for pilot chute deployment.

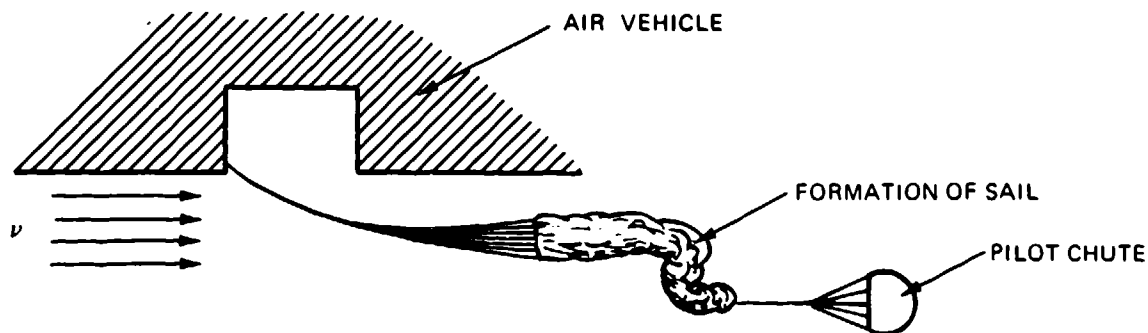


FIGURE 6-2. Pilot Chute Deployment.

6.1.4 Static-Line Deployment

In the static-line-deployment method, a line attached on one side to the air vehicle and on the other side to the parachute assembly will first open the parachute pack and then pull the parachute out of its deployment bag. A typical example is the T-10 paratrooper parachute used by the airborne troops of many western nations. The static-line deployment of the T-10 parachute is shown in Figure 6-3. After the jumper leaves the aircraft, a static line attached to the aircraft opens the parachute pack attached to the back of the paratrooper, extracts the parachute stowed in a bag attached to the static line, and deploys the parachute. The static line with the attached deployment bag stays with the aircraft. This parachute extraction method is limited to aircraft speeds of about 130 knots. Above 130 knots, sail formation will occur because the parachute is deployed at 90 degrees to the airflow, which pushes the front of the canopy skirt through the rear of the skirt and results in partial or full canopy inversion. Inversions on the T-10 parachute have been practically eliminated through introduction of the anti-inversion net around the skirt of the canopy (see section 6.3.4 for a description of the anti-inversion net).

Many variations of the static-line-deployment method have been used in operational systems. A related approach was used for deployment of the stabilization and retardation parachute for the nose section of the XS-2 research aircraft. In case of an emergency, explosive bolts were used to separate the nose section, which contained the pilot cockpit, from the aircraft. A static line attached to the aircraft fuselage extracted the drogue chute deployment bag and deployed the parachute. This system performed well in a high-speed emergency (Reference 5.11). However, a static-line-deployment method must be carefully analyzed to determine its suitability for the intended application. The controlled-deployment method described in the next paragraph is often a better approach.

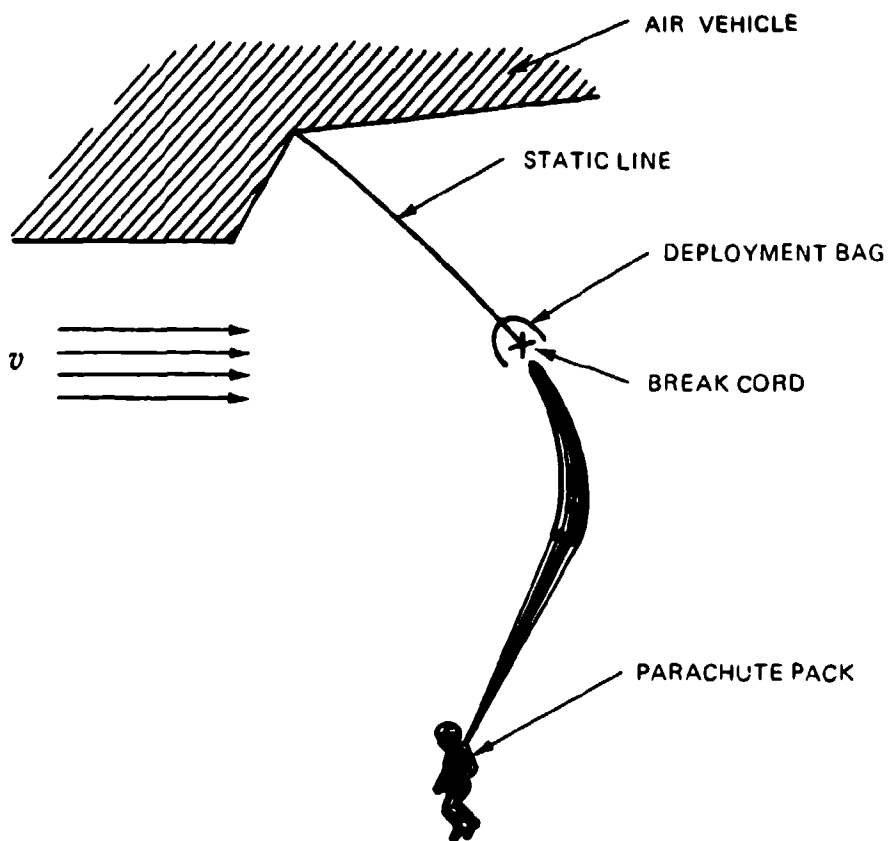


FIGURE 6-3. Parachute Static-Line Deployment.

6.1.5 Controlled Deployment

The controlled parachute deployment method, shown in conceptual form in Figure 6-4, is the basic deployment method for all parachute assemblies used for the recovery and retardation of air/space vehicles, ordnance items, and high-speed payloads. This method is also recommended, in an appropriate form, for other parachute assemblies, including personnel and aircrew emergency parachute systems.

Controlled parachute deployment starts with the forced ejection of a parachute compartment cover or a drogue gun slug that, in turn, pulls a pilot chute, or first-stage drogue chute, away from the air vehicle and into good airflow behind the vehicle. Mortar ejection or rocket extraction may also be used for forced deployment of pilot or drogue chutes.

Figure 6-4 shows a controlled deployment of a parachute assembly that starts with ejection of the compartment cover, which extracts the pilot chute stored in a small bag.

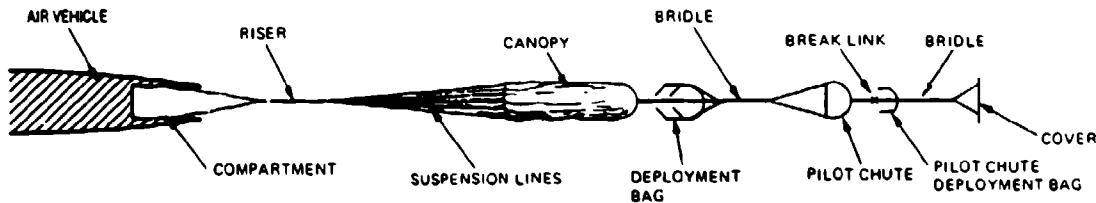


FIGURE 6-4. Controlled Parachute Deployment Concept.

Important in the deployment of the parachute assembly is the sequence: riser, suspension lines, and canopy. This type of sequence is called line-first deployment. The deployment bag of the main parachute contains two compartments, one for riser and suspension lines, and another for the canopy. All assembly components are retained in their respective compartments, using stow loops and tie cords. This arrangement ensures a controlled deployment with tension on all parts of the parachute assembly.

Figure 6-4 shows the pilot chute permanently attached to the main parachute canopy, an arrangement that has proven beneficial to all large reefed parachutes.

Mortar ejection or rocket extraction deploy the pilot or drogue chute directly. These two methods are described later.

Main parachutes are too large for forced deployment by mortar or rocket action. An intermediate, force-deployed pilot chute or the disconnected drogue chute are used for extracting main parachute assemblies.

6.1.6 Canopy-First Deployment

The canopy-first deployment method (Figure 6-5) should be avoided wherever possible; it results in high snatch forces and associated problems. This method had to be used on the landing deceleration parachute of the B-47 bomber to prevent the parachute deployment bag from falling and being dragged on the runway. The parachute deployment bag was permanently attached to the riser at a distance short enough to prevent the bag from contacting the ground. A large pilot chute extracted the canopy from the bag in a canopy-first process. The airflow around the canopy prevented dragging the canopy on the ground.

6.1.7 Drogue Gun Deployment

A positive ejection of the pilot chute or first-stage drogue chute, as provided by a drogue gun, mortar, or extraction rocket, is mandatory whenever the parachute must be deployed

from a spinning or tumbling vehicle or through the wake of a large forebody. Drogue gun deployment, the simplest of the three forced-ejection methods, is shown in Figure 6-6.

A drogue gun is similar in principle to a pistol. The gun body is attached to the primary vehicle. At deployment command, a piston, similar to the pistol shell, and called a drogue gun slug, is fired away and beyond the reach of the tumbling vehicle into good airflow behind the vehicle. The drogue gun slug attached to a bridle either extracts the pilot chute directly or extracts a small deployment bag containing the pilot chute.

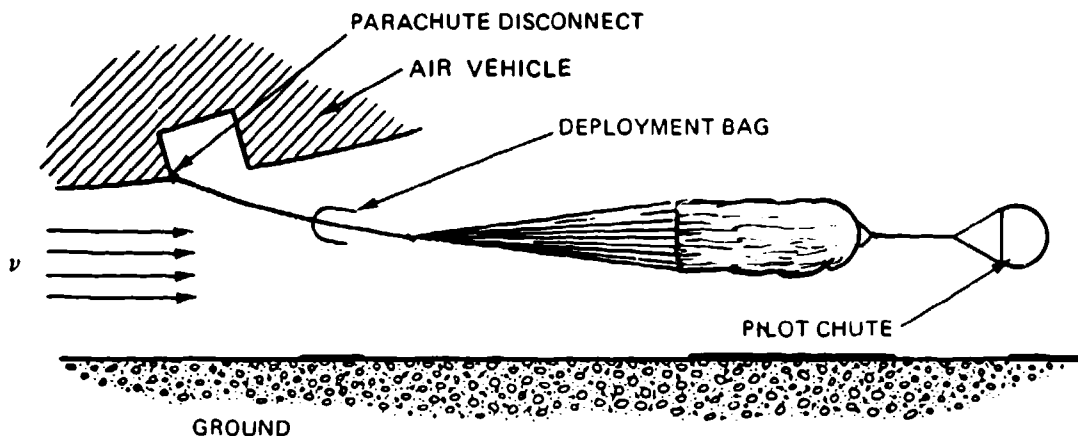


FIGURE 6-5. Canopy-First Deployment Method Used on the Landing Deceleration Parachute of the B-47 Bomber.

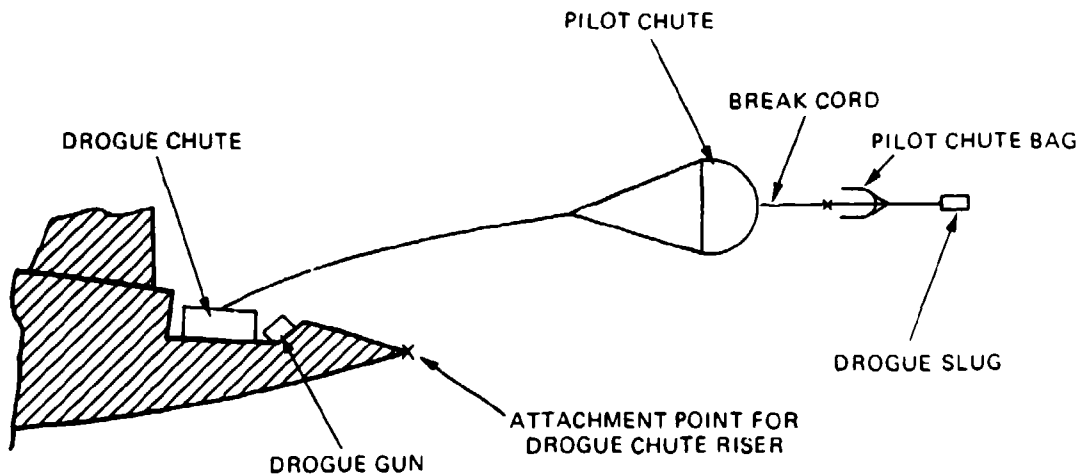


FIGURE 6-6. Drogue Gun Deployment.

Drogue gun slugs are limited in weight to about 2 pounds, restricting their use to lightweight pilot chutes. Drogue guns, which have a low reaction force, can be stowed conveniently at various locations on the primary vehicle. Figure 6-6 shows the drogue gun slug permanently attached to the pilot chute bag, with slug and bag breaking away after deployment is complete. This design is preferred because it prevents the drogue gun slug from becoming entangled with and damaging the pilot chute.

6.1.8 Parachute Mortar Deployment

If drogue gun deployment can be compared to firing a pistol, mortar deployment can be compared to firing a shell from a cannon. Drogue chute and main parachute assemblies in excess of 100 pounds have been mortar-deployed. Mortar deployment is a very positive means of getting a parachute assembly away from the effective range of a spinning or tumbling vehicle and into good airflow behind the vehicle. The disadvantages of mortar deployment are a large mortar reaction force; a relatively large mortar body; and a canopy deployment, not by the pull of a pilot or drogue chute, but by the inertia forces of the ejection. A large ejection velocity is required to accomplish bag stripoff and line and canopy stretch.

Figure 6-7 shows the mortar arrangement for the two Apollo drogue chutes. The Apollo command module was unstable and could rotate 90 degrees between the time the stabilization system was shut off and the time the drogue chutes could stabilize the command module. Contact between the red-hot heat shield and the drogue chute risers appeared possible. Firing the drogue chutes at 90 degrees to each other ensured that one drogue chute would be effective at all module attitudes. In addition, high-temperature-resistant steel cables were used in the contact range of the heat shield. Note that only one drogue chute was required for the primary landing system; the second drogue was part of the backup assembly.

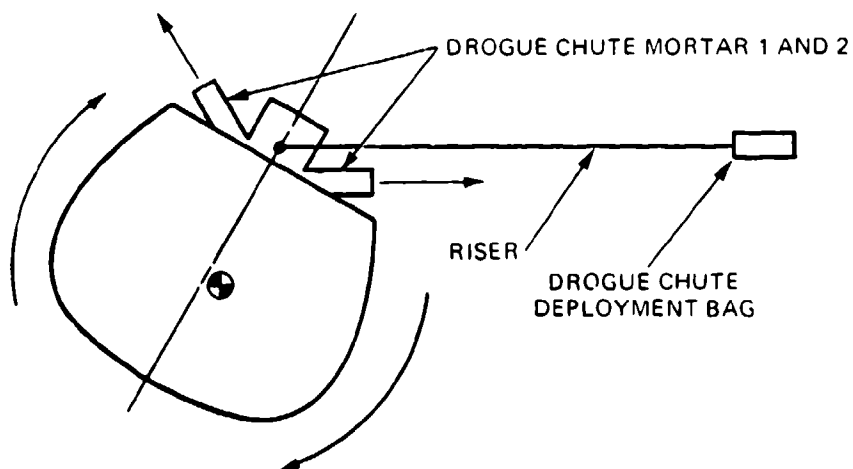


FIGURE 6-7. Mortar Arrangement of the Apollo Command Module.

Figure 6-8 shows the mortar assembly for the Apollo drogue chutes. The drogue chute is contained in a deployment bag stowed in a sabot (piston). The mortar tube has two cartridges firing into a common breech actuated from two individual sensor systems. Upon deployment command, both cartridges are fired. This firing builds up the pressure below the sabot, transmits the pressure to the cover, shears the pins holding the cover, and ejects the deployment bag and riser assembly. For the Apollo drogue chutes, the multiple steel cable risers were wound into a ring without turning the cables and were held in place by casting them in lightweight Styrofoam.

Static firings of the mortar confirmed bag stripoff and canopy stretch. Mortar cover, sabot, and the lightweight Styrofoam were lost after ejection. No interference between the loose parts and the drogue chutes was found. The high mortar-reaction loads were somewhat controlled by proper breech and orifice design (Reference 5.10). A variety of mortar concepts and designs have been used operationally. Reference 6.1 analyzes the design and performance of a parachute mortar.

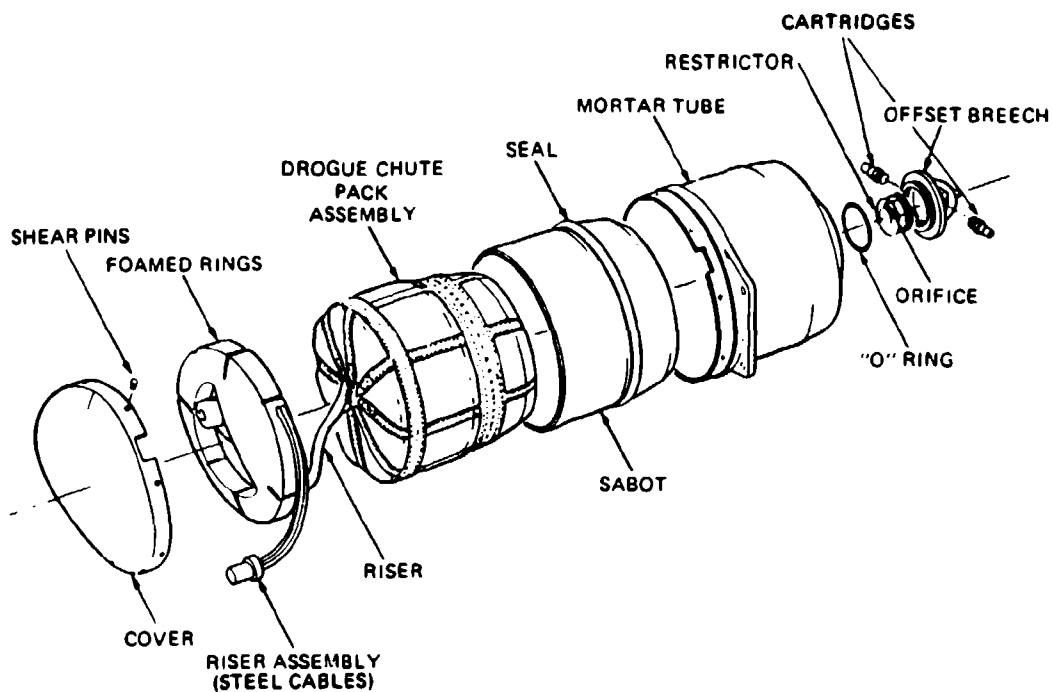


FIGURE 6-8. Mortar Assembly of the Apollo Drogue Chutes.

6.1.9 Deployment by Rocket Extraction

Figure 6-9 shows two typical rocket-extraction methods. Version 1 stows the rocket beside the parachute assembly, and version 2 stows the rocket in the middle of the doughnut-shaped deployment bag. Both versions have been used successfully. Rocket extraction provides favorable deployment by pulling the parachute bag from the top and providing a line-first deployment sequence. Rocket extraction creates no reaction forces that must be absorbed by the vehicle. Protection against the short-time rocket blast has not been a problem. References 6.2 and 6.3 describe several rocket-extraction systems.

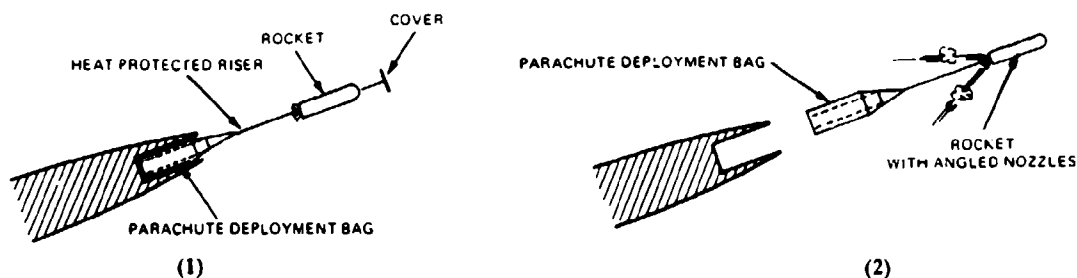


FIGURE 6-9. Two Typical Rocket-Extraction Methods.

6.1.10 Cross-Wind Deployment

Deployment bags that are stowed sideways in air vehicles need a means for ejecting the deployment-bag assembly into the airstream. Three methods that have been used operationally are shown in Figure 6-10. All three concepts require careful evaluation in bench deployment test.

A frequent problem with air-vehicle installation of parachute assemblies is a vertical stabilizer in the path of the deploying parachute assembly. One successful method for solving this problem is described in Reference 5.23.

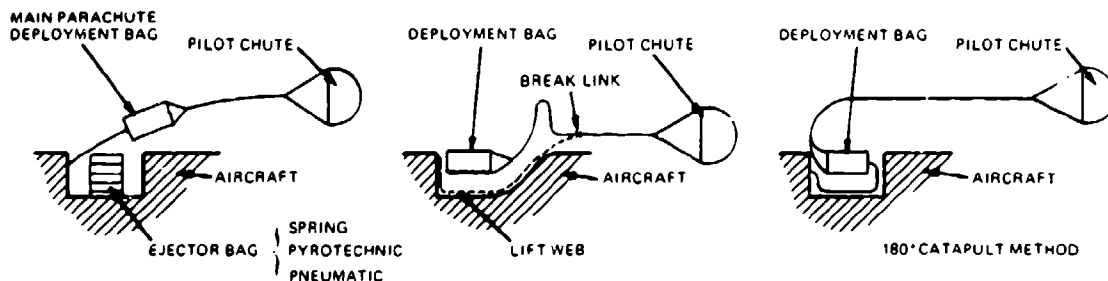


FIGURE 6-10. Cross-Wind Deployment-Bag Ejection Methods.

6.1.11 Parachute Assembly Installation

Parachute assemblies must be stowed inside or on top of the air vehicle or the payload that the parachute is to retard or recover. The location and shape of the stowage area or compartment for the parachute assembly should ensure favorable storage and deployment conditions for reliable parachute operation. The recovery-system engineer should get involved in the vehicle or payload design so that an acceptable compartment or stowage location and an unobstructed deployment path for the parachute can be obtained. Although parachute assemblies can be stowed in the last left-over hole in the aircraft or missile, odd compartment locations may require complex and expensive parachute ejection or extraction systems and difficult deployment concepts.

Airdrop platforms and airdrop equipment normally permit the parachute assembly to be located on top of the load, with sufficient space for hand-packed parachutes that have not been pressure-packed, and in a location that provides an unobstructed path for parachute deployment into good airflow.

Cylindrical or aerodynamically shaped slender vehicles, such as ordnance items, missiles, rockets, and aircraft, generally permit storage of the parachute assembly, or part of the assembly, in a compartment at the rear of the vehicle. However, this installation requires that the parachute be ejected from the container four to six forebody diameters behind the vehicle, through the reverse flow region into good airflow, to ensure proper canopy inflation.

Many missiles, target drones, and aircrew modules require a horizontal vehicle attitude for ground landing and an angled attitude for water landing. Most vehicle recovery systems require a drogue chute for high-speed deceleration and a main parachute assembly for final descent. Available vehicle space dictates stowage of the main parachute on the upper or lower side of the vehicle; the upper side is the preferred location. During descent on the drogue chute, the vehicle must be in a nose-down, minimum-drag attitude to avoid pendular and transverse oscillations. Vehicle rotation during drogue-chute descent, caused by ailerons not in zero position, can twist the risers and lead to squidding of the parachute. A swivel between the drogue chute and the vehicle may be necessary to prevent tangling. The drogue chute can deploy the main parachute by using a transfer bridle located in an indented channel in the vehicle skin, covered by a fly-away strip of plastic. The main parachute may also be deployed independently of the drogue chute by using one of the deployment methods previously discussed.

To avoid damage to the parachute assembly during installation and deployment, the parachute-stowage compartment must be smooth on the inside with no protrusions or sharp edges. If rough edges (such as those caused by compartment covers cut out by a detonating fuze cord) cannot be avoided, a plastic or textile inner liner may be used to cover the rough edges.

The deployment path of the parachute outside of the vehicle should be free of protrusions and obstacles, such as vertical fins. If anything is in the deployment path that the parachute can hang up on, the parachute will certainly do so at some time.

Most parachute compartments in air vehicles are rectangular, and, because space is limited, require pressure-packing of the parachute. Pressure-packing of parachutes into noncylindrical deployment bags requires the special knowledge and handling discussed in section 6.7.5.

Operational use has shown that it is practical to have removable parachute compartments. This arrangement allows parachute handling, packing, and installation in packing lofts to be away from other work on the vehicle, and provides ready-packed parachutes for quick turnaround as well as easy storage and protection of the parachutes under hostile environmental conditions.

Landing a vehicle in a stable horizontal or angled attitude requires three riser attack points, preferably two in front of and one behind the center of gravity of the vehicle. These hard points must be so arranged as not to interfere with parachute installation or deployment.

A very important but frequently overlooked point is the provision for parachute growth. Historically, air vehicles, crew modules, and payloads have grown in weight. The Apollo command module from its bidding specification to its first landing grew from 8100 to 13,000 pounds with no permissible increase in parachute storage, volume, or parachute loads. This weight increase has made extremely dense pressure-packing and multiple reefing stages necessary for all parachutes.

The permissible maximum landing velocity is usually based on the allowable impact deceleration. To accommodate a higher vehicle weight without increasing the rate of descent requires a larger parachute with even more dense pressure-packing. A limit exists as to how much pressure-packing a parachute can withstand without damage to the parachute and its components.

The following design details must not be overlooked:

1. Missiles, rockets, and drones that are accelerated on launchers in fractions of a second from zero velocity to flying speed press the parachute assembly with considerable force against the rear cover or door, necessitating proper design of the door restraint.
2. In cylindrical containers, parachute suspension lines that are attached at multiple points in the front end of the container easily chafe at the rear edge of the container. A wide webbing ring attached to all suspension lines at the rear location eliminates this problem.

3. Disconnecting the parachutes from the vehicle at landing is frequently necessary to avoid wind dragging. Pyro disconnects of various designs are available and in use. Sensors for initiating these devices include ground-impact and contact switches for ground landing, and impact and water-activated switches for water landing. It is important to activate the sensor circuitry only after all parachutes are open and the system is stabilized. This avoids disconnecting the parachutes by door ejection, parachute forces, and similar shock or electrical-signal sources.

Two interesting parachute installations in air vehicles, one with a 180-degree vehicle tip-over and the other with a vertical stabilizer in the parachute deployment path, are described in References 5.23 and 6.4.

Insisting on a good parachute installation and a clear parachute deployment path will pay multiple dividends in a more reliable parachute recovery system.

6.2 PARACHUTE DESIGN

6.2.1 Parachute Assembly Configuration

Parachutes constitute the primary elements of parachute recovery systems. These systems range from single parachutes used for the recovery of small loads at low speeds to multiple-parachute systems for the recovery and landing of heavy military loads, ordnance devices, and air vehicles.

Recovery from velocities below 150 to 200 knots can generally be accomplished with a parachute assembly consisting of one or several main descent parachutes deployed by static line or by aerodynamically deployed pilot chutes.

Recovery from velocities in excess of 200 knots, as a rule, requires a multiple-parachute system where the individual parachutes may be reefed in one or several steps. Such systems may include pilot chutes, first- and second-stage drogue chutes, and final descent parachutes that may be supported by ground-impact-attenuation systems.

Figure 6-11 shows a typical parachute recovery system that consists of a drogue-chute assembly and a main parachute assembly. The drogue chute, mortar-deployed in a deployment bag, is attached to the vehicle by a pyrotechnically actuated disconnect. A sequencer controls the firing of the disconnect and the release of the drogue chute. Upon drogue-chute disconnect, a jumper bridle extracts the pilot chute for the main parachute. After extraction of the pilot chute, the drogue chute with the attached pilot chute bag breaks away. The permanently attached pilot chute now deploys the main parachute, which is reefed in one or several steps. Depending on the type of vehicle to be recovered, a swivel and a transfer bridle may be required, the swivel to prevent a rotating forebody from twisting the main parachute, and the transfer bridle to shift the vehicle into a horizontal attitude for ground landing.

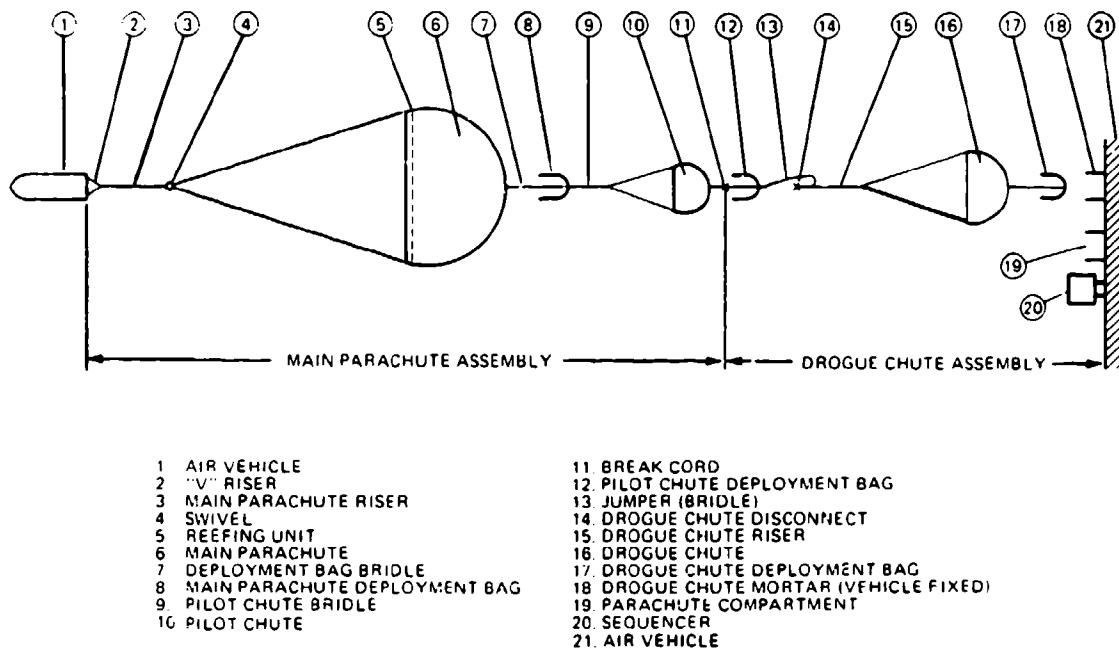


FIGURE 6-11. Typical Parachute Recovery System.

6.2.2 Parachute and Component Definition

Figures 6-12 to 6-14 show the components of a parachute labeled with generally accepted terminology. The two primary components of a parachute are the canopy and the suspension lines. The parachute canopy is the drag-producing component that provides the decelerating force. This force is guided through suspension lines to a riser that connects the parachute to the payload or air vehicle. Some payloads, such as cylindrical ordnance devices, connect the suspension lines, without a riser, directly to the vehicle. All circular parachute canopies are designed with more-or-less-triangular gores manufactured of sections cut from woven parachute cloth. The formerly 36-inch-wide parachute cloth is presently being replaced with cloth 48, 60, and 72 inches wide. Parachute cloth is available in a variety of weaves with strengths from about 40 to 500 pounds per inch-width.

Figure 6-13 shows details of a flat circular canopy. The layout, numbering system, and general definitions are in accordance with MIL-P-85710. The gores are numbered in a clockwise direction when viewed from the top of the canopy in the direction of flight. The gore with the highest number has in the right-hand corner above the gore number a decal containing such data as drawing number, date of manufacture, and contract number.

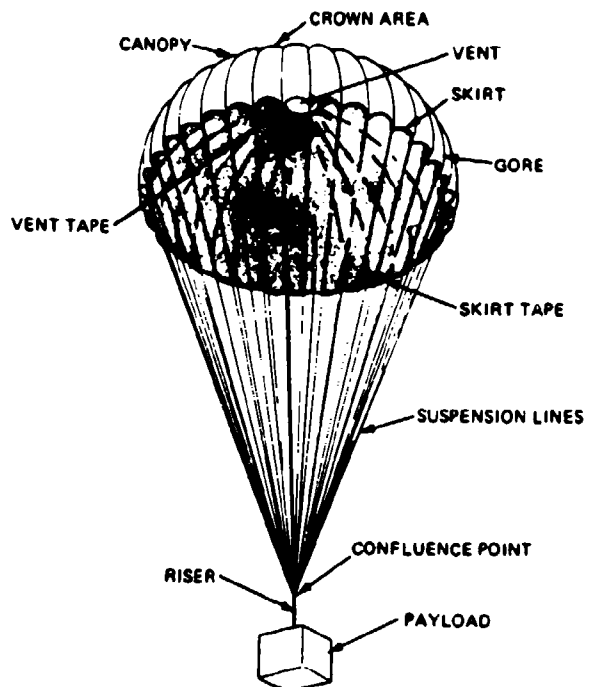


FIGURE 6-12. Components of a Parachute.

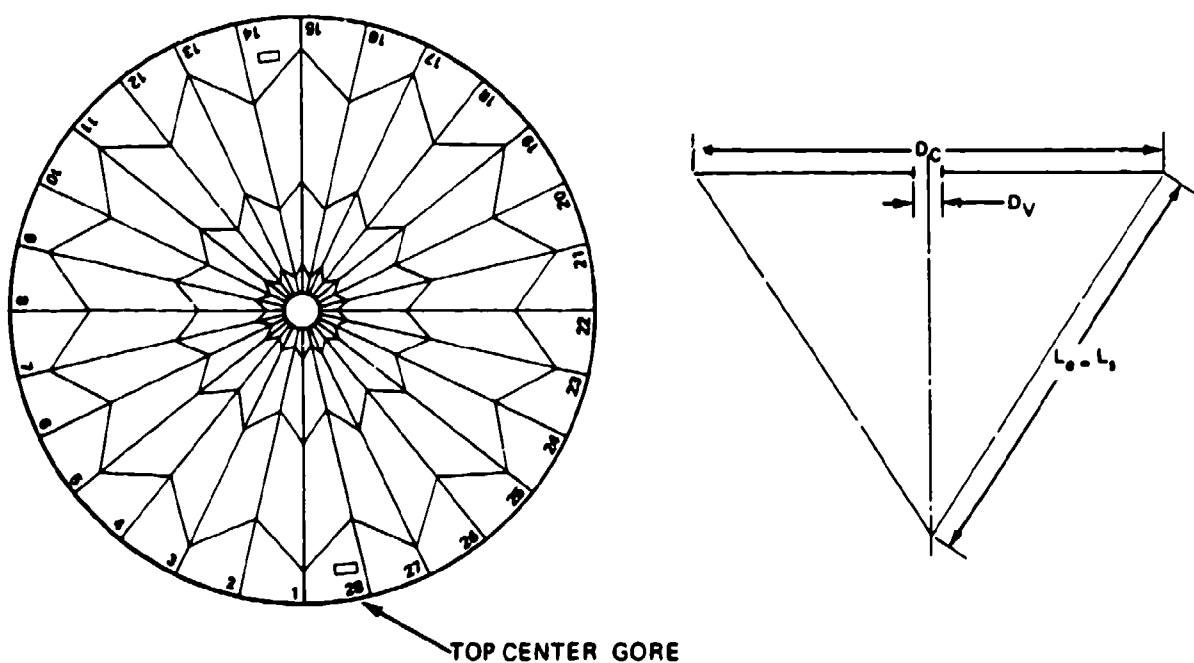


FIGURE 6-13. Typical Design of a Flat Circular Canopy.

Figure 6-14 shows two gore layouts with the sections cut in bias and block construction. Bias cut provides better stress distribution in the canopy and equalizes unavoidable small differences in manufacturing; this is the preferred construction method. Block construction, although simpler to design and manufacture, is primarily used for low-speed, low-load parachutes.

The individual gore sections are generally connected with a two-needle, 1/2-inch French fell seam with a 3/8-inch needle gage. A more efficient method uses a 3/8-inch fell seam with a 1/4-inch needle gage.

Most older parachutes use a 1-inch-wide, 4-needle fell radial seam to connect the individual gores to the suspension lines that run through a channel formed by a gap between the second and third rows of stitching. Many other radial-seam designs are in use today. One method runs the suspension lines on top of the radials over the canopy. Another has narrow radial seams with tapes sewn on top of the radials; the suspension lines are connected to the canopy skirt by sewing them to the tapes or running them through loops formed by the radials at the skirt of the canopy. Care must be taken to secure the suspension-line radial connection against side pull of the lines during deployment. Specification MIL-C-6635C, the ribbon parachute specification, shows several methods of connecting the suspension lines to the canopy skirt. Later sections of this chapter describe the design of the most commonly used parachute types and give references and specifications that describe the design of specific parachutes.

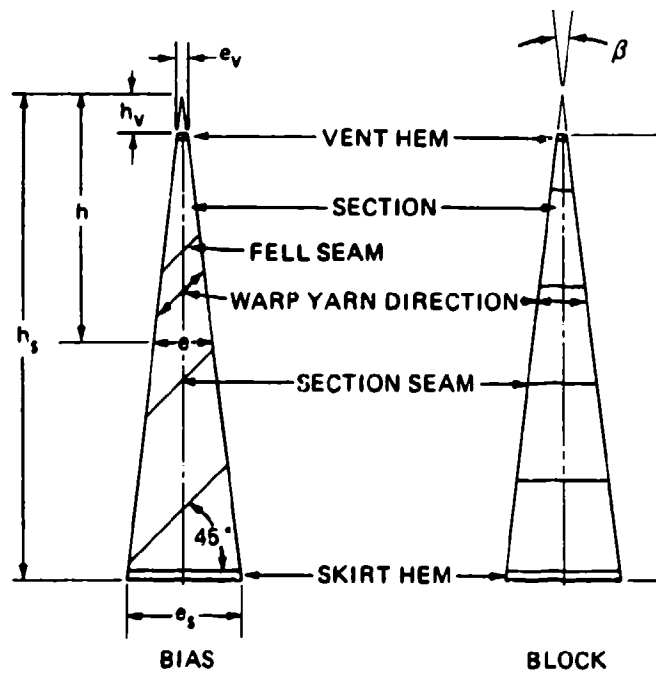


FIGURE 6-14. Gore Design of Bias and Block Construction.

6.2.3 Design of Solid Material Parachutes

Flat Circular and Conical Circular Parachutes. The flat circular parachute is the patriarch of all parachute designs and is still used for personnel and cargo-type parachutes, such as the 28-foot-diameter C-9 personnel parachute, and the 64-foot-diameter G-12 and 100-foot-diameter G-11 cargo parachutes. The flat circular parachute is simple to design, manufacture, and maintain, and has proven very reliable in operation. References 5.13 through 5.20, 5.95, 6.5, and 6.6 describe design and testing of circular flat parachutes of various diameters and for various applications.

Tests have established that conical and quarter-spherical parachute canopies, for the same canopy surface area, have a higher drag than flat parachutes (Reference 5.1). These results led to the design of conical parachute canopies; the best-known design is the Navy 26-foot-diameter conical parachute. References 6.7 and 6.8 describe conical parachutes.

Figure 6-15 shows the design and the nomenclature used for circular flat and circular conical parachutes. On flat parachutes, the canopy cone angle, μ , is zero and the gore angle, γ , is 360 degrees divided by N_G .

Section 6.4.5 discusses the benefits of relieving stress in the canopy by extending the calculated width of the gore, e_v , by 10% to e_v^* .

For large parachutes with long suspension lines, it has been proven practical to gather several lines in a single riser. This arrangement prevents length differences in the suspension lines that can be caused by differences in the elongation of adjacent lines. The effective suspension-line length, L_e , is always the distance from the skirt of the canopy to the real or hypothetical confluence point of the suspension lines.

Extended-Skirt Parachutes. Schematic drawings of three types of extended-skirt parachutes are shown in Figure 6-16: (a) the 10% extended-skirt designs, (b) the full (14.3%) extended skirt, and (c) the conical full extended skirt. The center part of the 10% extended-skirt designs is flat. Added to the skirt of the parachute is an inverted flat fabric ring with a width of 10% of the canopy diameter. The first extended-skirt parachute was a 28-foot-diameter circular flat parachute with 10% of the outer part of another 28-foot canopy sewn to the original canopy. The best known example of this type is the T-10 paratrooper parachute. A 12.5% flat extended-skirt parachute was tested at Wright Field. It was more stable than the 10% canopy but was slow to inflate and tended to delay opening.

The full extended skirt, flat and conical parachutes, designs (b) and (c) shown in Figure 6-16, have a 14.3% skirt extension. The angle of the extension coincides with the angle formed by the suspension lines. The conical full extended design has a conical center part; this design provides the highest drag coefficient of the three types.

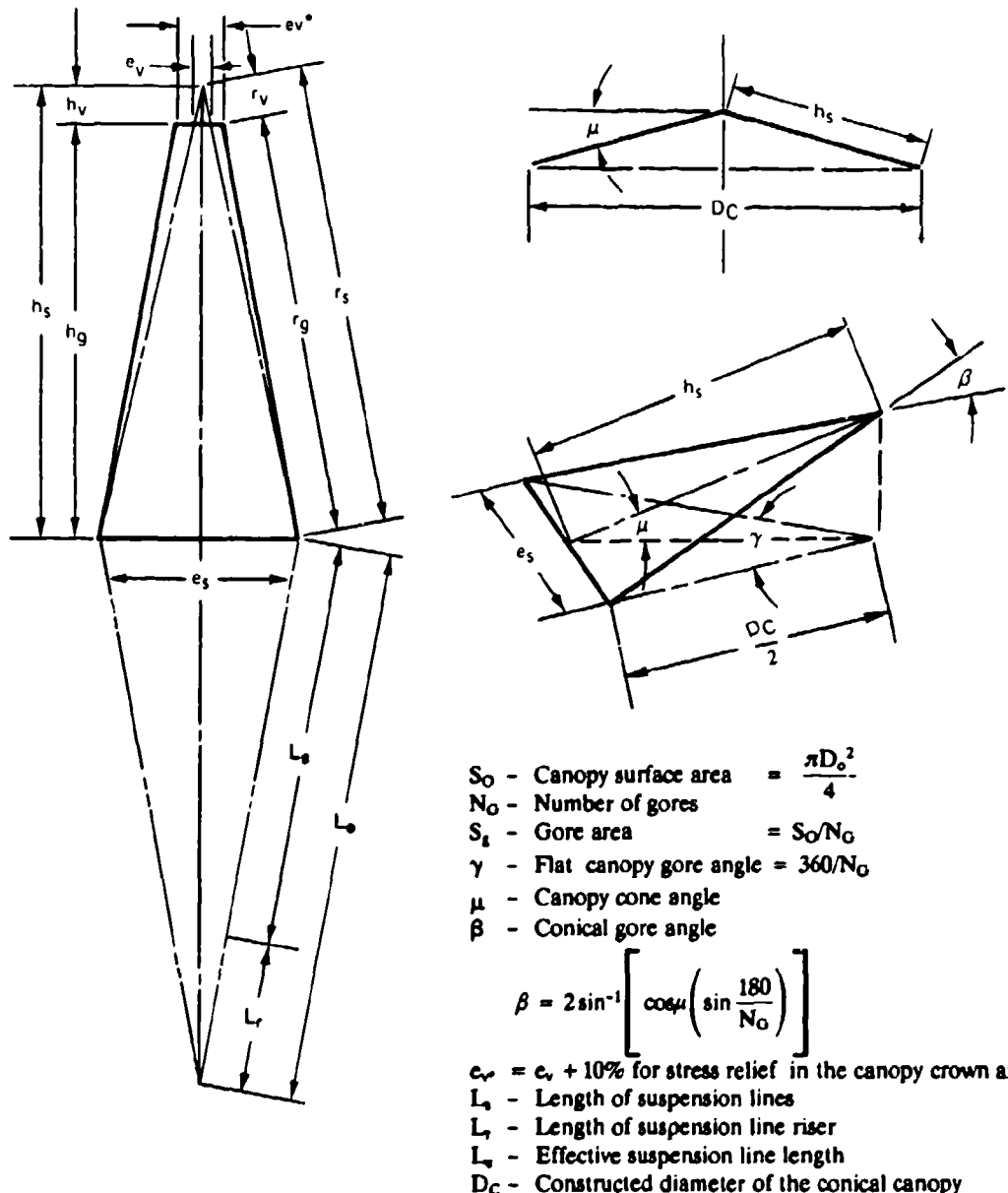


FIGURE 6-15. Circular Flat and Circular Conical Canopy Designs.

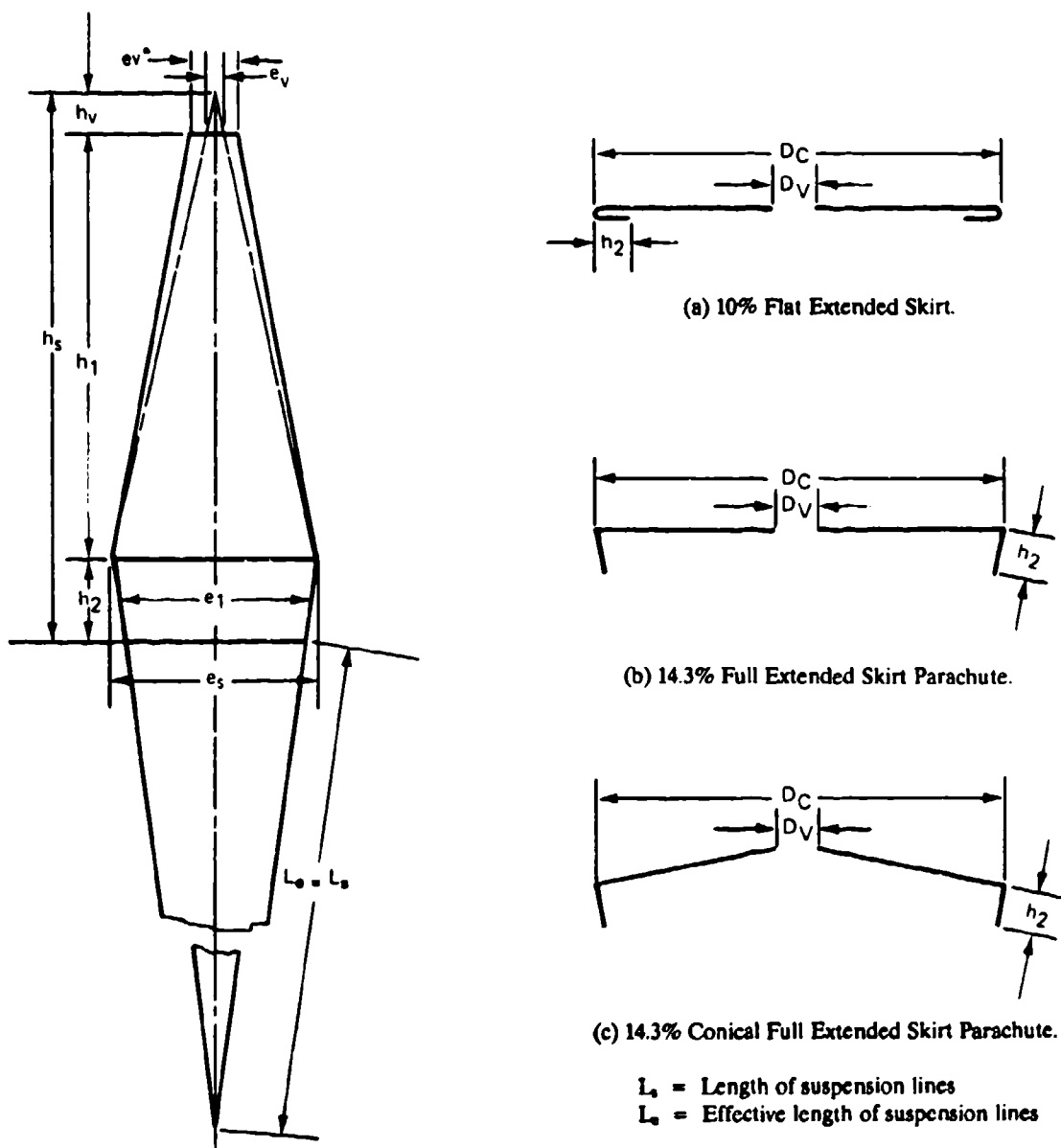


FIGURE 6-16. Design of Extended-Skirt Parachutes.

Figure 6-16 shows the design and the nomenclature, and Table 6-1 shows the dimensions for the different extended-skirt types.

The suspension-line length on the extended-skirt parachutes is usually equivalent to 0.95 to 1.0 diameter. Lengthening the suspension lines beyond $L_e/D_o = 1.0$ provides little gain in drag because the skirt extensions restrict the growth of the inflated-canopy diameter. This is contrary to flat circular and conical canopies, where longer lines notably increase the

TABLE 6-1. Determination of Gore Dimensions for Various Types of Parachutes.

Gore dimension	Type of parachute				
	Circular flat	Circular conical	10% flat extended skirt	14.3% full extended skirt	14.3% conical extended skirt
h_s	$\sqrt{\frac{S_o}{\tan \frac{\beta}{2} \cdot N_o}}$	$\sqrt{\frac{S_o}{\tan \frac{\gamma}{2} \cdot \cos \mu \cdot N_o}}$
h_1	$\sqrt{\frac{.735 S_o}{N_o \cdot \tan \frac{\beta}{2}}}$	$\sqrt{\frac{.653 S_o}{N_o \cdot \tan \frac{\beta}{2}}}$	$\sqrt{\frac{.653 S_o \cdot \cot \frac{\gamma}{2}}{N_o \cdot \cos \mu}}$
h_22 h_1	.286 h_1	.286 h_1
e_s	$2h_s \cdot \tan \frac{\beta}{2}$	$2h_s \cdot \tan \frac{\beta}{2}$	$2h_1 \cdot \tan \frac{\beta}{2}$	$2h_1 \cdot \tan \frac{\beta}{2}$	$2h_1 \cdot \tan \frac{\beta}{2}$
e_18 e_s	.857 e_s	.857 e_s
S_v	$\leq 0.0025 S_o$	$\leq 0.0025 S_o$	$\leq 0.0025 S_o$	$\leq 0.0025 S_o$	$\leq 0.0025 S_o$
e_v^*	1.1 e_v	1.1 e_v	1.1 e_v	1.1 e_v	1.1 e_v
L_e	.85 to 1.5 D_o	.85 to 1.5 D_o	.95 D_o	.95 D_o	.95 D_o

parachute drag (see Figure 5-20). For design details on extended-skirt parachutes, see References 5.21 through 5.24.

Polyconical Parachutes. Polyconical parachutes are a design modification of the high-drag quarter-spherical canopy discussed in section 5.2. Figure 5-16 shows the increased drag of this parachute compared to the circular flat parachute. The canopy profile is varied in a series of straight-line segments along a quarter-spherical arc. The triconical shape is the most commonly used design. Figure 6-17 shows the closeness of the quarter-spherical and triconical gore shapes. The number and length of the individual straight-cut gore sections can easily be varied to avoid material waste during manufacturing. Material waste is a problem on shaped-curvature gore designs.

The gore dimensions shown in Figure 6-17 are typical. No generally accepted standard designs have evolved. All companies that are designing polyconical parachutes have developed their own gore designs.

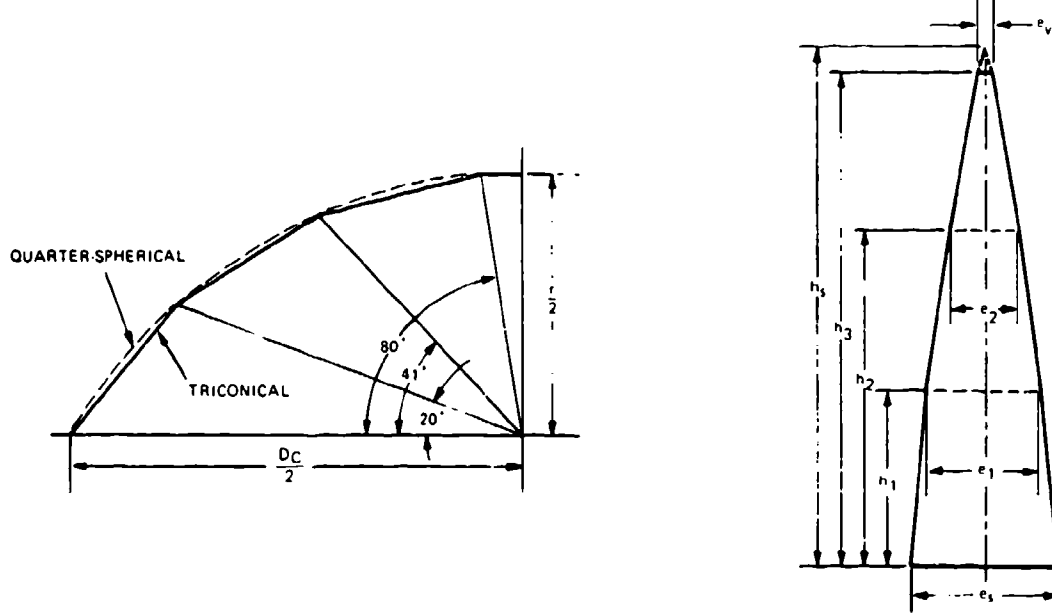


FIGURE 6-17. Typical Triconical Canopy Design Compared to Quarter-Spherical Shape.

Cross Parachutes. Cross parachutes, also called cruciform parachutes, were developed in the late 1940s by the Naval Ordnance Laboratory in Silver Spring, Md. Cross parachutes have had considerable use in recent years for the landing deceleration of aircraft, for stopping dragster racing cars, and for the retardation and stabilization of ordnance.

Figure 6-18 shows the simple design that consists of two layers of material connected in cross form. Drag, stability, and opening force are affected by the ratio of arm width, W , to arm length, L . A lower W/L ratio produces better stability and a lower opening-force coefficient, C_x ; however, a lower W/L ratio also produces a lower drag coefficient, C_{D_0} . References 5.25 through 5.35, 6.9, and 6.10 give design and aerodynamic information.

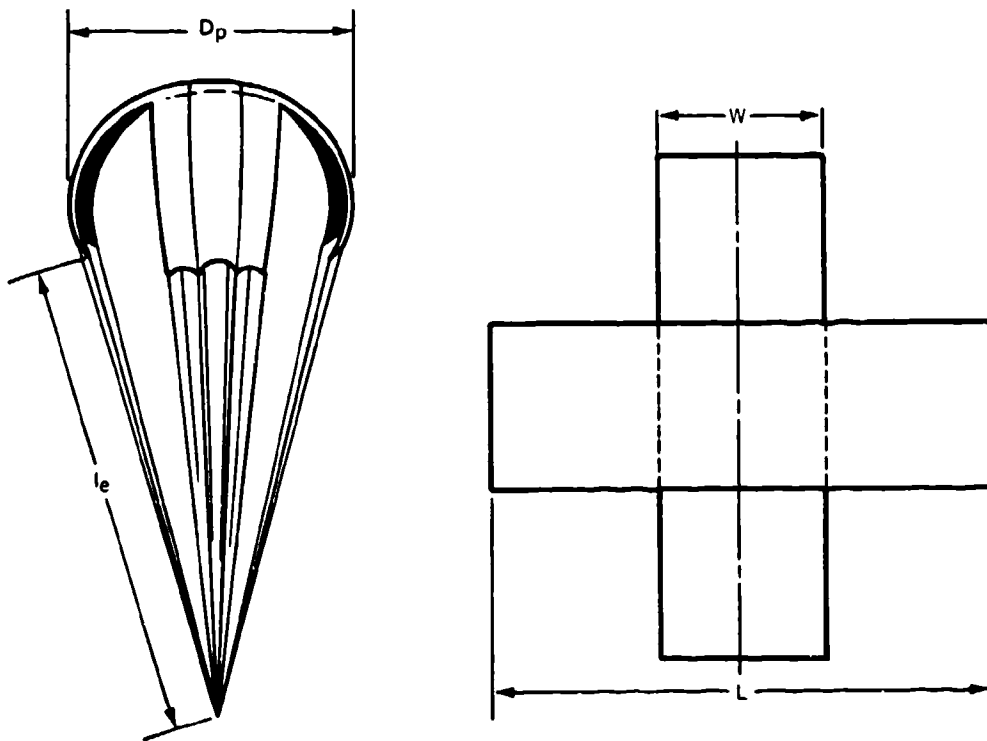
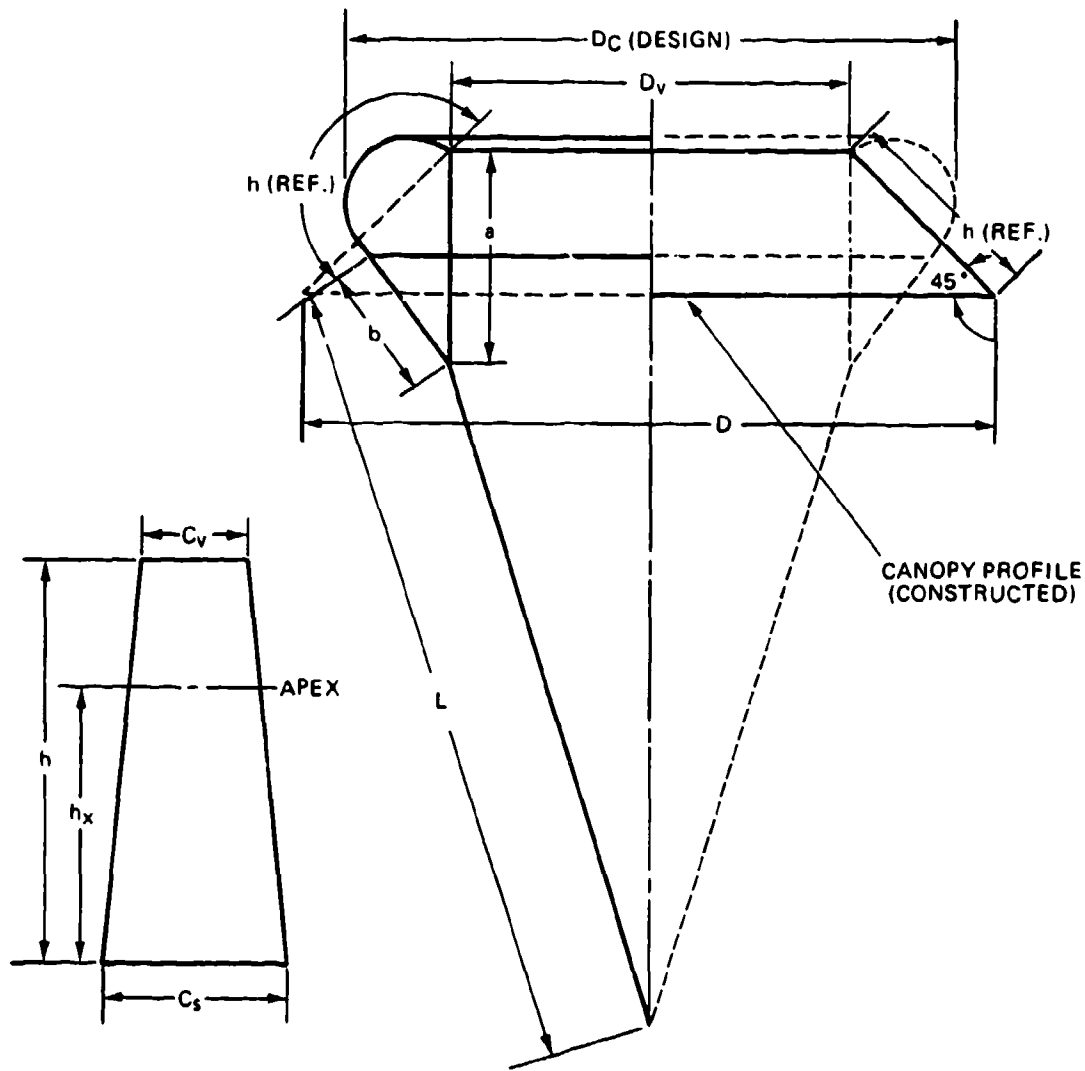


FIGURE 6-18. Typical Design of a Cross Parachute.

Cross parachutes have a tendency to rotate. Rotation can be diminished by connecting adjacent arm corners with a restricting line long enough to permit full canopy inflation but not long enough to permit overinflation. Parachutes used for the deceleration of dragsters frequently form the ends of the four arms into a pocket for faster canopy inflation. References 5.28 and 5.29 show that suspension-line length and number of suspension lines have a notable effect on the drag of cross parachutes.

Annular Parachute. The annular parachute, whose performance is discussed in section 5.2, evolved from the airfoil parachute and may be described as a conical parachute with a large pulled-down vent and with lines attached to the outer suspension lines (Reference 5.36). Figure 6-19, taken from Reference 5.36, demonstrates the design of the airfoil parachute.



Gore layout

Gore width:

$$C_v = \frac{\pi D_v}{N_G}$$

$$C_s = \frac{\pi D}{N_G}$$

 N_G = Number of gores

Apex height:

$$h_x = \frac{a + b + h}{2} - b$$

Vent/skirt elevation:

$$\frac{a - b}{h} = .392$$

$$D_o = 1.1284 \sqrt{s_o}$$

Dimension

Ratio, D_o

$$D_o \quad 1.000$$

$$D \quad 1.040$$

$$D_c \quad .940$$

$$D_v \quad .611$$

$$L \quad 1.250$$

$$h \quad .304$$

$$h_x \quad .209$$

$$a \quad .319$$

$$b \quad .200$$

FIGURE 6-19. Typical Design of Airfoil (Annular) Parachute.

Annular parachutes are used for midair retrieval with an engagement parachute attached above the open vent of the annular parachute, as shown in Figure 5-6 and described in References 5.37 and 5.38. A U.S. Army application is discussed in Reference 6.11.

Of all known parachute types, the annular and the polyconical parachutes have the highest drag coefficients related to the canopy surface area. Changing the relationship of the dimensions a and b in Figure 6-19 will notably affect the parachute performance.

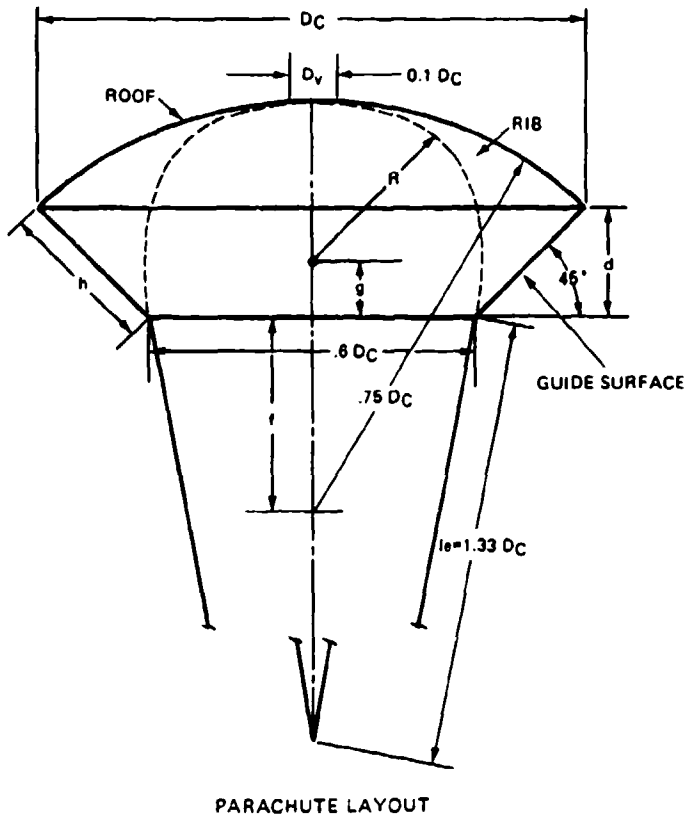
Guide Surface Parachute. Two types of guide surface parachutes are in use, the ribbed guide surface and the ribless guide surface. Both parachute types have a dome-shaped, rounded crown and an inverted cone-type guide surface in front of the dome. The guide surface causes uniform flow separation around the canopy edge and provides a strong restoring moment if the canopy is moved from the zero-angle attack position. Low-porosity canopy material is used for obtaining a fast, uniform inflation. Guide surface parachutes have the highest stability but the lowest drag of all known parachute types.

Ribbed Guide Surface Parachute. The ribbed guide surface parachute is the older type. It has a steeper $dc_m/d\alpha$ slope than the ribless type but it is more difficult to manufacture and has a slightly higher weight and volume. Figure 6-20 shows the general design of the ribbed guide surface parachute. References 5.53 and 6.12 detail design of two variations of the ribbed type of parachute, a stabilization type (the design shown in Figure 6-20), and a brake type with shorter guide surfaces.

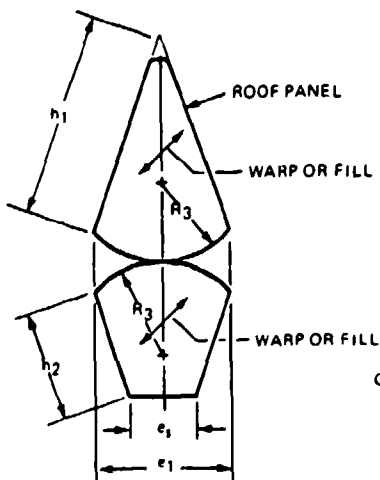
Guide surface parachutes, unlike most other parachute types, use the constructed parachute diameter, D_C , and the related canopy area, S_p , as reference for the drag coefficient, C_{Dp} .

Ribless Guide Surface Parachute. The ribless guide surface parachute eliminates the rib by extending the gore panel around the edges of the guide surface. Extending the gore creates more rounded corners on the guide surface and fewer sharp separation edges, resulting in a slightly lower $dc_m/d\alpha$ slope. A vent in the outer pocket of each gore ensures good inflation. Roof and guide surface dimensions vary with the number of gores. Figure 6-21 shows the general design. Panel dimensions for the various gore designs are listed in Table 6-2 taken from Reference 2.1. Additional design and performance data are found in References 5.53 and 5.54. Reference 5.54, a British report, gives slightly different panel dimensions but includes parachutes with more gores.

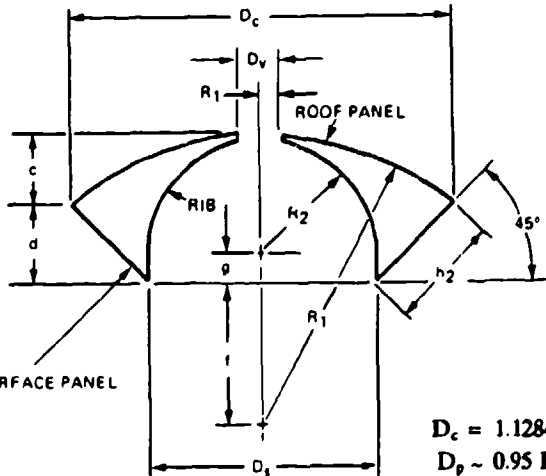
NWC TP 6575



PARACHUTE LAYOUT



ROOF PANEL AND GUIDE SURFACE LAYOUT



RIB LAYOUT

$$\begin{aligned}
 D_c &= 1.1284 \sqrt{s_0} \\
 D_p &\sim 0.95 D_c \\
 d &= 0.2 D_c \\
 \eta &= 0.28 D_c \\
 g &= 0.09 D_c
 \end{aligned}$$

FIGURE 6-20. Ribbed Guide Surface Parachute Design.

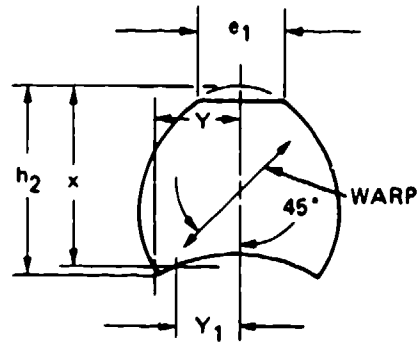
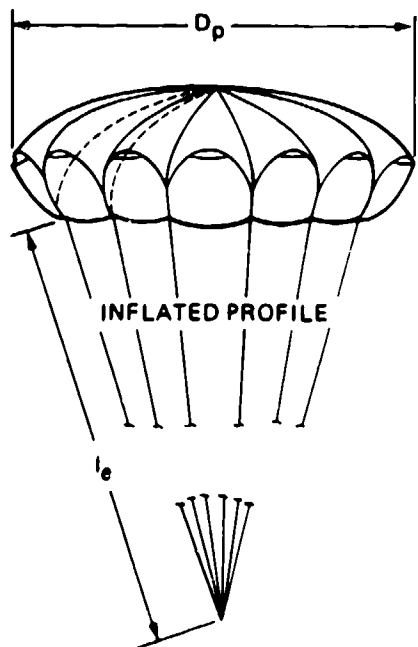
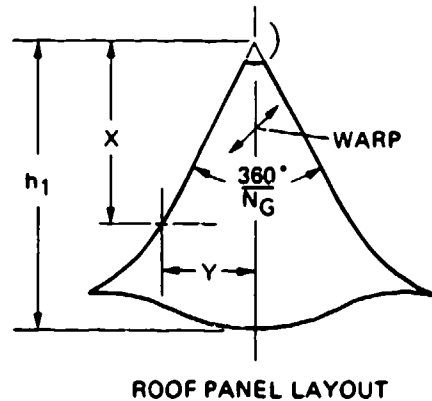
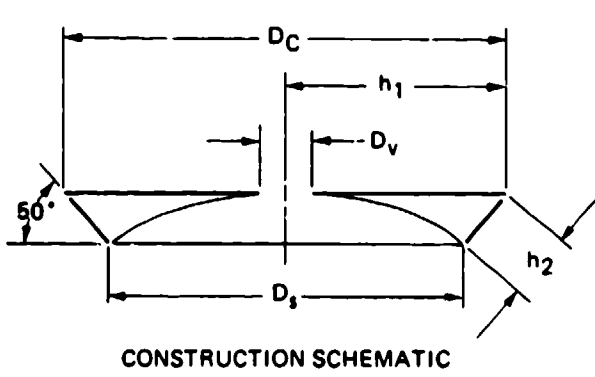


FIGURE 6-21. Ribless Guide Surface Parachute Design.

NWC TP 6575

TABLE 6-2. Roof Panel and Guide Surface Panel Pattern Dimensions.

		Roof Pattern						
Panels		6	8	10	12	14	16	20
X/h ₁	Y/X	Y/X	Y/X	Y/X	Y/X	Y/X	Y/X	Y/X
.10	.605	.532	.465	.394	.346	.303	.260	
.15	.605	.520	.464	.394	.344	.3045	.257	
.20	.605	.516	.461	.394	.348	.305	.258	
.30	.605	.514	.462	.407	.352	.307	.259	
.40	.605	.511	.459	.410	.354	.311	.263	
.50	.605	.511	.463	.416	.362	.317	.275	
.60	.605	.509	.469	.428	.378	.336	.294	
.70	.613	.525	.481	.441	.403	.366	.328	
.80	.676	.588	.545	.495	.464	.434	.402	
.832	.725							
.866		.713						
.875			.696	.676				
.882					.652		.622	
.888								.590
.896								
.90	.428	.496	.512	.527	.538	.554	.569	
.95	.280	.261	.261	.261	.261	.261	.261	
.975	.193	.1625	.1625	.1625	.1625	.1625	.1625	
1.0	0	0	0	0	0	0	0	

		Guide Surface Pattern						
Panels		6	8	10	12	14	16	20
X/H ₂	Y/X	Y/X	Y/X	Y/X	Y/X	Y/X	Y/X	Y/X
.05	5.56	5.52	4.83	4.33	4.12	3.85	3.535	
.10	3.85	3.81	3.52	3.21	3.01	2.77	2.42	
.15	3.08	2.98	2.76	2.58	2.37	2.18	1.90	
.20	2.54	2.43	2.285	2.13	1.975	1.82	1.605	
.30	1.93	1.80	1.69	1.58	1.48	1.37	1.215	
.40	1.56	1.42	1.335	1.25	1.18	1.075	.953	
.50	1.314	1.17	1.10	1.03	.965	.882	.772	
.60	1.138	.977	.919	.86	.80	.729	.636	
.70	1.01	.823	.769	.722	.672	.615	.528	
.80	.89	.705	.655	.61	.568	.517	.440	
.885	.808							
	.000							
.90	.796	.603	.558	.515	.472	.43	.3665	
	.278							
.919		.586						
		.000						
.922			.540					
			.000					
.93				.491				
				.000				
.937					.442			
					.000			
.944						.397		
						.000		
.95	.757	.559	.515	.472	.432	.394	.334	
	.613	.305	.261	.226	.161	.0896		
.954							.328	
							.000	
1.0	.72	.517	.474	.430	.393	.358	.3025	

6.2.4 Design of Slotted Parachutes

The slotted parachute family started with the design of the flat ribbon parachute, frequently called the FIST ribbon parachute after the Flugtechnisches Institute at T. H. Stuttgart where the parachute was developed in the late 1930s. In the late 1940s, the conical ribbon parachute was introduced at Wright Field; this parachute had, for the same canopy-surface area, a 10% higher drag than the flat canopy parachute (Reference 5.1). In 1949, Knacke and Hegele developed the ringslot parachute as a low-cost supplement to the ribbon parachute. The ringslot parachute, surprisingly, had a 10 to 15% higher drag than the ribbon parachute but the same stability and opening-force coefficient, C_x . The ringslot parachute has found wide application as a landing deceleration parachute for aircraft and as an extraction parachute for airdrop platforms.

In 1955, Ewing modified the ringslot parachute by changing its canopy shape and detail design. The resulting ringsail parachute had a larger drag and a shorter filling time, but also a slightly reduced stability.

An Air Force research program for the investigation of supersonic parachutes developed the hemisflo ribbon, the hyperflo, and the parasonic parachute. These parachutes proved to be superior to the conical ribbon parachute for longer application in the above-Mach 1.5 supersonic range.

Other slotted parachutes include the disk-gap-band parachute used for the Viking lander on Mars, and the square slot parachute.

Flat and Conical Ribbon Parachutes. The ribbon parachute was developed as a parachute suitable for the in-flight and landing deceleration of aircraft and missiles. It has good stability and a lower opening force than the solid flat circular parachute; however, its drag coefficient, C_{D_0} , is only 0.47 to 0.55, compared to 0.8 for the solid circular parachute. Because the conical canopy design is more efficient, the flat ribbon canopy design is considered obsolete. Conical ribbon parachutes are used successfully up to Mach 2 for the rapid deceleration of ordnance devices and for similar applications. If parachutes must operate for longer periods of time in the supersonic range, the hemisflo ribbon parachute is the better choice (see section 5.8).

The general construction of a ribbon parachute gore is shown in Figure 6-22. The individual gore is formed by a grid of horizontal and vertical ribbons. Radial ribbons are used to connect the individual gores. In recent years ribbon canopies have been designed with continuous horizontal ribbons; radial ribbons are used only as load-carrying members. Ribbons in accordance with specification MIL-STD-16213 are generally used for ribbon parachutes.

Figure 6-22 shows radial ribbons on the same side of the gore rather than on alternate sides. This arrangement eliminates the canopy's tendency to rotate because of the

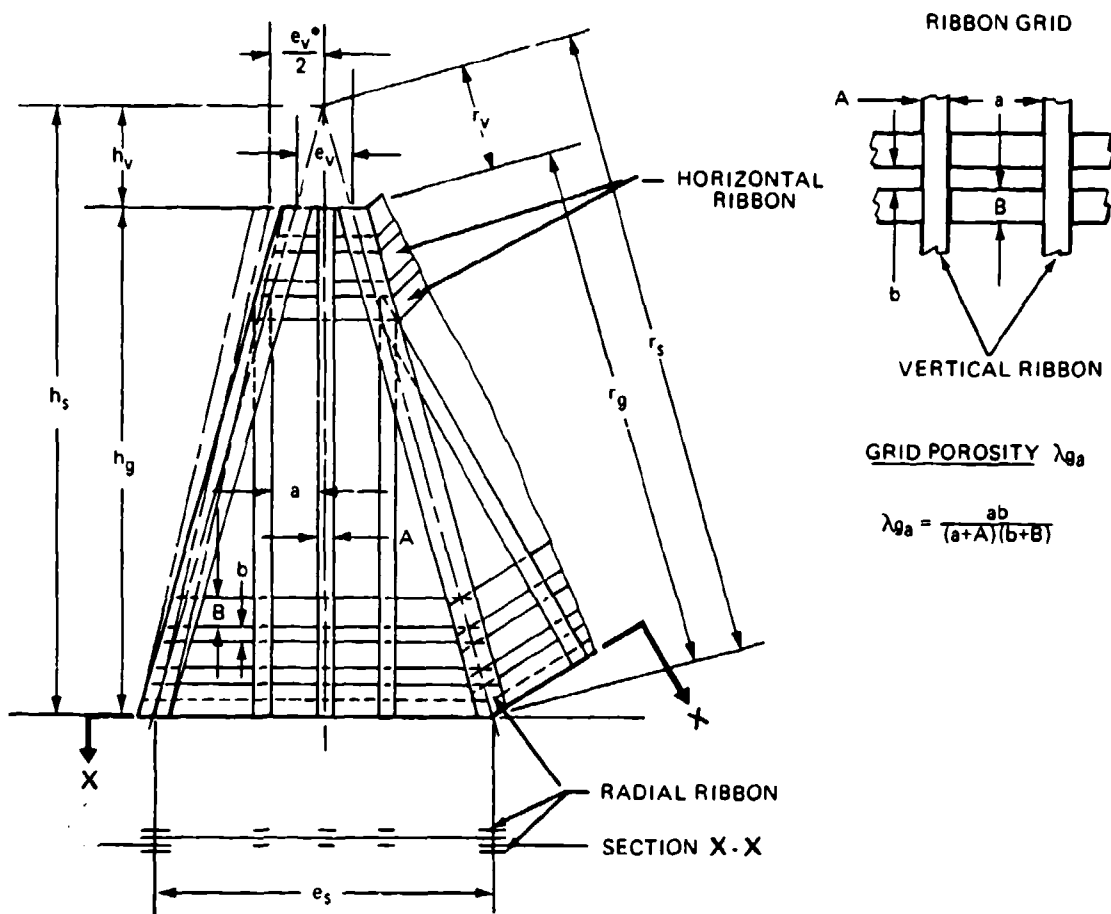


FIGURE 6-22. Typical Gore Design of a Flat or Conical Ribbon Parachute.

venetian-blind-type connection of gores. Double vertical ribbons on both sides of the horizontal ribbons are connected with three rows of stitching and are necessary for parachutes that operate for longer periods of time at high Mach speeds and high dynamic pressures. Single vertical ribbons are sufficient for low-speed operation, as for aircraft drag parachutes. Figure 6-22 shows fullness in the gore at the vent of the canopy, e_v^* , instead of at the gore width, e_v . The fullness in the upper part of the gore provides stress relief, as previously explained in connection with Figure 6-16.

Some older sources, such as Reference 5.39, recommend a vent area of 1% of the total canopy area, with a resultant 10% vent diameter. This vent area is too large, especially for reefed parachutes (Reference 6.13). A vent area that is 0.25% of the canopy area is a more practical approach.

All ribbon parachutes should be equipped with pocket bands to enhance reliability and uniformity of canopy inflation. Section 6.3 describes the design and operation of pocket bands. Figure 6-23 and Table 6-3 give the recommended total canopy porosity, λ_T , as a function of canopy diameter and application. The figure shows that a 3-foot-diameter ribbon parachute needs a total porosity of 33 to 35% for proper aerodynamic performance, whereas a 100-foot-diameter parachute must reduce the total porosity to about 12%. This reduction results in fast, uniform inflation; good stability; and the quoted aerodynamic coefficients.

The aerodynamic characteristics of ribbon parachutes are determined primarily by the total canopy porosity, λ_T , and the effective porosity, λ_e , or, more precisely, by the allowable change in effective porosity, λ_e . The total porosity is the product of the grid porosity of the gores, λ_g , and the material porosity of the textile members of the canopy, λ_m . The effective porosity defines in qualitative terms the increase in geometric porosity, λ_g , caused by the turning of the horizontal ribbons under high-pressure operation.

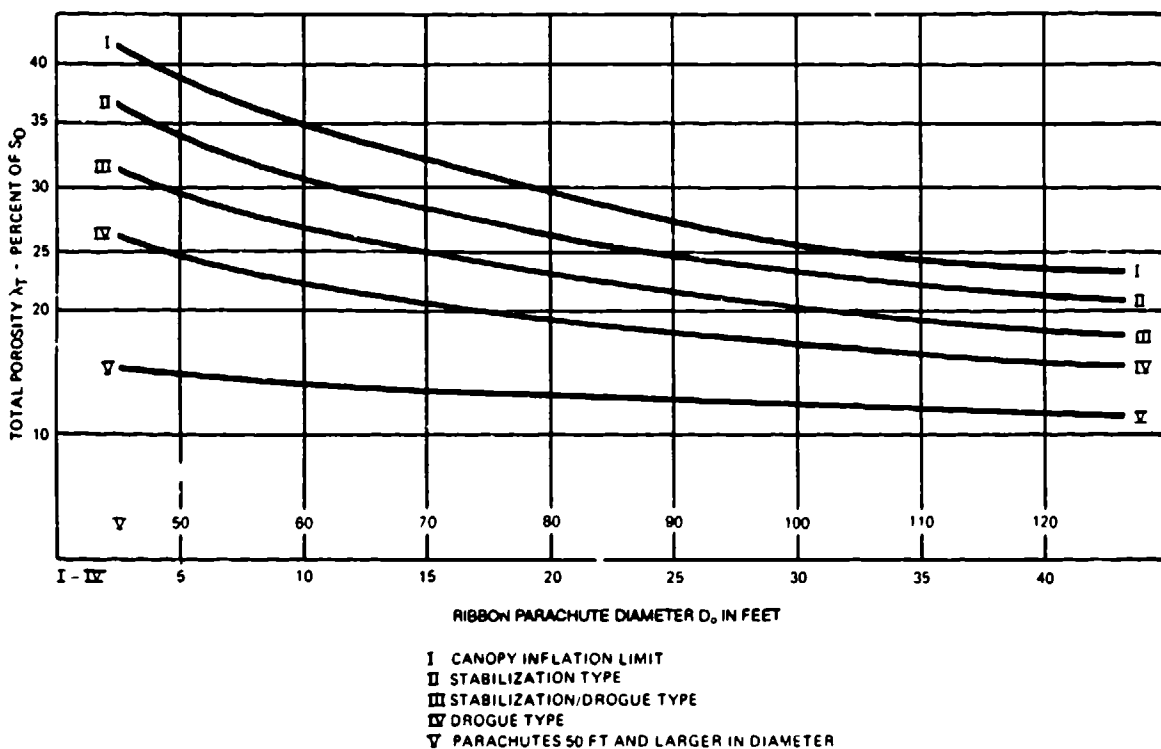


FIGURE 6-23. Recommended Total Canopy Porosity, λ_T , for Ribbon Parachutes as a Function of Parachute Diameter and Application (see Table 6-3 for Applications).

TABLE 6-3. Recommended Porosity Range and Vertical Ribbon Spacing
as a Function of Application and Velocity.

Parachute application	Canopy loading, $W/(C_D S)p$	Velocity range	Porosity curve, Figure 6-23	Ratio, a/b	Estimated oscillation degrees
Aircraft landing	High	Low	III	2.5	$\pm 0\text{-}3$
Aircraft approach	High	Medium	II-(I)	1.5	0
Missile brake up to $M = 2.0$	High	High	II-(III)	$1.0 \div 1.5$	2-3
Stabilization	High	High	II-I	1.5	0
Stabilization	Low	Low	III-II	2.5	0
Ordnance	Medium	High	IV-III	1.5	$\pm 5\text{-}8$

NOTE:

a = Distance between vertical ribbon

b = Width of horizontal ribbon

Figure 6-24 explains the effect of vertical ribbon spacing, a, and canopy loading, $W/(C_D S)p$, on the effective porosity change and the associated opening behavior of the canopy. The design porosity, λ_T , increases under internal canopy pressure because of the turning of the horizontal ribbons, called the venetian-blind effect. The increase in the porosity caused by the ribbon turning becomes greater as the ratio of vertical ribbon spacing, a, to horizontal ribbon width, b, and the dynamic pressure increase. The change in slot opening as a function of vertical ribbon distance is shown in lines I and II and the resultant change in effective porosity in line III of Figure 6-24. Lines IV and V of Figure 6-24 show how parachutes of different canopy loading react to the change in effective porosity. This increase in effective porosity, if not properly controlled in the design of the canopy, can reach the point of critical porosity, causing the canopy to open only partially or not at all.

Low-canopy-loading parachutes, such as large final descent parachutes, generally have sufficient drag, even with a partially inflated canopy, to reach lower velocities where the canopy will inflate fully. This may not be the case with high-canopy-loading parachutes, such as first-stage drogue chutes and ordnance retardation parachutes.

As a rule, high-canopy-loading parachutes require a short vertical ribbon spacing, whereas low-canopy-loading parachutes benefit from wider vertical ribbon spacing to obtain a slower, lower-force canopy inflation. The relationship of ribbon parachute application, canopy porosity, and vertical ribbon spacing is shown in Table 6-3.

Section 7.4 covers the design of a supersonic conical ribbon parachute, including several methods for determining the canopy porosity.

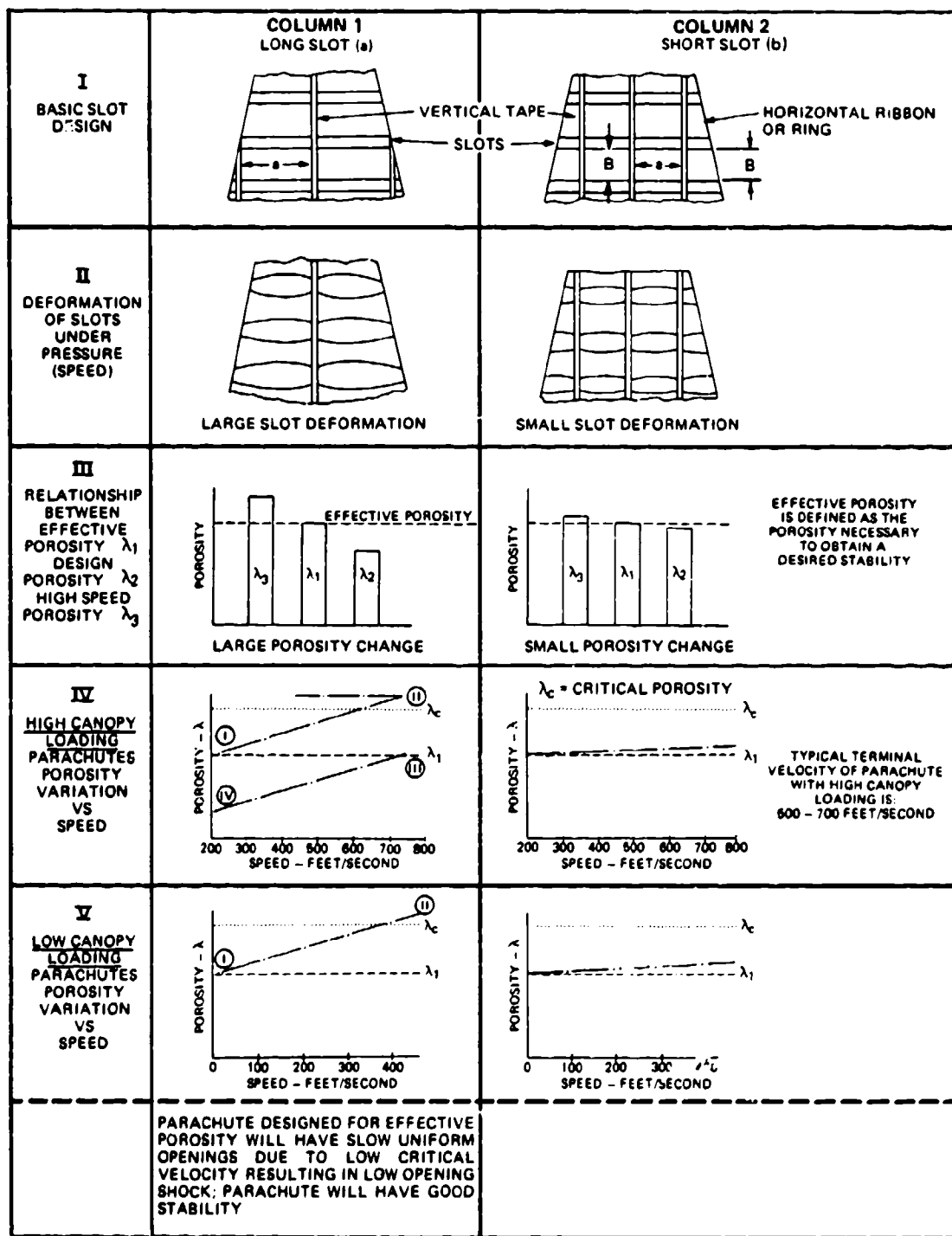


FIGURE 6-24. Change in Effective Porosity, λ_e , as a Function of Canopy Loading, $W/(C_D S)_p$, and Vertical Ribbon Spacing, a .

Reference 6.14 describes the design of a ribbon parachute with continuous horizontal ribbons and nonparallel vertical ribbons.

Computers are well suited to determine the geometric gore design of ribbon parachutes.

Ribbon parachutes that do not perform as expected may have been designed without following the generally known design principles that are presented in this manual.

Hemisflo Ribbon Parachute. Hemisflo ribbon parachutes have been used at velocities up to Mach 3, primarily as drogue and stabilization devices and for applications where the parachute must operate for longer periods of time in the supersonic region and often in the wake of a large forebody.

Typical applications are as stabilization and retardation parachutes for several types of ejection seats, for the encapsulated seats of the B-58 and B-70 bombers, and as first-stage drogue chutes for the F-111 and the B-1 crew modules.

The canopy of the hemisflo parachute forms part of a perfect sphere with the suspension lines connected tangentially to the sphere (see Figure 6-25),

where

$$L_e/D_o = 2.0$$

$$D_o = 1.1284 \sqrt{S_o}$$

$$D_p = D_c = \frac{\sqrt{360S_o}}{210\pi}$$

$$h_s = 0.916 D_o$$

$$L_e = 2.0 D_o$$

The point where the lines contact the canopy becomes the canopy skirt, resulting in a 210-degree canopy (see Figure 6-25). The hemispherical shape avoids the use of gores that can flutter in and out, as on flat or conical canopies, and eliminates the length difference in the leading and trailing edges of the horizontal ribbons. This greatly reduces canopy breathing and high-frequency ribbon flutter, both sources of canopy damage and drag decrease on conical ribbon parachutes operating at supersonic velocities. All detail design recommendations of conical ribbon parachutes also apply to hemisflo canopies. Figure 6-25 shows horizontal ribbons on alternate gore sides. As previously explained, this arrangement may cause a venetian-blind effect and can lead to canopy rotation. Having both radials on the same side will decrease rotational tendencies.

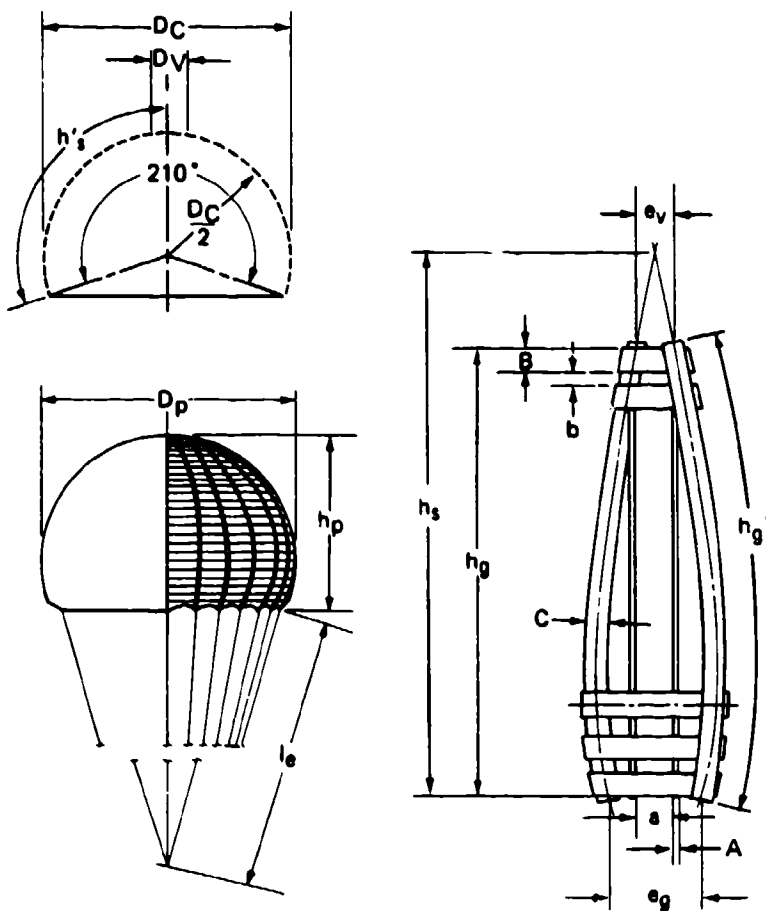


FIGURE 6-25. Typical Design of a Hemisflo Parachute.

Reefing of hemisflo canopies is similar to that of other ribbon parachutes. The reefing ratio and reefing-line force data for conical ribbon parachutes have been used with good results on hemisflo canopies. References 5.51, 5.52, and 6.15 through 6.18 give performance and design details for hemisflo ribbon parachutes.

Hyperflo Parachute. The hyperflo parachute was developed simultaneously with the hemisflo parachute by the Cook Research Laboratories in the supersonic decelerator program. The hyperflo parachute canopy has a flat ribbon grid crown and an inverted cone of solid material at the skirt, somewhat similar to the extended-skirt parachute. It has been tested in wind-tunnel, sled, and free-flight tests up to Mach 4. The hyperflo parachute is sensitive to variations in design, velocity, and dynamic pressure, and requires extensive testing before operational use; this need for testing has limited its application. Reference 6.17 and 6.19 describe hyperflo development, testing, and performance.

Ringslot Parachute. The ringslot parachute, developed as a low-cost supplement to the ribbon parachute, has similar aerodynamic characteristics, but has a 10 to 14% higher drag. The basic design shown in Figure 6-26 has been used with both a flat and a 25-degree conical canopy. The horizontal ribbons of the ribbon parachute are replaced with rings manufactured from full-, half-, or quarter-width standard parachute material. Individual segments are joined to rings that are reinforced on the upper and the lower edges; the rings are then joined using radial tapes. Specification MIL-C-9401 gives many design details. Rings have been manufactured from continuous pieces of material with V-type folds under the radial tapes. Landing deceleration and platform-load-extraction parachutes are multiple-use parachutes that need reinforcing between the rings and vertical tapes. As on ribbon parachutes, the number of vertical tapes in each gore depends on the canopy loading. Landing deceleration and platform-extraction parachutes that have a high canopy loading need three vertical tapes; low-canopy-loading ringslot parachutes, developed for the high-speed drop of supply containers, need only one vertical tape for a slower, lower-force opening. As with ribbon parachutes, the ringslot parachute's aerodynamic performance is controlled by the total

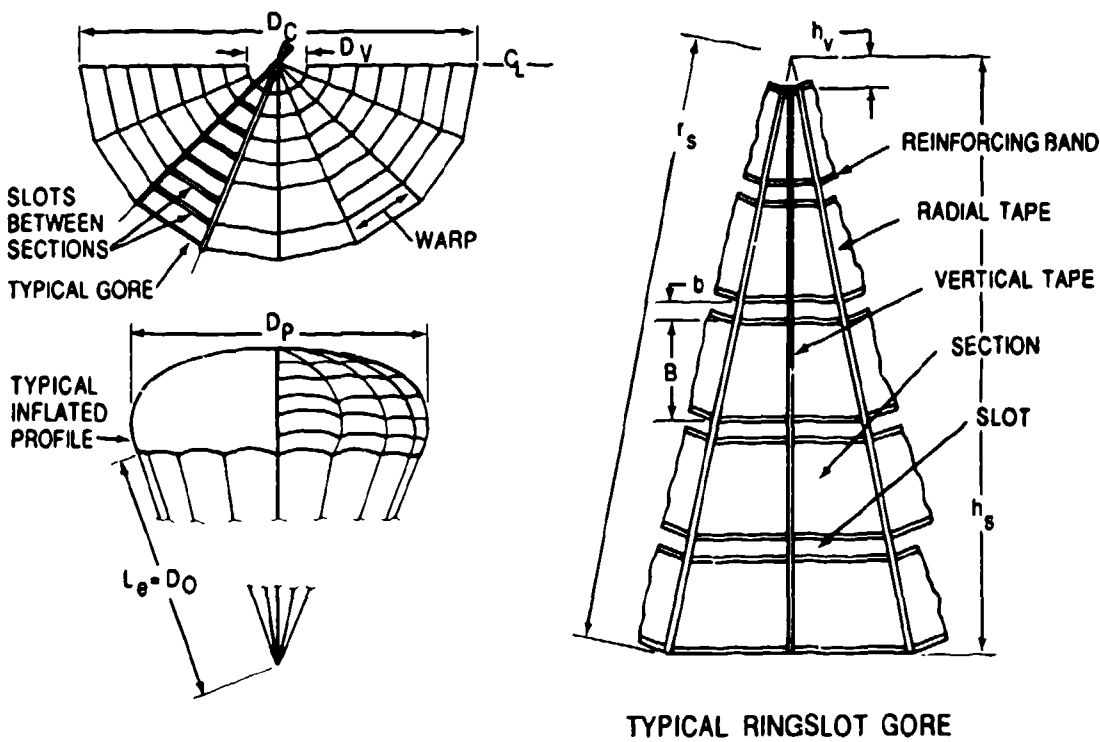
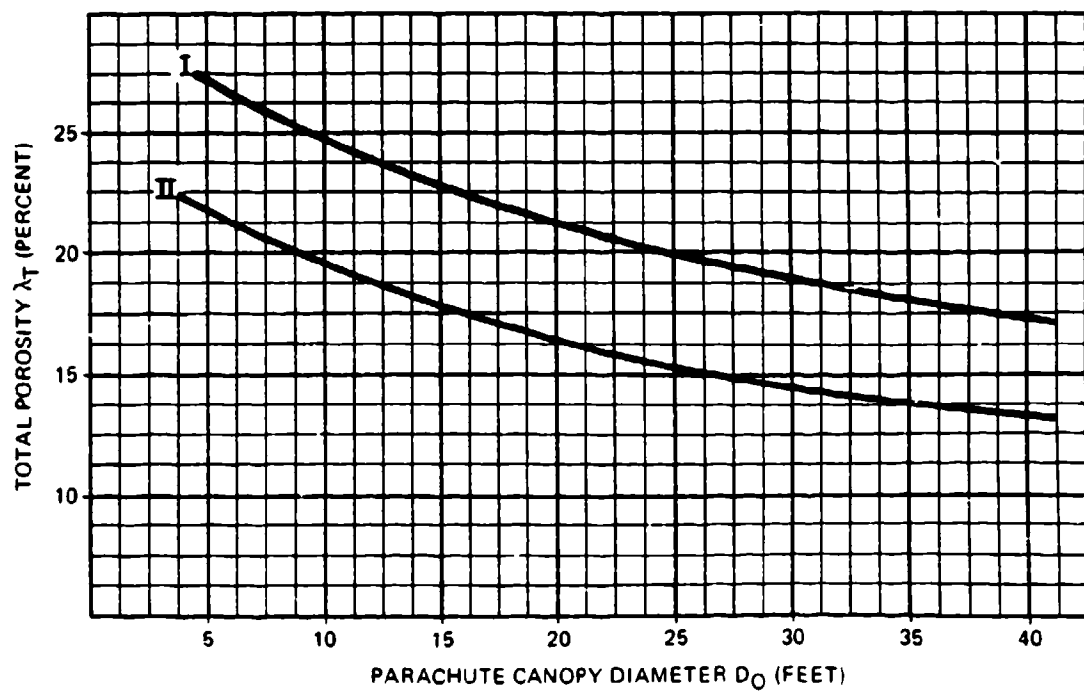


FIGURE 6-26. Typical Design of Ringslot Parachute.

porosity and the allowable increase in effective porosity. Figure 6-27 shows the total porosity as a function of parachute diameter, and number of vertical tapes.

Ringslot parachutes for platform extraction are being used in clusters of two and three parachutes (References 5.48 and 5.49).

Ringsail Parachute. The ringsail parachute, a modification of the ringslot parachute, has a quarter-spherical cross section in the lower part, and a conical cross section in the upper part of the canopy. The cut of the rings in the crown area is similar to that of the ringslot parachute. In the lower part of the canopy, each ring section has fullness in the leading edge of the ring that gives each section a positive angle of attack. This creates an outward-directed force that, in turn, provides a larger drag coefficient and a faster canopy inflation. The faster inflation increases the opening-force coefficient, C_x , to 1.2, compared to 1.05 to 1.1 for the ringslot parachute.



CURVE I. Porosity recommended for parachutes with three vertical tapes.

CURVE II. Porosity recommended for parachutes with one vertical tape.

FIGURE 6-27. Total Canopy Porosity, λ_T , Recommended for Ringslot Parachutes.

The ringsail parachute, whose basic design is shown in Figure 6-28 and described in detail in Reference 5.50, was used as main descent parachute for the three manned spacecraft, Mercury, Gemini, and Apollo (References 5.10, 6.90, and 6.91), and for the crew modules of the F-111 and B-1 bombers (References 5.169 and 5.170). After the Apollo program, NASA

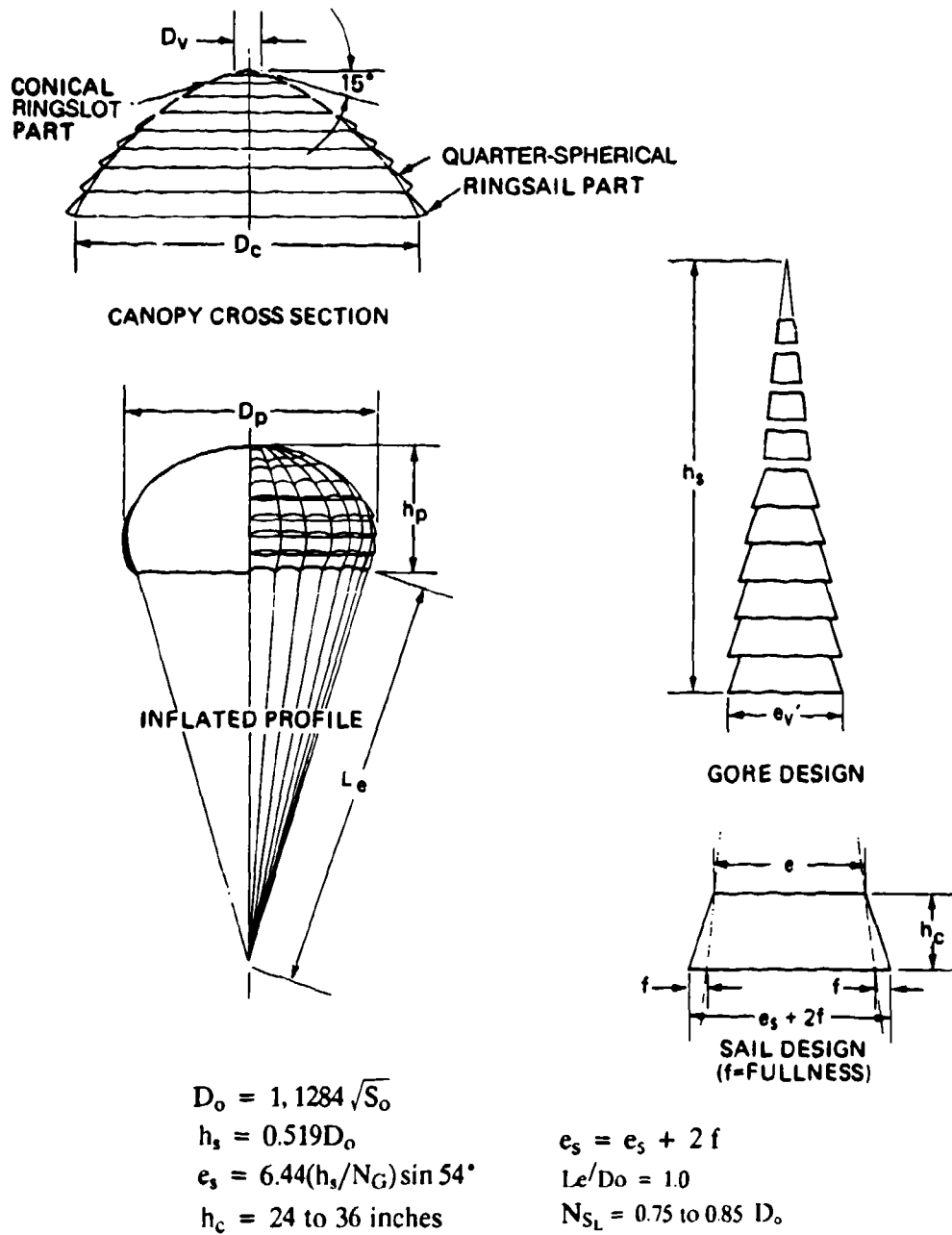


FIGURE 6-28. Typical Design of Ringsail Parachute.

funded programs for the development and testing of a cluster of approximately 125-foot-diameter ringsail parachutes and a single 189-foot-diameter parachute; both were successful programs (References 6.20 and 6.21).

The ringsail parachute has a characteristic that is beneficial for a single parachute but creates problems in cluster operation. Large, reefed ringsail parachutes open quickly into the first reefed stage; thereafter, additional rings inflate slowly before disreef. Quick opening is advantageous for single parachutes but creates a lead/lag chute situation in a cluster of three independently deployed Apollo main parachutes. The leading parachute or parachutes further increase in diameter during reefed inflation, crowding out the lagging chute or chutes and causing large differences in opening times and forces. To prevent this situation, a wide slot is placed between the fourth and fifth rings, preventing the leading chute or chutes from inflating further in the first reefed stage and permitting more uniform inflation of all three parachutes.

Disk-Gap-Band Parachutes. The disk-gap-band parachute, a NASA development, was used in the Viking program for assisting in the landing of two probes on Mars. The disk-gap-band parachute consists of a flat solid material top, a cylindrical extension on the canopy skirt, and a single slot or gap between the top and the extension, somewhat similar to a one-slot ringslot parachute. References 5.55 and 5.56 and 6.22 describe design and testing of this parachute.

6.3 Design of Parachute Assemblies and Components

A parachute assembly consists of several components (a typical assembly is shown in Figure 6-11). In addition, the total parachute system may consist of a cluster of several parachute assemblies. This section describes the design and operation of the various components that constitute a parachute assembly.

6.3.1 Parachute Clusters

6.3.1.1 Cluster Configurations

Three typical parachute cluster configurations are shown in Figure 6-29. Configuration (a) is used on parachute clusters for the airdrop of heavy military equipment and has been used successfully for loads up to 50,000 pounds and clusters of 10 100-foot-diameter G-11 cargo parachutes. Platforms containing the loads are extracted from the cargo compartment of the aircraft by a single parachute or a cluster of two or three ringslot parachutes. After the platform has left the aircraft, the extraction-parachute assembly is disconnected from the platform and lifts the tied-together main parachute deployment bags off the platform. The extraction parachute then serves as pilot chute for the deployment of the main parachutes. The extraction chute/pilot chute/bridle/deployment-bag assembly disconnects from the main parachutes and must be retrieved individually.

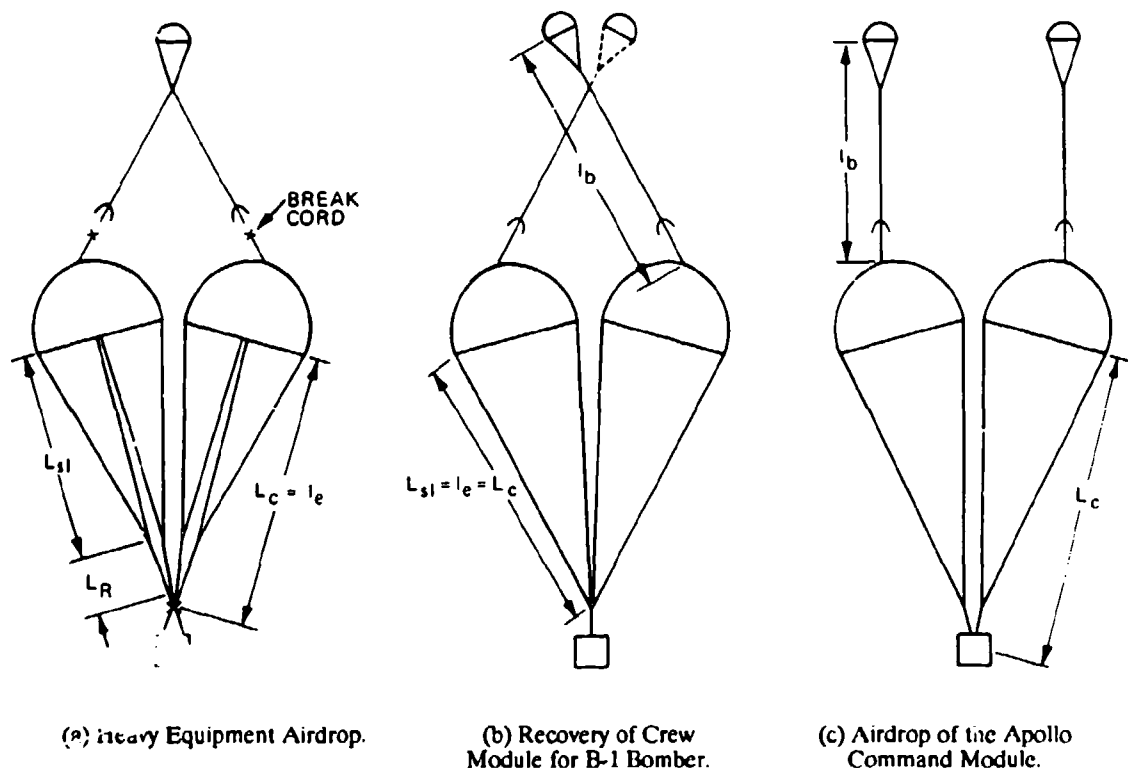


FIGURE 6-29. Typical Parachute Cluster Arrangements.

Cluster configuration (b) was used on the three ringsail main parachutes for landing the B-1 bomber crew escape module, a now discontinued concept. The cluster was begun using the independently deployed main parachute concept of the Apollo spacecraft but was changed to configuration (b), which stretches all parachutes simultaneously, resulting in more uniform deployment, canopy inflation, and opening forces. Each pilot chute was able to deploy the total cluster. The second pilot chute served as backup. References 5.169 and 5.170 describe the B-1 crew module parachute system.

Configuration (c) was used on the three 85.3-foot-diameter Apollo ringsail parachutes. Parachutes on manned spacecraft are the primary means for landing the astronauts. NASA, therefore, ruled that no failure of a subsystem or component should cause a catastrophic system failure. This ruled out common pilot chute and common riser connection points as on configurations (a) and (b). The two drogue chutes and the three main parachutes had to be individually deployed, connected, and disconnected, a major design complication.

Configuration (a) has three single failure points: a single pilot chute, a common pilot chute junction point, and a common riser connection fitting.

Configuration (b) has two single failure points: the fittings that connect the two pilot chutes to the bridles that lead to the main parachutes and the confluence point of the two main parachute risers. These single failure points were acceptable for the B-1 aircraft since the parachute-recovered crew module does not constitute the primary landing system, as do the parachutes on the Apollo spacecraft, but constitutes an emergency backup system. The pilot chute bridles on configuration (b) must be long enough to allow full inflation of all canopies plus a distance of about $0.1 D_p$ between adjacent parachutes.

Configuration (c) has no single failure points because of the independent deployment of each parachute assembly consisting of a permanently connected pilot chute, a pilot chute bridle, a main parachute deployment bag, a main parachute, and a riser. The independent deployment of the three main parachute assemblies of the Apollo spacecraft caused nonuniform parachute stretch and canopy inflation, resulting in opening-force variations. This problem is discussed in section 5.10.

A parachute cluster with two independently deployed main parachutes is described in Reference 5.23, shown in Figure 7.7, and detailed in section 7.3.

6.3.1.2 Effective Suspension-Line Riser Length

Section 5.10 discusses the loss of parachute drag in a cluster caused by interference between the parachutes and recommends using longer suspension lines or risers to recover some of the interference drag loss. Data on the drag gain caused by longer suspension lines can be found in section 5.2.

Both longer suspension lines and longer risers were used successfully on the Apollo main parachute cluster, with a negligible drag loss in the parachute assembly.

6.3.1.3 Permanently Attached Pilot Chutes

Large reefed parachutes often exhibit irregular canopy crown inflation; the inflated part of the canopy waves and the vent opening is not properly centered, which causes friction burn and damage in the canopy crown area. Permanently attached pilot chutes stabilize the canopy crown area, prevent friction burns, and support uniform canopy inflation. The distance between the vent of the main parachute and the leading edge of the pilot chute, L_p , should be long enough to permit inflation of the pilot chute in good airflow behind the vehicle (see Figure 6-29). Proper distance is especially important for deployment behind large, blunt forebodies. The forebody wake effect is discussed in detail in section 5.2. The pilot chute bridle

also must be long enough to permit full inflation of all parachutes in the cluster, allowing a space equal to about 10% of the inflated canopy diameter between the individual canopies. The pilot chute should stay inflated during the reefed canopy opening, but should collapse after full canopy inflation.

Several operational clusters with permanently attached pilot chutes used a pilot chute bridle line length of L_b equal to 0.4 to 0.55% of the diameter of the main parachute.

6.3.1.4 Canopy Ties

The individual parachutes in the cluster wander around slowly and change position in a random fashion, but seldom touch. This behavior has never caused any aerodynamic or stress problems, but looks awkward. Sandia National Laboratories has successfully used short tie lines to connect the canopies of ribbon and ringslot parachutes, but this technique has been tried unsuccessfully on clusters of less stable parachutes. Unstable canopies in a cluster appear to fight this restriction and cause large canopy deformations.

6.3.1.5 Canopy Vent Size

Most large parachutes use reefing for force control and for uniform inflation in the reefed stage. Experience has shown that the diameter of the vent of the reefed canopy must be substantially smaller than the diameter of the reefing-line circle to ensure good canopy inflation. The sometimes-used rule of thumb to make the vent area of the canopy equal to 1% of the total canopy area results in a vent too large for most reefed large parachutes. Problems with a large vent on the large ribbon parachutes for the recovery of the Space Shuttle solid booster rockets are discussed in Reference 6.13.

6.3.1.6 Cluster Parachute Deployment Bags

Cluster parachutes have been stowed successfully in individual bags as well as in a single compartmented bag. The choice of the deployment-bag configuration depends mostly on the shape of the payload and the type and shape of the compartment available for parachute storage.

Stowage of the parachutes in odd vehicle locations, parachute packing, rigging, and ground retrieval influence the selection of single or multiple deployment bags. Forced ejection of the parachutes in cross-wind deployment may favor the selection of a single, compartmented deployment bag.

6.3.1.7 Cluster Parachute Literature

Extensive literature is available on parachute cluster design and operation. References 5.1, 5.10, 5.23, and 5.164 to 5.179 provide information on many aspects of cluster design.

6.3.2 Pocket Bands

Pocket bands are an essential design element of all slotted parachutes and are beneficial to most solid material, standard-porosity canopies. Pocket bands support the inflation of high-porosity slotted canopies and make inflation times and forces of all parachutes more uniform by eliminating random long and short inflation times.

The author developed pocket bands during World War II to counteract the uncontrolled infolding of canopy gores of high-porosity ribbon parachutes. This gore infolding was especially pronounced in the wake of large forebodies. The design detailed in Figure 6-30 and Table 6-4 evolved from investigations of various pocket band configurations (References 5.39, and 6.23 to 6.25).

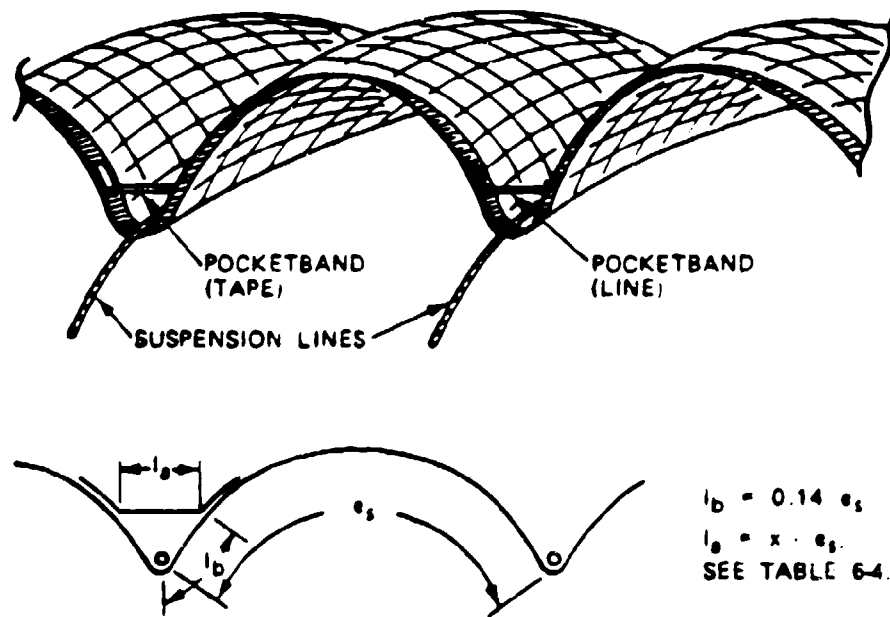


FIGURE 6-30. Pocket Band Design.

Sandia National Laboratories recently investigated, in wind-tunnel tests, the effect of pocket bands on the inflation of fully open and reefed ringslot parachutes. Sandia's conclusion reads, "The effect of pocket bands on any parachute is to produce repeatable minimized inflation times" (Reference 6.25). Pocket bands must be dimensioned so as not to restrict full canopy inflation. Different canopy types and different numbers of gores require different pocket band dimensions, as shown in Table 6-4. Extended-skirt parachutes, for example, have a flatter gore shape at the skirt than flat and conical canopies have and therefore need longer

TABLE 6-4. Pocket Band Dimensions.

Type of parachute	Number of gores, N_{SL}									
	12	16	20	24	28	32	36	40	48	60
Ribbon, heavy	.138	.127	.120	.115	.112	.110	.108	.105	.103	.102 $\times e_s$
Ribbon, light	.124	.114	.108	.104	.102	.100	.098	.097	.096	.095 $\times e_s$
Ribbon, conical	.132	.122	.115	.108	.105	.102	.099	.098	.097	.096 $\times e_s$
Solid flat circular	.140	.124	.116	.109	.104	.101	.099	.097	.095	.094 $\times e_s$
Extended skirt	.310	.285	.270	.260	.255	.250	.245	.242	.240	.239 $\times e_s$

pocket bands. Use of round lines or small tapes as pocket bands does not change the canopy inflation time, but 2-inch-wide pocket bands decrease the canopy inflation time by 15 to 25%.

Pocket bands should have a strength equivalent to 50% of that of the suspension lines or skirt tapes. Most parachute companies use pattern sewing machines for attaching the pocket band to the skirt of the parachute canopy.

The use of pocket bands for obtaining a small amount of canopy reefing, called "fixed reefing," is described in section 6.5.

6.3.3 Pilot Chutes

Pilot chutes are used to deploy large parachutes from their storage packs or containers into good airflow behind the jumper, load, or vehicle. A typical pilot chute and main parachute assembly is shown in Figure 6-4; the main parachute is stowed in a deployment bag. A pilot chute, attached to the bag, first extracts the parachute pack from the vehicle compartment and then deploys the main parachute from its deployment bag. The following requirements, based on experience, can be defined for pilot chutes:

1. Pilot chutes must open quickly and reliably.
2. Pilot chutes must be stable and must have sufficient drag to pull the main parachute pack away from the payload and extract the main parachute.
3. A pilot chute, ejected by its internal spring, drogue gun, or mortar into good airflow behind the forebody, must be able to extract and deploy the attached parachute or the parachute deployment bag.

Many types of pilot chutes have been used successfully and meet the requirements stated above. The most frequently used pilot chute for the deployment of military personnel emergency parachutes is the MA-1 type shown in Figure 6-31. This chute has a

30-inch-diameter canopy of low-porosity material. An internal coil spring ejects the pilot chute away from the jumper. Vanes attached between the suspension lines and the material cone that covers the internal spring orient the pilot chute in the direction of the airflow (Reference 6.26). A modified version with a simpler canopy design and a heavier spring than that of the MA-1 is used with sport parachutes.

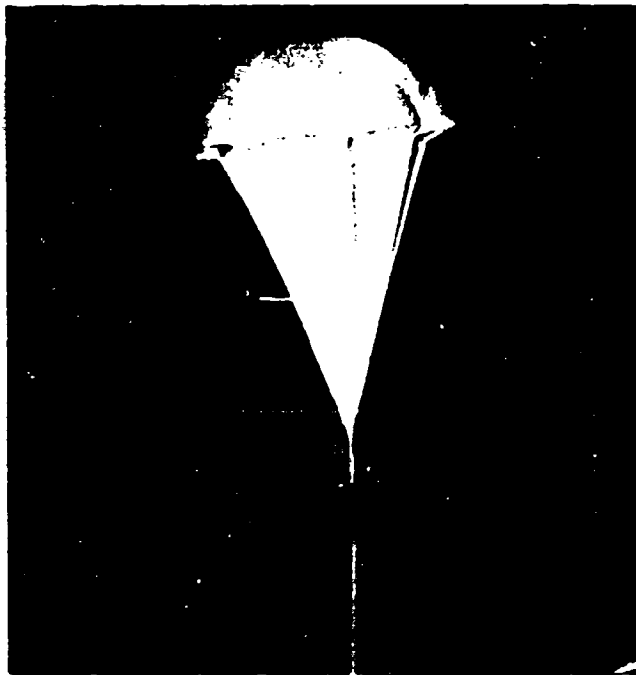


FIGURE 6-31. MA-1 Pilot Chute in Vertical Wind-Tunnel Tests.

A box-type pilot chute without an internal spring but with stabilizing vanes has been used for numerous applications where the pilot chute is extracted by a drogue gun slug or is mortar-ejected (Figure 6-32). Ribless guide surface and ringslot pilot chutes have been used successfully for many projects.

Mortar-ejected 7.5-foot-diameter ringslot parachutes were used as pilot chutes for disconnecting the Apollo main parachute deployment bags from the command module by means of a daisy chain, and for deploying the main parachutes. Pilot chutes must be ejected into good airflow behind the forebody. Tests conducted by several sources resulted in the recommendation to eject the pilot chute to a distance equivalent to at least four and, if possible, six times the forebody diameter behind the vehicle.

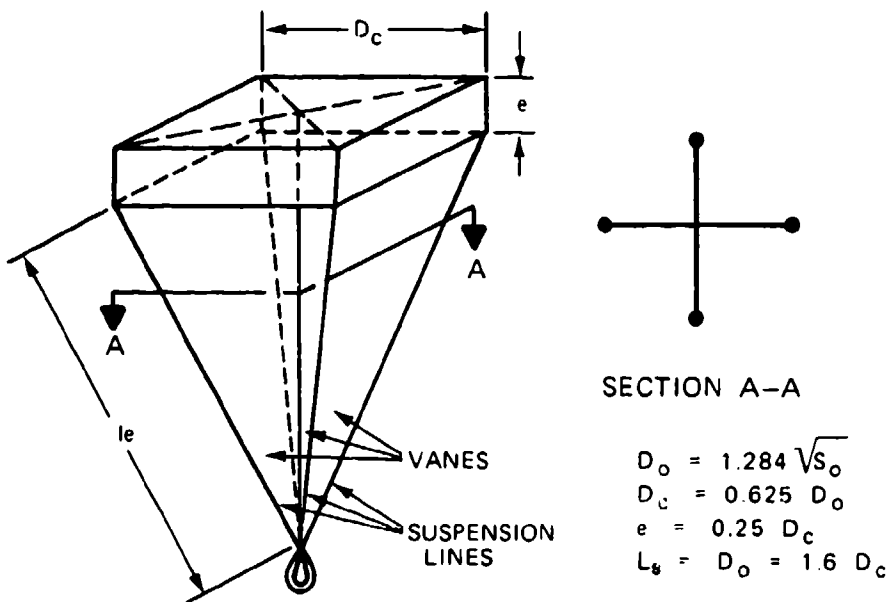


FIGURE 6-32. Box-Type Pilot Chute.

Evaluation of pilot chute failures at the El Centro parachute test range led to the rule of thumb that the pilot chute extraction force should be equal to or larger than four times the weight of the parachute assembly to be extracted.

Tests conducted with ribbon parachutes deployed behind a test-bed aircraft showed that a permanently attached pilot chute with a drag area equal to 6% of the main parachute drag area starts to squid the main parachute.

An evaluation of successful pilot chute applications established the pilot and main parachute drag-area ratio as a function of the deployment velocity listed in Table 6-5.

TABLE 6-5. Pilot and Main Parachute Drag-Area Ratios.

Deployment velocity, KEAS	Pilot-to-main-parachute drag-area ratio
< 150	0.03
150 to 250	0.02
> 250	0.005

Drag coefficients and opening-force coefficients for pilot chutes are shown in Table 6-6. The drag of a pilot chute close to a forebody may be less than that obtained from the Table 6-6 coefficients because of forebody wake. Figure 5-22 can be used to determine the drag loss.

TABLE 6-6. Pilot Chute-Drag and Opening-Force Coefficients.

Pilot chute type	Drag coefficient, C_D	Opening-force coefficient, C_X
Circular vane spring	0.55	2.05
Square box	0.60	2.0
Ribbon, conical	0.52	1.3 ^a
Ringslot	0.60	1.4 ^a
Guide surface, ribless	0.42	2.0 ^a

^a For normal applications, use C_X coefficients in Tables 5-1 and 5-2.

Table 6-5 recommends different sizes of pilot chutes for various deployment velocities. However, the size differences create problems for pilot chutes that must work over a wide velocity range. A single large pilot chute may satisfy the low-speed requirements but may create unacceptable snatch forces and pilot chute weights during high-speed deployment. A small pilot chute would work well at high speeds but would create a deployment problem at low speed. Some projects encountering this velocity-range deployment problem have used a two-step pilot chute or a pilot chute cluster.

Several multiple-step pilot chutes have been developed with low drag area at high-speed deployment and high drag area at low-speed deployment. One concept uses blow-out patches around the skirt of the pilot chute. These patches remain intact at low speeds but blow out at high speeds. Another concept uses a pilot chute with a strong inner canopy part and a weaker outer part. A second set of strong suspension lines is attached to the stronger canopy part at the inside of the canopy. At low-speed deployment, the entire canopy inflates; at high-speed deployment, the outer set of suspension lines breaks away and only the inner small part of the canopy inflates. A cluster of two pilot chutes, a larger light chute and a smaller strong pilot chute, performs the same two-speed function.

6.3.4 Anti-Inversion Net

The T-10 parachute, a 35-foot-diameter extended-skirt design, is used by several western nations as a paratrooper parachute. After the paratrooper exits the aircraft, the parachute is deployed by a static line attached to the aircraft, similar to the deployment procedure described in section 6.1 and shown in Figure 6-3. The cross-wind deployment of the parachute has a tendency to form a sail, causing canopy inversions when the upwind gore is pushed through two adjacent downwind suspension lines. The gore forms a pocket on the opposite

canopy side or pulls the entire canopy through the downwind side and turns the canopy inside out. Canopy inversion frequently causes extensive canopy damage.

The invention of the anti-inversion net by G.W. Stephens of Great Britain virtually eliminated T-10 inversions. Figure 6-33 shows a T-10 gore with the anti-inversion net installed. The U.S. version of the net uses nylon mesh with a 3.5-inch grid spacing. The net extends 18 inches down from the canopy skirt, forming an inverted cone extension. The British design uses a slightly smaller grid spacing.

Extensive tests conducted in Great Britain and by U.S. airborne troops have demonstrated the effectiveness of the anti-inversion net (References 6.27 through 6.29).

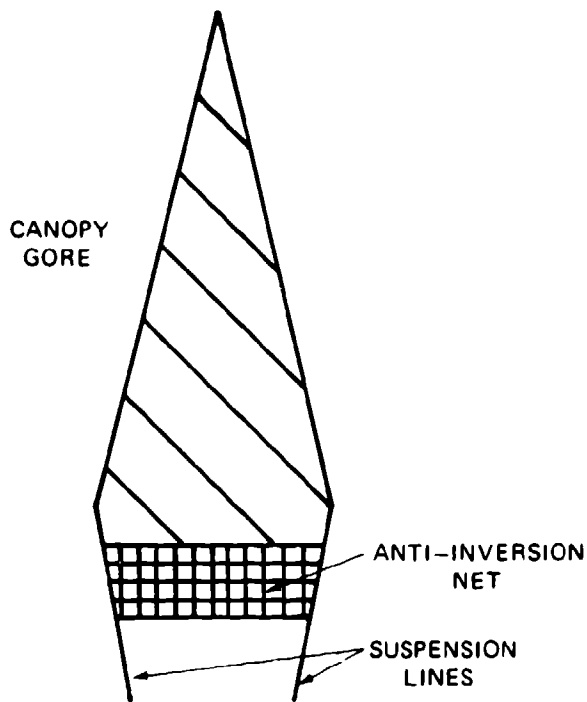


FIGURE 6-33. Canopy Gore with Anti-Inversion Net
(Only One Gore Shown).

6.3.5 Parachute Deployment Components

Section 6.1 describes various parachute deployment concepts and emphasizes that parachute deployment should proceed in the order of riser, suspension lines, and canopy, and that the mouth of the canopy should be closed until the suspension lines and the canopy are stretched to avoid high mass forces (snatch force). This deployment sequence, called line-first deployment, requires support equipment. Most frequently, a deployment bag is used to house

the parachute and riser. Deployment bags need compartments with round, rectangular, or related cross sections and a length-to-width ratio not to exceed about 4 to 1. For odd compartment shapes and locations, other means to support an orderly, sequential deployment have been developed; the most commonly used are skirt hesitators, quarter deployment bags, deployment sleeves, and sacrifice panels. However, this is a field where ingenuity frequently creates outstanding new approaches that ensure good deployment from odd parachute-compartment shapes and locations.

6.3.5.1 Parachute Deployment Bags

The most frequently and successfully used method for providing a controlled deployment is stowing the parachute in a flexible textile container, called a deployment bag, that becomes part of the parachute assembly (see Figures 6-4 and 6-11). The deployment bag must be shaped to the configuration of the parachute container or vehicle compartment and designed to control parachute deployment and permit easy handling, packing, rigging, and storage of the parachute assembly.

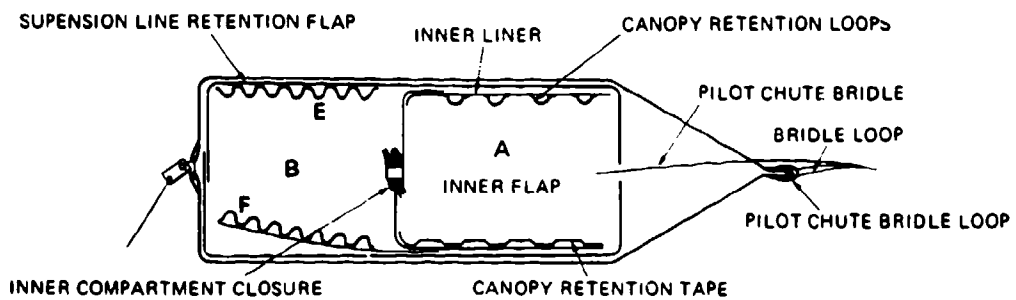
Pilot chutes or drogue chutes are used to extract the deployment bag and to deploy the parachutes. The deployment bag must provide a tight enclosure for the parachute assembly, but must be so designed that parachute and risers can deploy without friction damage caused by a bag that is too tight, or by protrusions in the bag. Reference 6.30 describes early ideas about the design and operation of deployment bags.

Many types of deployment bags have been used, ranging from a simple sack with a flap closure for small parachutes deployed at low velocity to a multiple-compartment, multiple-constraint bag for large, final descent parachutes such as those used for the Apollo and F-111 aircraft crew modules.

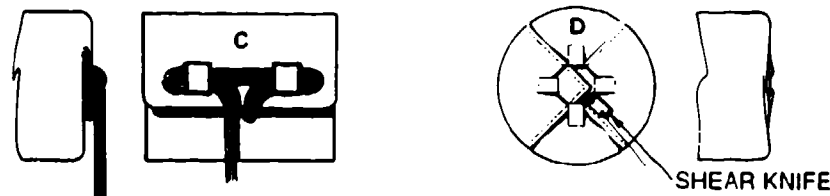
A typical deployment bag is shown in Figure 6-34. Detail (a) shows the deployment bag cross section consisting of two compartments, one for the parachute canopy (A) and a second for suspension lines and risers (B). The canopy and suspension lines are retained in their compartments with individual ties.

Detail (b) shows two bag closure methods. Method (b) (1) closes the flaps with line or riser stows. A line or riser bundle is routed through two loops that extend from the lower flap through openings in the upper flap. Care must be taken to prevent friction burns when extracting the line bundle. Wrapping the folded line bundle with wrapping paper or lining the stow loop with cotton or Teflon material are proven methods.

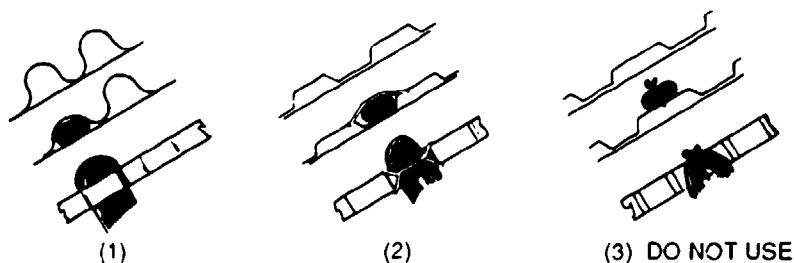
Method (b)(2) shows a circular bag closed with four flaps tied together with a heavy cord; the cord is severed with a shear knife upon deployment. The shear knife must be attached to the appropriate riser or line member that stretches before full riser or line stretch.



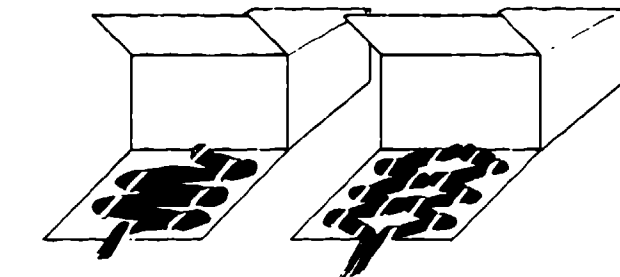
(a) Typical Deployment Bag.



(b) Typical Bag Closure.



(c) Canopy Stowage Methods.



(d) Typical Line Tie Downs.

FIGURE 6-34. Typical Deployment-Bag Details.

Typical ties for retention of the canopy and for stowage of suspension lines and risers are shown in Detail (c). Canopy ties must be designed to retain each or every second canopy accordion fold and to prevent slippage of the canopy under the ties; slippage will cause friction burns. Both light cords and rubber bands have been used for canopy ties and for tying lightweight suspension lines. Heavier lines and risers are best stowed in individual webbing loops sewn either to the wall of the bag or to fold-out flaps as shown in Detail (c), (1) and (2).

Stowing the suspension lines in two groups as shown in Detail (d) (2) prevents the bag from zigzagging during line deployment.

K. French has presented a theory for calculating the effect of line ties (Reference 6.31). Reference 6.32 presents an interesting approach to testing a deployment system.

A typical shear knife is shown in Figure 6-35. The knife must be installed so that no tension is exerted on the pull webbing before parachute deployment. The small hole in the shear knife secures the knife in a no-tension position before parachute deployment. The U.S. Army uses shear knives designed to cut multiple-layer webbings. Small shear knives have been made from half-inch-diameter rings.

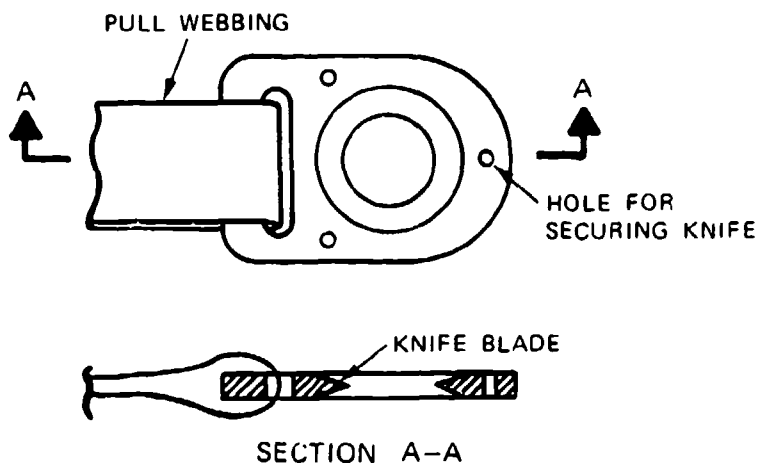


FIGURE 6-35. Typical Shear-Knife Design.

6.3.5.2 Banana-Peel Bag

The banana-peel bag, also called the longitudinal laced bag, was developed by the Sandia National Laboratories to meet a specific installation (Reference 6.33). This bag is suitable for heavy hand and mechanical pressure packing. The bag consists of a bottom part and several long flaps that form the actual bag (Figure 6-36). The flaps are tied together with strong tie

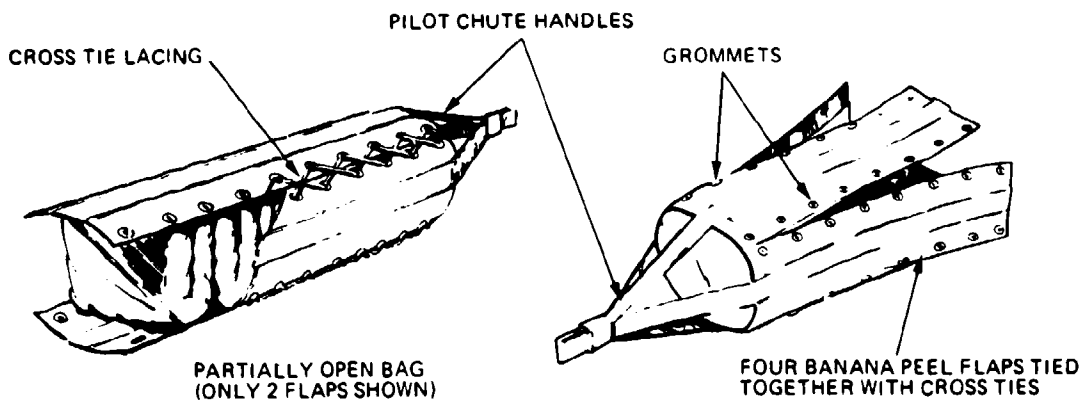


FIGURE 6-36. Banana-Peel Bag Design.

cords looped through grommets in the flaps. The parachute canopy and suspension lines are retained in the bag, with tie cords and loops on the inside of the flaps. At deployment, shear knives cut the flap tie cords and the bag unravels from the top.

Many variations of the bag shown are possible. However, all bag designs try to control the deployment of the parachute assembly in the sequence of riser, suspension lines, and canopy. All designs also try to keep the mouth of the canopy closed until suspension lines and canopy are fully stretched.

6.3.5.3 Deployment Sleeve

The deployment sleeve is a long cylindrical container that fits loosely over the parachute canopy (see Figure 6-37). Frequently the sleeve ends in a flap that folds over the lower part of the sleeve and is closed with suspension-line stow loops as shown in Figure 6-34, Detail (b). The suspension lines are stowed on the outside of the sleeve in a similar arrangement to that of Detail (d) in Figure 6-34. The deployment sleeve is extensively used by sport parachutists and

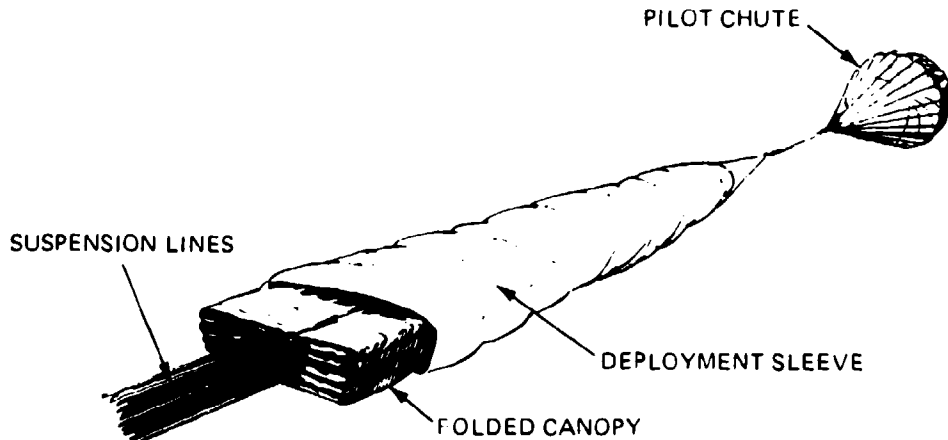


FIGURE 6-37. Typical Deployment Sleeve.

for parachutes that must be stowed in odd containers; for example, an aircraft spin recovery parachute that is stowed in a flat deployment container near the vertical stabilizer of a fighter aircraft. A closed sleeve is not suitable for deployment in excess of 200 knots because of the danger of friction burns.

6.3.5.4 Sacrifice Panel

The design of the sacrifice panel or wrap-around sleeve is shown in Figure 6-38. The sacrifice panel consists of an open sleeve attached to one of the canopy radials. The panel is wrapped around the folded canopy and tied together with light thread or a daisy-chain arrangement. Upon deployment, the panel closure is broken or opened, allowing the canopy to inflate. This design avoids friction burn between canopy and sleeve at high speed and retains the sleeve with the canopy.

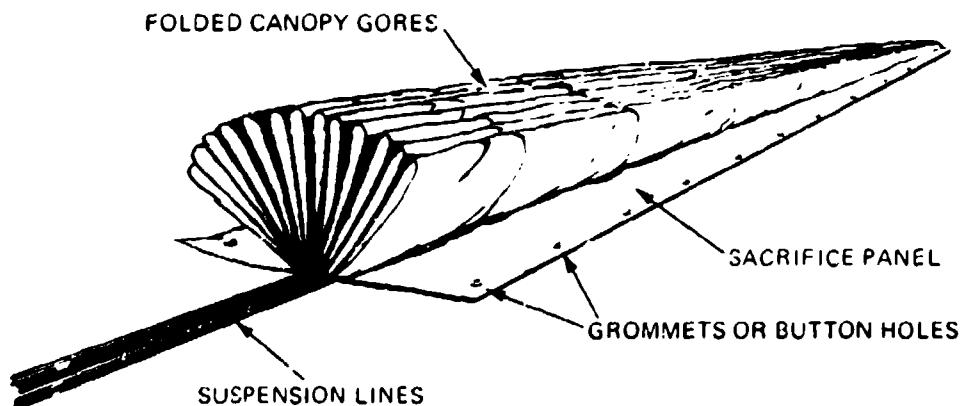


FIGURE 6-38. Sacrifice-Panel Design.

6.3.5.5 Skirt Hesitator and Quarter Deployment Bag

When a full deployment bag is not used, the skirt hesitator serves as a means for keeping the mouth of the canopy closed until suspension-line and canopy stretch occurs, thus preventing premature canopy inflation and a high mass shock. The skirt hesitator shown in Figure 6-39 incorporates two loops that fold around the canopy skirt and are tied together with a break cord that also encloses the bundled suspension lines. Stretching the canopy with a

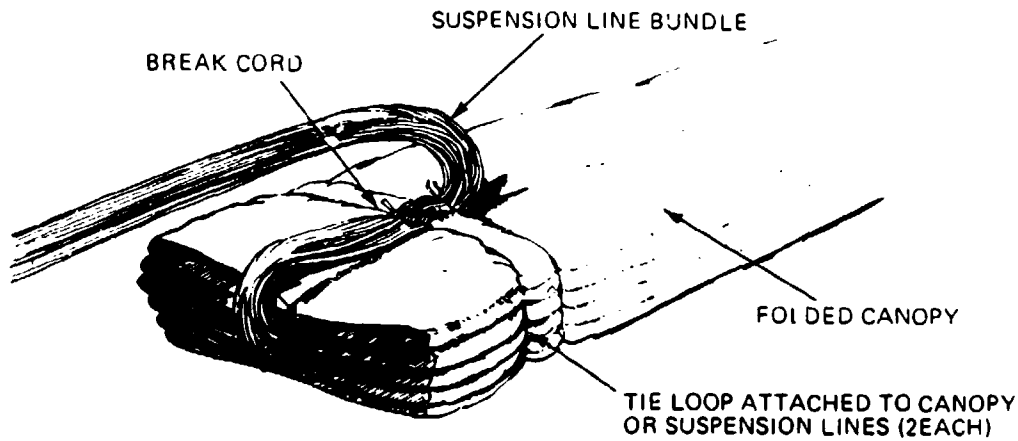


FIGURE 6-39. Skirt Hesitator.

pilot chute severs the break cord and allows the canopy to inflate. This concept prevents high snatch forces and makes canopy inflation more uniform.

A well-known modification of the skirt hesitator is the quarter deployment bag used on several types of personnel parachutes. The quarter bag is a short bag that encloses the skirt of the parachute canopy and stows the suspension lines in stow loops located under 45 degrees on the outside of the quarter bag, as shown in Figure 6-40. This design keeps the mouth of the canopy closed until canopy and line stretch occurs and ensures an orderly, low-snatch-force deployment.

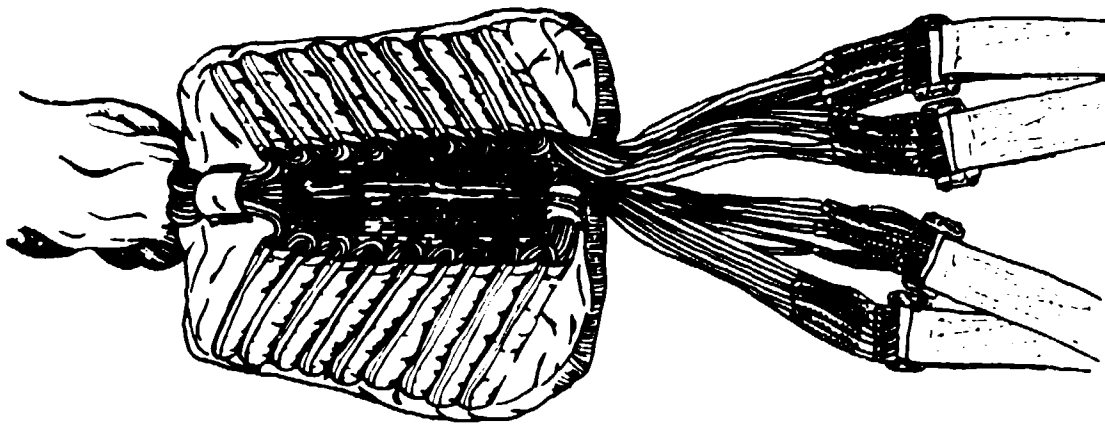


FIGURE 6-40. Deployment Bag Showing Suspension Lines in Stow Loops.

6.3.5.6 General Comments on Deployment

Friction burns from bags or sleeves during parachute deployment are a constant concern in the design of deployment methods. Bags, therefore, are frequently lined with low-friction material such as cotton or Teflon. This liner may be a fixed liner or a pull-out, turnaround sleeve. All protruding corners, such as the upper ends of the fold-out flaps, must be protected and smoothed to prevent canopy damage.

The design of the deployment bag must ensure that the extraction force of the pilot chute is properly guided around the bag and into the closure loops to prevent the bag from being ruptured by the extraction force.

6.4 PARACHUTE STRESS ANALYSIS

6.4.1 Stress Analysis of Parachute Textile Components

Methods established for aeronautical equipment are used to analyze the loads and stresses in the various components of a parachute assembly. However, because textiles are the primary materials used in parachutes, their special material and environmental characteristics must be known and considered in establishing design factors and in dimensioning the various elements of the parachute assembly. Textiles used include cloth and ribbons for the parachute canopy; webbings, lines, and tapes for suspension lines and canopy reinforcements; and various materials for deployment bags and related components. The strength of the woven material differs from the strength of the basic fiber because of the routing of the individual fibers in the manufacturing process of the material, and because of chemical treatment during weaving and finishing.

Textiles, as a rule, are connected by sewing and stitching, which introduces connection losses based on the type of connection used. Natural fibers, and, to a somewhat lesser degree, man-made fibers are affected much more than are metals by such environmental factors as temperature, humidity, radiation (light), chemicals, aging; and such mechanical factors as abrasion, handling, and packing.

It is very difficult to determine the load and stress distribution for a variable-geometry, variable-velocity inflating canopy. Many efforts in the 1950s and early 1960s did not provide a practical solution for stressing parachute canopies. During the Apollo program, Mullins and Reynolds developed a computerized system for calculating the stresses in horizontally slotted canopies in general, and for ribbon parachutes in particular (Reference 6.34). This method, called the CANO method, has been modified and improved by the University of Minnesota and the Sandia National Laboratories. A summary of efforts in this area and an analysis of the CANO program is presented with an extensive bibliography in Reference 6.35 and in

abbreviated form in Reference 6.36. The Sandia National Laboratories has recently published a modified and improved version of the CANO program called Canopy Load Analysis (CALA), a computer approach that gives good results for all slotted canopies and acceptable results for solid cloth canopies (Reference 6.37).

Prior to the CANO program, two methods were developed that give good approximations for determining the strength of cloth for solid material canopies and for the required strength of horizontal ribbons in ribbon parachutes. These two methods are described in sections 6.4.3 and 6.4.4. Both methods derive from the established procedure for calculating the hub stress in pressure vessels. These methods may still serve for a preliminary quick check.

6.4.2 Load and Design Factors

The determination of load and design factors follows established procedures in the aerospace industry. The recommended factors are shown in Table 6-7, but they may be changed by agreement between the prime contractor and subcontractor for specific operational or environmental requirements.

In agreement with common practice, a general safety factor of 1.5 is recommended for all nonmanrated parachute recovery systems. Primary manrated systems, those where the parachute assembly is part of the operational system and not a backup system, should use a slightly higher safety factor of 1.6. These systems include manned spacecraft parachute landing systems and parachutes for paratroopers, smoke jumpers, and sport parachutists. The same safety factor is recommended for ordnance devices where a failure of the parachute assembly could result in loss of the aircraft and the aircraft crew.

Parachutes for aircraft emergency escape are backup systems to the primary mode of landing the aircraft on its wheels. A safety factor of 1.5 should be satisfactory.

Dynamic Load Factor. The dynamic load factor was established at the request of the Stress Analysis Branch of the Aeronautical Systems Division at Wright Patterson AFB and used by NASA on the Apollo program. The dynamic load factor is used only for hard-to-determine loads, such as those encountered in the long bridle lines of the pilot chutes used to extract the Apollo main parachutes (Reference 6.38).

Line Convergence Factor. The forces in the parachute canopy are assumed to act parallel to the line of flight or to the canopy main axis. The suspension lines run at an angle to this axis, thereby experiencing a slightly higher load. For a suspension-line-to-nominal-parachute-diameter ratio, L_p/D_o , of 1.0, this factor is 1.05, but changes slightly with longer or shorter lines or inflated-canopy diameter.

TABLE 6-7. Recommended Design Factors for Parachute Assemblies.

Item	Safety factor, SF	Dynamic load, m	Line conversion, $\cos \phi$	Unsymmetrical load, s	Load factors			Loss factors			Ultimate design factor, DF
					Ultimate load factor	Joint loss, u	Abrasion loss, c	Fatigue, k	Water, oil, o	Total loss factor	
Emergency escape bailout, premied. seat, capsule	1.5	1.0	1.05	1.1	1.73	.6	.95	.95	.69	2.50	1.9
	1.5	1.0	1.05	1.0	1.575	.8	1.0	1.0	1.0	0.8	
Vehicle recovery UVs, drone manned, primary	1.5	1.0	1.05	1.0	1.575	.8	.97	.95	1.0	0.74	2.12
	1.6	1.0	1.05	1.0	1.68	.8	1.0	1.0	.95	0.76	
Airdrop paratrooper cargo	1.6	1.0	1.05	1.1	2.02	.8	.95	.95	.95	0.69	2.93
	1.5	1.0	1.05	1.0	1.575	.8	.95	.9	.95	0.65	
Aircraft deceleration	1.5	1.1	1.05	1.0	1.73	.8	.90	.9	.9	0.58	2.98
Ordnance	1.5	1.0	1.05	1.0	1.575	.8	1.0	1.0	1.0	0.8	1.97
torpedo, mines	1.6	1.0	1.05	1.0	1.84	.8	1.0	1.0	1.0	0.8	2.3
bombs, weapons											

Unsymmetrical Suspension-Line Load Distribution. A general assumption is that on circular parachutes, the parachute force is evenly distributed among the suspension lines. Although this assumption may not be correct, past experience has shown it to be acceptable for both reefed and full open canopies. If force measurements on suspension lines or uneven canopy deployment suggest an uneven load distribution, an appropriate factor should be used.

Ultimate Load Factor. The ultimate load factor is the sum of the individual load factors. Mechanical, environmental, and material conditions can cause strength losses that are not contained in the loss factors.

Joint Loss. Whenever textiles are connected to each other or to metals, a loss in joint strength occurs relative to the basic material strength. This loss is best determined by strength tests of the particular connections or established in relation to previously conducted tests. If no tests can be conducted, a loss factor of 0.8 should be used for all connections of nylon tapes, lines, and suspension lines to other elements of the parachute. A similar loss factor appears to be acceptable for the connection of Kevlar lines, tapes, and webbings, but not for Kevlar fabric. The efficiency of Kevlar fabric seams is lower than that of equivalent nylon seams. Section 6.6.5 discusses designing with Kevlar.

Abrasion Loss. One-time-use parachutes suffer little or no abrasion. However, aircraft landing deceleration parachutes that are used up to 50 times and are occasionally dragged on the ground suffer mechanical abrasion to various degrees.

Fatigue. Fatigue includes strength loss caused by multiple use, high-pressure packing, or a combination of both. Tests conducted during the Apollo program where nylon lines were loaded in short time intervals to 75% of their ultimate strength resulted in a strength reduction combined with a hysteresis-type loss in elongation.

Water, Oil, Sunlight, Vacuum, and Other Environmental Effects. Parachutes that are subjected to multiple use or exposed to sunlight, water, vacuum, and other environmental conditions will suffer a loss in strength. The loss differs for natural and man-made fibers and must be determined based on the operational environment and the materials used. Duplicating the translunar and re-entry environment on the Apollo parachute system did not produce a measurable material degradation from vacuum and radiation exposure. Effects of man-made radiation must be considered where appropriate.

Temperature. All natural and man-made fibers lose strength and melt, burn, or decompose when subjected to high temperatures. Dacron and Nomex are slightly superior and Kevlar is far superior to nylon in temperature resistance. Nylon parachutes in compartments close to engines or in nose cones that experience aerodynamic heating will lose 5 to 7% strength at the generally accepted 200°F compartment temperature. Section 6.6.1 provides information on the effects of environmental conditions on parachute textiles. The unstable Apollo

command module required steel-cable risers because of the possibility of contact between the red-hot heat shield and the drogue or main parachute risers.

Ultimate Design Factor. Combining the load, loss, and safety factors produces the ultimate design factor for the various parachute assembly components. A typical design-factor analysis is given in section 7.3. Most parachute textiles have an additional built-in safety factor. Textile specifications define a minimum strength. Manufacturers, to avoid rejections, generally weave the material 5 to 10% stronger than the specification strength, thus providing an additional margin of safety.

General Comments. Parachutes used in ejection seats and crew modules are permanently packed in well-protected containers and repacked only during major aircraft overhauls. Personnel emergency parachutes worn by aircraft crews are subjected to a certain amount of wear in the process of multiple repacking; the personnel parachutes are carried around and sometimes abused despite regulations to the contrary and therefore have a different design factor.

Aircraft landing deceleration parachutes are designed for high-speed emergency landings without the use of flaps or brakes. In normal use these parachutes are deployed at a dynamic pressure of about 55% of the design level, a considerably less severe operational environment.

6.4.3 Preliminary Stress-Analysis Method for Solid Material Canopies

The CANO and CALA computer programs are the final methods for determining loads and stresses in parachute canopies. However, two methods for approximate dimensioning of canopy fabric and horizontal ribbon strength, used successfully in the past, can be used for quick preliminary analysis.

In the first method, a comparative analysis can be made from the well-defined stress in a cylindrical vessel. The hub stress, t_c , in a cylinder is determined by

$$t_c = \frac{pr}{2} \text{ lb/unit width}$$

where p is the pressure in the vessel in lb/in^2 and r is the radius of the cylinder. The hub stress increases linearly with increased pressure, and decreases linearly with reduced radius.

Each gore of an inflating canopy may be considered part of a pressure vessel with variable radius, where the stress in the canopy increases linearly with the dynamic pressure or the related maximum parachute force, F_x , and decreases linearly with the radius or the related canopy diameter.

Using this approach, E. Ewing proposed the following formula for the stress-per-unit width for the fabric in a solid material canopy.

$$t_c = \frac{F_x}{D_p 12} DS \text{ (lb/in.)}$$

where

t_c = required material strength, lb/inch width

F_x = maximum parachute opening force, reefed or unreefed, lb

DS = ultimate design factor (see Table 6-7)

D_p = projected (inflated) canopy diameter, feet

The projected canopy diameter can be determined from Tables 5-1 to 5-4, which give the ratio D_p/D_o for the most common parachute types.

The inflated diameter of a reefed parachute, D_{pr} , can be calculated from the known reefed drag area, $(C_D S)_{pr}$. Assuming a 0.6 drag coefficient, C_{D_r} , for the reefed parachute for slotted canopies and an 0.8 drag coefficient for solid fabric canopies, the equivalent reefed canopy area is

$$S_{or} = \frac{(C_D S)_{pr}}{C_{D_r}}$$

and the equivalent reefed nominal diameter is

$$D_{or} = 1.1284, S_{or}, \text{ and } D_{pr} = D_o C \text{ with } C = 0.67$$

where a C_D of 0.65 is recommended. The value for the inflated full open canopy diameter is a good approximation. The projected diameter of the reefed canopy is less accurate. Therefore, a conservative approach should be used in the canopy material selection for the reefed parachute area.

6.4.4 Stressing of Horizontal Ribbons in Ribbon Parachutes

The second method is a somewhat similar analysis developed by the author for stressing the horizontal ribbons in ribbon parachutes. Using the determination of hub stresses in cylindrical pressure vessels as an analogy, a pressure definition

$$\frac{F_x}{(C_D S)_p}$$

is formed, with F_x again the maximum parachute force and $(C_D S)_p$ the parachute drag area. The radius relation is again expressed as gore width at the skirt of the canopy. Based on evaluation of numerous operational parachutes, curves have been plotted for the required ribbon strength (Figure 6-41).

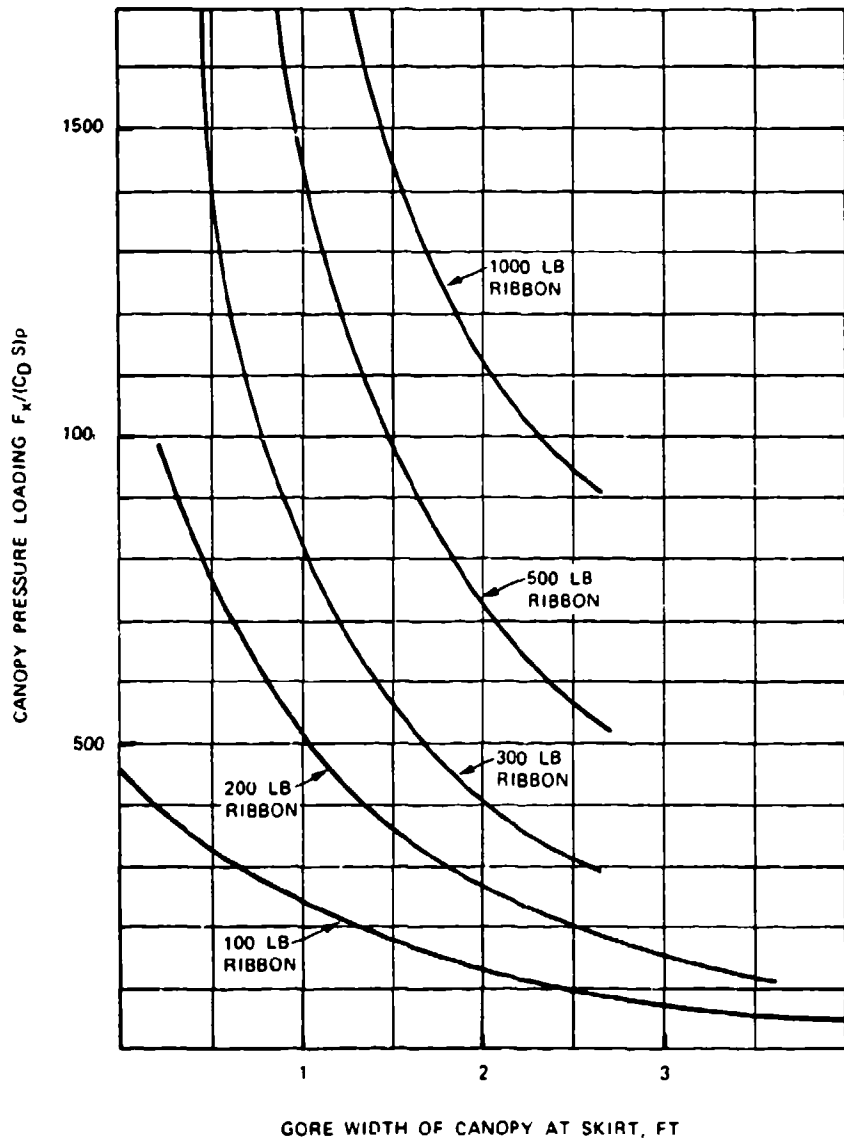


FIGURE 6-41. Boundary Curves for Horizontal Ribbon Strength.

Stress in reefed parachute canopies is calculated in the same manner as that in solid fabric canopies. The approach has provided good preliminary results for many ribbon parachutes. As previously stated, the availability of the CANO and CALA computer programs relegates this method to the quick, preliminary-approach status.

6.4.5 Stress Relief in the Canopy Crown Area

The hub-stress formula shows that the stress in a cylindrical pressure vessel as well as in the gore of an inflating canopy decreases with the gore radius. The inflating canopy gore has a radius in most of its length except at the vent of the canopy. A radius at the vent can be designed into the canopy by providing surplus canopy width in the vent area (see Figure 6-22) where the gore width at the vent, e_v , is increased to the dimension e_{v+} . Gathering the vent with the vent tape to the original dimension, e_v , now provides a radius at the vent.

The author conducted a weight-optimization analysis between the increase in gore radius, the decrease in required material strength, and the weight increase caused by the wider gore (Reference 5.39). This analysis showed that a 10% increase in gore width was an acceptable solution.

Section 7.3.9 describes the process of calculating the gore dimensions, including the gore widening at the vent, for a 74-foot-diameter extended-skirt parachute.

6.4.6 Dimensioning of Suspension Lines, Risers, and Canopy Vent and Skirt Tapes

Maximum parachute forces and the design factors discussed in section 6.4.2 govern the dimensioning of suspension lines, risers, and radial tapes. Dimensioning of vent and skirt tapes is a combination of experience and calculation. Chapter 7 of this manual includes the design of a solid material parachute cluster assembly and a ribbon parachute assembly. This design includes the dimensioning of all components including discussions of fullness in the canopy fabric as well as in skirt and vent tapes and in the vent bands.

Section 6.6.4, "Designing in Textiles," should be carefully studied before the design and dimensioning of a parachute assembly and all its components is started. The Sandia National Laboratories has developed a practical method for calculating the snatch force of a deploying parachute assembly (Reference 6.39).

6.5 REEFING SYSTEM DESIGN

6.5.1 General

Parachute reefing refers to a method of controlling the stepped inflation of a parachute canopy. The aerodynamics and the system aspects of reefing are discussed in section 5.6.

This section describes the design of the various reefing systems and the components used in the reefing installation, and discusses good and poor design approaches based on past experience. The reefing installation is a critical part of a parachute assembly, because a malfunctioning reefing system frequently causes a catastrophic system failure.

The sequence of reefing in this manual is defined by the number of reefing steps. A two-step reefing installation has two reefing steps but three parachute-inflation stages, or, aerodynamically speaking, three different drag-area levels: initial reefed-canopy inflation, an intermediate step, and final full open canopy.

Skirt reefing (see Figure 5-66 in section 5.6) is the most frequently used reefing concept for circular canopies. The introduction of noncircular parachutes, such as the Rogallo parawing and the parafoil (called the square chute by sport parachutists), has introduced slider reefing (shown in Figure 5-70) and modifications of the skirt reefing methods to fit these noncircular parachutes. Several unusual reefing concepts and attempts to develop a continuous disreefing system are described in the literature but have not been used.

6.5.2 Reefing System Installation

Figure 6-42 shows a typical skirt-reefing installation as viewed from under the inflated canopy. A reefing ring is attached to each connection point between the canopy skirt and suspension line, except on two opposite points where reefing cutters are installed. A continuous reefing line runs through all rings and two cutters. The length of the reefing line is determined by the required reduction in canopy drag area (reefing ratio). A typical reefing-line calculation is shown in section 7.3.

Figure 6-42 also shows a reefing ring installed in the middle of the upper right-hand gore. Additional reefing rings have been used on wide gores of large parachutes to restrict midgore flutter of the uninflated gore during the reefed phase. This arrangement is called midgore reefing.

The reefing cutters containing time-controlled, pyrochemically actuated knives sever the reefing line. The cutters are aligned with the reefing line by two guide rings, one installed on each side of the cutter. Figure 6-43 shows a typical reefing cutter installation with the two guide rings on either side of the cutter. Cutter action is begun by pulling a ring at one side of the cutter. A cord, attached on one side to the cutter ring and on the other side to an appropriate part of the parachute assembly, starts the cutter action.

Reefing cutters must be securely fastened to the canopy structure to prevent cutter shift or breakaway. Reefing cutter accelerations of up to 1000 g have been measured during high-speed deployment of parachutes. Two and sometimes three cutters have been used to ensure reliable cutting of the reefing line or lines. The Apollo main parachutes used two reefing

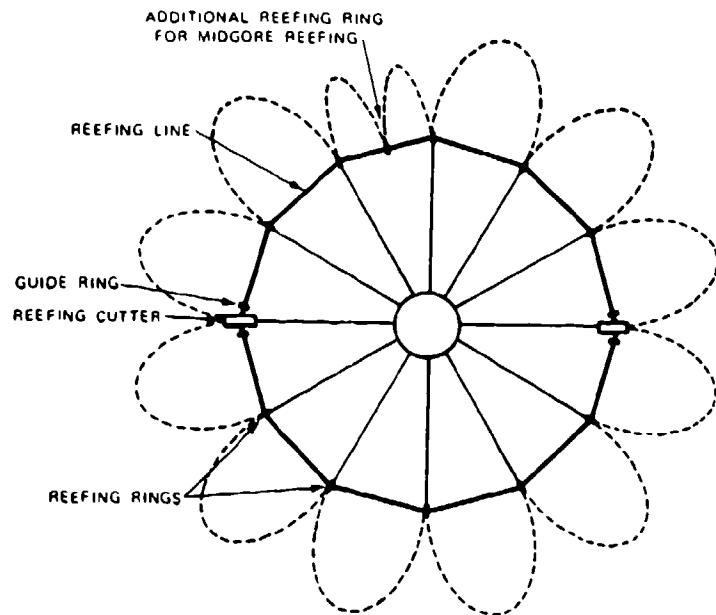


FIGURE 6-42. Typical Skirt Reefing Installation.

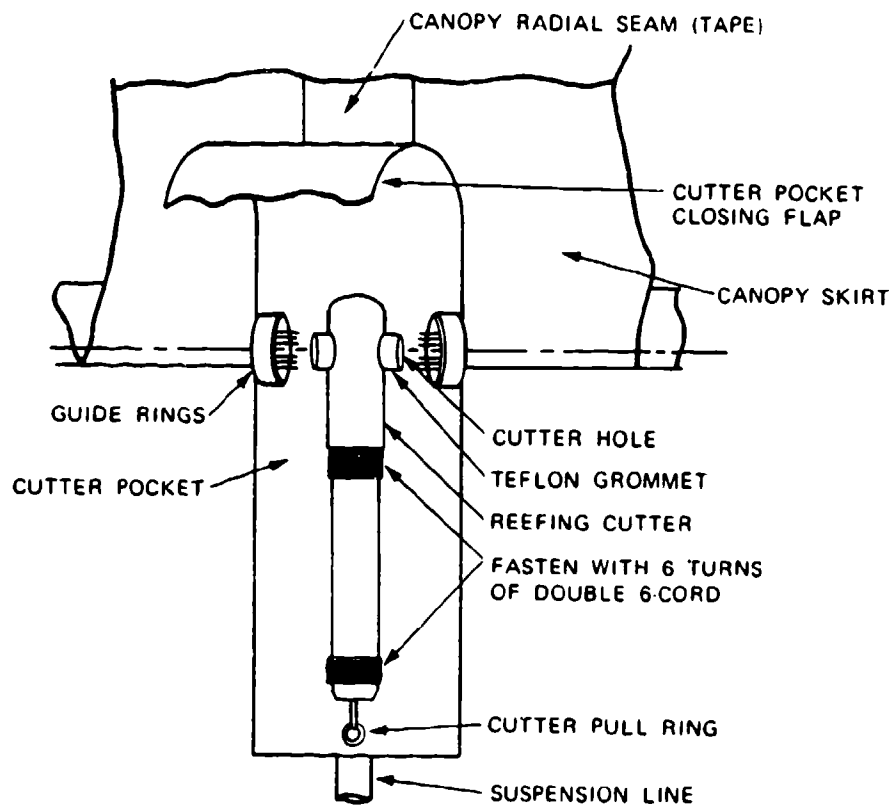


FIGURE 6-43. Reefing Cutter Installation.

lines in the first reefing stage as a safety measure against lines rupturing prematurely, or failure of one reefing cutter not to fire. This system results in a complex reefing system installation.

Three different methods of fastening the reefing-line cutters to the canopy are shown in Figure 6-44.

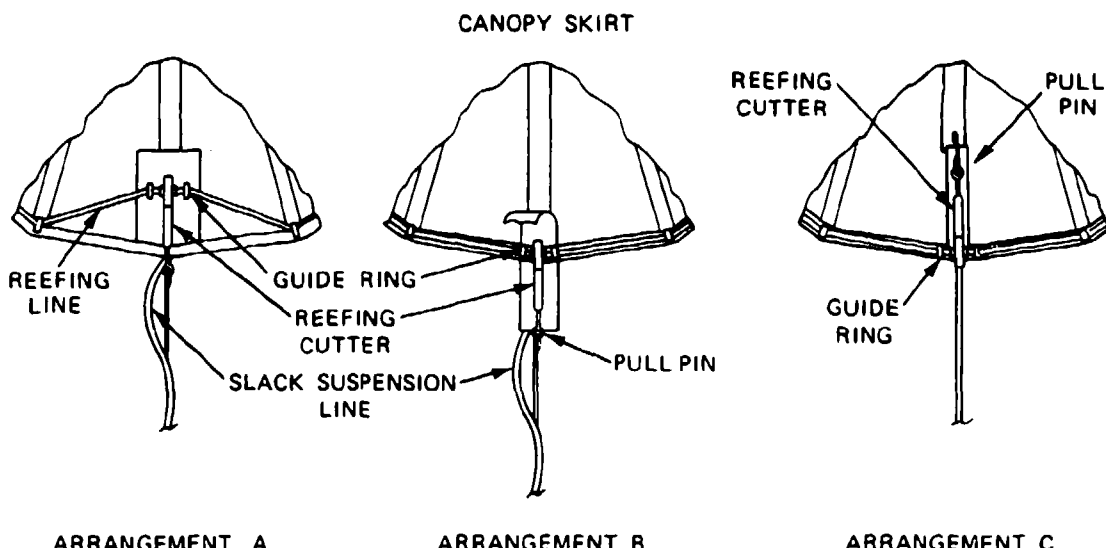


FIGURE 6-44. Three Methods of Reefing Cutter Installation.

Arrangement (A), used in the early days of reefing, requires little canopy modification, but routes the reefing line in a sharp angle from the reefing rings to the cutter hole. This arrangement can cause high longitudinal loads in the cutters, making the cutters rip out and damage or sever the reefing lines. Installation of strong guide rings on each side of the cutters will absorb the longitudinal forces and improve the installation, but this is not a completely satisfactory solution, especially when heavy cutters and heavy reefing lines are used.

Arrangement (B) is the most frequently used system. This arrangement aligns the reefing line as the line runs through the cutter and avoids radial forces and chafing of sharp edges of the cutters. However, arrangement (B) requires a modification of the canopy and necessitates care in packing the parachute since the cutter extends beyond the canopy.

Arrangement (C) reverses the cutter installation and attaches the pull cord for the cutter pin to the canopy instead of to the suspension lines. The U.S. Army successfully uses arrangement (C) for the G-11 and G-12 cargo parachutes. However, these parachutes are deployed at a relatively low velocity of 130 to 140 knots and experience low canopy-skirt accelerations. Using the same cutter installation on a 38-foot-diameter extended-skirt parachute for the encapsulated seat in the B-70 aircraft resulted in cutter malfunctions.

Deploying the parachutes using arrangement (C) at 250 knots resulted in cutter accelerations that prevented the firing pin in the cutter from properly indenting the percussion cap and initiating the cutter action. Similar results have been reported on other projects.

Many projects in the past have required multiple-step reefing. These have included the landing parachutes for the Apollo command module, the Space Shuttle solid boosters, the F-111 aircraft crew module, several Sandia projects, and especially large hi-glide parachutes for space vehicles and aircraft escape. These later parachutes need three or more reefing steps to handle the high opening forces associated with parachutes manufactured from low-porosity fabric. (References 6.40 to 6.42).

Figure 6-45 shows a typical reefing line and reefing cutter installation for a two-step reefing system. This installation introduces the problem of two lines running through the same

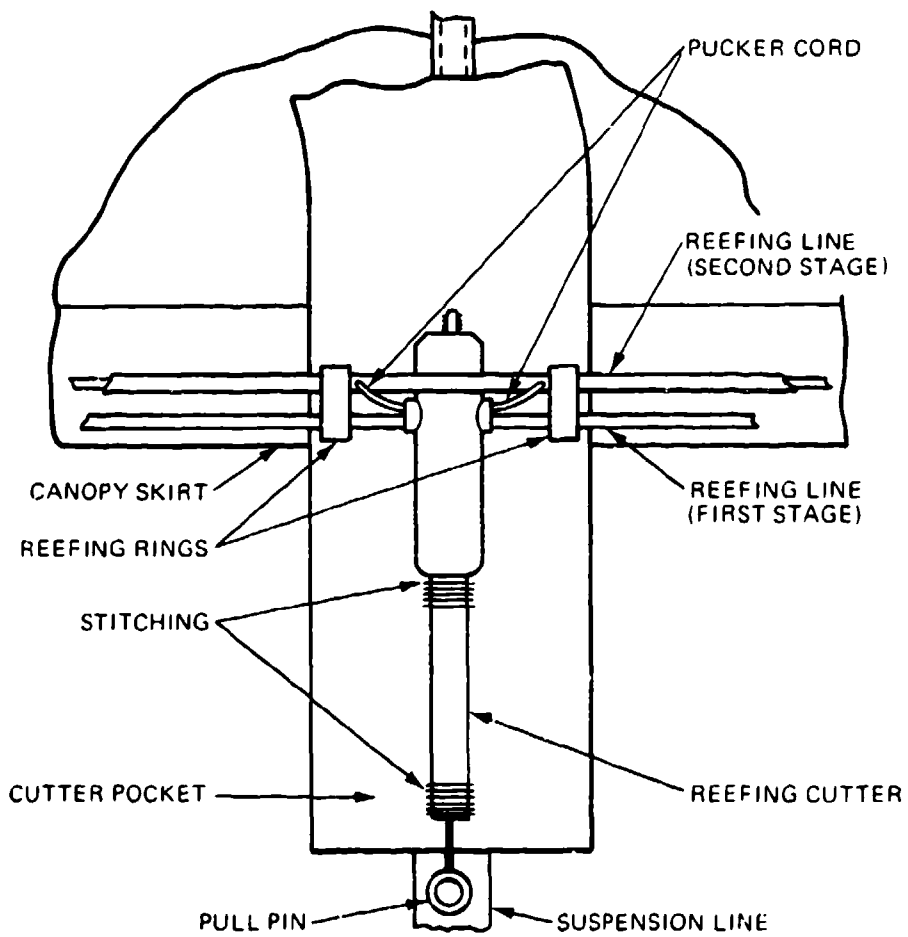


FIGURE 6-45. Cutter Installation for Two-Step Reefing.

reefing rings; entanglement can result when the second-stage reefing line is considerably longer than the first-stage line.

Two designs have been used successfully to overcome reefing line entanglement. Figure 6-45 shows a pucker cord needled through the hollow core of the second-stage reefing line. This pucker cord is the same length as the first-stage line and contracts the second-stage line to the length of the first-stage line. The pucker cord is then guided through the first-stage reefing cutters. Cutting the first-stage line also cuts the pucker cord of the second-stage line and allows the second-stage reefing line to extend fully.

Another method pulls the surplus length of the second-stage reefing line on four diagonally opposed places and stows the surplus line in small pockets from which it extracts when the first-stage reefing line is cut. Care must be exercised with this design to allow the free pull out of the stowed part of the second-stage reefing line. The reefing cutters for the second stage are usually placed under 45 degrees to the first stage cutters.

The heavy reefing lines for the two reefing stages of the drogue and main ribbon parachutes for the recovery of the solid rocket boosters for the NASA Space Shuttle cannot be guided through single reefing rings. The first-stage reefing line, therefore, is located 1 foot above the skirt of the drogue and main parachutes. This necessitates reinforcing this part of the canopy to accommodate the forces of the reefing system. On an overload test of the Space Shuttle solid rocket booster (SRB) drogue chute, the first-stage reefing assembly, including all rings, ripped away from the canopy without breaking the reefing line, causing immediate inflation into the second reefing stage and rupturing the second-stage reefing line, allowing the canopy to inflate fully. This action resulted in explosive destruction of the parachute canopy at a force in excess of 500,000 pounds; the highest parachute force ever measured in the western world. The SRB reefing system is described in References 6.40 and 6.41.

The Apollo main parachutes had a two-stage reefing system that included dual lines for the first-stage reefing, for a total of three reefing lines. This arrangement was necessary because of a NASA requirement to safeguard against not cutting and premature cutting. A probability analysis had shown that premature cutting of the first-stage line but not the second-stage line would result in a catastrophic failure of the parachute system. A dual reefing ring was developed to house the two first-stage reefing lines, Reference 6.43.

Hi-glide parachutes of the Rogallo parawing and the parafoil type have 60 to 70% higher opening forces than circular canopies manufactured from standard-porosity fabric. This requires more reefing stages to accommodate the higher opening forces.

A Rogallo parawing was investigated for an Apollo land landing system. This uncompleted program included aerial drop tests with a 4000-square-foot parawing airdropped at an altitude of 18,000 feet and a dynamic pressure of 90 lb/ft². Parachute opening forces were limited to the equivalent of 3.5 g, resulting in four reefing stages. The installation of the reefing

system with heavy reefing lines routed around different parts of the uneven skirt of the noncircular canopy, with rings and reefing cutters located at various distances from the skirt, was extremely difficult and prone to errors. Color coding was required for all parts belonging to a specific reefing stage, and multiple checking and rechecking was required to prevent reefing lines from running through and around the wrong reefing rings and cutters; this problem is usually not mentioned in final reports. References 6.44 and 6.45 describe this very successful program and its reefing system.

NWC investigated the use of a parafoil (square) parachute for aircrew escape as part of an ejection-seat system. The program, described in Reference 5.161, met the requirement of limiting the parachute opening force to 15 g when used at a 15,000-foot altitude and a speed of 300 KEAS. A three-step reefing system with a modified skirt-reefing concept was necessary to meet the requirements of this successful program.

Reference 6.46 describes how the problem of the reefing-line damage at the cutter was solved by running an independent line loop through the reefing cutter and tying the reefing line ends into this line loop. Firing the cutter cuts the line loop, which in turn releases the ends of the reefing line.

Reference 6.47 describes another reefing design developed by Sandia National Laboratories. This design uses a three-parachute cluster to replace the F-111 crew module main parachutes. All three parachutes are disreefed simultaneously from a single, centrally located reefing unit.

Variations in the pyro-time train of reefing cutters can cause different times in cluster disreefing, especially at long reefing times. This problem is discussed in more detail in section 6.5.3.

6.5.3 Reefing System Components

6.5.3.1 Reefing Rings

In the early days of reefing system applications, it was necessary to design the reefing rings with a flat profile to prevent the reefing rings from turning and squeezing the reefing line between the rings and the canopy. Figures 6-46 and 6-47 show three different designs for reefing rings. The type (a) rings in Figure 6-46 are the standard reefing rings in accordance with MIL-STD-MS 27762. The ring labeled Type (b) was developed by Northrop Ventura during the Apollo program to prevent reefing-ring deformation during heavy pressure packing, a common occurrence with type (a) rings. These type (b) rings are being manufactured from high-strength aluminum alloys.

Figure 6-47 shows a dual reefing ring also developed by Northrop during the Apollo program to accommodate the dual first-stage reefing lines of the main parachutes.

NWC TP 6575



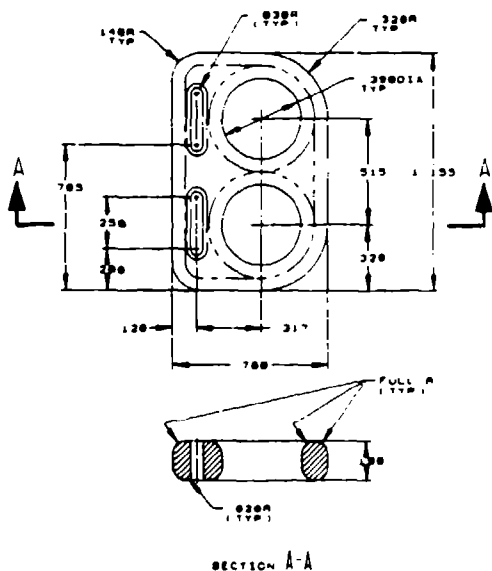
DASH NO	A	B	C	D	E	F	WT LBS	SUPERSEDES
-1	5/8	1/2	1/4	1/8	1/2	1/32	.007	4047995
-2	11/16	1/2	1/4	1/8	1/2	1/16	.011	4047995-1
-3	7/8	9/16	9/32	1/2	3/32	.023	4047995-2	
-4	7/8	1/2	1/4	1/8	1/2	1/32	.007	4047995-3
-5	5/8	1/2	1/4	1/8	1/2	1/32	.007	

DASH NO	A	B	C	SPEC	MATERIAL
-1				00-A-225/8	6061-T651
-2	300	100	25		AL ALT ROD
-3				00-S-783	3038E CRES
-4					COND B

(a) Standard Reefing Ring.
MIL-STD-MS2 7762.

(b) High-Strength Reefing Ring.
Northrop NV-STD-243.

FIGURE 6-46. Standard Circular Reefing Rings.



ITEM	RING	6061-T6 ALUMINUM ALLOY 101M BHT 1 00 3 1 20	00-A-250/11			
1	1	6061-T6 ALUMINUM ALLOY 101M BHT 1 00 3 1 20	00-A-250/11			
ITEM	CODE	PART OR IDENTIFYING NO. OR DESCRIPTION	REFERENCE OR DESCRIPTION	SPECIFICATION OR NOTE	MATERIAL	ITEM
2	2					40

FIGURE 6-47. Dual Reefing Ring (Northrop Ventura Dwg. DR 8127).

Special heavy-duty reefing lines have been developed by the Sandia National Laboratories.

6.5.3.2 Reefing Line Cutters

The reefing cutters that sever the textile reefing lines contain the following components: a reefing cutter body, a mechanical or electrical actuator, a pyro-initiator, a pyrochemical time train, a booster charge, a shear knife, and an anvil. Reference 6.48 gives a good description of the design and operation of reefing cutters.

The three primary groups of cutters used are shown in Figures 6-48 through 6-50.

The cutter in Figure 6-48 belongs to a series of commercially available cutters that are used for many applications, especially in lightweight main descent parachutes. These mechanically actuated cutters use a firing-pin spring that is unloaded before use and cocked by the extraction of the pull pin from the cutter body. The cutter pull pin line is attached to an appropriate part of the parachute assembly (see Figure 6-44). It is important that the hole in the reefing cutter is properly aligned with the reefing line, and that the cutter hole is smooth and well rounded to prevent damage to the reefing line. The reefing cutter must be properly

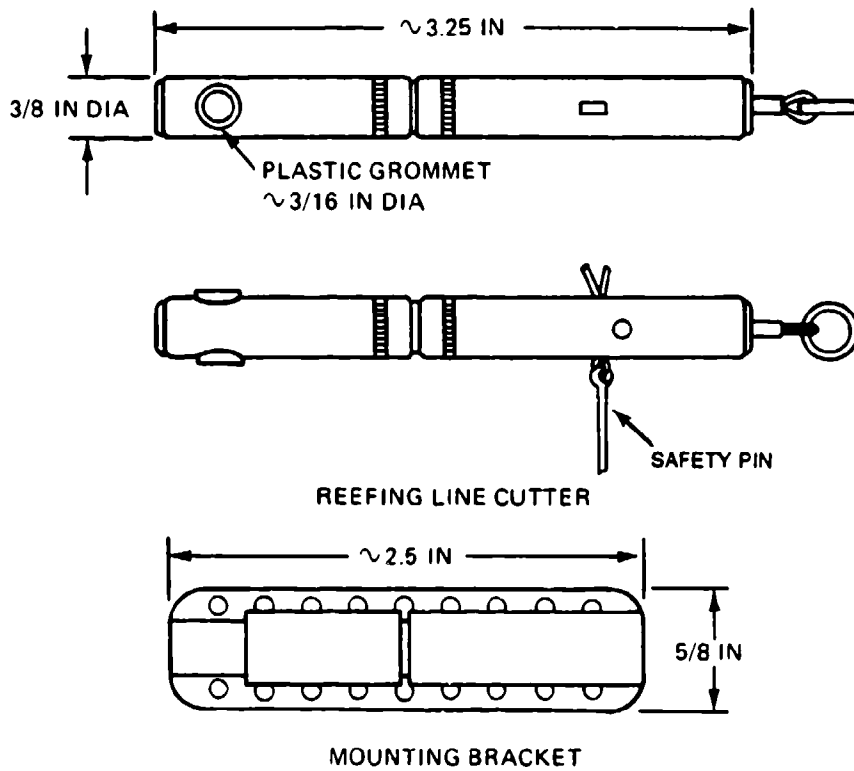


FIGURE 6-48. Typical Commercially Available Reefing-Line Cutter.



FIGURE 6-49. U.S. Army M21
Reefing Cutter.

secured to the canopy skirt to handle the high accelerations encountered during canopy deployment.

The cutter shown in Figure 6-49, called the M21 cutter, is the standard U.S. Army cutter used in the 1000-foot-diameter G-11 and the 64-foot-diameter G-12 cargo parachutes (see specification MIL-C-46992). Figure 6-49 shows that the U.S. Army cutter is installed in what may be called an upside-down position. The acceleration that these cutters experience at the low deployment velocity does not interfere with proper cutter action.

The Figure 6-50 reefing cutter is a heavy-duty cutter developed by the Sandia National Laboratories. This cutter is actuated by an electrical signal from the primary body. The development of this MC 3133 reefing cutter is described in References 6.49 and 6.50. The electrical signal is much more accurate than the pyrochemical time train. In addition, the temperature sensitivity of the time train is eliminated.

The reefing cutters specifically developed for the Apollo parachutes were highly reliable and of exceptional quality; however, nothing could be done to decrease the temperature sensitivity of the time train. Table 6-8 lists the time variation of the 10-second Apollo reefing cutter as a function of temperature. These data are taken from Northrop Ventura test memo 2211/67-74, dated 8 November 1967.

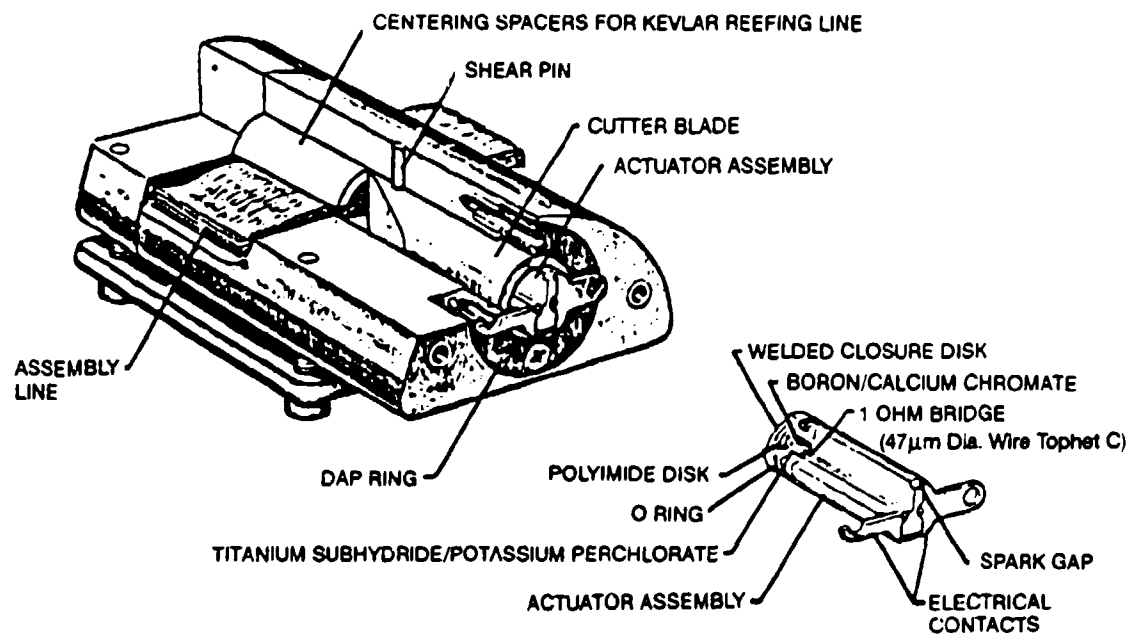


FIGURE 6-50. Sandia MC 3133 Reefing-Line-Cutter Installation.

TABLE 6-8. Variation of Reefing Cutter Time as a Function of Temperature for a 10-Second Apollo Reefing Cutter.

	+ 165°	+ 130°	+ 65°	- 10°	- 65°
Time delay	8.88 8.22 8.66 8.66 8.54 8.66 8.54 8.42	9.30 9.50 9.42 9.52 9.40 9.66 9.40 9.28	10.34 10.44 10.42 10.55 10.50 10.48 10.16 10.19	11.66 11.44 11.58 11.66 11.30 11.10 11.57 11.68	12.22 12.30 12.48 12.21 12.00 12.84 12.36 12.12
Mean	8.57	9.44	10.38	11.50	12.19
Standard deviation	0.195	0.124	0.144	0.206	0.203
3σ limits					
Upper	9.16	9.81	10.81	12.12	12.80
Lower	7.98	9.07	9.95	10.88	11.58

An analysis of test data on the Apollo reefing cutter indicated the possibility of a 1.1-second time difference in the 10-second second-stage cutters for the three Apollo main parachutes. To obtain uniform cutter firing, an investigation was conducted on firing the reefing cutters with an RF signal from the command module. This approach is described in Reference 6.51.

Firing the cutters by RF signal opened another possibility. The weight of the command module during the development cycle increased by 60% with no allowable increase in total parachute force taken by the command-module hard points. Electronic disreefing makes it possible to stagger disreefing of the three main parachutes, increasing the opening force of the first parachute to disreef, but decreasing the combined parachute force to be taken by the command-module hard points.

6.5.4 Special Reefing Concepts

6.5.4.1 Continuous Disreefing

As discussed in section 5.6.6, continuous disreefing is a method where the inflation of the canopy is controlled so as to produce a more-or-less constant or controlled parachute opening force. Many proposals have been made and prototypes have been tested. However, no practical solution has evolved so far.

6.5.4.2 Fixed Reefing by Pocket Bands

The aerodynamic effects of decreasing the inflated diameter of a slotted canopy by using pocket bands are explained in section 5.6.9. Decreasing the inflated diameter should increase stability, especially in the wake of a large forebody.

The mechanics of this process are explained by the example cited in section 5.6.9 (Figure 6-51). The effective porosity of a 6.8-foot-diameter parachute was increased from 26 to 33% by reefing the 6.8-foot-canopy diameter to the equivalent of a 6-foot-diameter canopy. Using the terminology from Figure 6-51, the skirt circumference of the 6.8-foot-diameter 16-gore canopy obtained by $16(2 e_x + L_a)$ is reduced to the skirt circumference of a 6-foot-diameter canopy, or $16(2 e_{x_1} + L_{a_1})$. The free length of the pocket band, L_a , is calculated for the 6-foot canopy and fastened to the 6.8-foot canopy at the distance, e_x . This arrangement greatly increases the length, L_{b_1} , thereby restricting the skirt circumference, $16(2 e_{x_1} + L_{a_1})$, to that of the 6-foot-diameter canopy and increasing the ratio of air leaving the canopy by the slots to the air going into the canopy at the skirt. Table 6-9 gives actual data for the fixed reef 6.8/6-foot canopy.

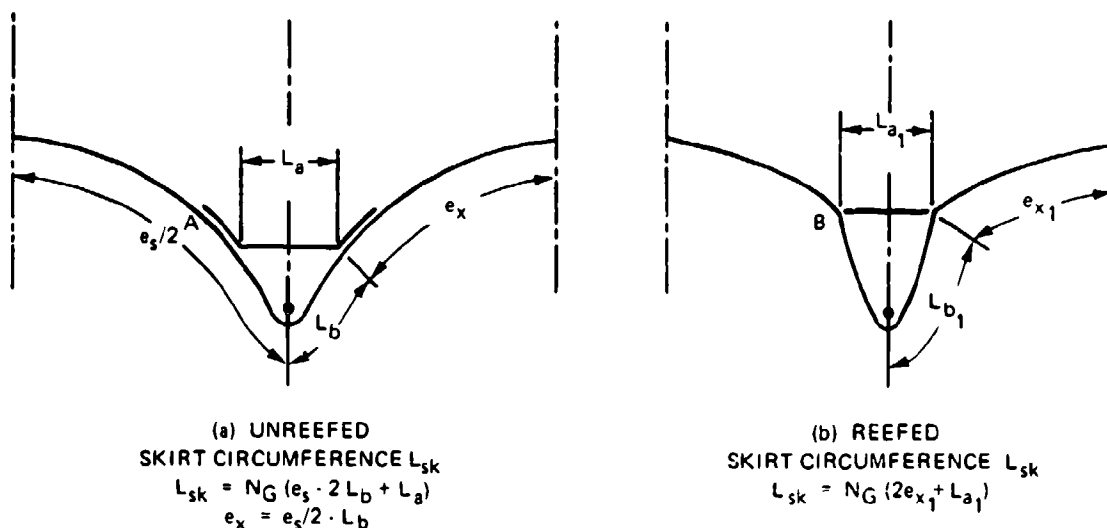


FIGURE 6-51. Diagram of Fixed Reefing by Pocket Bands.

TABLE 6-9. Dimensions for the Fixed Reefing of the 6.8-Foot-Diameter Conical Ribbon Parachute. (For nomenclature see Figures 6-51, 6-29, 6-30, and section 3.4.)

Unreefed						Reefed		
D_o , feet	μ , degrees	e_s , inches	L_a , inches	L_b , inches	e_x , inches	L_{a_1} , inches	L_{b_1} , inches	e_{x_1} , inches
6.8	30	14.99	1.8	2.1	5.4	1.59	3.33	4.17
6.0	30	13.23	1.59	1.85	4.17

6.5.4.3 Overinflation-Control Line (OC Line)

The OC line prevents overinflation of the parachute canopy by placing a line around the canopy skirt. The line permits the canopy to inflate fully, but restricts further inflation. The line can be a reefing line run through rings in a process similar to skirt reefing. A simpler approach is to fasten the line to the confluence point of suspension lines and radials at the skirt of the canopy. The effects of the OC line on limiting the parachute opening force are discussed in section 5.6.9.

6.6 DESIGNING AND FABRICATING IN TEXTILES

The laws of mechanics and aerodynamics apply to the performance and stress analysis of parachute recovery systems. However, the textile fabrics used in parachute construction have distinctly different mechanical and environmental characteristics than metals or composites. It is not the purpose of this manual to provide a detailed analysis of the complex area of textiles and fabrics, but rather to provide the parachute designer with a cursory survey of the textiles used in the design and manufacture of parachute assemblies. This section discusses the various processes of producing the fabrics and the mechanical and environmental properties of the fabrics. It also provides a list of the most frequently used Federal and military specifications, and presents feedback information on how to design parachutes that can be economically manufactured without problems in the manufacturing process.

The following references provide further information on textiles, designing in textiles, and the equipment and processes used in parachute manufacturing. References 2.17 and 2.18, two of the University of Minnesota short courses on parachute technology, contain extensive lectures on parachute textiles, including textile properties and the spinning, weaving, and braiding process of manufacturing fabrics. Reference 2.21, the Roxboro Seminars on Parachute Manufacturing, discusses the entire field of textiles; new materials; parachute hardware; manufacturing machinery; Government inspection, quality control, and configuration management; the role of computers in the manufacturing process; and related subjects. However, no papers are available on the sequential process of manufacturing a parachute, because parachute companies consider this proprietary information. The DuPont and Cellane companies have extensive literature on materials and fabric used in the manufacture of parachutes (Reference 6.52).

6.6.1 Textile Materials

The two primary groups of textiles are those of natural fibers and those of man-made fibers. Fiber is a generic name that refers to all materials used in the manufacture of textiles. Natural fibers include wool, cotton, silk, hemp, flax (linen), and many others. Only silk and cotton are of interest to parachute designers.

Man-made fibers are classified by their origins. Mineral fibers, the only nonorganic fibers, include glass fiber and metal thread used in woven metals such as metal shielding for electrical wiring. All other man-made fibers are based on cellulose, protein, or resin composites. The cellulose group includes rayon; the protein and resin groups include nylon, dacron, Kevlar, and others. Cellulose, protein, and resin are referred to as organic fibers.

6.6.1.1 Natural Fibers

Silk: Silk is produced by the silkworm, which spins a cylindrical cocoon from a thread less than 1/1000 of an inch in diameter, 800 to 1500 meters long, and triangular in cross section. Because the thread is so small in diameter, five to ten cocoons are unwound simultaneously and their threads spun together using the natural glue of the thread. The thread is then spun into yarn and woven into cloth. Silk is the strongest of all natural fibers, resists heat, and burns only as long as a flame is applied to it. The silk fiber is referred to as a long staple fiber, unlike cotton and wool, which are short staple fibers. Table 6-10 shows the characteristics of different materials.

Cotton: Cotton is a natural fiber 0.5 to 2.5 inches long depending on type and country of origin. The cotton fiber is irregular in shape and has a natural twist that makes it extremely suitable for fine yarns and for the fabrication of a large variety of textile fabrics. Cotton is abrasion resistant and is used in parachute assemblies for deployment bags, buffers, and friction-preventing items. All natural fibers can absorb a considerable amount of water without losing strength, but unless treated, they are affected by fungus, bacteria, and insects. Cotton burns without melting and loses 50% of its strength at a temperature of about 350°F.

6.6.1.2 Man-Made Fibers

Rayon: Rayon, the oldest man-made fiber, has a cellulose base that makes it economical to manufacture. Rayon has about half the strength of silk or cotton, loses 40% of its strength when wet, burns easily without melting, and decomposes at about 450°F. Rayon was used during World War II for cargo parachutes but is seldom used today for parachute assemblies.

Nylon: Nylon, developed shortly before World War II by DuPont for use in clothing, has become the primary fiber for parachute fabrics. Nylon is a synthetic resin (polyamide) with high tenacity caused by long, highly oriented molecules and high intermolecular forces that resist slippage. Nylon tenacity ranges from 2.5 to 9.5 grams per denier; its elongation ranges from 29 to 40%. Nylon type 6.6, used for parachute fabrics, is rated at 6.6 grams per/denier, approximately equivalent to a tenacity of 115,000 lb/inch², which compares favorably to other

TABLE 6-10. Characteristics of Various Materials.

Characteristic	Dimensions	Silk	Cotton	Rayon	Nylon	Dacron	Numex	Kevlar 29	Glass fiber "E"	Graphite	Stainless steel
Staple length	Inch lb/in ²	400-1300 yds	½-2½	Continuous	118,000	120,000	90,000	Continuous	370,000	350,000	285,000
Tensile strength	Gr/Denier	—	—	1.5-5.0	6.9	6.9	5	20-22	7.7	14.0	—
Tenacity	Gr./Cm ³	3.8-5.2	2.1-6.3	1.5-5.0	1.14	1.38	1.38	1.44	2.54	1.61	7.8
Specification weight	Gr./Cm ³	1.34	1.52	1.5	—	—	—	3	—	—	1.1
Ultimate elongation	%	13-31	3-7	15-25	25-40	12-20	16	3-5	—	—	—
Zero strength (melting point)	°F	302(D)	450(D)	350-450	490	485	800	850	1350	5000	2200
50% strength retention	°F	280	300	—	330	350	500	550	685	—	1800
Minimum yarn size	Denier	11/13	15	20	20	20	200	50	—	—	—
Filament diameter	Inch	0.0005	<0.001	0.0005	0.001	0.001	—	0.0005	0.0005	—	0.0005
Wet strength	%	75-95	110-130	45-55	85-90	95	65	100	95-100	—	—
Resistance to		P	G	P	P	G	G	D	E	—	E
Ultraviolet rays		G	G	E	E	E	G	E	E	—	—
Storage, aging		P	P	G	G	G	G	E	E	—	—
Fungus, bacteria		P	Burns	Burns	G	E	G	E	E	—	—
Flame		P									—

NOTE: P = poor, G = good, E = excellent
(D) decomposes

materials used in the aerospace industry. Figure 6-52 shows tenacity in grams per denier for a variety of industrial yarns. Nylon is abrasion resistant, durable, and little affected by humidity, fungus, bacteria, organic solvents, and alkalies. Nylon is sensitive to ultraviolet radiation (sunlight); this sensitivity can be reduced but not eliminated by appropriate treatment of the fabric. Nylon melts when subjected to fire but does not burn. This fabric can be used, with little loss in strength, at temperatures of up to 250°F (Table 6-10 and Figure 6-53). Nylon loses 50% of its strength at about 330°F, becomes sticky at higher temperatures, and melts at 480°F. If subjected to repeated stresses, nylon exhibits a certain hysteresis in its strain characteristics, but fully recovers after few minutes. However, long exposure to high stresses and high temperatures notably decreases the strength of the fabric. See Reference 2.21 for more information.

Dacron: Dacron is a polyester-based man-made fiber with characteristics somewhat similar to nylon, but dacron requires more treatment for good stability. Dacron has somewhat lower elongation than nylon but has better temperature characteristics and better resistance to nuclear radiation. Dacron has better low-porosity stability, more stable elongation for control lines, and slightly less weight and volume than nylon, characteristics that have made this material attractive for sport parachutes.

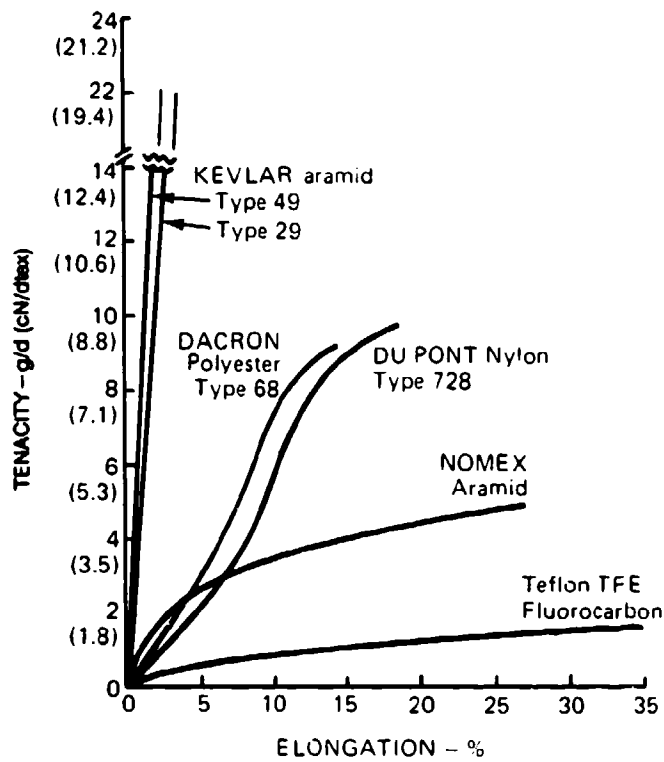


FIGURE 6-52. Tenacity in Grams Per Denier for Various Industrial Yarns.

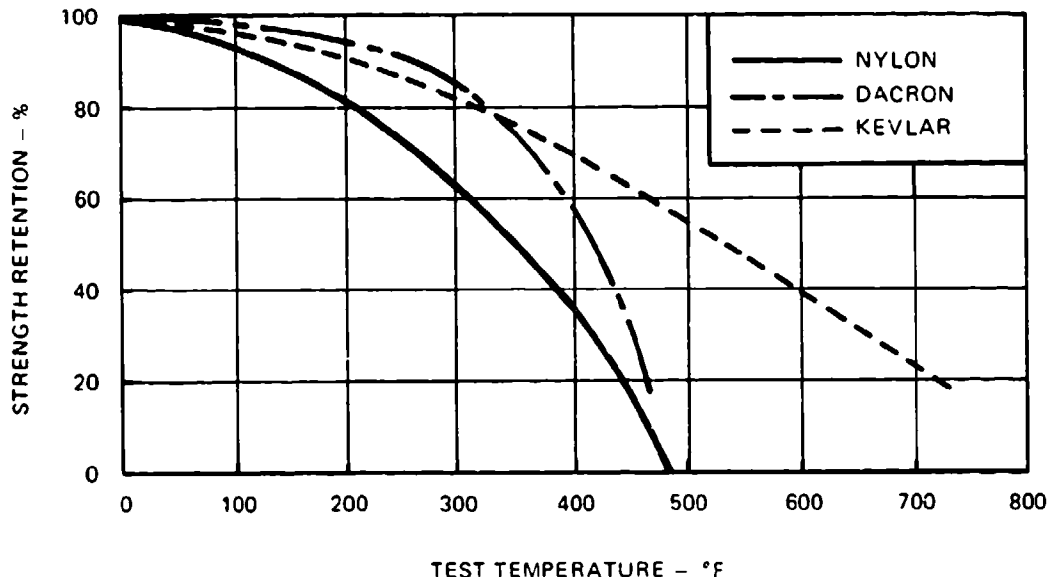


FIGURE 6-53. Loss of Tenacity Caused by Exposure to Temperature.

Teflon: The fluorocarbon fiber, Teflon, can be used at temperatures up to 450°F. Its low friction coefficient when in contact with other textile materials is Teflon's outstanding characteristic. Teflon is used as deployment-bag liner and as buffer material where high-speed contact between two nylon components of a parachute assembly may cause friction burns.

Kevlar: The para-aramid fiber, Kevlar, has become very prominent as high-tenacity material for parachute assemblies. Section 6.6.5 discusses Kevlar material and its application for parachutes.

6.6.2 Spinning and Weaving of Textiles

6.6.2.1 Spinning

Figure 6-54 shows a typical spinning process for man-made fibers. A spinning solution is formed of the basic material and then extruded through a number of very fine holes in the spinneret. The fine fibers (called filaments) are combined to filament yarns by twisting the fibers together, or by a glueing process called rotoset. The melt-spinning process shown in the figure is used for nylon, dacron, and glass fiber yarns. Related spinning processes are used for Kevlar, Nomes, rayon, and acetate yarns.

In the spinning process, fibers and yarns may be subjected to twisting, drawing, heat and chemical treatment, and other processes for obtaining desirable characteristics. Nylon

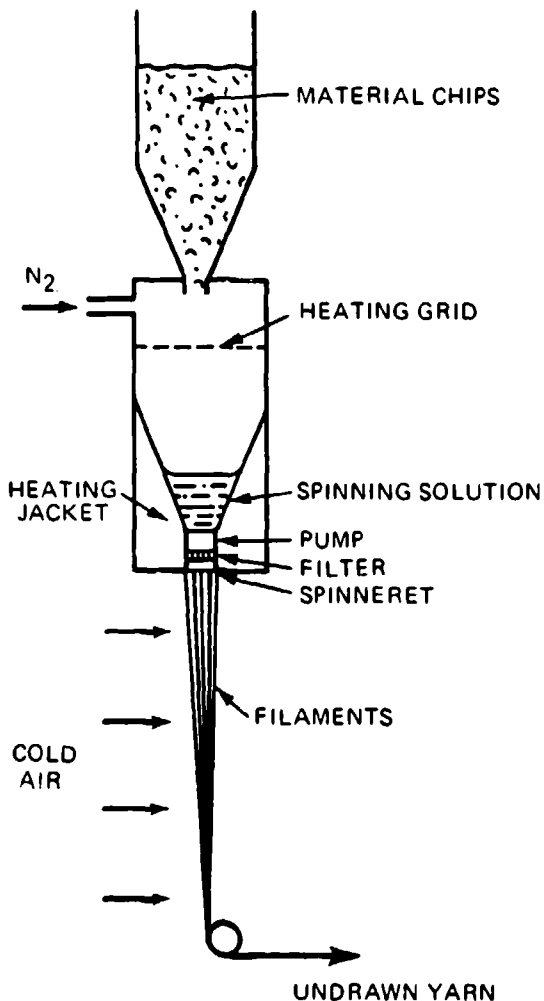


FIGURE 6-54. Melt-Spinning Process.

filaments, for example, are cold-drawn to four to seven times their original length to create a certain molecular orientation and increase tenacity.

Yarns are twisted together to obtain yarn stability and firmness and to improve mechanical characteristics of the yarn. Twist in yarn is defined by the number of twists per inch (TPI) and by the direction of the twist (Figure 6-55). A Z twist, shown in Figure 6-55 (a), is a right-handed, clockwise twist. An S twist, shown in Figure 6-55 (b), is a left-handed, counterclockwise twist. Figure 6-55 (c) shows Z-twist filaments twisted into an S-twist yarn. In addition to inducing stability and improving mechanical characteristics, twists can greatly change and improve the appearance of fabrics.

The size and strength of filaments and yarn is most frequently defined by a denier number; a denier is defined as the weight in grams of a fiber 9000 meters long. Although several other yarn-numbering systems are in use, the denier system is the one most frequently used for yarns in parachute fabrics.

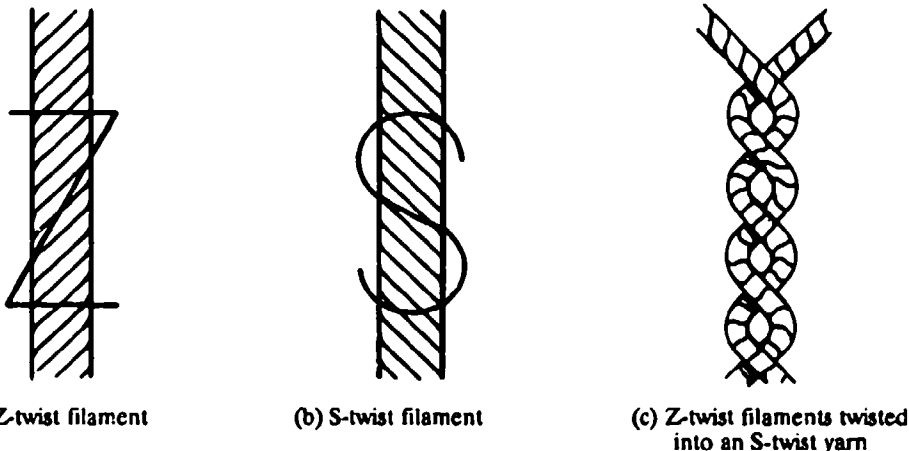


FIGURE 6-55. Examples of Z Twists and S Twists in Filaments and Yarns.

6.6.2.2 Fabric Weaving

All fabrics are produced on weaving machines called looms. The fabric produced on a loom has long yarns in the longitudinal direction of the fabric that are called warp. Yarns called fill are woven into the warp at a 90-degree angle.

Three types of looms are in use today. The shuttle loom uses a wooden bobbin to shuttle the fill yarn back and forth through the warp yarns that are fed into the loom from a large spool. This process produces a continuous fill yarn and a firm selvage edge on the fabric. The maximum bobbin speed is about 120 fill threads per minute.

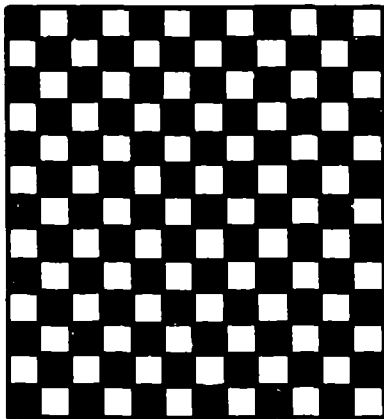
In recent years the rapier and the water-and-air jet weaving processes have been introduced. The rapier process pulls a fill thread by two needle-type rods from each side of the material through the warp threads and cuts the fill thread at each end at a speed of 400 fill threads per minute.

The water-and-air jet process shoots 800 to 1200 individual fill threads through the warp per minute. The economic advantages of the rapier and water-and-air-jet weaving processes are obvious.

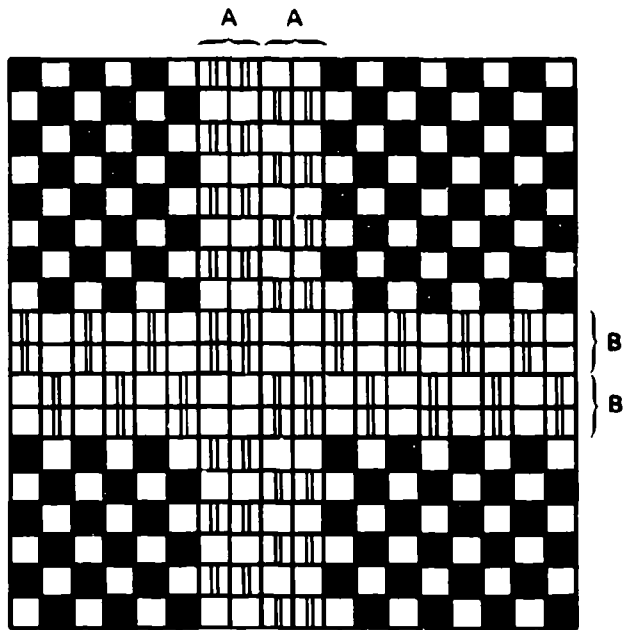
Parachute fabric is woven in 36-, 48-, 60-, and 72-inch widths. A typical parachute fabric has 122 warp threads, called ends, per inch width, resulting in 4392 ends for 36-inch-wide material. The warp ends are wound on a spool called a beam. The warp ends are guided

through the loom using several devices for straightening, lifting, and lowering the warp threads in preselected groups before inserting the fill thread. The sequence of lowering and raising the warp groups and inserting the fill thread determines the type of weave. The most common weaves are plain weaves where one fill thread goes over and under one warp thread, and the more complex are twill, taffeta, satin, and other weaves.

The type of weave desired is shown in a weave pattern in Figure 6-56. The black squares indicate the thread on top, and the white squares the thread on the bottom. The warp threads are called ends, and the fill threads are called picks. The pattern in Figure 6-56 (a) shows the weave pattern for a plain weave with one end going over and under one pick, and so on. Frequently the selvage edge of the fabric may have a slightly different pattern to ensure a more rigid, form-preserving edge.



(a) Plain Weave Pattern



A - TWO WARP ENDS WOVEN AS ONE
B - TWO FILLING PICKS PER SHED

(b) Ripstop Weave Pattern

FIGURE 6-56. Typical Weave Patterns for Parachute Fabric.

Figure 6-56 (b) shows the weaving pattern for 1.1-oz/y² ripstop nylon of MIL-C-7020, the material used in most military personnel parachutes. This fabric has a reinforcing rib woven in to stop small rips and prevent new rips from starting.

6.6.3 Parachute Fabric Specifications

The Department of Defense and other Government agencies have written specifications for all types of parachute fabrics. These specifications define the type of fabric (such as cloth, tapes, or lines), the mechanical properties, the weaving pattern, treatment during weaving, the finishing process, and inspection and testing procedures to ensure compliance with the specification requirements. Reference 2.1, the USAF *Recovery Systems Design Guide*; Reference 2.21, Piedmont Technical College Seminars on Parachute Manufacturing; and the Poynter *Parachute Manual*, Reference 2.22, list most of the parachute fabric specifications that would be sufficient for preliminary design. For final fabric selection, the specifications should be consulted.

This manual provides a current list of parachute fabric specifications but does not provide technical details.

6.6.3.1 Parachute Cloth

MIL-C-7020, cloth, parachute nylon (includes the standard 1.1 oz/y² ripstop)

MIL-C-7350, cloth, nylon, cargo parachutes (medium weight)

MIL-C-8021, cloth, parachutes, nylon, cargo and deceleration (heavyweight)

MIL-C-498, cloth, nylon (lightweight)

MIL-C-19262, cloth, nylon or rayon

MIL-C-7219, cloth, duck, nylon

MIL-C-3953, cloth, duck, nylon

MIL-C-26643, cloth, nylon, marquisette (pilot-chute vanes)

MIL-C-3395, cloth, netting, nylon (marquisette)

LP/P DES 81-1A, cloth, nylon, low porosity, US Forest Service Specification used in low porosity hi-glide parachutes

F-111, low-porosity cloth, nylon, G. Harris Corp.

MIL-C-5646, cloth, airplane, cotton

MIL-C-4279, cloth, cotton

CCC.D-419, cloth, duck, cotton, 12.28 oz/y²

SS 323244, polytetraflouoroethylene cloth (Teflon), Sandia specification. For Kevlar fabrics see section 6.6.5.3.

Low-porosity dacron cloth for sport jumper hi-glide parachutes is furnished by FWF Industries.

6.6.3.2 Thread

MIL-T-7807, thread, nylon, Fed. Spec. No. VT295

MIL-T-5660, thread, cotton, Fed. Spec. No. VT276

MIL-T-43636, thread, nylon, nonmelting

VT285, thread, polyester (dacron)

VT301, thread, silk

MIL-C-6635 and MIL-P-7567 discuss relationship of thread size, stitches per inch, and type of stitching.

6.6.3.3 Parachute Suspension Lines

MIL-C-5040, cord, nylon, cover and core line

MIL-C-7515, cord, nylon, coreless braided

MIL-C-17183, cord, nylon, braided tubular, spliceable

MIL-C-83243, cord, aromatic polyimide, nonmelting (Nomex)

Braided dacron suspension lines are available from FWF Industries.

For specifications for Kevlar lines, tapes, and webbings, see section 6.6.5.3.

6.6.3.4 Webbing and Tape

MIL-W-4088, webbing, textile, woven nylon

MIL-W-5038, webbing and tape, textile, reinforced nylon

MIL-W-27265, webbing, textile, woven nylon

MIL-W-5625, webbing, textile, nylon tubular

MIL-W-17337, webbing, textile, woven nylon

MIL-W-83144, webbing, textile, woven nylon, rolled selvage edge

MIL-W-83279, webbing, nylon

MIL-T-5666, tape, textile, nylon, multiple tubular

MIL-T-8363, tape and webbing, nylon

MIL-T-6134, tape, nylon

MIL-W-9049, webbing, textile, nylon, locking loop

MIL-W-5665, webbing, cotton

MIL-W-530, tape, cotton

MIL-W-5661, tape and webbing, textile, woven reinforced cotton

MIL-W-25339, webbing, polyester (dacron)

Ribbon for ribbon parachutes:

MIL-T-5608, tape, textile: webbing textile

SS 333416, ribbon, tape, and webbing; textile; nylon; Sandia specification

6.6.3.5 Related Specifications

MIL-STD-1520, Corrective Action and Disposition System for Nonconforming Materials

MIL-STD-1525, Verification Testing of Parachute Textile Materials

6.6.4 Designing in Textiles

Textile fabrics differ in several ways from other materials used in the aerospace industry. Textiles, as a rule, have a much higher elongation, are very flexible, and cannot be machined to a desired shape or cross section. The smallest building unit, the thread, already consists of a multitude of fibers. These characteristics introduce many design aspects not found in other materials.

6.6.4.1 Measuring Textiles

A metal rod has a length that can be measured with a measuring tape, and several people, even under different environmental conditions, will measure the same length. However, several people measuring the same piece of narrow or wide fabric at the same or different geographic locations will arrive at different dimensions, because textiles change in length depending on hand tension and environmental conditions. For this reason, a preload must be defined for measuring the lengths of different textiles. Although parachute canopy cloth is spread out on the cutting table and measured and marked under hand tension, all lines and tapes are measured under a preload. A preload of about 1% of the ultimate material strength is required to align all fibers in the woven or braided material before the individual fibers are stretched.

Military specifications, as a rule, comply with the 1% preload but limit the preload to a 5-pound minimum and a 40-pound maximum (see specifications MIL-P-25716 and MIL-C-6635).

Preloads up to 100 pounds are used for high-strength suspension lines on heavy-duty ribbon parachutes.

It is practical to let all fabrics relax for a short period after rewinding from the storage spool before measuring the material.

When NASA people found differences in the length of the same types of Apollo main parachute suspension lines measured at facilities in Southern California and Cape Kennedy, air conditioning was requested at all facilities. This was probably not necessary since all fabrics will elongate and contract about the same amount under similar atmospheric conditions.

6.6.4.2 Changes in Fabric Dimensions Caused by Sewing

Two pieces of wide fabric sewn together will become shorter in the seam than in the unsewn part of the fabric. This length change, shown in Figure 6-57, is called "take-up." The amount of take-up varies with the thickness of the fabric, the number of fabric layers in the seam, the number of rows of stitching, the size of the thread, the stitches per inch, the tension in the thread, and other factors. The take-up may range from 2% for lightweight fabrics connected with a simple fell seam to 10% for the radials of small, heavy ribbon parachutes with multiple radial ribbons and tapes and multiple rows of stitching.

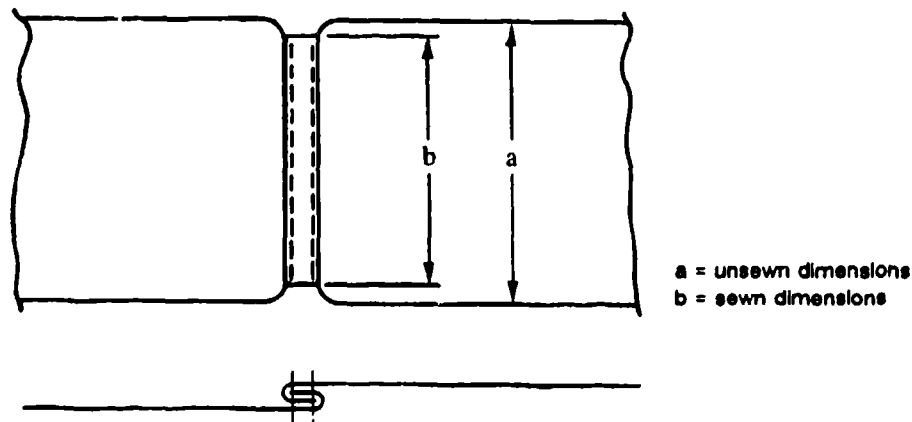


FIGURE 6-57. Changes in Fabric Length Caused by Sewing.

6.6.4.3 Finished Versus Pattern Dimensions

The shrinkage in fabric caused by sewing is somewhat similar to the shrinkage of metal castings when they are cooled. The design engineer must take the shrinkage into account.

All dimensions of a parachute assembly that are measured along a seam will shrink from the pattern dimensions. This shrinkage primarily affects radial seams, vent, skirt, and lateral tapes, and especially the radials of heavy ribbon parachutes with suspension lines sewn over the canopy with multiple rows of stitching.

Radials where the suspension lines run in channels through the canopy and are only attached at the vent and the skirt are less affected by this change.

The designer can specify the finished dimensions or the pattern dimensions, but not both. If finished dimensions are specified, then all pattern dimensions are reference dimensions. The ribbon parachute specification, for example, defines the finished length of the radials, and states that a certain amount of horizontal ribbons should be equally spaced in a finished distance, and defines the horizontal ribbon width and spacing only as reference dimensions.

A decision must be made for every parachute system whether it and its components, and which components, are to be manufactured to pattern or to finished dimensions.

Finished dimensions are necessary for parachutes that must have a repeatable precise aerodynamic performance (such as ordnance and aircraft landing deceleration parachutes). Air vehicle recovery parachutes, cargo parachutes, and most personnel parachutes used with a variation of loads and resultant rates of descent can accept less stringent tolerances. Pattern dimensions may be suitable for these types of parachute assemblies if the finished dimensions are held in acceptable tolerance limits.

6.6.4.4 Fullness

The designer of a parachute canopy may have established the geometric dimensions; for example, for the length of the radial seam. If the designer now adds a small amount of length to this dimension, the added material is called "fullness." Fullness serves two purposes: it creates a certain amount of stress relief in the canopy material, and it ensures that loads are carried in such primary load-carrying members as tapes and radials and are not being transferred to the canopy material. Sections 6.4.5 and 7.3.8 describe how adding fullness to the vent tape and then gathering it to the basic dimensions will create a certain amount of curvature to the canopy vent area, and will result in stress relief in the canopy fabric. The same is true for other parts of the canopy, as shown in Figure 7-12. Recommended amounts of fullness for solid material, circular canopies are 5% for the vent tape, 1% for the skirt tape, and no fullness for the radials.

The second purpose for fullness is to ensure that the main forces in the canopy are carried by the radials, the skirt, and vent tapes and are not being transferred to the canopy cloth. This is especially important for canopies with suspension lines or radial tapes sewn to the full length of the radial seam, and to canopies with cloth in block construction. If checks indicate that the elongation of the radials or tapes is higher than the elongation of the canopy fabric, negative fullness in the radials and tapes or positive fullness in the canopy material must be added.

To obtain load relief in the vent tapes, a common practice is to make the vent lines 5% shorter than the measured diameter of the completed vent. This diameter should be measured

after the canopy is completed, since the bunching of material in the vent connected with the multiple rows of sewing causes deviations from the drawing dimensions, especially on heavy-duty ribbon parachutes.

6.6.4.5 Tolerances

Several MIL specifications define the following tolerances for finished parachute parts:

Dimensions, inches	Tolerance, inches
0 to 0.5	1/16 (.06)
0.5 to 2.0	1/16 (.06)
2.0 to 10.0	1/8 (.12)
10.0 to 30.0	1/4 (.25)
30.0 to 60.0	3/8 (.37)
60.0 and up	1%

These tolerances have been satisfactory for personnel and cargo parachutes. However, they have caused problems on large parachutes for missile and booster recovery, and have been proven totally inadequate for the Apollo main and drogue parachutes.

It has been proven impossible to comply with a tolerance of 1/16 to 1/8 of an inch between radial centers on heavy-duty parachutes with radials 2 to 3 inches apart at the vent. On this type of parachute, the diameter of the vent should be the critical dimension.

The Apollo main parachutes had suspension lines 1440 inches long. Applying the 1% rule would have permitted a line variation of \pm 14.4 inches, or 29 inches between two adjacent suspension lines. The distance between two adjacent lines in the first reefing stage was 4 inches. This presented the unacceptable possibility that the reefing line could zig-zag in a 4-inch skirt distance up to 29 inches in the radial distance. In addition, the 29-inch length difference between two adjacent lines could create a dangerous stress concentration in the canopy skirt area. The allowable length difference between two adjacent Apollo suspension lines, therefore, was limited to 5 inches. The recommendation is to limit the free length of suspension lines in large parachutes by splitting the required total line length into (1) strictly a suspension line, and (2) a suspension line/riser part, as shown in Figure 6-29a.

In cooperation with NASA, a new system of tolerances was developed along with the definition of critical and noncritical dimensions. Critical dimensions as agreed upon included length of suspension lines, radials, vent diameters, length of skirt, vent and lateral tapes, and all leading and trailing edge ring dimensions. The tolerance system jointly agreed upon between Northrop, DCAS quality control personnel, and NASA is shown in Figure 6-58.

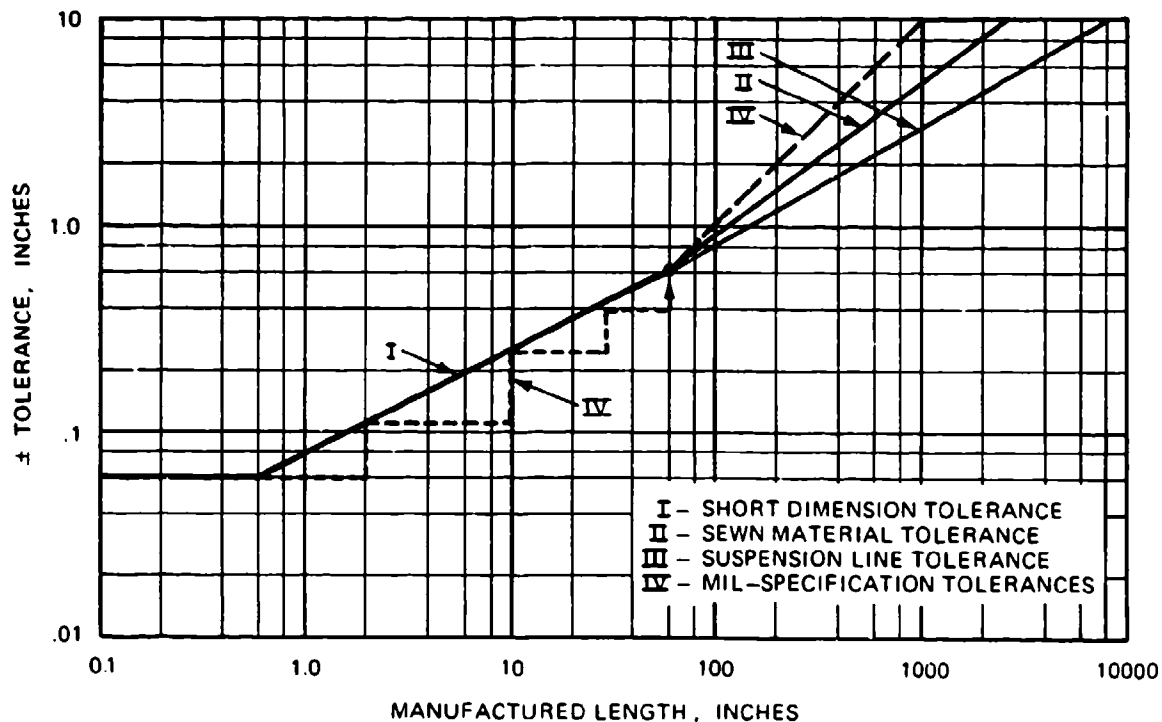


FIGURE 6-58. Tolerances for Manufactured Textile Parts, Apollo Program.

Small dimensional inaccuracies in large canopies with many gores can cause such canopy anomalies as canopy unfolding. The Gemini spacecraft astronaut capsule used an 84-foot-diameter, 72-gore, ringsail main descent parachute. A slide rule error of 0.6 inch in the trailing edge length of one of the 13 rings resulted in a surplus length in that ring of 43.2 inches and caused infolding of two canopy gores. A NASA aerodynamic study to find the reason for canopy infolding was terminated when the dimensional error in the gore design was found, corrected, and no more infoldings occurred.

6.6.5 Designing in Kevlar

6.6.5.1 General Information

Kevlar is about 2.5 to 3 times stronger than nylon and is considerably more heat resistant. Hybrid parachutes using nylon canopies and Kevlar suspension lines, risers, and canopy tapes will save up to 40% in weight and volume, depending on the amount of Kevlar used. Depending on the type of fabric, Kevlar may also be 5 times more expensive than nylon, and is not available in the wide range of fabrics as is nylon, especially not in lightweight, wide fabrics. New developments in lightweight, wide fabrics were recently reported in Reference 6.53. The

superior strength/volume characteristics make Kevlar extremely attractive for application where strength and volume requirements outweigh higher cost.

The Sandia National Laboratories in Reference 6.54 summarizes its experience in the use of Kevlar for all types of parachute application, placing emphasis on heavy-duty ribbon parachutes. Using Kevlar on heavy-duty ribbon parachutes for suspension lines and all canopy reinforcing elements, such as radial tapes, vent, and skirt tapes and vent lines, reduces the parachute weight and volume by 25 to 40% depending on the amount of Kevlar used. All-Kevlar ribbon parachutes were designed and tested, but Sandia decided, for the present, to use nylon canopies in connection with Kevlar suspension lines and canopy reinforcements. Kevlar ribbon canopies require considerable redesign because of the low elongation of Kevlar combined with sewing problems. Sandia also has successfully designed and tested large, lightweight, solid-fabric parachutes with Kevlar suspension lines and canopy reinforcements. Again, a weight and volume saving of 25 to 40% was achieved. This agrees well with the experience of the parachute industry.

The Naval Surface Warfare Center at Silver Spring, Md., replaced a nylon cross parachute for a low-altitude, 500-knot ordnance device with an all-Kevlar cross parachute. The Kevlar parachute required only 40% of the volume of the nylon parachute. However, new wide fabrics had to be developed for this application (Reference 6.55).

The Air Force, in Wright Aeronautical Laboratories at Wright Patterson AFB, investigated the use of Kevlar for ribbon parachutes. The investigation included the development of suitable fabrics, the design and manufacture of Kevlar ribbon parachutes, and the testing of the parachutes in high-speed airdrops. Reference 6.56 covers this investigation. Department of Defense agencies, the Sandia National Laboratories, DuPont, and the parachute industry have provided information on Kevlar and Kevlar applications in parachutes for this manual.

6.6.5.2 Kevlar Material

Kevlar was developed by the DuPont Co. Kevlar was originally to be used as a replacement for steel wire in automobile tires. Two Kevlar types, Kevlar 49 and Kevlar 29, have been used increasingly in the aerospace industry. Kevlar 49, with a tenacity of up to 23 grams per denier and a low elongation of 2 to 3%, is used extensively in high-strength composite structures for air vehicles, ground vehicles, boats, and for similar applications (Reference 6.57).

Kevlar 29, with a slightly higher elongation of 3.5% and a more flexible fiber, is used in high-strength textiles, including wide and narrow parachute fabrics. A Kevlar yarn consists of a large number of filaments extruded from an acid solution using a process slightly different from that for nylon. The individual fibers are held together by cohesion and natural glue. Later, the fibers are rotoset or twisted to enhance weaving capability. Twisting provides the yarn with firmness and stability, and contributes to yarn strength up to a certain number of twists. The

low elongation and firmness of the individual fiber require different methods of weaving and braiding than those used for nylon fabrics. The ratio of fabric strength to original yarn strength on Kevlar is about 70 to 90% compared to nylon, which obtains a yarn-to-fabric strength ratio of up to 100% (Reference 6.58).

Table 6-10 compares materials used in the aerospace industry with those used for parachute fabrics. The high tenacity of Kevlar of 22 to 23 grams per denier (shown in Figure 6-52) as compared to nylon with 6 to 9 grams per denier, is Kevlar's most outstanding characteristic. Figure 6-53 shows that Kevlar maintains about 55% of its strength at the melting point of nylon.

Figure 6-59, taken from Reference 6.56, shows the effect of twist on the tenacity of Kevlar yarn. Kevlar, similar to nylon, is affected by ultraviolet radiation. Figure 6-60, taken from an NWC investigation, Reference 6-59, shows the loss in strength caused by exposure to sunlight.

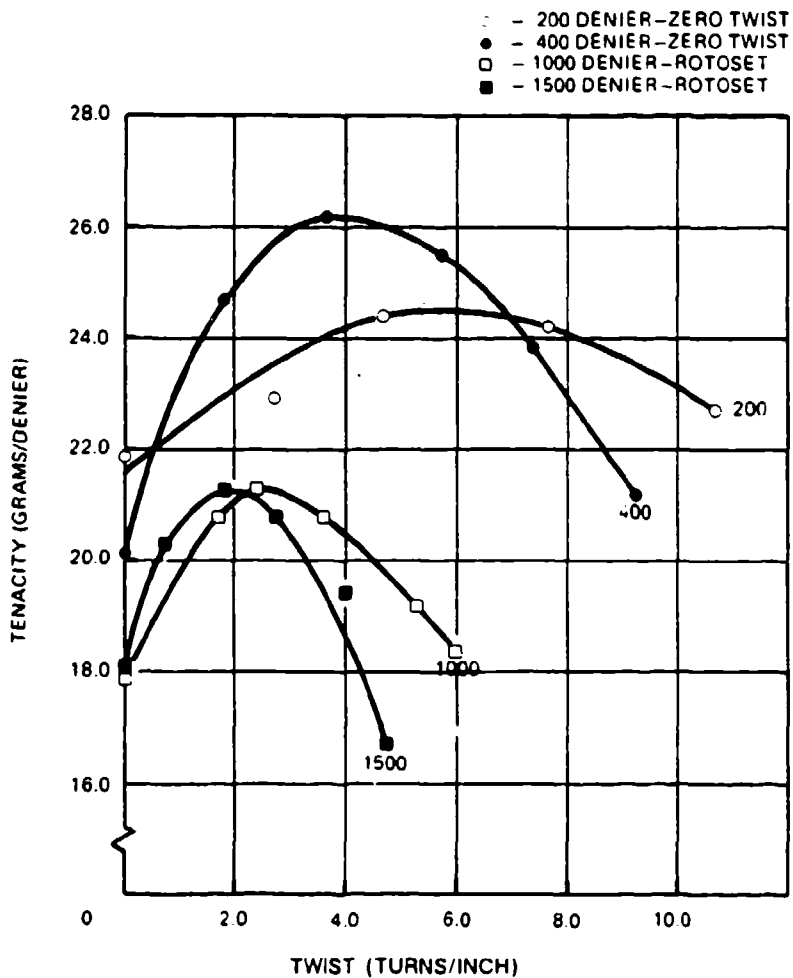


FIGURE 6-59. Tenacity of Four Kevlar Yarns as a Function of Yarn Twist.

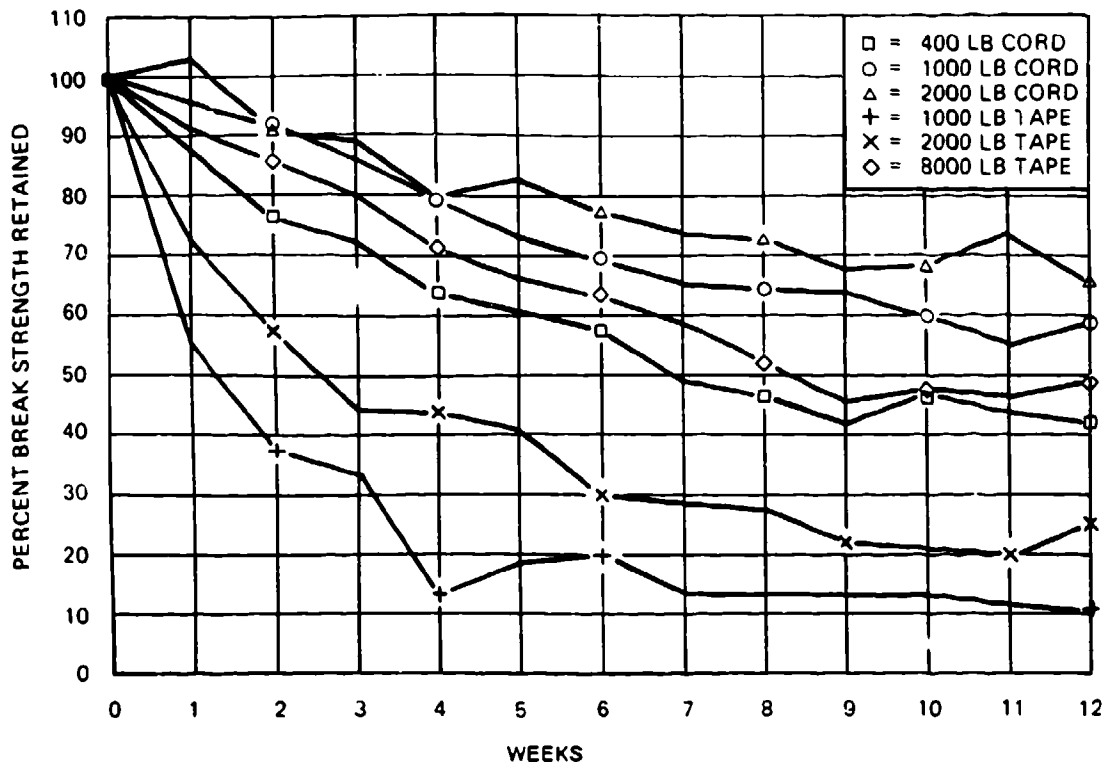


FIGURE 6-60. Loss in Strength of Six Different Kevlar Materials Caused by Weathering.

The lightest commercially available Kevlar yarn of 200 denier does not permit weaving a lightweight fabric that can compare with the widely used 1.1 oz/y² nylon ripstop fabric. However, the recently introduced 55-denier Kevlar yarn has been woven into lighter fabrics (Reference 6.57).

6.6.5.3 Kevlar Material Specifications

Parachute Cloth

MIL-C-8156, cloth, parachutes, aramid, intermediate modulus

MIL-C-38351, cloth, parachutes, aramid, low modulus

Thread

MIL-T-87128, thread, para-aramid, intermediate modulus

Suspension Lines

AMS 3814, cord, coreless braided, para-aramid, intermediate modulus

MIL-C-38282, tubular webbing, para-aramid, low modulus

Webbing, Tape

AMS 3793, tape, webbing textile, para-aramid, intermediate module

Sandia National Laboratories Specifications

SS 323279, cloth, textiles, Kevlar-aramid, intermediate modulus

SS 323241, tape and webbing, textiles, Kevlar-aramid, intermediate modulus

SS 323243, thread, textiles, Kevlar-aramid, intermediate modulus

SS 373117, waxing process, Kevlar and nylon thread

6.6.5.4 Design and Fabrication

Experience gained in the design and fabrication of all-Kevlar or Kevlar-nylon hybrid parachutes is discussed in References 6.57, 6.58, 6.59, and in several lectures of the Roxboro Parachute Manufacturing Seminar, Reference 2.21. General experience gained in the design and fabrication of nylon parachutes applies equally well to designing and manufacturing in Kevlar. However, the special Kevlar characteristics of low elongation and high strength require certain adjustments and changes, especially on parachutes manufactured entirely from Kevlar.

Hybrid parachutes using nylon canopies and Kevlar suspension lines, canopy reinforcing tapes, and radials have been used successfully for several applications with savings in weight and volume of 25 to 35%.

Parachutes manufactured totally from Kevlar do not have the benefit of stress normalization and load relaxations as do bias-constructed, high-elongation nylon canopies. Because of this, a stress-oriented design with special attention to the interface between canopy fabric and the load-carrying canopy tension members, radials, skirt, and vent tapes and vent lines is required.

Hybrid nylon-Kevlar canopies are best sewn with nylon thread, whereas Kevlar thread should be used for all-Kevlar canopies.

Low-elongation Kevlar lines are well suited for control lines, reefing lines, and for elements that require good dimensional stability. Indications are that Kevlar suspension lines decrease the rotational tendencies of cross parachutes.

The abrasion of Kevlar has been a controversial subject. Reference 6.60 and reports from the field rate Kevlar as the same or slightly better than nylon. High-speed extraction of Kevlar parachutes from deployment bags indicates that Kevlar parachutes suffer less from friction burns.

Kevlar seams in wide fabrics are less firm than nylon seams and have a tendency to pull out in a "rake type" fashion. To counteract this fault, Kevlar cloth can be slightly coated. The coating makes the cloth easier to work with and produces better seams. For uncoated fabrics to make a firmer seam, a binder such as segrine or a similar solution should be used in the seam

area. In Reference 6.61, seam efficiencies of Kevlar cloth using different seams, stitching, rows of stitches, and type of sewing were investigated. Kevlar seam efficiency is low compared with nylon; and more rows of stitching and longer stitch patterns are required for Kevlar.

Chinese finger splicing is possible with Kevlar lines; however, the length of the insert should be equal to 15 times the line diameter, instead of 10 times the line diameter as on nylon.

The same preloads can be used for Kevlar lines and tapes as for nylon. Kevlar cannot be hot cut with electric knives and standard cutters, and scissors require frequent sharpening. Special cutter blades and scissors are commercially available.

Sewing machines used for nylon fabrics are also used for Kevlar; however, thread tension needs adjustment to avoid damage to sewing machine parts by the strong Kevlar thread.

6.7 PARACHUTE RECOVERY SYSTEM WEIGHT AND VOLUME

6.7.1 Importance of Minimum Weight and Volume

A precise determination of the necessary parachute weight and volume is important early in any air vehicle development program requiring parachutes.

The relationship of weight and volume can be expressed by the amount of parachute weight that can be packed into 1 cubic foot of volume. This introduces the importance of pressure packing. The higher the pressure, the more weight can be stowed in a given space. Handpacked parachutes, such as those used for sport parachutists and personnel parachutes used for aircraft escape, stow about 22 to 23 pounds in 1 cubic foot of volume. Pressure-packing combined with suction to remove entrapped air can increase pack density to close to 50 pounds of parachute weight per cubic foot of compartment volume.

Hybrid nylon/Kevlar parachute assemblies and all-Kevlar parachutes will increase this value slightly because of the 26% higher specific weight of Kevlar. Sandia National Laboratories and industry sources state that packing methods and pack pressures developed for nylon parachutes are directly applicable to Kevlar/nylon and all-Kevlar parachutes.

Three methods for calculating the weight of a parachute or a parachute recovery system are

1. The preliminary design method
2. The drawing method
3. The TWK method

6.7.2 The Preliminary Design Method

Data on the weight of different types of parachutes and parachute recovery systems, including such components as storage containers, sequencers, and impact attenuation systems, are plotted in Figure 6-61, which shows the percentage weight of a parachute recovery system and its various subassemblies as functions of the primary vehicle weight.

The percentage weight of the parachute recovery system components decreases with an increase in vehicle weight caused by the relative weight decrease of the various components. Another reason for the weight decrease is that parachute recovery systems for larger air vehicles generally have lower permissible parachute forces expressed in g in relation to the weight of the air vehicle.

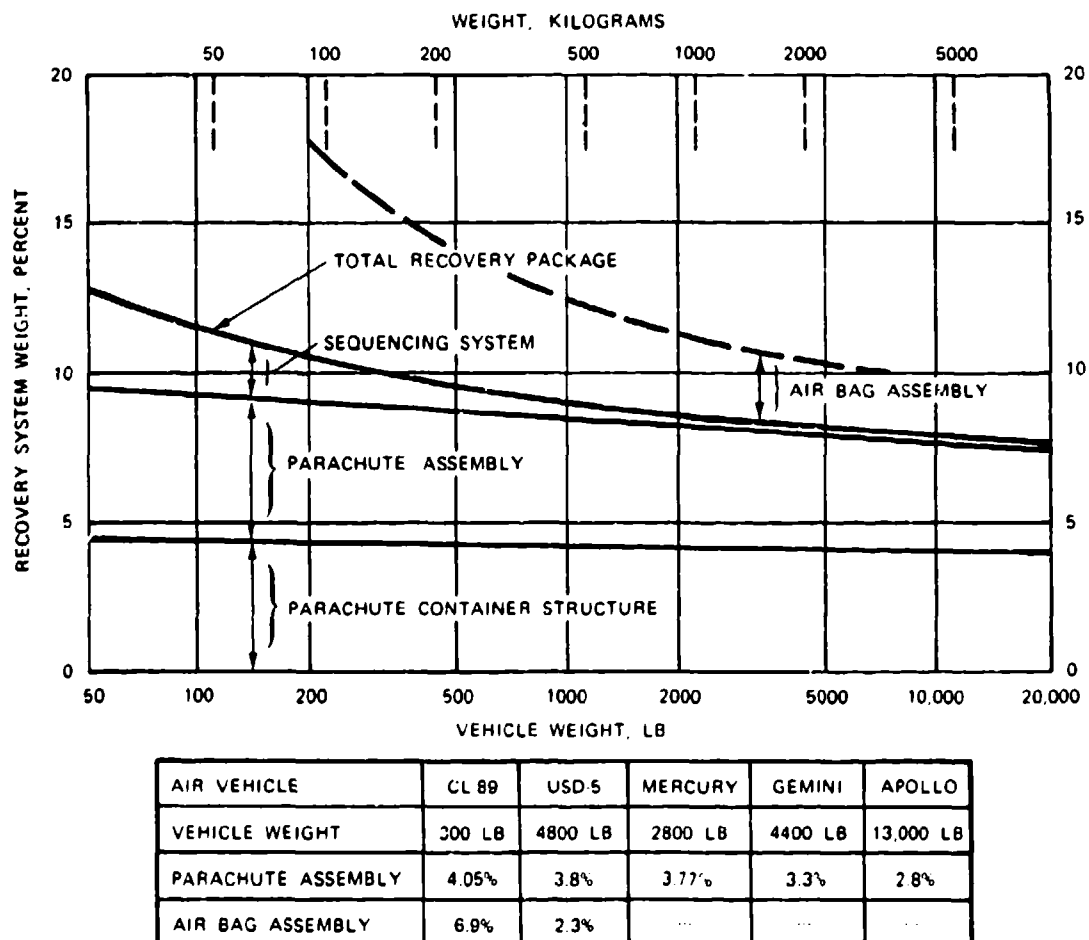


FIGURE 6-61. Parachute Recovery System Weight as Percentage of Air Vehicle Weight.

Figure 6-62 plots the weight of three groups of main descent parachutes. The I-curve is valid for extended-skirt and polyconical types of parachutes of all-nylon design deployed in the velocity range of 150 to 200 knots. Using a hybrid nylon/Kevlar design will decrease the parachute weight by 25 to 40%.

The data plotted in curve II refer to main descent parachutes that were deployed at velocities up to 300 knots, such as were used on the B-58 and B-70 crew modules, and may apply to some personnel parachutes used in ejection seat assemblies.

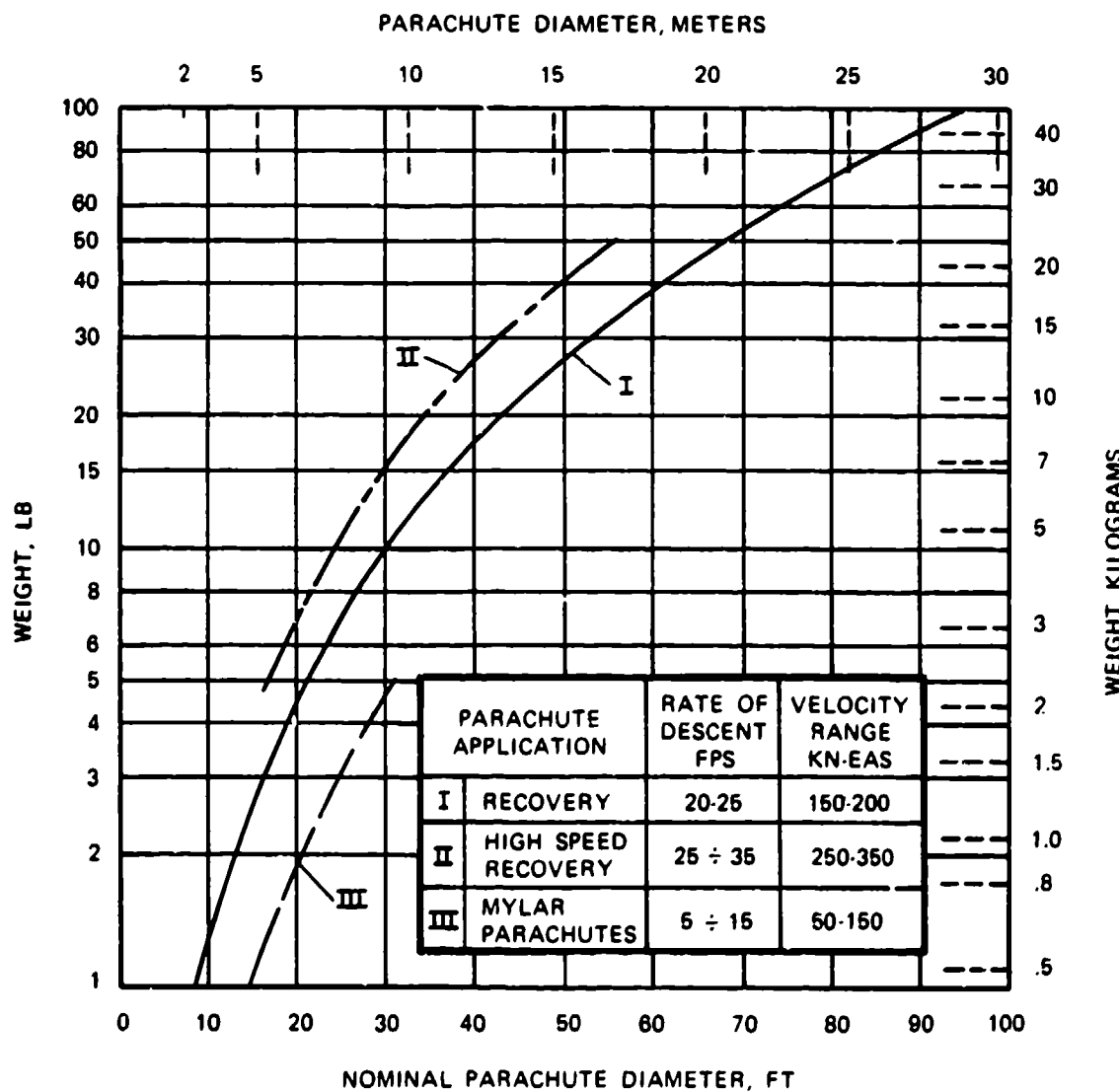


FIGURE 6-62. Weight of Final descent Parachutes.

The III-curve refers to a series of 0.25-mil mylar parachutes with 100-pound-strength suspension lines. These parachutes were designed for deployment at close to zero dynamic pressure at high altitudes.

These weight figures refer to the parachute itself, without deployment bags, pilot chutes, or other components. As a rule, deployment bags weigh 5 to 6% of the parachute, and deployment bags plus pilot chute and pilot chute bridle add 3 to 5%. First-stage drogue-chute assemblies will weigh from 25 to 40% of the main parachute weight depending on deployment dynamic pressure and riser length. A long riser behind a large-diameter forebody can add considerable weight.

Parachute clusters have 5 to 10% higher weight than a single parachute of equal drag area. This is because of the loss in drag caused by cluster interference (see section 5.10).

Figures 6-63 and 6-64 show the weight of all-nylon ribbon and ringsail parachutes versus diameter and strength range.

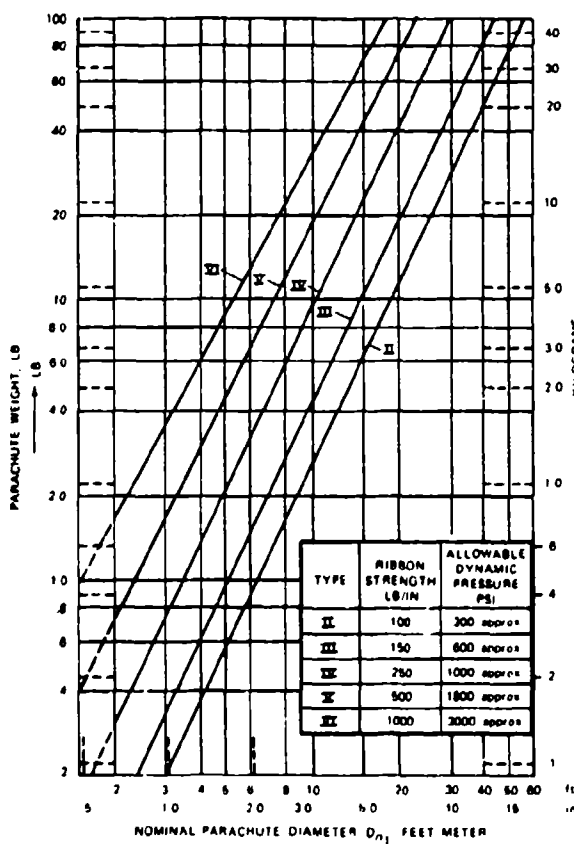


FIGURE 6-63. Ribbon Parachute, Weight Versus Diameter and Horizontal Ribbon Strength.

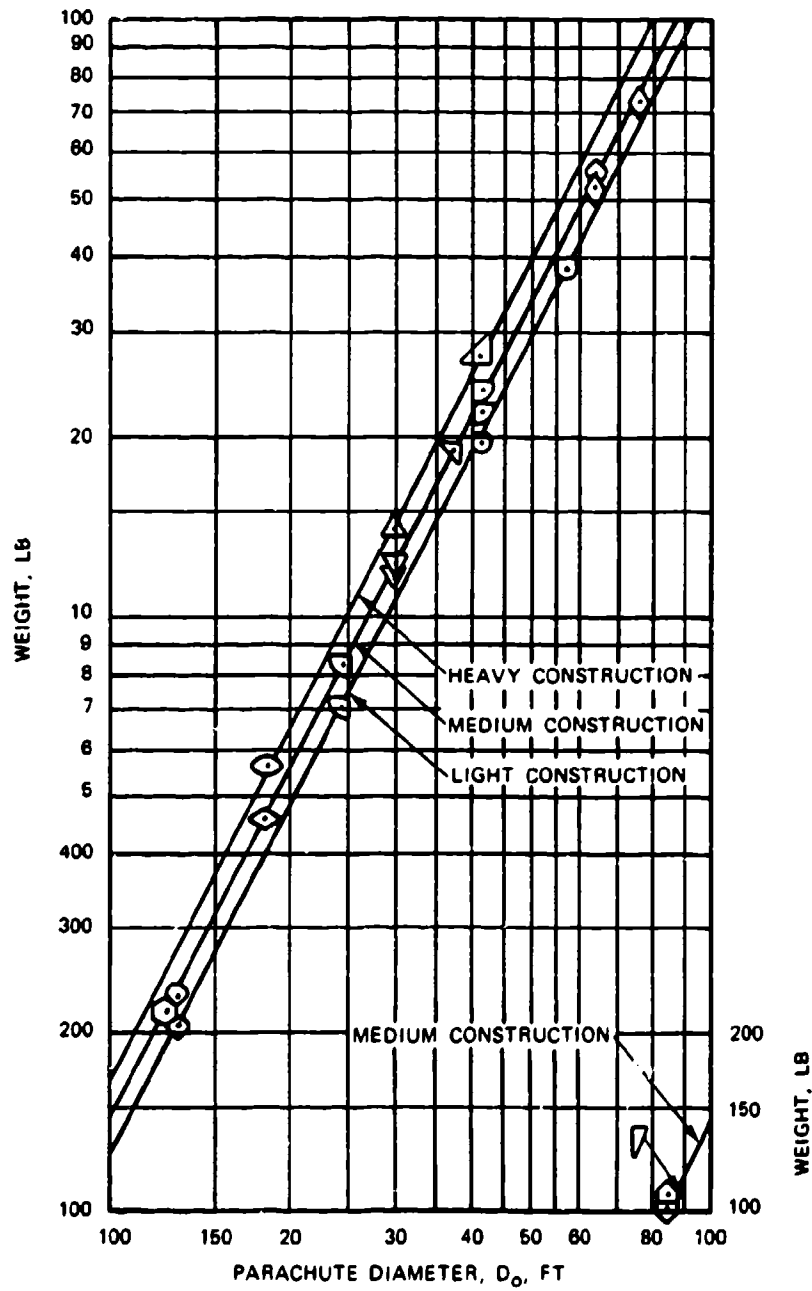


FIGURE 6-64. Weight of Ringsail Parachute as a Function of
Parachute Diameter (Reference 5.50).

6.7.3 The Drawing Method for Determination of Parachute Weight

If detailed drawings with material lists are available, the weight of the parachute assembly can be determined from the material and hardware specifications. Experience shows that this weight is frequently about 5% higher than the weight of the manufactured assembly.

6.7.4 The TWK Weight Determination Method

If no detailed drawing is available, but the primary dimensions of the parachute are known, the following method will give good weight data. The weight of a parachute can be written in following form:

$$W_p = S_o \cdot w_c + \underbrace{D_o/2 \cdot N_G \cdot w_{RT} \cdot F_{RT}/1000}_{\text{Canopy}} + \underbrace{N_{SL} \cdot L_S \cdot w_{SL} \cdot F_{SL}/1000}_{\text{Suspension lines}}$$

where

- W_p = Weight of the parachute, lb
- S_o = Surface area of the finished canopy, ft²
- w_c = Specific canopy weight, lb/ft²
- N_G = Number of gores (radials) in the canopy
- w_{RT} = Specific weight of radial tape, lb/ft/1000-lb strength
- F_{RT} = Strength of the radial tape, lb
- N_{SL} = Number of suspension lines
- L_S = Length of suspension lines, ft
- w_{SL} = Specific weight of suspension lines, lb/ft/1000-lb strength
- F_{SL} = Strength of suspension line, lb

In this formula D_o , S_o , N_G , N_{SL} , L_S , F_{RT} , and F_{SL} are known preliminary design data. The specific canopy weight, W_c , refers to the entire canopy including vent and skirt tape, but not to reinforcing radial tapes. The following specific canopy weights have been evaluated from manufactured canopies:

Canopy material	1.1 oz/y ² light design	1.1 oz/y ² standard design	1.1/2.25 oz/y ² combined design
Weight in lb/ft ²	0.092	0.105	0.0115

The 1.1/2.25 group refers to canopies where the canopy vent area uses 2.25-oz/y² as is common on reefed canopies.

The following is the specific weight of suspension lines, webbing, and tapes:

Woven nylon lines	$w_{SL} = 0.01 \text{ lb/ft}/1000\text{-lb strength}$
Braided nylon lines	$w_{SL} = 0.0075 \text{ lb/ft}/1000\text{-lb strength}$
Kevlar lines/webbing	$w_{SL} = 0.0035 \text{ lb/ft}/1000\text{-lb strength}$

The specific weight of lines and webbings decreases with increasing line/webbing strength. A 10,000-pound line has about 20% less specific weight than a 1000-pound line.

The weight calculation for suspension lines can be used also for risers using the quoted specific weights for lines and webbings.

For determining the weight of the parachute assembly, the percentage weight values in this section apply.

A method somewhat similar to the TWK method was presented by K. French in Reference 6.62.

6.7.5 Pressure Packing of Parachute Assemblies

The most commonly used methods for reduction in parachute stowage volume are lace-packing and pressure-packing using mechanical or hydraulic presses combined with suction to remove entrapped air, and autoclaving for heat setting.

Lace-packing is best suited for cylindrical compartments using the banana-peel type bags shown in Figure 6-36 and described in section 6.3.5.2. Using leverage-type tools or clam-shell forms with presses allows pack densities of up to 50 lb/ft^3 .

Air vehicle parachute compartments are frequently semirectangular or oddly shaped. An example is the storage area for the Apollo main parachutes that consisted of a quarter section of a truncated cone under the forward heat shield. An air gap of $\frac{1}{2}$ inch between deployment bags and the heat shield had to be maintained to prevent heat transfer between the heat shield and the parachutes. Pressure-packing in time intervals and air suction and autoclaving at 180°F for 24 hours was used. For transfer and storage, the parachutes were housed in a wooden form duplicating three sides of the storage area. The parachutes were then wrapped in two layers of plastic sheeting to prevent air entering the packed parachutes. The resultant pack density of 47 lb/ft^3 is equivalent to the density of maple tree wood.

Removal of the plastic covers and the opening of the daisy chain bag after 1 year did not result in any movement of the packed parachute; everything remained in the tightly packed position. The suspension lines, after having been extended to their full 120-foot length, snapped back to within 3 feet of their stowed position. The canopy behaved in a similar manner. Subsequent laboratory tests of components and parachute free-flight tests did not reveal any measurable strength degradation.

Early in the program, the heavy pressure-packing bent reefing rings and cutters and caused damage to the lightweight canopy cloth between adjacent reefing rings. Stronger reefing rings, proper cutter and ring location, combined with X-raying every packed parachute eliminated this problem. Figure 6-65 shows the packing presses used for packing the Apollo main parachutes, and Figure 6-66 shows an Apollo main parachute pressure-packed in its wooden storage form and wrapped in two plastic sheets.



FIGURE 6-65. Heavy Packing Presses Used for Packing the Apollo Main Parachutes.

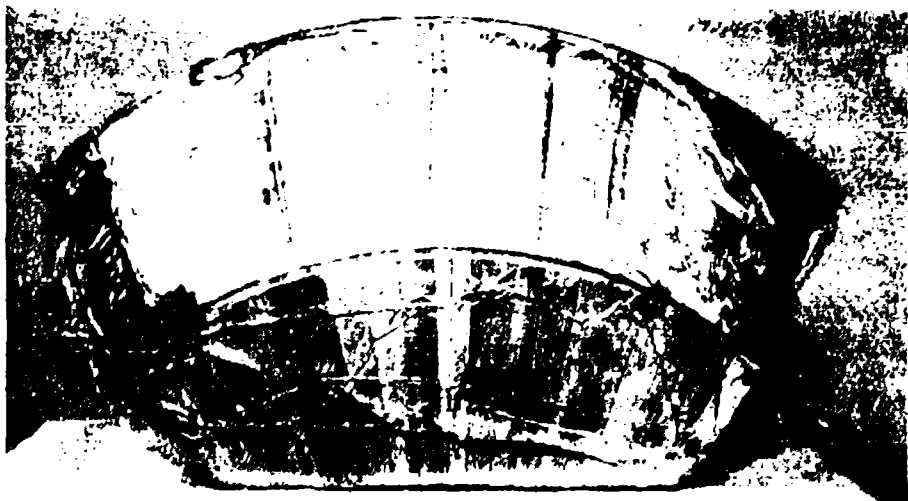


FIGURE 6-66. Apollo Main Parachute Pressure-Packed in its Storage Form.

6.7.6 Investigation of Pressure-Packaging

The results of an investigation of pressure-packaging are reported in Reference 6.63. The investigation found that the relationship of pack density as a function of pack pressure is relatively independent of the form of the packing container or the type of parachute—solid cloth, ribbon, lightweight, or heavyweight. Figure 6-67, taken from Reference 6.63, demonstrates this statement. An investigation of packing time intervals indicated that extending the time under pressure to several days provides a slight reduction in required packing volume, a fact that was later confirmed in the Apollo Program. Figure 6-67 also shows that little is gained by extending the specific pack pressure beyond 200 psi where a pack density of 45 lb/ft³ is obtained. The 47 lb/ft³ pack density on the Apollo parachutes required a specific pack pressure approaching 600 psi.

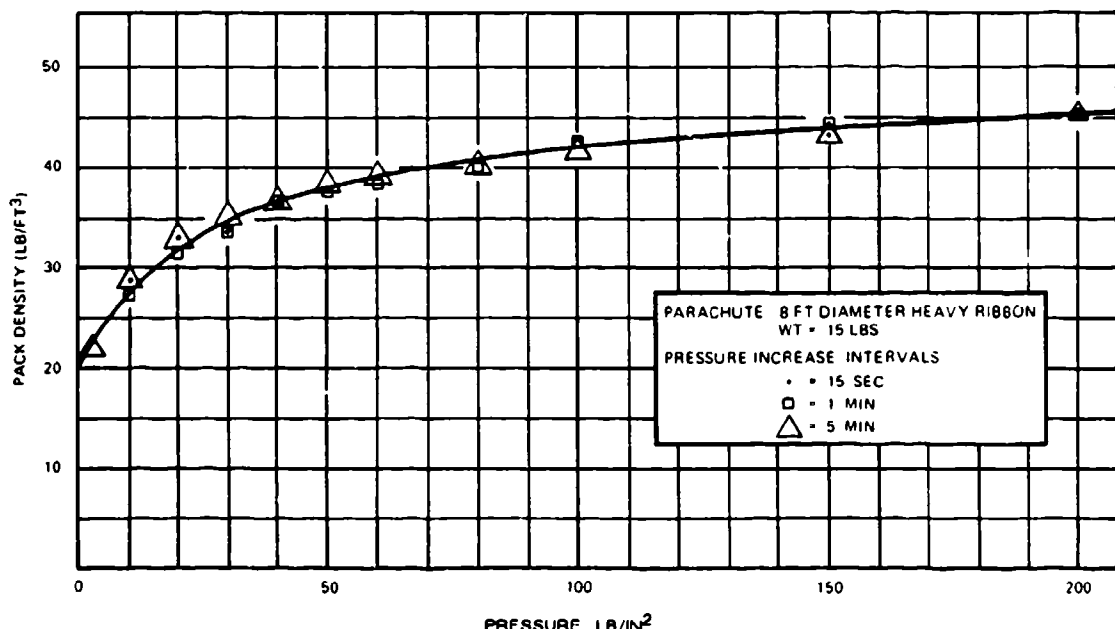


FIGURE 6-67. Pack Density as a Function of Pack Pressure and Packing Application Interval.

6.8 LANDING IMPACT ATTENUATION SYSTEMS

6.8.1 Landing Analysis

Every parachute landing of a vehicle or load requires that the vertical and horizontal landing energy be absorbed at ground contact. At slow descents and with rugged vehicles or loads, the vertical energy can be absorbed by elastic vehicle deformation and ground penetration, and the horizontal energy can be absorbed by sliding when the load has landed.

The energy to be absorbed at landing is equivalent to the decelerating force, F , acting over the deceleration distance, s , or

$$E = \int F(s) ds \quad (1)$$

F can be written $F = n W_s$, where W_s is the weight of the system to be decelerated and n is the allowable deceleration in multiples of the acceleration of gravity, or $n = \frac{F}{W_s}$. n will be called the allowable deceleration factor.

For most parachute-vehicle systems, the allowable impact deceleration is limited by structural and load considerations. Common practice is to refer to the impact deceleration factor, n , as the allowable deceleration.

The energy, E , to be absorbed at ground contact is $E = \frac{m V_h^2}{2}$ for horizontal deceleration, and $E = \frac{m V_v^2}{2} + W_s s$ for vertical deceleration.

Introducing the system weight $W_s = mg$ and the velocity limits, the energy is

$$E = \frac{W_s(V_1^2 - V_2^2)}{2g} + W_s s \quad (2)$$

Solving for the required deceleration distance, s , and introducing the allowable deceleration factor, n , and the efficiency of the impact attenuator, η , the required deceleration distance (stroke) is

$$s = \frac{(V_1^2 - V_2^2)}{2g(m\eta - 1)} \quad (3)$$

where

- s = required deceleration stroke (distance), ft
- V_1 = rate of descent at start of deceleration, ft/s
- V_2 = rate of descent at impact (generally zero), ft/s
- g = acceleration of gravity = 32.174 ft/s²
- n = allowable impact deceleration in multiples of g
- F = decelerating force, lb
- W_s = parachute-load system weight, lb
- η = efficiency of impact attenuator system, dimensionless

The required deceleration stroke depends primarily on the rate of descent, V_1 , and the allowable impact deceleration, n .

Equation 1 only accounts for the vertical deceleration. Movement in the horizontal plane caused by ground wind, use of a gliding parachute, or parachute oscillation necessitates (1) disconnecting the parachute assembly at ground contact to avoid dragging by the wind and possible vehicle damage, and (2) using an omnidirectional impact attenuator or attenuator arrangement. To predict or control the orientation of vehicles, loads, or platforms at landing has been proven impossible and so makes it difficult to depend on ground sliding in the longitudinal axis of the load. The requirement for an omnidirectional impact attenuation capability rules out certain types of shock absorbers.

The dynamics of the landing process of vehicles or loads with vertical, horizontal, and possibly tumbling motion is complex and dealt with in references 6.64 to 6.66.

6.8.2 Relationship of Deceleration Stroke, Rate of Descent, and Allowable Impact Deceleration

The required vertical deceleration stroke for any kind of vehicle as a function of the rate of descent, V_1 , and the allowable impact deceleration, n , is plotted in Figure 6.68, using the assumption that the velocity at impact, V_2 , is zero; and the impact attenuator used has an efficiency η of 0.65, the efficiency value of air bags.

Impact decelerations shown in Figure 6-68 labeled 1 were measured on the Radioplane OQ-19, a rugged target drone. Data labeled 2 refer to measurements on airdrop cargo platforms.

Figure 6-68 also defines application ranges for certain types of impact attenuators. Crushable and frangible attenuators, such as paper, plastic, and aluminum honeycomb, and metal cutting devices are suitable for required deceleration strokes in the up to 12-inch range. Inflatable air bags are best suited in the 12- to 36-inch deceleration stroke range. Longer deceleration strokes can be obtained with retrorockets. Such attenuators as crushable nose cones, ground penetration spikes, and others have been used successfully for special applications; however, most of these devices have design and application features that limit their operational usefulness.

Allowable impact decelerations based on measured data and experience are listed in Table 6-11.

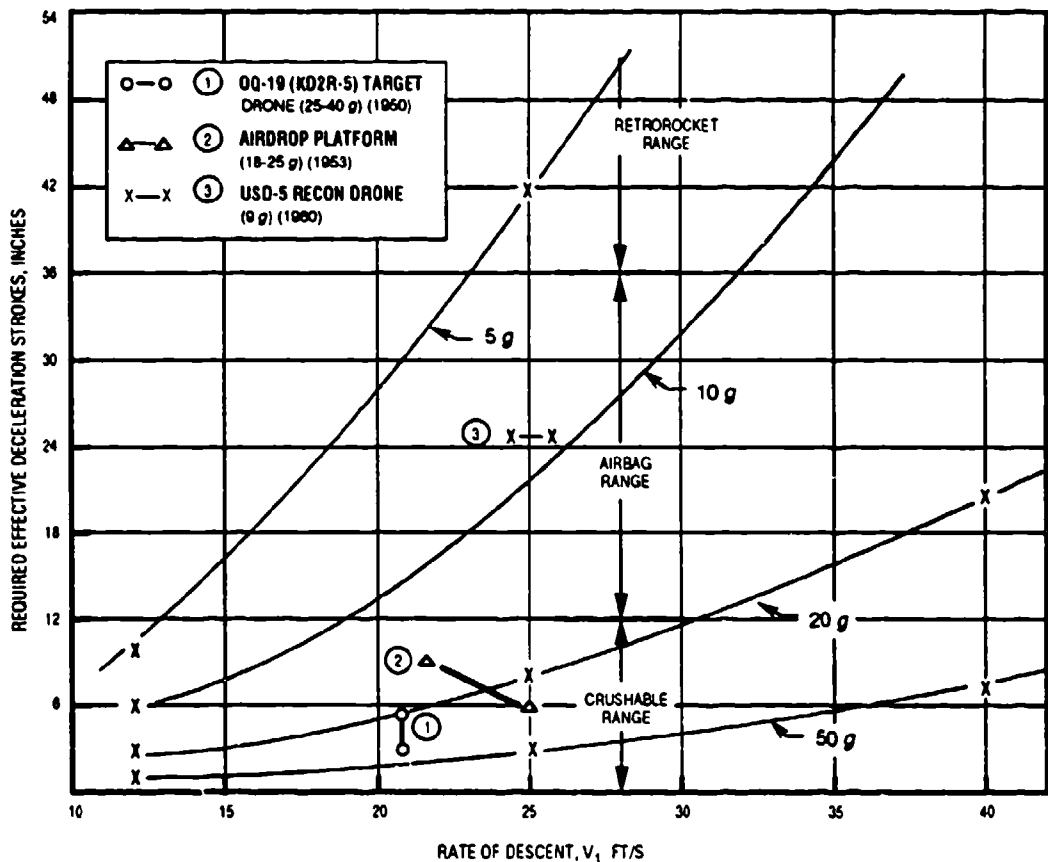


FIGURE 6-68. Deceleration Stroke Versus Rate of Descent and Allowable Impact Deceleration.

TABLE 6-11. Allowable Impact Decelerations.

Operation	Impact deceleration, g
Military airdrop cargo	20 to 35
Target drones, unmanned vehicle structures	20 to 30
Telemetry equipment	20 to 25
Sensitive electronics equipment	5 to 10
Aircrew members	6 to 10
Astronauts after long duration space flights	3 to 5

6.8.3 Selection and Description of Impact Decelerators

6.8.3.1 General

The rate of descent, allowable impact deceleration, type of vehicle, and operational landing condition are the factors that determine need for impact attenuation and the required deceleration stroke. The selection of the impact attenuator best suited for the operation depends on some or all of the following considerations:

- Required deceleration stroke
- Vertical and horizontal energy absorption requirement
- Possible variations in vehicle weight and rate of descent
- Energy absorption characteristics of attenuator
- Attenuator weight, volume, and stowage conditions
- Soil surface condition at landing
- Acquisition and life-cycle cost
- Reusability and cost of refurbishment
- Maintenance, recycling time
- Safety and maintenance during flight

Most of these requirements are self-explanatory. Weight and volume of the stored attenuators are of minor importance for military airdroppable cargo, but are of major importance (volume more often than weight) for air vehicles, crew modules, and missiles. Vehicles that are flown only over military test ranges usually land in less rough terrain than vehicles that fly in combat areas. The same can be said for aircrew escape modules that may land in flat terrain, mountains, forests, or water. Reusability, recycling times, and cost are important for target drones and unmanned reconnaissance vehicles, but are not required for airdroppable cargo or aircraft crew escape modules. Rocket fuel and high-pressure storage vessels may be a safety consideration for vehicles that fly in combat areas. Cost is of major importance for airdroppable cargo, but is less important for expensive manned and unmanned air vehicles. For manned air vehicles, reliability is the highest priority. Military airdroppable supplies may trade cost for reliability. Requirements for omnidirectional impact capability eliminate oleo and pneumatic strut type shock absorbers.

An ideal impact attenuator or impact-absorbing material would exhibit the load-deceleration stroke diagram shown in Figure 6-69. All impact attenuators and impact-absorbing materials deviate from this ideal energy absorption characteristic. A typical diagram for a crushable material in the honeycomb group is shown in Figure 6-70. Figure 6-70 demonstrates that an initial force, called the peak force, is necessary to start the compression of the material. The rise of the force curve, called the onset rate in g per second, is important for manned vehicles, since the onset rate is limited for the human body. The peak force determines the design load of the system. A high, steady average crushing force increases

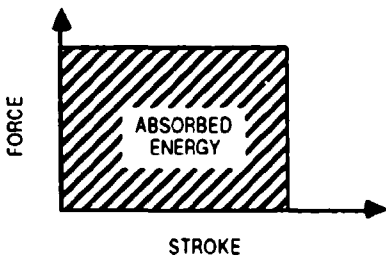


FIGURE 6-69. Ideal Energy Absorption Diagram.

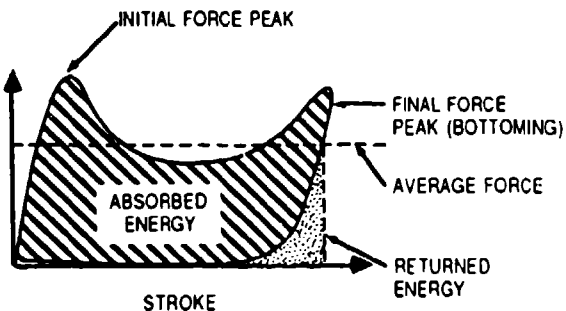


FIGURE 6-70. Typical Energy Absorption Diagram for Crushable Material.

the efficiency of the attenuator system. All energy should be absorbed before ground contact. Bottoming out of the attenuator results in a high final peak force. Stored elastic (returned) energy causes the system to bounce.

More than 100 reports are available that deal with impact attenuators used in connection with parachute descent systems.

6.8.3.2 Crushable Impact Attenuators

Crushable impact attenuators include paper, plastic, aluminum honeycomb (see Figure 6-71), and several types of foam material. All honeycomb material consists of a cell structure with variation in the cell size and material density. The energy absorption capability is higher in the x-direction, but remains at about 25% in the y-direction. The attenuator is delivered compressed in the y-direction and must be extended and covered with a top and bottom sheet prior to use. The primary application of the crushable impact attenuator is cushioning material for airdroppable cargo platforms that require energy absorption primarily in the vertical plane, with the horizontal energy being absorbed by sliding on the ground. Figure 6-72 shows a cargo platform loaded with a 42,000-pound AM551 armored

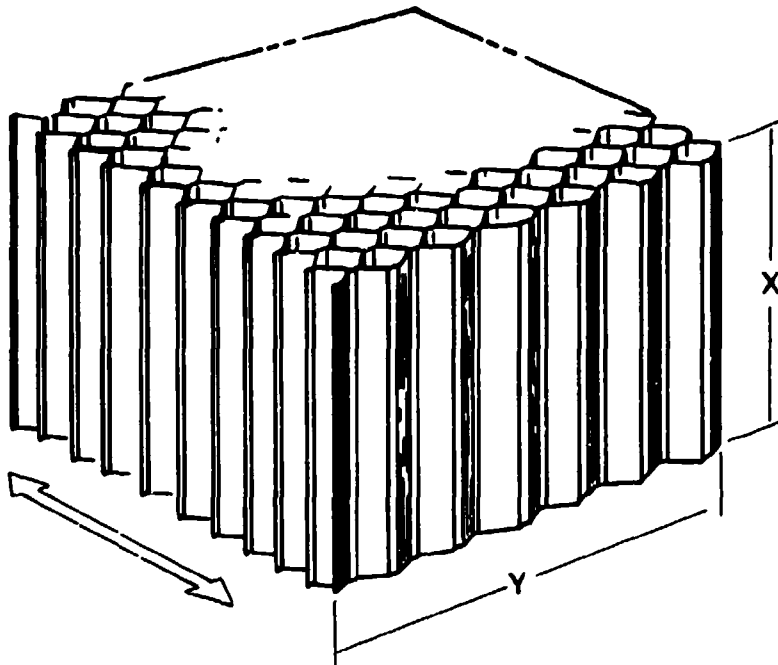


FIGURE 6-71. Typical Honeycomb Structure.



FIGURE 6-72. AM551 Armored Reconnaissance Assault Vehicle Loaded on a Cargo Platform Using Paper Honeycomb as Impact Attenuator.

reconnaissance assault vehicle using multiple layers of paper honeycomb for impact attenuation. References 6.67 and 6.68 detail the use of paper honeycombs for loads on airdrop cargo platforms.

Paper Honeycomb: The energy absorption characteristics of various types of paper honeycombs have been extensively investigated. References 6.69 to 6.71 give some of the results. Figure 6-73, taken from Reference 6.71, shows the stress-strain relationship of MIL-H-9884A paper honeycomb pads used by the U.S. Army for cargo platforms. The figure shows that this type of paper honeycomb can be compressed to about 30% of its height before bottoming out. A small peak force occurs at the beginning of the compression stroke, and a residual elastic force remains at the end of the stroke, which can cause a slight rebounce. If the total energy is not absorbed at the end of the 70% compression, a high ground-impact force will occur.

An investigated foldable paper honeycomb design used for military cargo platforms, as shown in Figure 6-74, is described in Reference 6.72.

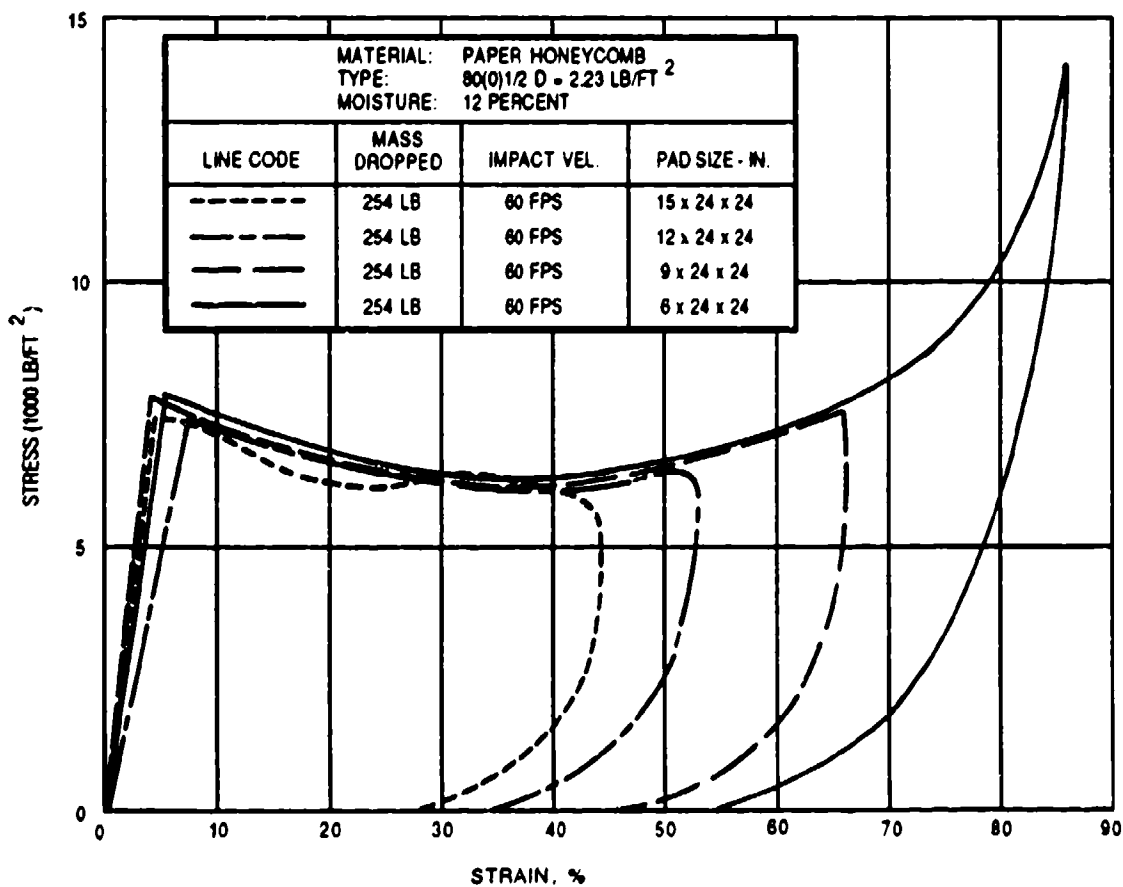


FIGURE 6-73. Stress-Strain Diagram of Paper Honeycomb Pads.

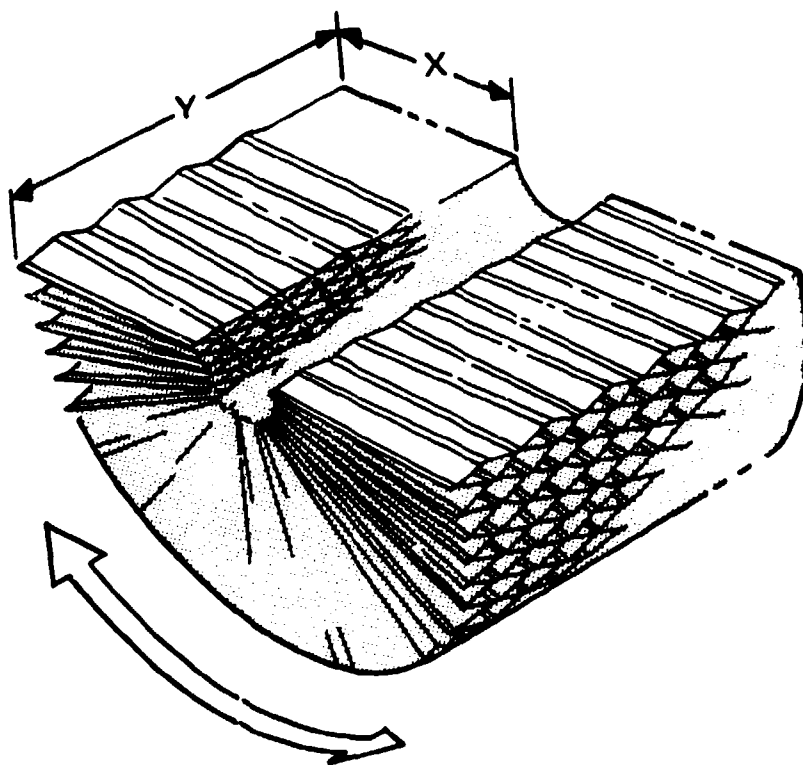
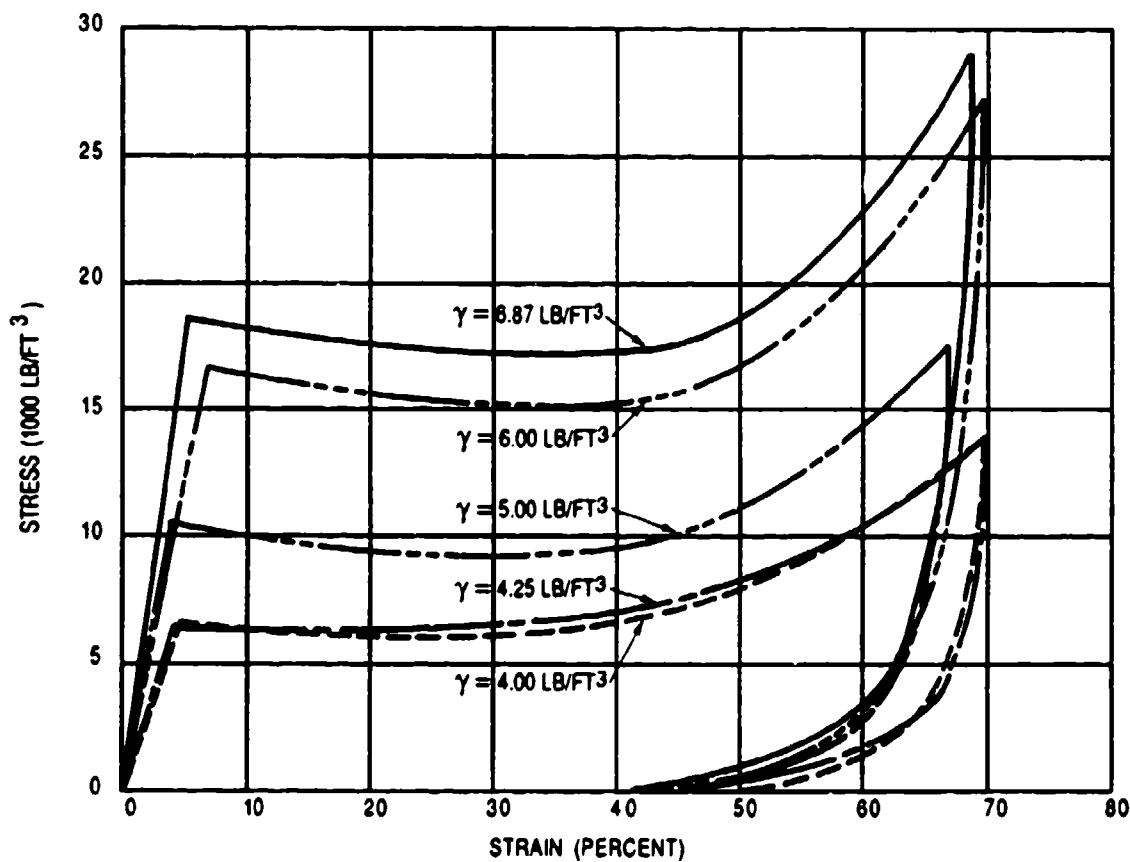


FIGURE 6-74. Paper Honeycomb Impact Attenuator.

Aluminum Honeycomb: Extensive investigations of crushable impact attenuators by the University of Texas, described in References 6.69 to 6.71, include aluminum honeycomb materials. The Northrop BQM-74 target drone uses extendable honeycomb pads for cushioning the impact on land landings.

Foam Plastics: Foam plastics as impact attenuators have also been investigated by the University of Texas (References 6.69 to 6.71). The stress-strain relationship of foam plastic is illustrated in Figure 6-75; taken from Reference 6.68. Foam plastic compared to paper honeycomb has a slightly lower peak force and bottoms out at about 50% of its height. Foam plastics are 100% omnidirectional in their energy absorption capability. Their energy absorption per pound of weight is low, they require relatively large storage volume in the uncompressed state, and they are not reusable.

A typical application for foam plastic is its use in cylindrical parachute test vehicles for the cushioning of telemetry and other electronic equipment. The electronic equipment is stored in a longitudinal cavity in the test vehicle and is held in place with light shear pins. A styrofoam pad of 10 to 20 inches in front of the telemetry box is compressed on landing impact and serves as an effective, low-cost shock absorber.



MATERIAL: FOAMED PLASTIC 108C PAD SIZE: 24 x 24 x 6 IN				
DENSITY (γ)	NO. OF TESTS	MASS DROPPED	IMPACT VELOCITY	LINE CODE
4.00 LB/FT ³	4	295 LB	50 FPS	-----
4.25 LB/FT ³	4	295 LB	50 FPS	- - - -
5.00 LB/FT ³	3	295 LB	58 FPS	- - - -
6.00 LB/FT ³	4	295 LB	71 FPS	- - - -
6.87 LB/FT ³	3	295 LB	75 FPS	=====

FIGURE 6-75. Effect of Density on Stress-Strain Curves for Polyurethane Foamed Plastic.

The development of a radio-frequency transparent, omnidirectional shock absorber for an instrument container is described in Reference 6.73.

The Air Force Flight Dynamics Laboratory at Wright Patterson AFB has investigated a foam-in-place impact attenuator for an unmanned reconnaissance vehicle. An extendable textile bag was attached to the underside of the vehicle and hardening plastic foam components were released into the bag. Hardening of the plastic took about one minute. The development and laboratory testing of this system is described in Reference 6.74. The advantage of this system is its small storage volume that can be located conveniently in the air vehicle. Its disadvantages include extensive plumbing and control equipment and a long, temperature-sensitive foam hardening time.

Figure 6-76 compares the effectiveness of several crushable materials by plotting the required compression force over the effective stroke. In analyzing Figure 6-76, you must remember that the compression stroke as part of total material height is different for the various materials.

Figure 6-77, taken from Reference 6.75, compares the efficiency of different types of impact attenuators.

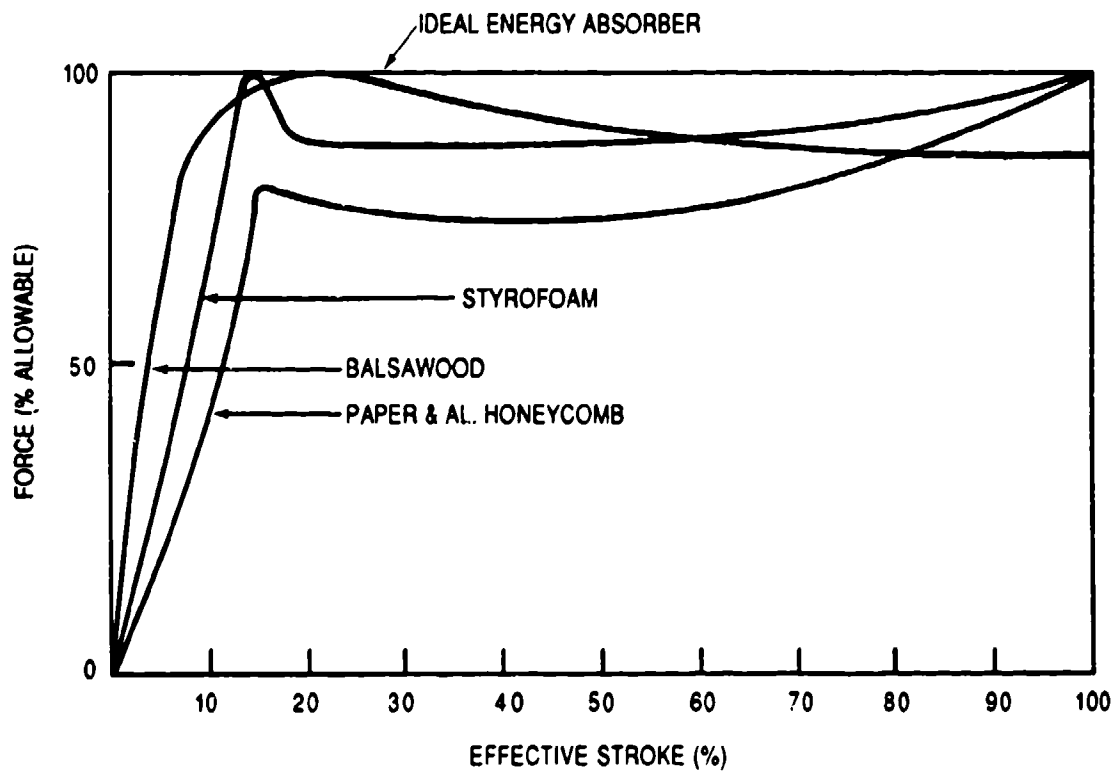


FIGURE 6-76. Force-Stroke Efficiency of Various Crushable Materials.

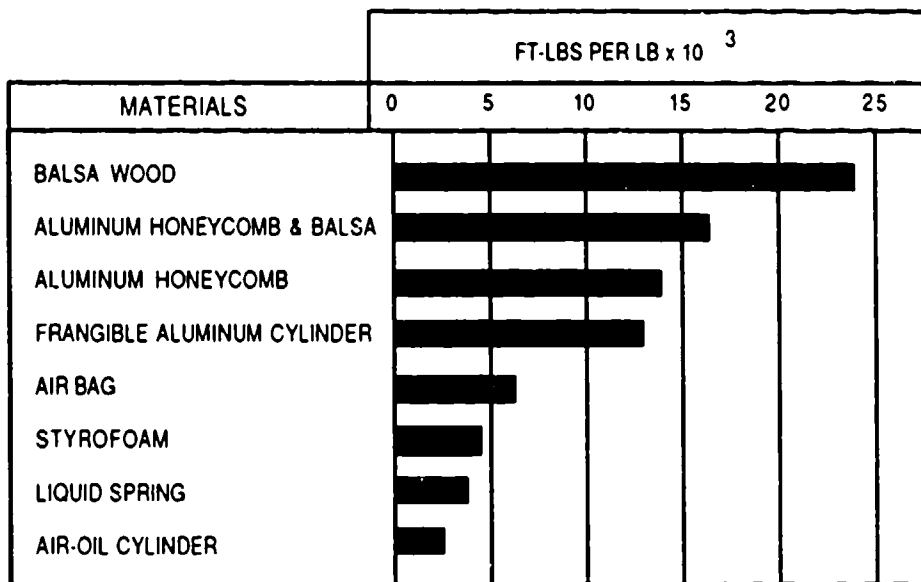


FIGURE 6-77. Energy Absorption Per Pound of Material Weight.

6.8.3.3 Air Bags

Air bags have increased in popularity for the impact attenuation of such air vehicles as target and reconnaissance drones, training missiles, and for the landing of aircrew escape modules. Figure 6-68 defines the required deceleration stroke range of 12 to 36 inches as the range best suited for air bag impact attenuators. Air bags require relatively little storage volume compared to crushables, are reusable, have a high energy absorption capability per pound of weight, and use almost 100% of the compression stroke for shock absorption.

The basic concept of the air bag consists of a textile bag coated with flexible plastic for zero porosity. The bag or bags are stored in the fuselage or wings of the air vehicle. After the main descent, parachutes are inflated, the bag compartment cover is ejected, and the bag is deployed and inflated to 1 to 2 psi to obtain a proper initial shape. At ground contact, the pressure in the bag rises adiabatically. At a predetermined level, pressure relief valves open and allow part of the compressed gas to escape, flattening the pressure force curve for better bag efficiency. Air bags are designed for one specific energy level. Changing the rate of descent, and thereby the energy to be absorbed, results in a bounce at the end of the deceleration stroke if the energy was higher than the design level; or, if the energy was lower than the design level, stopping the vehicle above the ground.

Dual-chamber air bags or small secondary bags have been used to keep the vehicle off the ground in rocky terrain or unsuitable ground conditions.

Figure 6-78 is a typical air bag pressure-stroke diagram. At ground contact, the bag starts to compress and the internal pressure increases until at Point A the pressure relief valves

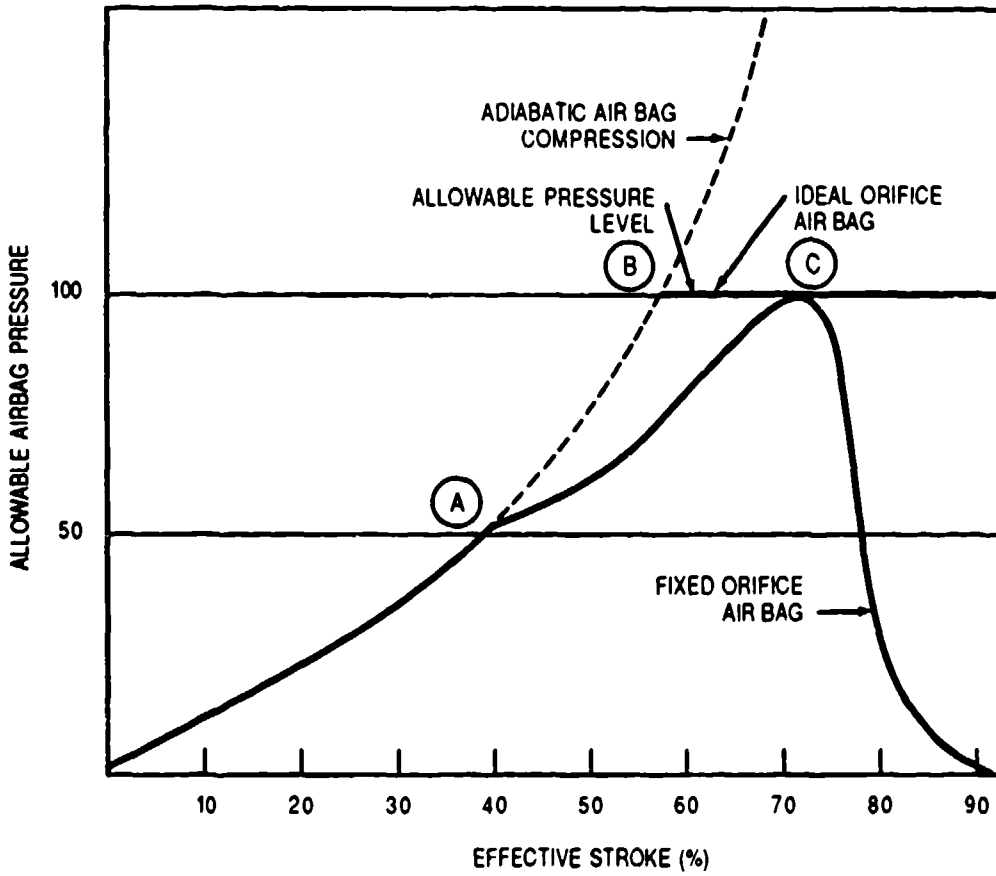


FIGURE 6-78. Air Bag Pressure Versus Stroke Characteristics.

open simultaneously, staggered, or pressure controlled. The pressure increase lessens until the allowable pressure level is reached at Point C. A gradual pressure decay follows.

The design of the pressure relief valve (orifice) contributes notably to the efficiency of the bag. Ideal orifices permit the bag pressure to rise to Point B and then remain constant until ground impact. Some recent orifice designs (described later in this section) have increased bag efficiency.

The height of the air bag is determined by the required deceleration stroke. The bag diameter is determined from the relationship that the bag cross section area times the bag pressure is equal to the allowable deceleration factor n times the vehicle weight, or

$$n W_v = p_b S_b$$

where

- n = allowable impact deceleration factor, dimensionless
- W_v = vehicle weight, lb
- P_b = bag pressure, psi
- S_b = air bag footprint area, inch²

The vehicle weight and the allowable vehicle deceleration at impact are fixed design values. The bag pressure and the bag cross section are variables and are influenced by the design rule that the bag height should not exceed 1.25 to 1.5 times the bag diameter. Both dimensions again depend on the shape of the bag, the bag design, and the bag installation.

Figure 6-79 shows several operational air bag designs and installations, and Table 6-12 provides technical data on the air bag systems shown in the figure. The air bags for the airdrop platforms were gravity deployed, weighted with lead to enhance bag stretch, and inflated by

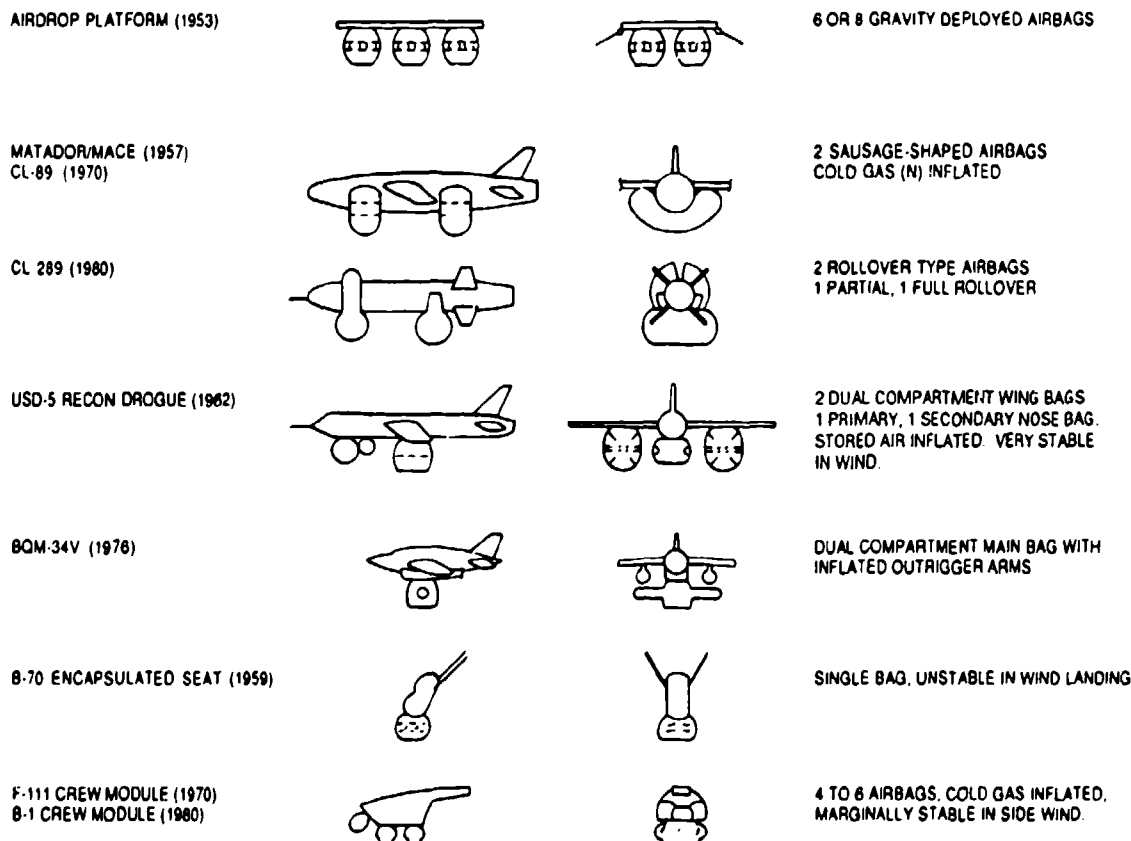


FIGURE 6-79. Air Bag Configurations for Various Air Vehicles.

TABLE 6-12. Air Bag System Data Related to Figure 6-78.

Application	Year	Vehicle weight, lb	Rate of descent, ft/s	Allowable impact deceleration, g	Reference
Aerial delivery	1952/53	10 to 20K	22	5 to 8	-
Matador/Mace cruise missile	1956	10,800	20	8	6.76
US-5 Reconnaissance drone (USA)	1960	4800	26	7	5.23
B-70 Encapsulated seat	1960	700	28	8	5.23
F-111 Crew module	1962	2700	26	8	6.77
B-1 Crew module	1973	8000	27	10	6.78
BQM-34V Unmanned vehicle	1977	4000	26	8	6.79
CL-289 Reconnaissance drone	1980	475	30	30 max	6.80

atmospheric pressure to eliminate the need for a pressurization system. These air bags had a poor initial shape, poor pressure onset rates, and a poor performance in general. All air bags shown have pressure relief valves. Some of the older bags had single-pressure, pop-out diaphragms. The USD-5 reconnaissance drone had diaphragms for two pressure levels. The recent Canadian CL-289 (USD-502) has pop-out sleeve-type pressure control valves detailed later in this section.

Stability of air bags in wind landings or on an oscillating parachute is a problem. Wind orientation of air bag systems for aligning the long axis of the vehicle with the wind has proven to be impossible. Any side motion must be absorbed by sliding on the ground. Sliding in plowed fields is almost impossible; the dust on dry lake beds acts like a lubricant. Air bags must stay under the vehicle with little deformation. Internal bag cross-bracing is used on the USD-5 bags. The CL-289 uses two pairs of sausage-shaped air bags with the front bag surrounding the vehicle. This arrangement permits a no-damage landing and a quick vehicle turn-around time. The USD-5 uses a wide base for air bag installation, which provides stability in sidewind landing and good sliding characteristics. The BQM-34V air bag design has two arms protecting the wing containers. Encapsulated seat bags as used on the B-70 were unsatisfactory in sidewind landings because of the poor relationship of bag diameter to vehicle height.

Figures 6-80 and 6-81 show two typical air bag valve designs. The Figure 6-80 design was used on the USD-5 dual-compartment air bags. Around the circumference of the air bag are two rows of dual-wall orifices reinforced with steel wire. Into each orifice is inserted a rubber disk with a circular groove. When the internal bag pressure reaches a predetermined level, the rubber diaphragm blows out along the circular groove and reduces bag pressure. It is important to have the valve blow out along the circular groove, thereby providing a controlled opening, rather than having an uncontrolled random blowout.

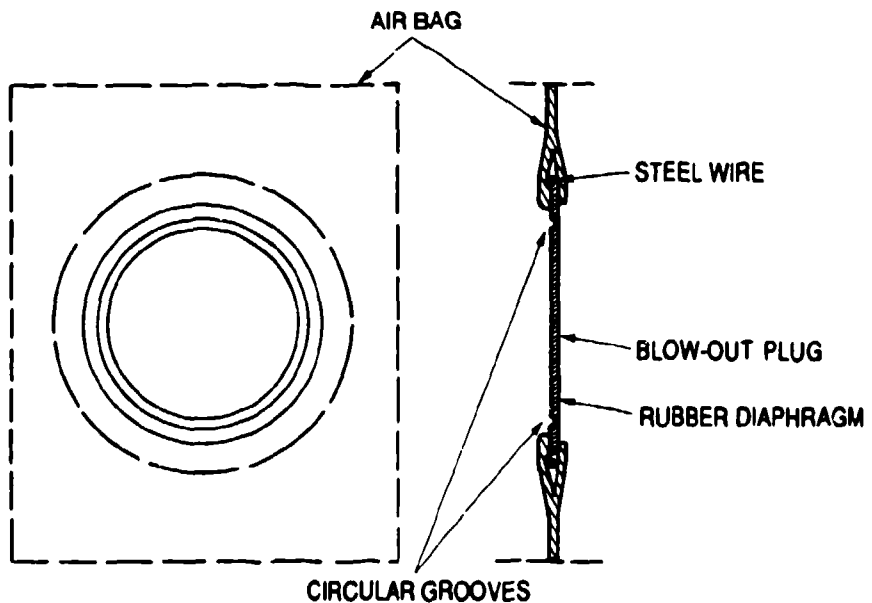


FIGURE 6-80. USD-5 Air Bag Pressure Relief Valve With Blow-Out Diaphragm.

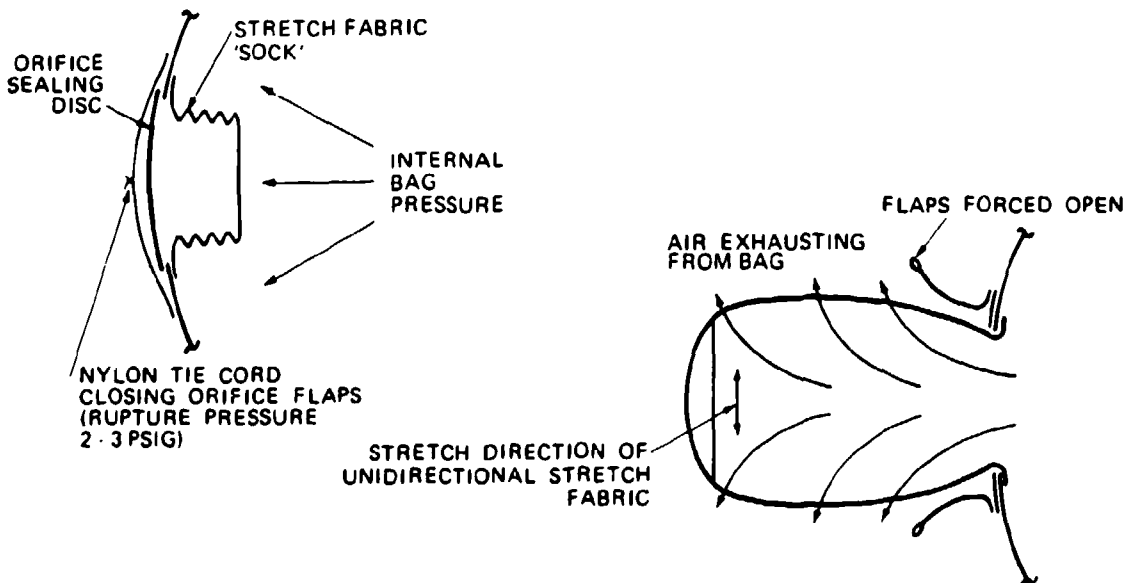


FIGURE 6-81. Pressure Relief Valves for the CL-289 Air Bags Using Stretch Fabric Sleeves.

Figure 6-81 illustrates the variable airflow pressure relief valve used on the CL-289 air bags. The bag orifice is covered by a blow-out disk, and a sleeve fabricated from stretch fabric pops out and meters the airflow from the bag. This stretch fabric sleeve opens at high internal pressure and restricts the airflow to a low pressure. Pop-out metal diaphragms are used on the F-111 air bags.

Most air bags are inflated with nitrogen stored in 3000-psi bottles. Nitrogen is available on most air bases. The USD-5 drone used dried air, stored at 3000 psi. Several air bag systems use injector nozzles with a 1:1 nitrogen-air mixture for inflation of the air bags; this saves considerable weight and volume and minimizes the effects of the temperature drop from the high-pressure storage condition during bag inflation.

6.8.3.4 Rerorocket Landing Attenuation System

Rerorockets may be called long-stroke impact attenuators. Rerorockets are well suited for loads and vehicles that have impact deceleration limits when landing in the 3- to 6-g range that normally results in required deceleration strokes of more than 3 feet. These long deceleration strokes cannot be obtained with air bags or crushable attenuators. Another advantage of rerorockets is their high energy-weight ratio and their capability of decelerating the vehicle before ground contact—a decided disadvantage of air bags and crushables.

The Soviet Union uses rerorocket parachute systems for land landing their cosmonauts on the South Russian plains. They also use rerorocket parachute systems for the airdrop of heavy military cargo.

The U.S. Army Redhead-Roadrunner target/missile is the only operational parachute rerorocket landing system used in the United States so far. The primary reason for the use of rerorockets as impact attenuators on the Redhead and Roadrunner was the resultant weight saving (Reference 6.81).

The Army Natick Research, Development, and Engineering Center in Natick, Mass., in the 1960s and 70s, funded extensive efforts to develop a rerorocket parachute system for landing heavy airdrop platforms. References 6.82 and 6.83 document this development work.

Many studies and some development work has been conducted by NASA, the Air Force, and industry for using rerorockets as impact attenuators for land landing the Gemini and Apollo spacecraft, for planetary landings, and for landing the B-1 bomber crew escape module.

Two rocket installation concepts that have been tested, called harness mounted and body mounted, are shown in Figure 6-82. The harness-mounted installation was used in the Redhead/Roadrunner missile; it is self-centering with relation to the center of gravity of the

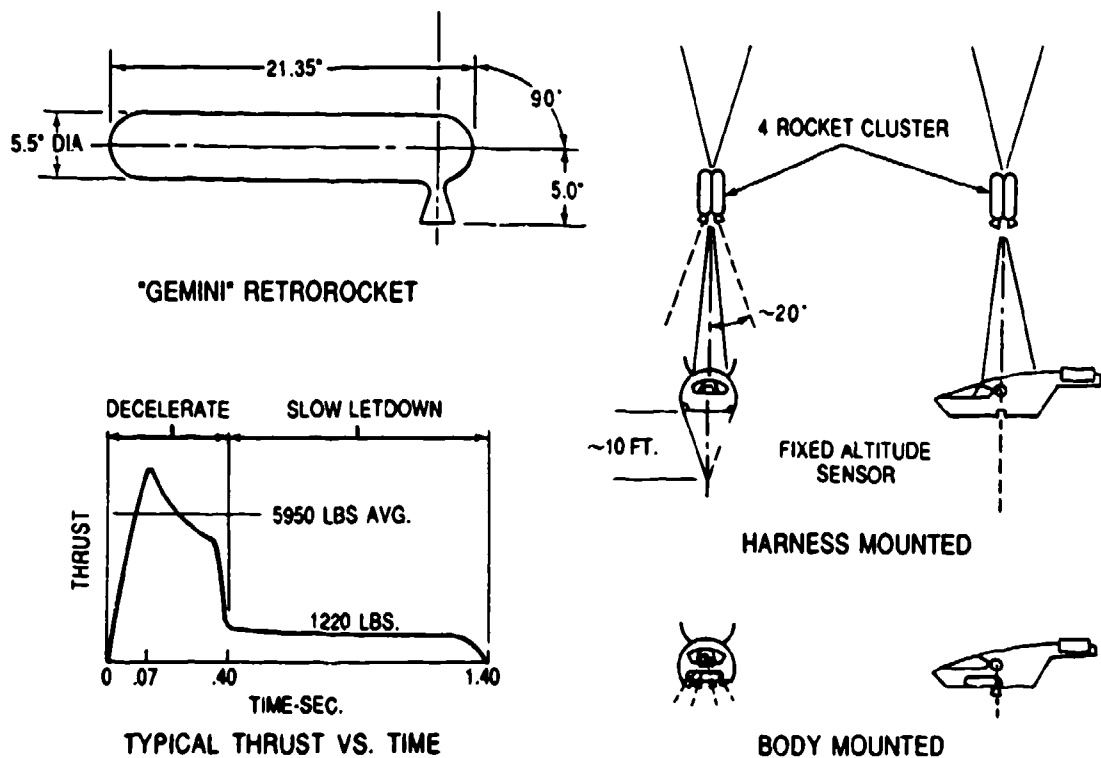


FIGURE 6-82. Details of Retrorocket Design and Installation.

vehicle-parachute system, and the rockets can be located in the parachute compartment. However, a clear deployment path is necessary for moving the retrorockets from the compartment to the operational location; also, some riser heat protection may be required. The body-mounted installation was used on NASA JSC tests for developing a gliding retrorocket parachute landing system for the Gemini spacecraft. The development and full-scale flight tests are described in Reference 6.84, and some work done on the Apollo is described in Reference 6.85. The body-mounted installation is sensitive to center of gravity shifts; and on the Lunar excursion module, retrorockets stirred surface dust so that visibility was impaired.

Retrorockets, like most other impact attenuators, are designed for one energy level. Increasing or decreasing the design rate of descent stops the load above ground or produces a high ground shock. To cope with this problem, NASA developed for the Gemini landing system a two-step rocket. The high thrust level is decreased to a 0.9-g deceleration at the lowest energy level; this low-energy deceleration stops the vehicle slightly above the ground and gently lowers it for final landing.

Air Force investigations for using retrorockets for landing retardation of aircraft crew escape modules are discussed in Reference 6.86. The presence of potentially explosive components in the crew module was a design consideration.

The ratio of parachute air bag and parachute retrorocket weight to total vehicle weight was investigated for the B-1 crew module as shown in Figure 6-83. The optimum weight ratio for a parachute air bag system is obtained at the rate of descent of 25 to 30 ft/s. The optimum weight for a parachute retrorocket system is in the range of 35 ft/s and above. This rate of descent may be too high for manned vehicles if the requirement exists for minimum aircrew injury at rocket malfunction.

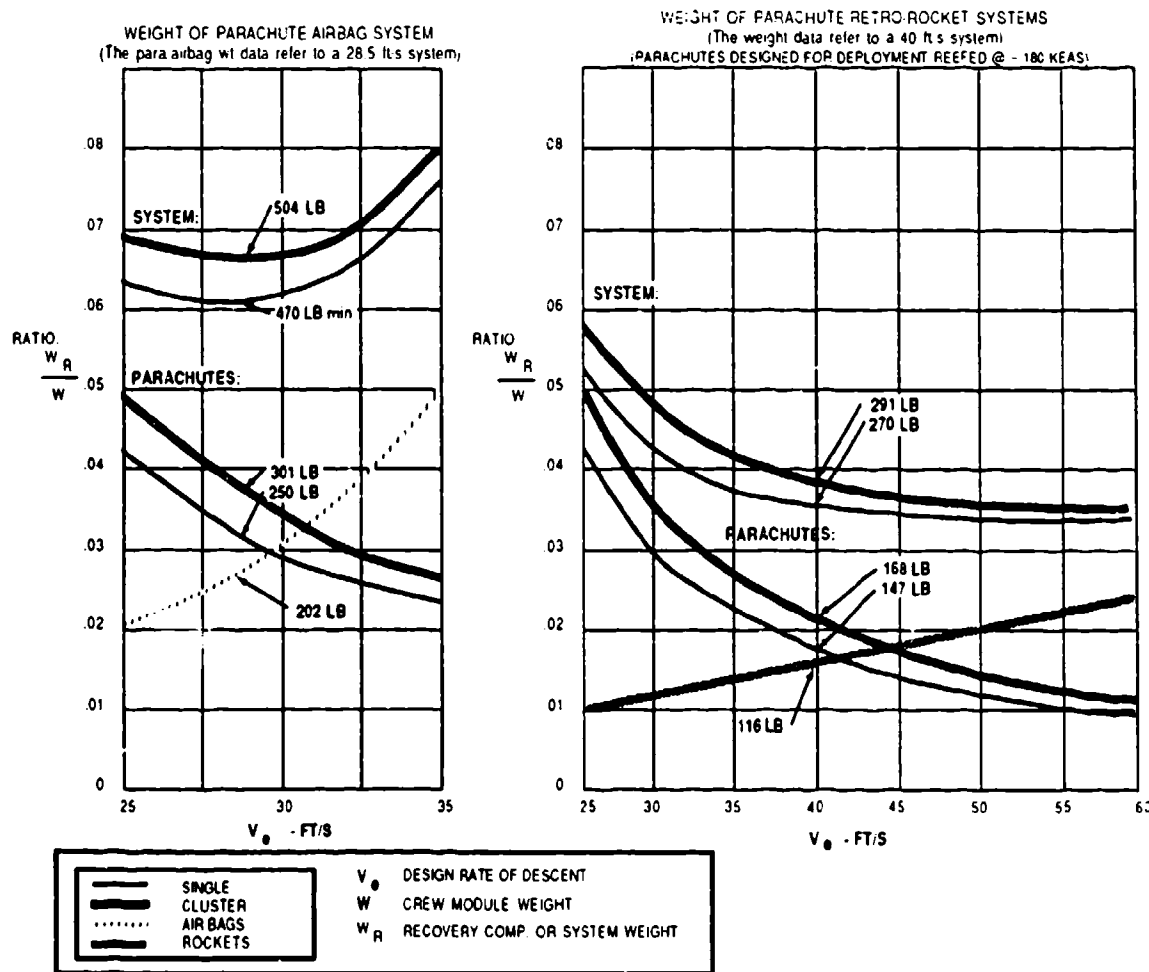


FIGURE 6-83. Weight Comparison of a Parachute-Air Bag and a Parachute-Retrorocket System for a 7800-Pound Crew Module.

Several methods have been investigated and used for determining the exact starting altitude for the retrorockets. The Redhead/Roadrunner drone used an extendable mechanical feeler with a microswitch at the end of the feeler. A similar approach was used for the NASA-tested Gemini retrorocket concept and is used by the Soviet Union for its retrorocket impact attenuators for airdrop of heavy vehicle-platform systems. The Apollo Lunar Excursion Module (LEM) used a highly sensitive radar for firing the retrorockets for the moon landing. An optical altitude sensor for firing retrorockets at a precise altitude is described in Reference 6.87.

6.8.3.5 Skirt Jet Retrorocket System

Northrop, during the Apollo development, tested an unusual retrorocket concept called the "skirt jet," which was tailored to the Apollo command module. Figure 6-84 illustrates the concept. A tube filled with rocket fuel, and having a slotted nozzle, was placed around the skirt of the command module. Tests proved that firing the rocket tube less than 30 degrees inward increased the thrust close to the ground. Development and testing of this approach is discussed in Reference 6.88.

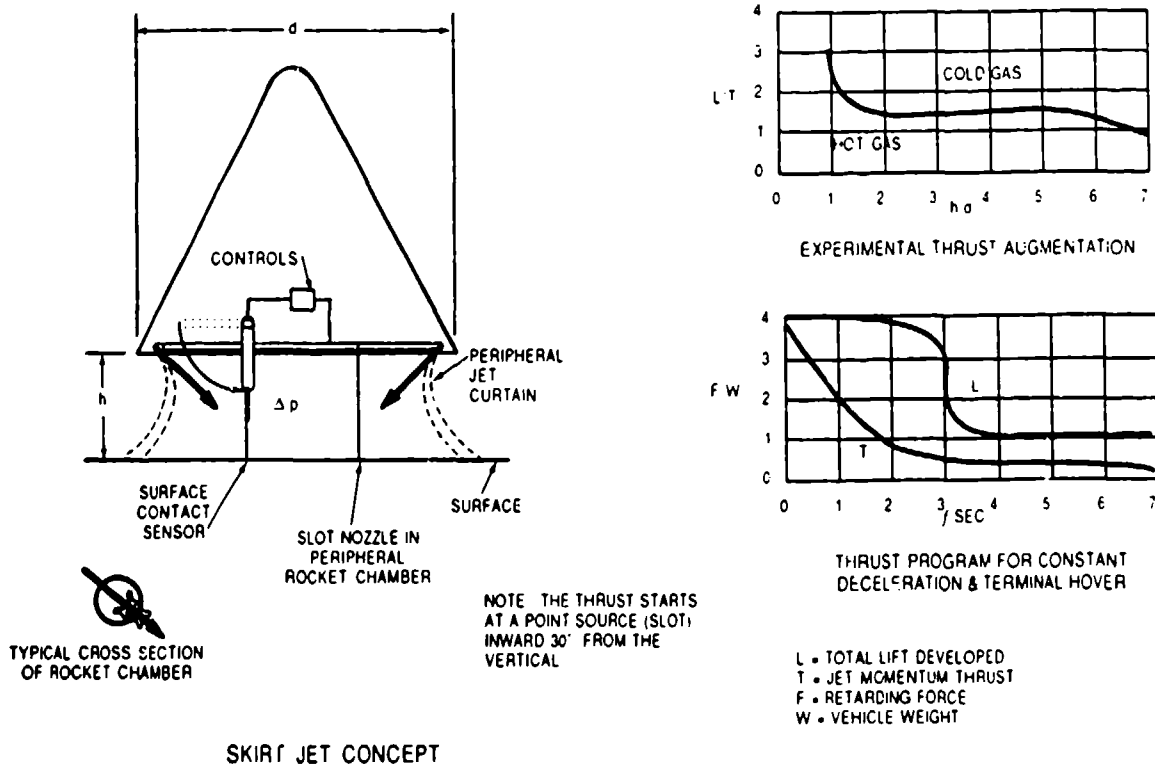


FIGURE 6-84. Design and Performance Details of the Skirt Jet Retrorocket System.

6.8.3.6 Special Impact Attenuators

Nose Cone Deformation: Several vehicles have used a crushable nose cone as an impact shock absorber. Use of a crushable nose cone requires that the vehicle or container descend in a nose-down attitude. The U.S. Army uses this concept on the airdroppable M4-A high-speed aerial delivery container. The container and the energy absorption characteristics are illustrated in Figure 6-85 taken from Reference 6.68.

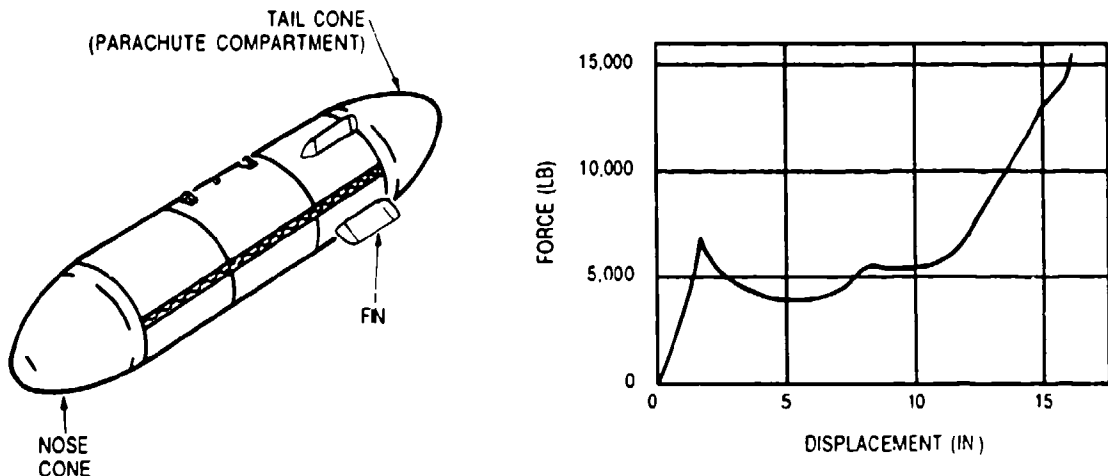


FIGURE 6-85. Army CTU-2A High-Speed Aerial Delivery Container With Crushable Nose Cone and Impact Decelerating Force Versus Cone Deformation.

Nose Spike: Nose spikes have been used successfully for impact attenuation of mostly cylindrical containers descending in a vertical position. Figure 6-86 illustrates a typical nose spike arrangement, and Reference 6.89 describes the use of a nose spike as impact attenuator on the Lockheed X-7 supersonic ramjet test vehicle.

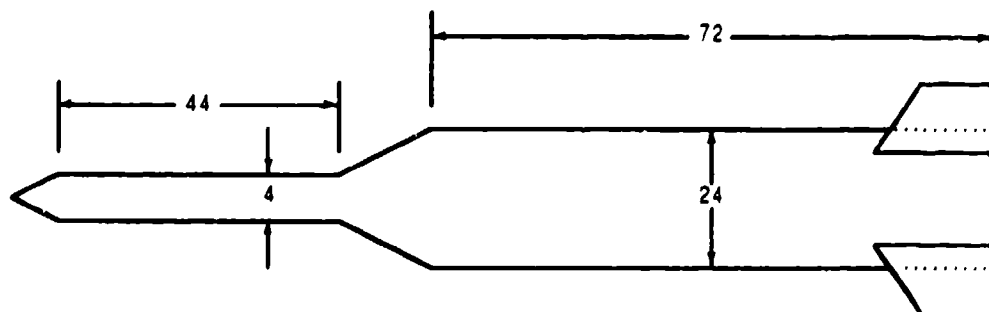


FIGURE 6-86. Typical Nose Spike Impact Attenuator.

Nose spike impact attenuators are simple in design, reusable, require no maintenance, but have operational limitations. Nose spikes cannot be used in rocky terrain. A rate of descent of 35 ft/s is necessary to ensure sufficient ground penetration for the vehicle to remain upright. The ratio of vertical to horizontal velocity in high-wind landings should be 2.5 or better to prevent the vehicle from falling over and being damaged.

Water Landing: The Mercury, Gemini, Apollo, and the Space Shuttle solid rocket boosters (SRB) land on parachutes in water. Water is an excellent hydraulic shock absorber. However, all three manned spacecraft landed on the flat heat shield but under an angle to obtain a wedge-type water entry for limiting the impact deceleration to less than 6 g (References 5.10, 6.84, 6.90, 6.91, and 8.5 through 8.11).

The Space Shuttle SRB originally parachute-descended into the water at a rate of descent of 85 ft/s, based on model test results. However, this rate of descent had to be reduced to 75 ft/s to minimize damage to the rocket structure.

Airdropped mines and torpedos use parachute retardation to limit water entry velocities to 200 ft/s or less to avoid structural damage and to obtain water entry angles that eliminate ricochet.

6.9 REFERENCE MATERIAL

- 6.1 T. P. Pawlikoski. "Drogue Mortar Simulation Development and Performance Evaluation." AIAA Paper, October 1986. (AIAA 86-2490.)
- 6.2 C. W. Peterson, et al. "Design and Performance of a Parachute for Supersonic and Subsonic Recovery of an 800-Lb Payload." AIAA Paper, October 1986. (AIAA 86-2435.)
- 6.3 J. L. Charleville. "The F-111 Crew Module Development." AIAA Paper, September 1970. (AIAA 70-1210.)
- 6.4 B. A. Engstroem and W. C. Buhler. "Mid Air Retrieval System for the Air Launched Cruise Missile (Boeing AGM 68)." AIAA Paper, October 1981. (AIAA 81-1915.)
- 6.5 U.S. Air Force. *G-11A Parachute Retardation System*, by I. Svoboda. USAF, February 1961. (USAF Report FTC-TM-61-102.)
- 6.6 ——. *Investigation of G-12D Parachute for Recovery of 8,000-Lb. Load*, by C. W. Marshall. USAF, July 1958. (USAF Report FTC-LR-59-110.)
- 6.7 U. S. Navy. *Investigation of Low Bulk Personnel Parachute, 26-Ft Conical*, by H. R. Moy. USN, El Centro, Calif., April 1953. (USNEC Report 7-53.)
- 6.8 U.S. Air Force. *Development of a Final Stage Recovery System for a 10,000 Lb. Weight*, by E. A. Gimelouski. USAF, December 1958. (USAF Report WADC-TR-59-109.)
- 6.9 G. A. Barnard. "Analysis of the Distribution of Load Among the Lines of an Inflating Cruciform Parachute." AIAA Paper. (AIAA 86-2441 CP.)
- 6.10 L. J. Long and Y. A. Staphenhill. "Development of a Large Cross Parachute with Deflation Pockets for a Water Landing Concept." AIAA paper, October 1986. (AIAA 86-2442 CP.)
- 6.11 A. J. Fallon, J. W. Watkins, and E. D. Vickery. "The Annular Parachute: An Approach to a Low Altitude Personnel Parachute." AIAA Paper, October 1986. (AIAA 86-2449.)
- 6.12 Specification MIL-P-5905A. "Parachute, Ribbed Guide Surface. General Specification for Construction of."
- 6.13 D. J. Kolega, W. R. Woodis, and J. D. Reuter. "Vent Modification of Large Ribbon Parachutes to Enhance Cluster Performance." AIAA Paper, October 1986. (AIAA 86-2433.)
- 6.14 D. W. Johnson. "All Radial Construction for Continuous Ribbon Parachutes." U.S. Patent No. 4-343-448.

- 6.15 General Dynamics. *B-58 Escape Capsule Stabilization Parachute System Development*, by T. H. Etherton, F. T. Burns, and L. C. Norman. GD, Fort Worth, Tex., February 1962. (GD Report FZA-4-408.)
- 6.16 J. L. Charleville. "The F-111 Crew Escape Module." AIAA Paper, March 1970. (AIAA 70-1210.)
- 6.17 U.S. Air Force. *Study and Exploratory Freeflight Investigation of Aerodynamic Decelerators Operating at High Altitudes and at High Mach Numbers*, by W. E. Nickel and L. W. Simms. USAF, July 1964. (USAF Report FDL-TDR-64-35, Vol. I.)
- 6.18 ———. *Study of Parachute Performance and Design Parameters for High Dynamic Pressure Operation*, by P. E. Pedersen. USAF, May 1964. (USAF Report FDL-TDR-64-66.)
- 6.19 L. W. Simms. "Concept, Aerodynamics, and Design Details of Hyper Flo Parachutes—A Summary." Paper presented at the University of Minnesota Short Course on Aerodynamic Deceleration, Minneapolis, Minn., July 1965.
- 6.20 National Aeronautics and Space Administration. *An Investigation of the Initial Century Series Ringsail Parachutes*, by L. C. Norman and K. L. Suit. NASA, August 1970. (NASA Report NASA-TND-5968.)
- 6.21 Irvin Industries, Inc. *20K Parachute System, Final Report*. II, August 1967. (IAC Report GIR 85-150.)
- 6.22 Naval Surface Warfare Center. *Wind Tunnel Tests of a 20-Gore Disk-Gap-Band Parachute*, by W. P. Lutke. NSWC, May 1989. (NSWC TR 89-180.)
- 6.23 Royal Aircraft Establishment. *A Geometric Basis for Taschengurt Design*, by H. J. Waters. RAE, Farnborough, England, December 1953. (Mech. Eng. Technical Note ME-162.)
- 6.24 ———. *Tests in the 24-Ft Wind Tunnel for Increasing the Critical Opening Speed of a Parachute*, by S. B. Jackson, C. H. Trent, and T. J. Nethrem. RAE, Farnborough, England. (Report AM-357.)
- 6.25 J. E. Purvis. "Pocket Band Effect on Ringslot Parachutes." Paper presented at the University of Minnesota-CCG lecture on parachute systems technology, Munich-Oberpfaffenhofen, June 1987.
- 6.26 U.S. Air Force. *Investigation of the Relative Efficiency of Pilot Chutes*, by R. C. Cory. USAF, March 1956. (USAF Report WADC-TR-56-147.)
- 6.27 G. W. Stevens. "The Net-Skirt to a Parachute as a Device to Prevent Inversions." AIAA Paper, October 1981. (AIAA 81-1927.)

- 6.28 Royal Aircraft Establishment. *The Net-Skirt Extension on Man-Carrying Type Parachutes*, by G. W. Stevens. RAE, Farnborough, England. (Report ME-389.)
- 6.29 U. S. Army. *Evaluation of T-10 Personnel Parachute With 3 3/5 Inch Mesh Net*. USANDC, Natick, Mass., April 1975. (PIT. TECOM Project No. 8-EG-060-010-003.)
- 6.30 U.S. Air Force. *Deployment Bags, Parachutes, General Development*, by R. W. Barnes. USAF, September 1949. (USAF Report MCREXE-672-23-L.)
- 6.31 K. French. "A First Order Theory for the Effect of Line Ties on Parachute Deployment." AIAA Paper, October 1974. (AIAA 74-0450.)
- 6.32 R. J. Speelman III. "Parachute Deployment Process Testing Technique," *AIAA Journal of Aircraft*, Vol. 14, No. 4, pp. 401 and 402, 1977.
- 6.33 H. E. Widdows. "Parachute Deployment Control Assembly." U.S. Patent No. 3-145-956, August 1964.
- 6.34 D. T. Reynolds and W. M. Mullins. "Stress Analysis of Ribbon Parachutes." AIAA Paper, November 1975. (AIAA 75-1372.)
- 6.35 W. L. Garrard. "Stress Analysis in Parachute Canopies." Paper presented at the University of Minnesota-CCG lecture on parachute systems technology, Munich-Oberpfaffenhofen, June 1987.
- 6.36 W. L. Garrard, M. L. Konicke, K. S. Wu, and K. K. Muramoto. "Measured and Calculated Stress in a Ribbon Parachute Canopy." *AIAA Journal of Aircraft*, Vol. 24, No. 2, pp. 65 to 72, February 1987.
- 6.37 W. D. Sundberg. "A New Solution Method for Steady-State Canopy Structural Loads." AIAA Paper. (AIAA 86-2489 CP.)
- 6.38 K. G. Lindh. "Tension Impact Tests on Nylon Webbing Structures." AIAA Paper, September 1970. (AIAA 70-1182.)
- 6.39 J. W. Purvis "Improved Prediction of Parachute Line Sail During Line-First Deployment," AIAA Paper, April 1984. (AIAA 84-0786.)
- 6.40 R. W. Rodier. "Reeling the Space Shuttle SRB-DSS Drogue Parachute." AIAA Paper, March 1979. (AIAA 79-0434.)
- 6.41 R. D. Moog, J. D. Sheppard, and D. A. Kross. "Space Shuttle Solid Rocket Booster Decelerator Subsystem Drop Test Results." AIAA Paper, March 1979. (AIAA 79-0463.)

- 6.42 D. W. Johnson. "Status Report of a New Recovery Parachute System for the F-111 Aircraft Crew Escape System." AIAA Paper. (AIAA 86-2437 CP.)
- 6.43 Northrop Ventura. *Reliability Trade-Off Analysis of Two-Stage Reefing System for Apollo Main Parachutes*, by A. E. Johnson. NV, September 1967. (NV Report NVR-6055.)
- 6.44 National Aeronautics and Space Administration. *Aerodynamic and Deployment Characteristics of Multi-Stage Canopy and Suspension Line Reefing System for a Twin-Keel All-Flexible Parawing*, by H. L. Morgan and A. D. McHatton, NASA, July 1971. (NASA Report NASA-TN-D-6306.)
- 6.45 ———. *Free Flight Investigation of Large All-Flexible Parawings and Performance Comparison With Small Parawings-Final Report*, by J. H. Moller, E. M. Linhart, W. M. Gran, and L. T. Parson. NASA, March 1970. (NASA Report NASA-CR-66918.)
- 6.46 E. D. Vickery, M. L. Eldredge, C. R. Vernet, and W. G. Jolly. "Development of a System of Six Clustered 137-Ft. Diameter Parachutes for Recovery of a 60,000 Lb Load." AIAA Paper, October 1986. (AIAA 86-2445.)
- 6.47 D. W. Johnson. "Apparatus for Simultaneously Disreefing a Centrally Reefed Clustered Parachute System." U.S. Patent No. 4-752-050, June 1988.
- 6.48 S. J. Barlog. "Practical Aspects of Reefing Cutter Design." AIAA Paper, March 1979. (AIAA 79-0418.)
- 6.49 Sandia National Laboratories. *Development of an Electronic Time Delay Reefing Line Cutter for Parachutes*, by W. B. Pepper, G. H. Bradley, and W. C. Jacoby. SNL, December 1973. (SNL Report SLA-73-0989.)
- 6.50 ———. *Development of the MC-3133 Reefing Line Cutter*, by J. R. Craig. SNL, September 1977. (SNL Report SA1 D77-0955.)
- 6.51 Northrop Ventura. *Apollo Main Cluster Reefing*, by D. W. Dunn, S. J. Axel, and W. M. Gran. NV, May 1964. (NV Report NVR-3538.)
- 6.52 DuPont de Nemours & Co. *Properties of DuPont Industrial Filament Yarns*. DuPont de Nemours & Co., Textile Fiber Department, Technical Service Section, Wilmington, Del. 19898, April 1982. (DuPont Bulletin X-267.)
- 6.53 Naval Weapons Center. *Evaluation of Lightweight Fabric Woven from 55 and 75 Denier Kevlar Yarn*, by R. W. Hunter. NWC, China Lake, Calif., 1 February 1984. (NWC TM 5170).
- 6.54 C. W. Peterson, W. R. Pepper, D. W. Johnson, and I. T. Holt. "Kevlar Parachute Design and Performance." AIAA Paper, April 1984. (AIAA 84-0810 CP.)

- 6.55 J. F. McNelia. "Relative Volumetric Efficiency of Kevlar vs. Nylon Parachute Designs." Paper presented at the Parachute Manufacturing Seminar, Piedmont Community College, Roxboro, N. C. 27573, March 1988.
- 6.56 U.S. Air Force. *Materials and Design Criteria for Kevlar Ribbon Parachutes*, by W. R. Pinnell. USAF, April 1982. (USAF Report AFWAL-TR-81-3138.)
- 6.57 S. Beare. "New Lightweight Parachute Fabrics of Kevlar Aramid Fiber," AIAA Paper, April 1989. (AIAA 89-0911.)
- 6.58 U.S. Air Force. *Development of Kevlar 29 Decelerator Systems Material*, by N. J. Abbott and R. J. Coskren. USAF, November 1978. (USAF Report AFFDL-TR-78-201.)
- 6.59 Naval Weapons Center. *Evaluation of Kevlar Materials, FY 83 to FY 85*, by R. I. Tubis. NWC, China Lake, Calif., August 1985. (NWC TM-5604.)
- 6.60 U.S. Air Force. *Kevlar Properties Investigation, High-Speed Abrasion Resistance*, by S. L. Goodwin and N. J. Abbott. USAF, February 1980. (AFWAL-TR-80-300.)
- 6.61 Naval Weapons Center. *Kevlar Stitching Patterns*, by R. I. Tubis. NWC, China Lake, Calif., September 1986. (NWC TP 6761.)
- 6.62 K. E. French. "A New Correlation of Parachute Weight Data." *AIAA Journal of Spacecraft and Rockets*, Vol. 8, No. 1, January 1971, pp. 71 and 72.
- 6.63 U.S. Air Force. *Study of Pressure Packing Techniques for Parachutes*, by W. J. Bridwell. USAF, September 1961. (USAF Report ASD-TR-61-426.)
- 6.64 National Aeronautics and Space Administration. *Analytical Investigation of an Inflatable Landing System Omnidirectional and Multiple Impact Capability*, by J. R. McGehee. NASA, May 1969. (NASA Report NASA-TN-D-5236.)
- 6.65 ——. *A Mathematical Procedure for Predicting the Touchdown Dynamics of a Soft-Landing Vehicle*, by G. A. Zupp. NASA, February 1971. (NASA Report NASA-TN-D-7045.)
- 6.66 U.S. Navy. *Application of Analog/Hybrid and Hybrid Computers to the Study of Shock Mitigation Systems*, by C. L. Patterson. NSRD, November 1970. (NSRD4A-6-28/70.)
- 6.67 U.S. Army. *Design of Cushioning Systems for Air Drop*, by M. P. Gionfriddo. USANDC, Natick, Mass., February 1967. (USANDC Report 67-59-AD.)
- 6.68 U.S. Army Material Command. "Design for Air Transport and Air Drop of Material," *Engineering Design Handbook*. USAMC, December 1967. (Pamphlet No. AMCP 706-130.)

- 6.69 University of Texas. *Design of Cushioning Systems for Air Delivery of Army Equipment*, by D. C. Ellus. UT, Austin, Tex., August 1961.
- 6.70 U.S. Army NLABS. *Variations in the Crushing Strength of Paper Honeycomb*, by E. P. Ripperger. USANLABS, December 1969. (USANLABS-TR-70-57-AD.)
- 6.71 University of Texas. *Cushioning for Air Drop, Parts I to VIII*, by J. W. Turnbow, et al. UT, Austin, Tex., 1955 to 1958. (Publications of UT, Structural Mechanics Research Laboratory.)
- 6.72 U.S. Air Force. *Development of a Paperboard Honeycomb Decelerator for Use With Large Platforms in Aerial Delivery Systems*, by H. W. Bixby. USAF. (USAF Report WADC-TR-59-776.)
- 6.73 National Aeronautics and Space Administration. *The Design and Development of Radio-Frequency Transparent Omnidirectional Energy-Absorbing Element Systems*, by R. H. Smith. NASA, January 1967. (NASA Report NASA-CR-66301.)
- 6.74 S. R. Mehaffie. "Foam Impact Attenuation System." AIAA Paper. (AIAA 79-0416.)
- 6.75 Northrop Ventura. *Impact Attenuation Systems*, by M. Neustadt. NV, December 1963. (NV Report NVR-2900.)
- 6.76 K. Idomir. "TM-76 Mace Landing Mat Design," *Aero/Space Engineering*, Vol. 19, February 1960, pp. 28 to 34.
- 6.77 U.S. Air Force. *Experimental Investigation of the Ground Impact Characteristics of a Full-Scale Aircraft Emergency Escape Capsule System (F-111)*, by R. L. Peterson and E. O. Roberts. USAF, July 1972. (USAF Report AFFDL-TR-72-34.)
- 6.78 ——. *Analysis of B-1 Crew Escape Module Impact Attenuation Test Results*, by E. O. Roberts. USAF, February 1974. (USAF Report AFFDL-TM-74-30-FER)
- 6.79 C. T. Turner and L. A. Girard, Jr. "Air Bag Impact Attenuation System for the AQM-34¹ Remote Piloted Vehicle." AIAA Paper, October 1981. (AIAA 81-1917.)
- 6.80 D. Webb and L. Palm. "Development of a Nylon-Kevlar Recovery System for the CL-289 (USD-502) Surveillance Drone." AIAA Paper, October 1981. (AIAA 81-1952.)
- 6.81 North American Aviation. *Redhead/Roadrunner Target/Missile System, Final Report*. NAA, February 1966. (NAA Report 64H-460 (AD 482 818).)
- 6.82 U. S. Army NLABS. *Parachute Retrorocket Airdrop System, Final Engineering Report*, by J. L. Michael, A. L. Oates, and A. L. Martinez. USANLABS, July 1972. (USANLABS-TR-72-16 (AD 736 361).)

- 6.83 U. S. Army NLABS. *Advanced Development of a Parachute Retrorocket Airdrop System*, by G. Chokoian. USANLABS, May 1973. (USANLABS-TR-73-59.)
- 6.84 National Aeronautics and Space Administration. *Gemini Land Landing System Development Program*, Vol. I and II, by L. C. Norman. NASA, March 1967. (NASA Report NASA-TN-D-3869.)
- 6.85 ———. *Attenuation of Land Landing for Manned Spacecraft*, by J. E. McCullough, F. A. Stafford, and F. A. Benson. NASA, April 1964. (NASA Report NASA-CR-53291.)
- 6.86 U.S. Air Force. *Design Analysis for a Parachute/Retrorocket Landing System for an Aircraft Crew Escape Module*, by C. A. Babisch. USAF, February 1973. (USAF Report AFFD/FER.)
- 6.87 ———. *An Active Optical Ground Sensor for a Parachute Retrorocket Airdrop System*, by R. Ulrich and A. J. D'Onofrio. USAF, February 1973. (USAF Report HDL-TM-73-2 (AD 911 216L).)
- 6.88 E. G. Ewing and G. Frank. "The 'Skirt Jet' Impact Attenuation System," *Proceedings of the ALAA Aerodynamic Deceleration Systems Conference*. Houston, Tex., September 1966.
- 6.89 U.S. Air Force. *X-7A Supersonic Ramjet Test Vehicle Parachute Recovery System*. USAF, June 1955. (USAF Report WADC-55-162.)
- 6.90 Northrop Ventura. *Project Mercury, Landing Parachute Development and Qualification*, by W. C. Buhler. NV, October 1961. (Northrop-Radioplane Report No. 2312.)
- 6.91 National Aeronautics and Space Administration. *Project Gemini, A Technical Summary*, by P. W. Malik and G. A. Souris. (NASA Report NASA-CR-1106.)

CHAPTER 7

DESIGN OF A PARACHUTE RECOVERY AND LANDING SYSTEM

This chapter deals with the design of a parachute recovery and landing attenuation system for a military reconnaissance drone. The prime emphasis in the design of this system is on undamaged recovery of the drone from the total flight performance envelope during the development and test phase, on undamaged recovery after a completed mission during military operations, and on multiple use of the recovery system. An engineering team conducts performance and system analyses and chooses what recovery concept to use, what types of parachutes to select for high-speed deceleration and for final recovery, and what impact-attenuation system is best for the particular application. This chapter covers the selection process for concepts and components. Different engineers may make different selections based on experiences with particular types of parachutes or deployment concepts; experience is always a viable reason for selecting a particular approach. However, using the selection criteria shown in Figure 2-6, the designer must put reliability of operation, undamaged recovery, reusability of the landing system, and minimum weight and volume at the top of the list of requirements.

7.1 REQUIREMENTS

7.1.1 System Requirements

An unmanned air vehicle used for military reconnaissance must be recovered after a completed mission in rough terrain, undamaged and ready for multiple reuse. The recovery system must be able to

1. Recover the air vehicle after the completed mission when the vehicle has landed in rough terrain at altitudes from sea level to 5000 feet.
2. Recover the drone during the engineering test phase from all controlled and uncontrolled flight conditions.
3. Serve as a range-safety device to prevent the air vehicle from leaving the boundaries of the test range.

The air vehicle has a takeoff weight of 7200 pounds and a landing weight, after the completed mission, of 4800 pounds. Undamaged landing shall be possible in rough terrain with rocks up to 8 inches in diameter. Replacement parts and refurbishment cost shall be kept to a minimum.

7.1.2 Requirements for Normal Operation

Drone weight at recovery after completed mission $W_d = 4800 \text{ lb}$
 Recovery velocity $v_0 = 150 \text{ to } 200 \text{ KEAS}$
 Minimum recovery altitude $H_o = 2000 \text{ ft above ground level (AGL)}$
 Maximum ground level $H = 5000 \text{ ft}$
 Maximum allowable total parachute force $F_o = 16,000 \text{ lb}$
 Maximum allowable impact deceleration at landing $a = 9.0 \text{ g's}$

7.1.3 Requirements for Emergency Operation

Emergency operation includes recovery during the test phase from takeoff to landing and also includes recovery for range-safety reasons.

Drone weight at takeoff $W_{d\max} = 7200 \text{ lb}$
 Maximum recovery velocity at
mean sea level (MSL) $v_0 = 490 \text{ KEAS}$
 Maximum recovery velocity at 38,000 to
50,000 ft altitude $v_0 = 1.5 \text{ Mach}$
 Maximum dynamic pressure $q_{\max} = 812 \text{ lb/ft}^2$
 Maximum allowable parachute force $F_o = 22,000 \text{ lb}$

7.1.4 Requirements Analysis

Three primary requirements pace the design of the recovery system:

1. The drone must be able to land in rocky but level terrain without damage.
2. Refurbishment cost and time shall be kept to a minimum.
3. Recovery must be possible from all flight conditions during the flight test phase, including cases where the out-of-control drone flies off the range.

7.2 LANDING ANALYSIS AND IMPACT-ATTENUATION SYSTEM

7.2.1 Landing Analysis

Three known recovery concepts prevent damage during landing in rocky terrain:

1. Midair retrieval.
2. Dual air bags or dual frangibles.
3. Retrorockets combined with small, nondeflatable air bags.

The need for retrieval helicopters or retrieval aircraft makes Method 1, midair retrieval, impractical. The other two methods are affected by the deceleration distance required to meet the 9-g limit.

In section 6.8 of this manual, the required deceleration distance(s) is determined to be

$$s = \frac{v_{e_1}^2 - v_{e_2}^2}{2g(n\eta - 1)}$$

where

v_{e_1} = velocity of the drone descending on the parachute (rate of descent), ft/s

v_{e_2} = permissible impact velocity, ft/s

g = acceleration of gravity, ft/s²

η = effectiveness of the impact attenuation system used, dimensionless

n = allowable impact deceleration, ratio $n = \frac{a}{g}$

Figure 6-68 of Chapter 6 shows the range of various impact attenuation systems as a function of rate of descent and allowable ground impact deceleration. The information indicates that air bags may be the most practical concept for this application. A cursory analysis indicates that a rate of descent of 25 ft/s at 5000 feet altitude will result in a close to optimum weight ratio of the combined parachute air bag system (see Figure 6-83). Properly designed air bags will have an effectiveness of 65% as shown in the stroke-pressure diagram in Figure 6-78 and allow ground contact or final velocity of close to 0 ft/s.

With these assumptions, the required effective air bag deceleration stroke is obtained

$$s = \frac{25^2 - 0}{(2 \cdot 32.174)(9.0 \cdot .65 - 1)} = 2.0 \text{ ft or } 24 \text{ in.}$$

This deceleration distance is too short for a parachute retrorocket system because of the required timing accuracy and rocket burning time. Retrorocket systems are most practical for deceleration distances greater than 4 or 5 feet. Crushable and frangible impact attenuators are suitable for deceleration distances of less than 15 inches. Air bag systems work best for deceleration distances of 24 to 48 inches. The original assumption that an air bag concept may be the most practical approach for this air vehicle is therefore confirmed.

7.2.2 Impact Attenuator System

The design of impact attenuator systems is discussed in section 6.8 of this manual. Figure 7-1 shows the reconnaissance drone and the air-bag attenuator systems that consist of two deflatable, two-compartment wing-bag bags (A); a single-compartment, deflatable nose bag (B); and a nondeflatable nose-buffer bag (C). The wing bags, the primary energy absorbers, need the already calculated 24-inch effective-deceleration stroke. For design reasons, 33 inches must be added to the bag height, 19 inches for the distance from the wing underside to the underside of the jet air ducts, 10 inches for ground clearance, and 4 inches for bag bottom curvature. These additions result in a total bag height of 57 inches. To ensure landing stability, an air bag height-to-diameter ratio of 1.25 is selected for the two wing bags, resulting in a bag diameter of 48 inches. The cross-hatched lower part of the two wing bags (see Figure 7-1) deflates at impact, but the upper part stays inflated and keeps the drone off the ground. The nose bag, B, helps to absorb the impact and deflates, and the nose of the drone comes to rest on the nondeflatable buffer bag, C. All air bags are inflated from 3000 psi nitrogen containers using aspirators for a 50/50 nitrogen air mixture. The air bags are prepressurized to 2 psi for full bag inflation prior to landing. Multiple blowout valves consisting of staggered blowout rubber disks around the circumference of the air bags control the bag deflation to stay within the 9-g deceleration limit.

The weight of the impact-attenuation system—air bags, nitrogen containers, plumbing, and A/C containers—is estimated from section 6.7 to be 2.2% of the total drone weight, or 105.6 pounds. The air bags should be stored in containers that can be easily removed from the drone for repacking. Air bags must be deployed after the main parachutes are fully open to prevent air-bag damage caused by high dynamic pressure. Air-bag deployment begins with simultaneous pyrojecting of the removable air-bag-container covers and opening of the nitrogen-container valves. The wing bags, the primary nose bag, and the nose-buffer bag inflate. At ground contact, the bags compress, increasing the pressure inside the bags. At a preselected pressure level, the blowout valves (rubber disks, metal disks, or rubber-type sleeves) open and limit the maximum drone deceleration to the preselected level.

Drone weight = 4,800 lb
 Drone wing area = 75 ft²

- A - Wing bags (2)
- B - Nose bag (1)
- C - Nose-buffer bag (1)
- D - Parachute compartment

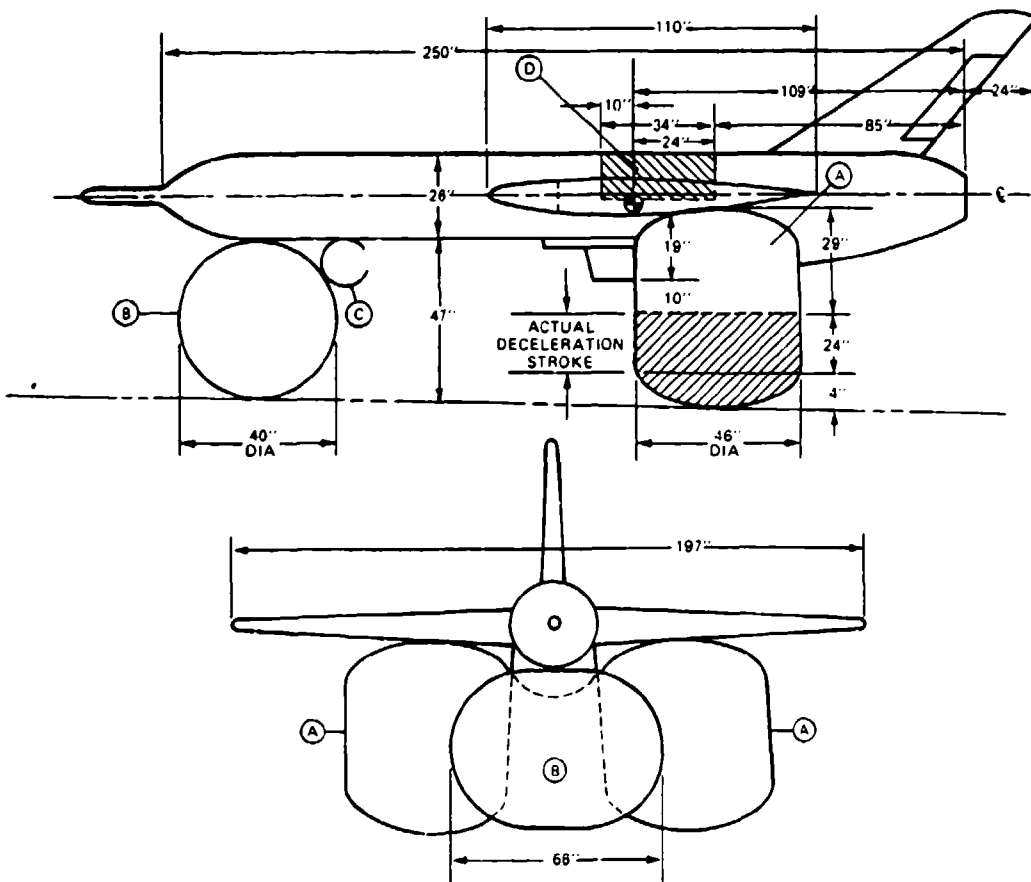


FIGURE 7-1. Reconnaissance-Drone and Air Bag Configurations.

$$\text{deceleration } a = \frac{\text{bag pressure} \cdot \text{bag ground contact area}}{\text{drone weight, } W_d}$$

The drone comes to rest on the upper compartment of the two wing bags and the nose-buffer bag.

The pressure increase in the bags at ground contact, in connection with a short time delay (0.5 to 1.0 second), may be used as a signal for disconnecting the main parachutes to prevent wind-dragging of the drone.

7.3 MAIN PARACHUTE SYSTEM

7.3.1 Main Parachute System Requirements

Weight to be recovered

Operational $W_d = 4800 \text{ lb}$

Test phase $W_{d \text{ max}} = 7200 \text{ lb}$

Recovery velocity $v_0 = 150 \text{ to } 200 \text{ KEAS}$

Recovery altitude $H_0 = 2000 \text{ ft AGL}$

Maximum ground level $H = 5000 \text{ ft}$

Rate of descent $v_e = 25 \text{ ft/s at } 5000 \text{ ft}$

Stability Oscillation of not more than $\pm 5 \text{ deg}$

Maximum total parachute force $F \leq 16,000 \text{ lb} = 3.8g$

Minimum recovery-system weight and volume are prime requirements.

7.3.2 Parachute-Assembly Selection

Section 2.4 defines the criteria for parachute type selection. Requirements for low weight and volume rule out the low-drag slotted parachutes (ribbon, ringslot, and ringsail) as well as guide-surface and cross parachutes (see Tables 5.2 and 5.3). Parachute deployment past the vertical stabilizer rules out a single parachute in favor of a cluster of two parachutes deployed independently left and right of the vertical stabilizer.

No cluster experience is available with annular or cross parachutes, and no reefing experience is available with annular parachutes. Cross parachutes cannot be reefed to the low reefing ratios required for this application. Extended-skirt and polyconical parachutes have been used successfully in clusters of large, reefed parachutes.

A cluster of two conical full extended skirt parachutes is most suitable for this system. In section 5.2, Figures 5-24 and 5-25 show that properly designed extended-skirt parachutes have drag coefficients equal to 0.8 to 0.9 in the 20- to 25-ft/s rate of descent range. Available data (Reference 5.23) indicate that a cluster of two extended-skirt parachutes is sufficiently stable for use with air bags. Extended-skirt parachutes have a low opening-force coefficient of 1.4, compared to an opening-force coefficient of 1.8 for conical and triconical parachutes. Extended-skirt parachutes can also be reefed to low reefing ratios, a requirement for final descent parachutes (see Chapter 5, Figure 5-72).

7.3.3 Parachute Diameter

The rate of descent at 5000 feet altitude was selected to 25 ft/s (see section 7.3.1). The equivalent rate of descent at sea level is

$$v_{e0} = v_e \sqrt{\rho/\rho_0} = 25 \text{ ft/s} \sqrt{\sigma}$$

$\sqrt{\sigma}$ at 5000 feet is 0.9283 (see Table 3-3); therefore,

$$v_{e0} = 25 \text{ ft/s} (0.9283) = 23.2 \text{ ft/s}$$

The required parachute drag area, $(C_{DS})_p$,* for one parachute is calculated

$$(C_{DS})_o = \frac{\text{Half the drone weight, } W_d}{\text{dynamic pressure, } q}$$

$$q = \frac{\rho}{2} v^2 = \frac{v^2}{x} \text{ (see section 5.11)}$$

$$q = \frac{(23.2)^2}{841.4} = 0.641 \text{ lb/ft}^2$$

and the single parachute drag area

$$(C_{DS})_o = \frac{2400}{0.641} = 3744 \text{ ft}^2$$

With this drag area, the parachute surface surface, S_o , is

$$S_o = \frac{(C_{DS})_o}{C_{D0}}$$

*In this manual, $(C_{DS})_p$ and $(C_{DS})_o$ are interchangeable.

The drag coefficient, C_{D_0} , for a conical full extended skirt parachute with a 23.2-ft/s rate of descent and a suspension-line ratio, L_e/D_o , of 1.0 is obtained from Figure 5-25:

$$C_{D_0} = 0.9 \text{ to } 0.92$$

In a cluster of two parachutes, a drag loss of 2% is experienced (see Figure 5-110). Longer suspension lines can somewhat compensate for the loss. Choosing a suspension line/canopy ratio of $L_e/D_o = 1.15$ (see Figure 5-20) results in a drag gain of 1.5%. A drag coefficient $C_{D_0} = 0.9$ is selected for this application.

If the drag coefficient is 0.9, the parachute surface area, S_o , is

$$S_o = \frac{(C_D S)_p}{C_{D_0}} = \frac{3744 \text{ ft}}{0.9} = 4160 \text{ ft}^2$$

and the nominal parachute diameter, D_o , is

$$D_o = \sqrt{\frac{4(S_o)}{\pi}} = 1.1273\sqrt{4160} = 72.7 \text{ ft}$$

A suspension-line ratio of 1.15 is selected. This is the longest practical length for extended skirt parachutes (see Figure 5-20).

The length of the riser, L_r , depends on its installation in the drone; the riser should be long enough to extend beyond the fuselage and vertical stabilizer of the drone (see Figure 7-2), which gives the final configuration of the parachute cluster, including risers and parachutes.

7.3.4 Parachute Deployment System

A cluster of two main parachutes is selected and deployed left and right of the vertical stabilizer to avoid hang-up or damage of a single parachute by the vertical stabilizer. Each parachute needs its own extraction and deployment system to properly deploy past the stabilizer and to avoid interference with the other main parachute during deployment and inflation.

Two fast-opening extraction parachutes are used on each main parachute. Stable parachutes will minimize interference during deployment. Experience with past recovery systems has shown that the most positive deployment is obtained by forced ejection of the extraction or pilot chutes into good airflow past the vertical stabilizer by either mortar or drogue gun ejection. A mortar can eject large, heavy parachutes but creates large reaction forces and needs considerable space for installation. Drogue gun ejection is effective, but is

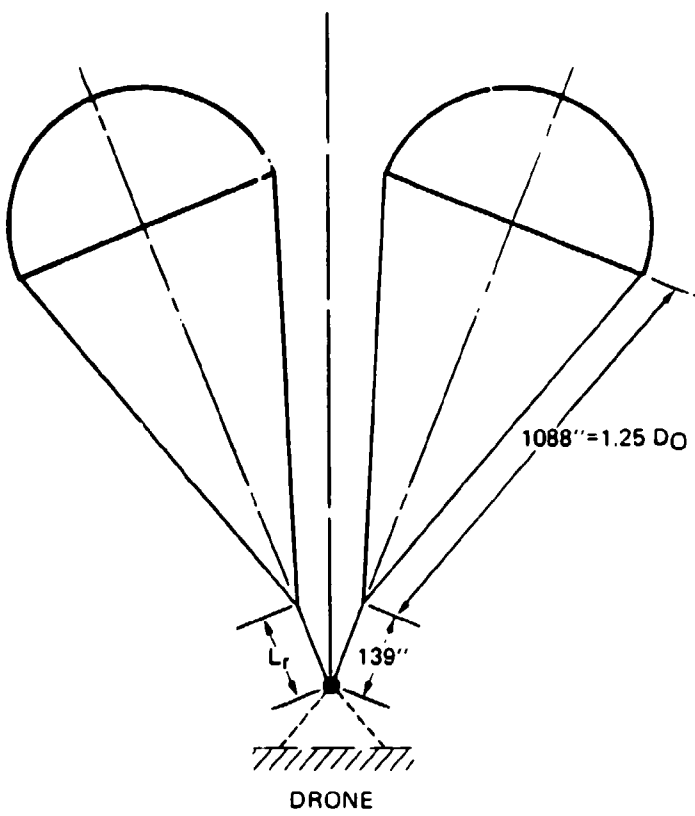


FIGURE 7-2. Cluster of Two 72.7-Foot-Diameter Extended-Skirt Parachutes (Drawn to Scale).

limited to the deployment of small, lightweight parachutes such as pilot chutes. Drogue gun ejected pilot chutes are selected for initiating main parachute deployment. To ensure proper clearance of the vertical stabilizer, the pilot chutes are ejected 45 degrees upward, backward and outward past the vertical stabilizer. The parachute installation in the drone fuselage requires cross-wind deployment and therefore forced ejection of the main parachute deployment bags. Four different methods have been used successfully to accomplish forced ejection: (1) using ejector springs enclosed in a textile cylinder, (2) gas-inflating nonporous ejector bags, (3) catapulting the bag out of the compartment, or (4) using a lift-web arrangement as discussed in section 6.1.

The deployment system selected consists of a drogue gun deployed pilot chute, an extraction parachute, and a main parachute deployment bag lifted from the parachute compartment by lift webs. When the hinged compartment doors open, two drogue gun slugs are fired 45 degrees upward and aft; each slug deploys a pilot chute sufficiently behind the drone into good airflow. These pilot chutes in turn extract two extraction chutes stowed on top

of the main parachute deployment bags. The extraction chutes extract and deploy the two main parachutes left and right of the vertical stabilizers. Lift webs and unsymmetrical bag handles lift the main parachute bags out of the drone compartment and extract the main parachute past the vertical stabilizer (see Figure 7-3).

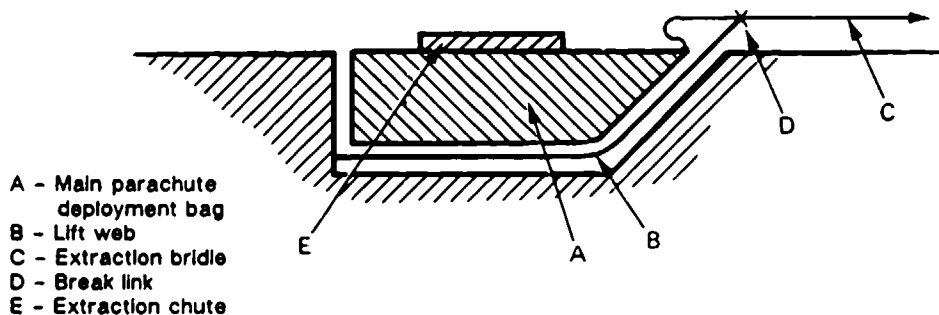


FIGURE 7-3. Parachute Assembly Installation and Extraction Concept.

7.3.5 Extraction Parachute Assembly

The two extraction parachutes must properly deploy the two main parachutes. The size of the extraction parachutes and their location in the wake of the drone is determined as follows:

1. The ratio of the drag area of the extraction parachute, $(C_{DS})_{EP}$, to the drag area of the main parachutes, $(C_{DS})_{MP}$, has been evaluated for various deployment velocities (see section 6.3, Table 6-5). For the 150- to 200-KEAS-velocity range, a $(C_{DS})_{EP}/(C_{DS})_{MP}$ ratio of 0.007 is selected.
2. The leading edge of the extraction parachute must be placed 6 forebody diameters behind the drone to ensure good inflation in the wake of the forebody.

The size of the extraction parachute is determined to be

$$(C_{DS})_{EP} = 0.007 \cdot 3744 \text{ ft}^2 = 26.20 \text{ ft}^2$$

The forebody diameter of the noncylindrical drone fuselage, shown in Figure 7-4 and discussed in section 5.2, is used to determine the location of the extraction parachute.

The equivalent forebody diameter is determined from the netted forebody area $S_{FB} = 4.9 \text{ ft}^2$ to

$$D_{FB} = \sqrt{\frac{4}{\pi} S_{FB}} = \sqrt{\frac{4}{\pi} 4.9 \text{ ft}^2} = 30 \text{ in.}$$

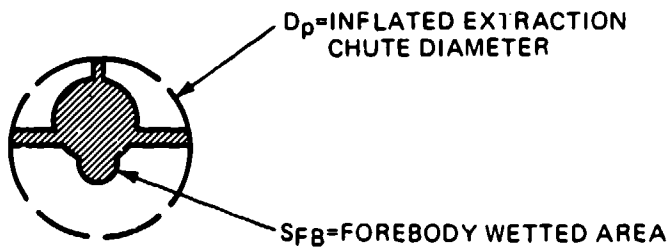


FIGURE 7-4. Determination of Equivalent Forebody Diameter.

The distance between the tail of the drone and the leading edge of the extraction parachute is

$$L = 6 \cdot D_{FB} = 6 \cdot 30 \text{ in.} = 180 \text{ in.}$$

The selected extraction parachute is a stable, reasonably high-drag ringslot parachute with long suspension lines. A ringslot parachute was used as an extraction chute for each Apollo main parachute. Table 5-2 in section 5.1 gives, for a ringslot parachute, a C_{D_0} of 0.56 to 0.65. A medium porosity canopy is selected with a $C_{D_0} = 0.65$. Using suspension lines with an L_e/D_0 ratio of 2 increases the drag coefficient by 10% (see Figure 5-20). Therefore, $C_{D_0} = 0.65 \cdot 1.1 = 0.715$.

The extraction parachute to forebody diameter ratio is

$$\frac{D_p}{D_{FB}} = \frac{5.0}{2.5} = 2.0$$

and the distance behind the forebody-to-forebody ratio is

$$\frac{L}{D_{FB}} = \frac{180 \text{ in.}}{30 \text{ in.}} = 6.0$$

resulting in a drag loss of 13% (see Figure 5-21) and a final C_{D_0} of $0.715 \cdot 0.87 = 0.62$.

The canopy surface area, S_0 , is

$$S_0 = \frac{(C_D S)_{EP}}{C_{D_0}} = \frac{26.20 \text{ ft}^2}{0.62} = 42.3 \text{ ft}^2$$

resulting in a nominal parachute diameter

$$D_0 = 1.1283 \sqrt{S_0} = 1.1283 \sqrt{42.3} = 7.34 \text{ ft}$$

A stable, 7.4-foot-diameter ringslot parachute is selected. The weight of the ringslot extraction parachute can be estimated from section 6.7 to 2.5 pounds, and the weight of the extraction parachute assembly including riser and deployment bag to $1.5 \cdot 2.5$ pounds = 3.75 pounds.

The weight of a single 72.7-foot-diameter main parachute, as determined from section 6.7, is 54 pounds. This weight estimate assumes an efficiently designed main canopy that has a combination of tape and radial seams to carry the radial loads and has other, similar weight-saving design features. The arrangement of the extraction parachute in relation to the drone is shown in Figure 7-5.

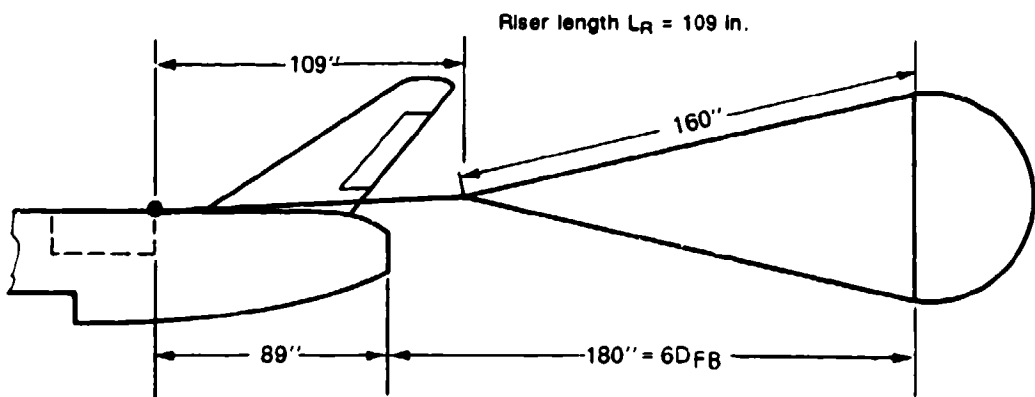


FIGURE 7-5. Extraction-Parachute Assembly.

7.3.6 Pilot Parachute Assembly

The extraction parachute assembly weight of 3.75 pounds is too heavy to be deployed by a drogue-gun slug; therefore, a small pilot chute is selected for initial deployment by the drogue-gun slug. This pilot chute, in turn, will deploy the extraction parachute.

Evaluation of past good and poor deployments has led to the rule that the extraction force of the pilot chute should be greater than or equal to four times the weight of the unit to be extracted; in this case, the extraction parachute assembly. So that the pilot chute has enough force, a pilot chute is selected that will produce, at the minimum deployment speed of 150 KEAS, an extraction force equal to five times the weight of the extraction parachute assembly: $5 \cdot 3.75$ pounds = 18.75 pounds.

The minimum dynamic pressure at 150 KEAS is

$$q_{(150 \text{ KEAS})} = \frac{v^2}{295} = \frac{150^2}{295} = 76.3 \text{ lb/ft}^2 \text{ (see section 5.11)}$$

This results in a pilot chute drag area of

$$(C_{DS})_{PC} = \frac{F_{PC}}{q} = \frac{18.75 \text{ lb}}{76.3 \text{ lb/ft}^2} = 0.25 \text{ ft}^2$$

A fast opening, stable, box-type pilot chute, see Figure 6-32, is selected with a drag coefficient of $C_{D0} = 0.55$. The pilot chute canopy area, S_0 , is

$$S_0 = \frac{0.25 \text{ ft}^2}{0.55} = 0.456 \text{ ft}^2$$

and the parachute diameter, D_0 , is

$$D_0 = 1.1283 \sqrt{S_0} = 1.1283 \sqrt{0.456} = 0.76 \text{ ft}$$

This is a very small parachute. A 2.0-foot-diameter box-type pilot chute with stabilizer vanes is selected. This pilot chute has a steady extraction force, F_{PC} :

$$\begin{aligned} F_{PC} &= (C_{DS})_{PC} q \\ &= 76 \text{ lb/ft}^2 1.73 \text{ ft}^2 = 131.3 \text{ lb for } 150 \text{ KEAS} \\ &= 135 \text{ lb/ft}^2 1.73 \text{ ft}^2 = 233.6 \text{ lb for } 200 \text{ KEAS} \end{aligned}$$

Figure 7-6 shows the pilot chute assembly in relation to the drone, and Figure 7-7 shows the total main parachute subsystem.

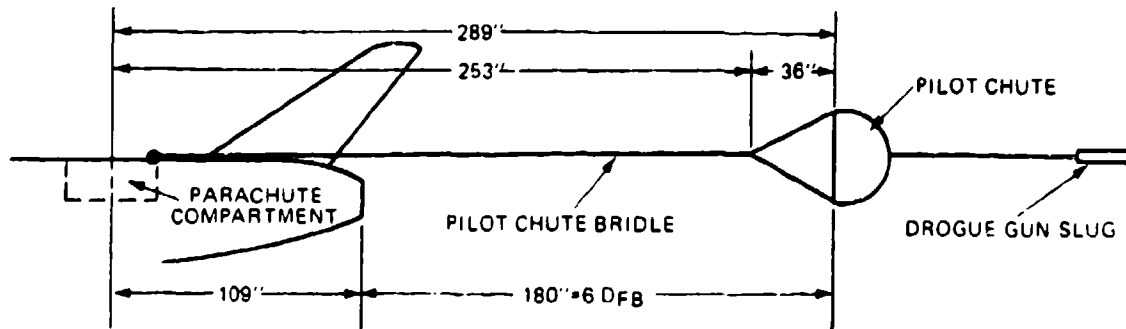


FIGURE 7-6. Pilot Chute Assembly.

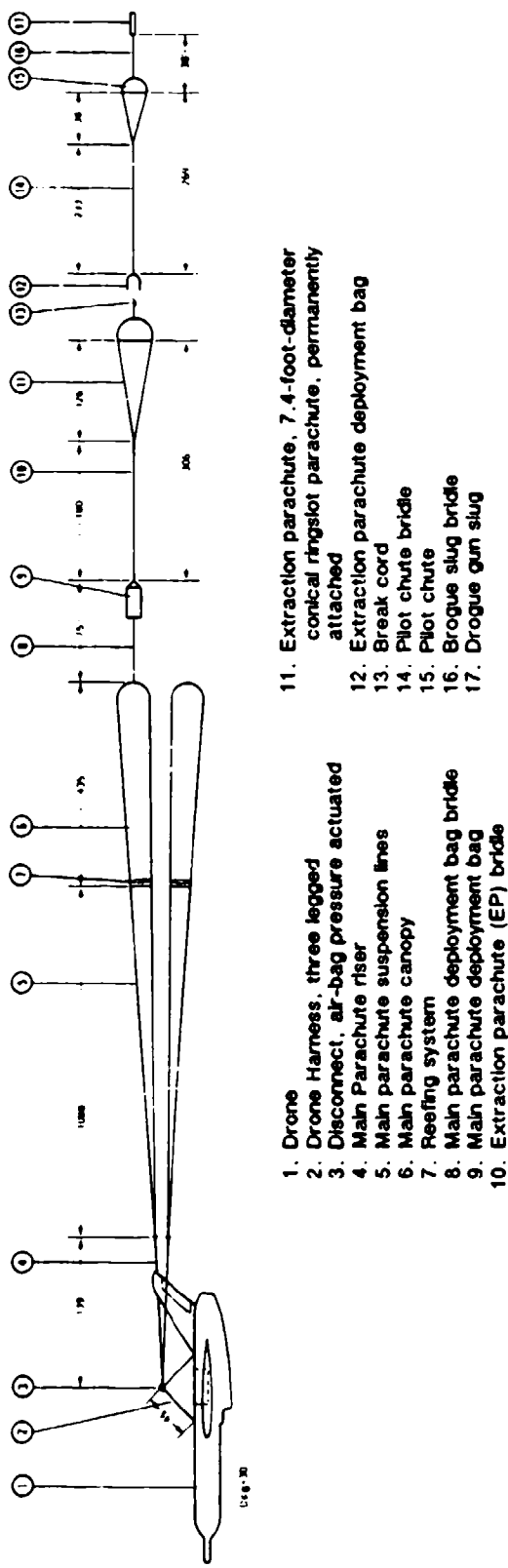


FIGURE 7-7. Main Parachute Assembly; Cluster of Two Parachutes.

7.3.7 Main Parachute Forces

7.3.7.1 Requirements

Drone weight	$W_D = 4800 \text{ lb}$
Maximum deployment speed	$v_o = 200 \text{ KEAS}$
Minimum deployment speed	$v_{o \text{ minimum}} = 150 \text{ KEAS}$
Maximum allowable total parachute force (two main parachutes)	$F_T = 16,000 \text{ lb}$
Deployment altitude	$H = 2000 \text{ to } 7000 \text{ ft}$

7.3.7.2 Velocity-Altitude Profile

Section 5.5 states that the maximum opening force of the main parachute occurs at maximum deployment altitude. Figure 7-8 shows a velocity-altitude-versus-time profile for a typical vehicle recovery system.

The maximum dynamic pressure, q_o , occurs at the 200-KEAS deployment velocity

$$q_o = q(200 \text{ KEAS}) = \frac{v^2}{296} = \frac{200^2}{296} = 135.14 \text{ lb/ft}^2$$

True velocity at maximum deployment altitude in feet per second is

$$v_o = v_{7000 \text{ ft}} = 200 \cdot 1.69 \frac{1}{\sqrt{\sigma}} = 200 \cdot 1.69 \cdot 1.1455 = 386.7 \text{ ft/s}$$

7.3.7.3 Force Calculation Methods

The opening forces of the reefed and full-open main parachutes will be determined by three different methods described in section 5.4.6.

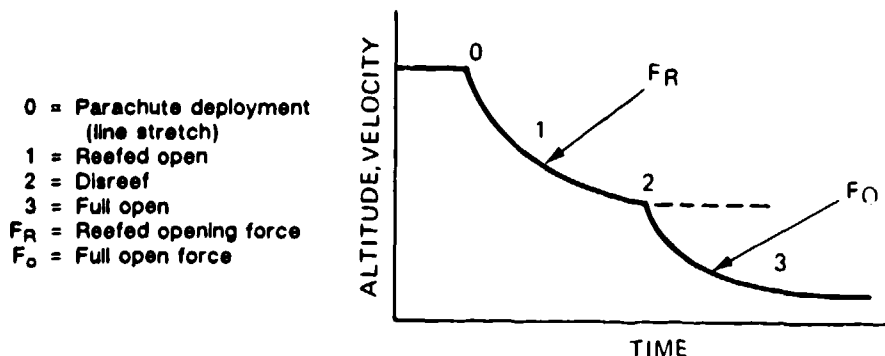


FIGURE 7-8. Velocity-Time Profile.

1. The $\left[\frac{W}{(C_{DS})_p} \right]$ method is accurate for high canopy loading $\left[\frac{W}{(C_{DS})_p} \right]$ parachutes, such as drogue chutes, and for the first stage of reefed parachutes. However, opening forces calculated by this method may be only $\pm 20\%$ accurate for unreefed main descent parachutes and for the disreef stage of large main parachutes.

2. The Pflanz method is quite accurate for all conditions including high altitude, but neglects the effect of gravity. Parachutes opened in vertical descent will have a 1-g (one weight unit) higher force than calculated. It is necessary to calculate the canopy filling times for the various reefed stages (see section 5.4.3) and to determine the drag-area-versus-time profile for the specific parachute (see section 5.4.4). This method permits the investigation of variations in filling times and drag-area-versus-time profiles.

3. The force-trajectory-time computer method includes the effects of altitude, gravity, and changing trajectory angle. This method requires determination of a drag-area-versus-time profile for the entire parachute opening sequence (see Figure 5-52). Computers permit multiple runs with changes in times, drag-area-versus-time profiles, starting velocities, and altitudes.

7.3.7.4 Reefed Opening Forces

When the $\left[\frac{W}{(C_{DS})_p} \right]$ method is used, the opening force of the reefed parachute, F_R , is

$$F_R = (C_{DS})_R \cdot q_o \cdot C_x \cdot X_1$$

where

$$F_R = \text{maximum allowable single parachute force } F_R = \frac{16,000 \text{ lb}}{2} = 8000 \text{ lb}$$

$(C_{DS})_R$ = reefed parachute drag area, ft^2

q_o = dynamic pressure at line stretch = $135.14 \text{ lb}/\text{ft}^2$ (see section 7.3.7.2)

C_x = opening-force coefficient at infinite mass (see Table 5-2)

X_1 = opening-force reduction factor (see Figure 5-48)

The allowable drag area of a single, reefed main parachute is

$$(C_{DS})_R = \frac{F_R \text{ allowable}}{q_o \cdot C_x \cdot X_1}$$

F_R allowable = 8000 pounds (see section 7.3.7.1). C_x for reefed opening of extended-skirt parachutes is 1.0 to 1.1 (see Figure 5-52). X_1 is obtained from Figure 5-48 as a function of canopy loading, $W/(C_{DS})_R$, that is calculated under the assumption that the reefed drag area of one main parachute is about 2.5% of the fully open drag area. Therefore, the canopy loading of the reefed parachute is

$$W/(C_{DS})_R = \frac{4800/2}{(0.025)(3744)} = 51.28 \text{ lb/ft}^2$$

For this canopy loading, X_1 is obtained from Figure 5-48 to 0.86 and

$$(C_{DS})_R = \frac{8000 \text{ lb}}{135.14 \text{ lb/ft}^2 \cdot 1.1 \cdot 0.86} = 62.58 \text{ ft}^2$$

This reefed drag area is less than 2% of the drag area of the full-open main parachute and may be too small for obtaining reliable, fully reefed canopy inflation. Therefore, a 2.2% drag area ratio is selected.

$$(C_{DS})_R = 2.2\% \text{ of } (C_{DS})_{PO} = 0.022(3744 \text{ ft}^2) = 82.37 \text{ ft}^2$$

The opening forces for this larger reefed drag area must be calculated. The canopy loading, $W/(C_{DS})$, of the reefed main parachute is

$$\frac{W}{(C_{DS})_R} = \frac{2400 \text{ lb}}{82.37 \text{ ft}^2} = 29.14 \text{ lb/ft}^2$$

For this canopy loading, Figure 5-48 shows a force-reduction factor, X_1 , of 0.75. The reefed opening force is now calculated

$$F_R = (C_{DS})_R \cdot q_0 \cdot C_x \cdot X_1 = (82.37 \text{ ft}^2)(135.14 \text{ lb/ft}^2)(1.1)(0.75) = 9183 \text{ lb}$$

$$2 F_R = 18,366 \text{ lb}; a = \frac{18,366}{4800} = 3.8 g$$

This force is higher than the allowable force of 8000 pounds per parachute (see Section 7.3.7.1).

When the second calculation method, the Pflanz method, is used, the reefed opening force is

$$F_R = (C_{DS})_R \cdot q_1 \cdot C_x \cdot X_1$$

X_1 is a function of the ballistic coefficient, A :

$$A = \frac{2W}{(C_{DS})_P \rho g t_f v_0}$$

In this equation, known values are W , $(C_{DS})_R$, g , and v_o .

The mass density of air, ρ , at a 7000-foot altitude is

$$\rho = f(H) = 0.0023769(0.8106) = 0.0019396 \text{ (see Table 3-3)}$$

Canopy inflation time, t_f , is calculated as follows (see [Section 5.4.3]):

$$t_f = t_{0-1} = \frac{nD_o}{v_o} \sqrt{\frac{(C_{DS})_R}{(C_{DS})_p}}$$

$$t_f = \frac{17(72.7)}{386.7} \cdot \sqrt{\frac{82.37}{3744}} = 0.49 \text{ seconds}$$

$$A = \frac{2(2400)}{(82.37 \text{ ft}^2)(0.0019396)(31.28)(0.49 \text{ s})(386.7 \text{ ft/s})} = 5.07$$

$X_1 = f(A)$ for $n = \frac{1}{2}$. $n = \frac{1}{2}$ is appropriate for reefed inflation (see Figure 5-39).

$X_1 = 0.77$ (see Figure 5-51)

$$F_R = (82.37 \text{ ft}^2)(135.14 \text{ lb}/\text{ft}^2)(1.1)(0.77) = 9428 \text{ lb}$$

It is interesting to investigate the effects of changing the canopy filling time $\pm 25\%$, and changing the slope of the drag area profile on the parachute opening force. For the change of the drag area slope, a profile factor of $n = 1.0$ instead of $n = \frac{1}{2}$ (see Figure 5-51) is selected. The resultant change in opening force is shown in Table 7.1.

TABLE 7-1. Reefed Opening Force as a Function of Filling Time and Drag-Area Profile.

$t_f, \text{ s}$	$n = f(C_{DS})$	A	X_1	$F_R, \text{ lb}$	% change
0.37	0.5	4.21	0.82	9956	+ 6.5
0.613	0.5	6.98	0.74	8985	-3.9
0.49	0.5	5.27	0.77	9428	0.0
0.49	1.0	5.27	0.79	9673	+ 2.6

Force data obtained with the force-trajectory-time computer method are shown in the force summary in section 7.3.7.5.

7.3.7.5 Main Parachute Disreef Opening Forces

A short reefing time, $t_R = t_{0-2}$, helps to limit altitude losses; however, in clusters, sufficient reefing time is required to permit all parachutes to reach full reefed inflation before disreef.

To save trajectory time, the reefed parachute is disreefed at a dynamic pressure 10 to 20% higher than the terminal reefed dynamic pressure. Therefore,

$$q_2 = 1.1 \frac{W}{(C_{DS})_R} \quad (\text{Figure 7-8})$$

$$q_2 = 1.1 \frac{4800 \text{ lb}}{2(82.37) + (C_{DS})_{\text{drone}}} = \frac{4800 \text{ lb}}{165.54 + 55} = \frac{4800}{220.54} = 23.94 \text{ lb/ft}^2, \text{ and}$$

$$v_2 = \sqrt{q \cdot y} \frac{1}{\sigma} = \sqrt{23.94(840)} \cdot 1.1455 = \text{ft/s} \quad (\text{see Figure 5-112})$$

Parachute opening force, F_o , by the $\left[\frac{W}{(C_{DS})_P} \right]$ method:

$$F_o = (C_{DS})_{2-3} \cdot q_2 \cdot C_x \cdot X_1$$

$$X_1 = f \left[\frac{W}{C_{DS}} \right]$$

$$\frac{W}{(C_{DS})_{2-3}} = \frac{2400 \text{ lb}}{(3744 - 82.4) \text{ ft}^2} = \frac{2400 \text{ lb}}{3661.3 \text{ ft}^2} = 0.656 \text{ lb/ft}^2$$

X_1 for 0.656 is 0.07 and

$$F_o = (3631)(23.94)(1.30)(0.07) = 7910 \text{ lb}$$

Opening force by the Pflaniz method:

$$F_o = (C_{DS})_{2-3} \cdot q_2 \cdot C_x \cdot X_1$$

$$X_1 = f(A)$$

$$A = \frac{2W}{(C_{DS})_{2-3} \cdot \rho \cdot g \cdot t_f \cdot v_2}$$

Known variables are W, ρ , g, and v_2 .

$$(C_{DS})_{2-3} = (C_{DS})_o - (C_{DS})_R = 3744 - 82.3 = 3661.7 \text{ ft}^2$$

A 6-second reefing time, t_f , is selected, and an altitude loss during the reefed stage of 500 feet is calculated (from 7000 feet to 6500 feet). Density, ρ , at 6500 feet is 0.0019569 slugs/ft³.

The disreef time, t_f , is obtained by

$$t_f = t_{2-3} = \frac{n D}{v_2} \cdot \sqrt{\frac{(C_D S)_o - (C_D S)_R}{(C_D S)_o}}$$

From Table 5-6 in section 5.4.3, a canopy fill constant $n = 6$ is selected; therefore,

$$t_f = \frac{6(72.7)}{155.6} \cdot \sqrt{\frac{3744 - 82.4}{3744}} = 2.80(0.988) = 2.87 \text{ s}$$

$$A = \frac{2(4800 \text{ lb})}{(2)(3.661 \text{ ft}^2)(0.0019569)(32.17)(2.87 \text{ s})(155.6 \text{ ft/s})} = 0.0471$$

From evaluation of test data, it is known that the drag-area-increase-versus-time of extended-skirt parachutes at disreef occurs in a concave form, denoted in Figure 5-51 by the definition $n = 2$. For a ballistic parameter $A = 0.0471$ and a drag area increase in accordance with $n = 2$, the force reduction factor, X_1 , is 0.067, and the parachute disreef force, F_o , is

$$F_o = (3.661 \text{ ft}^2)(21.76 \text{ lb/ft}^2)(1.4)(0.067) = 7472 \text{ lb}$$

Results of changing the canopy inflation time, t_f , and the drag-area-versus-time profile, n , are shown in Table 7-2.

Reference 5-76, the Pflanz report, provides a more detailed study of the effect of canopy fill time and drag-area-increase-versus-time profile on the magnitude of the parachute force.

TABLE 7-2. Disreef Opening Force as a Function of Disreef Time and Drag-Area Profile.

$t_f, \text{ s}$	$n = f(C_D S)$	A	X_1	$F_o, \text{ lb}$	% change
2.87	2.0	0.047	0.067	7472	0
3.29	2.0	0.00402	0.0595	6648	-11.0
2.35	2.0	0.0563	0.074	8268	+10.5
2.87	1.5	0.0487	0.080	8938	+19.6

Force-Trajectory-Time Computer Method

The program established by NWC determines as a function of time the parachute forces, the vehicle deceleration, and the space-positioning (trajectory) data in a two-axis system. The method requires a drag-area-versus-time profile for the individual parachutes and the total vehicle system (Figure 7-9). This profile was previously shown in Figure 5-52. Figure 7-9 includes the change in air-vehicle drag caused by the change in vehicle attitude during the parachute opening process.

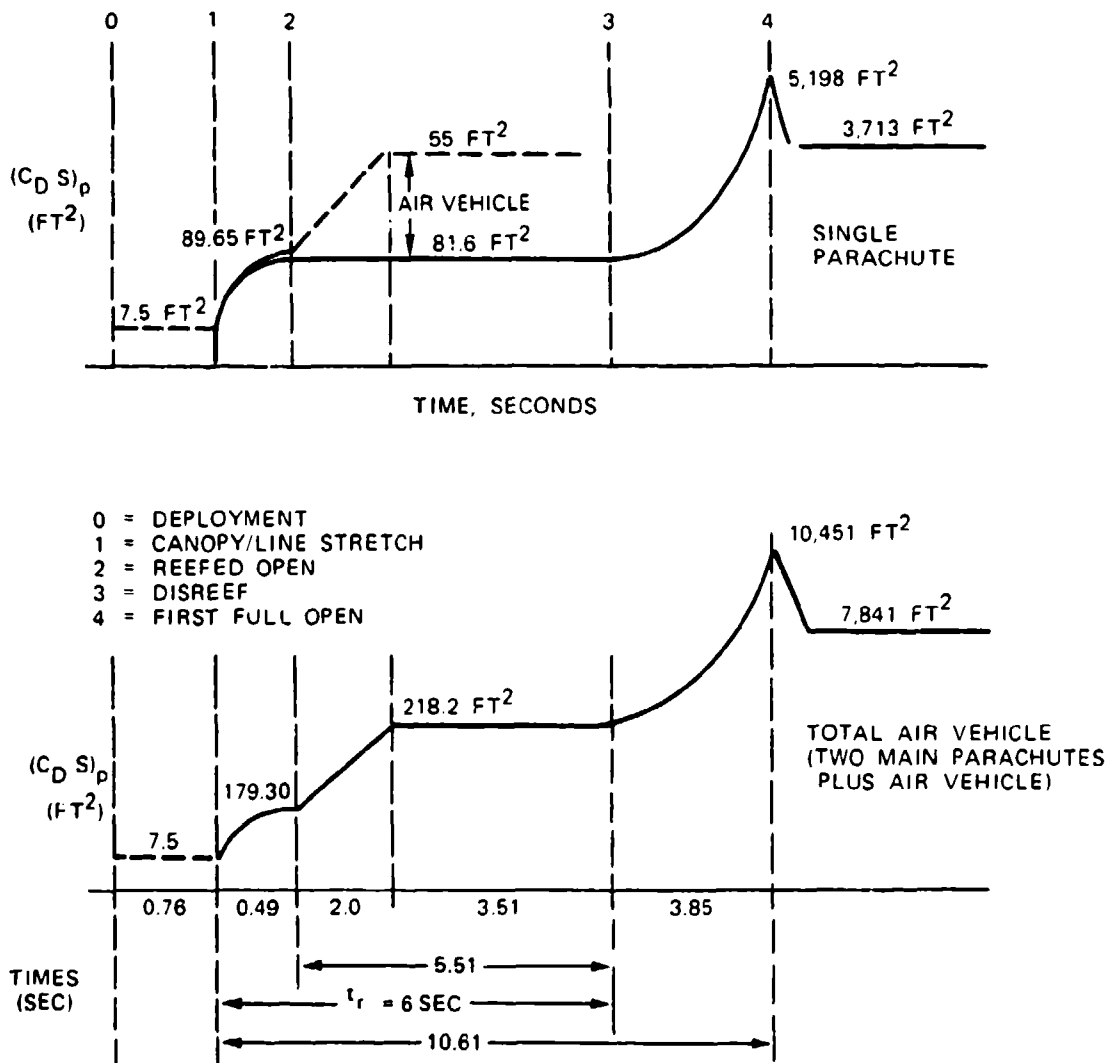


FIGURE 7-9. Drag-Area-Versus-Time Profile for a Single Parachute and the Total Drone.

Parachute force data calculated by the three methods are compared in Table 7-3.

7.3.7.6 Comments on Calculated Opening Forces

1. The reefed opening force for the single parachute is higher than the contractor-requested maximum allowable force per parachute of 8000 pounds.

TABLE 7-3. Comparison of Parachute Forces Calculated by the Three Methods.

	W/(C _D S) method, lb	Pflanz method, lb	Force-trajectory-time computer method, lb
Reefed Opening Forces			
	9107		
$t_f = 0.49 \text{ s}, n = \frac{1}{2}$		9428	9255 ^a
$t_f = 0.61 \text{ s}, n = \frac{1}{2}$		8985	
$t_f = 0.37 \text{ s}, n = \frac{1}{2}$		9956	
$t_f = 0.49 \text{ s}, n = 1.0$		9673	
Cluster of two parachutes			
$t_f = 0.49 \text{ s}, n = \frac{1}{2}$			19,133 ^a
$t_f = 0.39 \text{ s}, n = \frac{1}{2}$			19,058 ^b
$t_f = 0.61 \text{ s}, n = \frac{1}{2}$			20,132
			18,257
Disreef Opening Forces			
	7910		
$t_f = 2.87 \text{ s}, n = 2$		7472	7404
$t_f = 3.29 \text{ s}, n = 2$		6648	
$t_f = 2.35 \text{ s}, n = 2$		8268	
$t_f = 2.87 \text{ s}, n = 1.5$		8938	
Cluster of parachutes			
$t_f = 2.87 \text{ s}, n = 2$			13,120
$t_f = 3.25 \text{ s}, n = 2$			12,261
$t_f = 2.00 \text{ s}, n = 2$			16,115

^a Computer time steps $\Delta t = 1/100 \text{ s}$.

^b Computer time steps $\Delta t = 1/10 \text{ s}$.

2. The average disreef force is approximately 1500 pounds lower than the reefed force. Therefore, it appears logical to lower the reefed force and increase the disreef force. Although this adjustment probably cannot be made within the 8000-pound limit, 8500 pounds appears to be an obtainable goal.

3. To meet the contractor requirement of an 8000-pound maximum force limit per parachute, two-stage reefing is required.

4. It appears practical to determine in drop tests if a 2.0 to 2.1% reefed drag area can be obtained. This drag area would decrease the reefed opening force and somewhat increase the disreef force. However, reaching an average maximum force of less than 8000 pounds appears doubtful.

5. In the calculations, both parachutes are assumed to have equal opening forces. In reality, opening forces of the two parachutes can differ because of variations in filling time, lead-and-lag chute behavior caused by blanketing, and resultant nonuniform canopy inflation.

The fast-opening Apollo ringsail-type main parachutes had a load distribution among the three parachutes of 40-40-20. The individual parachutes, therefore, had to be overdesigned in a 40/33 ratio. However, the total parachute force load taken by the vehicle hard points did not exceed the calculated average load because of the high-low variation of the individual parachutes.

The two slower-opening extended-skirt parachutes used for this application are more uniform in their load distribution. A cursory analysis of available test data indicates that a 55/45 load distribution between the two parachutes and a no-overload condition for the vehicle hard points should be an acceptable load distribution.

A contractor-subcontractor agreement is required to determine whether the individual parachutes should be designed for the 55/45 load variation or whether this overload can be accommodated by the 1.5 safety factor and the additional safety provided by the normal overstrength of textile specification materials.

7.3.7.7 Snatch Forces

The snatch force is caused by the acceleration of the mass of the parachute assembly to the velocity of the forebody (drone). A canopy, partially inflated at line stretch, increases the mass of the parachute by the mass of the air included in the canopy; this can increase the snatch force (mass shock) considerably.

Two principal rules should be followed to keep the snatch force within allowable limits.

1. Keep the parachute canopy closed until line (canopy) stretch occurs by use of a deployment bag or skirt restrictor.
2. Accelerate the mass of the parachute assembly in incremental steps.

Known means of accomplishing these goals are discussed in Chapter 6.1.

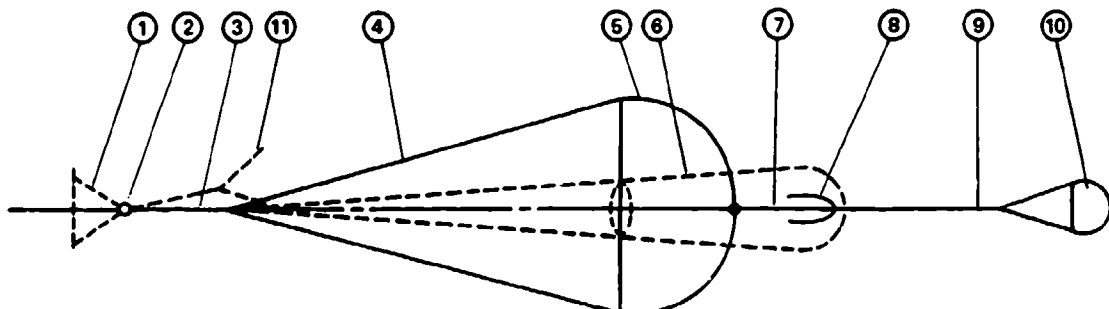
The difference between a poor deployment and a deployment that accomplishes the first rule and partially accomplishes the second is illustrated in Figure 5-54, which shows snatch and opening forces for the C-9 parachute with and without the quarter deployment bag. The deployment method outlined in section 7.3.4 should hold snatch forces at a level below the parachute opening forces.

A method for calculating snatch forces is described in Reference 2.2, the 1963 edition of the USAF parachute handbook. A preferred method for calculating parachute deployment, including the snatch force, is contained in J. W. Purvis's ALAA paper, "Improved Prediction of Parachute Line Sail During Lines-First Deployment" (Reference 5.86).

7.3.8 Parachute Stress Analysis

7.3.8.1 Parachute Design Data

A total parachute assembly is shown in Figure 7-10.



- | | |
|---|---------------------------------|
| 1. Drone bridle, two each | 7. Deployment bag bridle |
| 2. Disconnect, automatic at ground impact | 8. Deployment bag (DB) |
| 3. MP riser, two each | 9. Extraction parachute riser |
| 4. MP suspension lines, 64 per parachute | 10. Extraction parachute |
| 5. MP canopy | 11. Second parachute, not shown |
| 6. Parachute reefing system | |

FIGURE 7-10. Main-Parachute Assembly.

Parachute type: Conical full extended skirt

Diameter: $D_0 = 72.7 \text{ ft}$

Line-length ratio: $L_e/D_0 = 1.25; L_e = 1083 \text{ in.}$

7.3.8.2 Parachute Forces

The maximum reefed opening force, F_R , is 9255 pounds. The maximum disreef opening force, F_o , is 7404 pounds. The maximum design force for stressing the parachute assembly, F_x , is 9255 pounds.

The forces obtained in computer runs are selected as the most accurate forces for stressing the parachute assembly and its components. Based on multiple computer runs, a diligent choice must be made for the most likable forces.

7.3.8.3 Main-Parachute Safety and Design Factors

Section 6.4 is used as a guide for selecting the safety, load, loss, and design factors in Table 7-4.

TABLE 7-4. Determination of Design Factors for the Main Parachute Assembly (Section 6.4.2).

Assembly unit	Safety factor	Load factors				Loss factors					Design factor
		m	$\cos \phi$	s	LF	u	e	k	τ	σ	
Drone bridle	1.6	1.6	0.8	1.0	0.95	1.0	1.0	0.76
MP riser	1.6	1.6	0.8	1.0	↑	↑	↑	0.76
MP suspension lines	1.5	...	1.04	1.0	1.56	0.9	0.95	↑	↑	↑	0.81
MP canopy	1.5	1.0	1.5	0.9	0.95	↑	↑	↑	0.81
Reefing system	2.0	2.0	0.85	0.9	↑	↑	↑	0.73
Pilot chute	1.5	1.5	0.85	1.0	↓	↓	↓	0.81
EP riser	1.5	1.25	1.875	0.85	0.95	↓	↓	↓	0.77
EP suspension lines	1.5	...	1.02	1.0	1.53	0.85	0.95	0.95	1.0	1.0	0.77
EP canopy	1.5	1.0	1.5	0.9	0.95	0.95	1.0	1.0	0.81

NOTE: MP = main parachute; EP = extraction parachute.

7.3.8.4 Suspension-Line Selection and Strength

The following guidelines are used for selecting the suspension lines of the main parachutes (Table 7-5).

TABLE 7-5. Suspension-Line Selection.

Factors	Number of suspension lines				
	60	64	68	72	
Maximum parachute force, lb	F_x	9255	9255	9255	9255
Design factor (from Table 7-4)	DF	1.93	1.93	1.93	1.93
Required suspension-line strength, lb	F_{SL}	297.7	279.1	262.7	248.1
Gore width, ft	E_o	3.8	3.6	3.35	3.16

1. Connection of suspension lines to riser legs and drone hardpoints is made easier if the number of suspension lines are a multiple of 4 or 8.
2. The gore at the skirt should not be wider than 3.5 feet for packing reasons.
3. The canopy should have no fewer than 12 gores to avoid gore distortion during inflation.
4. Radial ribbons or radial seams should not overlap at the vent; overlapping causes bunching of material and associated sewing problems.
5. The strengths of available suspension-line types may affect the gore selection.

Table 7-5 shows the required suspension line strength and the resultant gore width as functions of the number of gore/suspension lines used.

The width of the gore of the skirt on conical, full-extended-skirt (CFES) parachutes is about 85% of the maximum gore width, E_0 .

Sixty-four suspension lines are selected in accordance with MIL-C-7515, Type XI, with 300-pound tensile strength.

This selection provides a margin of safety (MS) of

$$MS = \frac{\text{available strength}}{\text{required strength}} - 1 = \frac{300}{281.9} - 1 = 1.064 - 1 = 0.064$$

The suspension line will be attached to the canopy skirt in a loop connection.

7.3.8.5 Canopy Stress

No precise method has been developed for calculating the stress in a circular, solid-material, bias-construction canopy.

Section 6.4 describes a semi-empirical method for determining the required fabric strength of a solid material canopy in pounds per unit width using the stress in a pressure vessel as an analogy. The stress in a cylindrical vessel, expressed as force per unit length, is

$$t_c = \frac{pr}{2} (\text{lb/in.})$$

where p is the pressure in the cylindrical vessel and r is the vessel radius. Using this analogy and considering the canopy gore as part of a pressure vessel, the required material strength of the canopy per unit width is obtained

$$t_c = \frac{F_o}{D_p 12} DS$$

where

t_c = required material strength in lb/in. width

F_o = maximum parachute force = 9255 pounds

D_p = inflated parachute diameter = $D_o C$ (see Figure 5-78)

DS = design factor, 1.85 (see Table 7-4)

$$t_c = \frac{9255}{(\pi)(72.7)(0.7)(12)} 1.85 = \frac{9255}{1918} 1.85 = 8.9 \text{ lb/in.}$$

The maximum stress actually occurs during reefed inflation because of the smaller inflated diameter:

$$\text{Reefed inflated diameter} = D_p \sqrt{\frac{(C_D S)_R}{(C_D \cdot S)_p}} \cdot C = 72.7 \sqrt{0.02}(0.7) = 7.9 \text{ ft}$$

$$t_c \text{ reefed inflation} = \frac{9255}{9282.4} 1.85 = 60.6 \text{ lb/in.}$$

A 1.1 oz/yd² material is selected in accordance with MIL-C-7020, Type I, with 42 lb/in. breaking strength for the main part of the parachute canopy, and 2.2 oz/yd² material, MIL-C-7350, Type I, with 90-lb/in. strength for the crown area that is inflated during reefed opening.

7.3.8.6 Canopy Reinforcing Tapes

1. **Skirt Tape.** The skirt tape should be equal or greater in strength than the individual suspension lines but not less than 1000 pounds, and 1-inch-wide tape should be used for parachutes larger than 20 feet in diameter.

The nylon tape selected is 1-inch-wide MIL-T-5038, Type IV, with 1000-pound strength. Proper connection of the skirt tape to the radial seam (tape) and the suspension line must be ensured.

2. **Vent Tape.** From the geometric design of the parachute vent (Figure 7-11), the force in the vent tape, F_{VT} , is calculated

$$\begin{aligned} F_{VT} &= \frac{F_{RT}}{N_{SL} 2 \sin\left[\frac{360}{N_{SL}}\right]} DF \\ &= \frac{9255}{64\left(2 \sin \frac{360}{64}\right)} 1.85 = 1360 \text{ lb} \end{aligned}$$

A 1-inch-wide, 4000-pound webbing (MIL-W-5625) or 7/8-inch-wide, 3100-pound webbing (MIL-W-5625) is selected.

3. **Vent Lines.** The strength of the vent lines should be equal to or greater than 60% of the strength of the radials.

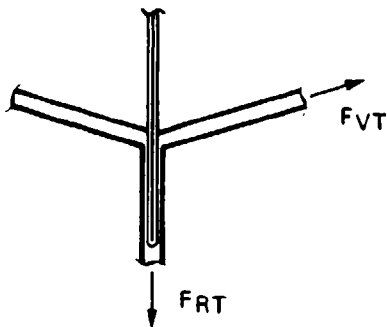


FIGURE 7-11. Vent-Tape Geometry.

7.3.8.7 Design of Radials

The following four types of radial designs are in use:

1. Radial seams with suspension lines running in channels over the canopy and attached at the vent and the skirt as on the canopy of the C-9 personnel parachute.
2. Suspension lines running on top of the radials over the canopy and sewn at full length to the canopy as on many heavy-duty ribbon parachutes.
3. Radial tapes sewn on top of or inside the radial seams, and suspension lines attached to the radial tapes by sewing or by skirt loops (NB-7 and T-10 canopies).
4. Radial ribbons on ribbon parachutes designed to take the total radial load with suspension lines sewn onto the radials or connected by a skirt loop.

The following are some comments on the design of radials:

1. Making the strength of the radials equal to 80% of the strength of the suspension lines has been satisfactory on thousands of ribbon parachutes.
2. When tapes or suspension lines are sewn at full length to the radials, care must be taken that fullness in the radials ensures that the radial tapes or the suspension lines are the primary load carrying members. For an explanation of fullness, see section 6.6.4.
3. Uniform material distribution is of utmost importance when sewn tapes or lines are used for radial reinforcement.

For the radial design of the main parachute, we use a tape with 80% strength of the suspension line ($0.8 \cdot 300 \text{ lb} = 240 \text{ lb}$) sewn on top of the radial seam. A 250-pound strength, $\frac{1}{2}$ -inch-wide tape is selected in accordance with MIL-T-5038, Type III. Tape and radial seams are marked every 24 inches for proper material distribution.

7.3.8.8 Check for Proper Gore Fullness

When the first parachute of a new design has been completed in the manufacturing shop, a gore fullness check in accordance with Figure 7-12 should be conducted. A slight amount of slack should be noticeable in the canopy fabric in both directions when all four corners of a gore are pulled radially outward. Slack indicates that the main loads are carried by the radials and reinforcing tapes and not by the canopy fabric. Stress folds in the canopy indicate faults in the design or manufacture of the parachute.

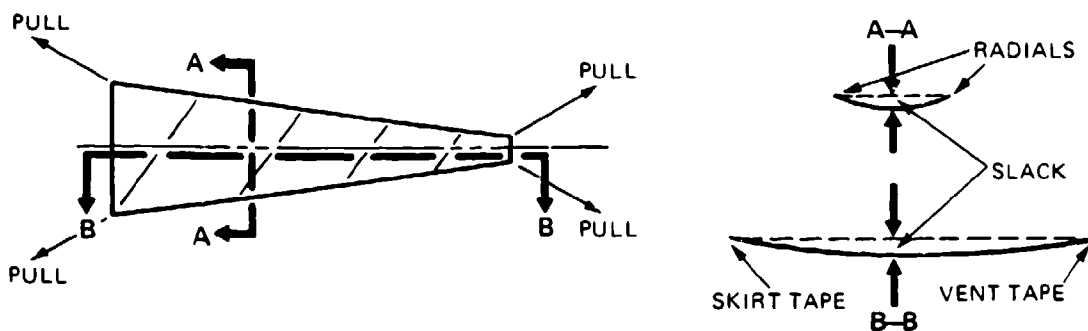


FIGURE 7-12. Bench Check on Gore Fullness.

7.3.9 Canopy Gore Shape

A full-extended-skirt parachute is selected that has a conical top with a 25-degree cone angle; a nominal diameter, D_o , of 72.7 feet; and 64 gores.

Based on the definitions in Figure 7-13, the canopy gore dimensions are

$$\text{Base gore angle } \gamma = \frac{360 \text{ deg}}{N_{SL}} = \frac{360}{64} = 5.625 \text{ deg}$$

$$\text{Cone angle } \mu = 25 \text{ deg}$$

$$\text{Gore Angle } \beta = \sin^{-1} \left[\cos \mu \left[\sin \frac{180}{N_{SL}} \right] \right]$$

$$\beta = \sin^{-1}[0.9063(\sin 2.8125 \text{ deg})]$$

$$\beta = \sin^{-1}(0.9063)(0.0491) = 2 \sin^{-1} = 0.04447$$

$$\beta = 5.1 \text{ deg}$$

Canopy surface area $S_o = 4160 \text{ ft}^2$ (see section 7.3.3)

$$\text{Gore height } h_1 = \sqrt{\frac{(0.653 S_o)(144) \cot \gamma/2}{N_{SL} \cdot \cos \mu}}$$

$$h_1 = \sqrt{\frac{(0.653)(4160)(144)(20.34)}{(64)(0.9063)}}$$

$$h_1 = 370.3 \text{ in.}$$

$$h_2 = 0.286h_1 = 0.286(372.73) = 105.9 \text{ in.}$$

$$e_1 = 2h_1 (\tan \beta/2) = (2)(372.73)(0.0445) = 32.96 \text{ in.}$$

$$e_2 = 0.857e_1 = 0.857(33.88) = 28.24 \text{ in.}$$

$$h_s = h_1 + h_2 = 370.3 + 105.9 = 476.2 \text{ in.}$$

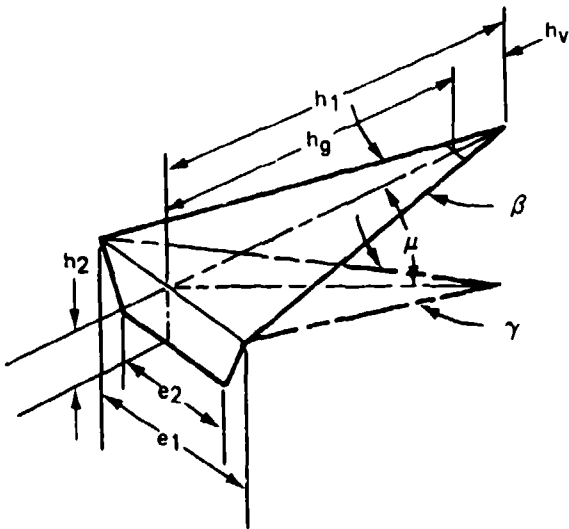


FIGURE 7-13. Gore Layout for Gore Dimensions.

7.3.9.1 Vent Area

A vent area, S_V , is selected that is equal to 0.25% of the total canopy surface area, S_o ; therefore,

$$S_V = (0.0025)S_o = 0.0025(4160) = 10.4 \text{ ft}^2 \text{ and the}$$

$$\text{vent diameter, } D_V = 1.1284 \sqrt{S_V} = 1.1284 \sqrt{10.4} = 3.64 \text{ ft}$$

This is a large vent opening for a reefed parachute. Several criteria may be used to determine the size of the canopy vent as follows:

1. Unreefed parachutes with vents up to 1% of the canopy surface area, S_0 , have been operated successfully.
2. Reefed parachutes require a vent diameter, D_V , smaller than the reefing line circle, diameter D_R , of the parachute; D_V is smaller than D_R (see section 5.6, Figure 5-66).
3. The radials at the vent should not overlap. A 1-inch free space between radials is desirable (see Figure 7-14).

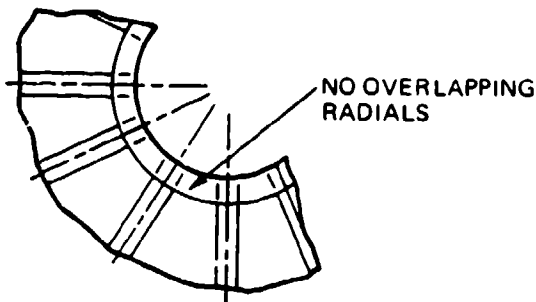


FIGURE 7-14. Vent Construction.

7.3.9.2 Vent Diameter

A vent construction is selected with a 1-inch free space between 1-inch-wide radials; this results in a vent circumference of $64 + 63 = 127$ in. and a vent diameter of

$$D_V = \frac{127}{\pi} = 40.43 \text{ in.}$$

A 3-foot vent diameter is selected. The radius is 18 inches, and vent height, h_V , is calculated

$$h_V = r(\cos \gamma/2); \text{ gore half angle } \gamma/2 = 2.55 \text{ deg}$$

$$h_V = 18(0.999) = 17.98 \text{ in.}$$

Manufactured gore height, h_g , is

$$h_g = h_1 - h_V = 370.3 - 17.98 = 352.32 \text{ in.}$$

Vent gore width, e_V ,

$$e_V = 2h_V \tan \beta/2 = 2(17.98)(0.0445) = 1.6 \text{ in.}$$

Stress in the canopy gore area can be relieved by making the gore at the vent 10% wider than the calculated gore dimension, e_V . Therefore, $e_V^* = 1.1 \cdot e_V = 1.1(1.6) = 1.76$ inches. The vent tape is sewn to the vent at the original e_V dimension, thereby gathering the vent 10% and creating a stress-relieving arcing in the gore fabric next to the vent. See Figure 7-15 for an example of final gore dimensions.

$$\begin{aligned}
 h_0 &= 476.2 \text{ in.} \\
 h_1 &= 370.3 \text{ in.} \\
 h_2 &= 105.9 \text{ in.} \\
 h_V &= 17.98 \text{ in.} \\
 e_1 &= 32.96 \text{ in.} \\
 e_2 &= 28.24 \text{ in.} \\
 e_V &= 1.6 \text{ in.} \\
 e_V^* &= 1.76 \text{ in.}
 \end{aligned}$$

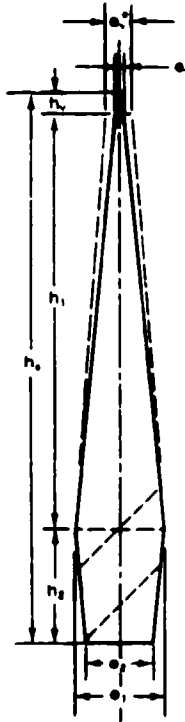


FIGURE 7-15. Final Gore Dimensions.

7.3.10 Pocket Bands

The pocket bands used on every gore make canopy inflation more uniform and eliminates long and short filling times. A narrow tape is used as the pocket band, which will not affect the average length of the canopy filling time. Data on the dimensioning of pocket bands are given in section 6.4. As shown in Figure 7-16, the pocket band dimensions are

$$e_S = e_2 = 28.24 \text{ in. (See Figure 7-15.)}$$

$$L_b = 0.14e_S = 0.14 \cdot 28.24 \approx 3.95 \text{ in.}$$

$$L_a = 0.238e_S = 0.238 \cdot 28.24 = 6.7 \text{ in.}$$

A 5/8-inch-wide tape, MIL-T-8363, Type I, is selected as pocket band material.

Important Note: Pocket band length, L_a , must be long enough to permit the full inflation of the parachute canopy.

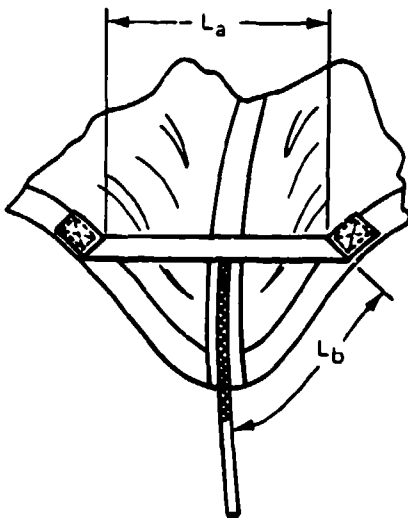


FIGURE 7-16. Pocket Band Arrangement.

7.3.11 Parachute Reefing

7.3.11.1 Length of Parachute Reefing Line

The drag area of a single reefed main parachute was calculated as $(C_{DS})_R = 82.37$ square feet (see section 7.3.7.4). This area results in the following reefing ratio:

$$\epsilon = \frac{(C_{DS})_R}{(C_{DS})_o} = \frac{82.37}{3744} = 0.022 = 2.2\% \text{ of } S_o$$

Reefing by the skirt-reefing method is selected (see section 5.6, Figure 5-66 and section 6.5).

From Figure 5-72, we obtain for an extended-skirt parachute with a reefing ratio $\epsilon = 0.22$, a reefing-line ratio:

$$\tau = D_R/D_o = 0.07$$

and the diameter of the reefing-line circle, D_R :

$$D_R = (0.07)D_o = 0.07 \cdot 72.7 \text{ ft} = 5.09 \text{ ft}$$

and the installed length of the reefing line, L_{RL} :

$$L_{RL} = D_R \pi = 5.09 \pi = 15.99 \text{ ft} = 191.88 \text{ in.}$$

The diameter of the reefing line circle, D_R , is larger than the 3.64-foot vent diameter of the canopy, D_V . This difference in diameters is an important design requirement (see section 7.3.9).

7.3.11.2 Strength of the Reefing Line

The force in the reefing line is determined according to information in section 5.6.8. Test items 22 and 23 in Figure 5-76 closely resemble the main parachute used here. A reefing-line-force-to-reefed-parachute-force ratio of 2.5% is selected for this assembly. Therefore, the force in the reefing line is

$$(0.025)F_R = 0.025(9255 \text{ lb}) = 231.4 \text{ lb}$$

The design factor, D_F , for the reefing system was determined in section 7.3.8, Table 7-4, to be 2.74.

Required reefing-line strength, $F_{RL_{\text{ultimate}}}$, is

$$F_{RL_{\text{ultimate}}} = D_F \cdot F_{RL} = 2.74 \cdot 231.4 \text{ lb} = 634 \text{ lb}$$

A coreless braided nylon line, MIL-C-7565, Type III, with a tensile strength of 750 pounds, is selected as reefing line.

Section 6.5 discusses reefing system design and installation details.

7.4 HIGH-SPEED DROGUE CHUTE ASSEMBLY

7.4.1 Requirements

The following operational requirements govern the design of the first-stage drogue chute:

1. The drone must be recoverable from any conceivable flight condition during the engineering test phase.
2. An out-of-control drone or a drone that loses radio contact with the controller must be prevented from flying off the range. Recovery is initiated by an independent range signal. This type of recovery requires a high-speed deceleration parachute that can be deployed and operated when the drone is moving at maximum speed, or is in a spin, or during any other abnormal flight condition.

This type of recovery established the following requirements for the type and size of the drogue chute:

1. The drogue chute must have reliable operation in the velocity range from 200 knots at sea level to Mach 1.5 at 50,000 feet.
2. Stability must be better than ± 3 degrees.
3. Minimum weight and volume is mandatory.
4. The drogue chute must be able to decelerate the drone to the permissible opening speed of the main parachute assemblies.
5. The drogue chute must be suitable for the operational environment.

Figure 7-17 shows the altitude-velocity flight envelope of the drone.

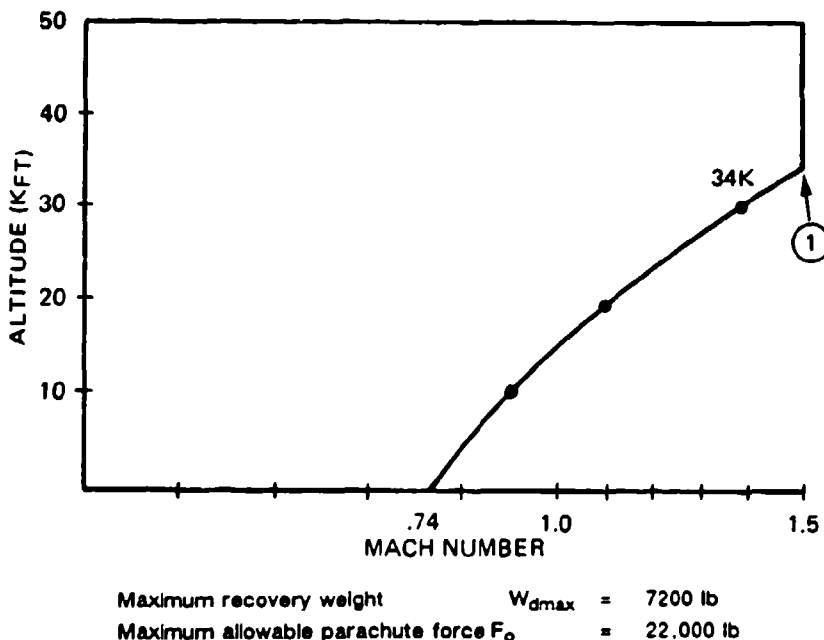


FIGURE 7-17. Drone Flight Envelope.

7.4.2 Drogue Chute Selection

Tables 5-1 through 5-5 in Chapter 5 list commonly used parachute types. Table 7-6 evaluates possible drogue chute candidates. Of the parachute candidates, only the conical ribbon and the hemisflo ribbon have been used successfully for similar applications.

A 25-degree conical ribbon parachute is selected for this application. The conical ribbon parachute meets all requirements and has a higher subsonic drag coefficient than the equally

TABLE 7-6. Drogue Chute Candidates.

Type	Stability	Supersonic experience	Drag coefficient		Supersonic load factor
			Subsonic	Supersonic	
Guide surface	0 to ± 2	Limited	0.3 to 0.4	0.2 to 0.3 ^a	1.7 to 2.0
Annual	< ± 6	None	0.85 to 0.95	Unknown	Unknown
Cross	0 to ± 3	Limited	0.6 to 0.85	Unknown	Unknown
Ribbon, conical	0 to ± 3	Extensive	0.55	0.4 to 0.55 ^a	1.5 ^b ; (1.2)
Ribbon, hemisflo	0 to ± 2	Extensive	0.45	0.3 to 0.45 ^a	1.25; (1.15)
Ringslot	0 to ± 5	None	0.65	Unknown	Unknown
Rotafoil	0 to ± 2	None	0.85 to 0.99	Unknown	Unknown

^a See section 5-8.^b See Figure 5-50.

suited hemisflo parachute. The subsonic drag coefficient determined the parachute size and its associated weight and volume. Numerous conical ribbon parachutes have been used successfully at this speed and diameter range.

Based on section 5.8, Figure 5-93, we obtain the following drag coefficients versus Mach number data:

Mach number	1.5	1.3	1.1	1.0	0.8
C_{D_0}	0.42	0.5	0.52	0.55	0.55

These C_{D_0} coefficients do not take into account a loss caused by forebody wake.

7.4.3 Required Drogue Chute Diameter

The size of the fully open drogue chute is determined by the requirement that it must decelerate the 7200-pound drone to the allowable opening speed of the main parachute, which is governed by the requirement that the opening force of the two main parachutes must stay within the 9350-pound-per-chute limit established for the 200-knot opening speed of the 4800-pound drone.

A preliminary calculation shows that a terminal velocity of about 175 KEAS is required to limit the opening load of the reefed main parachutes to 9350 pounds. A 13- to 14-foot-diameter drogue chute is needed to meet this requirement.

To reach 175 KEAS at main parachute line stretch, the drogue chute will be disconnected by an aneroid sensor at about 7000 feet mean sea level (MSL) while descending vertically from high altitude. The drone will free-fall for 0.8 second until main parachute line stretch occurs; the free-fall causes a 10-knot increase in velocity. In addition, the changing density, ρ , results in

about 5 KEAS Δv compared to equilibrium velocity. We therefore design for a terminal velocity of 175 - (10 + 5) knots, or 160 KEAS.

$$\text{Dynamic pressure, } q, \text{ at 160 KEAS} = \frac{160^2}{295} = 86.78 \text{ lb/ft}^2$$

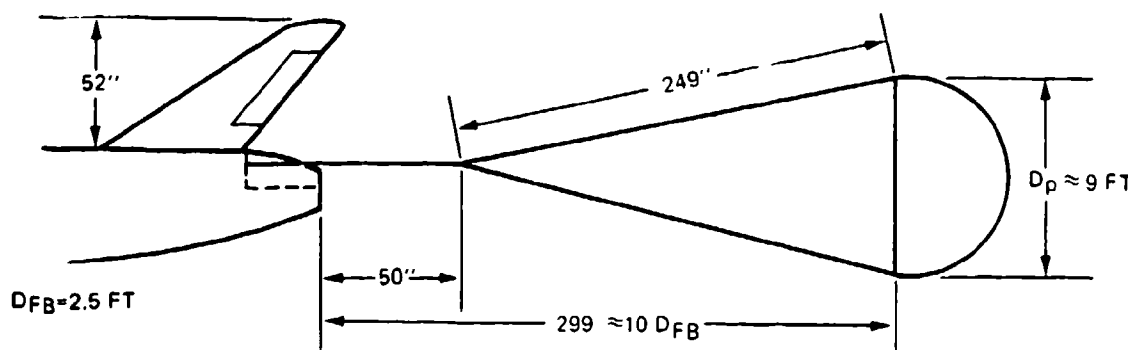
$$\text{Required drogue chute drag area, } (C_{DS})_p = \frac{W_{TO}}{q} = \frac{7200 \text{ lb}}{86.8 \text{ lb/ft}^2} = 82.95 \text{ lb/ft}^2$$

$$\text{Drogue chute canopy area, } S_o = \frac{(C_{DS})_p}{C_{D_o}} = \frac{82.95}{0.55} = 150.9 \text{ ft}^2$$

Nominal diameter, $D_o = 1.128\sqrt{S_o} = 1.128\sqrt{150.9} = 13.85 \text{ ft}$ and the inflated diameter $D_p = D_o C = 13.85 \cdot 0.65 = 9 \text{ ft}$.

The drag coefficient will be reduced because of the forebody wake and will increase if suspension lines are longer than $L_e/D_o = 1.0$.

Figure 7-18 shows the arrangement of the drogue chute.



$$\begin{aligned} L_e/D_o &= 1.5 (13.85 / 12) = 249 \text{ in.} \\ D_p/D_{FB} &= 9/2.5 = 3.6 \end{aligned}$$

FIGURE 7-18. Drogue Chute Arrangement.

Suspension lines equal in length to 1.5 D_o are selected, causing an 8.5% C_{D_o} gain, (see Figure 5-20). The loss in drag caused by forebody wake is determined from Figure 5-21. The ratio of inflated parachute diameter, D_p , to forebody diameter, D_{FB} , is 3.6, and the ratio of the distance between the leading edge of the inflated parachute and the aft end of the drone is 300/30 in. = 10 as shown in Figure 7-18.

The gain in drag caused by the longer suspension lines and the 5% loss in drag caused by forebody wake (Figure 5-21) result in a final drag coefficient, C_{D_0} , for the drogue chute of

$$C_{D_0} = 0.55 \cdot 1.085 \cdot 0.95 = 0.57$$

and a corrected drogue chute diameter

$$D_0 = 13.61 \text{ ft}$$

7.4.4 Computer Analysis of Drogue Chute Performance

At this point, a computer program should be established to determine the following performance conditions:

1. Balance reefed and disreef parachute forces and filling times. Start at Mach 1.5 at 34,000 feet (see point ① on Figure 7-17). Check final selection for a 10,000-foot-altitude condition.
2. Determine required opening altitude for high-speed, low-altitude deployment. This requires trajectory runs with both the drogue and main parachutes.
3. Determine maximum horizontal range, including prevailing wind conditions.
4. Verify that the selected main parachute opening speed of 175 KEAS is reached for all important flight conditions and that, for an opening velocity of 175 KEAS, the main parachute forces stay within the allowable force limit of 9255 pounds.
5. Include opening of the air bags with a 6.0-second inflation time in some of the trajectories. Inflation starts after main parachute opening.

The prime contractor should point out any special flight conditions that may require parachute recovery. The prime contractor will probably also perform recovery computer runs to determine for which flight conditions and from what altitudes recovery can be accomplished.

7.4.5 Flight Emergency Recovery Conditions

Certain flight conditions other than recovery command from the flight controller or the range safety officer may result in automatic on-board recovery command. These conditions include

1. Loss of RF link.
2. Loss of engine power (glide on internal power).
3. High accelerations in x, y, and z caused by out-of-control flight conditions or in-flight-afflicted damage on target drones.

7.4.6 Drogue Chute Opening Forces

Parachute opening forces should be obtained from the computer program. However, a hand calculation is required for defining the force range before setting up the computer program. Furthermore, canopy filling times and force coefficient, C_x , must be determined before computer runs (see section 5.4).

Determining the drogue chute opening forces with the W/C_{DS} method is normally sufficiently accurate for high-canopy-loading drogue chutes. If no computer backup is available, the Pflanz method (see section 5.4.6) will provide good force data.

7.4.6.1 Drogue Chute Reefed Opening Forces

When the W/C_{DS} method is used, the reefed opening force, F_R , is calculated to

$$F_R = (C_{DS})_R \cdot q \cdot C_x \cdot X_1$$

and the maximum allowable drogue chute drag area with a 22,000 force limit is calculated to

$$(C_{DS})_R = \frac{F_R}{q \cdot C_x \cdot X_1}$$

where

F_R , the maximum allowable force, is 22,000 lb

q , the maximum dynamic pressure, is 813.9 lb/ft²

For supersonic application, Figure 5-50 in section 5.4 shows $C_K = C_x \cdot X_1$ for the supersonic deployment of conical ribbon parachutes. Most applicable are the data for the Mercury and the Cook conical ribbon parachutes, which were deployed at velocities up to Mach 1.6. C_K factors of 1.3 to 1.75 have been measured in supersonic deployment of conical ribbon parachutes. Forebody wake and poor deployment greatly affect the force coefficient. Mortar deployment often produces bag strip-off before canopy stretch, causing premature partial canopy inflation and a high X_1 factor. Rocket extraction or drogue gun/pilot chute deployment, both resulting in canopy stretch before skirt inflation, generally avoid this problem. A force coefficient $C_x = 1.25$ is selected.

X_1 is a function of $\frac{W}{(C_{DS})_R}$ that is unknown at this time, but (based on experience) is estimated to be 0.95 and corrected afterward:

$$(C_{DS})_R = \frac{22,000 \text{ lb}}{(813.9 \text{ lb/ft}^2)(1.25)(0.95)} = 22.76 \text{ ft}^2$$

The canopy loading of the reefed drogue chute is

$$\frac{W_{d \text{ max}}}{(C_{DS})_R} = \frac{7200}{22.76} = \frac{7200}{22.76} = 316.3 \text{ lb/ft}^2$$

for this $\frac{W}{(C_{DS})_R}$. Figure 5-48 shows $X_1 = 1.0$; the corrected reefed-drogue-chute drag area is calculated

$$(C_{DS})_R = \frac{22,000 \text{ lb}}{(813.9 \text{ lb/ft}^2)(1.25)(1.0)} = 21.62 \text{ ft}^2$$

The required reefing-line length for obtaining this drag area can be determined from Figure 5-73, section 5.6.6, using the method of section 7.3.11.

7.4.6.2 Drogue Chute Disreef Opening Force

An important factor to determine is reefing time. A long time is required to reach close to terminal velocity before disreef. A practical approach, based on experience, is to select the 1.1-times-terminal-velocity point for disreef. If this time is too long, then a shorter reefing time is required, resulting in a higher disreef velocity and forces.

The terminal velocity of the reefed parachute is

$$q_{\text{terminal}} = \frac{W_{d \text{ max}}}{(C_{DS})_R + (C_{DS})_{\text{drone}}} = \frac{7200 \text{ lb}}{21.62 + 0.115 \cdot 75 \text{ ft}^2} = \frac{7200}{30.26}$$

$$q_{\text{terminal}} = 237.9 \text{ lb/ft}^2 = 265 \text{ KEAS}$$

Disreef occurs at 1.1 (q_{terminal}) = 1.1(237.9) = 261.7 lb/ft^2 .

The disreef force is

$$F_o = (C_{DS})_p \cdot q \cdot C_x \cdot X_1$$

C_x for disreef is 1.10

$$X_1 = f \left[\frac{W}{(C_{DS})_D} \right]$$

$$\frac{W}{(C_{DS})_D} = \frac{7200}{82.95} = 86.8 \text{ lb/ft}^2 \text{ and } X_1 \text{ from Figure 5-48} = 0.92$$

and disreef force, F_o , is calculated

$$F_o = (C_{DS})_D \cdot q \cdot C_x \cdot X_1$$

$$F_o = (82.95)(261.7)(1.10)(0.92) = 21,968 \text{ lb}$$

Both forces F_R and F_o are close to the allowable force limit of 22,000 pounds. Because loads vary 5 to 10%, slight overloads may occur. However, the 7200-pound drone weight is the take-off weight. Off-range recovery and conceivable emergencies will occur at lighter drone weights, resulting in lower parachute forces.

7.4.7 Drogue Chute Stress Analysis and Design

Dimensioning of the various components of the parachute assembly involves three primary tasks (1) establishing design and safety factors, (2) determining the loads and stresses in the assembly components, and (3) dimensioning all assembly members. The methods used for these tasks are described in section 6.4.

7.4.7.1 Drogue Chute Safety, Load, Loss, and Design Factors

The method used is similar to the one developed in section 6.4. Table 7-7 shows safety, load, and loss factors in relation to design factor.

TABLE 7-7. Determination of Design Factors for the Drogue Chute.

Drogue chute assembly unit	Safety factor	Load factors				Loss factors						Design factor
		m	$\cos \phi$	s	LF	u	e	k	τ	o	LF	
Riser	1.75	1.25	2.19	0.8	1.0	0.95	1.0	0.9	0.68	3.22
Suspension lines	1.7 ^a	1.1	1.04	...	1.94	0.8	1.0	0.9	0.68	2.86
Canopy	1.65	1.1	1.82	0.8	1.0	0.9	0.68	2.68
Reef system	2.0	2.0	0.8	1.0	0.9	0.68	2.94
Deployment means	1.75	1.75	0.8 ^b	0.95	0.9 ^c	0.65	2.69

^a A safety factor higher than 1.5 is used for supersonic parachute application.

^b Use 0.8 unless laboratory test results are available.

^c Closeness to the engine will determine this factor.

7.4.7.2 Number of Gores and Suspension-Line Strength

The drogue chute will be designed for a maximum force, F_o , of 22,000 pounds in the reefed and full-open stages. The suspension-line arrangement was selected in accordance with Table 7-8.

TABLE 7-8. Effect of Number of Suspension Lines/Gores on Required Suspension-Line Strength, GORE Width, and Vent Diameter.

Factors	Number of suspension lines			
	16	20	24	28
Design factor, D_F , from Table 7-7	2.78	2.78	2.78	2.78
Required suspension-line strength, lb ^a	3823	3058	2548	2184
Approximate gore width, ft	2.7	2.18	1.81	1.55
Minimum vent diameter, D_v , ft ^b	0.85	1.06	1.27	1.48
Area ratio (S_{vent}/S_{canopy}) · 100%	0.376	0.585	0.839	1.14
Suitable suspension line, MIL-C-7515 type	IX	IX	VIII	VII
Specification strength, lb	4000	4000	3000	2500

^a The suspension-line strength is determined by $F_{SL} = F_o/N_{SL}$.

^b The minimum vent diameter is determined by the requirement that radials do not overlap at the vent.

A canopy with 24 gores and 3000-pound-individual-strength suspension lines is selected primarily for gore width and vent diameter. The relatively large vent must be covered with wide vent lines held in place by proper connections.

The method described in section 6.4 is used for preliminary dimensioning of the horizontal ribbons. In this method, the expression $F_o/(C_{DS})_p$ is an indication of the pressure in the parachute canopy; the gore width, e_g , is an indication of the gore radius. A smaller gore width and resultant gore radius causes lower stress in the individual horizontal ribbons for a given internal pressure. Figure 6-41 shows boundary curves for the required horizontal ribbon strength. These data, based on analysis of many tested ribbon parachutes, were first presented in Reference 5.39 and subsequently updated by the author.

For the reefed parachute,

$$F_R/(C_{DS})_R = \frac{22,000 \text{ lb}}{21.62 \text{ ft}^2} = 1017.6 \text{ lb/ft}^2$$

The gore width of the reefed parachute is obtained from the following consideration. The reefed drag area is equivalent to the drag area of a parachute with the following nominal diameter (D_{RC}):

$$S_{o_{\text{reefed}}} = \frac{(C_{DS})_R}{C_{D_0}} = \frac{21.62 \text{ ft}^2}{0.55} = 39.31 \text{ ft}^2$$

The equivalent nominal diameter for the reefed parachute is

$$D_{R_0} = 1.128 \sqrt{S_o} = 1.128 \sqrt{39.31} = 7.07 \text{ ft}$$

and the gore width is

$$e_{rs} = \frac{D_{ro} \pi}{N_{SL}} = \frac{(7.07)\pi}{24} = 0.93 \text{ ft}$$

For an $\frac{F_{ro}}{(C_{DS})_p}$ of 1017.6 lb/ft² and gore width of 0.935, Figure 6-41 requires a horizontal ribbon strength of 500 pounds. For the fully open parachute, we obtain $\frac{F_o}{(C_{DS})_p}$ to $\frac{22,000 \text{ lb}}{82.95 \text{ ft}^2} = 265.2 \text{ lb/ft}^2$ and e_s to 1.8 feet. This condition requires a horizontal ribbon with 200-pound strength.

Two-inch-wide ribbon with 460-pound strength, MIL-T-5608, Type DII, is selected for the upper canopy part, and 2-inch-wide ribbon with 300-pound strength, MIL-T-5608, Type CV, is used for the lower part of the canopy. This drogue parachute will be subjected to high-frequency ribbon flutter during its high-speed descent from altitude, which may include a descent on the drogue chute from 50,000 to 7000 feet. Disintegration of horizontal and vertical ribbon and the stitching connecting the ribbons has occurred in the past during long-duration, high-speed applications of reefed and unreefed ribbon chutes. This high-frequency flutter is especially pronounced on the uninflated part of reefed ribbon parachutes.

Experience has shown that the following design features will counteract this problem:

1. Tight spacing of vertical ribbons.
2. Two vertical ribbons, one on each side of horizontal ribbon.
3. Three rows of stitching with F-F thread in the vertical ribbon.

All three features are used in this canopy design.

7.4.7.3 Design of Radials, Vent and Skirt Tape, and Vent Lines

Radials. Based on experience, radials are designed to have 80% of the strength of the suspension lines; $0.8 \cdot 3000 = 2400$ pounds. Three 2-inch-wide tapes of MIL-T-5608 form each radial; two 1000-pound Class EII tapes and one 460-pound Class DII tape give each radial a combined strength of 2460 pounds. It may be possible to use only two 1000-pound strength tapes that have 80% of the actual load of 2548 pounds.

Skirt and Vent Tape. In accordance with the discussion in section 7.6.6, the selected skirt tape is equal in strength to the suspension line but is 2 inches wide. Nylon tape (MIL-T-5608, Class E, Type V) with 3000-pound strength meets this requirement.

The required strength of the vent tape is

$$F_{VZ} = \frac{F_{RT} DF}{2 \sin \frac{360}{N_{SL}}} = \frac{(2548)(0.8)(2.68)}{2 \sin 15 \text{ deg}} = \frac{5463}{0.5176} = 10,554 \text{ lb}$$

Because some of this load will be taken by the vent lines, a double 4000-pound webbing is chosen in accordance with MIL-W-2756, Type II.

Special attention is required to obtain a design that achieves proper connection between radial tape, vent tape, and vent lines.

Vent Lines. The vent lines should have 60% of the strength of the radial tapes and be 5% shorter than the finished vent diameter.

7.4.7.4 Drogue Chute Riser Design

The drogue chute riser is formed of bundled suspension lines. This design eliminates the 20% connection loss, u , on the parachute side and permits a highly efficient connection on the drone side. The individual lines must be secured against each other to prevent flutter abrasion. Each line runs from a loop on the canopy radial, down the riser, around the drone connection point, and up the riser to an opposite radial-tape loop. Tests should be made to determine the strength of the radial-tape and suspension-line-loop connection and the individual loop around the drone hard point. A wrap-around keeper is used on the riser suspension line transfer point.

7.4.8 Aerodynamic Design of Ribbon Parachute Canopies

The two most important aerodynamic features that determine the design of a ribbon canopy are (1) canopy porosity, λ_T ; and (2) vertical ribbon spacing, a , which influences effective porosity, λ_e .

7.4.8.1 Canopy Porosity

The porosity of a ribbon canopy is defined as the percentage ratio of openings in the canopy plus the material porosity divided by the total canopy surface area. Canopy porosity affects parachute stability, drag, and opening process. A canopy with high porosity provides for good parachute stability, and uniform, low force inflation, but also lower drag than a canopy with lower porosity. Too high a canopy porosity may result in no or only partial canopy inflation.

The operational porosity limit decreases with decreasing parachute diameter from about 35% total porosity for a stable 3-foot-diameter parachute to about 12% porosity for a 100-foot-diameter parachute (see Figure 6-23 (a) and Table 6-3). Section 6.2.4 discusses the effect of canopy porosity on the design and performance of ribbon parachutes.

Properly designed conical ribbon parachutes with the correct porosity have an oscillation equal to or less than 2 to 3 degrees; a drag coefficient, C_{D_0} , of 0.55; and an opening-force coefficient, C_x , of 1.05 to 1.07 for subsonic applications with low forebody drag, such as experienced in wind-tunnel tests.

The vertical ribbon spacing discussed in section 7.4.8.2 is of utmost importance for supersonic application. A canopy porosity of 25 to 26% in accordance with Figure 6-23, Curve III, and Table 6-3 is recommended for this application.

7.4.8.2 Vertical Ribbon Spacing

Ribbon parachutes in the past were designed with individual gores, and the gores were connected with radial ribbons and several rows of stitching. This arrangement created the "venetian blind effect" shown in Figure 7-19. The venetian blind effect increases the effective canopy porosity discussed in section 6.2.4.

More recently, ribbon canopies have been designed with continuous horizontal ribbons, a design that offers savings in weight and cost. This design is described in detail in section 7.4.10.

Figure 7-20 shows the basic arrangement of a canopy gore and ribbon grid consisting of horizontal and vertical ribbons.

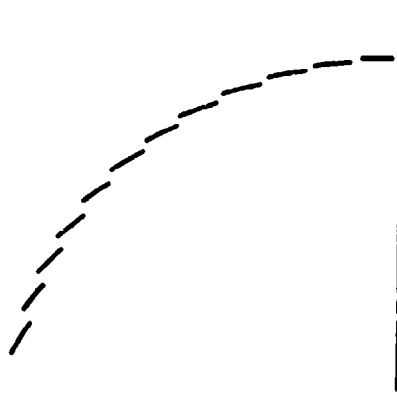


FIGURE 7-19. Venetian-Blind Effect of Horizontal Ribbon in a Ribbon Canopy.

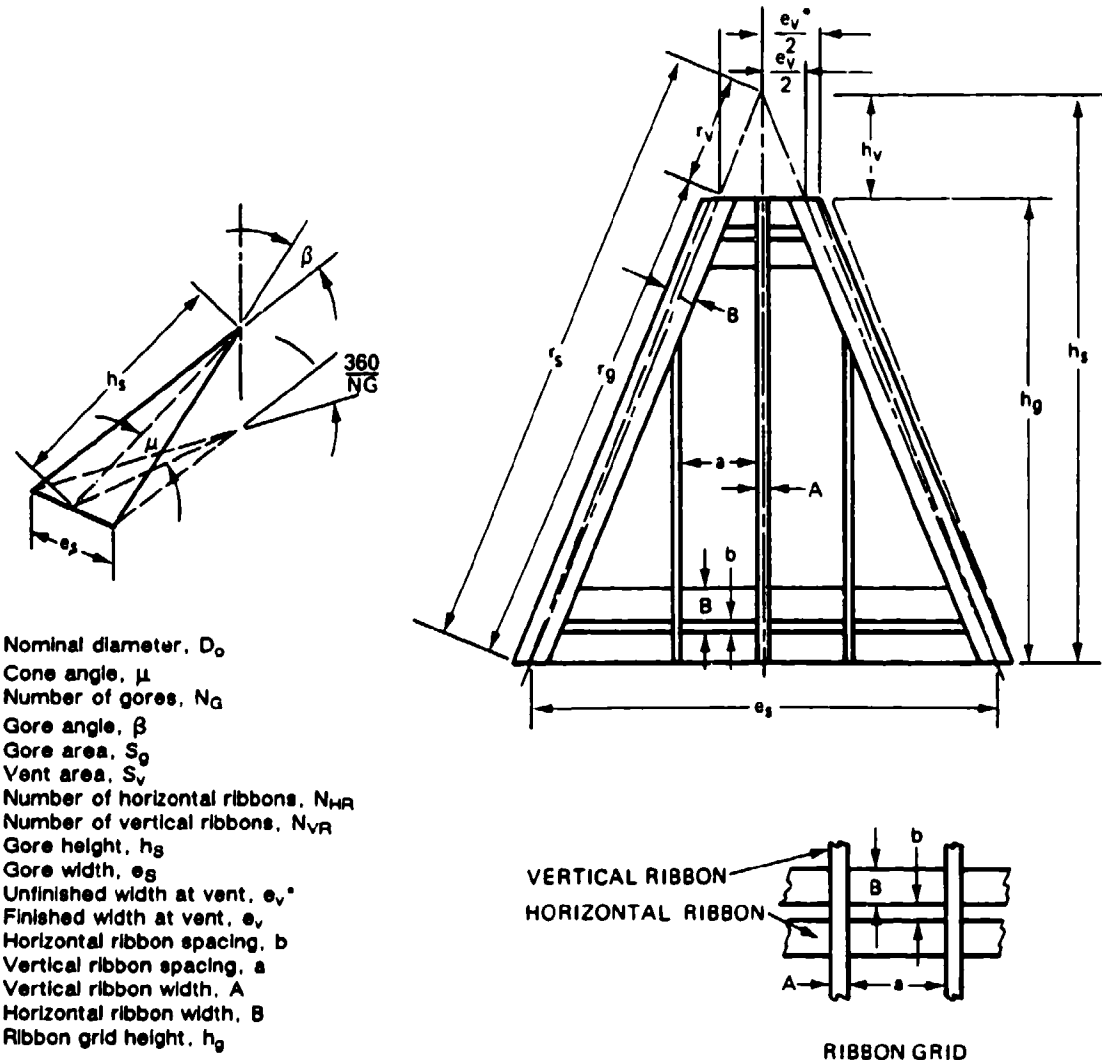


FIGURE 7-20. Canopy Gore Layout.

Section 6.2.4 explains the relationship of canopy loading, $W/(C_{DS})_p$; effective porosity, λ_e ; and vertical ribbon spacing, a . Ribbon parachutes used as final descent parachutes use a vertical ribbon spacing to horizontal ribbon width a/B of 2.5 to 4.0. This spacing allows advantage to be taken of the change in effective porosity. High-canopy-loading ribbon parachutes, such as first-stage drogue chutes, use a vertical ribbon spacing of 1 to 2 to avoid the negative effects of the change in effective porosity. A narrow vertical ribbon spacing of 1.25 times the width of the horizontal ribbon width will be used for the drogue chute.

7.4.8.3 Drogue Chute Summary

Parachute type	30-deg conical ribbon	
Parachute diameter	D_o	13.61 feet
Suspension-line ratio		$L_e/D_o = 1.5$
Canopy porosity	λ_T	25 to 26%
Vertical to horizontal ribbon spacing	a/B	1.25

7.4.9 Canopy Gore Design and Porosity Check

7.4.9.1 Canopy Gore Calculation

Preliminary nominal parachute	$D_o = 13.61 \text{ ft}$ (Section 7.4.3)
Number of gores	$N_G = 24$
Canopy cone angle	$\lambda = 30 \text{ deg}$
Canopy surface area	$S_o = 145.48 \text{ ft}^2$
Vent area	$S_v < 0.01 S_o$

Labeled with the definitions from Figure 7-20, the individual gore dimensions are as follows:

$$\text{Gore area, } S_g = \frac{S_o}{N_G} = \frac{145.48 \text{ ft}^2}{24} = 6.06 \text{ ft}^2 = 872.9 \text{ in}^2$$

Gore half angle, $\beta/2$:

$$\sin \beta/2 = \cos \mu \left[\sin \frac{360}{2 N_G} \right]$$

$$\sin \beta/2 = \cos 30 \text{ deg} \left[\sin \frac{360}{2.24} \right] = 0.866(0.1305) = 0.113$$

$$\beta/2 = 6^\circ 29' = 6.48 \text{ deg}$$

$$\text{gore angle } \beta = 12.96 \text{ deg}$$

$$\cos \beta/2 = 0.99361$$

$$\tan \beta/2 = 0.11368$$

Gore radius, r_S :

$$r_S = \left[\frac{S_g}{\sin \beta/2(\cos \beta/2)} \right]^{1/2} = \left[\frac{872.9 \text{ in.}^2}{0.1130(0.9936)} \right]^{1/2}$$

$$r_S = 88.44 \text{ in.}$$

$$\text{Gore height, } h_S = r_S (\cos \beta/2) = (88.44 \text{ in.})(0.99361) = 87.87 \text{ in.}$$

$$\text{Gore width, } e_S = 2r_S(\sin \beta/2) = (2)(88.44)(0.1137) = 20.11 \text{ in.}$$

Vent area criteria:

$$1. S_V < 0.01 S_o$$

$$S_V < 0.01(145.48 \text{ ft}^2) = 1.45 \text{ ft}^2$$

$$2. D_V \pi \geq 24 \cdot \text{width of radial ribbon with no between spacing at vent}$$

$$\pi \cdot D_V \geq 24(2.0) = 48 \text{ in.}$$

$$D_V = \frac{48 \text{ in.}}{\pi} = 15.28 \text{ in.} = 1.27 \text{ ft}$$

$$S_V = (15.28)^2(0.7854) = 183.37 \text{ in}^2 = 1.273 \text{ ft}^2$$

$$\frac{S_V}{S_o} = \frac{1.273}{145.48} = 0.00875$$

Therefore, $\frac{S_V}{S_o}$ is less than 1%.

Vent height, h_V :

$$h_V = r_V \left(\cos \frac{\beta}{2} \right) = \frac{D_V}{2} \left(\cos \frac{\beta}{2} \right)$$

$$h_V = 7.64(0.9936) = 7.59 \text{ in.}$$

$$\text{Ribbon grid height, } h_g = 87.87 - 7.59 = 80.28 \text{ in.}$$

All previous gore dimensions and the dimensions shown in Figure 7-21 are preliminary. The horizontal ribbon spacing, b , is controlled by the required porosity, λ . Required changes in horizontal ribbon spacing may result in slight changes in gore and canopy dimensions.

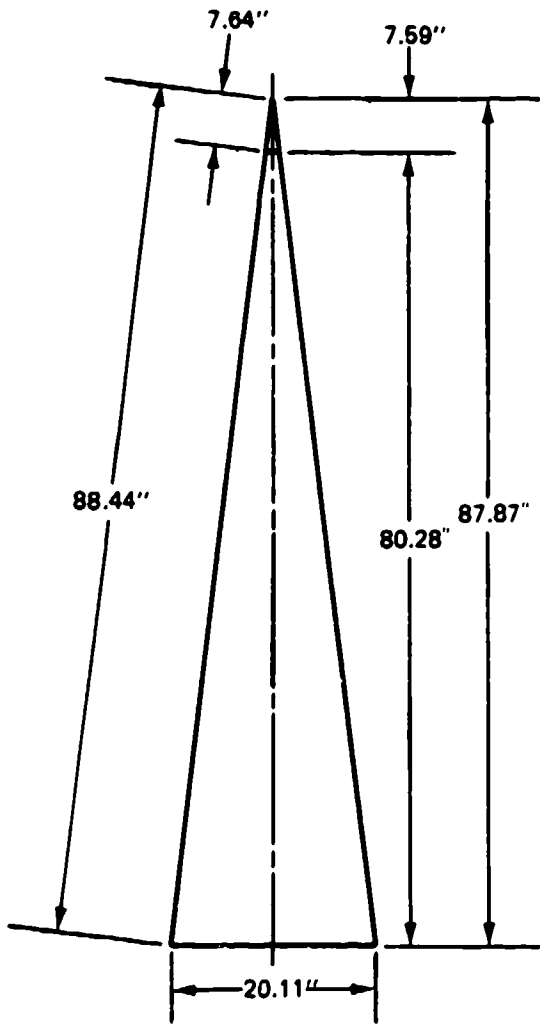


FIGURE 7-21. Preliminary Gore Dimensions.

7.4.9.2 Preliminary Gore-Porosity Check

Two methods of calculating gore porosity are in use. The older method, described in Reference 5.39, has been updated in this chapter. This method allows calculation of the porosity for preliminary design purposes when no final gore drawings are available. Reference 2.2 shows how to calculate canopy porosity if a drawing is available based on the ratio of open spaces to total canopy area. Both methods include an estimation of the ribbon (material) porosity.

The total canopy porosity, $\lambda_T = \lambda_g + \lambda_m$ where

λ_g = gore porosity, %

λ_m = canopy fabric porosity, %

Figure 7-20 shows that the porosity of a perfect ribbon grid, λ_{ga} , can be calculated as:

$$\lambda_{ga} = \frac{\text{porosity of slot area}}{\text{total grid area}} = \frac{ab}{(a + A)(b + B)}$$

From the evaluation of numerous porosity calculations, the following estimate can be made:

$$\lambda_T = \lambda_{ga} - \Delta\lambda$$

where

$$\Delta\lambda = 2 \text{ to } 3\%$$

The porosity of a ribbon grid with variations in the distance of the horizontal ribbons is now calculated. The total porosity is estimated, and the most likable horizontal ribbon distance is selected for the first gore-porosity check (Table 7-9). The widths of the vertical ribbon, A, and the horizontal ribbon, B, are fixed values. The ratio of vertical ribbon spacing, to horizontal ribbon width, a/B, was previously selected to 1.25, which is equal to 2.5 inches. A horizontal ribbon distance, b, of 1.1 inches is selected as first approach based on data in Table 7-9.

TABLE 7-9. Grid Porosity as Function of Horizontal Ribbon Distance, b.

Desired total porosity, λ_T	% inches	25 to 26% (see section 7.10.8.2)			
		1.0	1.05	1.1	1.15
Selected horizontal ribbon spacing, b	%	26.67	27.54	28.39	29.21
Calculated grid porosity, λ_{ga}	%	1.17	2.04	2.89	3.71
$\Delta\lambda = \lambda_{ga} - 25.5\% (\lambda_T)$	%				

7.4.9.3 Recheck of Gore Dimensions with Vertical Ribbon Spacing, b, Equal to 1.1 Inches

With b equal to 1.1 inches, a gore recheck is required to determine the resultant number of horizontal ribbons and the gore height. The number of horizontal ribbons, N_{HR} , that can be spaced in the gore grid height, h_g , is

$$N_{HR} = \frac{h_g - B}{(B + b)} = \frac{80.28 - 2.0}{(2.0 + 1.1)} = 25.25 \text{ (see Figure 7-20)}$$

To avoid a decrease in parachute diameter, 26 horizontal ribbons are selected, changing the gore dimensions from those shown in Figure 7-21 to those shown in Figure 7-22.

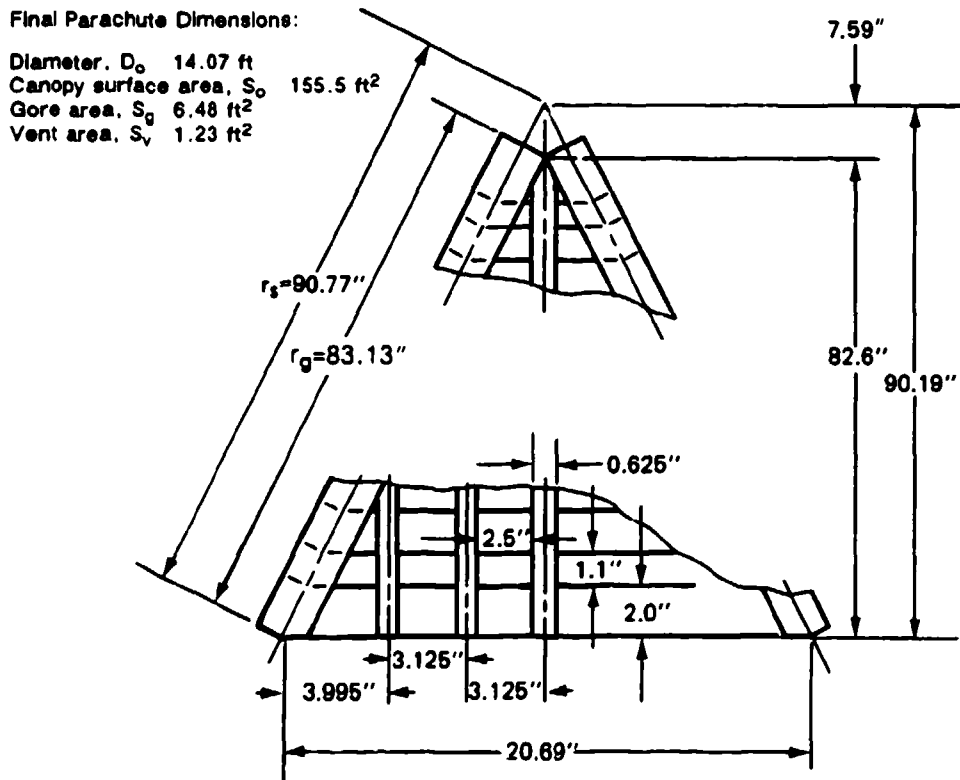


FIGURE 7-22. Final Gore Dimensions.

$$h_g = 26(2.0 + 1.1) + 2.0 = [(26)(3.1)] + 2 = 80.6 + 2.0$$

$$h_g = 82.6 \text{ in.}$$

$$e_S = 20.11 \frac{82.6}{80.28} = 20.69 \text{ in.}$$

$$h_S = h_g + h_v = 82.6 + 7.59 = 90.19$$

$$S_g = \frac{e_S h_S}{2} = \frac{20.69(90.19)}{2} = 933.02 \text{ in}^2 = 6.48 \text{ ft}^2$$

$$S_o = 24 S_g = 24(6.48 \text{ ft}^2) = 155.5 \text{ ft}^2$$

$$D_o = 1.1284 \sqrt{S_o} = 1.1284 \sqrt{155.5} = 14.07 \text{ ft}$$

Gore radius, $r_S = h_S \frac{1}{\cos \beta/2}$

$$r_S = 90.19 \frac{1}{0.99361} = 90.77 \text{ in.}$$

Radius of ribbon grid height, $r_g = h_g \frac{1}{\cos \beta/2} = \frac{82.60}{0.99361} = 83.13 \text{ in.}$ The number of vertical ribbons, N_{VR} , is five, based on free spacing of 2.5 inches and horizontal ribbon spacing, b , of 1.1 inches.

This change in diameter from 13.67 to 14.07 feet increases the parachute drag area by 6%, decreases the final rate of descent by about 3%, leaves the reefed opening force unchanged, and slightly increases the disreef opening force.

7.4.9.4 Gore-Porosity Recheck

$$\text{Geometric gore porosity, } \lambda_g = \lambda_{ga} + \left[\frac{S_v *}{S_o} \left[\frac{100 - \lambda_{ga}}{100} \right] \right] - \left[\frac{S_{RR}}{S_o} \lambda_{ga} \right]$$

Grid porosity, $\lambda_{ga} = 28.39\%$ (See Table 7-9.)

Open vent area, $S_v = 1.272 \cdot 0.59^* = 0.683 \text{ ft}^2$

Canopy area, $S_o = 155.50 \text{ ft}^2$

Area of radial ribbons, $S_{RR} = (r_g)(B)(N_{SL}) = (83.7 \text{ in.})(2.0 \text{ in.})(24) = 4017.6^2 \text{ in.} = 27.90 \text{ ft}^2$

$$\begin{aligned} \lambda_g &= 28.39 + \left[\frac{0.683}{155.50} \left[\frac{100 - 28.39}{100} \right] \right] = \left[\frac{27.90}{155.50} 28.39 \right] \\ &= 28.39 + [(0.0044)(0.7161)] - [(0.179)(28.39)] \\ &= 28.39 + 0.0032 - 5.08 = 23.31\% \end{aligned}$$

* Area covered by vent bands.

Material porosity,

$$\lambda_m = \frac{\lambda_m^*}{27.4} \left[1.0 - \left[\frac{\lambda_g}{100.0} + \frac{S_V + S_{RR} + S_{VR} + S_{ST}}{S_o} \right] \right]$$

Ribbon Specification Porosity, λ_m^* :

The upper half of the gore uses 500-pound ribbon; $\lambda = 0$. The lower half, encompassing 75% of the gore area, uses 300-pound ribbon; $\lambda = 150 \text{ ft}^3/\text{ft}^2/\text{min}$.

The conversion from material porosity to geometric porosity at 1/2-inch H₂O pressure is $27.4 \text{ ft}^3/\text{ft}^2 \text{ min} = 1\% \lambda$. Therefore,

$$\lambda_{m_{\text{gnd}}} = \frac{150(0.75)}{27.4} = 4.1\%$$

$$S_V = 0.683 \text{ ft}^2$$

$$S_{RR} = 27.90 \text{ ft}^2$$

Area of vertical ribbon covering horizontal ribbon, S_{VR} :

$$\begin{aligned} S_{VR} &= N_G \frac{N_{VR}}{2} A [h_g - ((N_{HR} - 1)6)] = (24) \left(\frac{5}{2} \right) (0.625)[82.6((27 - 1)1.1)] \\ &= 38.7[82.60 - ((26)(1.1))] = (38.7)(54.0) = 2089.80 \text{ in}^2 \\ &= 14.51 \text{ ft}^2 \end{aligned}$$

Area of skirt band, S_{SB} :

$$S_{SB} = N_g e_S = (24)(20.69 \text{ in.}) = 496.56 \text{ in}^2 = 3.45 \text{ ft}^2$$

$$\begin{aligned} \lambda_m &= \frac{(150)(0.75)}{27.4} \left[1.0 - \left(\frac{23.31}{100} + \frac{0.683 + 27.90 + 14.51 + 3.45}{155.50} \right) \right] \\ &= 4.106 \left[1.0 - \left(0.2331 + \frac{46.543}{155.50} \right) \right] = 4.106[1.0 - 0.5324] \\ &= (4.106)(0.4676) = 1.92\% \end{aligned}$$

Total canopy porosity, $\lambda_T = \lambda_g + \lambda_m = 23.31 + 1.92 = 25.23\%$. This porosity falls into the specified range of 25 to 26% as established in Table 7-6. Porosity should be cross-checked with the method outlined in Reference 2.2.

7.4.9.5 General Comments on Gore Design and Porosity Selection

The canopy gore design—total canopy porosity, λ_T ; spacing of vertical ribbon; size of vent; and pocket-band arrangement—are the primary design features that determine the aerodynamic performance of the parachute. The most important characteristics of parachute performance are stability, smooth opening, drag, and opening-force coefficients.

Determining porosity under a no-load condition is rather unrealistic, because most of the important aerodynamic characteristics occur under high-load conditions (opening shock) or medium-load conditions (descent). However, since the beginning of parachute development, aerodynamic parachute characteristics obtained in wind-tunnel and free-flight tests have been related to fixed design dimensions such as diameter and porosity.

Determining the effective porosity caused by the changing load during the opening process and by the venetian-blind effect of the ribbon grid design is practically impossible. Furthermore, the change in effective porosity is similar on all ribbon parachutes because of the similarities of the ribbon grid designs, load factors, and related changes in material elongation that cause deformation of the ribbon grids and the parachute canopies.

7.4.9.6 Computer Programs for Determining Gore Design and Porosity Calculation

Both gore design and porosity calculations can be determined by computer programs. Organizations involved in frequent design of ribbon parachutes should establish these programs.

7.4.10 Ribbon Parachute Canopies with Continuous Horizontal Ribbons

Ribbon parachute canopies are frequently designed and manufactured with continuous horizontal ribbons either in single or two-section canopies. The continuous ribbon design decreases weight and volume, increases the strength of the horizontal ribbon-radial connection, and simplifies manufacturing. Continuous horizontal ribbons change the porosity characteristics of the canopy.

Figure 7-19 shows how the individual horizontal ribbons orient themselves in a canopy manufactured from individual triangular gores. In the inflated canopy, the horizontal ribbons in the canopy crown area orient parallel to the canopy design. However, in the skirt area, the canopy design line is almost parallel to the airflow. This design, usually called the "venetian blind effect," causes the longer leading edge of each horizontal ribbon to bulge out and position the ribbon with a positive angle of attack to the airflow. The result is an increase in effective porosity under high dynamic pressure conditions. The venetian blind effect is discussed in section 6.2.4, and the influence of canopy loading on the change in effective porosity is shown in Figure 6-24.

Designing canopies with continuous horizontal ribbons changes the venetian blind effect. Returning to Figure 7-19, it is obvious that continuous horizontal ribbons in the canopy skirt area do not bulge out since leading and trailing ribbon edges have the same length and do not position themselves with an angle of attack to the airflow. However, in the crown area of the canopy where each gore forms a triangle, the equal length of the leading and trailing ribbon edges now gives each ribbon a negative angle of attack thereby increasing the effective porosity in the canopy crown area. The effect is minimized by large number of gores and by the use of a center vertical ribbon, or a miniradial, as Sandia engineers call it.

Discussion with Sandia and industry personnel indicates that no measurable difference has been found in the aerodynamic characteristics of ribbon parachute canopies designed with individual gores or with continuous horizontal ribbons so long as the canopies contain a large number of gores and a center vertical ribbon. However, a slight delay in initial inflation seems to occur on small parachutes with a small number of gores. Closer spacing of vertical ribbons in the canopy crown area should counteract this delay. Another method of counteracting the delay is by gathering the trailing edges of horizontal ribbons with several rows of stitching and using a lower porosity in the crown area.

7.4.11 Use of Kevlar Fabrics

Many modern ribbon parachutes use Kevlar suspension lines, risers, and canopy skirt, lateral, and vent tapes, which results in a decrease in weight and volume. Section 6.5.5 discusses all aspects of working with Kevlar in the design of parachute assemblies. This includes physical characteristics of Kevlar fibers and fabrics, available Kevlar fabrics, and experience in designing in Kevlar. Section 6.6.5 should be studied before designing in Kevlar.

CHAPTER 8

PARACHUTE RECOVERY SYSTEM APPLICATIONS

8.1 APPLICATIONS ANALYSIS

Parachutes are the primary means of aerial recovery and landing of air and space vehicles; aircrew emergency escape; retardation of ordnance; airdrop of military troops and supplies; premeditated use by sport parachutists, rescue personnel, and smoke jumpers; and other applications.

The *Recovery Systems Design Guide* (Reference 2.1) describes many parachute recovery systems applications in use through 1977. This chapter describes parachute applications in use or being developed since 1978.

Different applications require a variety of parachute types. Tables 5-1 through 5-5 list 29 different parachute and inflatable decelerator types. Table 8-1 lists parachute design criteria that apply to all parachute applications. These criteria are useful in understanding why a particular parachute was used for a specific application described in this chapter.

TABLE 8-1. Parachute Criteria.

<ul style="list-style-type: none"> • Reliability • Stability • High drag • Low opening shock • High Mach capability • Low weight and volume • Repeatability of performance • Environmental adaptability • Growth potential • Indifference to damage • Simplicity of design and manufacturing 	<ul style="list-style-type: none"> • Simplicity of maintenance and service • Low acquisition cost • Low life-cycle cost • Weight efficiency $\frac{(C_{DS})_o}{W_p}$ • Volume efficiency $\frac{(C_{DS})_o}{V_p}$ • Cost efficiency $\frac{(C_{DS})_o}{\\$}$ • $(C_{DS})_o$ Parachute drag area, ft²
	W_p Parachute weight, lb V_p Parachute volume, ft ³

Reliability of operation is understandably the number one requirement for all parachute applications. Each parachute listed in the tables opens reliably when deployed in good airflow in the velocity range suitable for that particular parachute. Parachute inflation problems are introduced by installation, forebody wake, air vehicle instability, interference with vehicle protrusion in the path of the deploying parachute, and velocity and altitude problems—all factors that must be considered in the preliminary selection of the parachute assembly, installation, and deployment concept. Other criteria, such as stability, low opening forces, simplicity of design, suitability for the mission velocity, altitude, and environmental profile narrow the choices but frequently leave several candidates for the choice of main descent parachute(s). This main descent parachute contributes the largest percentage of the weight and volume of the parachute assembly. For otherwise equal performance, weight and volume are generally the deciding factors for main descent parachute selection. The use of parachute reefing and parachute clusters gives the design engineer a chance to control parachute opening forces and stability and allows the use of high drag parachutes that, as a rule, have high opening forces and poor stability.

For specific parachute applications (air vehicles, aircrew escape, ordnance retardation), the requirements of minimum weight and especially of minimum volume outweigh parachute assembly cost considerations. Parachute assemblies, as shown in Figure 6-61, constitute 8 to 12% of the total vehicle weight; this increases to 12 to 15% if an impact-attenuation system is added. The parachute recovery system, ballast during the operational mission, is needed only for final recovery. Every pound saved in the parachute assembly allows greater payload, range, or mission-oriented on-board equipment. The ever-increasing use of Kevlar in primary load carrying members, a very important step in parachute development, can reduce the weight of parachute assemblies by 25 to 40%, depending on the amount of Kevlar used. Newer materials, such as Specktra, may further reduce weight and volume.

One criterion for judging the weight effectiveness of parachutes is the amount of parachute drag area produced per pound of parachute weight, $(C_{DS})_P/W_P$. This criterion is called the "weight effectiveness" in this manual. Weight effectiveness is automatically related to volume effectiveness: the lower the parachute assembly weight, the lower the required volume for storing the parachute assembly. The size, and hence the required drag area and resultant weight of the main parachute(s), are determined by the permissible rate of descent at landing. Table 8-2 compares the weight effectiveness of parachutes manufactured from nylon fabric and from a hybrid nylon/Kevlar fabric. The weight effectiveness of well-designed nylon parachutes reaches 65 square feet (ft^2) of drag area per pound of parachute weight. Hybrid parachutes using nylon for the canopy and Kevlar for suspension lines, canopy tapes, and radials reach 85 ft^2 of drag area per pound of parachute weight. Kevlar will help alleviate the ever-present problem of vehicle weight growth during development and vehicle life. The weight of the F-111 aircraft crew module, the Teledyne Ryan Firebee target drone, and the Mercury and Apollo spacecraft grew by 25 to 80% with no permissible increase in vehicle rate of descent, parachute compartment volume, or parachute opening forces taken by the vehicle

TABLE 8-2 Drag Area/Weight Efficiency ($C_D S_p/W_p$) for Several Operational Parachutes.

Parachute type	Application	Recovery weight, lb	Parachute D ₀ , ft	V _{eo} , fps	IAS, kft	Parachute performance	Max. force, lb	Parachute weight, lb	Drag coefficient, C _{D0}	Parachute drag area, ft ²	Weight effectiveness C _D S _p W _p /lb
Solid flat (G-1A)	Aerial delivery	3000	100	23	150	2000	...	215	0.66	5200	25.2
10% extended skirt (T-10C)	Army troop chute	360	34.9	21	150	2000	low	13.75	0.89	885	64
Fully extended skirt	Q2-B drone	1800	67.5	22.5	275	15,000	...	62	0.85	3050	49.2
Ringsail	Mercury capsule	2300	63.1	26	150	10,000	10,000	55.4	0.75	2350	42.5
Extended skirt (cluster of two)	USD-5 drone	4800	78	22.3	225	2500	15,000	64.5	0.825 (cluster)	3940	61.0
Ringsail (cluster of two)	Apollo	13,000	85.2	28.8	165	10,000	23,000	110	0.74 (cluster)	4400	40.0
Ringsail	Experimental	9786	128.8	26.4	225	16,000	25,650	230.3	0.87	11,300	48.5
AIM	CL-289 drone	475	31	32	300	1000	...	11.08	0.55	416	38.5*
Triconical	Teledyne-Ryan RPV	1465	76.4	19.7	54.5	0.93	4273	77.3**
Polyconical	SLAT	1200	63	18	200	5000	6000	35.8	0.96	3109	70.3*
Triconical	AGM-109	1900	71.8	25	200	10,000	8000	44.1	0.91	3682	83.7*
Cross	Aries	2000	59.4	27.3	150	10,000	...	47.5	0.8	2250	46.7
Cross	High-altitude meteorology	...	23.0	3.0	...	>100,000	...	1.3	...	320	246 ^c

^aNylon canopy, Kevlar suspension lines.^bPioneer Aerospace information.^cNSWC drawing 2A21730.

hard points. Past attempted solutions have often involved higher parachute pack density. When initial design of the parachute recovery system must include a high pack density for the parachute assembly, costly and time consuming vehicle redesign may be necessary to accommodate the required larger parachute(s). For new vehicles, the prime contractor and the recovery system subcontractor should take into account unavoidable vehicle growth. A pack density in the 30- to 35-lb/ft³ range allows an increase in parachute size, weight, and volume of approximately 35% using a pack density in the 45-lb/ft³ range. Planning for vehicle weight increase and the requirement for a larger, more voluminous parachute assembly appear to be the rule in designing parachute recovery and retardation systems.

8.2 AIR AND SPACE VEHICLE RECOVERY

This section describes the parachute recovery systems for the U.S. Navy supersonic low-altitude target drone (SLAT), the Navy and Air Force cruise missile midair retrieval systems, and the Canadian CL 289 reconnaissance drone.

8.. AQM-127A Supersonic Low-Altitude Target (SLAT)

The SLAT vehicle duplicates the attack of a fast, on-the-deck flying missile against Navy ships. The SLAT can fly at supersonic speed and high altitude and dive from outside the effective range of ship defenses for an on-the-deck attack. Parachute recovery is initiated by vehicle pull up about 1 mile prior to target contact, and parachute deployment is initiated at Mach 0.5 at an altitude of 5000 to 10,000 feet. Drone recovery is possible over land and water. The parachute system consists of a drogue-chute assembly and a single main parachute assembly with different main parachutes for land or water landing. Parachute deployment starts with the pyro-ejection of the parachute compartment cover located on the upper side of the vehicle, shown in Figure 8-1; this ejection also extracts a small pilot chute that, in turn, deploys a 4.2-foot-diameter, conical ribbon drogue-chute. This drogue chute has a small amount of fixed reefing for increased stability in the wake of the drone forebody. The drogue chute decelerates the drone, pulls it into a high angle of attack attitude, and, after 13 seconds, disconnects and deploys the main recovery parachute. Both the drogue and the main parachute are reefed in two stages for opening-force control to a 3-g level. A 48-foot-diameter polyconical, solid fabric parachute is used for water landing. Two flotation bags located in the parachute compartment and inflated with nitrogen to 3000 psi are deployed 36 seconds after the recovery command. The flotation bags float the missile in a 30-degree, nose-high attitude.

A bridle connecting the tops of the two flotation bags serves as the contact point for helicopter hookup during water retrieval.

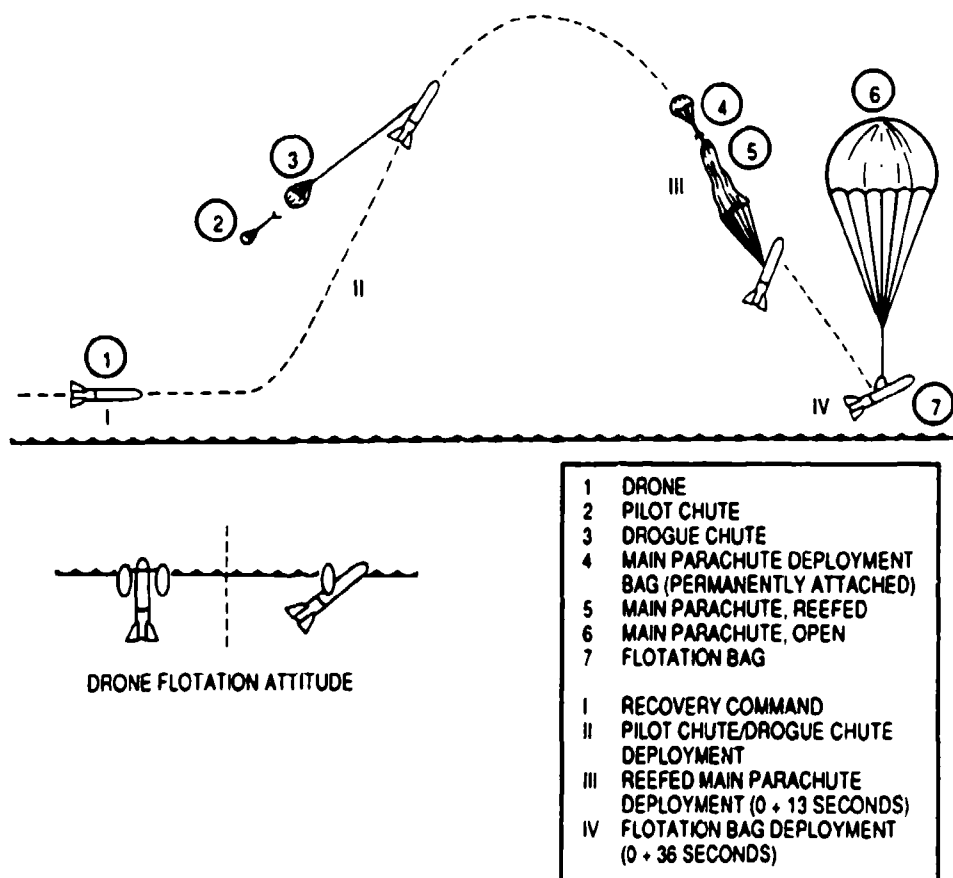


FIGURE 8-1. Slat Drone Parachute Recovery Sequence.

A 63-foot-diameter polyconical parachute is used to land the 1200-pound target drone on land at a rate of descent of 18 ft/s in a slightly nose-high attitude. Both main parachutes use standard-porosity nylon fabric for the canopy and Kevlar for canopy tapes, radials, suspension lines, and risers. The weight effectiveness (square foot of drag area per pound of parachute weight) is 70.5 lb/ft², a good value. No impact attenuation system is required at the 18 ft/s rate of descent.

8.2.2 CL 289 Reconnaissance Drone

The CL 289 reconnaissance drone with a recovery weight of approximately 375 pounds is the successor to the CL 89 reconnaissance drone developed in the early 1960s in Canada. The parachute landing system, developed by Irvin Canada, uses parachutes for deceleration and descent, and air bags for ground impact attenuation; the recovery system incorporates several innovative features.

Figure 8-2 (from Reference 8.1) shows the landing sequence. A fast drone turnaround time necessitates a precise landing in a preselected area, an undamaged drone after landing,

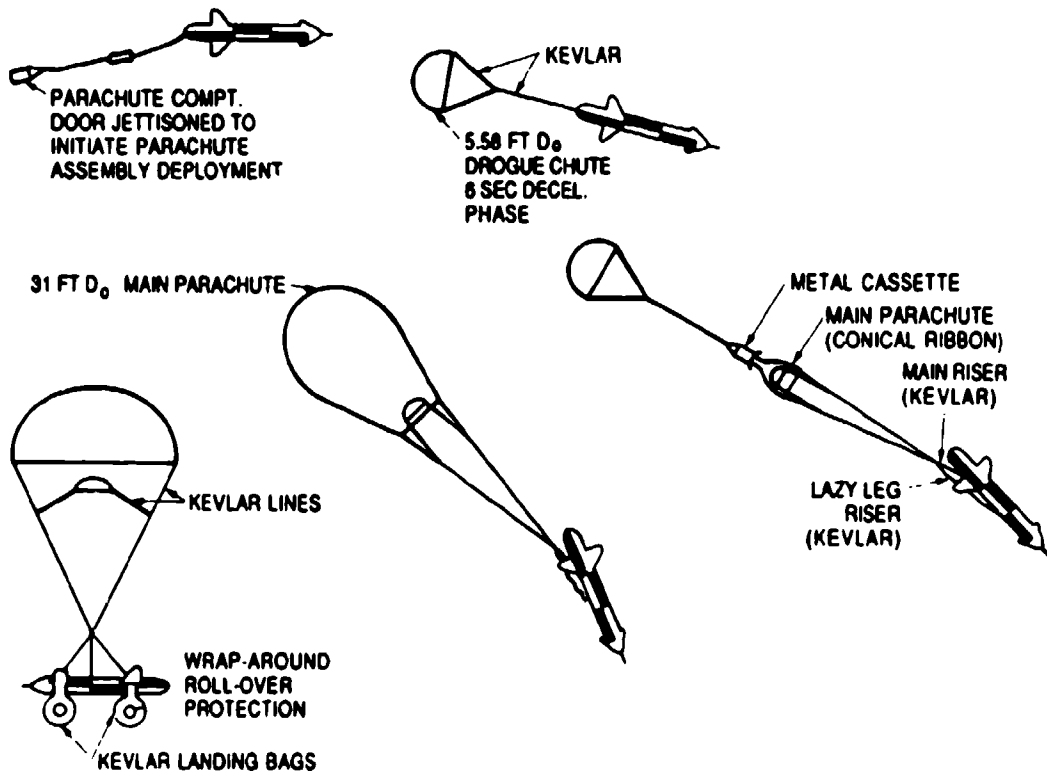


FIGURE 8-2. Sequence of CL 289 Drone Recovery.

and quick removal of the used and fast installation of a refurbished parachute air bag system. Recovery after a completed mission starts at about 250 knots with ejection of the parachute compartment cover located on the aft underside of the vehicle. The cover extracts a 5.58-foot-diameter, conical ribbon drogue chute that decelerates and stabilizes the drone and, after 6 seconds, disconnects and deploys the 31-foot-diameter conical ribbon main parachute that lowers the drone at a rate of descent of 31 ft/s. Both ribbon parachutes have variable porosity nylon canopies with lower porosity at the crown and higher porosity at the skirt area. The main parachute is equipped with an internal web chute for inflation control. The developer states that both features, the varied canopy porosity and the internal web chute, provide a more controlled and uniform canopy inflation. The working of the internal web chute is explained in Reference 5.89. A stable main descent parachute is required for proper air bag operation. The ribbon parachute was probably chosen based upon the positive experience with a similar parachute on the CL 89 drone. Both the drogue and the ribbon main parachutes are modern designs with continuous horizontal ribbons; a mostly nylon canopy; and Kevlar risers, suspension lines, and canopy reinforcing tapes. The parachute assembly is stored in a removable metal container packed to a density of 53 lb/ft³, a very high value. Using today's knowledge, a reefed cross parachute with good stability and with a 29% higher drag than the ribbon main parachute may somewhat relieve the high pack density problem.

The air bag design is shown in Figure 8-3. Both the nose and tail bags are two-compartment bags. One compartment works as the impact attenuator and the other compartment stays inflated and keeps the drone off the ground. Two interesting air bag features are the rollover protection provided by the nose air bag that wraps around the cylindrical drone body (shown in Figure 8-3) and the design of the air bag pressure relief valves (shown in Figure 8-4 and shown previously as Figure 6-81). When the internal bag pressure reaches the operational pressure level, sleeves manufactured from stretch fabric expand and meter the air out of the bags, using the variable porosity characteristics of the stretch fabric to control the permissible deceleration level for various landing conditions, an elegant design approach. Reference 8.1 documents the design and testing of the parachute air bag landing system. The weight effectiveness of the main parachute, approximately $39 \text{ lb}/\text{ft}^2$, is relatively low. However, the use of air bag attenuators necessitates the use of a stable, and therefore low-drag, main parachute. Ribbon parachutes are stronger and heavier and can stand a lot of abuse, including high deployment speed and multiple reuse.

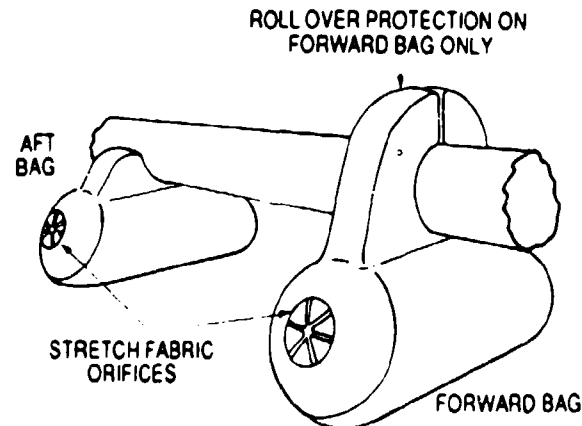


FIGURE 8-3. Impact Attenuation Bag Configuration.

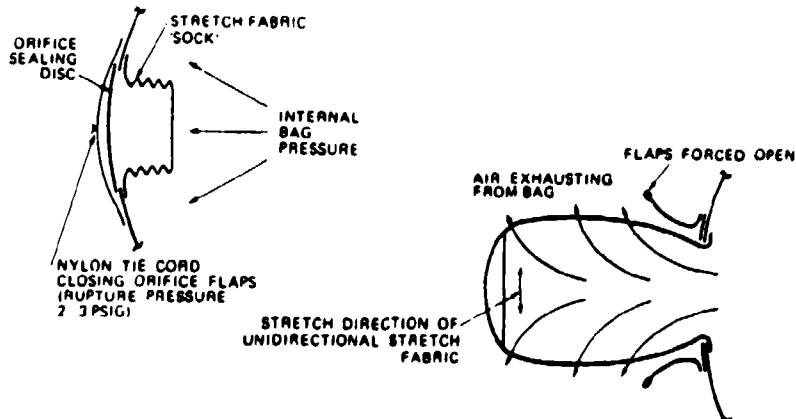


FIGURE 8-4. Pressure Relief Valves for the CL 289 Air Bags
Using Stretch Fabric Sleeves. (Repeat of Figure 6-81
for purposes of accessibility.)

8.2.3 Midair Retrieval of the USAF AGM-86B Air Launched Cruise Missile

The midair retrieval system (MARS) for the Air Force air launched cruise missile (ALCM) has two functions. MARS allows retrieval by helicopter after a training mission is completed and allows ground recovery of the missile if the training flight must be aborted. An annular parachute as main descent parachute and a ringsail engagement parachute form an effective MARS parachute assembly.

In the flight termination mode, a drogue chute is used for high-speed deceleration at dynamic pressures up to $900 \text{ lb}/\text{ft}^2$ and altitudes up to 40,000 feet. The annular parachute is deployed at 15,000 feet and ground-recovers the missile. In the MARS mode, the drogue chute is bypassed and midair retrieval takes place starting at 19,000 feet. The annular main and ringsail engagement parachute assembly is shown in Figure 8-5. A vehicle weighing up to 2000 pounds can be lowered by the 71.6-foot-diameter annular parachute at a rate of descent of 23.6 ft/s from an altitude of 10,000 feet. The development of the annular parachute concept and related airfoil parachute is described in References 5.37 and 5.38. The 22.3-foot-diameter ringsail engagement parachute is located above and is closely coupled to the main parachute. The annular parachute has a vent opening equal to 65% of the inflated canopy diameter. Airflow through this large vent inflates the ringsail engagement parachute, resulting in a very stable parachute assembly with no independent movement in the engagement parachute.

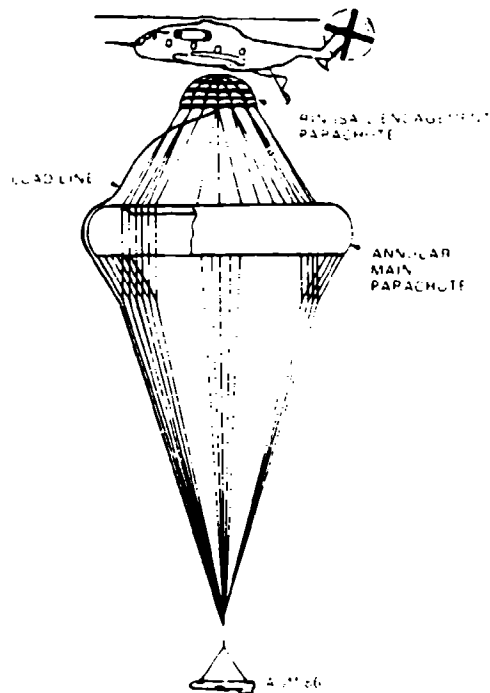


FIGURE 8-5. Midair Retrieval Parachute Assembly.

Figure 8-6 shows the parachute deployment sequence. Different signals initiate either the midair retrieval mode or the flight termination ground recovery mode. Both signals initiate ejection of the parachute compartment cover located on the vehicle underside. The cover simultaneously extracts a light design, 5.9-foot-diameter ringslot pilot chute and a strong, 1.8-foot-diameter ribbon pilot chute. At high-speed deployment, the large, light design pilot chute breaks away and the ribbon pilot chute deploys a 6.6-foot-diameter ribbon drogue chute. The missile descends on this drogue chute and, at 15,000 feet, disconnects and deploys the main parachute assembly for ground recovery. The MARS mode deployment sequence begins at 19,000 feet and at a low deployment speed. The large pilot chute bypasses the ribbon drogue chute and deploys the main parachute assembly as demonstrated in Figure 8-6. The time from cover ejection to ready-for-action main parachute is 24 seconds and is tailored to limit the parachute opening forces to 3 g for a 2000-pound vehicle. The vehicle turns over during the parachute deployment process. The helicopter, upon making contact with the engagement parachute, hooks a load line that runs around the engagement parachute, down the engagement parachute suspension line and the main parachute, to a disconnect located at the V-riser junction point. The intricate deployment, reefing, engagement, and parachute disconnect systems are described in Reference 8.3. Extensive use of Kevlar for the ribbon drogue and, where appropriate, for the main parachute assembly, decreases weight and volume, allowing stowage in a very limited parachute compartment at a pack density of 51 lb/ft³ (using form setting by autoclaving under vacuum and heat application). A 6-foot-diameter cross parachute is used for stabilizing the missile during helicopter tow.

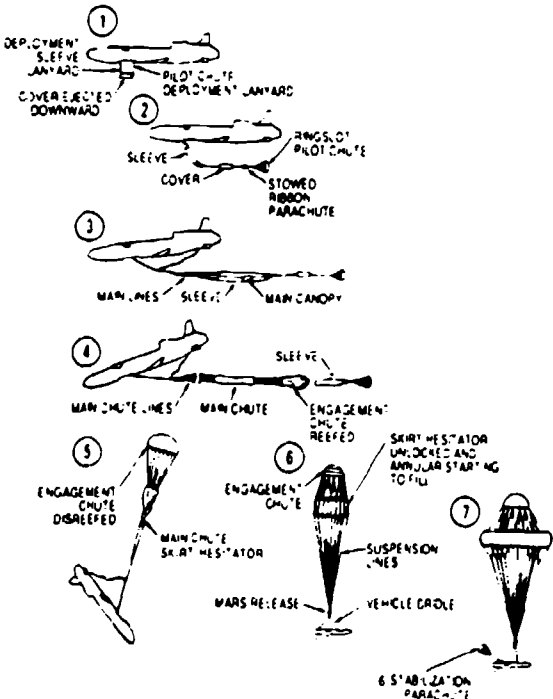


FIGURE 8-6. Deployment Sequence of the MARS Parachute System.

8.2.4 Midair Retrieval System for the Navy AGM-109 Cruise Missile

The Navy AGM-109 cruise missile uses the tandem parachute concept for helicopter midair retrieval after training missions are completed. Figure 8-7 shows the parachute deployment and midair retrieval sequence. The parachute system consists of a 71.8-foot-diameter triconical, gliding, main descent parachute and a 16.4-foot-diameter ringslot engagement parachute connected to the main parachute; the missile has a 13,600-pound Kevlar load line. Previous tandem systems for midair retrieval had problems maintaining tension in the heavy load line, poor yaw stability of the main parachute, and the engagement parachute trailing outside the wake of the main parachute.

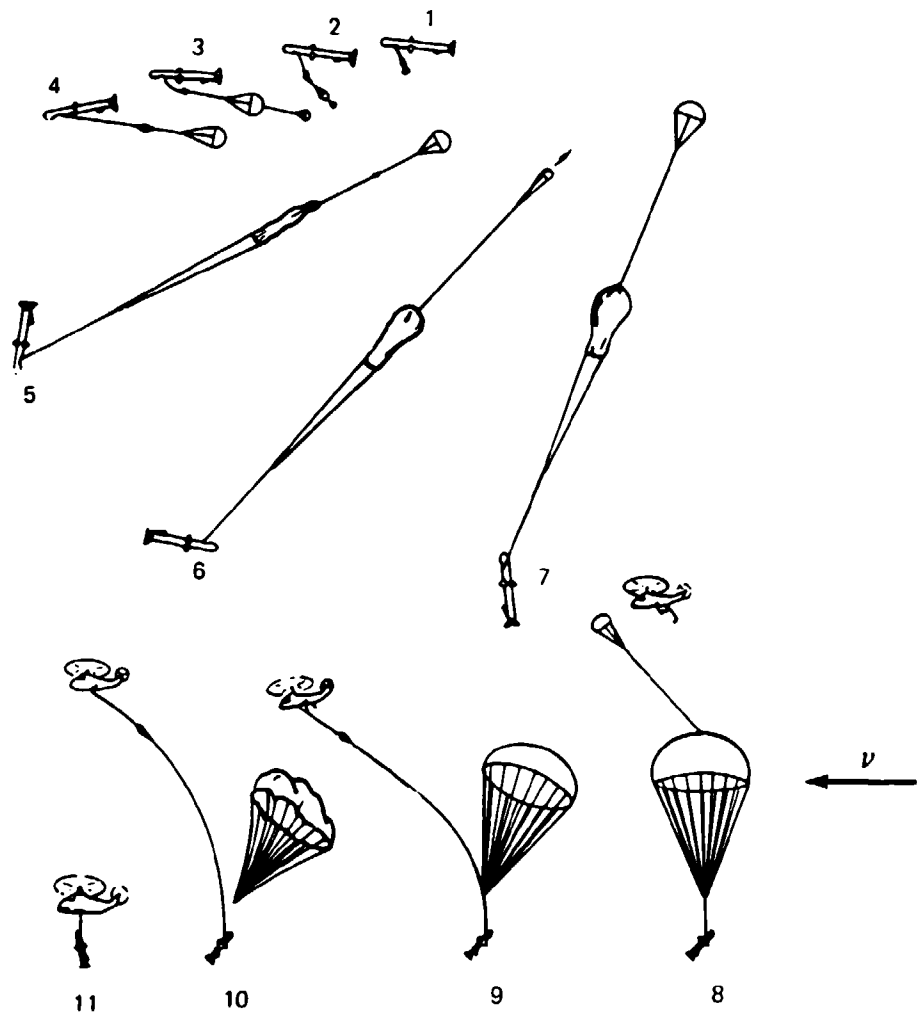


FIGURE 8-7. Parachute Deployment and Engagement Sequence.

These are characteristics that make it difficult for the helicopter to catch the engagement parachute in the proper position to disconnect the load line. Pioneer Parachute Co., Inc., Manchester, Conn., developed a tandem parachute system for the AGM-109 missile that overcomes the problems mentioned above. This system includes a lightweight Kevlar load line and a gliding main parachute with a glide ratio of 0.65 and a yaw stability of better than 1 degree per second. Gliding is obtained by venting two sections in each of 16 gores in the 64-gore canopy; this, together with stabilizing vents, provides for a stable gliding parachute with the engagement parachute trailing at a 65-degree attitude toward the main parachute, shown in sequence 8 of Figure 8-7. The tandem parachute assembly is detailed in Figure 8-8 and the vented canopy in Figure 8-9. Figures 8-7 through 8-9 are taken from Reference 8.4, which gives a detailed description of the development and testing of this tandem concept.

Upon deployment command, the missile performs a pull-up maneuver. When the dynamic pressure decreases to 80 lb/ft², the cover of the parachute compartment is pyro-ejected, and an attached lanyard deploys a 24-inch pilot chute that in turn deploys a 60-inch-diameter guide surface parachute, which then extracts the main parachute assembly. The tandem parachute assembly uses nylon for the parachute canopy and Kevlar for the load line, main parachute suspension lines, and canopy reinforcing tapes. The parachute assembly is pressure packed to a density of 43 lb/ft³, heat cycled during packing, and autoclaved at 180°F after packing for 20 hours to maintain form stability of the packed parachute. The weight effectiveness of the triconical main parachute expressed in square feet of drag area produced per pound of weight is 83.7 ft²/lb, a high value.

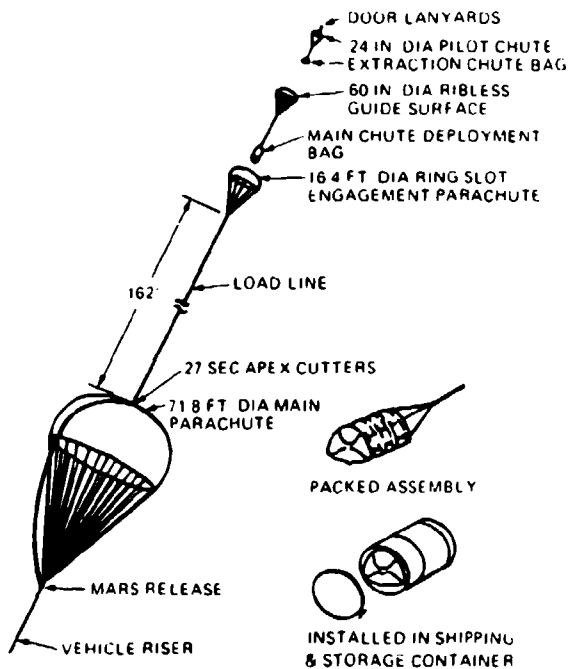


FIGURE 8-8. AGM-109 Tandem Parachute Assembly.

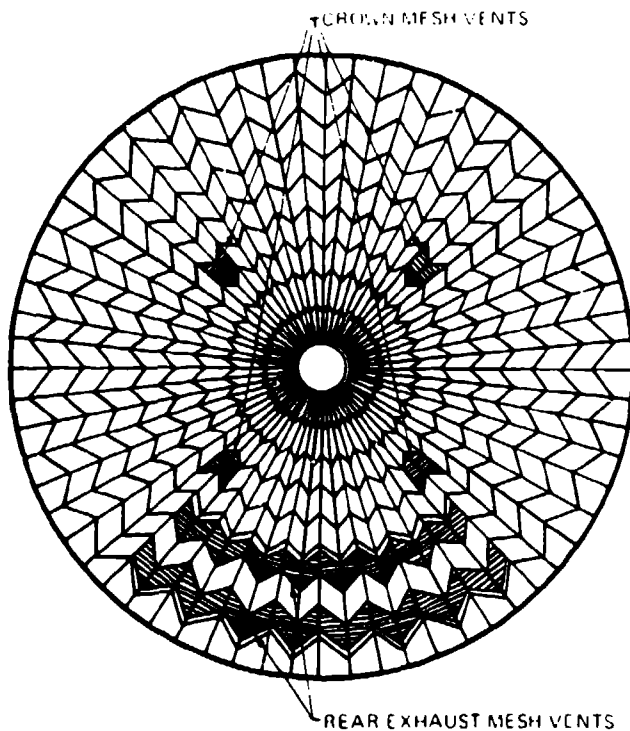


FIGURE 8-9. Main Canopy Plan.

8.2.5 Space Shuttle Solid Booster Rocket Parachute Recovery

The parachute recovery system for the three solid rocket boosters (SRBs) of the NASA Space Shuttle is described in Chapter 2 of Reference 2.1. The 175,000-pound steel casing boosters descend into the atmosphere broadside, thereby decelerating the booster to about Mach 0.6 at altitude of 16,000 feet. A single, 56-foot-diameter conical ribbon parachute, reefed in two steps, decelerates and stabilizes the booster. At 6000 feet, three 115-foot-diameter conical ribbon parachutes decelerate the booster to a water entry velocity of 85 ft/s. This system successfully recovered the SRBs in 10 out of 11 flights. References 6.41 and 8.5 to 8.11 detail individual development and test phases of the SRB parachute recovery system.

Two problems developed. (1) The water entry velocity, 85 ft/s, established in model drop tests did not prevent structural damage in the booster shells. (2) The development of a carbon-epoxy filament-wound booster casing decreased the booster weight and changed its mass properties, which resulted in higher reentry velocities and necessitated the development of a stronger, first-stage drogue chute.

To solve the water entry problem, the diameter of each of the three main descent parachutes was increased to 136 feet. The result was a 20-degree conical ribbon parachute with a canopy porosity of 15%, having 160 gores, suspension lines with a length 1.5 times the diameter, and weighing 2159 pounds.

The parachute is reefed in two steps, with the opening force per parachute limited to 175,000 pounds. To avoid differential elongation in the 204-foot-long suspension lines (discussed in section 6.6), the lines are interspaced in three sections. The parachute is packed to a density of 39 lb/ft³. Reference 8.10 describes the development and testing of the 136-foot-diameter ribbon main parachute.

As of January 1989, both boosters were recovered on 27 out of 29 Space Shuttle flights, with the first 13 flights using the 115-foot-diameter ribbon main parachutes and the remaining flights using the larger 136-foot-diameter parachutes. Individual drogue chutes have been used five times and the main parachutes, designed for 20 uses, have been used four times so far without having reached their useful life limits.

Future Space Shuttle launches from Vandenberg Air Force Base, Calif., will use the carbon-epoxy filament-wound case SRBs that are approximately 30,000 pounds lighter than the present 175,000-pound steel casing SRBs. A change in the mass properties of this booster will cause a change in a wide range of drogue chute deployment conditions, from low speed to deployment close to Mach 1 at 16,000 feet. This requires a stronger drogue chute to accommodate the higher dynamic pressure. The drogue chute diameter was reduced to 52.5 feet, and the design load increased to 375,000 pounds. The 20-degree conical ribbon parachute has a porosity of 20% and has 72 gores and suspension lines, with a 15,000-pound strength and a length equal to 1.8 times the diameter of the canopy. The parachute is reefed in two steps with Kevlar reefing lines; the rest of the parachute and riser are manufactured from nylon. The diameter of the pilot chute was reduced to 10 feet to comply with the available compartment volume. Deployment of the pilot chute/drogue chute combination over the required velocity range was investigated in pilot chute deployment tests at the Supersonic Naval Ordnance Research Track (SNORT), Naval Weapons Center, Calif. (Reference 8.11).

Aerial tests using a 50,000-pound test vehicle dropped from a B-52 aircraft were also conducted at the Naval Weapons Center. During one of these aerial drop tests in an overload condition, a parachute force of 471,000 pounds was recorded—probably the highest parachute load ever measured on a successful test. Numerous design, installation, and deployment problems encountered during the development of this almost 2000-pound drogue chute had to be solved as described in References 8.10 and 8.11. Use of this stronger drogue chute awaits use of the filament-wound composite booster casings.

8.3 AIRCREW EMERGENCY ESCAPE PARACHUTE SYSTEMS

8.3.1 Escape System Concepts

In Chapter 2 of Reference 2.1, requirements for and methods of recovering aircrews in case of aircraft emergencies are discussed in detail. Following are five methods of aircrew emergency escape now being used.

Manual Bailout. The aircrew exits the aircraft over the side of the cockpit, through a door or an escape hatch. A manually or automatically opening parachute, equipped with a lock set above 15,000 feet, is used for deceleration, descent, and landing. The manual bailout method is still used on military trainers and on transport aircraft. Manual bailout is limited to velocities below 300 knots because of difficulties in leaving the aircraft and the danger of contact with the aircraft. Tables 8-3 and 8-4 list Navy and Air Force personnel emergency parachutes used for manual bailout.

Tractor Rocket Extraction. As the name implies, the aircrew is pulled out and away from the aircraft by a tractor rocket. This extraction method uses an automatic parachute for recovery and landing. Often called the Yankee system, this method is used for military trainers, and has been used for emergency escape during flight testing of commercial aircraft. The danger of contact with the aircraft limits the velocity in this concept.

Ejection Seat. In the ejection-seat method, the crew member and the seat are ejected out of the aircraft on rails and then shot upward and away from the aircraft by rockets. A multiple parachute assembly decelerates and stabilizes the seat with the crew member remaining in the seat. At the proper altitude, or at the proper speed at low altitude, seat and crew member separate and the main descent parachute opens. Frequently, the opening main parachute is used to pull the crew member away from the seat. The separation of the crew member from the seat, and proper timing of main parachute deployment, require altitude and pressure sensors and multimode sequences for control of parachute deployment in the velocity-altitude range from zero on-the-deck to Mach 3 at altitudes approaching 100,000 feet. High dynamic pressure makes it difficult to restrain the limbs of the crew member and retain protective headgear. Multiple crew member ejection requires staggered timing and proper seat separation to avoid seat collisions and parachute interference.

Encapsulated Seat. The encapsulated seat method uses an ejection seat where the crew member is protected against air blast (high dynamic pressure) by a clamshell-type shield that folds over the seat from top and bottom or from the sides. Encapsulated seats used on the B-58 and B-70 bombers required parachute stabilization and retardation at high speeds and altitude, main parachutes for descent and landing, and impact attenuation for absorbing the landing impact. Crew members using both seats appreciated the protected environment and that some of the rescue and survival gear was moved from the parachute harness assembly to the encapsulated seats.

Crew Module. A crew module permits the aircraft crew to fly in a semishort sleeve environment. The crew module normally encompasses the aircraft cockpit cut from the fuselage by pyrocord, rocket-ejected from the aircraft, and rocket- or fin-stabilized until the stabilization and retardation drogue chute becomes effective. The drogue chute assembly lowers the crew module to the allowable opening speed or altitude for main parachute deployment. Crew modules need ground-impact/attenuation systems. The ground-

impact/attenuation systems, in turn, require a stable main parachute assembly. High drag parachutes in clusters are frequently used for the crew module method. Crew module parachute systems are designed for low g forces related to the deceleration limit of the human body.

Parachute assemblies designed for low opening forces using multiple reefing also result in a decrease in the weight of the parachute system. A parachute assembly designed for 3- g equivalent opening forces weighs 40% less than a parachute assembly designed for 6- g equivalent forces. A main parachute assembly designed for ground impact forces not to exceed 6 g would require a very low rate of descent and would result in excessively large and heavy parachutes. Frangible impact attenuators have been used on the B-58 encapsulated seat, and air bags on the B-70 encapsulated seat and the F-111 crew modules. Studies indicate that a parachute retrorocket impact attenuation systems will provide the minimum weight system. Parachute/air bag and parachute retrorocket systems are not very flexible with regard to rate-of-descent variations caused by weight increases and changes in landing altitude (see section 6.8). The main parachute assembly should be installed at a low pack density in the 30-lb/ft³ range, allowing the installation of a larger parachute at a higher pack density.

Operational escape vehicles had the following empty weights per crew member:

Ejection seats	150 to 175 lb/crew member
Encapsulated seats	400 to 500 lb/crew member
Crew modules	1200 to 1400 lb/crew member

References 8.12 to 8.14 describe past and present aircrew emergency situations as well as possible development trends.

8.3.2 Military Personnel Emergency Parachute Types

The Navy and Air Force personnel emergency parachute assemblies used for individual bailout and for bailout in ejection seats are listed in Tables 8-3 and 8-4, respectively. These tables update information contained in Tables 1-4 and 1-5 in the *Air Force Recovery System Design Guide*. In the 12 years since the publication of the *Air Force Recovery System Design Guide*, the Navy has eliminated four personnel emergency parachute assemblies and has added ten new assemblies to comply with changes in the aircraft inventory. However, 18 of the 19 assemblies listed still use the 28-foot-diameter flat and the 26-foot-diameter conical personnel parachutes somewhat tailored to the individual application. The Martin Baker ejection seat in the F-18 fighter uses a 5.2-meter-diameter aeroconical parachute. The newest version of the ejection seat uses a 6.2-meter aeroconical parachute, designed by Martin Baker.

The Air Force has eliminated four personnel emergency parachute assemblies and has added seven new assemblies. The F-15 and F-16 fighters and the B-1 bomber use the McDonnell Douglas ACES II ejection seat. This seat uses a reefed 28-foot standard personnel

TABLE 8-3. Navy Emergency Escape Parachute Information and Utilization.

Relative equipment	Parachute and quantity in service (Note 2)	NB-6 (1043)	NB-7 (814)	NB-TD (192)	NB-8 (1,562)	NC-3 (378)	NES-8B (667)	NES-12 (1723)	NES-14 (2219)	NES-16 (62)
Type aircraft and quantity used per aircraft (Note 1)	C-1 (9) T-34 (2) C-2 (4)	A-3 (8) E-2 (5)	A-3 (5)	A-3 (8) C-2 (4) C-130 (5) P-3 (27)	C-130 (2) C-131 (6)	F-4 (2)	A-4 (1) TA-4 (2) S-3 (4)	F-14 (2) A-6 (2) EA-6B (4)	A-4E (1)	
Ejection seat (manufacturer)	None	None	None	None	Mk-H7 (M-B)	IG-3 (A-4/TA-4) IG-1 (S-3) (MACDAC)	Mk GRU-7 (A-6) Mk EAGRU-7 (EA-6B) Mk GRU-7A (F-14) (M-B)	IG-3 (A-4/TA-4) IG-1 (S-3) (MACDAC)	IA-1 (MAC/DAC)	
Type canopy (Part number)	26-foot conical 60A114E3-1	28-foot flat 60A113E5-18	28-foot flat 60A113E5-18	28-foot flat 60A113E5-18	28-foot flat 60A113E5-18	28-foot flat 60A113E5-18	28-foot flat 107AS106-22	28-foot flat 60A113E5-18	28-foot flat 107AS106-22	28-foot flat 107AS106-22
Type harness	60A113E3-14 60A113E4-14	PCU-33/P	PCU-33/P	60A113E3-14 60A113E4-14	675AS102-1 675AS103-1	PCU-33/P	PCU-33/P	PCU-33/P	PCU-33/P	PCU-33/P
Drogue parachute	None	None	None	None	None	None	MBEU 38272	None	MBEU 38272	None
Canopy opening aid	None	None	None	None	None	None	PDVL	-10/12 BSG	PDVL	-10/12 BSG
Auxiliary equipment	-30 APRR -34 APRR	PHSRU -34 APRR	PHSRU -34 APRR	SPEC	-34 APRR SPEC	None	PHSRU -34 APRR	PHSRU -34 APRR	PHSRU -34 APRR	PHSRU -34 APRR
Work unit code	91A2300	91A2400	91A2400	91A2500	91A2100	91A2800	91A2B00	91A2C00	91A2E00	
NA 13-1-6.2 W/P	0013 00-018 00	019 00-024 00	025 00-030 00	031 00-036 00	008 00-012 00	043 00-048 00	070 00-074 00	054 00-058 00	075 00-080 00	
Seat PAN/RKT/Unit	SP-1A	HSSP SSP	SP-1A	SSP	RSSK-1A	RSSK-8	SKU-2	SKU-1/A		
Cognizant field activity	Design	NWC	NWC	NWC	NWC	NWC	NWC	NWC	NWC	NWC
	Log mgt.	NWC	NWC	NWC	NWC	NWC	NWC	NWC	NWC	NWC

NOTES:

1. Maximum number of parachutes per type aircraft.
2. Total Navy emergency escape parachutes in service: (includes operational, spares, and storage) 24,790 through FY 1985. (Figures do not include NACES, AFIP2SS-29.)

DEFINITIONS:

SEU/SJU	=	Seat ejection unit
NES	=	Navy ejection seat/system
NB	=	Navy back
NC	=	Navy chest
LS	=	Low speed
PHSRU	=	Parachute harness sensing release unit (SEAWARDS)
VCL	=	Vent control line
MAC/DAC	=	McDonnell/Douglas
GAC	=	Grumman Aerospace Corp
NAMER	=	North American
M-B	=	Martin Baker Aircraft

LW	=	Lightweight
BSG	=	Spreading gun assembly
PDVL	=	Pull down vent line
APRR	=	Automatic parachute ripcord release (Model 7000)
SPEC	=	Special application
NWC	=	Naval Weapon Center, Code 6415, China Lake, CA
UPCO	=	Universal Propulsion Co.
NAVAR	=	Naval Air Systems Command
M-B	=	Martin Baker Aircraft

NWC TP 6575

TABLE 8-3. (Contd.)

Relative equipment	Purchase and quantity in service (Note 2)	NFS-25 (904)	LW-3B (72)	AP28S-24 (523)	AP28S-25 (383)	AP28S-27 (113)	AP28S-28 (123)	AP28S-29 (TBD)	AP28S-30 (31)	AP28S-31 (31)	AP28S-31 (150)
Ejection seat (manufacturer)	Type aircraft and quantity used per aircraft (Note 1)	T-2C (2)	QV-10 (2)	F/A-18A (1)	A-7E (1)	TA-7C (2)	AV-8B	A-4F (2)	TAV-8B (1)	TAV-8B (1)	E-2C (5)
LS-1 (N/AMER)	LW-3B (N/AMER)			SJU-5/A SJU-6/A (M-B)	SJU-8/A (UPCO)	SJU-11/A SJU-12/A (UPCO)	SJU-4/A (UPCO)	SJU-17/A (UPCO)	SJU-13/A (UPCO)	SJU-14/A (UPCO)	None
Type canopy (Part number)	28-foot flat	42. Meter aerocomical flat	28 foot modified	28 foot modified	28 foot modified	28 foot modified	28 foot modified	28 foot modified	28 foot modified	28-foot modified	26-foot modified
Type harness	PCU-33/P	PCU-33/P	PCU-33/P	PCU-33/P	PCU-33/P	PCU-33/P	PCU-33/P	PCU-33/P	PCU-33/P	PCU-33/P	PCU-33/P
Drogue parachute	1.900 SGR3 None U 65700	PCU-31/A	PCU-31/A	PCU-29/A	PCU-28/A	PCU-29/A	PCU-29/A	PCU-29/A	PCU-29/A	PCU-29/A
Canopy opening aid	-11/13 BSG None	VCL	-4 BSG	-4 BSG	-9 BSG	VCL	-9 BSG	-9 BSG	-9 BSG	-9 BSG	None
Auxiliary equipment	PHSRU -30 APRR	PHSRU	PHSRU	PHSRU	PHSRU	PHSRU	PHSRU	PHSRU	PHSRU	PHSRU	None
Work unit code	91A2K00	91A2L00	91A2M00	91A300	91A4500	1744000	1744000	TBD	TBD	TBD	91D1000
NA 13-1-6-2 W/P	081 00-006 00	071 00-002 00	063 00-068 00	100 00-106 00	105 00-111 00	113 00-119 00	113 00-119 00	TBD	113 00-119 00	113 00-119 00	123 00-130 00
Seat PAN/T/T/N/nit	RSSK-3	RSSK 9	SKU-3/A	SKU-4/A	SKU-6/A	SKU-7/A	SKU-6/A	SKU-6/A	SKU-6/A	SKU-6/A	SKK-9/P22P-11
Cognizant field activity	Design	NWC	NWC	NAVAIR (NWC) (limited)	NAVAIR	NAVAIR	NAVAIR	NAVAIR	NAVAIR	NAVAIR	NAVAIR
Long m/s	NWC	NWC	NWC	NWC	NWC	NWC	NWC	NAVAIR	NAVAIR	NAVAIR	NAVAIR

TABLE 8-4. Air Force Personnel Emergency Parachutes, Man Mounted.

Code	Part number	Canopy type	Deployment aid	Opening aid	Manual ripcord	Automatic opener	Canopy release	Harness type	Container	Aircraft application	Remarks
BA-18	50C7024-18	C-9	1/4 D-bag	None	Yes	F-1B	Capewell	Class H #59K6259	Soft	B-52, C-130, C-135, C-141 B-52	Line first deployment
BA-21	50C7024-21	C-9	1/4 D-bag	None	Yes	F-1B	Capewell	Class H #59K6710	Soft	T-33, B-1, F-5, A-37 T-37, T-38, C-141 T-38, T-37	Line first deployment
BA-22	50C7024-21A	C-9	1/4 D-bag	None	Yes	F-1B	Capewell	Class H #65K1533-101	Soft	T-33, B-1, F-5, A-37 T-37, T-38, C-141 T-38, T-37	Line first deployment
BA-22	50C7024-22A	C-9	1/4 D-bag	None	Yes	F-1B	Capewell	Class H #65K1533-101	Soft	T-33, B-1, F-5, A-37 T-37, T-38, C-141 T-38, T-37	Line first deployment
BA-25	50C7024-25A	C-9P	1/4 D-bag	PDVL	Yes	F-1B	Capewell	Class H #65K1533-101	Soft	B-52	Line first deployment
BA-27	50C7024-27	C-9P	1/4 D-bag	PDVL	Yes	F-1B	Capewell	Class H #59K6710	Soft	B-52	Line first deployment
BA-27	50C7024-27A	C-9	1/4 D-bag	None	Yes	F-1B	Capewell	Class H #7747210-10	Soft	Small-statured crews Premeditated personnel drops only F-106	Line first deployment
BA-29	50C7024-29	C-9	1/4 D-bag	None	Yes	None	Capewell	Class H #65K153-101	Soft	Canopy first deployment	Canopy first deployment
BA-222	50C7024-222	C-9	1/4 D-bag	None	Yes	Seat sequencing	Capewell	Class H #67534640-1	Soft	C-131, H-1, H-3, H-53	Canopy first deployment
B-20	50C7024-20	C-9	Deployment gun	None	Yes	None	Capewell	Class H #59K6706-30	Soft	C-130, C-140, H-1 H-3, RC-135	Canopy first deployment
CA-12	50C7023-12	C-9	None	None	Yes	F-1B or Scott	Capewell	Class H #68J420	Soft	C-130, C-131, H-3	Canopy first deployment
C-12	50C7023-9	C-9	None	None	Yes	None	Capewell	Class H #68J420	Soft	F-111A, JF-111A, T-33	Line first deployment
SA-20	50C7025-20	C-9	1/4 D-bag	None	Yes	F-1B	Capewell	Class H #58K6260-21	Soft	HH-3E	Canopy first deployment
S-21	50C7025-21	C-9	None	None	Yes	None	Capewell	Class H #58K6260-21	PCU-15/P	Semi-rigid	Canopy first deployment SEAWARS
ESCAPAC	AP28S-20	C-9	None	None	Yes	Model 7000	Koch	PCU-15/P	PCU-15/P	Semi-rigid	Canopy first deployment SEAWARS
ESCAPAC	AP28S-21	C-9	None	None	Yes	Seal sequencing	Koch	PCU-15/P	PCU-15/P	Semi-rigid	Canopy first deployment SEAWARS
I.W.-3B	300-535040-101 3MN-535040-201	C-9	Mortar slug/ static line	None	Yes	Seal sequencing	Koch	PCU-15/P	PCU-15/P	Rigid	Early F-15
MKA17	32-621552-307, -311, -313 32C821552-13	C-9P	Drogue gun	PDVL	Yes	Seal sequencing	Koch	PCU-15/P	PCU-15/P	Rigid	OV-10
ACES II	J114509-515	C-9	Catapult	Reeling line	No	Seal sequencer	Koch	PCU-15/P	PCU-15/P	Rigid	F-15
ACES II	J114509-517	C-9	Catapult	Reeling line	No	Seal sequencer	Koch	PCU-15/P	PCU-15/P	Rigid	A-10
ACES II	J114509-523	C-9	Catapult	Reeling line	No	Seal sequencer	Frost	PCU-15A/P	PCU-15A/P	Rigid	F-16
ACES II	8311719-401	C-9	Catapult	Reeling line	No	Seal sequencer	Frost	PCU-15A/P	PCU-15A/P	Rigid	B-1

parachute where the reefing greatly reduces the maximum opening force. Figure 5-53 in section 5.4.7 compares parachute opening forces as a function of velocity for several personnel emergency parachutes presently in use.

8.3.3 Navy Aircrew Common Ejection Seat (NACES)

In 1983, the Navy started developing an ejection seat to be used in all present and future Navy aircraft. The contract was awarded to the Martin Baker Aircraft Company, Ltd., in Great Britain. A subcontract was to the GQ Parachutes, Ltd., for the development of the parachute assembly to be used with the seat. The seat is designed for recovery of aircrew from the 5th percentile Oriental female to the 98th percentile American male, resulting in a maximum test weight of 291 pounds. Emergency recover covers from close to zero speed on the deck to Mach 2.5 at altitudes approaching 100,000 feet.

The parachute assembly consists of a drogue chute for initial seat stabilization and deceleration, and a main parachute assembly for final recovery.

The drogue chute, a 5-foot-diameter (D_0) conical ribbon parachute, stabilizes and retards the seat for descent from high altitude with the crew member remaining in the seat, and for deceleration at high speeds at altitudes below 18,000 feet. The main parachute assembly consists of a 6.2-meter-constructed diameter, aeroconical parachute of G. Q. design. The canopy is manufactured from low-porosity nylon fabric in block construction, with four gore sections covered with nylon mesh to improve stability and lower opening forces. Two LeMoigne type slots with attached control lines provide maneuverability on demand with a maximum glide ratio of $L/D = 0.65$ and a turn rate of 13 seconds per 360-degree turn. The canopy is equipped with a 3-foot-diameter conical ribbon controller drogue chute, permanently attached around the crown area of the canopy for inflation control. Figures 8-10 and 8-11 show the canopy plan form and the main parachute assembly with controller parachute and deployment sleeve. Parachute deployment is controlled by altitude and pressure sensors feeding into an electronic sequencer that provides five different deployment modes, depending on aircraft altitude and velocity.

A typical mode sequence for up to 8000 feet altitude and 500 to 600 KEAS velocity appears as follows: after 35 inches of seat travel, the electrical sequencer is activated. At zero + 0.22 second, the drogue gun fires and extracts the drogue chute. After 0.45 second, the triple drogue chute bridle is disconnected from the upper and lower attachment points. At 1.3 seconds (0.15 second prior to drogue chute disconnect), the extractor rocket for main parachute deployment is fired; at 1.5 seconds, the crew member harness disconnects and the inflating main parachute pulls the crew member from the seat. The main parachute inflates quickly because the low-porosity canopy fabric is somewhat controlled by the controller parachute. References 8.15 and 8.16 discuss the extensive testing program conducted by the Naval Weapons Center at China Lake. These tests include whirl-tower drops, aerial drops of

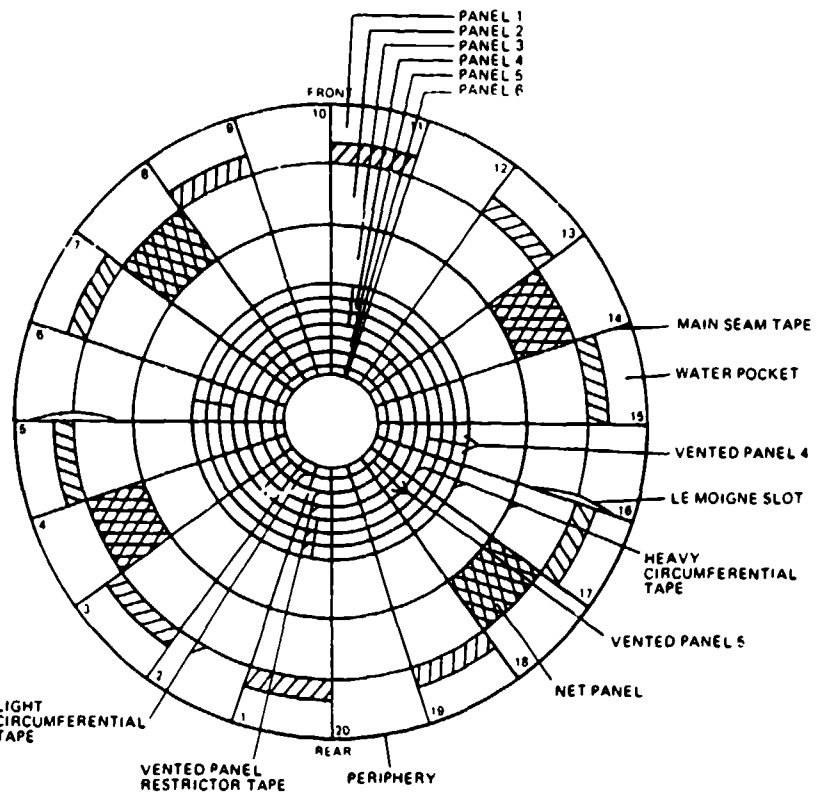


FIGURE 8-10. Plan Form of the 6.2-Meter Aeroconical.

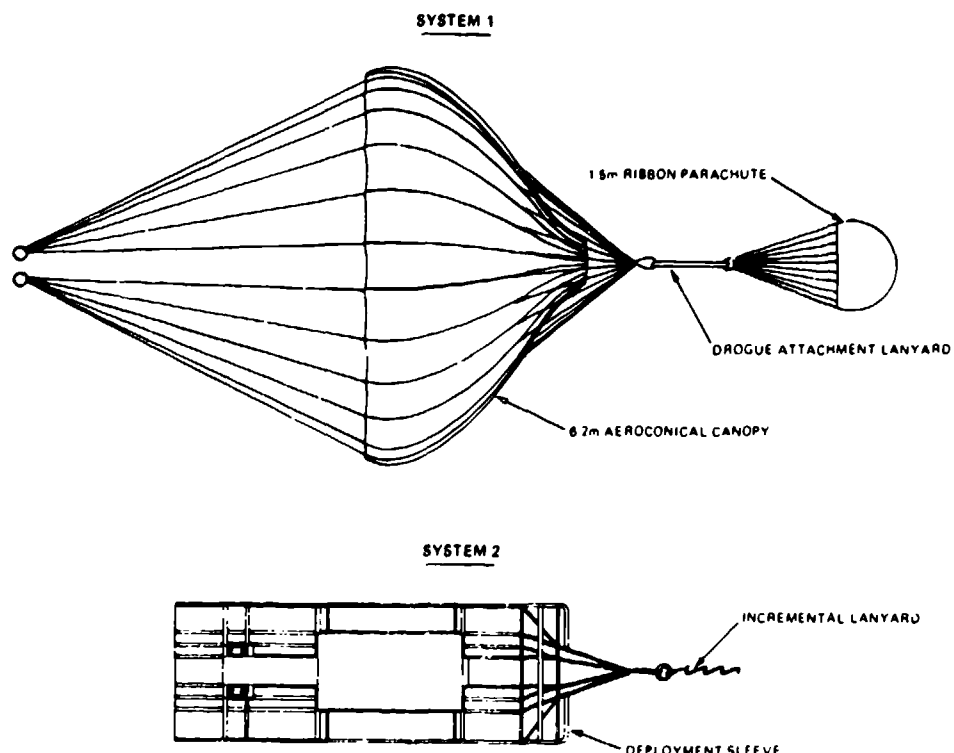


FIGURE 8-11. Assembly Components of the 6.2-Meter Aeroconical.

torso dummies, and tests with cylindrical test vehicles (CTVs) as well as numerous live jumps over land and water. Water deflation pockets worked well in wind speeds up to 10 knots (the maximum wind speed encountered during these jumps).

Figure 5-53 in Chapter 5 shows parachute opening forces versus velocity for several personnel escape parachutes presently in service. The opening forces for the 6.2-meter aeroconical parachute are from References 8.15 and 8.16. The force data in Figure 5-53 are comparable only up to a certain point because of the lack of a common testing standard for personnel emergency escape parachutes. An analysis of ejection seats presently in service indicates that the sequencing modes used on these seats limit the parachute canopy inflation speeds to 240 knots and below.

The main parachute is housed in a sleeve-type deployment bag, shown in Figure 8-11, with the suspension-lines stowed in a pocket on the outside of the sleeve. The last two suspension-line stows close the deployment sleeve. Photo evaluation of aerial drop tests and cross-wind deployment in high-speed ejection-seat track tests gave good line first deployment, with the canopy remaining closed until line stretch occurred.

Angled rocket operation and ripple timing will provide seat separation in multiple seat ejections.

8.3.4 Aircrew Gliding Escape System (AGES)

In 1983, the Aerosystems Department of the Naval Weapons Center started to investigate the use of hi-glide parachutes for aircraft emergency escape. The reasons for this investigation were to find methods to lower rate of descent and opening forces, decrease the parachute assembly weight and volume, and permit the crew member to select a suitable landing area and conduct evasive maneuvers under wartime conditions.

The obvious parachute choice was the ram-air inflated parafoil parachute widely used for special military applications and by sport parachutists and paratroopers.

The requirements included parachute opening at 300 KEAS at 15,000 feet altitude without exceeding a 15-g opening force related to a 98th percentile American male crew member; a hands-off landing with speeds not to exceed 21 ft/s vertical and 8 ft/s horizontal; and easy controllability and design, packing, and maintenance within present operational limits.

The development program was conducted in two phases. The first phase covered the modification of an existing parafoil personnel parachute to meet performance and stress requirements. Testing of the various modifications required numerous aerial drop tests starting with helicopter drops and extending to drop of an instrumented CTV from an F-4 aircraft at 15,000 feet altitude at 300 knots. The second phase tested the parachute assembly in a high-speed set ejection test from an F-4 aircraft.

The development started with a 280-square-foot, heavy-duty, Strato-Cloud parachute equipped with deployment bag, ropes, and a reefing system. It became obvious after the first high-speed tests that more data had to be gathered in the fields of deployment, opening dynamics, and canopy stress design.

The parachute, in its 13 modifications, went through changes in configuration, fabrics, canopy reinforcement, development of a suitable reefing system with two steps of reefing, and changes in deployment and pack configuration. The final version had 270 square feet of canopy area, a Lissaman 7808 airfoil, an aspect ratio of 2, 1.1 oz/y² ripstop nylon fabric with close to zero porosity, and a two-step reefing. The first-stage reefing line was 3.2 feet long and passed through rings on the lower surface periphery of the canopy and through reefing rings on the top leading edge of each half-cell. The second-stage reefing line was 6 feet long and passed through the four grommets of the slider and through the four slider stop rings on the lower edge of the stabilizer panels. The maximum opening force measured at drop speed up to 300 KEAS at 15,000 feet never exceeded 3800 pounds when tested in a CTV dropped from an F-4 aircraft. The schematic opening sequence of the parachute is demonstrated in Figure 8-12.

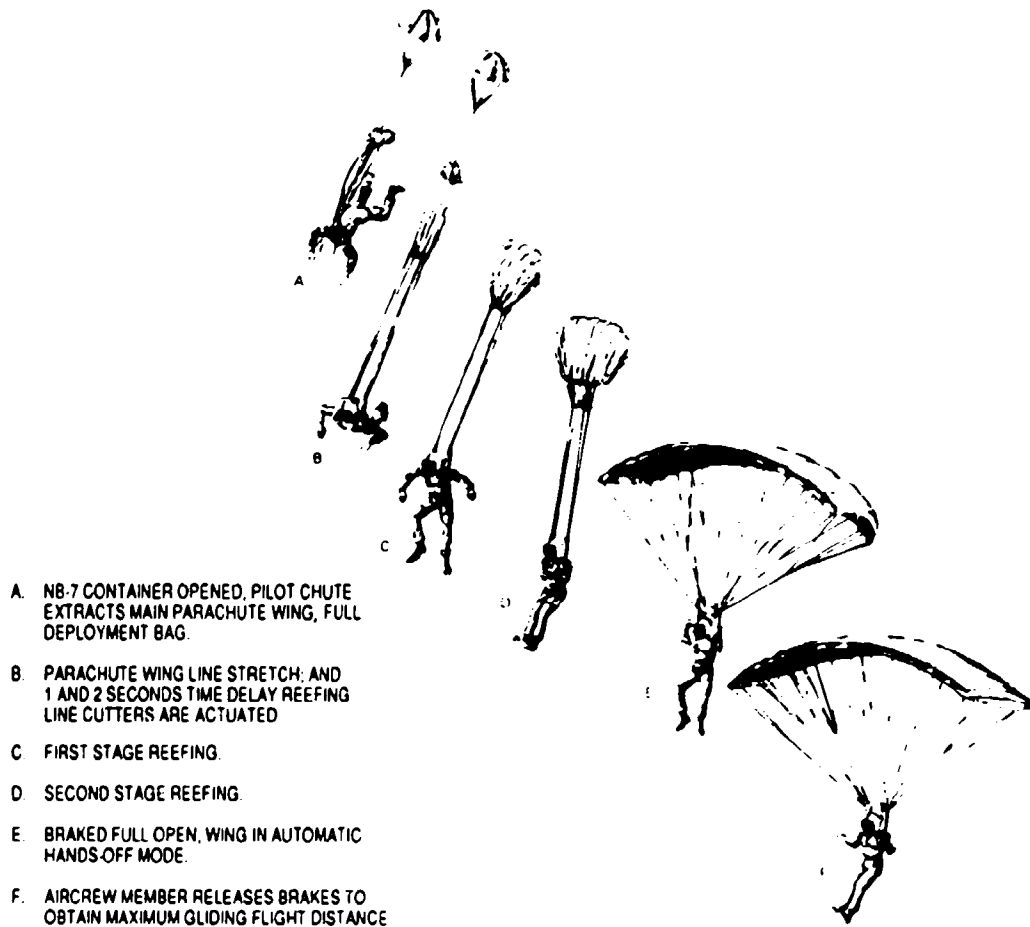


FIGURE 8-12. Opening Sequence of AGES Parachute Assembly.

A single-flight ejection test was performed with a Stencil SIIIS-3-er seat ejected from a specially equipped two-seat F-4 flying at an altitude of 7500 feet and a velocity of 500 KEAS. The parachute used was the No. 13 version with minor modification to the deployment system to fit into the headrest container and to connect with the seat drogue chute and the sequencing system. A 155-pound dummy was used (the weight was dictated by aircraft safety considerations). The main parachute performed well and was undamaged. Reference 8.17 describes this test. The maximum opening force of the two-step reefed parachute was below 2000 pounds. This low force is explained by the fact that the main parachute has a line-stretch velocity of about 220 KEAS, as demonstrated in Figure 3 of Reference 8.18.

8.3.5 Space Shuttle Crew Escape System

The NASA Space Shuttle orbiter has been equipped with an emergency escape system for individual astronaut bailout. This system consists of an escape hatch in the orbiter and a telescoping pole for the astronauts to slide down to avoid contact with the orbiter wing.

The January 1986 loss of the Space Shuttle Challenger and its crew started an extensive NASA investigation of emergency escape concepts for the orbiter astronauts. The orbiter is structurally not suited for an emergency landing on water or unsuited terrain.

The investigation showed that a crew module or individual ejection seat would require unacceptable orbiter modifications and weight penalties. Instead, individual crew bailout through a side hatch in the orbiter was selected as the most practical approach. However, this procedure introduced the possibility of astronaut contact with the orbiter wing or the orbiter maneuvering unit. Both are in the flight path of the exiting crew member.

To overcome this problem two methods were investigated: (1) the astronaut would be pulled from the orbiter by an extraction rocket in a flight path above the wing, and (2) the astronaut would slide down an aluminum pole that would lead to a flight path below the wing.

NASA investigated both exit methods. A contract was awarded to the Aerosystems Department of the Naval Weapons Center at China Lake, Calif., for development of a personal parachute assembly (PPA) and for laboratory and flight testing of the two escape modes. Both systems went through the preliminary design and testing phase. The curved-pole exit method, shown in Figures 8-13 and 8-14, was selected as the mechanically simplest and lightest approach.

The pole consists of three telescoping tubes with one section permanently attached in the orbiter and two sections extending 8.5 feet downward out of the escape hatch.

The PPA includes most of the survival gear and all bailout, stabilization, descent, and water flotation gear. The primary components of the PPA are

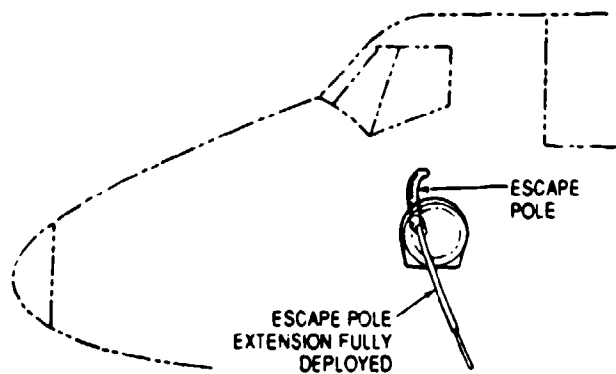


FIGURE 8-13. Side View of Escape Pole Deployed Through Side Hatch.

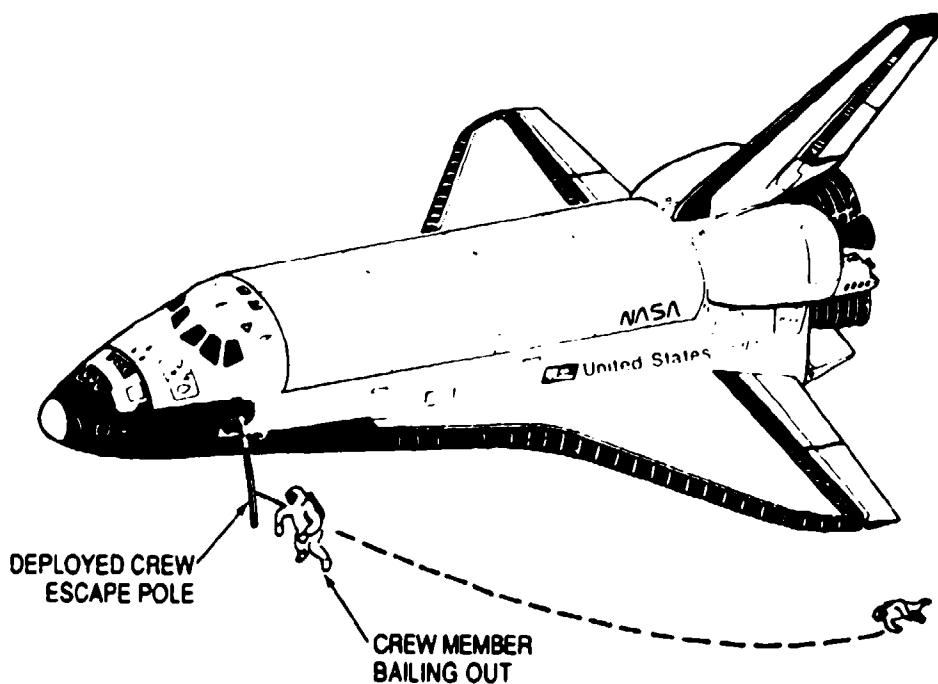


FIGURE 8-14. Crew Bailout Mode—Crew Escape Pole.

1. A harness that fits the 5th percentile Oriental female to the 95th percentile American male. This harness is worn over the partial-pressure suit donned by the astronauts on takeoff and landing. Ten-minute bailout oxygen is stored on the harness.
2. A survival vest that contains some of the survival equipment customarily worn by military pilots on over-water flights.

3. A personal life vest with two underarm flotation bladders that keep the crew member's head out of the water. This life vest is automatically inflated on impact with the water.
4. A backpack containing the parachute assembly, and, in a separate pack, the life raft. The parachute assembly consists of a pilot chute; a 4.5-foot-diameter guide surface stabilization parachute; and a 23.6-foot-diameter conical solid fabric parachute, a modification of the Navy 26-foot conical parachute, for final descent and parachute sequencing hardware. The life raft and the emergency locator beacon are stored in a separate compartment of the backpack.

The bailout procedure starts at 60,000 feet altitude after the decision to make an emergency landing has been made. The orbiter is flown on autopilot and stabilized at a 15-degree angle of attack and a flight velocity of 200 KEAS. At 25,000 feet, the cabin is depressurized, and shortly thereafter the escape hatch is pyro-ejected and the escape pole is extended. Bailout starts at 20,000 feet. Each crew member hooks an extraction bridle connected to the top of the parachute pack to the escape pole and slides out the hatch and down the pole. Crew members leave the hatch at intervals of 15 to 20 seconds.

After exit, the extraction bridle starts the automatic sequencer for the parachute assembly and then disconnects from the pole.

Three seconds after exit, the pilot chute is deployed, which in turn extracts the stabilization and drogue chute, which lets the crew member descend in a stable attitude to 14,000 feet where the drogue chute automatically disconnects and deploys the reefed main parachute. After 2 seconds, the main parachute disreefs and lowers the crew member at a rate of descent of about 22 ft/s.

At water impact, the main parachute automatically disconnects, flotation vest and life raft are inflated, and the crew member boards the life raft.

The crew member has a manual override for parachute deployment in case of malfunction of the automatic deployment system.

The short time available for development dictated the use or modification of existing equipment for all PPA components.

The Naval Weapons Center conducted an extensive test program including dummy drops and life bailout tests with Navy test jumpers.

Figures 8-13 to 8-15 show the exit arrangement, the bailout procedure, and a Navy test jumper sliding down the pole.



FIGURE 8-15. Navy Test Jumper Using Crew Escape Pole.

References 8.19 and 8.20 describe the orbiter escape system and the equipment used.

8.3.6 F-111 Crew Escape Module Parachute Recovery System

The parachute recovery system for the two-person crew escape module of the F-111 bomber was developed in the late 1960s. The 2800-pound module uses for its final descent a 5-foot-diameter hemisflo ribbon drogue chute for initial deceleration and stabilization, and a 70-foot-diameter ringsail main descent parachute deployed at a velocity of 300 KEAS from sea level to 18,000 feet altitude. Air bags cushion the landing impact.

Earlier in this chapter it was discussed that air vehicles, as a rule (and the F-111 crew module falls into this group), grow in weight during their operational life because of the addition of black boxes and environmental and operational equipment. The weight of the F-111 crew module has grown to close to 3200 pounds, resulting in a higher rate of descent and an increase in crew injuries during parachute-air bag landings.

The Air Force awarded a contract for the development of an improved final-rate-of-descent assembly to the Sandia National Laboratories (SNL) in Albuquerque, N. Mex. The SNL designed a new parachute assembly consisting of a cluster of three 52.5-foot-diameter, 20-degree conical solid-ringslot parachutes, where the crown of the solid fabric canopy is replaced with a ringslot insert for better stability and improved opening force control. The hybrid-material parachute uses a nylon canopy and Kevlar risers, suspension lines, and canopy tapes. A unique centrally located and controlled disreefing system permits simultaneous disreefing of the two reefing stages of all three parachutes. The development and testing of this interesting parachute assembly is described in Reference 6.42.

The major design problems were the very limited parachute compartment volume, low permissible parachute opening forces, and cross-wind parachute deployment at 300 knots. Since publication of the referenced paper, SNL has decreased the diameter of the three 52.5-foot-diameter parachutes to 49.0 feet. This reduction was made possible by the higher than expected drag coefficient of $C_{D_0} = 0.9$ instead of the anticipated 0.77. The smaller parachute diameter also decreased the weight and volume of the parachute assembly, permitted a more civilized pack density, and lessened parachute installation problems.

The weight effectiveness of the main parachutes without added assembly components is 54.8 cubic feet of parachute drag area per pound of parachute weight, a good value considering the high deployment velocity of 300 KEAS and the allowable parachute force of only 6 g related to the crew module weight.

The performance requirements for the main parachute assembly were based on the condition that the existing hemisflo drogue chute could be retained without change. The new parachute assembly was tested up to 275 knots. It did not meet the requirement of 300 knots at an 18,000-foot altitude for a 3120-pound crew module and, therefore, was not accepted by the Air Force.

8.4 AIRDROP OF CARGO AND PERSONNEL

8.4.1 Scope of Airdrop Operations

The airdrop of cargo and personnel encompasses the transport to the drop zone, the extraction and drop of cargo and personnel from the cargo aircraft, the stabilization and retardation during descent, and the landing of cargo and personnel undamaged and ready for use or action. Training exercises involve retrieval and refurbishment of platforms, containers, parachute assemblies, and equipment. Airdrop operations and the equipment used are detailed in the U.S. Army *Engineering Design Handbook for Air Transport and Airdrop*, Reference 6.68; the USAF AFSC *Design Manual, DH 1-11*, section 4A, Reference 8.21; and MIL-STD-669B, Reference 8.22.

The U.S. Army Natick Research, Development and Engineering Center at Natick, Mass., in November 1988, conducted an Industry Airdrop Systems Briefing that outlined requirements and goals for military airdrops. Reference 8.23 details the proceedings of the briefing, and Reference 8.24 is a subsequent paper on the subject.

In recent years the scope of airdrop operations has been extended by (1) the expected introduction in the mid-1990s of the C-17 cargo aircraft that will have a total load-carrying capacity of 110,000 pounds and an individual drop capability of 60,000 pounds as compared to the single and total airdrop capability of 42,000 pounds for the C-130 aircraft; (2) the need to approach the drop zone below radar detection altitude that will require drops from 300 feet or below, technically a very difficult task; and (3) the need for high-altitude airdrop capability.

Cargo and personnel in military airdrop operations often must land in unprepared, hostile terrain. This task requires rugged, reliable, well-designed equipment suitable for rough handling and field operations.

In the 1970s the author prepared the airdrop section in the *Air Force Recovery Systems Design Guide*, Reference 2.1. The airdrop section in this manual is an updated version of the write-up in the *Air Force Design Guide*.

8.4.2 Airdrop Aircraft and Procedures

Table 8-5 lists the primary aircraft used in military airdrop operations. Smaller aircraft that are used in commercial as well as charitable airdrops, and occasionally in military operations, are not included in the table. The C-130, the "airdrop workhorse," is rated for a total as well as an individual airdrop load of 42,000 pounds. It is used for all forms of airdrop operations from LAPES on-the-ground platform extraction to high-altitude container and personnel drops. References 8.25 to 8.29 describe C-130 airdrop characteristics and capabilities. In the early 1990s, the McDonnell-Douglas C-17 cargo aircraft will become available. This aircraft has a total load-carrying capacity of 110,000 pounds, a single airdrop load capacity of 60,000 pounds, a wider and larger cargo area, and an improved unprepared-field landing capability. Similar to the C-130, the C-17 will permit airdrops of all presently used airdrop systems. The C-141 handles all airdrops with the exception of LAPES (References 8.30 to 8.32). The C-5, being primarily a transport aircraft, is used only occasionally for airdrop operations (Reference 8.33 and 8.34). The DeHavilland CV-7A is mostly used by the Air Force Reserve for airdrop of cargo and personnel.

Helicopters are used by the Army and the Marine Corps for personnel and cargo drops. Table 8-6 gives weight ranges, parachutes used, aircraft speeds, and minimum altitude for containers dropped from CH-46 and CH-53 helicopters.

TABLE 8-5. Primary Aircraft Used in Military Airdrop Operations.

Aircraft	Maximum compartment size, in., L/W/H	Airdrop capacity, lb	Unit airdrop capacity, lb	Airdrop speed, KEAS	Aircraft installation	Airdrop system	Paratroopers
C-130, Lockheed	492/108/100	42,000	42,000	130	Dual rail, automatic restraint	LAPES, CDS, standard, hi-alt, special	64
C-141, Lockheed	840/123/109	70,000	38,500	150	Dual rail, automatic restraint	CDS, standard, hi-alt, special	120
C-5A, Lockheed	1450/228/162	220,000	42,000	150 ± 10	Dual rail, automatic restraint		75
C-17, McDonnell-Douglas	1056/216/162	110,000	60,000	150	Dual rail, automatic restraint	LAPES, CDS, standard, hi-alt, special	102
CV-7A, DeHavilland	373/92/78	12,000	12,000	100-120	Skate wheel buffer board	Standard airdrop	25
CH-53, Sikorski	360/96/77	20,000	20,000	50-120	Container handling	Gravity	
CH-47, Boeing	366/90/78	16,000	12,000	50-120	Container	Gravity	

TABLE 8-6. Container Summary for Helicopter Airdrop.

Container weight, lb	Cargo type	Parachute type	Pilot chute size	Drop speed, knots	Drop altitude, ft
300 to 500	A-7A Cargo sling	G-13 or G-14	None	80 to 120	500
800 to 1000	A-22 Cargo bag	2 × G-13 2 × G-14	None	80 to 120	500
1000 to 2000	A-22 Cargo bag	G-12D	68 in.	80 to 120	600

Each airdrop of heavy cargo, such as vehicles, guns, and heavy equipment, requires restraining the cargo and the parachute assemblies on a cargo platform and then restraining the cargo platform in the aircraft using the aircraft dual-rail restraint system (References 8.26 and 8.35). This semiautomatic dual-rail restraint system replaces the skate-wheel conveyors and buffer boards used in the C-119 cargo aircraft. The dual-rail system is used in connection with the Army Type II standard platform and the Air Force Type A/E 23H-1 extended aluminum platform used for LAPES extraction (Reference 8.36).

In the C-130, the left-hand restraining rail has detent notches that engage corresponding indents in the platform for fore and aft restraint in accordance with MIL-A-8421 tiedown requirements of 3 g forward, 1.5 g aft, 2 g up, and 1.5 g lateral. These tiedown restraints refer to the load on the platform as well as the restraint of the platform in the aircraft. For the LAPES extraction method, the load-to-platform and platform-to-aircraft tiedowns increase to 8 to 12 g forward and 6 g in all other directions.

Under adverse weather conditions, the pilot reaches the computed airdrop release point (CARP) by use of the Advanced Weather Aerial Delivery System (AWARDS). The AWARDS is a combined aircraft radar navigation and computer system used in Pathfinder C-130 aircraft (Reference 8.37). Upon reaching the CARP, the pilot commands "airdrop." This command starts the platform extraction process (Reference 8.38). The platform extraction parachute, stored in a deployment bag attached to the pendulum release, falls free and swings in an arc to the rear where the extraction parachute deploys and inflates behind the aircraft. A long extraction line (60 feet long for the C-130 and 120 feet long for the C-141) connects the extraction parachute to the platform to be extracted. Before the extraction parachute deployment, manual detents on the left dual rail are removed and the platform is restrained in the aircraft only by the spring-loaded detents in the right-hand rail. As soon as the parachute extraction force reaches a preset level, the preloaded detents release the platform, and the platform is extracted. After the platform leaves the aircraft, the extraction parachute is disconnected from the platform and deploys the main parachutes for standard airdrop.

Figure 8-16 shows the parachute extraction system for a standard Army platform. Reference 6.68 also gives considerable details of cargo platform installation and extraction.

In sequential platform drops, the extraction parachute for the follow-on platform is stored on the preceding platform and deployed upon separation of the first platform from the aircraft.

The parachute extraction force will vary somewhat for different weight platforms but is tailored to an average extraction force of about 1.5 g.

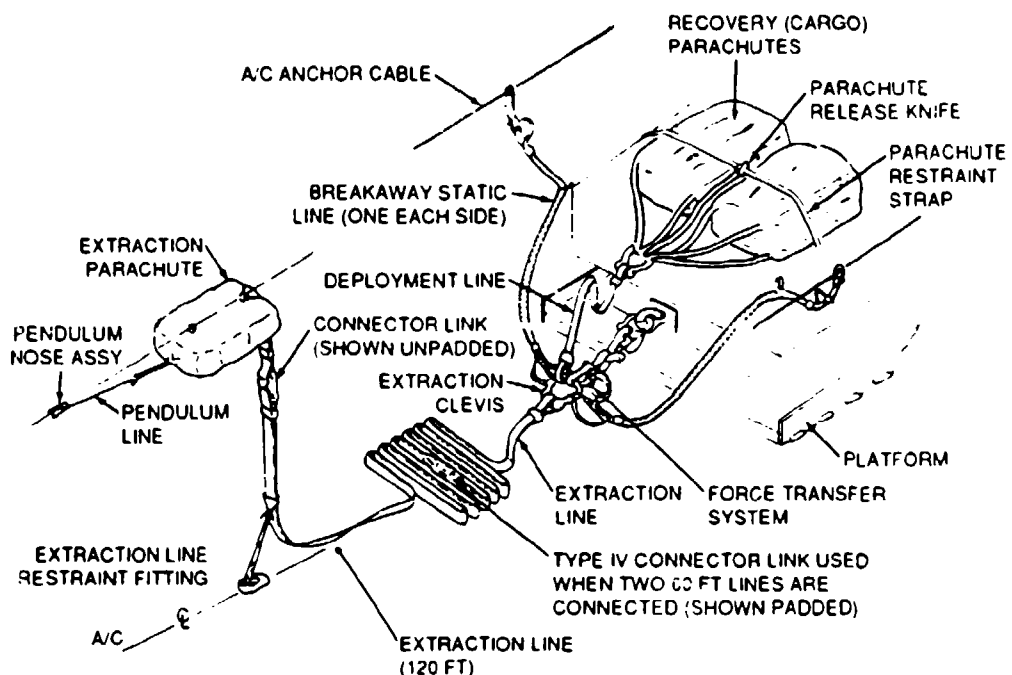


FIGURE 8-16. Parachute Extraction System for Cargo Platforms.

8.4.3 Cargo Airdrop

In World War II, personnel and cargo were dropped from altitudes of 1000 to 2000 feet at aircraft velocities of 80 to 100 knots. This method was modified in the post-war years for several reasons: (1) enemy counteraction as experienced in Southeast Asia made it desirable for aircraft to approach below radar detection altitude or above the range of the antiaircraft artillery, (2) the minimum speed of today's aircraft used for military airdrop has increased to about 130 knots, and (3) the weight of individual items to be dropped has grown to 42,000 pounds and will reach 60,000 pounds when the C-17 is put into service.

These requirements have resulted in supplementing the standard airdrop system, where cargo and personnel are dropped from 500 to 1500 feet, with the LAPES and high-altitude airdrop systems. Larger and more effective parachutes and cargo platforms have been developed that can handle the higher drop speeds and heavier loads.

Three methods are presently in use for airdropping military cargo from medium and low altitudes: (1) standard airdrop method, (2) CDS (container delivery system), and (3) LAPES.

Standard Airdrop Method. Figure 8-17 shows the operational sequence of the standard airdrop method. The cargo to be dropped is loaded and restrained on a standard cargo platform, which, in turn, is loaded and restrained in the aircraft using the dual-rail aircraft

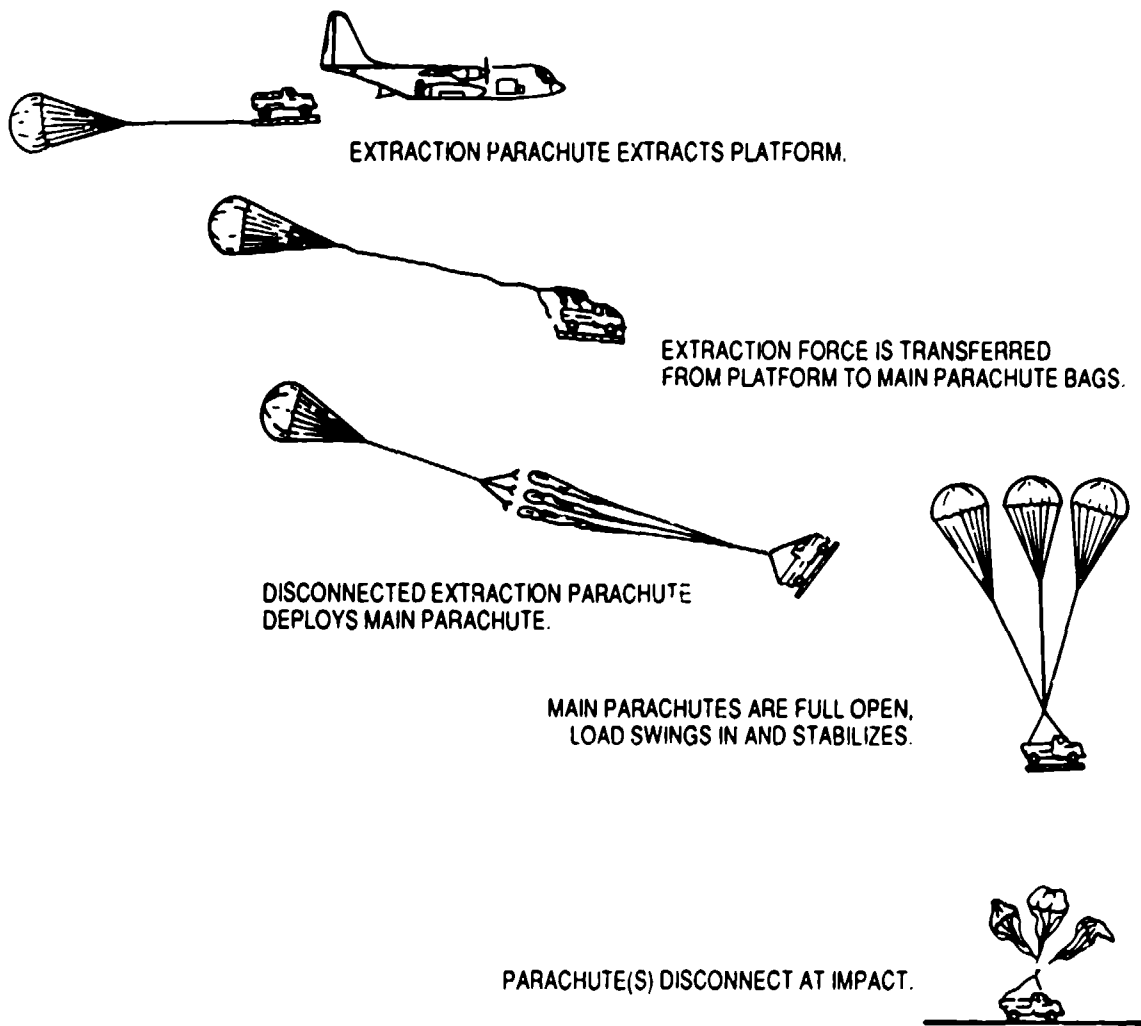


FIGURE 8-17. Standard Airdrop Method.

cargo handling system, as described in Reference 8.26. Upon reaching the drop area, the pilot commands "drop." The drop begins with the pendulum ejection of the extraction parachute. The extraction parachute pulls the load platform out of the aircraft and, after disconnecting from the platform, pulls the main parachute packs away from the platform and deploys the main parachutes. The size and number of main parachutes are selected for rates of descent of 20 to 25 ft/s, depending on the type of load dropped and the amount of cushioning material used.

Impact attenuation methods, including crushable materials such as paper honeycomb, are discussed in section 6.8. Figure 6.72 shows a military vehicle loaded on a standard platform using multiple layers of paper honeycomb for cushioning the landing impact. Several platforms may be extracted sequentially from the C-130 or C-141 aircraft, depending on the

size and weight of the cargo to be dropped. Platforms in the 2300- to 42,000-pound range use single or clusters of up to three 64-foot-diameter G-12 parachutes, or clusters of up to eight 100-foot-diameter G-11 parachutes. The required drop altitude for standard airdrop is 800 to 1500 feet, depending on platform size, weight, type, and number of parachutes used. This drop altitude is undesirable in today's operational environment; however, the standard airdrop method is a well-developed and well-equipped approach and is used for single loads of up to 42,000 pounds (Reference 8.39).

The Army is working on a method of decreasing the dispersion of sequentially dropped platforms by tying them together and having them descend on a cluster of parachutes. This method, called Aircraft Controlled Exit System (ACES), is described in Reference 8.40.

Container Delivery System. Methods for the delivery of multiple A-22 containers have been developed for the C-130 and C-141 aircraft (Reference 6.68). The goal of this method is to drop the containers in the shortest possible distance. The C-130 can drop 16 A-22 containers, and the C-141 can drop up to forty 2200-pound A-22 containers in two rows from the rear of the aircraft. The containers are restrained in the aircraft with chains and sheer webs. Shortly before the drop, the chains are removed and the aircraft is placed in a slightly nose-high altitude of 3 to 4 degrees. Upon pilot "drop" command, the restraining webs are cut by shear knives. Cutting the webs allows the two most rearward containers to leave the aircraft by gravity drop, with a static-line-deployed pilot chute initiating extraction and deployment of the G-12 main parachute. This method of gravity container drop and static-line-actuated pilot and main parachute deployment is repeated until all containers have left the aircraft.

LAPES. The extraction sequence for this extremely low-altitude-platform-extraction method is shown in Figure 8-18. The C-130, the only aircraft used for LAPES, approaches the drop zone below radar detection altitude. At the drop zone, the pilot deploys a 15-foot-diameter ringslot parachute using the pendulum extraction method. This parachute, by means of a 60-foot riser and a tow release, is attached to the rear of the aircraft. Upon reaching the drop zone, the pilot lowers the aircraft to about 5 feet above the ground and disconnects the ringslot parachutes, which, in turn, deploy a large single or a cluster of several extraction parachutes that pull the platform out of the rear of the aircraft cargo compartment. The platform drops to the ground and is stabilized and decelerated by the force of the large extraction parachute(s) and ground friction. Up to three platforms, connected with flexible couplings, can be extracted using this system. Depending on the type of load to be extracted, the extraction riser is attached close to the center of gravity of the platform-cargo assembly.

USAF Technical Order T.O. 1C-130.9 defines the LAPES rigging, restraint, and extraction procedure. The Air Force Type A/E 28H-1 (metric) platform was specifically developed to accommodate the high vertical loads frequently associated with the LAPES platform extraction method.

Loads up to 45,000 pounds have been extracted with the LAPES system.

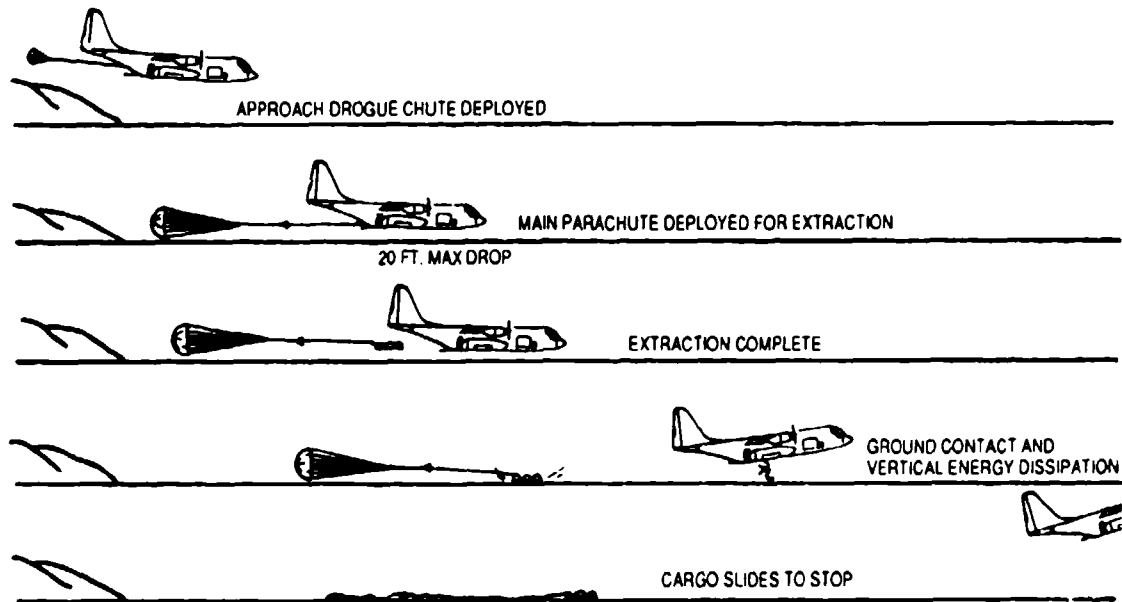


FIGURE 8-18. The LAPES C-130 Platform Extraction System.

The advantages of the LAPES airdrop method are obvious. The exposure of the aircraft to the antiaircraft and rocket fire is greatly reduced, the cargo delivery is very accurate, and large main parachute assemblies are eliminated. The disadvantages of the LAPES airdrop method are the need to fly at extremely low altitudes and the need for a large, level drop area for extraction and ground deceleration. References 8.41 to 8.44 describe development and testing of the LAPES airdrop method.

High-Speed, Low-Altitude Container Drop. A finned aluminum cargo container, Type CTU-2A, a successor to the M4-A container, has been developed for underwing carriage by fighter type aircraft. The container can be flown at speeds up to 550 knots and dropped at speeds up to 400 knots. A reefed 34-foot-diameter ringslot parachute is used for retardation and recovery of the 500-pound container that is equipped with a crushable nose cone for impact attenuation. The development of the container, shown in Figure 6-85, is discussed in References 6.68 and 8.45.

High-Speed, Low-Altitude C-130 Container Delivery. This container delivery method, also referred to as high-speed, low-level airdrop system (HSLLADS), delivers A-21 containers from a specially equipped C-130 (COMBAT TALON). The A-21 containers are stored at the rear of the aircraft compartment and ejected from the cargo ramp by a slingshot ejection delivery system (SEDS). A static line attached to the aircraft deploys the 22- or 28-foot-diameter ringslot extraction parachute used as the main parachute for each container. The slingshot delivery method can eject four modified 500-pound A-21 containers at velocities

up to 250 knots. Several layers of paper honeycomb on the bottom of the containers are used to cushion the impact shock (References 8.46 and 8.47).

High-Altitude Airdrop Methods. High-altitude airdrops allow the drop aircraft to fly above the effective range of small- and medium-caliber antiaircraft and rocket fire. The problem is to drop with sufficient accuracy without overly complex drop equipment.

Several high-altitude airdrop concepts have been investigated (References 8.48 to 8.53). The U.S. Army developed in-house the High-Altitude Airdrop Resupply System (HAARS). This system is an A-22 container dropped at altitudes above 10,000 feet and stabilized with a standard 68-inch pilot chute at a descent speed of about 250 ft/s. At 800 to 100 feet above the ground, a baro-switch-actuated pyro disconnect releases the pilot chute and deploys the 64-foot-diameter G-12 main parachute attached to the container by an inner V-sling. The G-12 parachute is equipped with a pull-down vent line for faster opening and higher drag. Figure 8-19 shows the HAARS system with the first-stage pilot chute deployed.

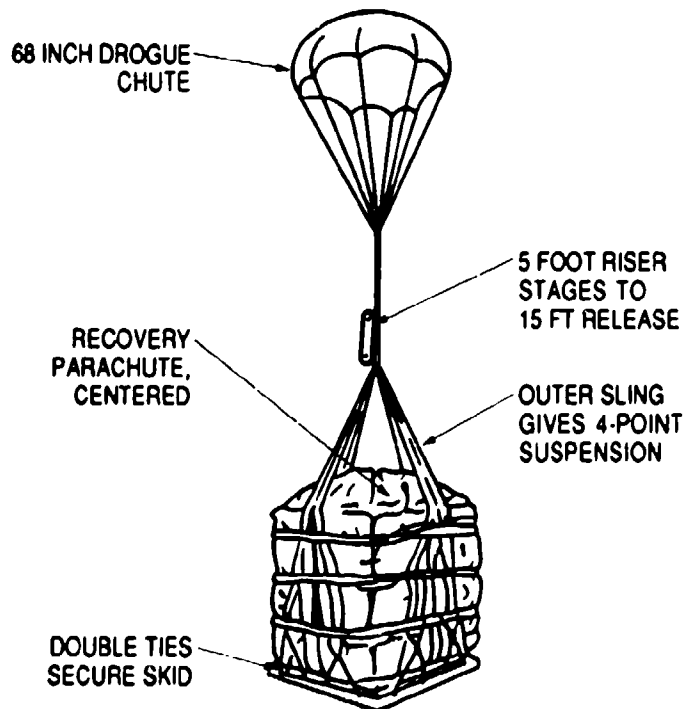


FIGURE 8-19. High-Altitude Airdrop Resupply System (HAARS), First-Stage Configuration.

8.4.4 Containers Used in Military Airdrop Operations

Table 8-7 lists containers used in military airdrop operations. Troops in the field have frequently modified military airdrop containers to meet their specific requirements. Reference 6.68 provides detailed information on containers and platforms and on their rigging and installation procedures.

TABLE 8-7. Airdrop Containers.

Container, platform	Weight range, lb	Parachute(s) used
A-7A, A-21	200 to 500	Single G-13, G-14
A-22	500 to 2200 500 to 1000 (2 Chutes) 1000 to 15000 (3 Chutes)	Single G-12 Clustered, G-14 Clustered, G-13
Platform	2500 to 42,000	Single & Clustered G-11

8.4.5 Airdrop Parachute Assemblies

Airdrop parachute assemblies include pilot chutes, extraction parachutes, and main parachute assemblies ranging from a single 30-foot-diameter G-13 parachute to clusters of up to eight 100-foot-diameter G-11 parachutes. Storage, packing, rigging, and installation of these parachutes are basically similar to those for parachute assemblies used in other fields. However, maintenance of airdrop parachute assemblies must frequently be conducted under adverse conditions caused by poor facilities, weather, retrieval from rough terrain, and lack of equipment and personnel. Refurbishment of parachute assemblies for repeated use is a vital peacetime requirement.

This operational environment establishes design requirements somewhat different from those governing the design and use of recovery parachutes for missiles, air vehicles, and spacecraft. Low acquisition cost and simplicity of maintenance, packing, rigging, and retrieval for reuse pace the requirements for parachutes used in airdrop operations.

The following requirements govern the selection, design, and use of parachutes for airdrop operations:

1. Reliability of parachute operation and suitability for system integration.
2. Safety of the aircraft during rigging, flight, load extraction, and parachute deployment.
3. High drag for low rate of descent coupled with a low weight and simplicity of manufacturing from low-cost material.

4. Uniformity and repeatability of performance under multiple reuse and suitability for cluster operation.
5. Ease and simplicity of packing, rigging, maintenance, and repair of the parachute assembly.
6. Low cost.

Some specialized requirements may include the following:

1. Ultrafast deployment, canopy inflation, and system damping for low-altitude airdrops.
2. Fast and uniform operation of extraction parachutes, including load transfer from the platform to main parachute deployment.
3. Uniform, simultaneous deployment and opening of cluster parachutes.
4. Reliable parachute ground disconnect and deflation in high surface winds.
5. Easy retrieval of large parachutes dropped over cargo equipment and collapsing in rocky, brushy terrain.

Figure 2-6 of Chapter 2 lists general design criteria; many of these criteria apply also to cargo parachute assemblies.

Main Descent Parachutes. Operational experience has defined certain parachute design restraints. The size and weight of the 100-foot-diameter G-11 parachute assembly, weighing about 250 pounds, may be the upper practical limit for handling, packing, rigging, and retrieval after use.

The U.S. Air Force, in the early 1950s, developed and tested a 150- and a 200-foot-diameter parachute for the airdrop of heavy cargo platforms. The tests showed the parachutes to be technically feasible but impractical in several aspects. The size and weight of the parachutes required large facilities and made handling, packing, and rigging difficult. The 200-foot parachute had canopy inflation times of over 20 seconds that resulted in canopy twisting, damage, and destruction. Ground retrieval of the parachutes by conventional methods resulted in excessive damage to the lightweight canopy fabric. At that time, the parachutes were judged unsuitable for military airdrop use. References 5.14 and 8.54 describe the testing of the large parachutes at the El Centro Test Range. Reference 8.55 lists the reports that cover the extensive testing done at the El Centro Test Range on airdrop assemblies and cargo parachutes. Table 8-8 lists cargo parachutes presently in use by the U.S. Armed Forces.

TABLE 8-8. Military Cargo Parachutes.

Parachute type	Nominal diameter, D _o , ft	Number of gores and suspension lines	Effective L _e /D _o	Material canopy		Material suspension lines		Wt., lb ^a	Max. vel., knots	Performance	
				Type	Str., lb/in.	Type	Str., lb/in.			Wt., lb	V _e , ft/s
G-13 hemispherical	32.4	20	0.93	Cotton		Rayon	400	40	150	500 ^b	20 ^c
G-14 ^d single-slot biconical	34	32	0.8	Cotton ^e	48	Cotton ^f	400	37.5	150	500	27
G-12D solid flat	64	64	0.8	Nylon	90	Nylon	1000	130	200	2200	28
G-12E	64	64	0.8	Nylon	90	Nylon	1000	130	250	2200	28 ^c
G-11A	100	120	0.9	Nylon	50	Nylon	550	250	150	3500	22
G-11B ^f	100	120	0.9	Nylon	50	Nylon	550	275	150	5000	25 ^c
G-11C	100	120	0.9	Nylon	50	Nylon	550	275	150	5000	25 ^c
137-ft ^g triconical	136	120	1.25	Nylon	50	Nylon	550	300	150	10,000	25 ^c

^a Assembly weight includes deployment bag, bridle, static line.^b Maximum payload weight.^c For quoted maximum payload.^d Replacement for G-13.^e Cotton or polyester.^f Pull-down vent line.^g Experimental.

The 32-foot-diameter G-13, the 64-foot G-12, and the 100-foot G-11 parachutes were all developed in the 1940s and early 1950s. All attempts to replace the design of these old parachutes with better designed parachutes have failed so far, with the exception of the 34-foot-diameter biconical G-14 parachute developed in the 1960s as a replacement for the G-13 parachute. New parachutes must be either lower in cost for the same performance or higher in performance for the same cost. Cost has proven to be a very important factor for cargo parachutes. Material accounts for about 70 to 80% of the acquisition costs of cargo parachute assemblies.

Rates of descent of 20 to 30 ft/s are normal for cargo parachutes. Single parachutes should not oscillate more than 10 to 15 degrees and should have good damping characteristics.

The G-13 and the G-14 parachutes are used in unreefed condition for the airdrop of A-7 and A-21 containers and cargo bundles weighing up to 500 pounds (References 8.56 and 8.57).

The G-12 parachute with a canopy manufactured from 90-lb/in. material is well suited for rough handling and multiple reuse. It is used singly and in clusters (Reference 8.58).

The 100-foot-diameter G-11 parachute is the Army workhorse for platform drops. The solid flat canopy uses 1.6 oz/y² nylon fabric, and has 120 gores and suspension lines of 550-pound strength. It became clear early in the development of this parachute that reefing was necessary for proper single-canopy inflation and even more necessary for proper cluster operation. For a single parachute, reefing provides an in-between inflation stop that permits all canopies to obtain a proper circular canopy inflation prior to disreef.

The author, in the late 1940s, observed a cluster drop of four unreefed G-11 parachutes. One lead chute opened ahead of the others, overloaded and broke away. A second and third chute followed until all parachutes had either broken away or were destroyed. Reefing gives all canopies a chance to obtain a reasonably uniform reefed inflation. Disreefing from this position supports a more uniform final inflation of all parachutes. The first version of the parachute, the G-11A, uses a 20-foot-long reefing line and two 2-second, M-21-type reefing cutters. This parachute has been successfully dropped in clusters of up to eight parachutes (References 8.59 and 8.60).

Several modifications have been investigated to improve performance and to shorten the canopy inflation time, a prerequisite for lowering the airdrop altitude. One successful modification is the pull-down vent line (PDVL), also called the center line. A line connecting the vent of the canopy with the confluence point of the suspension lines pulls the vent of the canopy toward the skirt. This creates a toroidal, annular type canopy shape; increases the inflated canopy diameter; and reduces the inflation time. The G-11B uses a 95-foot-long PDVL in connection with a 60-foot reefing line and four 2-second reefing cutters. The G-11C has a 100-foot PDVL, a 20-foot reefing line, and two 4-second cutters. References 8.61 and 8.62 describe the development of the pull-down vent line for the G-11, quoting as primary gain the reduction of the parachute opening time. The pull-down vent line permits the drop of cargo using a single parachute or a cluster of two G-11C parachutes from an altitude of 500 feet.

The Air Force investigated the addition of an internal parachute canopy for better inflation control and shorter inflation time. Reference 8.63, which discusses these tests, states that the marginal reduction in canopy filling time did not justify the added complexity.

C-17 Parachute. The airdrop of a single 60,000-pound load will become a reality with the introduction of the C-17 cargo aircraft. Use of a cluster of 10 to 12 100-foot-diameter G-11 parachutes is technically difficult and operationally impractical. The U.S. Army is investigating two approaches. First, the development of a cluster of six 137-foot-diameter parachutes, and second, a parachute-retrorocket system. The parachute system is in the final development state; the retrorocket program, a revival of a program of the 1960s, has just been started.

Requirements for the 137-foot cluster assembly include an individual parachute assembly weight of less than 350 pounds; a rate of descent of not more than 25 ft/s for a single parachute dropped with a 10,000-pound load; short parachute opening time including deployment, canopy inflation, and system stabilization; and handling, packing, rigging, and load installation procedures similar to present procedures. The design, development, and testing of the final cluster of six 136.9-foot-diameter triconical parachutes with a single circumferential slot in each canopy is described in References 8.64 and 8.65. Each canopy is equipped with a pull-down vent line, has 120 gores, and has suspension lines of 550-pound strength. The parachute assembly underwent major modifications to overcome cluster inflation, interference, and related canopy stress problems. The Army states that the parachute assembly is undergoing final refinements prior to qualification.

Several previous programs have dropped loads in excess of 42,000 pounds. The Air Force extracted an 87,500-pound Minuteman missile from the rear of the C-5 aircraft (Reference 8.66). Investigations of dropping loads in excess of 50,000 pounds are described in References 8.67 and 8.68.

NASA developed the water recovery system for the 180,000-pound solid-rocket boosters of the Space Shuttle. Each of the two boosters is decelerated with a 56-foot-diameter ribbon drogue chute and lowered into the water on three 135-foot-diameter ribbon parachutes at a rate of descent of 75 ft/s. This parachute system is described in section 8.2 and References 8.5 to 8.11. These programs indicate that airdropping even a 60,000-pound single load may not be the upper limit.

Experience from World War II, Korea, and Vietnam indicates that cargo parachutes are never recovered in a battlefield environment. This fact instigated the development of one-time-use, expendable parachutes. Both the Army and the Air Force started development programs for obtaining such one-time-use parachutes substantially lower in cost than existing cargo parachutes. Materials investigated included paper, plastic film, laminated spun nylon, and others. Special canopy designs tailored to these materials were investigated. Difficulties developed in connecting these materials, in attaching suspension lines to the canopy, in packing the relatively stiff materials, and in handling and rigging. Canopies manufactured from imporous material were unstable and had high opening forces. Designing porosity into the canopies in the form of slots and openings defeated the low-cost aspect. Efforts in this area were discontinued after several unsuccessful programs (References 8.69 to 8.71).

Extraction Parachutes. Extracting heavy loads and load platforms from the rear of cargo aircraft was demonstrated in the late 1940s with the C-82 cargo airplane. In the early 1950s the pendulum-swing-arm method was developed for deploying extraction parachutes. Large extraction parachutes and a precise control of the extraction process became mandatory with the introduction of LAPES. An extraction force equal to 0.75 to 1.5 times the weight of the load to be extracted was found to be a practical approach for platforms using the standard airdrop

method. The LAPES method required extraction forces equivalent to about 3 g to decrease platform extraction and aircraft response time.

A high degree of reliability and uniformity of inflation is required for the operation of the extraction parachute to comply with aircraft safety, stability, and control requirements. The extraction parachute, be it single or a cluster of parachutes, must be sufficiently stable that it does not interfere with aircraft control and smooth platform extraction. Only stable ribbon and ringslot parachutes meet these requirements and are used for this application.

Table 8-9 lists standardized extraction parachutes that are in the inventory or that have been qualified.

TABLE 8-9. Extraction Parachute Types.

Nominal diameter, ft	Type	Number of gores	L_s/D_o ratio	Canopy material	Suspension line breaking strength, lb	Parachute weight, lb	Used for	Drawing number
15	Ringslot	16	1.0	2.25-oz nylon	1000	8.0	Standard/LAPES	57J6032
22	Ringslot	28	1.0	3.5-oz nylon	1500	27.5	Standard/LAPES	52K6329
28	Ringslot	30	1.0	2.25-oz nylon	2000	36.5	Standard/LAPES	58K6326
28	Ringslot	36	1.0	3.5-oz nylon	2300	68.5	Standard/LAPES	67K1901
35	Single-Slot	32	1.0	3.5-oz nylon	4000	96.0	Special	68K373
35	Ringslot	32	1.0	3.5-oz nylon	4000	90.0	Special	68K372
35	Ribbon	48	1.0	500-16 Ribbon	4000	150.0	LAPES	11I3766

The group of 15- to 28-foot-diameter ringslot extraction parachutes was developed for use with the standard airdrop method. Depending on the weight to be extracted, the parachutes are used singly or in clusters. Reference 8.72 recommends the proper load-extraction parachute combinations. The heavy 28-foot-diameter ringslot and the 35-foot-diameter ribbon parachutes were developed for LAPES, which requires a fast extraction for aircraft stability. References 8.73 to 8.78 document the extensive work conducted for the development of safe extraction methods and extraction parachutes.

Figure 8-20 shows the parachute extraction force and the platform extraction velocity of a 50,000-pound load platform extracted with the 35-foot ringslot parachute. The platform was held in the aircraft by the rail release mechanism until the parachute extraction force reached 15,000 pounds; this resulted in a fast platform extraction and avoided excessive aircraft pitch-up caused by the platform moving aft in the aircraft.

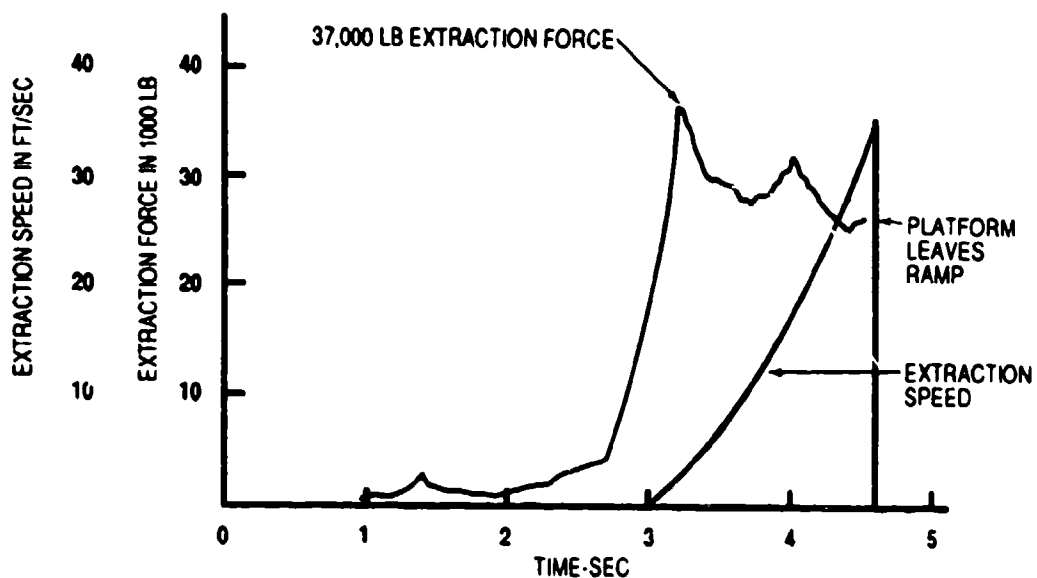


FIGURE 8-20. Parachute Extraction Force and Extraction Speed vs. Time for a 35-Foot Parachute Extracting a 50,000-Pound Load.

8.4.6 Parachute-Retrorocket Airdrop System

Section 6.8 discusses the technical aspects of retrorockets as long-stroke, low-deceleration impact attenuators. Retrorockets may be either body- or harness-mounted in parachute retrorocket systems as shown in Figure 6-82. Both arrangements have their advantages and disadvantages. However, for airdrop systems, the harness-mounted arrangement is the best approach. Retrorockets as impact attenuators provide the maximum amount of energy per pound of weight or cubic foot of volume. However, retrorockets also add some complexity because of the need for a ground sensor and for exact rocket ignition timing, and because an explosive material is added to an otherwise benign system. Also, a retrorocket system is most likely higher in acquisition costs than paper honeycomb, the presently used impact cushioning material for heavy loads on airdrop platforms.

The U.S. Army, in the 1960s, conducted an extensive development and test program of a parachute-retrorocket airdrop system (References 8.79 to 8.82). The feasibility of the concept was proven; however, the development was temporarily shelved in favor of the LAPES development, which was, at that time, operationally more desirable.

The U.S. Army has reevaluated the retrorocket concept. One of the advantages of the retrorocket as compared to the present approach with mountains of paper honeycomb (see Figure 6-72) is the saving of time. Storing, transporting, and building up the paper honeycomb cushions is a logistics problem and a time-consuming process. The total airdrop mechanism

using loads and platforms with its many restraints and cushioning material is a labor-sensitive process. Retrorockets can easily provide the 8-ft/s rate of descent required by the Army for the landing of sensitive loads and military vehicles (Reference 8.83). The Army, as a result of these considerations, has established a new program for developing a parachute-retrorocket airdrop system.

8.4.7 Cargo Point Delivery With Maneuverable Parachutes

Besides cargo delivery with the standard airdrop and the LAPES methods, the need exists for cargo delivery and resupply of small units in isolated areas. This can be accomplished by dropping cargo from high altitudes toward a marker or beacon on the ground using maneuverable parachutes. The first attempts to develop such a system are as old as the introduction of gliding, maneuverable parachutes. However, practical systems had to wait for the development of hi-glide parachutes, especially the ram-air inflated parafoil. The technical aspect of hi-glide parachutes is discussed in section 5.9. The U.S. Army, in a 1969 paper, Reference 8.84, defined requirements for and discussed such a cargo point delivery system. None of the attempts in the 1970s and early 1980s to develop such a system were operationally acceptable (References 8.85 to 8.87).

Watching sport jumpers perform precision landings raises the question: Why not use the same approach for cargo point delivery? Sport jumpers have an excellent on-board guidance and control system that allows them to judge altitude, location with regard to the landing zone, and wind direction and velocity. From those data the necessary glide angle and approach direction can be estimated and control lines can be manipulated for a perfect flareout point landing. However, to duplicate these functions in a guidance and control unit attached to the airdrop package is difficult and expensive.

Only recently have two cargo point delivery systems been developed that provide acceptable performance. They can be dropped at speeds up to 150 knots and altitudes up to 20,000 feet. An on-board guidance and control unit flies the cargo toward a beacon on the ground. A 99% landing accuracy in 100-yard circle around the beacon is claimed by the manufacturer.

The development of a 10,000-pound point delivery system, using the same design approach, is described in Reference 8.88. References 8.89 and 8.90 describe the recovery of large spacecraft and and spacecraft components using maneuverable parachutes.

8.4.8 Airdrop of Military Personnel

The U.S. Army and other service branches use personnel parachute assemblies for premeditated jumps of paratroopers, paramedics, and special-forces personnel. The primary requirement of these parachute assemblies is to land the jumper uninjured and ready for action.

In World War II the paratroopers used a 28-foot-diameter, solid flat parachute, the T-7, in connection with a 24-foot-diameter reserve parachute that was only used in training jumps. In the 1950s the T-7 was replaced with a 35-foot-diameter, 10% extended skirt parachute, the T-10—still today the paratrooper's workhorse (Reference 5.22). The 24-foot T-7 reserve parachute has been maintained with the T-10 assembly. Several T-10 versions are in use today. The original T-10 parachute is shown in Figure 8-21, and the maneuverable version, the MC1-1B with glide and control slots and the anti-inversion net, in Figure 8-22.

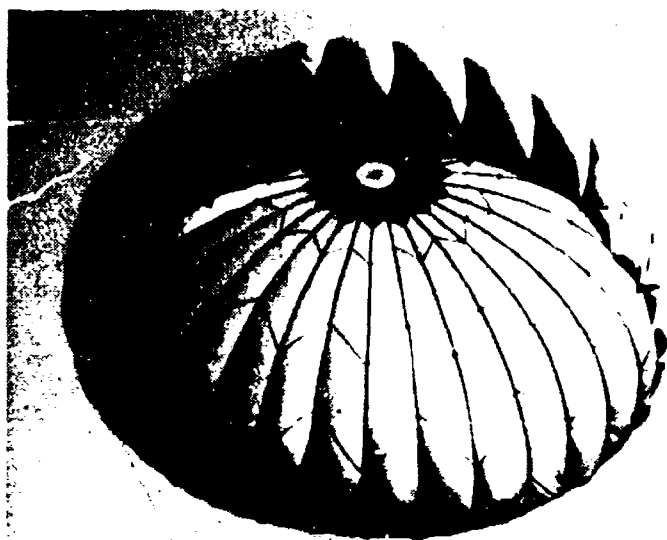


FIGURE 8-21. T-10 Paratrooper Parachute.



**FIGURE 8-22. MC1-1B Maneuverable Paratrooper Parachute
With Glide and Control Slots and Anti-Inversion Net.**

The standard version of the T-10, used by paratroopers, is housed in a deployment bag with the suspension lines stowed on the outside of the bag. The bag is housed in a pack attached to the harness of the paratrooper. When exiting the aircraft, a static line attached to the aircraft breaks the pack closing cord, pulls the parachute deployment bag from the pack, and deploys the parachute. The static line with the empty deployment bag trails behind the aircraft.

This method ensures a reasonably uniform opening of all parachutes behind the aircraft. Paratroopers exit the C-130 and the C-141 in two rows from the rear of the fuselage at timed intervals of about 0.5 second. At a jump speed of 130 knots, this creates a considerable spread of the paratroopers on the ground. A closer spacing of the troopers is highly desirable but hard to accomplish. Most paratroopers carry a considerable amount of equipment that increases the rate of descent and requires adaptation of the parachute harness and the component location.

In recent years new requirements have necessitated modifications of the T-10 assembly and have probably formulated requirements for a new parachute assembly. The weight of some jumpers has increased to close to 400 pounds because of the special equipment carried. Table 8-10 lists the various versions of the T-10 parachute presently used by the military services of the United States. The basic dimensions of the T-10 parachute are listed in Table 8-11.

TABLE 8-10. List of Military Premeditated Jump Parachutes.

Type	T-10	T-10A	T-10B	T-10C	T-10C(2)	MC-1	MC1-1	MC1-1B	MC1-1C	MC1-2	MC-2	MC-3
Main parachute	35-ft extended skirt	35-ft	35-ft	35-ft	35-ft	35-ft	35-ft	35-ft	35-ft	35-ft	35-ft	Para- Com- mander
Reserve parachute	24-ft solid flat canopy	24-ft	24-ft	24-ft	24-ft	24-ft	24-ft	24-ft	24-ft	24-ft	24-ft	24-ft
Anti- inversion net		x	x	x	x			x	x			
TU maneuver slots							x	x	x	x		
Elliptical opening (Tojo)						x					x	
Pilot chute										36 in.	36 in.	40 in.
Static line deployment	x	x	x	x	x		x	x	x			
Manual deployment						x				x	x	x
Barostat deployment						x				x	x	x

The T-10, T-10A, and MC-1 have the harness with the central release lock; all other parachute harnesses have 2 canopy disconnects.

The T-10A has the anti-inversion net and the central harness release lock.

The T-10B has the anti-inversion net and individual canopy releases.

The T-10C adds the modified pocket bands.

All MC-types are maneuverable parachutes.

The MC-1 is similar to the Navy NSP-1.

The MC1-2 is similar to the Navy NSP-2.

The MC1-1C is similar to the MC1-1B but uses low-porosity canopy material.

The MC1, MC1-2, MC-2, and MC-3 are freefall parachutes.

The T-10C and the MC1-1B are the standard paratrooper parachutes, with the latter being phased out for use in mass assault.

TABLE 8-11. Basic T-10 Assembly Dimensions.

Type	T-10	T-10 Reserve
Design	10% extended skirt	Solid flat
Diameter, D_0	35.0 ft	24.0 ft
Number of gores	30 ea	24 ea
Length of suspensions lines	25.5 ft	20 ft
Strength of suspension lines	375 lb	550 lb
Effective L_s/D_0	0.84	0.9
Canopy material	1.1 oz/yd ² nylon	1.1 oz/yd ² nylon
Parachute weight	13.85 lb	10.4 lb
Maximum jump speed	150 knots	150 knots
Pocket bands	50%	...

The first major T-10 modification was the addition of the anti-inversion net. Static-line, cross-wind-deployed parachute canopies have a tendency to form the canopy in a sail-like fashion resulting in canopy inversions and malfunctions. This problem is discussed in section 6.1.4. The anti-inversion net, a wide mesh nylon netting extending 18 inches down from the canopy skirt, has reduced T-10 canopy inversion in a ratio better than 1 to 1000. Design and testing of the anti-inversion net is described in section 6.3.4 and References 6.27 to 6.29 and 8.91. This modification created the T-10B. The T-10C, in addition to the anti-inversion net, modified the canopy pocket bands, which resulted in about a 1.5 ft/s reduction in rate of descent.

Several approaches have been investigated for decreasing the rate of descent and the jump altitude. It is possible to design a larger parachute to slow the rate of descent, and it is probably possible to design a canopy that will open faster, but a larger canopy will also increase the canopy inflation time unless the design of the canopy is changed. An example of design change would be the use of a pull-down vent line. However, because the same amount of energy must be absorbed in a shorter time, every decrease in canopy inflation time will increase the opening force. Also, time to recognize a malfunction and activate the reserve parachute must be available. A 300-foot drop altitude leaves little time for malfunction recognition and reserve parachute deployment.

To solve these problems, a British-German team tried to use a cluster of three small parachutes. Using the Apollo spacecraft approach, two parachutes met the rate of descent requirements; and the third parachute, the reserve parachute, was simultaneously deployed and provided not only the reserve safety, but also a slower rate of descent. The final version of this assembly, however, was not operationally acceptable.

One of the concepts to obtain a low-altitude jump parachute, investigated by the U.S. Army, is the annular/airfoil parachute assembly described in Reference 8.92.

The deployment of the reserve parachute, in case of a main parachute malfunction, has been plagued by interference and entanglement with the malfunctioning main parachute. Many investigations have been conducted to obtain reliable reserve parachute deployment and inflation. Some of these investigations are described in References 8.93 to 8.96.

The military has a need for parachutes that can be dropped offset and flown to a selected landing area. Another application is the precision parachute landing for rescue and special missions.

The first maneuverable parachute, the so-called "Tojo" gliding parachute, standardized as the MC-1 and MC-2 parachute assemblies, resulted from an Air Force investigation of several early gliding parachutes (Reference 8.97). The canopy has an elliptical hole in the rear. Air escaping horizontally from the hole creates a reaction force and causes gliding in the opposite direction. Two slots and attached control lines provide turn control.

The MC1-1B is a T-10 canopy with TU-slots covering 11 gores. Seven center slots are glide slots and two long and two short slots are turn slots that are activated by two control lines. This parachute, shown in Figure 8-22, has a glide ratio of close to one, and turns 180 degrees in 8 seconds. The MC1-1C is similar in design to the MC1-1B but uses low-porosity canopy material. References 8.98 and 8.99 refer to development and testing of the MC1-1B parachute.

The MC-3 is the military version of the paracommander parachute used extensively by sport parachutists in the 1970s before the introduction of the ram-air inflated canopies. The MC-3 has a glide ratio of 1.1 and excellent stability and turn control (Reference 8.100).

Three types of maneuverable parachutes are standardized and are listed in Table 8-10. However, the maneuverable parachute almost exclusively used is a commercially available ram-air inflated parafoil personnel parachute with seven-cell canopy area of 375 ft². This parachute is in the process of being standardized by the U.S. Army Natick Research, Development and Engineering Center at Natick, Mass. The parachute, well known from the demonstrations of the Army Golden Knights and sport jumpers, has a glide ratio equal to or better than 3, and has excellent stability and turn control. Section 5.9 discusses its performance, and References 5.152 to 5.161 discuss its design and development and its application as a military personnel parachute.

8.4.9 Multiple Personnel Drop

The idea for airdropping small military units in a container with all their equipment was first suggested at the end of World War II. This idea has been proposed and investigated several times in different countries. This concept overcomes the situation where paratroopers are spread out over considerable distances. References 8.101, 8.102, and 8.103 discuss proposals for multiple paratrooper drops.

8.5 AIRCRAFT IN-FLIGHT AND LANDING DECELERATION BY PARACHUTE

8.5.1 General Application

Parachutes are very effective when used to decelerate landing aircraft, to steepen the landing approach, and to help aircraft recover from unfavorable spin and deep stall flight conditions.

The ribbon parachute was especially developed as a stable, low-opening-shock parachute for the in-flight and landing deceleration of aircraft. The first ribbon-parachute-decelerated landing was performed in 1939. During World War II, ribbon parachutes were used as landing deceleration parachutes and retractable aircraft dive brakes, and were used for the recovery of aircraft from spin and high-speed emergency conditions during the development flight test phases.

The B-47 jet bomber was the first United States aircraft to be equipped with a landing deceleration parachute. When the landing approach of the B-47 proved to be too shallow for an accurate landing, a small parachute was installed as a dive brake to steepen the landing approach.

Today many military and some civilian (Concorde, for example) aircraft use landing deceleration parachutes. Also, most military and some civilian aircraft must demonstrate their capability to be able to recover from spin and deep stall flight conditions. If recovery problems occur, parachutes are used to restore the airplane to a controllable flight condition.

Parachutes are also used to decelerate dragsters (racing automobiles) and to recover high-speed-racing-boat crews.

8.5.2 Landing Deceleration Parachutes

8.5.2.1 Landing Roll Analysis. Aircraft use flaps and slots to decrease the landing approach velocity, and wheel brakes for deceleration after touchdown. Originally, parachutes were used as a backup to wheel brakes when runways were wet and icy, for such emergencies as

landing without flaps or brakes, and in cases of aborted takeoffs. However, emergency use soon developed into normal use when it was found that using parachutes during the high-speed phase of the landing roll, and wheel brakes during the low-speed phases, resulted in considerable savings in brakes and tires.

The effectiveness of landing parachutes is demonstrated in Figure 8-23, which shows the length of the landing roll of a 100,000-pound bomber using wheel brakes and parachutes of various diameters for different runway conditions. A friction coefficient $\mu = 0.3$ is valid for a good, dry runway; a coefficient $\mu = 0.1$ for wet conditions; and $\mu = 0.05$ for icy conditions.

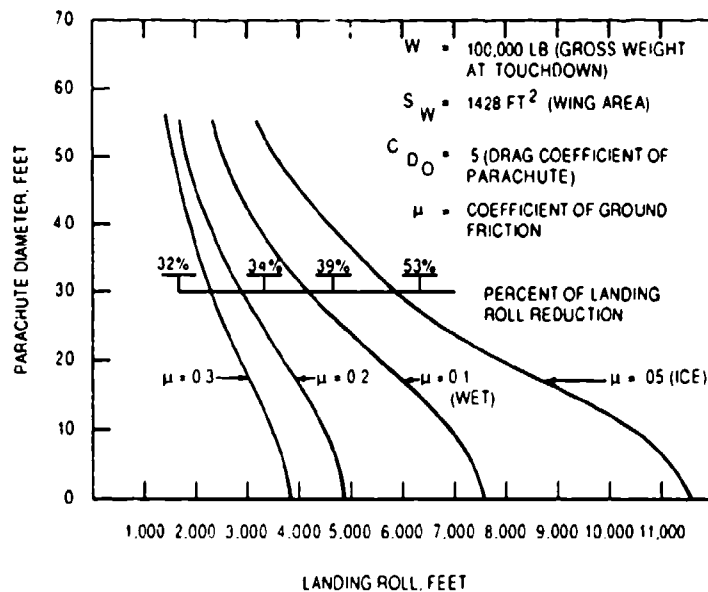


FIGURE 8-23. Aircraft Landing Roll as a Function of Parachute Diameter and Runway Conditions.

In operation, the pilot makes a normal approach and landing and deploys the landing deceleration parachute at, or shortly after, touchdown. The inflated parachute will trail behind the aircraft and will stay inflated as long as the aircraft is in motion or the engines are running. The airflow around the canopy will keep the parachute off the ground even if the parachute attachment point is low on the airplane. At the end of the landing roll, the pilot keeps the parachute inflated by slowly rolling to a designated drop-off area at the end of the runway, where the parachute is jettisoned.

Figure 8-24 shows the landing of a B-52 bomber with its 44-foot-diameter ribbon landing deceleration parachute deployed.



FIGURE 8-24. B-52 With 44-Foot-Diameter Landing Deceleration Parachute.

8.5.2.2 Landing Deceleration Parachute Design. Figure 8-25 shows a typical landing deceleration parachute assembly consisting of pilot chute, pilot chute bridle, main parachute deployment bag, main parachute, riser, and aircraft parachute compartment and attach fitting.

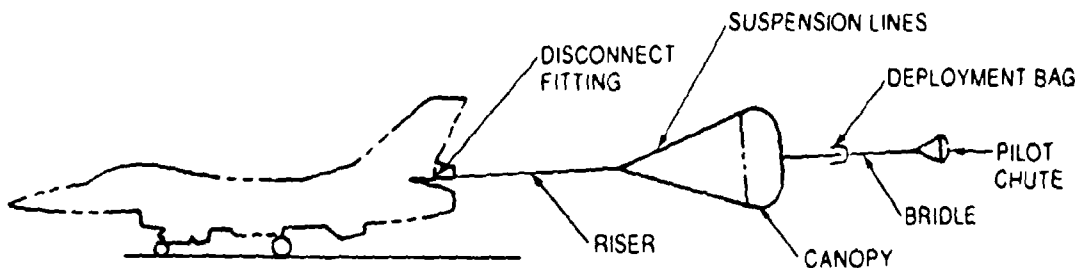


FIGURE 8-25. Typical Landing Deceleration Parachute Installation.

Landing deceleration parachutes must be free of oscillation and must have a low opening-force coefficient, C_x . Parachute oscillations as small as 3 to 5 degrees start interfering with the control of the aircraft. The stable ribbon parachute was used exclusively in the late 1940s and early 1950s. At that time, the ringslot parachute was developed as a low-cost substitute for the ribbon parachute. The ringslot parachute is used for aircraft landing deceleration on many military airplanes in the United States and abroad. Several nations use the stable cross parachute for this application. Ribbon parachutes usually can be used for fifty landings or more, whereas ringslot parachutes are generally replaced after 25 landings. The longer service life of the ribbon parachutes has resulted in their use on modern military aircraft.

The required parachute diameter must be calculated based on the characteristics of the aircraft and the required landing roll. Operational experience has established the relationship

of parachute drag area to aircraft wing area of about 0.25 to 0.5. The higher value is used on fighter aircraft and the lower value is used for bombers. Table 8-12 lists aircraft deceleration parachutes presently in use or in development.

TABLE 8-12. Aircraft Deceleration Parachutes.

Type	Aircraft	Diameter, ft	Type	Number of gores	Deployment velocity, knots
MB-5	F-100	16	Ringslot	20	190
MB-6	F-101 F-4	15.5	Ringslot	20	200
MB-7	F-104	16	Ringslot	20	200
MB-8	F-105	20	Ribbon	24	225
A-28A-1	F-106	14.5	Ringslot	20	220
-	F-5	15	Ringslot	20	180
MB-1	B-47 (approach)	16	Ringslot	20	195
D-1	B-47	32	Ribbon	36	160
D-2	B-52	44	Ribbon	48	170
	F-16 ^a	23	Ribbon	24	180
	TA-7E	15	Ringslot	20	180
	Space Shuttle orbiter	40	Ribbon ^b	44	230

^a Norwegian version

^b Continuous ribbon

The size of the main parachute is affected by the often large wake of the aircraft. This wake will cause a loss in drag because of the velocity decrease behind the aircraft. The large wake will also cause a reduction in stability. Section 5.5.2 discusses the wake effect and shows how to calculate the drag loss. Lengthening of the riser and use of suspension lines longer than the nominal parachute diameter (see Figure 5-21) will somewhat compensate for drag loss. However, design limitations exist in riser and suspension-line length. The parachute and all its components must be designed with multiple use in mind.

All components of the parachute assembly must be designed for rough handling and easy replacement of interchangeable parts. Heat protection will be necessary for some assemblies.

The pilot chute that starts the deployment sequence of the parachute assembly must be large enough to prevent the main deployment bag from falling and being dragged on the runway, but it must also not delay the inflation of the main canopy if the pilot chute is

permanently attached to the main parachute, the most frequently used design. Experience has shown that pilot chutes with a drag area equivalent to 3% of the drag area of the main parachute meet these requirements. This size limitation does not apply to pilot chutes that are not attached to the parachute assembly. Ejection of the pilot chute into good airflow behind the airplane is of utmost importance for proper assembly deployment. Spring-loaded pilot chutes usually meet this requirement. However, drogue-gun or mortar deployment of the pilot chute is necessary for aircraft with large, flat tail ends, such as the Space Shuttle orbiter. The pilot chute bridle must be long enough to place the leading edge of the pilot chute into good airflow behind the airplane.

The main parachute deployment bag should contain compartments for canopy, suspension lines, and risers. Stow loops and tie cords should be used to obtain a controlled, incremental, orderly deployment of all parts of the parachute assembly. This will ensure a low mass shock (snatch force) at canopy and line stretch as well as proper canopy inflation. The deployment bag should fit tightly in the parachute compartment, and the parachute assembly should be handpacked. Pressure packing, so extensively used in missile and drone recovery systems, requires presses and tools as well as long packing times. Pressure packing is unsuitable for frequently repacked landing deceleration parachutes.

Parachute risers for landing parachutes are formed from multiple layered webbings or from bundled continuous suspension lines. The latter design is used mostly for large, high load parachutes, such as those of the B-52 and the Space Shuttle orbiter where multiple layer webbing risers proved to be not strong nor flexible enough. The length of the riser is determined from two considerations: The leading edge of the main parachute must be far enough behind the wake of the aircraft to avoid a large drag loss, and the parachute force line should go as close as possible through the C.G. of the airplane. A low location of the riser attachment point, together with a large diameter parachute, may cause the parachute force line to run below the C.G. of the aircraft and cause high loads on the forward landing gear. This can be somewhat overcome by lengthening the riser. The inflated parachute canopy will trail about 0.25 of the inflated canopy diameter above the runway. Since the canopy diameter is constant, lengthening the riser will decrease the riser angle and lower the load on the forward landing gear. Landing parachutes for fighter aircraft usually have long risers of 1 to 1.5 times the nominal parachute diameter. These long risers are used to avoid drag losses on a parachute too close to the aircraft and to protect the parachute from the heat plume of the jet engine. A parachute assembly installation close to the jet engine requires special heat protection for parachute compartment and riser. Most landing parachutes for fighter aircraft use coated woven metal sleeving for heat protection.

8.5.2.3 Aircraft Installation. The parachute assembly installation must conform to the aircraft. A good installation must provide a suitable parachute compartment configuration and location and a safe parachute lock, deploy, and jettison mechanism. The parachute compartment should be located on the upper side and to the rear of the fuselage; it should be

smooth on the inside with rounded corners and with walls either straight or slightly conical toward the rear for good parachute extraction by the pilot chute. The deployment path of the pilot chute and the parachute bag must be clear of obstacles and protrusions that can cause hang-ups or damage. The pilot chute installation should ensure immediate ejection after compartment door opening. A good location for the pilot chute is on the inside of the compartment doors, or on top of the main parachute bag, with the pilot chute held in place by flaps that are actuated by the opening of the compartment doors. The pilot chute controlled deployment of the parachute assembly should proceed in the sequence of riser, suspension lines, and canopy. This sequence, called riser-first deployment, keeps the canopy closed until line and canopy stretch occurs and prevents a large snatch force that would be caused by the canopy being partially inflated before line stretch.

If the parachute compartment is on the side or the bottom of the fuselage, the main parachute bag must be held in place by flaps that are actuated by the pilot chute. An under-fuselage installation, as was used on the B-47 bomber, should be avoided. Overhead installation of a large, heavy parachute assembly is difficult and requires the undesirable canopy-first deployment concept (see section 6.1.1).

The parachute installation should permit easy installation and access by maintenance personnel. Safety precautions must be taken to prevent maintenance personnel from inadvertently opening the compartment door and releasing the pilot chute. Two approaches have been used to avoid inadvertent parachute operation during flight: (1) the disconnect-mechanism hook that connects the parachute to the aircraft is not closed until the pilot is ready to deploy the parachute, or (2) a fail-safe break link is installed in the riser attachment fitting that breaks if the parachute is deployed above a safe velocity. The first approach is preferred.

The following process for operation of the parachute has evolved as the most practical system. A single handle in the cockpit, accessible to both pilot and copilot, provides three functions for parachute operation: (1) A short pull on the handle engages the hook that connects the parachute to the airplane, (2) a further pull opens the parachute compartment door and starts the deployment process, and (3) a 90-degree turn of the handle disconnects the parachute.

The parachute compartment must be protected against engine heat and high humidity, and the door(s) must open under icing conditions. Maximum allowable compartment temperature (Reference 8.104) is 250°F for nylon parachutes. However, the temperature should be limited to 200°F. The specification that governs parachute installations in aircraft is also found in Reference 8.104.

Use of Kevlar textile material for risers, suspension lines, and canopy reinforcing tapes has reduced the weight and volume of missile and ordnance parachutes by 25 to 40%. An equal

saving in weight and volume is possible for landing-deceleration parachutes. Kevlar has a temperature limit almost twice as high as nylon.

A modern landing deceleration parachute developed for the Space Shuttle orbiter is configured as follows: Maximum orbiter landing weight is 240,000 pounds. The maximum parachute deployment velocity is 230 knots. A 40-foot-diameter conical ribbon parachute has a canopy porosity of 16%, and continuous horizontal ribbons varying in strength from 200 pounds at the canopy skirt to 500 pounds in the crown. Six lateral tapes reinforce the canopy. Horizontal and vertical ribbons are made of nylon. Suspension lines, risers, vent, skirt, and lateral tapes are Kevlar. The 44 suspension lines have an effective length of $1.24 D_0$. The 67.5-foot-long riser is formed from suspension lines for flexibility, and is connected to the suspension lines by a wrap-around keeper. The distance from forebody to the leading edge of the canopy is equal to five times the blunt forebody diameter of about 25 feet. A 9-foot-diameter ringslot pilot chute is mortar-ejected into good airflow behind the blunt forebody. To avoid delays in opening the main parachute, the large pilot chute is not connected to the main parachute.

8.5.3 Landing Approach Parachutes

Parachutes have been used in the past when either the flaps of the aircraft were not sufficient to steepen the landing approach or when dive brakes were needed as an afterthought. The only known aircraft that used a landing approach parachute was the B-47 bomber. The approach angle of the aerodynamically clean aircraft within allowable velocity limits was reduced to about 2 to 3 degrees. This angle made a point touchdown at the end of the runway very difficult. A 15-foot-diameter ringslot approach parachute deployed at high altitude at the start of the letdown increased the approach angle to about 5 degrees, permitting a more precise touchdown. Reference 8.105 is a detailed description of the design, development, testing, and operation of the B-47 approach parachute.

The Germans, during World War II, developed adjustable, retractable parachute dive brakes for bombers, and reefed parachutes for diving and landing military attack gliders. Both applications are described in Reference 8.2. The use of parachutes as dive and approach brakes is now considered obsolete.

8.5.4 Aircraft Spin and Deep Stall Recovery Parachutes

8.5.4.1 Aircraft Spin Characteristics. Most military and some civilian aircraft must prove the ability to recover from spin and deep stall flight attitudes. An aircraft in full spin descends vertically in a rotational mode with the wings fully stalled at angles of attack of 40 to 90 degrees. Spinning is mostly a yawing motion. Fighter aircraft have been observed to make six turns in 7 seconds and change during that time to inverted spin and back again. A recovery parachute

must be large enough to stop the gyroscopic yawing motion and pull the airplane into a stable nose-down attitude. This is best accomplished by a parachute attached to and pulling on the tail of the aircraft. Such a parachute must be ejected into good airflow outside the effective spinning range, and behind the large wake of the spinning aircraft. In the installation of the parachute assembly, consideration must be given to the gyroscopic mass forces created by the spinning airplane, the deployment of the parachute assembly, and the necessity for the inflating parachute to pull on the tail of the aircraft at an angle of 40 to 90 degrees.

8.5.4.2 Aircraft Deep Stall Characteristics. Recovery from a deep stall must be proven for most military and civilian aircraft during development flight tests. In a known instance, control surfaces and engine power were not sufficient to correct a deep stall on a commercial airplane. A parachute installed in the tail of the aircraft is frequently used as an emergency means for pulling the tail of the aircraft up and returning the aircraft to a controllable flight attitude.

8.5.4.3 System Considerations. Aircraft spin and deep stall recovery parachute systems must meet requirements similar to those for aircraft landing deceleration parachutes. Spin and stall recovery parachutes must be stable and have a low opening shock so as not to interfere with the controllability of the aircraft; ribbon, ringslot, and cross parachutes meet these requirements and have been successfully used for this application.

The required parachute size is best determined in aircraft model spin tests in a vertical wind tunnel. Such a wind tunnel is available at the NASA Langley Research Center. References 8.106 and 8.107 summarize wind-tunnel test, design, and flight-test experience on spin recovery parachutes.

Other important design considerations include the location of the parachute canopy in relation to the tail of the aircraft to ensure operation of the parachute in good airflow behind the wake of the aircraft, the aircraft installation and parachute ejection system, and the mechanism for connecting and jettisoning the parachute.

Table 8-13 lists data on a number of operational spin/stall recovery parachute assemblies. A cursory parachute size analysis indicates a ratio of parachute drag area to aircraft wing area of 0.5 to 0.7 for large aircraft in the 50,000-pound range, and a ratio of 0.7 to 1.0 for lighter aircraft. Spin recovery parachutes are generally sized to the lower ratio level, and stall recovery parachutes to the upper level.

The length of the parachute riser, or more precisely, the distance from the leading edge of the canopy to the tail of the aircraft, is important to ensure good inflation in the wake of the spinning or stalled aircraft. No precise analytical method is available to determine the aircraft wake and the location of the parachute canopy behind the airplane. Table 8-13 shows the distance used in operational aircraft as the ratio of riser-plus-suspension-line length divided by the nominal parachute diameter. This ratio is 3 to 4 for spin recovery and 5.5 to 7 for stall

recovery parachutes. The riser of the DC-9 stall recovery parachute had to be lengthened to ensure good parachute inflation in flight tests with wheels and flaps extended. It has been proven to be advisable to conduct in-flight deployment tests of all spin and stall recovery parachutes to ensure good operation in the wake of the aircraft before use in actual spin/stall tests.

TABLE 8-13. Spin and Deep Stall Recovery Parachutes.

Aircraft	Aircraft gross weight, lb	Deployment velocity, kts	Parachute size, D_o , ft	Line length, L_e , ft	Riser length, L_R , ft	Trailing distance, L_t/D_o	Parachute type	Deployment method (Fig. 8.26)	Function
DC-9	108,000	210	24	24	136	6.3	Ribbon	A	Stall rec.
T-38	11,000	185	24.8	35	45	3.2	Ribbon	C	Spin rec.
F-105	50,000	200	21	21	45	3.7	Ringslot	C	Spin rec.
F-14	53,000	185	26	26	74	3.8	Ribbon	A	Spin rec.
S-3A	42,500	140	28	28	47	2.7	Ribbon	A	Spin rec.
F-16	20,000	188	28	28	50	2.8	Ribbon	A	Spin rec.
F-5E	15,000	185	24.8	25	45	3.2	Ribbon	B	Spin rec.
F-18	36,000	180	33.5	33.5	68	3.0	Ribbon	D	Spin rec.
X-29	17,800	180	19	27	38	3.4	Ribbon	C	Spin rec.
Concorde	-	200	35.1	36.1	164	5.7	Cross		Stall rec.

NOTE: L_t = Forebody - canopy distance

8.5.4.4 Aircraft Installation and Deployment. The discussion of landing-deceleration parachute installation in section 8.5.2 applies equally well to spin/stall parachute installations. Again, it is emphasized that spin parachutes may pull at angles of up to 90 degrees in all planes. Stall parachutes may pull at angles of up to 30 degrees, primarily in the vertical plane on the tail of the aircraft. Also, all parts of the parachute assembly must have a free deployment path to avoid damage to parachute and aircraft and associated parachute malfunction. It is important to mention again that ejection of the parachute through the wake of the aircraft into good airflow is of utmost importance.

Figure 8-26 shows a typical spin/stall recovery parachute assembly and four different deployment methods. Mortar deployment is the simplest and most direct deployment method. Bench mortar ejection tests must show that the mortar ejection is powerful enough to accomplish deployment-bag strip off. Parachute assemblies weighing 130 pounds have been deployed using the mortar deployment method. A relatively large mortar reaction force is a drawback to this deployment method.

Method A shown in Figure 8-26 is a mortar deployment design that deploys the parachute directly without using a pilot chute.

Method B uses a mortar-deployed pilot chute for extraction of the main parachute. This design has more components and a slightly longer deployment time, but it also has a smaller

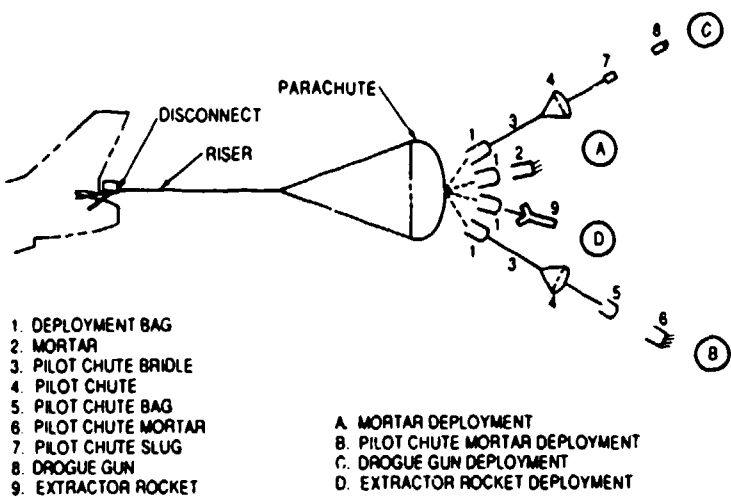


FIGURE 8-26. Typical Spin/Stall Recovery Parachute Assembly and Deployment Concept.

mortar and a lower mortar reaction load. This method was used for the F-5 fighter spin recovery parachute installation.

Method C is similar to Method B, but the pilot chute is deployed with a drogue-gun slug. Method C also uses more components and has a longer deployment time. This design was used successfully on the T-38 jet trainer in actual spin recovery flight tests. This approach permits installation of the parachute assembly in a flat plane.

Method D uses rocket extraction. A rocket fires, and extracts the main parachute bag, and the parachute deploys. The advantage of this method is that the main parachute is immediately deployed without the mortar reaction. However, Method D uses more components and requires heat protection of the parachute assembly from the rocket thrust. The Method D design was used on the F-18 and F-15 spin recovery parachutes.

Section 6.1 discusses in detail the design and operation of these four deployment methods.

The parachute attach fitting on the aircraft must be designed for a 360-degree circular, 90-degree angular pull for spin parachutes, and for a 30-degree upward pull for deep stall recovery parachutes. The attach fitting should be open during flight and closed before parachute deployment, and must be able to jettison the parachute under full load.

Figure 8-27 shows the in-flight deployment of the F-18 spin recovery parachute assembly.

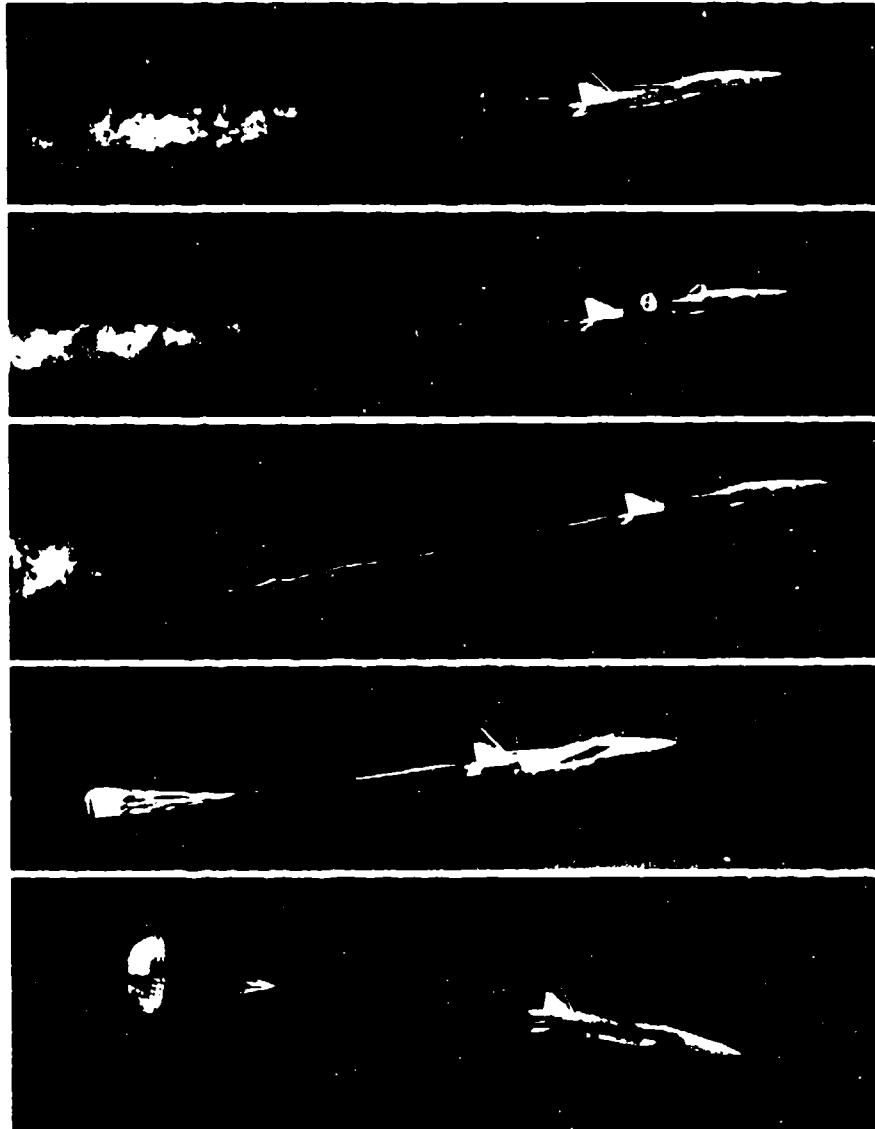


FIGURE 8-27. Deployment Sequence of the F-18 Spin Recovery Parachute.

8.6 ORDNANCE STABILIZATION AND RETARDATION BY INFLATABLE DECELERATORS

8.6.1 Scope of Application

Ordnance stabilization and retardation by inflatable aerodynamic decelerators cover a variety of applications and devices. Bombs dropped from low altitude need retardation to permit the aircraft to escape before the bomb explodes. Mines dropped from aircraft need stabilization and retardation to obtain water entry angles and velocities that avoid ricochet and damage to the ordnance. Aerial torpedoes dropped from high and low altitude at various velocities need stabilization and water entry velocity and entry angle control to avoid damage and to ensure that the torpedo mechanism functions properly. Flares fired from guns and dropped from aircraft for battlefield and target illumination require a low descent rate.

Parachutes of special design and material are used as targets for gunnery and missile firing practice and for special tracking purposes. Airdroppable sonar buoys use parachutes for stabilization and for slow water entry to avoid equipment damage.

Cluster bombs and antitank and antirunway bomblet ammunition, grouped under the name of submunition, use parachutes for retardation, dispersion, scanning, and guided approach to the target.

Some ordnance devices use foldable metal retarders. However, the use of inflatable textile retarders, such as parachutes or ballutes, is the more common approach. Inflatable aerodynamic decelerators manufactured from textiles provide more drag area per pound of weight or storage volume than any other stabilizing or decelerating retarder.

8.6.2 Stabilization and Retardation of Bombs, Mines, and Torpedoes

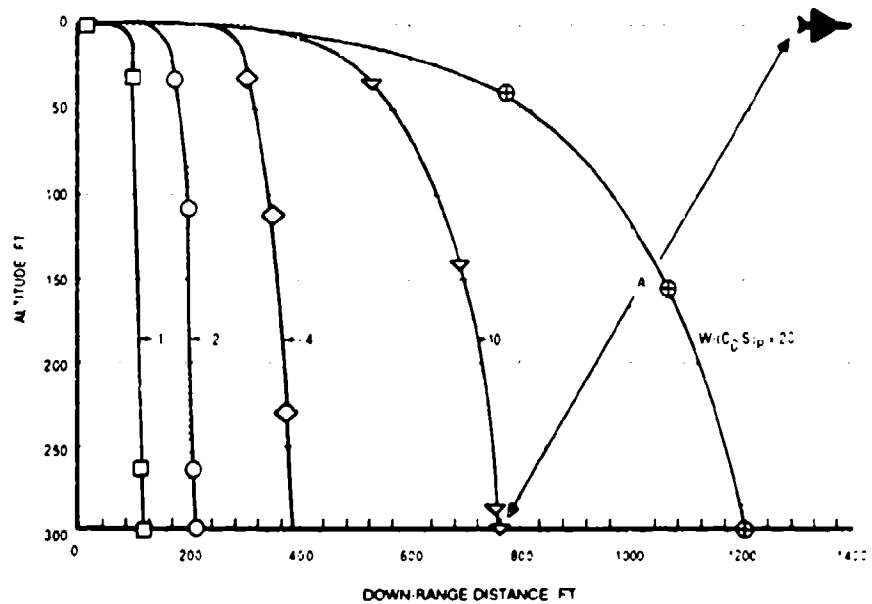
Self-inflatable aerodynamic decelerators for the stabilization and retardation of aerial bombs, mines, and torpedoes are generally quite similar with regard to drop altitudes and velocities, in-flight stabilization and retardation, ground and water entry velocities, and water entry angle. This similarity results in related performance, design, and operational requirements for the retarders used.

The drag of the retarder must be large enough to ensure sufficient separation between the aircraft and the exploding bomb or an inadvertently exploding mine or torpedo.

The retarder must stabilize the ordnance in flight to ensure a precise, repeatable trajectory and a stable water entry for mines and torpedoes. The ground or water impact angle must be steep enough, and the impact velocity low enough, to obtain a desired explosive effect for bombs and to avoid ricochet, broaching, and water entry damage to mines and torpedoes.

Reliability of the retarder operation is of utmost importance. A malfunctioning retarder can result in aircraft and aircrew loss. The retarder should have a high drag, but a low initial opening force, coupled with low weight and volume. Fast, reliable, and repeatable retarder inflation is especially important for ordnance dropped at high speed from low altitudes. Retarder manufacturing should be simple and inexpensive. Handling, packing, and maintenance should be easy and should require a minimum of special tooling. The retarder must be suitable for stowage in a compartment compatible with the configuration of the ordnance, and must be suitable for long-term storage under field and shipboard conditions.

Figure 8-28 plots, for any kind of ordnance, the down-range distance, the impact angle, and the distance between the drop aircraft and the exploding bomb as a function of altitude, and the ratio of ordnance weight to retarder drag area $W/(C_{DS})_p$. The figure assumes that the retarder will inflate instantaneously at drop. The table below the figure gives, for a 2000-pound ordnance device and various ratios, $W/(C_{DS})$, the down-range distance, the impact angle, and the separation distance of aircraft-to-ordnance impact for drop altitudes of 100 and 300 feet, as well as the required diameter, D_o , of a conical ribbon parachute retarder with a drag coefficient, C_{D_o} , of 0.55.



BALLISTIC PARAMETER $W/(C_{DS})_p$	$W/(C_{DS})^2$	10	20	40	100	200
IMPACT ANGLE γ 100 FT	DEGREE	-90	86	83	64	52
IMPACT ANGLE γ 300 FT	DEGREE	-90	-90	88	61	74
DISTANCE TO AC 100 FT AL ^a A	FEET	3100	3500	2500	2100	1700
DISTANCE TO AC 300 FT AL ^a A	FEET	9400	7700	5700	4400	3700

FIGURE 8-28. Effect of Ratio Vehicle Weight, W , to Decelerator Drag Area (C_{DS}) on Down-Range Distance, Impact Angle, and Aircraft Separation Distance.

The figure demonstrates the known fact that airdropped bombs that explode on ground contact need larger decelerators than mines and torpedoes that are retarded primarily to avoid ricochet and damage at water entry.

Two types of inflatable aerodynamic decelerators are used as ordnance retarders: (1) parachutes of ribbon, ringslot, guide surface, and cross type design, and (2) inflatable balloon-type decelerators, called ballutes. Performance characteristics and design details of these two types of decelerators are discussed in Chapters 5 and 6. Textile retarders for ordnance devices are generally housed in metal containers that are part of the ordnance, or are attached to the ordnance. Retarder deployment is accomplished by pyro or spring mechanisms that either eject the parachute directly or use a compartment cover that deploys the parachute or an intermediate pilot chute.

Textile retarders are stored individually or in tail housings in single or multiple containers, frequently hermetically sealed. Field or shipboard storage lives can be 10 to 20 years.

8.6.3 Bomb Retardation

The most important ballistic requirements for bomb retardation, especially for bombs dropped from low altitude at high subsonic and low supersonic velocities, are stabilization for obtaining a precise trajectory and sufficient separation between the aircraft and the exploding bomb.

Two typical bomb retardation systems are the parachute retardation assembly for the B-61 nuclear bomb and the ballute retarder system for the Air Force Mark 82 and Mark 84 and the Navy Mark 83 conventional bombs.

B-61 Parachute Retardation System. The B-61 nuclear ordnance device can be used alternately with a 17-foot-diameter, all nylon, conical ribbon parachute or with a hybrid nylon-Kevlar 24-foot-diameter conical ribbon parachute. Both parachutes have the same weight and fit into the same compartment. The 765-pound bomb has a final rate of descent of 75 ft/s with the 17-foot parachute, and 50 ft/s with the 24-foot parachute. The 24-foot parachute uses Kevlar for suspension lines, radials, skirt, and vent tape, and for all vertical and some of the horizontal ribbons. The larger retarding force of the 24-foot parachute is a distinct advantage for high-speed, low-altitude drops. References 5.42 and 8.108 and Table 8-14 describe the development and list data on both parachute assemblies.

The B-61 parachute deployment system may be called a modified mortar ejection system (see section 6.1.9). The parachutes are packed in leaf-type cylindrical bags, split in the middle, and are pressure-packed with mechanical tools and corset-type lacing. The deployment bag has a cylindrical opening along its center for placing it around the telescoping ejector tube by

means of two heavy webbing straps placed around the deployment bag. Upon ejection, the tube ruptures six shear pins that hold the rear cover in place and ejects the deployment bag by means of the pressure plate and the two webbing straps. At full bag stretch, shear knives cut the bag lacing. An ejection velocity of 150 to 170 ft/s produces full suspension-line and canopy stretch. The two webbing straps and the pressure plate stay attached to the vent of the parachute.

TABLE 8-14. Comparison of the 17-Foot-Diameter Nylon and the 24-Foot-Diameter Nylon-Kevlar Parachutes for the B-61 Nuclear Bomb.

Characteristics	Nylon parachute	Nylon/Kevlar parachute
Parachute diameter, D_0 (ft)	17.0	24.0
Parachute type	Conical ribbon	Conical ribbon
Number of suspension lines	24	24
Suspension-line strength (lb)	10,000	13,500
Horizontal ribbon strength (lb)	3000/2000/1000	3000/2000/1000
Porosity (geometric) (%)	21.5	20
Impact velocity (ft/s)	75	50
Parachute weight (lb)	84	85
Parachute volume (ft^3)	2.12	2.12
Ballistic coefficient $W/(C_D S)$, lb/ ft^2	6.1	3.1

A simpler deployment system, called in this manual a forced pilot chute ejection system, is used successfully on several other ordnance devices. A rear cover is pyro-ejected with several ejector bolts. The cover forms the vent of a pilot chute that in turn extracts the main parachute. Another tested version connects the ejected rear cover with several short straps to the deployment bag of a cluster of three ribbon pilot chutes that then deploy the main parachute. The cluster of three pilot chutes, that has been successfully tested up to low supersonic velocities, provides for a fast, uniform pilot chute action. This method is obviously simpler than the ejector tube method and eliminates the need for the central opening in the main-parachute deployment bag.

All parachutes used for ordnance retardation are manufactured to finished dimensions (see section 6.6.4). This assures that the parachutes will have a high degree of uniformity resulting in a precise, repeatable trajectory—an absolute necessity for dropping bombs with fully automated weapons management systems. References 5.41 to 5.47 describe the development of ribbon parachute assemblies used for ordnance retardation.

Mark 82-84 Ballute Retarder Systems. The Navy and the Air Force have developed ballute retarder assemblies for the Mark 82, 83, and 84 conventional bombs. The ballute retarder, frequently called an attached inflatable decelerator (AID) or a ram-air-inflated

decelerator (RAID), is shown in Figure 8-29. The ballute inflates somewhat faster than a conventional parachute but requires more weight and volume for the same degree of retardation. All three bomb retarder systems have been tested up to low supersonic velocities and at altitudes as low as 100 feet. References 8.109 to 8.111 describe the development of the ballute retarders for the Mark 82 and Mark 84 bombs. Deployment of the retarder is started by a steel cable lanyard attached to the aircraft. Upon lanyard stretch, spring-loaded clips that hold the rear cover in place are released. The rear cover is ejected and extracts the retarder. Four scoops around the periphery of the ballute inflate the Mark 83 retarder in 0.1 to 0.2 second.

Lifting Parachute Type Retarder. The Sandia National Laboratories have developed an interesting concept: A conical ribbon parachute is equipped with a lifting section consisting of horizontal ribbons with a high angle of attack. This produces a lifting trajectory and results in a larger distance between bomb and aircraft for low-altitude bomb drops. Since parachutes are not stable in roll, a roll control system was developed consisting of a reference unit, a gas generator, and several exhaust nozzles that control bomb roll during lifting flight. The development of this concept is described in References 8.112 and 8.113.

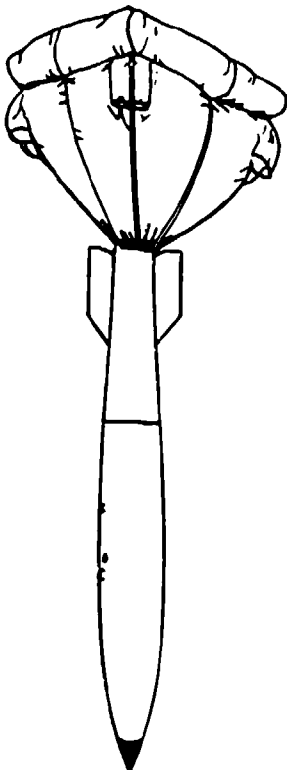


FIGURE 8-29. Mark 83 Bomb With
Ballute-Type Retarder.

8.6.4 Retardation of Aerial Mines

Aerial mines carried by fixed-wing or rotary-wing aircraft in underwing or fuselage installations require a low drag, somewhat streamlined shape, similar to torpedoes. Mines weigh from 500 to 2500 pounds and are being airdropped from close-to-the-deck to high altitudes at speeds from 50 to 500 knots.

Mine retarders must meet requirements similar to those for bomb retarders. The mine must be stabilized from drop to water impact and decelerated to 100 to 300 ft/s at stable water entry. The water entry velocity is governed by mine design, the operational concept, and the need to avoid damage at water entry. The water entry angle must be steep enough to prevent ricochet and broaching. One requirement is for precision mine drops into narrow water channels with sufficient aircraft-to-mine-impact distance to avoid inadvertently exploding mines.

Guide surface and ringslot parachutes are still used as retarders on older mines. Newer mine designs use the stable, low opening shock, cross parachute that is inexpensive and simple in design.

Mine retarder parachutes are usually housed in the tail fairing of the mine. These tail fairings are stored in hermetically sealed containers and are attached to the mine with channel-type metal bands consisting of three to four link-connected pieces.

The size of the retarder is determined by the weight of the mine and the allowable water entry velocity. The retarder must be disconnected at or slightly after water entry. The disconnect may be a mechanical device actuated by a paddle, or a pyrotechnical disconnect actuated by an impact deceleration sensor.

Textile retarders for mines have a shelf life of 20 years when stored in their hermetically sealed containers.

A typical parachute retarder for a 2400-pound mine has the following performance and design data: The retarder is a cross parachute with a surface area of $S_0 = 180.7 \text{ ft}^2$, equivalent to a nominal parachute diameter of $D_0 = 13.17 \text{ feet}$, and a drag area of $(C_D S)_p = 108 \text{ ft}^2$. These parameters result in a ballistic coefficient of $W/(C_D S)_p = 22.2 \text{ lb}/\text{ft}^2$, and a water entry velocity of 137 ft/s. The parachute canopy material has a strength of 500 pounds per inch width, and the parachute has 24 suspension lines of 5500-pound strength each.

The parachute has been manufactured both in nylon and in all-Kevlar. The nylon parachute weighs 23.9 pounds, and the Kevlar parachute weighs 9.32 pounds, a weight saving of 61%. More detailed data on these two parachutes can be found in Reference 6.55. Both parachutes were tested at low and high altitudes at speeds up to 550 knots.

Figure 8-30 shows a typical mine cross parachute assembly in flight. Reference 8.114 describes the development of mine retarder parachutes by the Naval Surface Warfare Center at Silver Spring, Maryland, the primary Naval agency responsible for mine development. Reference 8.115 lists the military specifications for mine parachutes.



FIGURE 8-30. Typical Mine Cross Parachute Assembly in Flight.

8.6.5 Stabilization and Retardation of Aerial Torpedoes

Aerial torpedoes weigh from 400 to 800 pounds, are dropped from 50 to 40,000 feet altitude and from zero up to high subsonic speeds, and enter the water at a velocity of from 50 to 200 ft/s. This lower water entry velocity, compared to mines, reflects the less rugged torpedo design.

The aircraft drop procedure is similar to the drop procedure for bombs and mines: safe aircraft flight with the torpedo carried externally or internally and protected against premature deployment of the retarder; safe torpedo drop and separation from the aircraft; fast and reliable retarder deployment and inflation; and stable, predictable retarder descent until water impact and retarder disconnect. In some cases water retardation is also required. Stable water entry at an angle of 30 to 60 degrees without nose cap, and 30 to 90 degrees with nose cap, is especially important to avoid ricochet or broaching and torpedo damage.

Guide surface, cross, and ribbon parachutes are used as retarders for various types of torpedoes. Reliable in-air and sometimes in-water performance of the retarder, timely separation, and long-term storage capability are prime retarder requirements. The operational modes and sensor systems of the torpedo affect the launch altitude and airspeed.

The retarder assembly is housed in a special container behind the propulsion section of the torpedo. The retarder disconnect may be of mechanical, pyrotechnical, or combined designs actuated by an impact inertia sensor. The retarder assembly is presently stored up to 20 years in a sealed storage container and attached to the torpedo prior to use.

A typical aerial torpedo retarder system has the following data:

Torpedo weight, 510 pounds

Water entry velocity, 150 ft/s

Retarder type ribbon parachute

Retarder diameter, $D_0 = 7.5$ feet

Number and strength of suspension lines, 12 lines, 3000 pounds each

Retarder drag areas, $C_{DS} = 22 \text{ ft}^2$

Retarder ballistic coefficient, $W/C_{DS} = 23.6 \text{ lb}/\text{ft}^2$

Deployment method, static-line initiated

Parachute assembly weight, 20 pounds

Figure 8-31 shows a torpedo ribbon parachute retarder in flight.

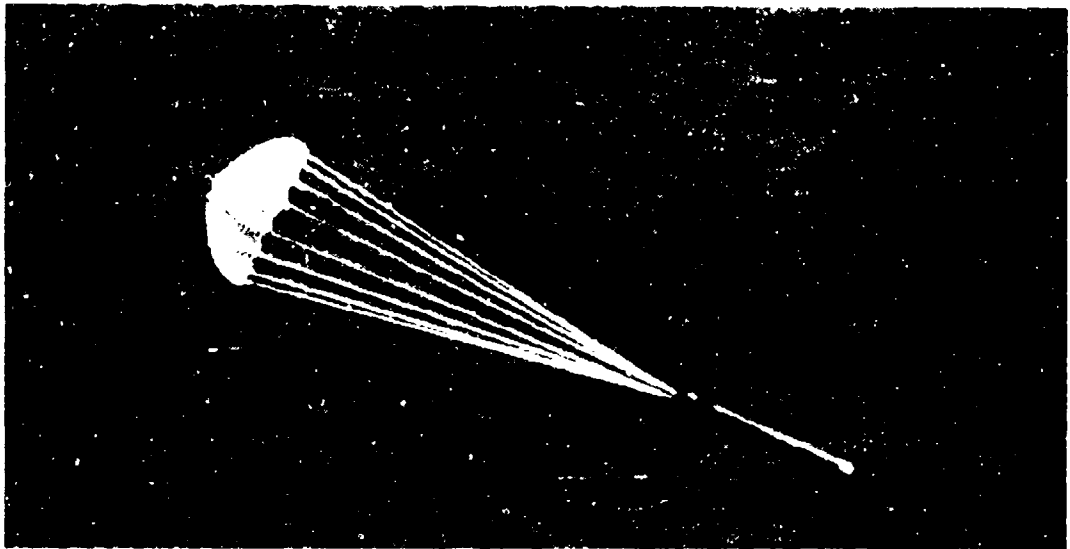


FIGURE 8-31 Torpedo With Ribbon Parachute Retarder in Flight.

8.6.6 Retardation of Illuminating Flares

Flares are used for battlefield illumination, aerial night photography, runway illumination for night landings, and similar applications. Gun-fired flares and aerial flares dropped from a variety of aircraft were used in large quantities in World War II and in the Southeast Asia conflicts.

Flare shells are fired from 60-mm, 105-mm, and 155-mm guns, and from 81-mm mortars. A flare shell consists of the flare housing, the candle, the descent parachute assembly, and a mechanism that ejects candle and descent parachute at a preset time after firing or airdrop. The flare shell, at or after firing from the gun, is subjected to accelerations of 10,000 to 20,000 g, a deceleration that the total flare shell assembly must be able to withstand, a high rotational acceleration, and candle and parachute ejection at shell rotations of 200 to 300 revolutions per second and shell speeds up to 2400 ft/s.

Flare assemblies weigh from 2.4 pounds for the 60-mm flare shells to 50 pounds for airdropped flares. High drag, low oscillation parachutes are used for maximum descent time on the burning candle. Slightly oscillating parachutes are claimed to provide a better resolution for target details. Solid material parachutes of special design are usually used for this application. Parachute diameters range from 24 inches for 60-mm flare shells to over 12 feet for aerial flares. Steel cable risers, and on some flares steel cable suspension lines, of sufficient length are used to protect the parachute from the heat of the candle.

The military agency responsible for flare development is the U.S. Army Armament Research, Development, and Engineering Center at Picatinny, NJ.

8.6.7 Sonar-Buoy Deceleration

Sonar buoys are underwater listening devices that are dropped from rotary- and fixed-wing aircraft. After aircraft separation, stabilization and retardation of the buoy is necessary to achieve a predictable trajectory and an allowable water entry velocity. Sonar buoys range in weight from 12 to 39 pounds. Drop speeds vary from hover for helicopters to about 400 knots for modern antisubmarine warfare (ASW) aircraft, such as the Navy P-30 aircraft. The launch angle of the store relative to the aircraft is between 45 and 90 degrees, depending on the type of drop aircraft. Drop altitudes range from 30 feet for helicopter drops to 30,000 feet for patrol aircraft. The sensing equipment in the sonar buoys restricts the allowable water entry velocity to 120 ft/s and below.

A typical sonar buoy assembly is a tubular container 4.87 inches in diameter and 36 inches long. A parachute is housed in the rear of the tubular container. The store is ejected into the airstream by a pyrotechnic or pneumatic power source. A wind flap is mounted on the parachute end of the container. When the container enters the airstream, the wind flap is pulled away from the container, and, by means of a bridle between the wind flap and the parachute deployment bag, the wind flap extracts and sequentially deploys the suspension lines and the canopy, ensuring an orderly parachute inflation. The parachute opens in 0.1 to 0.15 second and stabilizes the store in 2 to 3 seconds. Equilibrium velocity of the store is reached in 10 to 12 seconds, followed by a stable descent to water impact. At water entry, the parachute is disconnected to avoid entanglement with the buoy.

A safety-of-flight requirement limits the length of the uninflated decelerator to 36 inches for all sonar-buoy configurations. A wind-tunnel and flight-test program was conducted with closely coupled cross, rectangular, and square parachutes of 1.5 to 5 ft² of canopy area. The data obtained were used to define parachute designs that comply with a ballistic coefficient requirement of $18.0 \pm 1.5 \text{ lb}/\text{ft}^2$ for stores between 32 and 39 pounds, and a ballistic coefficient of $12.3 \pm 1.0 \text{ lb}/\text{ft}^2$ for all other stores.

A slotted square parachute that meets all requirements is being produced. Development of this type of decelerator is continuing.

References 8.116 to 8.120 describe development and test work on sonar-buoy parachute decelerator systems. Figure 8-32 shows a typical sonar-buoy parachute system.

The U.S. Navy organization primarily responsible for sonar-buoy decelerator systems is the Naval Air Development Center, Air Vehicle and Crew Systems Development Department, in Warminster, Pa.

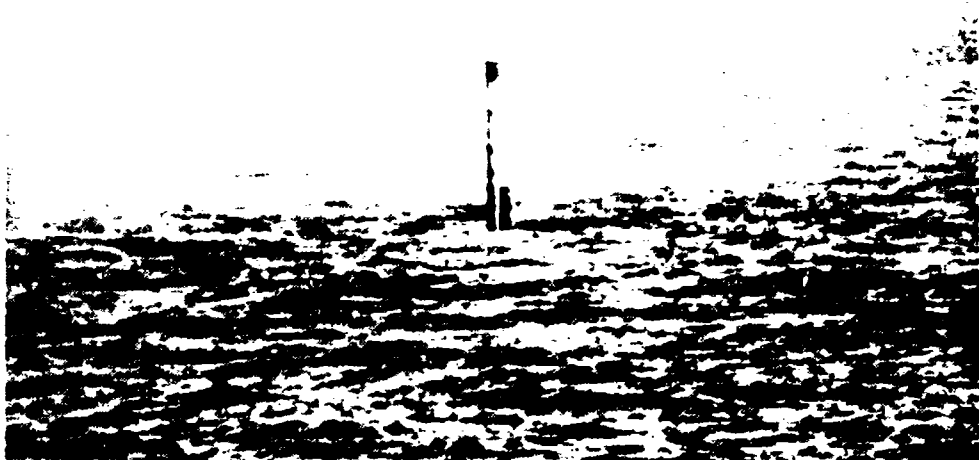


FIGURE 8-32. A Typical Sonar-Buoy-Parachute System in Stable Descent.

8.6.8 Retardation of Electronic Countermeasure (ECM) Jammers

ECM jammers are small electronic devices that block electrical signal propagation and return. Such jammers were used in great numbers in the Southeast Asia conflicts. These devices, weighing less than 10 pounds, are dropped from aircraft in dispenser-type containers and are ejected by centrifugal force or by pyrotechnic units.

Small parachutes of ballistic, gliding, or rotating design are used to provide maximum operating time at the desired altitude. Light weight, high drag, simplicity of design and manufacturing, and low cost are the prime requirements of these parachutes. These small parachutes are ideally suited for computer controlled, automated, mass production processes.

8.6.9 Shell Recovery

Malfunctioning fuzes or components in gun- or mortar-fired shells are impossible to inspect or analyze because they are destroyed at impact. It is desirable during the development and test phase to recover certain types of munition for hardware inspection and functional analysis.

Parachute assemblies for the recovery of shells are subjected to the extreme environment of shell firing, with horizontal accelerations at firing of 10,000 to 20,000 g, radial accelerations of up to 400,000 rad/s², parachute deployment at shell velocities of 1000 to 2000 ft/s, and shell rotation of up to 300 RPS. During firing, the high acceleration may result in a high hydrostatic pressure on parachute components and the parachute compartment.

The parachute usually is installed in the warhead at the tip of the shell. Parachute deployment, initiated by a shell fuze or timer, is accomplished by separating the warhead from the shell by pyro action. The parachute must stabilize the shell and decelerate it to ground impact velocities of 30 to 100 ft/s, depending on the sensitivity of the equipment to be recovered. The rotation of the shell during parachute deployment has caused system mutation before system stabilization. It has been found practical in some cases to use a steel-cable riser between parachute and shell, slightly longer than the shell, to avoid textile riser damage caused by contact with the tumbling shell section. A swivel between shell and riser is required to prevent riser and/or suspension-line wrap-up. Commercially available swivels frequently cannot handle the high loads and high RPS, necessitating the design of special swivels.

References 8.121 to 8.124 describe the development and testing of several shell-recovery systems, including such design details as swivels, steel-cable risers, and warhead separation methods. For long steel-cable risers, it may be practical to cast the wound steel cable in lightweight styrofoam to prevent cable twisting and kinking. This approach was used successfully on the long multiple-steel-cable risers of the Apollo drogue and main parachutes (Reference 5.10 and section 6.1.8). The type of parachute, number of parachutes, and parachute assembly layout depend on the type and weight of the munition to be recovered, the altitude and velocity at the start of the recovery, and the necessary impact velocity. As with most rocket and missile recovery systems, weight and volume of the parachute assembly is at a premium. Extensive use of high-strength Kevlar material and a high degree of pressure packing are recommended. Parachutes for this application seldom exceed 12 feet in diameter and may be considered one-time-use items not subjected to extreme environmental requirements.

8.6.10 Submunition Retardation by Parachute

Submunition refers to small cluster-type bomblets that are carried in airdroppable containers. After aircraft drop and a predetermined time, the container ejects the parachute-retarded bomblets.

The submunition may range from ballistic-parachute-retarded bomblets or mines to sophisticated, self-seeking, sensor fuzed, self-forging, fragment-type destructors descending on rotating, scanning parachutes with the capability to glide toward the target.

The submunition delivery system may be a simple, two-shell cylindrical container; a container with provisions for rearward or sideward ejection of the submunition in a preselected pattern; a winged vehicle with rocket propulsion for a 10- to 20-mile standoff drop; or an engine-equipped, self-guided vehicle with a 100- to 500-mile range for attacking isolated military and supply concentrations. References 8.125 and 8.126 describe several such concepts.

Figure 8-33 shows a submunition delivery system. A standoff container, airdropped and retarded by parachute, lands and scans the area to find and identify suitable targets. Submunition is then rocketed toward the target, descends on a parachute in a scanning motion, flies toward the target, and explodes at a lethal distance. Such systems carry names like anti-armor cluster ammunition (AACA), extended range anti-armor mines (ERAM), and modular standoff weapon (MSOW).

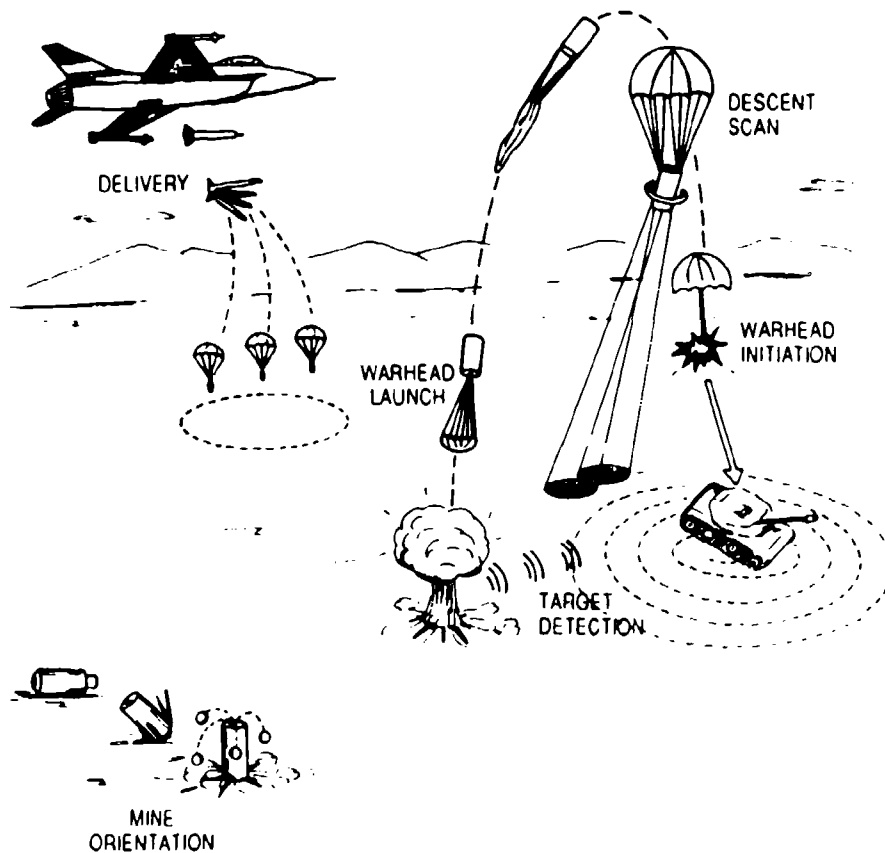


FIGURE 8-33. Typical Configuration of an Extended Range Anti-Armor Mine.

Parachute requirements range from simple ballistic cross parachutes to a parachute that rotates and scans in a predetermined fashion. A considerable amount of theoretical and retarder hardware development work has been accomplished to define the operational characteristics and the dynamic behavior of rotating, scanning (conning), and gliding parachutes suitable for this application. This work includes a rotating guide surface parachute, the rotfoil, the vortex ring parachutes, and samara wing (maple leaf) type decelerators. The aerodynamic and inertia characteristics of the ammunition parachute system are frequently affected in a negative way by the wake of the forebody and gyroscopic forces.

References 8.127 to 8.134 describe theoretical and applied investigations of these types of retarders.

8.6.11 Radar Reflecting Target Parachutes

Specially designed parachutes have been used in the past as radar targets. These parachutes use silver- or aluminum-coated material in the canopy and arrange the material in a pattern that provides a desired radar return signal. An attempt was made to duplicate glint and scintillation of the radar return signals by parachute oscillation and/or rotation. Figure 8-34 shows the radar cross section of one of the parachutes investigated in References 8.135 and 8.136. Use of these parachutes was discontinued in the late 1960s when better radar targets became available.

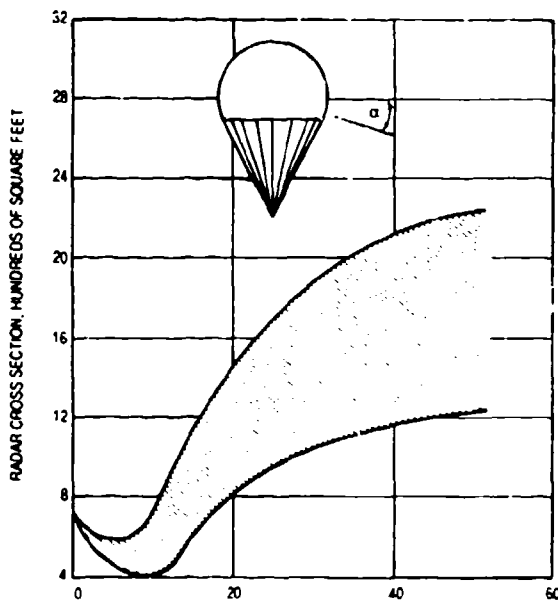


FIGURE 8-34. Radar Reflectivity of a 220-Degree Spherical Canopy, 36 Feet in Diameter Versus Aspect Angle.

In several recent applications, parachutes were equipped with a radar reflecting segment to enhance radar tracking. References 8.135 and 8.136 provide information that is useful for this type of application.

8.7 PREMEDITATED PARACHUTE JUMPING

8.7.1 Scope of Application

Premeditated jumping with parachutes was first used in the 15th century in China and Siam. The parachutists jumped from high towers for show purposes.

The introduction of aerial balloons in the late 18th century in France instigated the competitive development of parachutes, first for saving the lives of balloonists in distress, followed by premeditated parachute jumps in air shows. Parachuting from balloons culminated around 1900 with the relatively modern parachutes and jump techniques of Tinny Broadwick in the United States and Kaethe Paulus in Germany (Reference 8.137).

The introduction and extensive use of military observation balloons in World War I necessitated the use of parachutes for escape from balloons destroyed by enemy action. Parachutes were used for the recovery of balloons, gondolas, and personnel. Records indicate that balloon personnel emergency parachutes were also life tested for premeditated jumps.

The development and use of emergency escape parachutes for aircraft crew members started at the end of World War I. The need to test parachutes to prove that they met the operational and performance requirements of the established specifications brought about the profession of the parachute test jumper.

The widest application of premeditated jumps and associated development of equipment and jump techniques occurred when airborne military units were established to use parachutes for transporting troops to areas of military operations.

The U.S. Bureau of Land Management (BLM) and Forest Service use maneuverable parachutes for transportation of fire fighters (called "smoke jumpers") to remote fire areas. Also, maneuverable parachutes are widely used by the "sky divers"—sport jumpers.

8.7.2 Military Test Jumpers

At the end of World War I, when the development and use of emergency escape parachutes for aircraft crew members began, German pilots started using static-line-operated parachutes similar to parachutes used by military balloon observers (Reference 8.138).

The first documented test jump using a manually operated freefall parachute was performed by Leslie Irvin, the founder of the Irvin Airchute Company, on 28 April 1919, at McCook Field in Dayton, Ohio. The parachute used was developed by a team headed by Major Hoffman. Floyd Smith was the chief parachute designer. The development of the parachute and the jump is described in Reference 8.139.

The introduction of high-performance aircraft during and after World War II led to the development of ejection seats and crew escape modules. Parachutes developed for these new safety measures were (1) personnel emergency escape parachutes for individual aircraft escape, and (2) parachute systems to be used with ejection seats and crew modules. All parachute assemblies and parachute systems undergo extensive development and qualification tests, including live jumps by test jumpers. Ejection seats and crew modules and their parachute systems must permit emergency escape throughout the total aircraft flight performance envelope from zero velocity on the deck to maximum velocity and altitude, including such adverse flight conditions as aircraft being out of control, dives, spinning, etc. The personnel emergency escape parachute, as part of the ejection seat, is limited to deployment below 18,000 feet MSL and 250 KEAS.

Wilhelm Buss in Germany performed the first premeditated live ejection seat test in October 1941 from a Ju 87 bomber using a Heinkel-designed ejection seat (References 8.140 and 8.141). Bernard Lynch in June 1946 made the first live ejection seat test in Great Britain using a Martin-Baker-designed ejection seat (Reference 8.141), followed by Sgt. Larry Lambert who, in August 1946, at Wright Patterson AFB, ejected from a Northrop P-61 with a Wright-Field-designed seat (Reference 8.142). Warrant Officer E. Murray, in September 1959, made live ejection seat tests with the B-58 encapsulated seat, a small crew module.

The U.S. Navy, Army, and Air Force have test jumper units qualified to do live-jump tests of personnel parachutes. Testing emergency escape personnel parachutes involves developing aircraft exit procedures and testing extensive personnel rescue and survival equipment. Rescue and survival equipment may include pressure and temperature protective gear, emergency oxygen equipment, life rafts, emergency radio beacons, and related equipment fashioned for male and female aircrews, from the 5th percentile to the 98th percentile individual with a weight range from 150 to about 300 pounds.

The Naval Weapons Center at China Lake, Calif., has a fine-tuned program for training test parachutists. Training starts with a ground indoctrination program that acquaints the trainee with the equipment used. This training is followed by five static-line jumps using paratrooper parachutes, a procedure that all military parachutists follow. The static-line jumps take place at Ft. Benning, Ga. The program continues with Phase 1 of a two-phase

program at the Naval Weapons Center that includes 14 jumps with freefalls up to 15 seconds, using most of the Navy's personnel emergency escape parachute assemblies listed in Table 8-3 as well as the Army's MC1-1B (gliding T-10) and the aeroconical parachute used in the F-18 aircraft Martin Baker ejection seat.

During or after Phase 1 the trainee is introduced to the ram-air-inflated, maneuverable, gliding parafoil parachute in the "Parascension Program" (Reference 8.143). The trainee ascends from a towed launching platform on the inflated parafoil. During tow the trainee is instructed on the use of parachute controls and how to perform a landing. This has proven to be a safe, effective, and economic method of training parachutists and aircrew members in the use of high-performance, maneuverable parachutes.

In Phase 2 of the training program, the trainee is instructed in body control during long freefalls followed by gliding descent. Such maneuverable parachutes as the U.S. Army MC-3 (paracommander) and the MT-1XS/SL parafoil are used.

Table 8-15 contains information on maneuverable parachutes used by the U.S. military services.

TABLE 8-15. Military Maneuverable Parafoil Parachutes.

Parachute designation	Main parachute area, ft ²	Reserve parachute area, ft ²	Deployment method
MT-1SS	270	270	Manual
MT-1XS	370	270	Manual
MT-1XX	370	370	U.S. Army MC-4, manual
MT-1XS/SL	370	270	U.S. Navy, manual or S/L.

All of the listed parachute assemblies use parafoils as main and reserve parachutes. Figure 8-35 shows a typical parafoil in descent, ready to land with the jumper pulling full brakes. The design and the aerodynamic aspects of maneuverable parachutes in general and the parafoil in particular are discussed in section 5.9.

Some of the parachute assemblies listed in Table 8-15 are used by military rescue and paramedics teams and by special forces of all services.



FIGURE 8-35. Parachutist Landing Parafoil With "Full Brakes."

8.7.3 Paratroopers

In the early 1930s, the Soviet Union established the first airborne troops that were transported by aircraft to the war zone and dropped by parachute. In 1936, the German Air Force established an Airborne Division and began training paratroopers.

German airborne troops were used in the 1940 offensive against France and the low countries. Transported by gliders and dropped by parachutes, the troops overpowered a Belgian Fort and occupied some Dutch Rhine bridges. In 1941, the Germans dropped 8700 paratroopers on the Island of Crete. In 1943, the Germans introduced a modified Hoffman triangle gliding parachute. This parachute worked well in individual jumps, but in the first mass jump, fatalities occurred because paratroopers glided into each other and became entangled.

In the United States, the idea of dropping troops into military zones is credited to General Mitchell. In fact, to demonstrate the feasibility of this concept, a group of soldiers parachuted from the bomb bay of an aircraft.

U.S. and British paratrooper divisions, established at the beginning of World War II, were used in the conquest of Italy, on D-Day in France, and later in an attempt to gain some of the bridges on the Rhine. Paratroopers also played an important part in the more recent invasions of Granada and Panama.

Paratroopers who jumped at Normandy found that the planned 700-foot jump altitude actually varied from 500 to 1500 feet because of the evasive maneuvers of the aircraft to avoid antiaircraft fire. Dropping troops from a 300-foot altitude is now the aim of military strategists to avoid radar detection and minimize the effect of antiaircraft fire.

Paratroopers carry ammunition, rifle, rockets, and other equipment, but the gear restricts the mobility of the paratrooper. The equipment and the low drop altitude leave little chance for maneuvering other than to obtain a favorable landing position.

During the invasion of Normandy in World War II, U.S. paratroopers, because they used main parachutes with canopy-first deployment, used reserve parachutes. However, British paratroopers, who used main parachutes with lines-first deployment, used no reserve parachutes.

Paratrooper training consists of ground training, tower jumps, and five static-line jumps using the T-10 paratrooper parachute. Following this training, the paratrooper is ready for military airdrop operations. During the average enlistment of 3 to 4 years, a paratrooper may accumulate up to 35 jumps. Reserve parachutes are worn on all of these jumps.

A detailed discussion of the development, testing, and use of parachute assemblies for paratroopers can be found in section 8.4.8.

A distinct difference exists in the use of parachutes by paratroopers compared to parachute use by military test jumpers and sport parachutists. Where test jumpers use parachutes for investigation, and sport parachutists use parachutes for recreation, paratroopers use parachutes as a means of transportation from an aircraft to the landing area, uninjured and ready for action.

The U.S. Army is interested in developing a reliable, fast-opening, low-opening-force parachute that will lower a 390-pound paratrooper from an aircraft flying at 300 feet altitude at a rate of descent of 15 ft/s to a landing site 5000 feet above sea level. Low weight and volume must be considered when developing a new paratrooper parachute assembly.

8.7.4 Smoke Jumper Parachuting

The U.S. BLM and Forest Service use aircraft and parachutes to transport fire fighters to remote and inaccessible fire areas. In this case, similar to the case of paratroopers, parachutes

are used strictly as a means of reaching the fire area. In the past 10 years the BLM and Forest Service have changed to low rate of descent, highly maneuverable parachute assemblies.

Smoke jumpers carry equipment that can amount to as much as 80 pounds, bringing the average weight for the parachute to carry to about 250 pounds. The BLM Interagency Fire Center in Boise, Idaho, in conjunction with a parachute company, has developed a 330-ft², seven-cell parafoil parachute that is similar in construction to the military MT-1SS parafoil but differs in the method of deployment.

After the jumper exits the aircraft, a static line attached to the airplane deploys a large pilot chute. The pilot chute, attached to the jumper, decelerates and stabilizes the jumper. After a predetermined length of time, the jumper disconnects the pilot chute, and the pilot chute extracts and deploys the main parafoil. A kill line then deactivates the pilot chute.

The reserve parachute is a five-cell, 270-ft² parafoil. This type of parafoil follows the trend in recent years of using a parafoil reserve with a parafoil main parachute.

The Forest Service Technology & Development Center in Missoula, Mont., has recently changed from the FS-10 (maneuverable T-10) to a newly developed parachute assembly, the FS-12. The FS-12 has an approximately round canopy 32 feet in diameter. This parachute uses low porosity material in front and high porosity material and openings in the rear to obtain glide, and Derry-type slots connected to control lines for maneuverability. The FS-12, when carrying a smoke-jumper weight of 250 pounds, has a measured rate of descent of 15.8 ft/s at MSL and a turn rate of 60 degrees/s.

The Forest Service and BLM have both developed sophisticated ground training programs including tower jumps, cable sliders for aircraft exit, parachute flight control, and a landing training mechanism with the jumper descending at a constant speed.

The Forest Service has a computergraphic maneuvering simulator for jump training. This simulator uses an IBM-compatible personal computer, software that permits variation in jump conditions and terrain, and a VCR and TV screen. The trainee goes through an entire jump, maneuver, and landing in typical forest-fire terrain. An instructor supervises and corrects the trainee's performance. This preliminary training is followed by ten to fifteen training jumps before actual fire jumps. Each year, smoke jumpers returning to fire duty make several training jumps and a proficiency jump every 14 days during periods of no fire fighting. Reserve parachutes are worn on all jumps.

Figure 8-36 shows a Forest Service smoke jumper wearing the FS-12 parachute assembly and standard jump gear.



FIGURE 8-36. Forest Service Smoke Jumper
Ready to Jump.

8.7.5 Sport Parachuting

Sport parachuting started in the late 1920s in the Soviet Union and was sponsored by the government as paramilitary training for subsequent service as paratroopers. After World War II, the French government established several sport parachuting centers that were followed by sport-jumping activities in several European countries and the United States.

Two developments helped to make parachuting a popular sport. The first was the development of sky-diving techniques in the early 1950s in France; the second was the invention in 1964 in the United States of the ram-air-inflated, maneuverable, hi-glide parafoil parachute by Domina Jalbert.

The sport parachute jump consists of two distinctly different phases. The first is a freefall phase where the parachutist, by body positioning and arm and leg movement, controls the freefall and performs glides, turns, loops, and other maneuvers. In the second phase, the jumper pulls the ripcord that opens the parachute pack and deploys the parachute. The parachutist then glides, turns, performs maneuvers, and prepares for and performs a spot landing.

Sky diving has grown so popular that it has become necessary to establish rules and regulations for the safety of the divers. The regulations encompass drop aircraft, sport parachuting centers, the training and licensing of instructors, jump masters, safety inspectors, parachute riggers, and the use of the airspace. The U.S. Parachute Association (USPA) was formed by the sky divers and, in cooperation with the Federal Aviation Agency (FAA), establishes operational and safety regulations for sport parachuting.

Dan Poynter's book, *Parachuting*, and the *Parachute Manual*, References 8.137 and 2.22, describe all aspects of sky diving and parachuting, including the equipment used and the regulations that govern the sport.

In the 1950s and early 1960s, converted military parachutes, such as the standard 28-foot-diameter circular flat modified parachute with openings and slots for glide and turn control, were commonly used for sport parachuting. These parachutes obtained glide ratios of about 0.6 to 0.8 to 1. These were followed by the French LeMoigne and its offspring, the paracommander parachute, shown in Figure 5-103. The paracommander has glide ratios of slightly better than 1 to 1. For a short time, versions of the Rogallo wing, shown in Figure 5-104, were used. The Rogallo wing produced glide ratios of up to 2.5 to 1. Parafoil parachutes are used almost exclusively now for sport parachuting.

Section 5.9 discusses the development and aerodynamics of maneuverable parachutes, all of which have certain technical aspects in common, such as the materials used and the means for obtaining glide and turn control.

Government agencies, including the military, have benefitted from the improvements in equipment and the training methods developed by the sport parachuting community. At first the assumption was that these high-performance, maneuverable parachutes would be difficult to operate and would require extensive training. Time and experience have overcome these problems. Advanced low porosity materi.'s, new sewing techniques, prestretched Dacron suspension lines, and lines manufactured with the super-strong Spectra material have greatly improved dimensional stability, decreased weight and volume, increased performance, and simplified the flying and control of high-performance parafoils.

The sport parachuting community calls the parafoil a ram-air-inflated, square parachute. This is a misnomer. All parachutes are ram-air inflated. Parafoils with a wing-span-to-wing-depth ratio of 2 to 3 are actually rectangular in wing planform, not square. The planform wing area of parafoils ranges from about 150 ft^2 to more than 400 ft^2 . Parafoil canopies are manufactured from low porosity or nonporous fabrics. They behave aerodynamically, the same as rough surface, low-aspect-ratio aircraft wings. Wing loading as the ratio of jumper plus equipment weight divided by the area of the wing (W/S) affects the trajectory velocity of the aircraft. The same is true for parafoils—the higher the wing loading, the faster the forward velocity and the descent rate. The maneuverability is also greatly increased with higher wing loading.

High-wing-loading small canopies should be used only by experienced jumpers. Paratroopers and smoke jumpers (parachutists that use parafoils primarily as a means of transportation) use large, low-wing-loading parachutes that are slower in flight and landing, are easier to control, and are more forgiving of control errors.

Most parafoils use aspect ratios of 2 to 2.5. Higher aspect ratios result in more slender wings, lower wing drag, and better glide ratios. However, parachute deployment and control become more demanding. High-aspect-ratio parafoils, called parawings, are now being used for slope gliding and soaring in the manner of hang gliders.

Several methods are used to deploy parafoils and other maneuverable parachutes. Static-line deployment of the main parachute is used for student jumps with no freefalls. For freefall jumps, a manually or automatically deployed spring-loaded pilot chute is ejected into the airstream. After the pilot chute is inflated, it extracts and deploys the main parachute. Some parachutists prefer to hand-deploy an all-flexible pilot chute. The tandem parachute system uses a method similar to the smoke jumper method.

The nonporous canopy material used for the parafoil and other hi-glide parachutes affects the opening behavior of the canopy. Wind-tunnel and aerial drop tests of low porosity or nonporous material canopies show that the canopy filling time is shorter than the filling time of standard porosity or slotted canopies. The shorter filling time results in about 50% higher opening forces than those of the standard material, round, flat canopies, and a 140% higher force than that of slotted canopies of ribbon or ringslot design.

To decrease the opening shock of parafoils, a slider is used. A slider is a rectangular piece of cloth with grommets on the four corners. The suspension lines are guided in four equally numbered groups through the grommets. The slider can thus move up and down on the suspension lines. When the parachute is deployed, the slider is up on the canopy keeping the canopy closed until line stretch occurs. This arrangement avoids a high snatch force (mass shock). The inflating canopy forces the slider down the suspension lines, controlling and slightly delaying canopy inflation to maintain a low opening force.

The left and right trailing edges of the parafoil are attached to control lines that a jumper can manipulate. Pulling down the left or right control line, thereby the left or right canopy trailing edge, increases the drag on the respective side and causes the parachute to turn in that direction. Pulling both control lines increases the drag as well as the lift of the canopy by increasing the airfoil curvature. This process, similar in action to aircraft flaps, is used during landing. The action of pulling both control lines is called "brakes." Half brakes may be used for the landing approach, and full brakes for landing. Reference 8.137 discusses in detail aircraft exit, freefall maneuvering, parachute glide, and landing.

The Basic Safety Regulations (BSR), published by the USPA and approved by the FAA, mandate the use of reserve parachutes for all sport parachuting. In the early days, round

canopy parachutes of 22 to 26 feet in diameter were used as reserve parachutes, preferably the Navy 26-foot-diameter conical parachute. More recently, sport jumpers, the military, and the BLM fire fighters have used parafoil reserves whenever a parafoil main parachute is used.

Usually a malfunctioning main parachute is disconnected (cut away) before the reserve parachute is deployed. An altitude controlled automatic activation device (AAD) is used by most parachute centers for reserve deployment during student training jumps. This automatic opener deploys the reserve parachute using a spring-loaded pilot chute. The AAD automatically deactivates if a pressure unit senses proper main parachute inflation. All reserve parachutes must be repacked every 120 days by an FAA certified parachute rigger.

Three training methods are in use for becoming a licensed sky diver: (1) the standard method, (2) the accelerated freefall method, and (3) the tandem jump method. The latter is frequently used in connection with the first two, usually as an introduction to sky diving.

The standard training method starts with ground training followed by five static line jumps, normally using a hi-glide parachute. The next steps are training in freefall, freefall maneuvers, parachute glide, and spot landing. After about 20 freefall jumps, the parachutist is eligible to apply for a USPA "A" license (Novice).

The sky diver, in subsequent jumps that include longer freefalls, more complex maneuvers, and precision landings, acquires USPA licenses B to D. These can be earned with a minimum of 200 jumps. Experienced sky divers perform freefall maneuvers forming stars and other formations with large numbers of sky divers participating. All these activities are sanctioned and supervised by the USPA, with strong emphasis on safety. The numerous awards available for extended freefalls, canopy relative work, and competitions are described in Chapter 9 of Reference 8.137.

The accelerated freefall method starts immediately with freefall jumps. The trainee is accompanied on the first jump by two certified jump instructors who advise the student on freefall body control, parachute deployment, parachute control, and landing. As the parachutist learns, the training changes to one accompanying instructor and then to unaccompanied freefalls.

Tandem Jumping. In the tandem training method, two persons freefall, descend, and land on the same parachute. An experienced parachutist, a rated "tandem master," is the parachute operator. A passenger is attached to the front of the instructor with four snaps and D-rings. This allows the passenger to enjoy a parachute jump, or a trainee to get the feel of freefall and operating and landing the parachute. Parafoils with 375 to 425 ft² canopy area are used to obtain the same rate of descent as a single jumper. Tandem parachutes use hand-deployed large 52-inch-diameter pilot chutes that stabilize and decelerate the parachutists before the main parachute deploys. Manually disconnecting the pilot chute opens the parachute pack and deploys the main parachute. This tandem jump method is enjoying

increased use for passenger jumping as well as for the accelerated training of sky divers. Reference 8.144 describes the tandem parachute concept.

Sport parachutists have developed three jump methods: the tandem jump method; BASE (buildings, antenna towers, spans (bridges), and earth (mountain cliffs)); and paragliding.

BASE Parachuting. Experienced parachutists jump from buildings, antenna towers, bridges, and mountain cliffs, all the locations inherent in the acronym, BASE. This type of parachuting requires a reliable, fast-opening, gliding canopy that opens away from the obstacle, often followed by a precision landing in a limited area. Canopies that open quickly at low deployment velocities and modified packing procedures have been developed from the sport of BASE parachuting. Reference 8.145 describes the sport of BASE parachuting.

Paragliding. Parafoil parachutes are used for gliding down steep slopes and in ridge and thermal soaring. When the slope of a hill is steeper than the glide ratio of a parachute, or the rate of descent of a parachute is slower than the updraft on a mountain ridge or a thermal, the parachute can be used for gliding and soaring. This activity is called paragliding.

High-performance gliders approach glide ratios of 50 to 1, hang gliders glide at up to 15 to 1, and parafoil paragliders now reach and surpass glide ratios of 5 to 1. This ratio is obtained through high-aspect-ratio wings; nine-cell canopies; better airfoils; and better airfoil shapes achieved by using plastic stiffeners, winglet type end cells, and other refinements. Parawings of this type are not suitable for sport parachuting because the paragliders lack maneuverability and have more critical stall characteristics (Reference 8.146).

Several technical innovations have been developed by the sky-diving community and associated industry. These innovations include the three-ring parachute disconnect; the canopy slider; the dual parachute pack; and excellent integration of harness, parachute pack, clothing, and related equipment.

8.8 REFERENCE MATERIAL

- 8.1 D. Webb and L. Palm. "Development of a Nylon-Kevlar Recovery System for the CL 289 (AN/USD-502) Surveillance Drone." AIAA Paper, October 1981. (AIAA81-1952.)
- 8.2 T. W. Knacke. "Report on the Work of the Parachute Department, Forschungsanstalt Graf Zeppelin." USAF translation F-SU-1107-ND, June 1946.
- 8.3 P. R. Delurgio, B. A. Engstrom, and W. C. Buhler. "The Mid-Air Recovery System for the Air Launched Cruise Missile." AIAA Paper, October 1981. (AIAA 81-1915.)
- 8.4 W. J. Everett and D. W. Henke. "Design & Development of a Light-Weight Mid-Air Retrieval Parachute System for Cruise Missiles." AIAA Paper, October 1981. (AIAA 81-1914.)
- 8.5 R. E. Runkle and W. R. Woodis. "Space Shuttle Solid Rocket Booster Decelerator Subsystems Drop Test 3—Anatomy of a Failure." AIAA Paper, March 1979. (AIAA 79-0431.)
- 8.6 R. W. Rodier. "Reeling the Space Shuttle SRB-DSS Drogue Parachute." AIAA Paper, March 1979. (AIAA 79-0434.)
- 8.7 D. A. Kross and R. W. Webb. "Space Shuttle Solid Rocket Booster Decelerator Subsystem Rocket Sled Test Program." AIAA Paper, March 1979. (AIAA 79-0437.)
- 8.8 R. D. Moog, D. L. Bachus, and R. L. Utreja. "Performance Evaluation of Space Shuttle SRB Parachutes From Airdrops and Scaled Model Wind Tunnel Tests." AIAA Paper, March 1979. (AIAA 79-0464.)
- 8.9 R. E. Runkle and R. F. Drobnik. "Space Shuttle Solid Rocket Booster Decelerator Subsystem-Airdrop Test Vehicle/B-52 Design." AIAA Paper, March 1979. (AIAA 79-0466.)
- 8.10 R. W. Rodier, R. D. Moog, and D. R. Kross. "136-Foot Main Parachute for Recovery of Space Shuttle Solid Rocket Boosters." AIAA Paper, April 1984. (AIAA 84-0804 CP.)
- 8.11 R. A. Corvin, W. R. Woodis, and J. R. Reuter. "Design and Development of High Strength Parachute for Recovery of Filament Wound Case Space Shuttle Solid Rocket Booster." AIAA Paper. (AIAA 86-2432.)
- 8.12 U. S. Air Force. *Compilation of Data on Crew Emergency Escape Systems*, by J. O. Bull, E. L. Senocki, and H. L. McDonnell. USAF, September 1966. (USAF Report AFFDL-TR-66-150.)

- 8.13 D. N. DeSimone. "Escape System Decelerator Technology." AIAA Paper, October 1981. (AIAA 81-1913.)
- 8.14 A. B. McDonald. "Ejection Seats in the Year 2000." Proceedings of the 16th Annual SAFE Symposium, San Diego, Calif., October 1978.
- 8.15 Naval Weapons Center. *Conduct and Result of the GQ Type 1000 Aeroconical Parachute Assembly Qualification Program for Service Release in the NACES System*, by F. H. Richards. China Lake, Calif., NWC, March 1988. (NWC TP 6906.)
- 8.16 T. Chadderton and J. S. Lingard. "Development of the 6.2-M Aeroconical Ejection Seat Parachute System." AIAA Paper. (AIAA 86-2454 CP.)
- 8.17 Naval Weapons Center. *Aircrew Gliding Escape System (AGES) Exploratory Development Investigation of Aircrew Emergency Escape Ram-Inflated Flexible Wing*, by J. T. Matsuo and M. C. Butler. China Lake, Calif., NWC, September 1983. (NWC TP 6098.)
- 8.18 _____. *In-Flight Ejection Seat Test Using the Aircrew Gliding Escape System (AGES) Parachute*, by M. C. Butler. China Lake, Calif., NWC, September 1986. (NWC TP 6741.)
- 8.19 M. Herr. "Development of the Personal Parachute Assembly for the Space Shuttle Crew Escape System." AIAA Paper, April 1980. (AIAA 89-0922.)
- 8.20 R. Hauck. "The New Crew Escape System, What Can it do for the Discovery Five?" *Countdown*, publication of the NASA Johnson Space Center, October 1988.
- 8.21 U. S. Air Force. *Design Manual*. USAF, February 1980. (USAF AFSC DH1-11.)
- 8.22 Military Standard. "Loading Environment and Related Requirements for Platform Rigged Airdrop Material." August 1968. (MIL-STD-669B.)
- 8.23 U. S. Army. *Proceedings of Airdrop Systems, an Advanced Planning Briefing for Industry*. USANRDEC, Natick, Mass., November 1988.
- 8.24 M. Gionfriddo. "U. S. Army Airdrop Technology Needs for the Future." AIAA Paper, November 1989. (AIAA 89-0977.)
- 8.25 U. S. Air Force. *Evaluation of the C-130E Stability and Control Characteristics During Tandem, Sequential, and Single Platform LAPES Deliveries and Airdrop Deliveries*, by E. L. Rutan and F. B. Stroup. USAF, November 1967. (USAF Report AFFTC-TR-67-18.)
- 8.26 _____. *A C-130 Dual Rail Aerial Delivery System for Heavy Equipment Drop*, by T. A. Olson. USAF, May 1962. (USAF Report AFTC-TR-62-17.)

- 8.27 U. S. Air Force. *Airdrop Tests of the XM-551 Army Full-Tracked Vehicle From a C-130 Aircraft*, by R. P. Hastings. USAF, October 1964. (USAF Report AFTC-TR-64-30.)
- 8.28 U. S. Air Force. *Development of a High-Speed, Low Altitude, Aerial Delivery Parachute System for Use With a Modified C-130 Aircraft*, by F. B. Morris. USAF, December 1970. (USAF Report AFTC-TR-70-33.)
- 8.29 F. B. Stroup and E. L. Rutan. "Stability and Control During Heavy Weight, Low Level Cargo Delivery From a C-130E Aircraft." *Society of Experimental Test Pilots, Technical Review*, Vol. 8, No. 4. Pp. 1-22. 1967.
- 8.30 U. S. Air Force. *Performance Evaluation of a 25,000 to 35,000 Pound Capacity Extraction System for the C-141A Aircraft*, by H. J. Hunter. USAF, August 1947. (USAF Report AFTC-TR-67-23.)
- 8.31 _____. *C-141 Aircraft Aerial Delivery System, Category I Evaluation Tests*, by H. J. Hunter. USAF, December 1966. (USAF Report AFTC-TR-66-32.)
- 8.32 U. S. Army. *Joint Initial Operational Tests and Evaluation Developmental Check Tests of C-141 Container Delivery Systems*. by J. P. Ford, et al. TECOM Project No. 4, April 1975. (Report 4-ES-065-000-001.)
- 8.33 U. S. Air Force. *Evaluation Tests of C-5A Airplane Aerial Delivery System, Phase II Airdrop and Jettison Capability*, by H. J. Hunter and G. E. Boyer. USAF, November 1971. (USAF Report AFTC-TR-71-47.)
- 8.34 _____. *Evaluation Tests of C-5A Airplane Aerial Delivery, Phase III, Modified Aerial Delivery System Components*, by M. A. Tingdahl and H. J. Hunter. USAF, December 1972. (USAF Report AFTC-TR-72-52.)
- 8.35 _____. *Cargo Handling System A/A32H-4*, by M. A. Tingdahl. USAF, February 1964. (USAF Report AFTC-TR-63-46.)
- 8.36 _____. *Evaluation of A/32H-4 Dual Rail Cargo Handling System for Airdrop and Low Level Cargo Delivery*, by R. J. Ducote. USAF, December 1964. (USAF Report AFTC-TR-67-35.)
- 8.37 _____. *Advanced Weather Aerial Delivery System*, by B. D. Ferrier. USAF, November 1971. (USAF Report TAC Test 70A-037A (AD 889 197L).)
- 8.38 _____. *Pendulum Release Parachute Extraction System (PREPS)*, by P. A. Dehmer. USAF, June 1969. (USAF Report TAC Test 68-224 (AD 853 569L).)
- 8.39 _____. *463L Universal Cargo Handling System*, by T. A. Olson. August 1962. (USAF Report AFTC-TR-62-27.)

- 8.40 B. C. Bonaceto and J. F. Schroeder. "Aircraft Controlled Exit System (ACES)." AIAA Paper, October 1984. (AIAA 84-0821.)
- 8.41 U. S. Air Force. *Development and Evaluation of a C-130 Aircraft Low Altitude Parachute Extraction System (LAPES) for Aerial Delivery of Single and Tandem Cargo Platforms at Ground Proximity*, by C. O. Laine. USAF, March 1968. (USAF Report AFTR-68-3.)
- 8.42 _____. *Comparison Study of the Ground Proximity Extraction System and the Low Altitude Parachute Extraction System (LAPES) as Method of Tactical Aerial Delivery of Combat Forces*, by J. W. Worley and D. R. Hughes. USAF, August 1969. (Air Force Institute of Technology Report SLSR-40-69.)
- 8.43 _____. *Joint Tests of 1528 LAPES, Phase I*, by R. W. Hink. USAF, June 1973. (TAC Project 72B-203T.)
- 8.44 _____. *Joint Tests of 1528 LAPES, Phase II*, by W. Foss. USAF, September 1973. (TAC Project 73TB-102X.)
- 8.45 _____. *Low Altitude Aerial Delivery (Fighter Aircraft). Results of Qualification Testing of the M-4A Modified Container Aerial Delivery System*, by P. L. Weintraub. USAF, November 1966. (USAF Report AFTR-66-36.)
- 8.46 _____. *Development of a High Speed, Low Altitude Aerial Delivery System for Use With a Modified C-130 Aircraft*, by F. B. Morris. USAF, November 1970. (USAF Report AFTR-70-33.)
- 8.47 _____. *High Speed, Low Level Aerial Delivery System (HSLLADS)*, by I. L. Franklin. USAF, March 1974. (TAC Project 73A-079T.)
- 8.48 _____. *Evaluation of a Radar and Barometric Altimeter Activated Two-Stage Airdrop System*, by M. J. Wuest. USAF, August 1975. (USAF Report AFFTC-TR-75-25.)
- 8.49 _____. *Military Potential Tests of Interim High Level Container Airdrop System (HLCADS)*, by E. J. Barnicle. USAF, August 1975. (USAF Report ASD-TR-74-23.)
- 8.50 _____. *Feasibility Investigation of a Two-Stage Platform Mounted Airdrop System*, by J. Krizauskas. USAF, July 1975. (USAF Report AFFTC-TR-75-22.)
- 8.51 _____. *Development and Evaluation of a Two-Stage, High Altitude Airdrop Container System*, by W. N. Massey and J. Krizauskas, et al. USAF, November 1974. (USAF Report AFFTC-TR-74-32.)
- 8.52 G. A. Barnard. "Development of a High Level Airdrop Container System." AIAA Paper, November 1975. (AIAA 75-1386.)

- 8.53 W. B. Pepper, et al. "Adaptation of a 15-Foot-Diameter Ribbon Parachute and a 73-Foot Cross Main Recovery Parachute for Cargo Delivery From High Altitude." AIAA Paper. (AIAA 84-0790.)
- 8.54 U. S. Air Force. *150-Foot-Diameter Straight Gore, Solid Flat Parachute*, by C. R. Graham. USAF, February 1954. (USAF FTL-54-16 (AD 289 123).)
- 8.55 _____. *Bibliography of 6511th Test Squadron (Parachute) Technical Publications 1952-1975*, by W. H. Packard. USAF, January 1976. (USAF Report AFFTC-TIM-76-1.)
- 8.56 _____. *Acceptance Tests of G-13 Parachutes*, by R. H. Rice. USAF, January 1954. (USAF Report AFTC-TN-53-7.)
- 8.57 _____. *G-13, 500-Pound Cargo Parachute*, by C. R. Graham, USAF, August 1954. (USAF Report FTC-LR-54-20.)
- 8.58 _____. *G-12B, 64-Foot Cargo Parachute Cluster Tests*, by C. W. Marshall. USAF, March 1958. (USAF Report AFTC-LR-58-102.)
- 8.59 _____. *G-11A Parachute Ultimate Drop Test Conditions*, by C. R. Graham. USAF, September 1954. (USAF Report FTC-TN-54-23.)
- 8.60 _____. *Evaluation Tests of C-5A Airplane Aerial Delivery System, Phase II, Airdrop and Jettison Capability*, by J. B. Hunter and J. E. Boyer. USAF, November 1971. (USAF Report AFFTC-TR-71-43.)
- 8.61 U. S. Army. *Development Tests II (Service Phase) of G-11A Vent Control System for Division Ready Force (DRF)*, by K. T. Cooksley. TECOM Project No. 4, April 1975. (Report 4-ES-60-011-005 (ADV 003 848).)
- 8.62 _____. *A Discussion of the Applicability of Parachutes With Pull Down Vent Lines for Airdrops of Supplies and Equipment From a 500-Foot Altitude*, by E. J. Giebutowski. USA, October 1971. (Report 72-23-(AD 750-585).)
- 8.63 U. S. Air Force. *Internal Parachute Study, Phase II (Clusters)*, by M. A. Tingdahl. USAF, May 1967. (USAF Report FTC-TM-67-109 (AD 289 123).)
- 8.64 W. J. Everett, E. D. Vickery, and R. A. Vernet. "Recovery of 60,000 Pounds Using a Cluster of Six 137-Foot-Diameter Parachutes." AIAA Paper, March 1964. (AIAA 84-0800 CP.)
- 8.65 E. D. Vickery, M. L. Eldridge, and R. A. Vernet. "Development of a System of Six Clustered 137-Foot-Diameter Parachutes to Recover 60,000 Pounds." AIAA Paper, October 1986. (AIAA 86-2445.)

- 8.66 U. S. Air Force. *Development of a Parachute System for Minuteman I Missile Launched From a C-5 Aircraft*, by C. W. Marshall, et al. USAF, April 1975. (USAF Report AFFTC-TR-75-2.)
- 8.67 U. S. Army. *Prototype Cluster Parachute System for a Unit Load of 50,000 Pounds, Volumes I and II*, by R. A. Toni. ANLABS. (Report NLABS-TR-69-83-AD.)
- 8.68 H. J. Hunter, "An Airdrop System for Testing Large Parachutes for Recovery of Loads in Excess of 50,000 Pounds." AIAA Paper, May 1973. (AIAA 72-471.)
- 8.69 U. S. Air Force. *A Study of Design and Materials for Low Cost Aerial Delivery Parachutes*. USAF, September 1959. (USAF Report WAD-TR-59-385.)
- 8.70 _____. *A Study of Design and Materials for Low Cost Aerial Delivery Parachutes*, by F. A. Ruprecht. USAF, June 1962. (USAF Report ASD-TDR-62-309.)
- 8.71 U. S. Army. *Letter of Report of Engineering Design Tests (Airdrops) of the 500-Pound-Capacity Plastic Film Low Cost Parachute*. TECOM Project No. 4, November 1966. (Report 4-S-7498-02.)
- 8.72 U. S. Air Force. *The Criteria for Non-Standard Airdrop Loads*. USAF, December 1977. (USAF Report AFD-TM-ENE-77-1.)
- 8.73 _____. *Extraction Systems*, by C. W. Marshall. USAF, July 1958. (USAF Report AFFTC-TR-58-6.)
- 8.74 _____. *Extraction Parachute Clustering Techniques*, by C. W. Marshall. USAF, October 1958. (USAF Report AFTC-TM-58-18.)
- 8.75 _____. *35-Foot Ringslot Parachute Extraction System Development*, by H. J. Hunter and R. P. Hastings. USF, July 1964. (USAF Report FTC-TR-64-17.)
- 8.76 _____. *Performance Evaluation of a Cluster of Two 28-Foot D₀ Ringslot Extraction Parachutes Towed From a C-130 Aircraft*. USAF, August 1965. (USAF Report FTC-TR-65-25.)
- 8.77 _____. *Performance Evaluation of Heavy Duty 28-Foot D₀ Ringslot Extraction Parachute*, by F. B. Morris. USAF, December 1968. (USAF Report AFFTC-TR-69-43.)
- 8.78 _____. *Development, Test and Evaluation of an Extraction Parachute Subsystem for Airdrop From the C-5A Aircraft*, by J. M. Black. USAF, October 1969. (USAF Report AFFTC-TR-69-29.)
- 8.79 U. S. Army. *A Parachute Retrorocket Recovery System for Airdrop of Heavy Loads*, by G. A. Chakoian. USANLABS, November 1969. (USANLABS-TR-70-34AD.)

- 8.80 _____. *Final Engineering Report-Parachute Retrorocket Airdrop System*, by J. L. Michal, et al. USA, December 1970. (USA Report TR-72-16(AD736 361).)
- 8.81 U. S. Army. *An Active Optical Ground Sensor for a Parachute Retrorocket Airdrop System*, by R. R. Ulrich and A. J. D'Onofrio. USA, February 1973. (USA Report HDL-TM-73-2.)
- 8.82 _____. *Plan for Advanced Development of a Parachute Retrorocket Airdrop System*, by G. A. Chakoian. USA, October 1972. (USA Report TR-73-59-AD.)
- 8.83 J. D. Cyrus. "Retrorocket-Assisted Parachute In-Flight Delivery (RAPID) System Development Update." AIAA Paper. (AIAA 86-2465-CP.)
- 8.84 U. S. Air Force. "The Precision Drop Glider (PDG)," by J. E. Forehand, U.S. Army. Paper presented at the Symposium on Parachute Technology and Evaluation, El Centro, Calif., USAF, April 1969. (USAF Report FTC-TR-64-12, pp. 34-44.)
- 8.85 Sandia National Laboratories. *Controlled Recovery of Payloads at Large Gliding Distances Using the Parafoil*, by C. P. Knapp and W. R. Batron, SNL, November 1967. (SNL Report SC-R-67-1049.)
- 8.86 U. S. Air Force. *Parafoil Steerable Parachute Exploratory Development for Airdrop System Applications*, by R. J. Speelman. USAF, April 1972. (USAF Report AFFDL-TR-71-347.)
- 8.87 Sandia National Laboratories. *A Study of Gliding Parachutes for Accurate Cargo Delivery*, by W. B Pepper. SNL, July 1971. (SNL Report SC-TM-72-0298.)
- 8.88 E. Puskas. "The development of a 10,000-Pound-Capacity Ram Air Parachute." AIAA Paper, April 1989. (AIAA 89-0904.)
- 8.89 R. T. Mayer. "Terminal Descent Controlled Vehicle Recovery." AIAA Paper. (AIAA 84-0801.)
- 8.90 R. T. Mayer, E. Puskas, and P. Lissaman. "Controlled Terminal Descent of Large Aerospace Components." AIAA Paper. (AIAA 86-2467 CP.)
- 8.91 U. S. Army. *Product Improvement Test (Service Phase) of T-10 Personnel Parachute (Modified With 3½-Inch Mesh Net)*, by K. P. Foster. TECOM Project No. 8-EG-0, March 1975. (Report 8-EG-060-010-003(ADB 004 284L).)
- 8.92 A. J. Fallon and J. W. Watkins. "The Annular Parachute—an Approach to a Low Altitude Personnel Parachute." AIAA Paper. (AIAA 86-2449-CP.)
- 8.93 U. S. Air Force. *Quick Opening Reserve Parachutes*, by M. B. Kanowski. USAF, July 1959. (USAF Report AFFTC-TN-59-10.)

- 8.94 U. S. Air Force. *Army Troop Reserve Parachute, Ballistically Deployed Pilot Chute*, by C. O. Laine. USAF, March 1963. (USAF Report FTC-TR-63-4.)
- 8.95 U. S. Air Force. *Performance Evaluation of a Gas-Deployed Reserve Parachute*, by R. B. Calkins. USAF, April 1971. (USAF Report FTC-TDR-71-10.)
- 8.96 U. S. Army. *Check Test of Reserve Parachute Personnel, Troop Chest, Ballistically Deployed*, by D. E. Wolstenholme and T. Dolighan. USA, November 1971. (Report AB 1470-2 (AD 892 431L).)
- 8.97 U. S. Air Force. *Steerable Parachutes*, by D. Gold and J. Rosenberg. USAF, January 1955. (USAF Report FTC-TN-55-1.)
- 8.98 Naval Weapons Center. *Performance Evaluation 35-Foot Diameter Extended Skirt Maneuverable Personnel Parachute*, by G. R. C. Menard. China Lake, Calif., NWC, April 1967. (NWC TR-8-66.)
- 8.99 U. S. Army. *Service Tests of Maneuverable Troop Back Personnel Parachute, Modified*, by B. R. Franklin. TECOM Project No. 8, March 1970. (Report 8-EG-065-000-001 (AD868 721L).)
- 8.100 U. S. Air Force. *Performance Evaluation of Para-Commander Mark 1 Personnel Parachute*, by C. W. Nichols. (USAF Report FTC-TR-66-16.)
- 8.101 H. J. Hunter and M. J. Wuest, "Aerial Delivery of Personnel in Ground Proximity." AIAA Paper. (AIAA 89-0887-CP.)
- 8.102 U. S. Air Force. *Low Level Multiple Personnel Delivery Capsule*, by J. O. Deering. USAF, October 1966. (USAF Report SEG-TR-66-10 (AD 880 624).)
- 8.103 _____. *Concept for a Multiple Personnel Airdrop System*, by J. F. Falcone. USAF, November 1973. (USAF Report FTC-TR-74-15-AD (AD 771 945).)
- 8.104 Military Specification. "Parachutes." MIL-P-87141A, November 1986.
- 8.105 U. S. Air Force. *B-47 Approach Control Parachute*, by J. W. Kiker. USAF, July 1954. (USAF Report ARDC-TN-WCLE-54-18.)
- 8.106 National Aeronautics and Space Administration. *Summary of Design Considerations for Airplane Spin-Recovery Parachute Systems*, by M. B. Sanger, Jr. NASA, August 1972. (NASA Report NASA-TN-D-6866.)
- 8.107 H. P. Stough. "A Summary of Spin-Recovery Parachute Experience on Light Airplanes." AIAA Paper, 1990. (AIAA 90-1317-CP).

- 8.108 W. B. Pepper, "Design and Development of a 24-Foot Diameter Hybrid Kevlar/Nylon Parachute," *AIAA Journal of Aircraft*, Vol. 17, pp 45 to 52, January 1980.
- 8.109 P. G. McGirr and A. C. Aebisher, "Development and Testing of Ballute Stabiliser/Decelerator for Aircraft Delivery of a 500-Pound Munition." AIAA Paper, May 1973. (AIAA 73-485.)
- 8.110 U. S. Air Force, *Evaluation of a Ballute Retarder System for the Mark-82 Bomb*, by R. A. Evors. USAF, May 1973. (USAF Report ADTC-TR-73-31.)
- 8.111 _____. *Preliminary Investigation for Applying a Ram-Air Inflatable Decelerator (RAID) as the Retardation System for the 800-Pound Modular Bomb—Summary Report*, by M. C. Miller. USAF, February 1974. (USAF Report EC-TR-73052.)
- 8.112 W. B. Pepper and J. R. Bistervbold, "An Omnidirectional Gliding Ribbon Parachute and Control System." AIAA Paper, May 1973. (AIAA 73-486.)
- 8.113 R. E. Rychnowski, "A Lifting Parachute for Very-Low-Altitude, Very-High-Speed Deliveries." *AIAA Journal of Aircraft*, Vol. 14, No. 2, February 1977.
- 8.114 Naval Surface Warfare Center, *Some Highlights of the United States Naval Surface Weapons Center—White Oak in the Field of Retardation Systems*, by W. P. Luttko. White Oak, Md., NSWC, October 1982. (NSWC-MP-82-446.)
- 8.115 Military Specification, "Parachutes for Underwater Mines." MIL-P-21904A(OS), March 1987.
- 8.116 C. T. Caliano, "Aeroballistic Characteristics of a Sonarbuoy Parachute Limited to a Length of Three Feet." AIAA Paper, October 1981. (AIAA 81-1950.)
- 8.117 Naval Air Development Center, *AN/SSQ-41, Two Stage Parachute System*, by E. A. Reed, III. Johnsville, Pa., NADC, October 1972. (NADC-72174-VT.)
- 8.118 _____. *AN/SSQ-41A/53 Sonardrop Q41 System Qualification Tests Q53 Developmental Tests*, by E. R. Gombos and E. A. Reed, III. Johnsville, Pa., NADC, December 1972. (NADC-72209-VT.)
- 8.119 _____. *Sonarbuoy Effective Drag Area Ballistic Coefficient, and Parachute Construction Requirements*. Sonarbuoy Production Document, Johnsville, Pa., NADC, 15 April 1988. (NADC SPD-13C.)
- 8.120 C. T. Caliano, "Drag and Stability Improvements of a Square Parachute." AIAA Paper, October 1986. (AIAA 86-2471.)

- 8.121 Sandia National Laboratories. *Parachute System to Recovery of A Spinning (250 RPS) 155-mm Shell Subjected to 20,000 gs Launch Condition*, by W. B. Pepper and R. D. Fellerhoff. SNL, September 1968. (SNL Report SC-R-68-1806.)
- 8.122 D. E. Waye, C. W. Peterson, and W. T. Botner. "Design and Performance of a Parachute Recovery System to Recover 155-mm and 8-Inch Diameter Artillery Shells." AIAA Paper. (AIAA 86-2444.)
- 8.123 C. A. Moehler and D. W. Pillasch. "Development of a Two-Stage Projectile Payload Deceleration System." AIAA Paper. (AIAA 86-2443 CP.)
- 8.124 J. A. Buckley. "Missile Recovery System for High-Speed Small-Caliber Missiles." AIAA Paper, October 1986. (AIAA 86-2462.)
- 8.125 S. K. Ibrahim. "An Overview of Munition Decelerator Technology With Recent Applications at Honeywell." AIAA Paper, May 1984. (AIAA 84-0780.)
- 8.126 H. Wanstell. "Flying Dispensers for Stand-Off Attack." Interavia Aerospace Review, July 1989, Pp.717 to 720.
- 8.127 R. J. Kingsley and J. Reuter. "Development of a Lifting Parachute to Provide Self-Dispersing Capability for an AVCO Designed Tactical Ammunition." AIAA Paper, October 1981. (AIAA 81-1928.)
- 8.128 R. Kline and W. Koenig. "Samara Type Decelerator." AIAA Paper, April 1984. (AIAA 84-0807.)
- 8.129 D. W. Pillash, J. C. Shen, and N. Valero. "Parachute/Submunition Coupled Dynamics." AIAA Paper, April 1984. (AIAA 84-0784.)
- 8.130 P. Crimi. "Analytical Modelling of a Samara-Wing Decelerator." AIAA Paper, October 1986. (AIAA 86-2439.)
- 8.131 Z. Shpund and D. Levin. "Improved Measurements of the Dynamic Loads Acting on Rotating Parachutes." AIAA Paper, October 1986. (AIAA 86-2473.)
- 8.132 K. F. Doherr and R. Synofzik. "Investigation of Rotating Parachutes for Submunition." AIAA Paper, October 1986. (AIAA 86-2438.)
- 8.133 J. Reiff. "Parachute Studies Conducted at MRB, Aeromechanical Two-Body Model With Nine Degrees of Freedom." Paper presented at the University of Minnesota/Carl Cranz Gesellschaft Lecture on "Parachute Technology: Fundamentals, Concepts and Applications," Munich-Oberpfaffenhofen, July 1987.

- 8.134 W. H. Koenig. "A Flexible Fin Deployment Simulation." AIAA Paper, April 1989. (AIAA 89-0919.)
- 8.135 Hughes Aircraft Co. *Missile Target Systems Pogo-Hi*, Vol. 4, by H. K. Epple. HAC, January 1960. (Report TM603.)
- 8.136 University of Texas. *Reflecting Characteristics of Pogo Parachute Models D556, D503, and P/B 509-330*, by C. O. Britt, L. C. Kraus, and W. W. Bahn. UT Electrical Engineering Research Laboratory, January 1960. (Report EERL 3-24.)
- 8.137 D. F. Poynter. *Parachuting*. Book published by Para Publishing, P. O. Box 4232, Santa Barbara, Calif., 93140. Fifth edition, 1989.
- 8.138 T. W. Knacke. "Technical-Historical Development of Parachutes and Their Applications Since WWI." AIAA Paper, October 1986. (AIAA 86-2423.)
- 8.139 P. Hearn. *Sky High Irvin*. Book published by Robert Hale Limited, Clerkenwell House, Clerkenwell Green, London EC1R OHT, 1983.
- 8.140 S. Ruff, M. Ruck, and G. Sedlmayr. *Sicherheit und Rettung in der Luftfahrt*. Bernhard Graefe Verlag, Karl-Mand Strasse 2, 5400 Koblenz, West Germany, 1989.
- 8.141 Bryan Philpott. *Eject, Eject*, Ian Allan Ltd. Publishers, London. Sole U.S. distributor: Motorbook International, Osceola, Wis. 54020, 1989.
- 8.142 U. S. Army Air Force. *Human Subject Ejection Test From a P-61 Airplane*, by H. Fouch. USAAFMC, August 1946. (Report No. TSEAC-45341-2-1.)
- 8.143 Naval Weapons Center. *Parascension Training Program*, by M. C. Butler and M. A. Peltz. China Lake, Calif., NWC, September 1986. (NWC TP 6728.)
- 8.144 B. Booth. "Tandem Jumping." AIAA Paper. (AIAA 86-2485-CP.)
- 8.145 J. Boenish. "BASEic Sport Parachuting; We Will Cross (Jump Off) That Bridge When We Come to It." AIAA Paper. (AIAA 86-2484-CP.)
- 8.146 M. J. Ravnitzky. "Today's Slope Soaring Technology Previews the Future of Advanced Ram-Air Canopies for Parachutists." *Skydiving*, Vol. 9, No. 10, Issue 106, April 1990.

LIMITED INDEX

- Aeroconical parachute, 5-63, 8-19
 Aerodynamic forces, steady, 4-9
 Aerodynamic heating, 5-102
 Air Bags, 6-112, 7-4, 8-7
 Aircraft
 crew module, 5-38, 8-26
 escape, general, 8-13
 landing approach parachute, 8-55
 landing deceleration parachute, 8-49
 spin/stall recovery parachute, 8-55, 56
 AIM parachute, 5-63, 8-6
 Airdrop
 containers, 8-33
 LAPES, 8-33
 personnel, 8-43
 platforms, 8-28
 systems, general, 8-27
 Airflow around canopies, 5-33
 Air-to-air retrieval (*see* midair retrieval)
 Anti-inversion net, 6-46
 Apollo Earth landing system, 5-23, 66, 6-8
 Atmospheric properties, 4-1
- Ballute, 5-5, 107, 8-63
 BASE parachuting, 8-84
 Bomb ballute retarder, 8-63
 Bomb lifting decelerator, 8-64
 Bomb retardation, 8-60
 Bomblet parachute (*see* submunition)
 Booster recovery, 8-12
 Bridle, 6-6, 14
- CALA, CANO, 6-61
 Canopy
 apex pull down, 5-78
 filling time, 5-42
 geometry, 6-17, 36
 hi-glide, 5-110, 8-21, 76
 inflation process, 5-41
 loading, 5-49
 nominal diameter, 5-2, 129
 porosity, 5-71
 pressure distribution, 5-93
 reefing, 5-74, 6-61
 shapes, 5-91
 spreader gun, 5-64
 surface area, 5-2, 129
 types, 5-3
 Cloverleaf parachute, 5-112, 118
 Cluster parachutes, 5-121, 6-38
 Coefficients (*see* specific use)
- Conical parachutes, 5-3, 6-17
 Conversion tables, 3-5
 Cotton, 6-75
 Crew modules, 5-38, 8-26
 Critical opening speed, 6-32
 Crushable materials, 6-106
- Dacron, 6-76
 Deployment, 6-1
 bags, 6-48
 controlled, 6-5
 cross-wind, 6-10
 drogue gun, 6-6
 forces (snatch force), 5-64, 6-2
 methods, 6-1
 mortar, 6-8
 sequence, 6-1
- Design criteria, 2-5
 Design factors, 6-55, 7-24
 Diameter, nominal, 5-2, 129
- Dimensioning, parachute assembly, 6-58
 Dimensions, finished, 6-85
 Disconnect, 6-13
 Drag area variation, 5-45, 61
 Drag coefficients, 5-2
 Drogue chute, 5-66, 8-4
 design, 7-34
 Dynamic load factor, 6-55
 Dynamic pressure, 3-15, 4-7, 5-128
 Dynamic stability, 5-32
- ECM jammer deceleration, 8-70
 Effective forebody diameter, 5-24
 Effective length of suspension lines, 5-20
 Effective porosity, 6-31
 Effects of environment on textiles, 6-54, 76
 Ejection methods devices, 6-5, 10
 Ejection seats, 2-2, 5-38, 8-14, 19
 Encapsulated seats, 5-38, 8-14
 Environment, Earth, 4-1
 Extraction parachutes, 8-40
- Fabrics, 6-74
 fabrication, 6-80
 Filling distance, 5-42
 Filling time, 5-43
 Flare parachutes, 8-68
 Forebody wake effect, 5-21, 55
 Formulas, frequently used, 5-128
 Fullness, 6-86

- Geodetic line system, 5-36
- Gliding parachutes, 4-17, 5-5, 110, 6-24, 8-76
- Gore shapes, 6-17
- Gravity, 4-2
- Guide surface parachute, 5-3, 29
- Hardware (see specific items)**
- Heating, aerodynamic, 5-102
- Hi glide parachutes, 5-5, 13, 110
- Hi glide systems (see section 8.7)
- History of parachutes, Ref. 2.2, 8.137
- Impact attenuation, 6-101
- Impact attenuation systems, 6-117, 7-4
- Induced drag, 4-18
- Infinite mass condition, 5-49
- Infinite mass opening force coefficient, 5-50
- Inflation
 - air bags, 6-112
 - canopies, 5-42
- Inversion (canopy), 6-46
- Joint efficiency, 6-57
- Kevlar
 - designing in, 6-88
 - materials, 6-89
 - environmental effects, 6-57
- Landing approach parachutes, 8-55
- Landing deceleration parachutes, 8-49
- Landing impact dynamics, 6-103
- LAPES airdrop system, 8-33
- Lift, 4-10
- Lift/drag (glide ratio), 4-19, 5-5, 117, 8-48
- Load (opening force) analysis, 5-38, 7-15
- Load distribution (canopy), 6-58
- Mach number, 4-4
- Main parachute system, 6-14, 7-6
- Maneuverable parachutes, 5-13, 110, 8-76
- Manufacturing (parachutes), 6-74
- Materials
 - crushables, 6-106
 - fabrics, 6-82, 89
 - honeycomb, 6-106
 - low-cost, 8-40
- Mass, finite, 5-49
- Mass, infinite, 5-49
- Midair retrieval, 8-8, 10
- Military test jumpers, 8-74
- Mine retardation, 8-65
- Missile recovery, 8-4
- Mortars, 6-8
- Newton's laws, 4-7
- Nominal diameter, 5-2, 129
- Nose, crushable, 6-121
- Nose spike, 6-121
- Opening force**
 - altitude effects, 5-67
 - coefficient, 5-2, 50
 - calculations, 5-50
 - diagrams, 5-62
 - hi-glide parachutes, 5-120
 - overinflation control line, 6-74
 - porosity effects, 5-67
- Ordnance retardation, 8-60
- Oscillation, 5-31
- Parachute**
 - annular, 5-3, 8, 28, 6-22, 8-48
 - applications, 2-3, 8-1
 - circular flat, 5-3, 6, 25, 63, 6-18
 - cloverleaf, 5-112, 118
 - conical, 5-3, 6-17
 - cross, 5-3, 9, 44, 6-21, 8-65
 - definitions, 6-14
 - disk-gap land, 5-4, 29, 6-38
 - extended-skirt, 5-3, 7, 6-17, 7-7
 - growth potential, 2-6, 6-12
 - guide surface, 5-3, 8, 29, 6-24, 7-6
 - hemisflo, 5-4, 29, 101, 6-33
 - hyperflo, 5-101, 6-34
 - Le Moigne, 5-5, 112
 - paracommander, 5-5, 113
 - parafoil, 5-5, 13, 114, 8-21, 76
 - parawing, 5-5, 13, 114
 - ribbon, 5-4, 9, 56, 6-28, 7-35, 8-57
 - ringsail, 5-4, 10, 29, 6-36
 - ringslot, 5-4, 10, 29, 6-35
 - Rogallo wing, 5-115
 - rotifoil, 5-11, 8-73
 - tojo, 5-5, 8-46
 - vortex ring, 5-4, 12, 8-70
- Paragliding, 8-84
- Paratroopers, 8-43, 77
- Pilot chutes, 6-3, 43
- Pocket bands, 5-87, 6-42, 7-32
- Premeditated parachuting, 8-74
- Pressure packing, 6-99
- Pull-down vent line, 5-65, 8-38
- Quarter deployment bag, 6-52
- Rate of descent, 4-14, 5-128
- Release (see disconnect)
- Recovery systems, see Chapter 8
- Reconnaissance drone recovery, 8-5

Reefing

general, 5-74, 6-61
 continuous disreefing, 5-79
 hi-glide parachutes, 6-66, 8-21
 installation, 6-64
 line cutters, 6-69
 multiple stage, 6-65
 rings, 6-67
 simultaneous, 6-66, 8-27
 slider, 5-79

Retrorockets, 6-118, 8-42

Reynolds number, 4-4, 5-29

Ribbon parachutes, 5-4, 6-28, 7-44, 8-51

Risers, 6-6

Sacrifice sleeve, 6-52

Sailwing parachute, 5-5

Seams, textiles, 6-85, 92

Shear knives, 6-50

Silk, 6-75

Skirt hesitator, 6-52

Skirt jet, 6-120

Sleeve, deployment, 6-51

Smoke jumpers, 8-78

Snatch force, 5-64

Sonar-buoy retardation, 8-69

Space Shuttle escape system, 8-23

Spin recovery, 8-55

Sport parachuting, 5-112, 8-80

Spreader gun, 5-63

Stability, parachute, 5-30

Stabilization parachutes, 5-30

Stall recovery, 8-56

Steady aerodynamic forces, 4-9

Stitching types, 6-83

Strength of materials, 6-80, 92

Submunition retardation, 8-71

Supersonic parachutes, 5-97

Supersonic drag devices, 5-109

System analysis, 7-2

Symbols, list of, 3-16

Tandem parachuting, 8-83

Target drone recovery, 8-4

Target parachutes, 8-73

Temperature conversion tables, 3-10

Temperature effects on textiles, 6-78

Test jumpers, 8-74

Textiles

cotton, 6-75

dacron, 6-76

designing in, 6-84

fabrics, 6-74

fibers, natural, 6-75

fibers, man-made, 6-75

spinning, 6-78

tapes, 6-83, 91

threads, 6-83

weaving, 6-80

webbing, 6-83, 91

Tolerances, textile manufacturing, 6-87

Torpedo retardation, 8-67

Units of measurement, 3-1

Unmanned vehicle recovery, 8-4

Volume of parachutes, 6-93

Volplan parachute, 5-5

Wake effect, 5-21

Wake, supersonic, 5-99

Weight of parachutes, 6-93

Weight of deceleration systems, 6-93

Wind-tunnel testing, 4-20

Warning-Disclaimer

Whenever a person leaves the ground, he or she risks injury or even death. Whether to accept or reject this risk and its accompanying challenge must be a personal decision; one must weigh the risk and the reward. This book is designed to promote safety through education.

This is not a do-it-yourself text. The information contained here is intended as an introduction to parachute engineering and design and as a source of reference. It is not the only source of information.

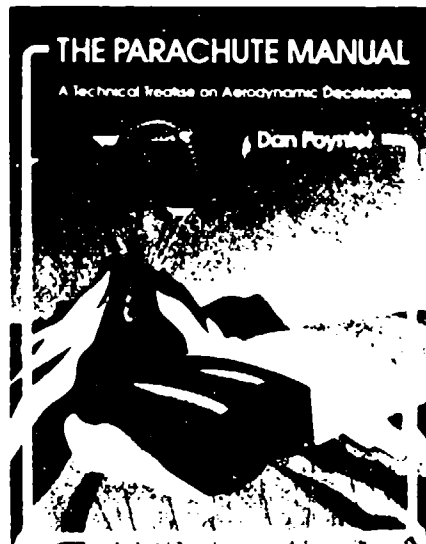
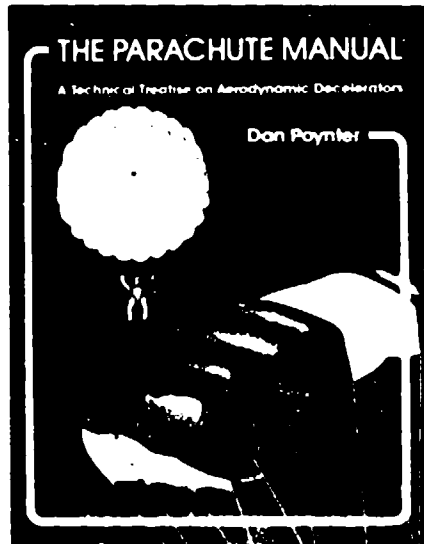
This book is designed to provide accurate and authoritative information in regard to the subject matter covered. It is not the purpose of this manual to reprint all the information that is otherwise available, but to complement, amplify and supplement other courses and texts. For more information, see the many listed references.

The purpose of this manual is to educate and entertain. Every effort has been made to make this book as complete and as accurate as possible. However, there may be mistakes both typographical and in content. Therefore, this text should be used only as a general guide and not as the ultimate source of parachute information. Furthermore, this manual contains information only up to the printing date.

Para Publishing warrants this book to be free of defects in materials and workmanship. This warranty shall be in lieu of any other warranty, express or implied.

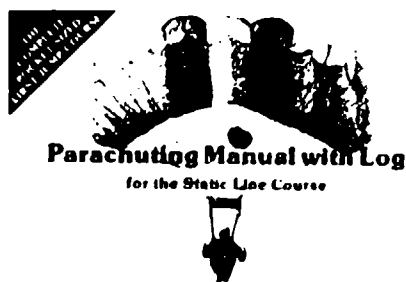
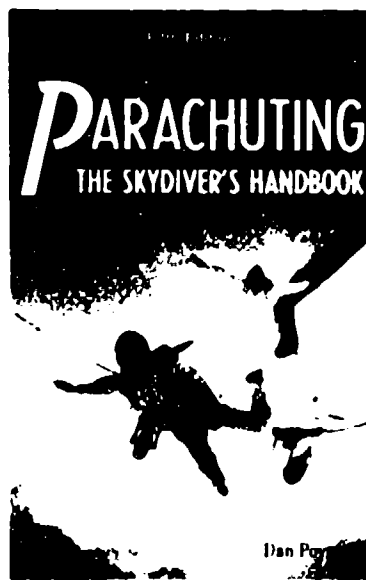
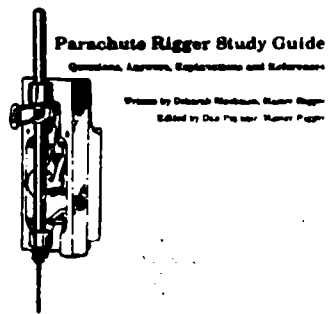
The author and Para Publishing shall have neither liability for, nor responsibility to, any person or entity with respect to any loss or damage caused or alleged to be caused directly or indirectly by the information contained in this book.

If you do not agree with the above, you may return this book to the publisher for a full refund.



PARACHUTE RIGGING COURSE

A COURSE OF STUDY FOR THE PARACHUTE RIGGING COURSE



Parachuting Manual with Log
for Accelerated Freefall



Order Blank

Telephone orders

From the U.S.: (800) PARAPUB. (727-2782).

From other countries: (805) 968-7277

Have your MasterCard, Visa, Discover, Optima or American Express card ready.

Fax orders

(805) 968-1379. (Send this order blank.)

Postal orders

Para Publishing, P.O. Box 4232-P, Santa Barbara, CA 93140-4232, USA.

Please send me the following books:

- The Parachute Manual, Volume I (to 1984) by Dan Poynter @ \$49.95
- The Parachute Manual, Volume II (since 1985) by Dan Poynter @ \$49.95
- The Parachute Recovery Systems Design Manual by T.W. Knacke @ \$49.95
- Parachute Rigging Course by Dan Poynter @ \$11.95
- Parachute Rigger Study Guide by Deborah Blackmon @ \$14.95
- Parachuting Instructor/Examiner Course by Dan Poynter @ \$14.95
- Parachuting, The Skydiver's Handbook by Dan Poynter @ \$19.95
- Parachuting Manual with Log for the Static Line Course by Dan Poynter @ \$2.50
- Parachuting Manual with Log for AFF by Jan Meyer @ \$3.95

Company name: _____

Your name: _____ Telephone: (_____) _____

Address: _____

ZIP: _____

Payment:

Cheque. (Foreign orders, use credit card, send cheque drawn on a U.S. bank or send an International Postal money order.)

Credit card. Expiration date: ____/____

Type of card: _____ Card number: _____

Name on card: _____ Signature: _____

Sales tax:

Add 7.75% for books sent to California addresses (only).

Shipping: (Overpayments for lighter books and multiple-book shipments will be refunded.)

U.S.-	Surface:	\$3.00 for the first book, \$1.00 for each additional book.
	Air:	\$4.75 per book.
Foreign-	Surface:	\$5.50 for the first book, \$4.00 for each additional book.
	Air:	\$29.00 per book.

Prices subject to change without notice. SBN 216-8981. Fed ID 95-6582285. DUNS: 09-141-9360. Street address: 530 Ellwood Ridge, Santa Barbara, CA 93117-9700, USA.

Send for FREE descriptive brochures on individual books

Order Blank

Telephone orders

From the U.S.: (800) PARAPUB. (727-2782).

From other countries: (805) 968-7277

Have your MasterCard, Visa, Discover, Optima or American Express card ready.

Fax orders

(805) 968-1379. (Send this order blank.)

Postal orders

Para Publishing, P.O. Box 4232-P, Santa Barbara, CA 93140-4232, USA.

Please send me the following books:

- The Parachute Manual, Volume I (to 1984) by Dan Poynter @ \$49.95
- The Parachute Manual, Volume II (since 1985) by Dan Poynter @ \$49.95
- The Parachute Recovery Systems Design Manual by T.W. Knacke @ \$49.95
- Parachute Rigging Course by Dan Poynter @ \$11.95
- Parachute Rigger Study Guide by Deborah Blackmon @ \$14.95
- Parachuting Instructor/Examiner Course by Dan Poynter @ \$14.95
- Parachuting, The Skydiver's Handbook by Dan Poynter @ \$19.95
- Parachuting Manual with Log for the Static Line Course by Dan Poynter @ \$2.50
- Parachuting Manual with Log for AFF by Jan Meyer @ \$3.95

Company name: _____

Your name: _____ Telephone: (_____) _____

Address: _____

ZIP: _____

Payment:

Cheque. (Foreign orders, use credit card, send cheque drawn on a U.S. bank or send an International Postal money order.)

Credit card. Expiration date: ____/____

Type of card: _____ Card number: _____

Name on card: _____ Signature: _____

Sales tax:

Add 7.75% for books sent to California addresses (only).

Shipping: (Overpayments for lighter books and multiple-book shipments will be refunded.)

U.S.- Surface: \$3.00 for the first book, \$1.00 for each additional book.

Air: \$4.75 per book.

Foreign- Surface: \$5.50 for the first book, \$4.00 for each additional book.

Air: \$29.00 per book.

Prices subject to change without notice. SBN 215-9981. Fed ID 85-6532286. DUNS: 09-111-9356. Street address: 530 Ellwood Ridge, Santa Barbara, CA 93117-9700, USA.

Send for FREE descriptive brochures on individual books

Here is everything there is to know about recovery systems from the earliest models to the latest, most advanced parachutes.

This incredible compilation of parachute design information provides you with tools to evaluate, select, design, test, manufacture, and operate parachute recovery systems. These systems range from simple, one-parachute assemblies to multiple-parachute systems. All aspects are discussed, including the need for parachute recovery, the selection of the most suitable recovery system concept, a computerized approach to parachute performance, force and stress analysis, geometric gore design, component layout, material selection, system design, manufacturing, and in-service maintenance. In short, this is the last word in technical design manuals for recovery systems.

"Theo Knacke has made major contributions to Sandia's high performance parachute programs since 1954 through his publications, design manuals, parachute short courses and generous advice. This excellent design manual adds even more stature to his international reputation as a parachute expert."

— Randy Maydew, Manager, Aerodynamics,
Sandia National Laboratories (retired).

"This book provides the necessary tools to evaluate, select, design, test, manufacture and operate parachute recovery systems, laying stress on contemporary practice. A 'must' for parachute engineers."

— David Cockrell, University of Leicester, England.
Recipient of the 1989 AIAA Aerodynamic Decelerator Award.

"Here is an outstanding and exhaustive study of round parachutes by the pre-eminent engineer in the field."

— Dan Poynter, author, *The Parachute Manual*.



Theo Knacke is the parachute engineer's engineer. He has spent a lifetime working in all phases of parachute research, development and application in both Germany and the United States. He is the authority on escape systems, landing deceleration canopies, aerial delivery clusters, personnel parachutes and spacecraft recovery systems. Mr. Knacke served as Chief of the Technical Staff for both the Gemini and Apollo Spacecraft Landing Systems. He is known worldwide for his lectures sponsored by the American Institute of Aeronautics and Astronautics and hosted by the University of Minnesota.

**This handy reference will provide
you with everything there is to
know about parachute
engineering and design.**

ISBN 0-915516-85-3



9 780915 516858

END
FILMED

DATE:
4-92

DTIC